UNIVERSITÄT LEIPZIG

REPORT
Institute für Physik
The Physics Institutes

2014

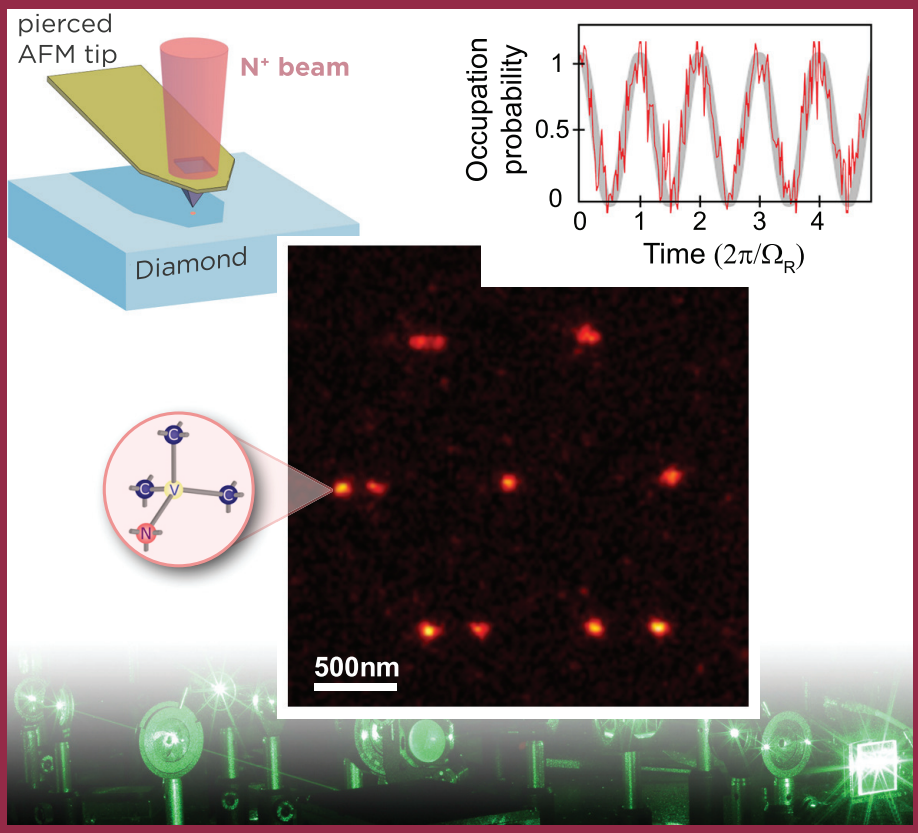

The Physics Institutes of Universität Leipzig, Report 2014
M. Grundmann (Ed.)

Technical Editor: Anja Heck

Printed in Germany by
MERKUR Druck und Kopierzentrum GmbH, Leipzig

online available at
http://nbn-resolving.de/urn:nbn:de:bsz:15-qucosa-148925

Front cover

■ Optical centres in diamond for quantum-information processing and high-sensitivity high-resolution magnetometry: The central image is a fluorescence scan of a high-purity diamond substrate implanted with nitrogen atoms to produce a pattern of single nitrogen-vacancy (NV) centres (the structure of the defect is shown). The image was obtained by Stimulated Emission Depletion (STED) microscopy at Stephan Hell's group (Max Planck Institute, Göttingen). The top left scheme shows the "nano-implanter" setup used to create the pattern of NV centres. The top right inset shows Rabi oscillations measured at room temperature between two magnetic sublevels of one of the single NV centres. (The contributions of NFP 8.1)

Institut für Experimentelle Physik I
Institut für Experimentelle Physik II
Institut für Theoretische Physik

Fakultät für
Physik und Geowissenschaften

Universität Leipzig

Institute for Experimental Physics I
Institute for Experimental Physics II
Institute for Theoretical Physics

Faculty of Physics and Earth Sciences

Universität Leipzig

Report 2014

Addresses

Institute for Experimental Physics I

Linnéstraße 5
D-04103 Leipzig, Germany
Phone: +49 341 97-32470
Fax: +49 341 97-32479
WWW: http://www.uni-leipzig.de/~physik/exp1.html

Institute for Experimental Physics II

Linnéstraße 5
D-04103 Leipzig, Germany
Phone: +49 341 97-32650
Fax: +49 341 97-32668
WWW: http://exp2.physgeo.uni-leipzig.de/start/

Institute for Theoretical Physics

Brüderstr. 14 - 16
D-04103 Leipzig, Germany
Phone: +49 341 97-32420
Fax: +49 341 97-32548
WWW: http://www.uni-leipzig.de/~physik/thph.html

Preface

The 2014 Report of the Physics Institutes of the Universität Leipzig presents a hopefully interesting overview of our research activities in the past year. It is also testimony of our scientific interaction with colleagues and partners worldwide. We are grateful to our guests for enriching our academic year with their contributions in the colloquium and within the work groups.

The open full professorship in the Institute for Experimental Physics I has been filled with an outstanding candidate. We could attract Prof. Ralf Seidel from the University of Münster. He is an expert in molecular biophysics that complements the existing strength in cellular biophysics.

Prof. Hollands could fill all positions of his ERC Starting Grant, so that the work on the project "Quantum Fields and Curvature – Novel Constructive Approach via Operator Product Expansion" is now running at full pace.

Within the Horizon 2020 project LOMID "Large Cost-effective OLED Microdisplays and their Applications" (2015-2017) with eight European partners including industry the semiconductor physics group contributes with transparent oxide devices.

A joint laboratory for single ion implantation was established between the Leibniz-Institute for Surface Modification (IOM) and the university under the guidance of Profs. Rauschenbach and Meijer.

The EU IRSES Network DIONICOS "Dynamics of and in Complex Systems", a consortium of 6 European and 12 non-European partners, including sites in England, France and Germany as well as in Russia, Ukraine, India, the United States and Venezuela, started in February 2014. In the next four years the Leipzig node headed by Prof. Janke will profit from the numerous international contacts this network provides.

With a joint project, Prof. Kroy and Prof. Cichos participate in the newly established priority research programme SPP 1726 "Microswimmers", which started with a kick-off workshop in October 2014.

In 2014 the International Graduate College "Statistical Physics of Complex Systems" run by the computational physics group has commenced its third 3-years granting period funded by Deutsch-Französische Hochschule (DFH-UFA). Besides the main partner Université de Lorraine in Nancy, France, now also Coventry University, UK, and the Institute for Condensed Matter Physis of the National Academy of Sciences of Ukraine in Lviv, Ukraine, participate as associated partners.

During the last week of September the TCO2014 conference "Transparent Conductive Oxides – Fundamentals and Applications" took place in honor of the 100th anniversary of the death of Prof. Dr. Karl W. Bädeker. In 1907 Karl Bädeker had discovered transparent conductive materials and oxides in Leipzig. About a hundred participants joined for many invited talks from international experts, intense discussion and new

cooperations.

At the end of November the by now traditional 15th International Workshop on Recent Developments in Computational Physics "CompPhys14" organized by Prof. Janke took place in Leipzig. Around 60 scientists from over 10 different countries exchanged ideas and discussed recent progress in several fields of computational physics.

Work has successfully continued in the Centers of Excellence (Sonderforschungsbereiche) SFB 762 "Functionality of Oxide Interfaces" and SFB TRR 102 "Polymers under Multiple Constraints: Restricted and Controlled Molecular Order and Mobility" (just renewed for 2015-2019).

Our activities and success are only possible with the generous support from various funding agencies for which we are very grateful and which is individually acknowledged in the brief reports.

Leipzig,
July 2015

M. Grundmann
W. Janke
J. Käs
Directors

Contents

III Institute for Theoretical Physics 243

1

Structure and Staff of the Institutes

1.1 Institute for Experimental Physics I

1.1.1 Office of the Director

Prof. Dr. Josef A. Käs (director)

1.1.2 Molecular Nano-Photonics, Molekulare Nanophotonik [MON]

Prof. Dr. Frank Cichos

Technical staff

Dipl.-Phys. Uwe Weber

Academic staff

Dr. Markus Selmke

PhD candidates

Subhasis Adhikari, M.Sc.
Dipl.-Phys. Nicole Amecke
Dipl.-Phys. Marco Braun
Dipl.-Phys. Andreas Bregulla
André Heber, M.Sc.
Dipl.-Phys. Martin Pumpa
Dipl.-Phys. Romy Schachoff
Dipl.-Phys. Rebecca Wagner

Students

Alice Abend
Tanja Jawinski

Nikolai Kortenbruck
Sascha Loebel
Irene Neugebauer
David Plotzki
Erik Wiedemann

1.1.3 Molecular Physics, Molekülphysik [MOP]

Prof. Dr. F. Kremer

Secretary

Kerstin Lohse

Technical staff

Dipl.-Phys. Cordula Bärbel Krause
Dipl.-Ing. (FH) Jörg Reinmuth
Dipl.-Phys. Wiktor Skokow

Academic staff

Dr. Mahdy M. Elmahdy

PhD candidates

Dipl.-Phys. Markus Anton
Wycliffe Kiprop Kipnusu, M.Sc.
Dipl.-Phys. Wilhelm Kossack
Emmanuel Urandu Mapesa, M.Sc.
Dipl.-Phys. Nils Neubauer
Dipl.-Phys. Tim Stangner
Dipl.-Phys. Martin Treß

Students

Falk Frenzel
Ludwig Popp
Benjamin Suttner

1.1.4 Physics of Interfaces, Grenzflächenphysik [GFP]

PD. Dr. Frank Stallmach
Prof. Dr. Jörg Kärger (retired)

Prof. Dr. Dieter Freude (retired)

Technical staff

Lutz Moschkowitz

Academic staff

Dr. Christian Chmelik
Dr. Anne-Kristin Pusch
Dr. Rustem Valiullin

PhD candidates

Dipl.-Phys. Carsten Horch
Dipl.-Math. Daria Kondrashova
Alexander Lauerer, M.Sc.
Dipl.-Phys. Dirk Mehlhorn
Mgr. Mikulas Peksa
Tobias Splith, M.Sc.
Dipl.-Phys. Tobias Tietze

1.1.5 Soft Matter Physics, Physik der weichen Materie [PWM]

Prof. Dr. Josef A. Käs

Secretary

Claudia Brück

Technical staff

Dr. Undine Dietrich
Dipl.-Phys. Bernd Kohlstrunk
Ing. Elke Westphal

Academic staff

Dr. Mareike Zink

PhD candidates

Uta Allenstein, M.Sc. (zusammen mit Prof. Mayr)
Dipl.-Phys. Anatol Fritsch
Martin Glaser, M.Sc.
Tom Golde, M.Sc.
Dipl.-Phys. Chris Händel

Dipl.-Phys. Tina Händler
Paul Heine, M.Sc.
Dipl.-Phys. Tobias Kießling
Dipl.-Math. Melanie Knorr
Hans Kubitschke, M.Sc.
Jürgen Lippoldt, M.Sc.
Erik Morawetz, M.Sc.
Dipl.-Phys. Steve Pawlizak
Saddam Moyazur Rahman, M.Sc. (BBZ, Forschergruppe M. Zink)
Dipl.-Phys. Sebastian Schmidt
Dipl.-Phys. Jörg Schnauß
Dipl.-Phys. Carsten Schuldt
Dipl.-Phys. Enrico Warmt
Emilia Wisotzki, M.Sc.

Students

Dave Ahrens
Paul Birkenmeier
Tobias Eggebrecht
Sabrina Friebe
Gregor Haider
Konrad Jahn
Till Möhn
Linda Oswald
Florian Rämisch
Lydia Reuter
Erik Schmidt
Markus Sommerfeld
Tobias Thalheim
Astrid Weidt
Iris Wenzel

1.1.6 Biological Physics, Biologische Physik [BIP]

Prof. Dr. Claudia Mierke

Secretary

Kerstin Lohse

Technical staff

Dipl.-Ing. Kathrin Koch

Academic staff

PhD candidates

Stefanie Puder, M.Sc.
Dipl.-Phys. Tony Kurth
Tom Kunschmann, M.Sc.

Students

Faranak Zamani
Stefanie Riedel
Tamara Heredia
Yadav Bashyal
Alexander Hayn
Jeremy Perez
Sebastian Haupt
Jacek Zlotowski
Mirko Kirchner

1.2 Institute for Experimental Physics II

1.2.1 Office of the Director

Prof. Dr. Marius Grundmann (director)

1.2.2 Magnetic Resonance of Complex Quantum Solids, Magnetische Resonanz Komplexer Quantenfestkörper [MQF]

Prof. Dr. Jürgen Haase

Secretary

Sophie Kirchner

Technical staff

Gert Klotzsche
Tilo Pilling
Stefan Schlayer
Horst Voigt

Academic staff

PD Dr. Marko Bertmer
Prof. Dr. Dieter Freude
Prof. Dr. Andreas Pöppl

PhD candidates

Nina Dvoyashkina, M.Sc.
Stefan Friedländer, M.Sc.
Nataliya Georgieva, M.Sc.
Robin Gühne, M.Sc.
Dipl.-Phys. Alexander Jäger
Michael Jurkutat, M.Sc.
Arafat Hossain Khan, M.Sc.
Dipl.-Phys. Jonas Kohlrautz
Anastasiia Kultaeva, M.Sc.
Anusree V. Kuttatheyil, M.Sc.
Alexander Lauerer, M.Sc.
Kathrin Lorenz, M.Sc.
Thomas Meier, M.Sc.
Dipl.-Phys. Matthias Mendt
Steven Reichardt, M.Sc.
Dipl.-Phys. Sebastian Sambale
Daniel Schneider, M.Sc.
Emmanouil Veroutis, M.Sc.
Marufa Zahan, M.Sc.

1.2.3 Nuclear Solid State Physics, Nukleare Festkörperphysik [NFP]

Prof. Dr. Jan Meijer

Technical staff

Dipl.-Phys. Steffen Jankuhn
Carsten Pahnke
Dipl.-Ing. Joachim Starke

Academic staff

Dr. Sébastien Pezzagna
Dr. Daniel Spemann (since October 2014)
Dr. Jürgen Vogt

PhD candidates

Dipl.-Math. Roger John, B.Sc.
Jan Lehnert, M.Sc.
Nicole Raatz, M.Sc.
Ralf Wunderlich, M.Sc.

Students

Youssef Albanay, B.Sc. (since October 2014)
Sascha Becker, B.Sc.
Christopher Eames (since May 2014)
Jakob Helbig (since May 2014)
Johannes Küpper (since May 2014)
Tobias Lühmann, B.Sc.
Michael Mensing, B.Sc.
Maximilian Quaas (since October 2014)
Marcel Ritzschke (May – October 2014)
Lukas Rogée (till April 2014)
Clemens Scheuner (April – October 2014)
Julian Vogel, B.Sc. (since May 2014)
Erik Wiedemann, B.Sc. (since August 2014)

1.2.4 Semiconductor Physics, Halbleiterphysik [HLP]

Prof. Dr. Marius Grundmann

Secretary

Anja Heck
Birgit Wendisch

Technical staff

Dipl.-Phys. Gabriele Benndorf
Monika Hahn
Dipl.-Ing. Holger Hochmuth
Dipl.-Phys. Jörg Lenzner
Dipl.-Phys. Axel Märcker
Gabriele Ramm
Roswitha Riedel

Academic staff

Dr. Kerstin Brachwitz
Dr. Helena Franke
Dr. Heiko Frenzel
Prof. Dr. Michael Lorenz
PD Dr. Rainer Pickenhain
Prof. Dr. Bernd Rheinländer (retired)
Dr. Rüdiger Schmidt-Grund
Dr. Chris Sturm
Dr. Holger von Wenckstern
Dr. Chang Yang

PhD candidates

Henner Bieligk, M.Sc.
Michael Bonholzer, M.Sc.
Dipl.-Phys. Eike Lennart Fricke
Marcus Jenderka, M.Sc.
Robert Karsthof, M.Sc.
Sherzod Khujanov, M.Sc.
Tom Michalsky, M.Sc.
Dipl.-Phys. Fabian Klüpfel
Dipl.-Phys. Christian Kranert
Abdurashid Mavlonov, M.Sc.
Dipl.-Phys. Stefan Müller
Anna Reinhardt, M.Sc.
Steffen Richter, M.Sc.
Dipl.-Phys. Friedrich-Leonhard Schein
Peter Schlupp, M.Sc.
Dipl.-Phys. Florian Schmidt
Peter Schwinkendorf, M.Sc.
Alexander Shkurmanov, M.Sc.
Daniel Splith, M.Sc.
Dipl.-Phys. Marko Stölzel
Martin Thunert, M.Sc.
Haoming Wei, M.Sc.
Marcel Wille, M.Sc.
Zhang Zhipeng, M.Sc.
Vitaly Zviagin, M.Sc.

Students

Sofie Bitter
Raffael Deichsel
David Diering
Tobias Dörfler
Oliver Herrfurth
Alexander Hohn
Agnes Holtz
Max Kneiß
Hannes Krauß
Silvia Kunz
Stefan Lange
Steffen Lanzinger
Lisa Paller
Paul Räcke
Katharina Rudisch
Michael Scheibe
Thorsten Schultz

Robert Staacke
Anna Werner

1.2.5 Superconductivity and Magnetism, Supraleitung und Magnetismus [SUM]

Prof. Dr. Pablo Esquinazi

Secretary

Sandy Ehlers

Technical staff

Dr. Winfried Böhlmann
Dipl.-Krist. Annette Setzer

Academic staff

Prof. Dr. Michael Ziese
Dr. José Barzola-Quiquia
Dr. Israel Lorite Villalba
Dr. Yogesh Kumar

PhD candidates

Ana Ballestar, M.Sc.
Francis Bern, M.Sc.
Santiago Muiños Landín, M.Sc.
Bogdan Semenenko, M.Sc.
Christian Eike Precker

Students

Tiago Rafael Silva Cordeiro
Markus Stiller, B.Sc.
Mahsa Zoraghi, B.Sc.

1.3 Institute for Theoretical Physics

1.3.1 Office of the Director

Prof. Dr. Wolfhard Janke

Secretary

Susan Hussack
Gabriele Menge
Lea Voigt

1.3.2 Computational Quantum Field Theory, Computerorientierte Quantenfeldtheorie [CQT]

Prof. Dr. Wolfhard Janke

Academic staff

Dr. Stefan Schnabel
Dr. Jonathan Gross
Dr. Suman Majumder

PhD candidates

M.Sc. Johannes Bock
Dipl.-Phys. Niklas Fricke
M.Sc. Momchil Ivanov
M.Sc. Ravinder Kumar ("co-tutelle" with Coventry University, UK)
Dipl.-Phys. Martin Marenz
Dipl.-Phys. Marco Müller
Dipl.-Phys. Hannes Nagel
Dipl.-Phys. Andreas Nußbaumer
Dipl.-Phys. Jeremi Ochab (jointly with Jagiellonian University Krakow)
M.Sc. Philipp Schierz
M.Sc. Johannes Zierenberg

Students

Kieran Austin
Marius Bause
Jan Meischner
Benjamin Schott
Henrik Christiansen
Karl Horn
Felix Neduck
Dorian Nothaaß
David Oberthür
Simon Schneider
Paul Spitzner
Robert Wiesen
Sandesh Bhat
Tobias Weiss

1.3.3 Quantum Field Theory and Gravity, Quantenfeldtheorie und Gravitation [QFG]

Prof. Dr. Gerd Rudolph (Speaker)
Prof. Dr. Rainer Verch

Academic staff

Prof. Dr. Gerd Rudolph
Prof. Dr. Rainer Verch
Priv.-Doz. Dr. Michael Bordag
Dr. Gandalf Lechner
Dr. Matthias Schmidt

Retired

Prof. em. Bodo Geyer
Prof. em. Armin Uhlmann

PhD candidates

Andreas Andersson, M.Sc.
Tobias Diez, M.Sc.
Erik Fuchs, M.Sc.
Michael Gransee, M.Sc.
Mathias Hänsel, M.Sc.

Students

Richard Busch
Bärbel Hanle
Sophia Helmrich
Maximilian Kähler
Stanislaw Kazmin
Sebastian Knappe
Richard Neidhardt
Johannes Zähle

1.3.4 Statistical Physics, Statistische Physik [STP]

Prof. Dr. Bernd Rosenow

Academic staff

Dr. Daniel D. Scherer
Dr. Björn Zocher

PhD candidates

Dipl. Phys. Alexander Janot
Lukas Kimme, M.Sc.
Martin Treffkorn, M.Sc.

Students

Enrico Lohman
Florian Knoop
Johann Schmidt
Alexander Schneider
Alexander Uhlig
Heinrich-Gregor Zirnstein

1.3.5 Theory of Condensed Matter, Theorie der kondensierten Materie [TKM]

Prof. Dr. Ulrich Behn (Speaker)
Prof. Dr. Klaus Kroy

Prof. Dr. Dieter Ihle (retired)
Prof. Dr. Adolf Kühnel (retired)

PhD candidates

Dipl.-Phys. Jakob T. Bullerjahn
Gianmaria Falasco, M.Sc.
Dipl.-Phys. Andrea Kramer
Rüdiger Kürsten, M.Sc.
Dipl.-Phys. Marc Lämmel
Anne Meiwald, M.Sc.
Dipl.-Phys. Holger Schmidtchen
Dipl.-Phys. Sebastian Sturm
Guillermo Zecua, M.Sc.

Students

Sven Auschra, B.Sc.
Mona Guthardt, B.Sc.
Andreas Hübner, B.Sc.
Michaela Kettner, B.Sc.
Richard Pfaller, B.Sc.
Nicolas Preuß, B.Sc.
Felix Schramm, B.Sc.
Robert Schulz, M.A.
Benjamin Streitz, B.Sc.

Maik Weßling, B.Sc.
Meike Will, B.Sc.

1.3.6 Theory of Elementary Particles, Theorie der Elementarteilchen [TET]

Prof. Dr. Stefan Hollands

Academic staff

Dr. Markus Fröb
Dr. Jan Holland
PD Dr. Roland Kirchner
Dr. Ko Sanders
PD Dr. Arwed Schiller
Dr. Jochen Zahn

PhD candidates

Giovanni Collini, M.Sc.
Steffen Pottel, M.Sc.
Mojtaba Taslimitehrani

Students

Tobias Jerabek, B.Sc.

I

Institute for Experimental Physics I

2

Molecular Nano-Photonics

2.1 Introduction

Studying dynamic processes at the level of single molecules and particles in soft materials, the group has recently started to explore the release of heat from single molecules and nanoparticles. These absorbing chromophores are able to convert optical energy into heat, if their fluorescence quantum yield is low. This released heat is generating a steady state spatial temperature profile as they are embedded in a large heat bath, which is their solvent environment. This local temperature profile allows a number of new studies, which range from fundamental physical aspects of Hot Brownian Motion (HBM) to the active motion of self-propelled particles. In particular this field of research of the group addresses

- Thermally propelled particles and micromachines
- Manipulation and trapping of single nano-objects in solution
- Transmission microscopy of Rayleigh- and Mie-particles
- Manipulation of living cells by local temperature fields
- Heat conduction at the nanoscale

During the year 2014 the Molecular Nanophotonics Group has celebrated a number of achievements. Among them are:

- Prof. Dr. Cichos has been a guest professor at Princeton University working with Prof. Dr. Haw Yang at the Department of Chemistry.
- The group has successfully applied for a grant within the priority program SPP 1726 "Microswimmers".
- Marco Braun has been awarded with the 2nd BuildMoNa price for his research on single particle trapping in temperature fields.

Collaborations with the group of Prof. Dr. Klaus Kroy (Universität Leipzig), Prof. Dr. Michael Mertig (TU Dresden) and Prof. Dr. Haw Yang (Princeton University) have been very fruitful. Collaborative measurements with the groups of Prof. Dr. Friedrich Kremer and Prof. Dr. Marius Grundmann have been carried out.

Frank Cichos

2.2 Thermophoretic Trapping of Single and Multiple DNA Molecules

M. Braun, A.P. Bregulla, F. Cichos

The manipulation and trapping of single molecules that undergo Brownian motion are of considerable interest to soft-matter sciences as it for example would allow for controlled studies of protein aggregation dynamics or molecular reactions or interactions. Optical tweezing is the most common technique for the trapping of individual particles in solution and is based on the optical gradient force. As particles become nanometer sized, optical tweezing, however, becomes unsuitable as the required polarizability contrast with the environment is lost. Molecular trapping can be achieved e.g. by a

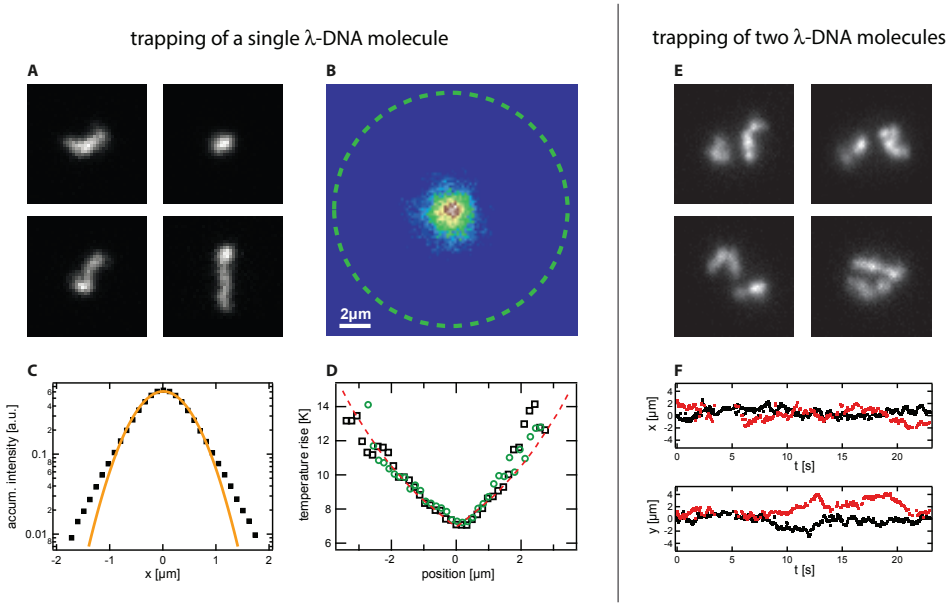

Figure 2.1: A) Four snapshots ($4.6\times4.6\,\mu m^2$) of a trapped single λ-DNA molecule. **B)** Probability density of the trapped molecule with a width $\sigma = 0.75\,\mu m$ at 3.0 mW heating laser power. **C)** Accumulated fluorescence intensity after shifting each frame by the molecules center of mass and normalization, showing a non-Gaussian mass distribution about the center of mass. Gaussian fit in orange ($R_G = (0.66 \pm 0.02)\,\mu m$). **D)** Temperature field in the trap reconstructed from the probability density of the molecule in x (black) and y (green) direction for a measured Soret coefficient of $S_T = 0.8\,K^{-1}$ and theoretical temperature field (red dashed curve). **E)** Four snapshots ($6.9\times6.9\,\mu m^2$) of the trapping of two single λ-DNA molecules. **F)** x and y components of the trajectories of the two DNA molecules trapped in a $d_{trap} = 15\,\mu m$ trap.

technique called Anti-Brownian Electrokinetic trap (ABEL trap), which exploits the feedback controlled electric field of four electrodes. However, the latter technique requires electrical contacts, which introduce difficulties when fabricating multiple traps. In this project we have developed an all-optical technique which replaces the electric fields by highly localized thermal fields and is therefore scalable to large arrays [1, 2]. The so-called thermophoretic trap exploits thermophoretic interactions of a molecule placed in a temperature gradient in solution. In our approach, the temperature field is generated by an optically heated gold nanostructure. Due to the small dimensions of

the gold heat sources, even a small temperature increase introduces large temperature gradients causing a strong thermophoretic drift through which the motion of a diffusing particle can be manipulated. To realize this trap, a circular hole in a gold film (~ 8 nm in diameter and 50 nm in height) is manufactured by microsphere lithography, where gold is thermally evaporated onto a monolayer of polystyrene microspheres, which are later removed by sonification. Single DNA molecules carrying out 2-dimensional Brownian motion are then confined between a cover slide carrying the gold array and a blank cover slide. By means of a focussed laser beam the circumference of the gold structure is heated, resulting in a strongly localized temperature field and steep temperature gradients. Real time tracking of the DNA in the trap allows to apply heating laser pulses to push the DNA towards a well defined target position in the trap (see Figure 2.1A). Doing so enables a restriction of the Brownian motion of the DNA to a small trapping region as shown in Figure 2.1B. As the trapping is determined by the feedback, almost arbitrarily shaped trapping potentials can be generated in one gold structure (Figure 2.1F). In addition, the trap allows to hold an exact number of molecules in the trap enabling controlled multimolecular interaction studies. This new all-optical technique for the manipulation of nano-objects enables long-time observations of not only single but also multiple nano-objects without applying strong optical or electric fields.

[1] M. Braun, F. Cichos: *Optically controlled thermophoretic trapping of single nano-objects*, ACS nano 7(12): 11200-11206 (2013).
[2] M. Braun, A. Würger, F. Cichos: *Trapping of single nano-objects in dynamic temperature fields*, PCCP 16(29): 15207 (2014).

2.3 Interactions of Janus-type Microswimmers studied by Photon Nudging

A.P. Bregulla, F. Cichos

Within the project we employ feedback mechanisms to explore the interaction of artificial microswimmers among each other. The microswimmers are constructed of colloidal particles covered on one side with a thin gold layer. By the absorption of light in the gold layer and its conversion into heat we are able to control the temperature gradient along the surface of micro- and nanoparticles in solution to cause an interfacial liquid flow, which leads finally to a phoretic motion of particles. What is so far not understood is how such swimmers, which generate a temperature and an hydrodynamic flow field interact in an ensemble to form a collective motion. To explore this interaction in detail, we have developed with the group of Prof. Haw Yang at Princeton University a feedback based technique called photon nudging [1]. This feedback mechanism analyzes the orientation and position of a Janus particle in real time. If the particle direction is pointing towards a target, a laser is switched on to drive the self-propelled motion towards the target. Thus the rotational diffusion is used to stochastically drive the particle at the right times. Thereby, trapping and steering have been demonstrated [1] and an assay has been created in which we place a single microswimmer close to a heat source. Doing so we are able to extract the interaction of a point like heat source with the Janus

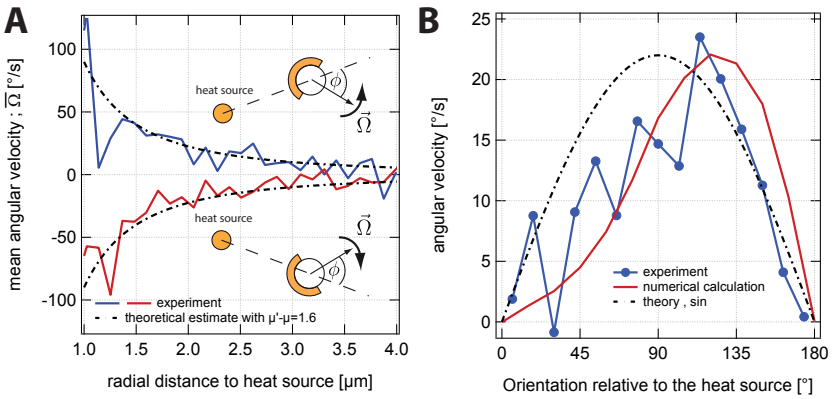

Figure 2.2: A) Dependence of the mean angular velocity that reorients the microswimmer in the temperature field of a gold nanoparticle at a certain distance from the nanoparticle. A distinction is made by the relative location of the particles orientation $\mathbf{n_o}$ relative to the radial vector $\mathbf{e_r}$. This leads to a clockwise (blue curve) or counter clockwise rotation (red curve). **B)** Magnitude of the angular velocity for different relative orientations ϕ in comparison to the theory (dashed line) and numerical estimate (red curve).

particles which gives rise to a repulsive interaction and an orientational polarization of the swimmer in the temperature field. This is the first experimental proof on a thermophoretic torque on an asymmetric particle (see Figure 2.2). In summary, this switchable self-propelled motion of Janus particles delivers new ways to control particle motion by feedback mechanisms. Thus new studies of the interaction and dynamics of swarming particles become possible.

[1] A. P. Bregulla, H. Yang: *Stochastic localization of microswimmers by photon nudging*, ACS nano 8(7): 6542-6550 (2014).

2.4 All-optical Switching using Photothermal Effects

A. Heber, M. Selmke, F. Cichos

The modulation of light intensities with the help of light is typically very difficult, as photons hardly interact with each other without involving non-linear dielectric materials. Within this project, we have explored the modulation of light intensity by light with the help of a heat induced phase transition in liquid crystals. To do so, we mount a single gold nanoparticle on a glass slide which is further covered with a liquid crystal (Figure 2.3A). The liquid crystal is in its nematic phase and the thickness of the liquid crystal film has been adjusted in such a way that it resembles a half-wave-plate rotating the incident light of linear polarization by 90 degree. Thus if an analyzing polarizer is placed behind the liquid crystal film, no light is transmitted through the structure. If light is now absorbed by the gold nanoparticle in the film, the released heat induces a phase transition into an isotropic liquid in a well defined region around the nanoparticle. This isotropic liquid has no anisotropic optical properties and allows the light to pass the liquid crystal structure unmodified. Thus the transmission of the modulator structure is increased up to a maximum of 100 percent (see Figure 2.3B). It has been

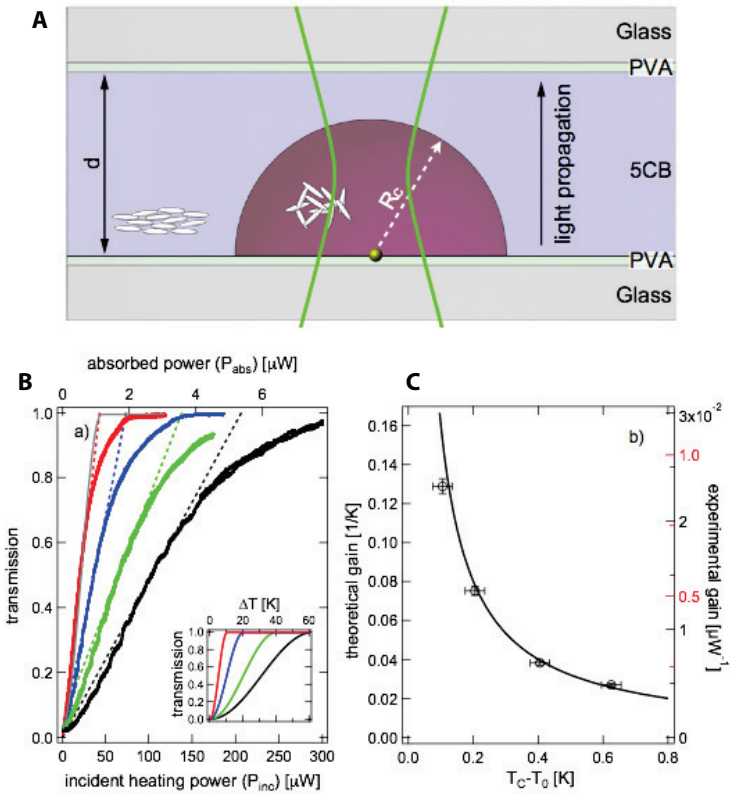

Figure 2.3: A) Sketch of the photothermal modulator structure. **B)** Steady state response: The transmission of the probe laser beam is plotted against the incident heating power. It is varied sufficiently slowly to achieve a steady state transmission signal of the system at each incident heating power. The transmission is shown at different temperatures $T_C - T_0$ being 0.11 K (red), 0.21 K (blue), 0.43 K (green) and 0.63 K (black) below the nematic to isotropic phase transition temperature $T_C = 307.5$ K. The corresponding dashed lines are tangents of the maximum slopes indicating the linear regime and determining the experimental gain. The inset shows the theoretically derived transmission as a function of the temperature increase at the nanoparticle's surface. **C)** Gain factors: Comparison of theoretical (line) and experimental gain factors (markers), which correspond to the maximum transmission increase per temperature and incident heating/absorbed power. The labels on the right axis correspond to the experimental gain with respect to P_{inc} (black) and P_{abs} (red).

shown in [1] that this type of structure is able to control large intensities by small control light intensities (see Figure 2.3), which is in most of the other current existing structures not possible. However, due to the use of a phase transition, switching is only possible with kilohertz rates. On the other hand, the preparation of such structures is extremely easy and thus large arrays can be constructed. Further, the structure combined with the technique may be used to study local phase transitions in liquid crystals at the nanoscale.

[1] A. Heber, F. Cichos: *Metal nanoparticle based all-optical photothermal light modulator*, ACS nano 8(2): 1893-1898 (2007).

2.5 Photothermal Single Particle Microscopy

M. Selmke, R. Schachoff, A. Heber, M. Braun, F. Cichos

The detection of single molecules and nanoparticles which do not emit light is very difficult as the absorption cross sections of such objects are in general very low and thus the absorption signal is very weak as compared to the background and noise in a common absorption measurement. A way to reduce the optical background and to make absorption measurements on even single molecules possible is photothermal microscopy. In

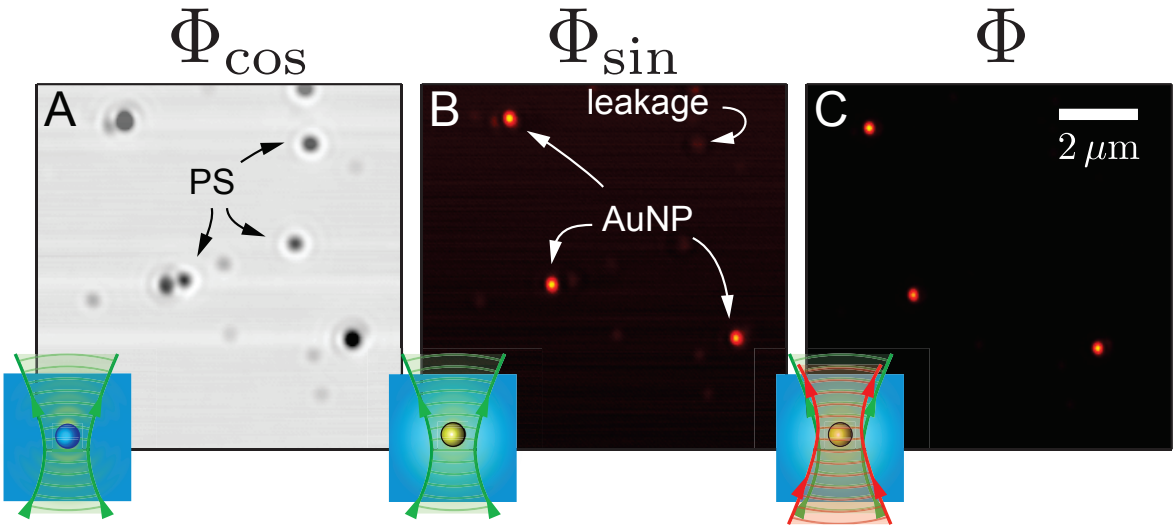

Figure 2.4: A) The self-lensing in-phase signal $\Phi_{\cos}$ showing the constant background, $R = 10\,\text{nm}$ and 30 nm AuNPs and $R = 100\,\text{nm}$ polystyrene scatterers. **B)** The out-of-phase PT signal $\Phi_{\sin}$ showing the AuNPs and minor leakage of the scatterers due to the anharmonicity in the excitation $P(t)$. **C)** The PT signal using a separate probe-beam (no leakage). The SNR is better by a factor ~ 7.6.

photothermal microscopy, absorbing chromophores release the optical energy not as photons but as heat. The heat changes the local temperature around the chromophore and thus the refractive index as well. This local refractive index change can be effectively detected by scattering a laser which is not absorbed by the chromphore. Therefore photothermal microscopy typically relies on two laser beams, one which is absorbed by the chromophore and the second being used to detect the local refractive index change. The use of these two lasers of different wavelength make an alignment very difficult and the application for example in complex media complicated. Within this project, we have developed a photothermal single particle microscopy scheme, which allows for an absorption detection of down to 5 nm single gold nanopartciles by a single laser beam. The method is based on the fact that even a single laser beam is modified in its propagation by the thermally induced refractive index profile. To separate the heat induced scattering and the scattering due to other refractive index inhomogeneities, we use the finite heat diffusivity of the material. Modulating the heat at the certain frequency modulates also the refractive index change. The finite heat diffusivity now delays the response of the system and thus the scattering of the incident laser. This out-of-phase signal is now maximum, when the heat just traverses the extent of the laser focus. Thus by looking at an out-of-phase photothermal signal we are able to

discriminate between absorbing and scattering objects in the sample (see Figure 2.4, [1]). In this way, the developed method is free of chromatic aberrations and allows easy scanning and access scattering samples as for example living cells.

[1] M. Selmke, A. Heber, M. Braun, F. Cichos: *Photothermal single particle microscopy using a single laser beam*, Appl. Phys. Lett. 105(1): 013511 (2014).

2.6 Funding

FOR 877, TP 1: Hot Brownian Motion
F. Cichos in collaboration with K. Kroy, M. Mertig (TU Dresden)
DFG, CI 33/7-2

FOR 877, TP 2: Static and Dynamic Properties of DNA-based Polymer Structures under Constraints and Confinement
F. Cichos in collaboration with M. Mertig (TU Dresden), R. Seidel
DFG, CI 33/11-2

FOR 877: From Local Constraints to Macroscopic Transport
F. Cichos et al.
DFG, CI 33/12-1

DFG-ANR: Thermoelectric Effects at the Nanoscale
F. Cichos in collaboration with A. Würger (Université de Bordeaux, France)
DFG, CI 33/14-1

DFG SPP 1726, TP Propulsion and Interaction of Hot Brownian Swimmers
F. Cichos in collaboration with K. Kroy
DFG, CI 33/16-1

SFB/TRR 102, TP B10: Interaction of Single Polymer Chains in a Thermophoretic Trap
F. Cichos
DFG SFB/TRR 102

Leipzig School of Natural Sciences – Building with Molecules and Nano-objects (BuildMoNa)
F. Cichos (Principal Investigator)
DFG GSC 185

ESF-NFG Effiziente Energienutzung: Neue Konzepte und Materialien, TP 3: Wärmetransport auf der Nanoskala
F. Cichos
ESF-Nachwuchsforschergruppe des Freistaates Sachsen im Rahmen des Europäischen Sozialfonds

2.7 Organizational Duties

Frank Cichos

- Speaker of the DFG Research Unit 877 "From Local Constrainst to Macroscopic Transport"
- Member of the Steering Committee of the graduate school BuildMoNa
- Head of the Eignungsfeststellungskommission Fakultät für Physik und Geowissenschaften
- Vice head Promotionsausschuss
- Vice head of the Qualitätssicherungskommission
- Member of the Prüfungsausschuss
- Referee: Phys. Rev. B, Phys. Rev. Lett., Nature, Chem. Phys. Lett., Appl. Phys. Lett., ACS Petroleum Research Fund; Medical Research Council

2.8 External Cooperations

Academic

- TU Dresden
  Prof. Dr. Michael Mertig
- Unviversité Bordeaux
  Prof. Dr. Alois Würger
- Universität Münster
  Prof. Dr. Ralf Seidel
- TU Chemnitz
  Prof. Dr. Christian von Borczyskowski
- Universität Mainz
  Prof. Dr. Thomas Basché
- Princeton University
  Prof. Dr. Haw Yang
- MPI Kohlenforschung Mühlheim
  Dr. Frank Marlow
- Universität Stuttgart
  Prof. Dr. Clemens Bechinger
- MPI Intelligenete Systeme
  Prof. Dr. Peer Fischer

2.9 Publications

Journals

M. Braun, A. Würger, F. Cichos: *Trapping of single nano-objects in dynamic temperature fields*, Phys. Chem. Chem. Phys. **16**, 15207–15213 (2014)

A.P. Bregulla, H. Yang, F. Cichos: *Stochastic localization of microswimmers by photon nudging*, ACS Nano **8**, 6542–6550 (2014)

M. Selmke, A. Heber, M. Braun, F. Cichos: *Photothermal single particle microscopy using a single laser beam*, Appl. Phys. Lett. **105**, 013511 (2014)

A. Heber, M. Selmke, F. Cichos: *Metal nanoparticle based all-optical photothermal light modulator*, ACS Nano **8**, 1893–1898 (2014)

M. Selmke, F. Cichos: *Energy-redistribution signatures in transmission microscopy of Rayleigh and Mie particles*, JOSA A **31**, 2370–2384 (2014)

N. Amecke, A. Heber, F. Cichos: *Distortion of power law blinking with binning and thresholding*, J. Chem. Phys. **140**, 114306 (2014)

Talks

M. Selmke, F. Cichos: *Single particle interferometry in the generalized Lorenz-Mie framework*, DPG Spring Meeting, Berlin, 17–21 March 2014

F. Cichos, A. Bregulla, M. Braun, H. Yang: *Thermophoretic trapping and steering of single nano-objects with plasmonic nanostructures*, DPG Spring Meeting, Dresden, 30 March–04 April 2014

M. Braun, F. Cichos: *Gold nano-structure assisted thermophoretic trapping of single nano-objects*, DPG Spring Meeting, Dresden, 30 March–04 April 2014

A. Bregulla, F. Cichos: *Efficiency of optically heated Janus particles*, DPG Spring Meeting, Dresden, 30 March–04 April 2014

A. Heber, M. Selmke, F. Cichos: *Thermal diffusivity measured with a single nanoparticle*, DPG Spring Meeting, Dresden, 30 March–04 April 2014

F. Cichos: *Trapping and steering of individual nano-objects*, Micro- and Nanomachines Conference 2014, Hannover, 02–05 July 2014, invited

A. Heber, M. Selmke, F. Cichos: *Thermal diffusivity measured with a single nanoparticle*, Condensed Matter, Paris, France, 24–29 August 2014

Posters

M. Braun, F. Cichos: *Gold nanostructure assisted thermophoretic trapping of single nano-objects*, Annual BuildMoNa Conference, Leipzig, 03–04 March 2014

I. Neugebauer, M. Selmke, F. Cichos: *Nanoparticle characterization by laser transmission microscopy*, DPG Spring Meeting, Berlin, 17–21 March 2014

M. Selmke, F. Cichos: *Energy redistribution in single particle interference microscopy*, 10th International Conference Series on: Laser-Light and Interactions with Particles (LIP2014), Marseille, France, 25–29 August 2014

A. Heber, M. Selmke, F. Cichos: *Thermal diffusivity measured with a single nanoparticle*, European Optical Society Annual Meeting (EOSAM 2014), Berlin, 15–19 September 2014

A. Heber, M. Selmke, R. Schachoff, F. Cichos: *Application of photothermal microscopy to the study of cells*, Advances in Live Single-Cell Thermal Imaging and Manipulation (ALSCTIM), Onna, Okinawa, Japan, 10–12 November 2014

R. Schachoff, M. Selmke, M. Braun, F. Cichos: *Photothermal detection and correlation spectroscopy of single gold nano particles in living cells*, Advances in Live Single-Cell Thermal Imaging and Manipulation (ALSCTIM), Onna, Okinawa, Japan, 10–12 November 2014

2.10 Graduations

Bachelor

- Alice Abend
  Thermophoretic Tapping
  March 2014
- Tanja Jawinski
  3-Dimensional Photothermal Single Particle Velocimetry
  July 2014
- Erik Wiedemann
  Interactions of Gold Coated Janus-Particles?
  January 2014

2.11 Guests

- Ulrich F. Keyser
  University of Cambridge, UK
  4–6 October 2014
- Tim Liedl
  LMU Munich
  5–6 October 2014
- W. E. Moerner
  Stanford University, USA
  10–12 July 2014
- Haw Yang
  Princeton University, USA
  3–9 October 2014

3

Molecular Physics

3.1 Introduction

This is my last report as an active professor; in March 2015 I shall retire. But this does not mean that I intend to move away from research. Instead, I plan to focus on the fields of Broadband Dielectric and Fourier Transform Infrared Spectroscopy; in both we have profound expertise and the two have proven to be complementary and highly versatile in the physics of soft and hard condensed matter. In detail it is planned to study the dielectric properties of polymeric Ionic Liquids (PIL), a project already being funded by the German Science Foundation within a "Knowledge-transfer-project (Erkenntnistransferprojekt)" together with Prof. Veronika Strehmel, FH Krefeld and Merck KGaA in Darmstadt. Currently under review for the second funding period (2015 - 2019) is an application - titled "Broadband Dielectric and IR Spectroscopy to study molecular dynamics and order in nanometer domains of end-fixed polymers" - within the Collaborative Research Center (CRC) of the universities in Halle and Leipzig, "Polymers under multiple constraints: restricted and controlled molecular order and mobility". Furthermore a common endeavor together with researchers from veterinary medicine is under discussion and might soon become concretized. In summary, I plan to have a research team of about 4 PhD students and one Postdoc. Additionally, several book projects are envisaged within the series "Advances in Dielectrics". So I look forward to pursue research in soft matter physics with utmost engagement and ambition.

Friedrich Kremer

3.2 Data analysis for nano-structured electrode arrangements

M. Treß, N. Neubauer, R. Winkler[*], P. Uhlmann[*], E.U. Mapesa, M. Reiche[†], F. Kremer

[*]Leibnitz-Institut für Polymerforschung, Dresden

[†]Max-Planck-Institute for Microstructure Physics, Halle an der Saale

The development of nano-structured electrodes [1] moved Broadband Dielectric Spectroscopy into the field of interfacial techniques [2–8] and recent refinements succeeded to employ this method to block copolymers [9], polymer brushes [10] and even isolated

polymer chains [11]. Such systems cannot be studied with conventional methods since only the free surface i) enables mesoscopic structural rearrangements (block copolymers, brushes) and ii) avoids electrical short cuts in un-continuously covered samples (isolated chains). On the other hand, as a result the probe volume contains several different materials which contribute in a non-trivial way to the total response.

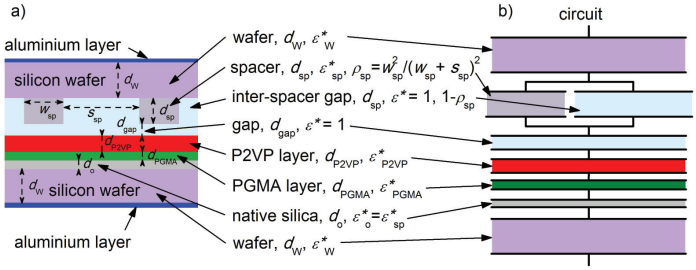

Figure 3.1: a) Schematic cross-section of P2VP brushes in the nano-structured electrode arrangement anchored on a PGMA layer. b) Equivalent circuit.

To unwrap the latter and extract the net dielectric properties of the sample material, a sophisticated fit function is employed. For that, an equivalent circuit describing the spatial distribution of all components is created [12]. Exemplarily, Fig. 3.1 displays the cross section of poly(2-vinylpyridine) (P2VP) brushes grafted to an poly(glycidyl methacrylate) (PGMA) anchoring layer and the respective equivalent circuit. Consequently, the fit function derived from the latter does not only contain parameters for the dielectric properties of all components but also implements their geometrical distribution. This enables a quantitative description of the data which can explain features like the polarization process induced by the conductivity of P2VP (Fig. 3.2).

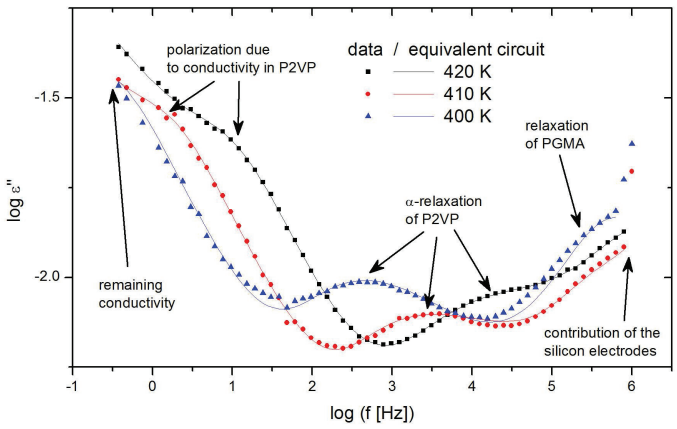

Figure 3.2: Dielectric loss spectra of 6.4-nm-thick P2VP polymer brushes grafted to an PGMA anchoring layer (2.5 nm) in the nano-structured electrode arrangement (temperatures as indicated). Solid lines represent fits with the equivalent circuit model which contains the geometrical measures of the sample.

[1] A. Serghei and F. Kremer, Rev Sci Inst 79 026101 (2008)

[2] A. Serghei, H. Huth, C. Schick and F. Kremer, Macromol 41 3636 (2008)
[3] M. Erber, M. Tress, E.U. Mapesa, A. Serghei, K.-J. Eichhorn, B. Voit and F. Kremer, Macromol 43 7729 (2010)
[4] M. Tress, M. Erber, E.U. Mapesa, H. Huth, J. Müller, A. Serghei, C. Schick, K.-J. Eichhorn, B. Voit and F. Kremer, Macromol 43 9937 (2010)
[5] E.U. Mapesa, M. Erber, M. Tress, K.J. Eichhorn, A. Serghei, B. Voit and F. Kremer, Eur Phys J: Spec Top 189 173 (2010)
[6] E.U. Mapesa, M. Tress, G. Schulz, H. Huth, C. Schick, M. Reiche, and F. Kremer, Soft Matter 9 10592 (2013)
[7] E.U. Mapesa, L. Popp, W.K. Kipnusu, M. Tress, and F. Kremer, Soft Materials 12 S22 (2014)
[8] E.U. Mapesa, M. Tarnacka, E. Kaminska, K. Adrjanowicz, M. Dulski, M. Tress, W. Kossack, W.K. Kipnusu, K. Kaminski, and F.Kremer, RSC Adv. 4 28432 (2014)
[9] W.K. Kipnusu, M.M. Elmahdy, M. Tress, M. Fuchs, E.U. Mapesa, D.-M. Smilgies, J. Zhang, C.M. Papadakis, and F. Kremer, Macromol 46 9729 (2013)
[10] N. Neubauer, R. Winkler, M. Tress, P. Uhlmann, M. Reiche, and F. Kremer, Soft Matter 11 3062 (2015)
[11] M. Tress, E.U. Mapesa, W. Kossack, W.K. Kipnusu, M. Reiche and F. Kremer, Science 341 1371 (2013)
[12] M. Tress, E.U. Mapesa, W. Kossack, W.K. Kipnusu, M. Reiche, and F. Kremer in Kremer, F. (Ed.) Dynamics in Geometrical Confinement, Springer International Publishing, 2014, 61-93

3.3 Dielectric properties of high permittivity siloxanes

S.J. Dünki[*†], M. Treß, F. Kremer, S.Y. Ko[*†], F.A. Nüesch[*†], C. Racles[‡], D.M. Opris[*]

[*]Swiss Federal Laboratories for Materials Science and Technology, Switzerland
[†]Ecole Polytechnique Fédérale de Lausanne, Switzerland
[‡]Poni Institute of Macromolecular Chemistry, Romania

A homologous series of novel siloxane polymers with fine-tuned glass transition temperatures and dielectric properties by utilizing thiol-ene post-polymerization reactions is presented [1]. The pendent vinyl groups of a high molecular weight polymethylvinylsiloxane were exhaustively reacted with the thiol compounds 1-butanethiol and 3-mercaptopropionitrile both separately to give polymers P2 and P3, respectively, as well as in various ratios x, y so as to create materials $P2_x3_y$ with greatly differing contents of the polar nitrile group y (Fig. 3.3 scheme). Because of the presence of the polarizable thioether and nitrile groups, the resulting siloxane polymers exhibit permittivity ranging from $\varepsilon' = 4.7$ to 18.4 for P2 and P3, respectively. Due to their high permittivity, these polymers are attractive candidates for dielectric elastomer actuators and flexible electronics.

The BDS measurements in a broad frequency and temperature range reveal the segmental relaxation of the siloxane backbone (Fig. 3.3); the scaling with T_g verifies that this is the structural relaxation underlying glassy dynamics. Another process with non-Arrhenius type thermal activation is, according to other studies of PDMS, ascribed

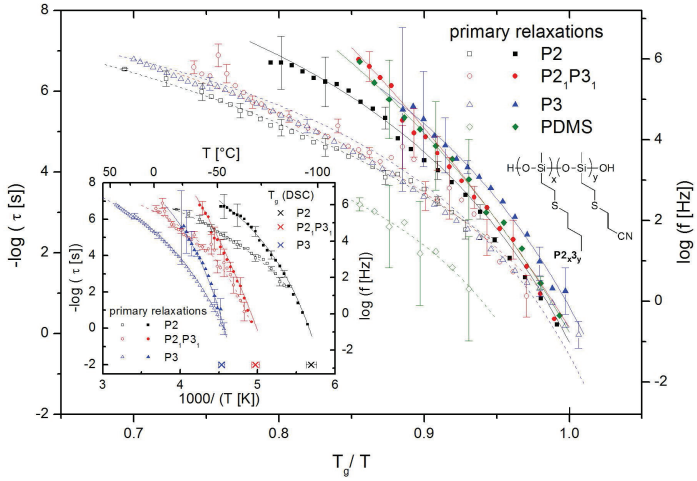

Figure 3.3: Mean relaxation time τ of the primary relaxations of the polymers P2, $P2_1P3_1$ and P3 as a function of absolute inverse temperature (inset) and rescaled with respect to the corresponding calorimetric glass transition temperature T_g (main frame). Solid and dashed lines are fits of the Vogel-Fulcher-Tammann equation to the data of the α-relaxation in the amorphous phase (solid symbols) and the segments neighbouring the crystallites (open symbols), respectively. In the main frame, also the chemical structure of $P2_xP3_y$ is depicted.

to the relaxation of segments neighbouring crystallites. Two secondary relaxations (Fig. 3.4), a fast and a slow one, can be assigned to local fluctuations of the two types of side chain end groups (methyl and nitrile groups, respectively). This is evident from the differences in the dynamics, in the activation energies and in the dielectric relaxation strength.

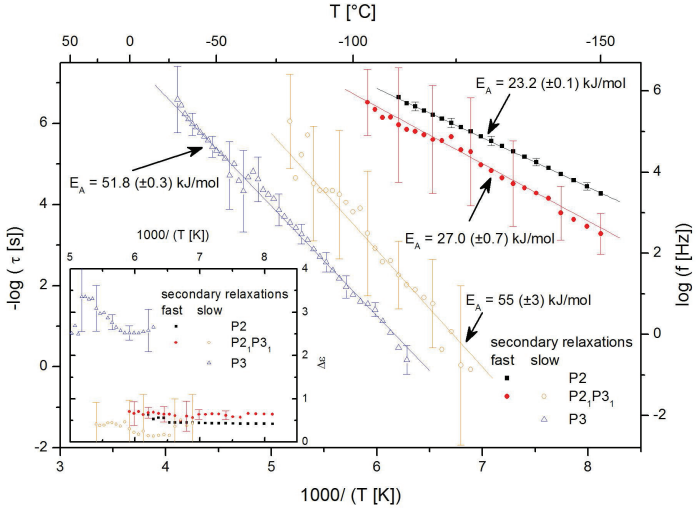

Figure 3.4: Mean relaxation time τ as a function of inverse temperature of the secondary relaxations of the polymers P2, $P2_1P3_1$ and P3. Inset: Dielectric relaxation strength $\Delta\varepsilon$ of these relaxations as a function of inverse temperature.

[1] J. Dünki, M. Tress, F. Kremer, S. Y. Ko, F. A. Nüesch, C. Racles and D. M. Opris, submitted (2015)

3.4 Molecular dynamics of itraconazole confined in thin supported layers

E.U. Mapesa, M. Tarnacka*, M. Treß, W.K. Kipnusu, K. Kamiński*, F. Kremer

*Institute of Physics, University of Silesia, ul. Uniwersytecka 4, 40-007 Katowice, Poland

For the first time, we studied a liquid crystalline material under one-dimensional nano-confinement. Broadband Dielectric Spectroscopy (BDS) was used to study the molecular dynamics of thin layers of itraconazole - an active pharmaceutical ingredient with rod-like structure and whose Differential Scanning Calorimetry (DSC) scans reveal liquid crystalline-like phase transitions. It is found that (i) the structural relaxation process remains bulk like, within the limits of experimental accuracy, in its mean relaxation rate (Figure 3.5), while (ii) its shape is governed by two competing events (Figure 3.6): interfacial interactions, and crystalline ordering. Additionally, (iii) the dynamics of the δ-relaxation - assigned to the flip-flop rotation of the molecule about its short axis - deviate from bulk behaviour as the glass transition is approached for the confined material. In a recently published paper [1], these observations are rationalized within the framework of molecular dynamics as currently understood.

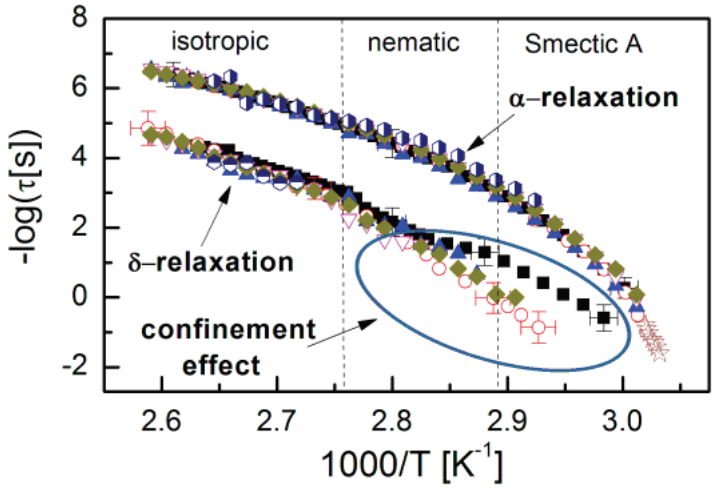

Figure 3.5: The temperature-dependence of the mean relaxation times for the α- and δ-processes for different layer thicknesses. The star symbols represent data obtained by temperature-modulated DSC for the bulk sample.

[1] E.U. Mapesa, M. Tarnacka, E. Kamińska, K. Adrjanowicz, M. Dulski, W. Kossack, M. Tress, W.K. Kipnusu, K. Kamiński, and F. Kremer, RSC Adv. 4, 28432 (2014)

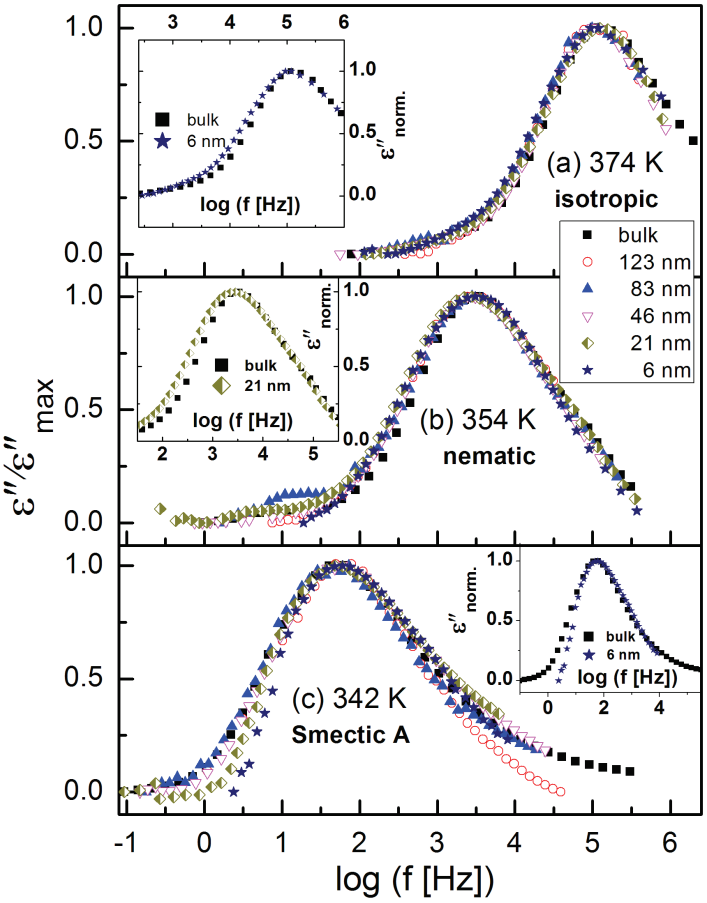

Figure 3.6: Dielectric spectra normalized with respect to the maximum of dielectric loss (ε''_{max}) of the α-process at temperatures where the (a) isotropic, (b) nematic and (c) smectic A mesophases are expected. The insets in (a) and (b) compare data for bulk sample and thin films (thicknesses as indicated) at 374 and 354 K, respectively.

3.5 Structure and Dynamics of Asymmetric Poly(styrene-b-1,4-isoprene) Diblock Copolymer under 1D and 2D Nanoconfinement

W.K. Kipnusu, M.M. Elmahdy*, E.U. Mapesa, J. Zhang†, W. Böhlmann, D-M. Smilgies‡, C.M. Papadakis†, F. Kremer

*Department of Physics, Mansoura University, Mansoura 35516, Egypt
†Physik-Department, Physik weicher Materie, Technische Universität München
‡Cornell High Energy Synchrotron Source (CHESS), Wilson Laboratory, Cornell University, Ithaca, New York 14853, United States

From both technological and fundamental view points, studies of structure and dynamics of confined block copolymers (BCPs) is of great interest. In most technological applications, BCPs are constrained within nano-scale spaces of different dimensions. The question of how dimensionality of nanoconfinement affects the morphologies and

the dynamical properties such as glass transition temperature of BCPs therefore become weighty. In this work the impact of 1-and 2-dimensional (2D) confinement on the structure and dynamics of asymmetric poly(styrene-*b*-1,4-isoprene) P(S-*b*-I) with f_{PI} = 0.73 diblock copolymer is investigated by a combination of Scanning Electron Microscopy (SEM), Atomic Force Microscopy (AFM), Grazing-Incidence Small-Angle X-ray Scattering (GISAXS), and Broadband Dielectric Spectroscopy (BDS). 1D confinement is achieved by spin coating the P(S-*b*-I) to form nanometric thin films on silicon substrates, while in the 2D confinement, the copolymer is infiltrated into cylindrical anodized aluminum oxide (AAO) nanopores. Figure 3.7 shows the SEM and GISAXS results for the sample confined in AAO pores and in thin films respectively. The SEM micrograph reveal copolymer nanorods. GISAXS images of thin films show hexagonally packed cylinders. Three dielectrically active relaxation modes assigned to the two segmental modes of the styrene and isoprene blocks and the normal mode of the latter are studied selectively by BDS. The dynamic glass transition, related to the segmental modes of the styrene and isoprene blocks is independent of the dimensionality and the finite sizes (down to 18 nm) of confinement but the normal mode is influenced by both factors with 2D geometrical constraints exerting greater impact. This reflects the considerable difference in the length scales on which the two kinds of fluctuations take place. [1]

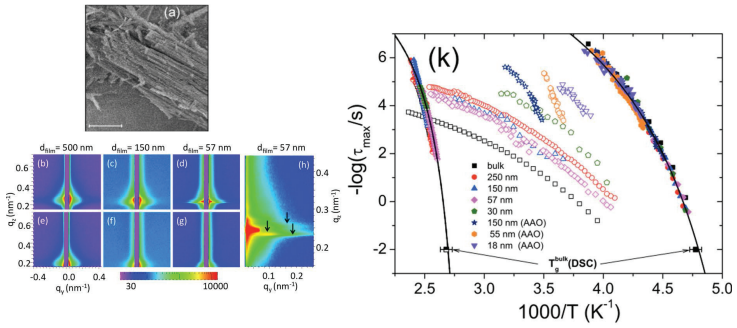

Figure 3.7: SEM micrograph of the nanorods of P(S-*b*-I) that was contained in 150 nm AAO pores (a); 2D GISAXS images of P(S-*b*-I) films with f_{PI} = 0.73 (b-d,h) α_i = 0.14° and (e-g) α_i = 0.09° and activation plot for the relaxation processes in P(S-*b*-I (k).The film thicknesses and pore sizes are indicated.

[1] W.K. Kipnusu, M.M. Elmahdy, J. Zhang, W.Böhlmann, D-M. Smilgies, C. M. Papadakis and F. Kremer, Submitted to ACS Appl. Mater. Interfaces, (2014).

3.6 Hydrogen-bonded chain length equilibria in mono-hydroxyl alcohol under nano-confinement

W.K. Kipnusu, K. Kamiński*, F. Kremer

*Institute of Physics, University of Silesia, ul. Uniwersytecka 4, 40-007 Katowice, Poland

The effect of 2-D confinement of 2-ethyl-1-hexanol (2E1H) in unidirectional nano-pores having diameters of 4, 6, and 8 nm as studied by means of Broadband Dielectric (BDS) and Fourier Transform Infrared (FTIR) spectroscopies. The glassy dynamics of confined 2E1H is faster than bulk at the vicinity of T_g while the Debye relaxation is minimally affected. The decrease in the ratio of dielectric strength of these two processes, and a weakening of the dipolar correlation is accompanied by a concomitant increase in the population of isolated molecules as revealed by FTIR. In hydrophilic pores, the apparent thickness of interfacial layer obtained from BDS decreases with temperature in accord with the FTIR data. This proves that geometrical constraints and the surface interactions break the linear chains in 2E1H resulting in shorter Hydrogen bonded structures that still exhibit Debye-like relaxation. [1]

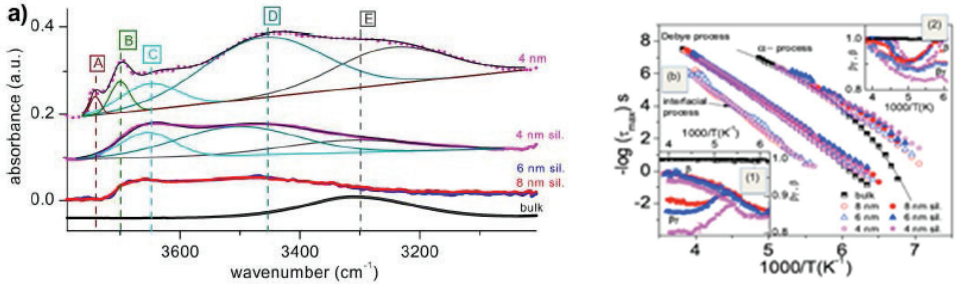

Figure 3.8: (a) shows stacked infrared spectra of 2E1H at 255 K (thick lines) in bulk and when confined in different pore sizes being modeled as a sum (black, thin lines) of independent pseudo-voigt peaks (colored thin lines). (a) All absorption peaks are assigned to (OH) of the various hydroxyl groups present in the system: silica surface (non H-bonded): A; silica surface (H-bond donor): B; isolated 2E1H: C; terminal 2E1H in chains (H-bond donor): D; and bulky 2E1H (H-bond donor and acceptor): E. (b) Activation plots for 2E1H; in bulk state (halffilled symbols), in native silica pores (open symbols) and in silanized pores (filled symbols). Insets: Temperature dependence of the HN shape parameters of the Debye process: β and $\beta\gamma$ for: (1) silanized (crossed symbols) and (2) native silca nanopores.

[1] W.K.Kipnusu, K. Kamiński, and F. Kremer under preparation

3.7 Inter- and intra-molecular dynamics in polyalcohols during glass transition

L. Popp, W. Kossack, M. Treß, W.K. Kipnusu, F. Kremer

The molecular dynamics of a homologous series of glass forming polyalcohols is studied by Broadband dielectric spectroscopy (BDS) and Fourier transform infrared spectroscopy (FTIR) during the dynamic glass transition around the calorimetric glass transition temperature, T_g [1]. Using BDS, the dynamics of dielectric relaxation processes are investigated in sorbitol, xylitol, threitol and glycerol over a wide frequency range (10^{-2} to 10^6 Hz). Additionally, FTIR is utilized to characterize the temperature dependence of intra-molecular vibrations of different atom bonds [2]. Therefore, the

temperature dependencies of specific IR absorption bands are studied in terms of their spectral position and the corresponding oscillator strength. By comparison of the results from BDS and FTIR the different properties and the interplay between inter- and intra-molecular dynamics can be examined [3]. With decreasing temperature the IR band positions of the CCO and CO stretching vibration and the CH_2 twisting vibration, show a blue shift with a distinct kink at the calorimetric glass transition temperature. The OH stretching vibration again exhibits a different temperature dependency, namely a strong redshift with decreasing temperature. Additionally, a qualitative model of the underlying molecular causes to the obtained vibrational dynamics is developed.

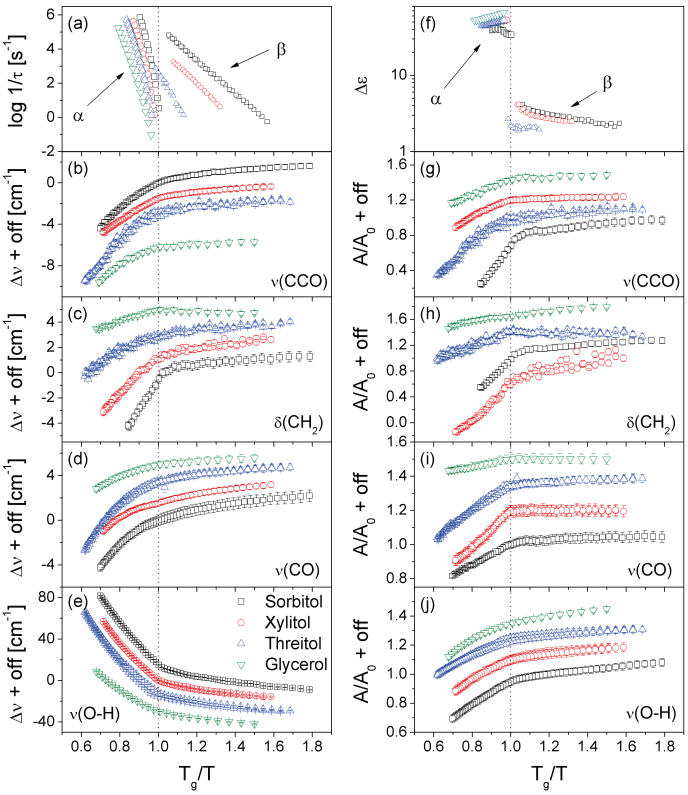

Figure 3.9: Comparison of the IR vibrational properties (from FTIR) and the relaxation dynamics (from BDS) of sorbitol, xylitol, threitol and glycerol as a function of scaled T (with respective T_g). The (a) activation plots and (f) the relaxation strengths (from BDS) of the α- and β-relaxations are shown as well as the temperature dependencies of the peak positions (b-e) of the different investigated intra-molecular vibrations and their corresponding oscillator strengths (g-j) (with arbitrary offsets between curves).

[1] P. Papadopoulos et al., Soft Matter (2013) 9, 1600-1603
[2] W. Kossack et al., Phys Chem Chem Phys (2013), 15(47): 20641-50
[3] W. K. Kipnusu et al., Soft Matter (2013) 9, 4681-4686

3.8 Relaxations and charge transport in Polymeric Ionic Liquids

F. Frenzel, M.Y. Folikumah*, M. Schulz*, W.H. Binder*, F. Kremer

*Institute of Chemistry, Martin-Luther-University Halle-Wittenberg

Broadband Dielectric Spectroscopy (frequency range: 10^{-2}-10^{7} Hz, temperature range: 200-400K) as well as calorimetry are employed to unravel relaxations and charge transport in a homologous series of monovalent or bivalent N,N,N-triethyl-ammonium and 1-methylpyrrolidinium telechelic polyiso-butylene (PIB) based Polymeric Ionic Liquids (PIL) (Fig. 3.10) having four different anions (Br, NTf_2, OTf, pTOS).

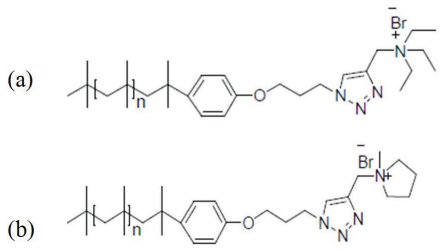

Figure 3.10: Chemical structure of N,N,N- triethylammonium telechelic PIB (a) and of 1-methylpyrrolidinium telechelic PIB (b) (here with bromide as anion).

Two relaxation processes are observed, being assigned to the dynamic glass transitions of the polymeric part of the PIL and to the moieties having the character of Ionic liquids. The former (Fig. 3.11) scales well with the calorimetric glass transition temperature as measured calorimetrically; the latter (Fig. 3.12) is proportional in its relaxation rate to the DC conductivity, hence following a Barton-Nakajima-Namikawa (BNN) relation as well established for low molecular weight systems.

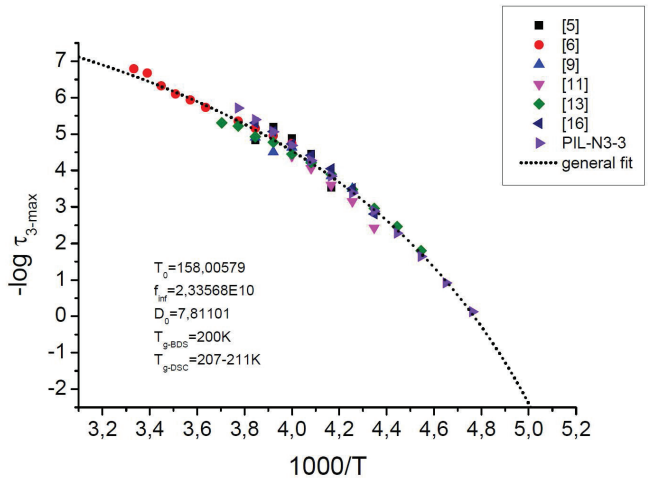

Figure 3.11: Five samples, where the dynamic glass transition relaxation can be observed, as well as the polymeric part of the PIL and a general Vogel-Fulcher-Tamman-fit.

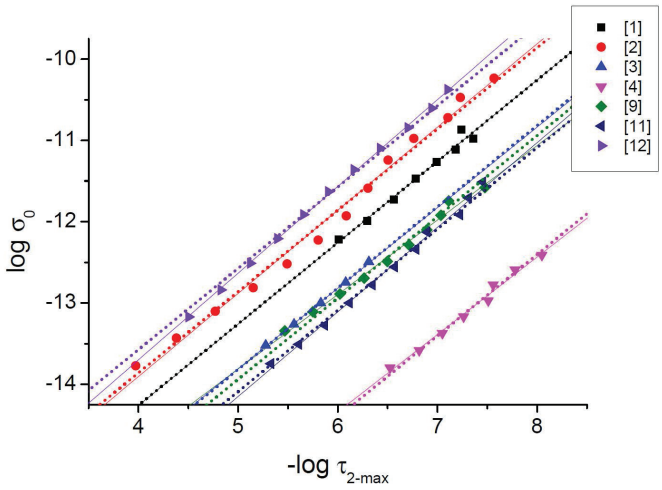

Figure 3.12: Seven selected samples that show strongly the linear dependency between relaxation time of the second process and the DC-conductivity, whereat the straight lines reveal a linear fit resp. to the data and the dotted line resp. to slope value 1.

[1] Sangoro, J.R., C. Iacob, A.L. Agapov, Y. Wang, S. Berdzinski, H. Rexhausen, V. Strehmel, C. Friedrich, A.P. Sokolov, F. Kremer, Soft Matter 10, (20) 3536-402014 (2014)
[2] Sangoro, J.R., F. Kremer, Acc. Chem. Res. 45 (4), 525-532 (2012)
[3] Sangoro, J.R., M. Mierzwa, C. Iacob, M. Paluch, F. Kremer, RSC Adv. 2, 5047-5050 (2012)

3.9 Strain induced, anisotropic crystallization studied by FTIR

W. Kossack, A. Seidlitz*, T. Thurn-Albrecht*, F. Kremer

*Institut für Physik, Martin-Luther-Universität Halle-Wittenberg

The orientation of crystalline and amorphous building blocks in strain-recrystallized Poly-Capro-Lactone (PCL, Fig. 3.13 b) is studied by Infrared-Transition Moment Orientational Analysis (Fig. 3.13 a shows the corresponding IR-spectra) [1]. To do so a cast film is stretched by approximately 10% leading to a plastically (PDR, $\sim 2\mu$m thick) and an elastically deformed region (EDR, $\sim 11\mu$m). As apparent from Polarized optical microscopy (POM) both regions exhibit anisotropic optical properties on the length-scale of the wavelength (Fig. 3.13 c,d). In the PDR the initially centrosymmetrically grown spherulites are broken up and linear structures are formed (Fig. 3.13 d), exhibiting a strong macroscopic ($\sim$cm^2) and biaxial order of crystalline and amorphous moieties. This is quantified by the nematic order parameter S, being ≤ 0.76 for the crystalline c-axes and ≤ 0.5 for the amorphous chains' backbones. The respective biaxiality, b, is found to be ~ 0.25 and $\beta \sim 0.1$ [1].This is in contrast to the EDR, where $S \sim b \sim 0$.

[1] W. Kossack, P. Papadopoulos, P. Heinze, H. Finkelmann and F. Kremer, Macromolecules, vol. 43, no. 18, 7532, 2010.

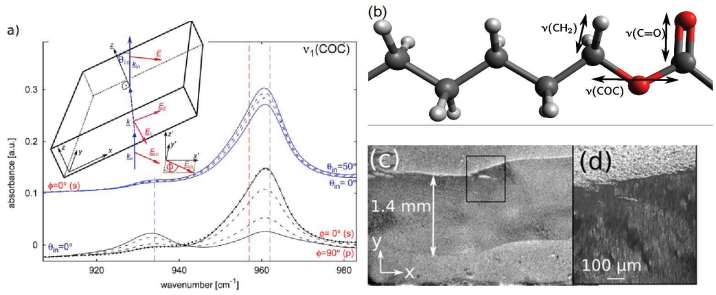

Figure 3.13: a) IR-spectra of the PDR measured for different polarizations ϕ and inclinations θ_{in}in as given in the graph; The inset shows the geometry of the measurement including the electric fields, $\vec{E}$ and the wavevectors, $\vec{k}$. b) IR spectra chemical structure (stick and ball model) and transition moments (arrows) of the PCL monomer (light grey: H, dark grey C and red O); c) micrograph of the PDR; The framed region is depicted in d) showing a POM picture.

3.10 Glassy dynamics of Poly(2-Vinyl-Pyridine) brushes with varying grafting density

N. Neubauer, R. Winkler*, M. Treß, P. Uhlmann*, M. Reiche†, F. Kremer

*Leibnitz-Institut für Polymerforschung, Dresden

†Max-Planck-Institute for Microstructure Physics, Halle an der Saale

The molecular dynamics of poly(2-vinyl-pyridine) (P2VP) brushes is measured by Broadband Dielectric Spectroscopy (BDS) in a wide temperature (250K - 440K) and broad spectral (0.1 Hz - 1 MHz) range [1]. This is realized using a nanostructured electrode arrangement. Two highly conductive silicon electrodes ($\rho < 0.01\Omega$cm) are assembled to form the capacitor. Silicon dioxide pistons having a height of 35 nm serve as spacers, leading to a distance of around 40 - 50 nm between the solid surfaces of the electrodes. The grafting of P2VP on a highly conductive silicon layer is realized in a two-step "grafting-to" preparation. A thin layer ($\approx$ 2.5 nm) of poly(glycidyl methacrylate) (PGMA) serves as anchors for carboxyl terminated poly(2-vinylpyridine) (P2VP-COOH). By applying different annealing times, P2VP-brushes with different grafting densities are formed. In the present study P2VP-brushes with five grafting densities (0.03 - 0.117 chains/nm^2) and layer thicknesses from 2 nm to 7 nm were investigated. This corresponds to distances between the grafting points of about 3 - 6 nm (smaller than $2R_g \sim 10$ nm). The quality of the prepared films is checked by ellipsometry and Atomic Force Microscopy (AFM). The dielectric loss (ε'') spectra show two well separated relaxation modes, an Arrhenius-like process being attributed to fluctuations in the poly(glycidyl methacrylate) (PGMA) linker used for the grafting reaction and the segmental dynamics (dynamic glass transition) of the P2VP brushes (Fig. 3.14 a). The latter is characterized by a Vogel-Fulcher-Tammann dependence similar to bulk P2VP (Fig. 3.14 b). The results can be comprehended considering the length scale on which the dynamic glass transition ($\leq$ 1 nm) takes place.

[1] N. Neubauer, R. Winkler, M. Tress, P. Uhlmann, M. Reiche, and F. Kremer, Soft Matter, 11, 3062, 2015

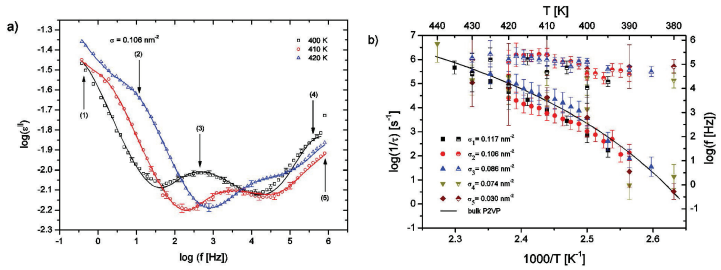

Figure 3.14: a) Dielectric loss ε'' spectra of P2VP brushes with σ = 0.106 nm^{-2} on a PGMA anchoring layer at varying temperatures as indicated. Several contributions are observed and marked by arrows in the spectra. (1) a linear contribution due to a parasitic conductivity of the spacers or contaminating particles between the electrodes, (2) a polarization which originates from the conductivity of P2VP, (3) the α-relaxation of P2VP, (4) a PGMA-relaxation, (5) and a linear contribution due to the limited conductivity of the silicon electrodes. The fit function (solid lines) is deduced from an equivalent circuit model. b) Activation plot of the P2VP α-relaxation (filled symbols) and the PGMA-relaxation (half-filled symbols) for five different grafting densities as indicated. For all grafting densities the PGMA relaxation has an Arrhenius-like thermal activation while the P2VP-brushes follow a Vogel-Fulcher-Tammann temperature dependence. The solid line shows the mean relaxation rates of bulk P2VP. The error bars show the accuracy for determining the mean relaxation rate.

3.11 Methods to determine the pressure dependence of the molecular order parameter in (bio)macromolecular fibers

A.M. Anton, C. Gutsche, W. Kossack, F. Kremer

The experimental realization and an algorithm for analyzing the pressure dependence of the molecular order parameter of specific structural moieties in (bio)macromolecular fibers has been developed [1]. By employing a diamond anvil cell (DAC) the polarization-dependent IR-transmission at hydrostatic pressure is recorded. In parallel, using an integrated microscope, the macroscopic orientation of the fibers is determined. Because the apparent spectral dichroism originates from the convolution of the macroscopic distribution of the fibers and the microscopic distribution of transition moments within one fiber, one is able to separate between order and disorder at macroscopic and microscopic scales. Using the example of major ampullate spider silk the pressure dependence of the molecular order parameter of alanine groups located within nanocrystalline building blocks is deduced and found to decrease reversibly by 0.01 GPa^1 when varying the external hydrostatic pressure between 0 and 3 GPa.

[1] A. M. Anton, C. Gutsche, W. Kossack, F. Kremer, Soft Matter (2014) DOI: 10.1039/C4SM01142B

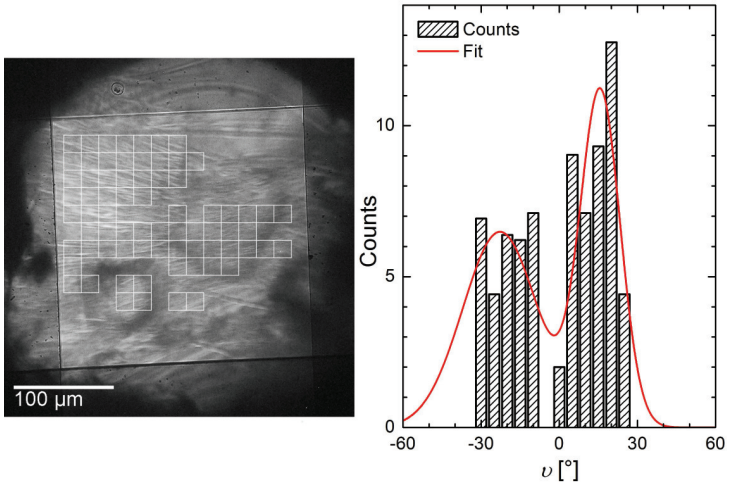

Figure 3.15: The macroscopic orientation distribution of the fibers is evaluated by determining the mean orientation within a reference volume (square region) and compiling a histogram or distribution function of these reference volumina.

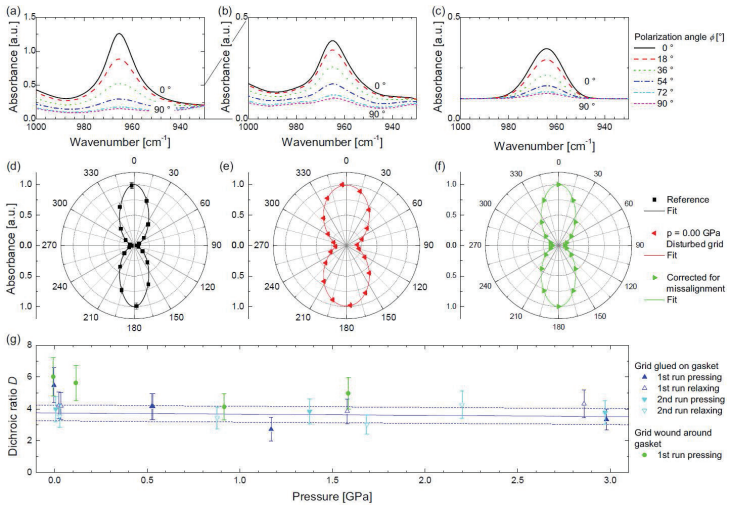

Figure 3.16: (a) The spectral dichroism of parallel fibers is used as a standard for the microscopic distribution of transition moments at ambient conditions (d). (b) Applying hydrostatic pressure causes the grating of parallel fibers to distort on expense of the apparent dichroism (e). (c) Utilizing the macroscopic distribution of the fibers (Fig. 3.15) and anticipate the apparent dichroism as the convolution of the macroscopic distribution and the microscopic distribution of the transition moments within one fiber one is able to separate pressure effects on the macroscopic and microscopic scale and to extract the microscopic transition moment distribution for a deformed grating. (g) This procedure is used to determine the pressure dependence of the molecular order parameter of an alanine-specific vibration located within the nanocrystalites. [1]

3.12 The influence of shear processing on the morphology orientation and mechanical properties of styrene butadiene triblock copolymers

N. Mahmood[*], A.M. Anton, G. Gupta[*], T. Babur[*], K. Knoll[†], T. Thurn-Albrecht[*], F. Kremer, M. Beiner[*‡], R. Weidisch[*‡]

[*]Martin-Luther-Universität Halle-Wittenberg, Halle
[†]BASF, Ludwigshafen
[‡]Fraunhofer-Institut für Werkstoffmechanik IWM, Halle

The influence of ram extrusion on structure and mechanical properties of a triblock copolymer consisting of polystyrene (S) outer blocks and poly(styrene-stat-butadiene) (S/B) middle block is studied for a wide range of shear rates [1]. Structural features on the mesoscale (10 100 nm) are investigated by small angle X-ray scattering (SAXS) and transmission electron mircoscopy (TEM). Transition Moment Orientational Analysis (TMOA) is applied to quantify the orientation on the molecular (segmental) scale (< 1 nm). All extruded samples microphase-separate and show a lamellar morphology with periodicities of about 33 nm. Significant orientation is observed on the mesoscale where the surface normals of the lamellae are preferentially perpendicular to the extrusion direction. The corresponding degree of orientation drops slightly at elevated shear rates of about 600 s^1. In contrast, significant orientation on the molecular scale is absent for styrene and butadiene units indicating basically random orientation of the chain segments. The mechanical properties are, however, strongly anisotropic. In general, the results demonstrate that orientation effects on the mesoscale have a strong influence on the mechanical properties and must be considered during the optimization of extruded or injection-molded components made from microphase-separated block polymers.

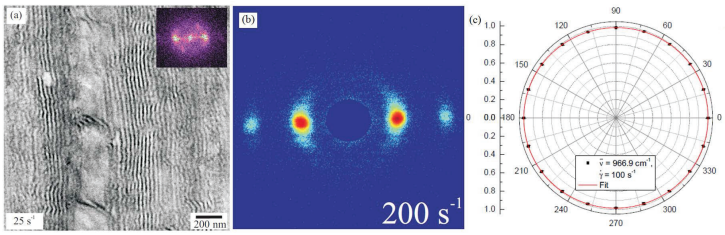

Figure 3.17: TEM (a), IR-TMOA (b), and SAXS (c) measurement on S-S/B-S triblock copolymer. On the mesoscale well-defined and well-aligned lamella structures are evident (a and c). In contrast, the circular shape of the polarization-dependent oscillator strength indicates absence of any molecular orientation on the segmental scale (b).

[1] N. Mahmood, A. M. Anton, G. Gupta, Tm Bambur, K. Knoll, T. Thurn-Albrecht, F. Kremer, M. Beiner, R. Weidisch, Polymer (2014) 55, 3782-3791

3.13 IR transition moment orientaional analysis (IR-TMOA) on the surface-induced orientation in thin layers of a high electron mobility n type copolymer (P[NDI2OD-T2])

A.M. Anton, R. Steyrleuthner*, W. Kossack, D. Neher†, F. Kremer

*Freie Universität Berlin
†Universität Potsdam

The novel IR-based method of infrared transition moment orientational analysis (IR TMOA) is employed to unravel the molecular order in thin layers of the semiconducting polymer poly[N,N′-bis(2-octyldodecyl)-1,4,5,8-naphthalenediimide-2,6-diyl]-alt-5,5′-(2,2′-bithiophene) (P[NDI2OD-T2]). Structure-specific vibrational bands are analyzed in dependence on polarization and inclination of the sample with respect to the optical axis. By that the molecular order parameter tensor for the respective molecular moieties with regard to the sample coordinate system is deduced. Making use of the specificity of the IR spectral range, we are able to determine separately the orientation of atomistic planes defined through the naphthalenediimide (NDI) and bithiophene (T2) units relative to the substrate, and hence, relative to each other. A pronounced solvent effect has been observed: While chlorobenzene causes the T2 planes to align preferentially parallel to the substrate (angle of 29°), 1:1 chloronaphthalene:xylene mixture as solvent results in a reorientation of the T2 units from a face on into an edge on arrangement. In contrast the NDI part remains unaffected.[1] The derived orientation is well correlated with the direction of π-π stacking.[2] For both solvents evidence for the aggregation of chains in accord with recently published results is obtained by UV/Vis absorption spectroscopy.[1,2]

[1] A. M. Anton, R. Steyrleuthner, W. Kossack, D. Neher, F. Kremer, JACS (accepted)
[2] R. Steyrleuthner, R. Di Pietro, et al., D. Neher, J. Am. Chem. Soc. (2014) 136, 4245-4256

3.14 Epitope-Scans of monoclonal antibody HPT-101 using dynamic force spectroscopy and ELISA

T. Stangner, S. Angioletti-Uberti*, D. Knappe†, D. Singer†, C. Wagner, C. Gutsche, J. Dzubiella*, R. Hoffmann†, F. Kremer

*TU Berlin
†Biotechnologisch-Biomedizinisches Zentrum Leipzig

Monoclonal antibodies (mAbs) are nowadays widely used as medical agents in therapy and diagnostics. Especially in the context of neurodegenerative diseases (e.g. Alzheimer's disease), when symptoms are heterogeneous or their initial manifestation is ambiguous and can be mistaken with that of other conditions, the specificity

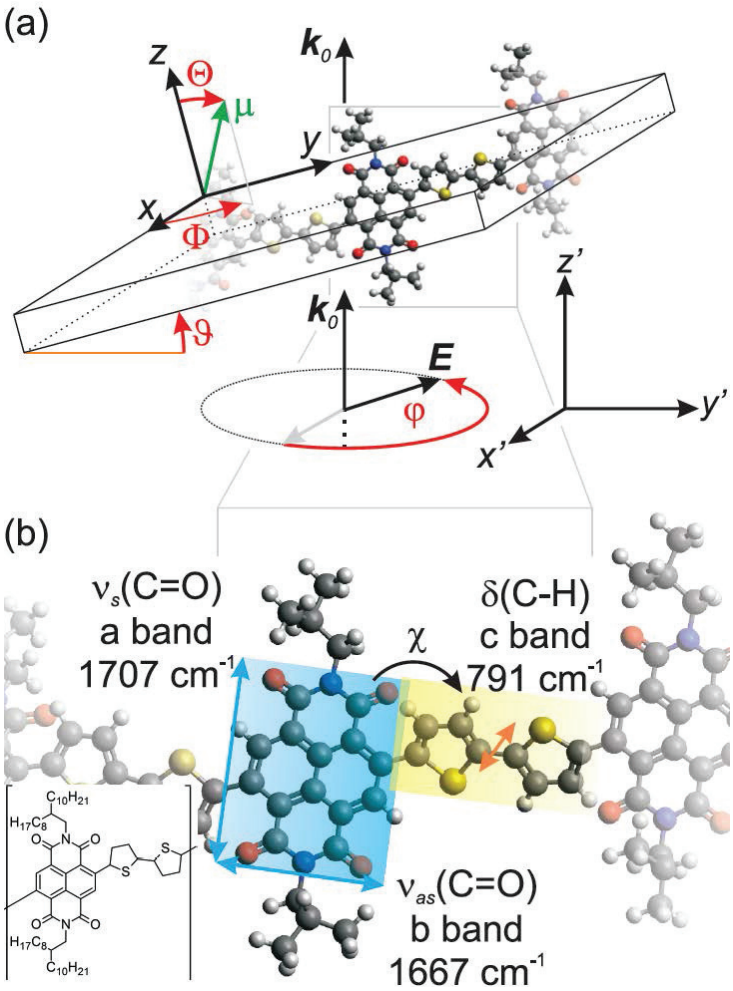

Figure 3.18: (a) For IR-TMOA the sample coordinate system (x,y,z) is inclined relative to the laboratory frame (x′,y′,z′) while the polarization(φ)- and inclination(ϑ)-dependent absorbance is measured. (b) Schematic of a sample fragment and the transition moments (arrows). The C_8H_{17} and $C_{10}H_{21}$ alkyl side chains are replaced by methyl groups.

of mAbs is a key feature for the early stage diagnosis of the disease [1]. Therefore, we analyze binding of the phosphorylation-specific monoclonal antibody HPT-101 to the peptide tau[pThr231/pSer235] carrying two potential phosphorylation sites (Thr231 and Ser235), being the most probable markers for Alzheimer's disease. In order to determine the antibody epitope, seven tau-isoforms were synthesized from the parent peptide by replacing binding relevant amino acids with a neutral alanine (alanine-scan). The interactions between the modified peptides and mAb HPT-101 were investigated using ELISA and optical tweezers-assisted dynamic force spectroscopy. The latter allows characterizing the binding between the peptide and antibody on a single-molecule level [2, 3]. By comparing the results from both methods, we were able to categorize the importance of each amino acid. Thereby, we found four essential, two beneficial (secondary) and one non-essential amino acid for the interaction between the mAb and the parent peptide. In conclusion, we were able to identify the target epitope of the monoclonal antibody HPT-101 by means of single amino acids.

[1] D.J. Cahill, Journal of Immunological Methodes, 2001, 250, 81-91.

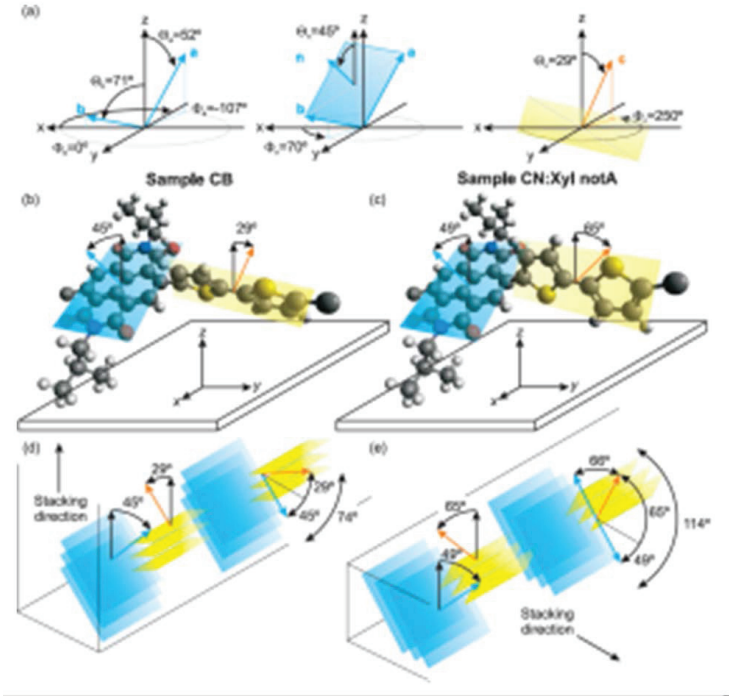

Figure 3.19: (a) Microscopic orientation of the molecular planes. (b) Using chlorobenzene, the NDI unit (blue) is inclined by 45° relative to the substrate, whereas the T2 part (yellow) features an angle of 29 and a face on orientation. (c) Using a chloronaphthalene:xylene mixture results in a distinct edge on orientation of the T2 unit. The NDI block, instead, retains its alignment. For sake of clarity the C8H17 and C10H21 alkyl chains are replaced by methyl groups. (d,e) Interpretation of the π-π stacking direction correlated to the orientation of the T2 unit.

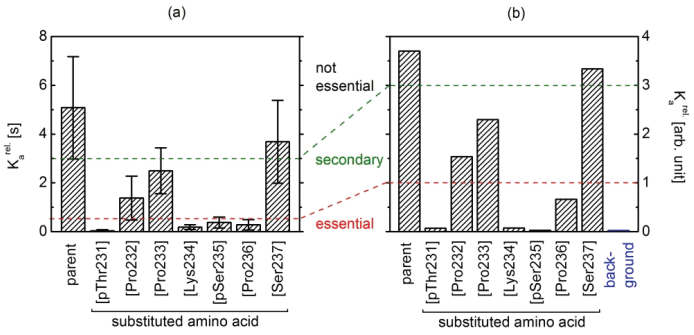

Figure 3.20: Comparison of the affinity constant Karel. of mAb HPT-101 to the parent peptide and its isoforms using dynamic force spectroscopy (a) and ELISA (b) measurements. In agreement of both approaches, four essential, two secondary and one non-essential amino acid can be determined for the interaction between mAb HPT-101 and the parent peptide tau[pThr231/pSer235].

[2] Wagner et al., Soft Matter, 2011, 7, 4370-4378
[3] Stangner et al., ACS Nano 2013, 7, 12, 11388

3.15 Funding

FOR 877 "From local constraints to macroscopic transport" TP 7 "Electric field driven motion of single polyelectrolyte grafted colloids"
Prof. Dr. F. Kremer
KR 1138/21-2 (2011-2014)

SPP 1369 "Polymer-Solid Contacts: Interfaces and Interphases" TP "Interfacial dynamics of polymers in interaction with solid substrates"
Prof. Dr. F. Kremer
KR 1138/23-2 (2011-2014)

Graduate School "Leipzig School of Natural Sciences - Building with Molecules and Nano-objects" BuildMoNa, TP 15 "Dynamics of DNA under tension and in confinement"
Prof. Dr. F. Kremer
GSC 185/1 (2008-2014)

SFB/TRR 102 "Polymers under multiple constraints: restricted and controlled molecular order and mobility", TP B05 "Structural levels of organisation in spider-silk - a combined mechanical and IR-spectroscopic study" (2011-2015), TP B08 "Broadband Dielectric Spectroscopy to study the molecular dynamics in nanometer thin layers of block copolymers" (2011-2015)
Prof. Dr. F. Kremer

New Polymer Materials on the Basis of Functionalized Ionic Liquids for Application in Membranes "Knowledge Transfer Project"
Prof. Dr. F. Kremer, Prof. Dr. Veronika Strehmel (Hochschule Niederrhein)
KR 1138/24-1; STR 437/5-3; (2014- 2017)

3.16 Organizational Duties

Friedrich Kremer

- Principal Investigator in the "Leipzig School of Natural Sciences - Building with Molecules and Nano-Objects" in the framework of a Graduate School funded by the "Ferderal Excellence Initiative". This supports several Ph.D. projects.
- Deputy chairman of the SFB-TRR 102 on "Polymers under multiple constraints: restricted and cotrolled molecular order and mobility" of the Universities of Halle and Leipzig

3.17 External Cooperations

Academic

- Max-Planck-Institute for Microstructure Physics, Halle
  Dr. Manfred Reiche

- Cornell University, Ithaca, New York
  D.M. Smilgies
- Technische Universität München
  Prof. Dr. C.M. Papadakis, J. Zhang
- Leibniz-Institut für Polymerforschung Dresden
  Dr. P. Uhlmann, R. Winkler
- University of Silesia, Katowice
  Prof. Dr. M. Paluch, Dr. K. Kaminski
- Martin-Luther-Universität Halle-Wittenberg
  PD Dr. M. Beiner, N. Mahmood
- Fraunhofer Institut für Werkstomechanik IWM, Halle
  PD Dr. M. Beiner
- Helmholtz-Zentrum Berlin für Materialien und Energie, Berlin
  Prof. Dr. J. Dzubiella, Dr. S. Angioletti-Uberti
- Department of Chemical and Biomolecular Engineering, University of Tennessee, Knoxville
  Dr. J. R. Sangoro
- Department of Materials Science and Engineering, Penn State University
  C. Iacob, Ph. D.
- Hochschule Niederrhein, Institute of Organic Chemistry
  Prof. Dr. Strehmel

Industry

- Novocontrol, Hundsangen, Germany
- BOREALIS Polyolefine GmbH, Linz, Austria
- Süd-Chemie AG, München, Germany
- MERCK KGaA, Darmstadt, Germany
- Goretex, Ottobrunn, Germany

3.18 Publications

Journals

Griffin, P.J., A.P. Holt, Y. Wang, V.N. Novikov, J.R. Sangoro, F. Kremer, A.P. Sokolov "Interplay Between Hydrophobic Aggregation and Charge Transport in the Ionic Liquid Methyltrioctylammonium Bis(trifluoromethylsulfonyl)imide" J. Phys. Chem. B 118, 783-790 (2014) DOI: 10.1021/jp412365n

Sangoro, J.R., C. Iacob, A.L. Agapov, Y. Wang, S. Berdzinski, H. Rexhausen, V. Strehmel, C. Friedrich, A.P. Sokolov, F. Kremer "Decoupling of ionic conductivity from structural dynamics in polymerized ionic liquids" Soft Matter 10, (20) 3536-402014 (2014) DOI: 10.1039/c3sm53202j

Kossack, W., W.K. Kipnusu, M. Dulski, K. Adrjanowicz, O., E. Kaminska, E.U. Mapesa, M. Tress, K. Kaminski, F. Kremer "The kinetics of mutarotation in L-fucose as monitored by dielectric and infrared spectroscopy" J. Chem. Phys. 140, 215101 (2014) DOI: 10.1063/1.4880718

Mapesa, E.U., L. Popp, W.K. Kipnusu, M. Tress, F. Kremer "Molecular dynamics in 1- and 2-D confinement as studied for the case of poly(cis-1,4-isoprene)" Soft Materials 12, 22-30 DOI: 10.1080/1539445X.2014.928320

Mahmood, N., A.M. Anton, G. Gupta, T. Babur, K. Knoll, T. Thurn-Albrecht, F. Kremer, M. Beiner, R. Weidisch "Influence of shear processing on morphology orientation and mechanical properties of styrene butadiene triblock copolymers" Polymer 55, 3782-3791 (2014) DOI: 10.1016/j.polymer.2014.05.062

Mapesa, E.U., M. Tarnacka, E. Kaminska, K. Adrjanowicz, M. Dulski, W. Kossack, M. Tress, W.K. Kipnusu, K. Kaminski, F. Kremer "Molecular dynamics of itraconazole confined in thin supported layers" RSC Adv. 4, 28432 (2014) DOI: 10.1039/c4ra01544d

Kipnusu W.K., P. Zeigermann, C. Iacob, F. Kremer, M. Schoen, M.G. Mazza, R. Valiullin "Experimental evidence of enhanced transport in supernematics" Soft Condensed Matter (2014) arXiv:1406.5868v1

Books

Tress, M., E.U. Mapesa, W. Kossack, W.K. Kipnusu, M. Reiche, F. Kremer "Molecular dynamics of condensed (semi-) isolated polymer chains" in: "Dynamics in Geometrical Confinement", F. Kremer (Ed.) Springer-Verlag (2014) ISBN 978-3-319-06099-6

Mapesa. E.U., M. Tress, M. Reiche, F. Kremer "Molecular dynamics of poly(cis-1,4-isoprene) in 1- and 2-dimensional confinement" in: "Dynamics in Geometrical Confinement", F. Kremer (Ed.) Springer-Verlag (2014) ISBN 978-3-319-06099-6

Kipnusu, W.K., C. Iacob, M. Jasiurkowska-Delaporte, W. Kossack, J.R. Sangoro, F. Kremer "Rotational diffusion of guest molecules confined in uni-directional nanopores" in: "Dynamics in Geometrical Confinement", F. Kremer (Ed.) Springer-Verlag (2014) ISBN 978-3-319-06099-6

Iacob, C., J.R. Sangoro, W.K. Kipnusu, F. Kremer "Rotational and Translation Diffusion of Ionic Liquids in Silica Nanopores" in: "Dynamics in Geometrical Confinement", F. Kremer (Ed.) Springer-Verlag (2014) ISBN 978-3-319-06099-6

3.19 Graduations

Habilitation

- Dr. Periklis Papadopoulos
  Active swimmers - selbstgetriebene Bewegung von Kolloiden
  XX/2014

Doctorate

- Emmanuel Urandu Mapesa
  Molecular dynamics of nanometric layers of glass formers in interaction with solid substrates
  11/2014
- Martin Treß
  Breitbandige dielektrische Spektroskopie zur Untersuchung der molekularen Dynamik von Nanometer-dünnen Polymerschichten
  12/2014

Bachelor

- Benjamin Suttner
  Intramolekulare Dynamik von niedermolekularen organischen Glasbildnern
  XX/2014

3.20 Guests

- Dr. Jun Ma
  Institution 1
  01-06/2014

4

Physics of Interfaces

4.1 Introduction

The department of Physics of Interfaces (Grenzflächenphysik, GFP) is in a transition state since April 2009. From the 10 scientists employed in the group at the end of 2014, 8 were financed as PhD students or post-docs via third party funding. The good situation with respect to third party funding allowed us to successfully contribute to teaching and research within the Institute of Experimental Physics I. During the winter term, the Experimental Physics freshmen courses *Mechanics* (IPSP) and *Mechanics and its mathematical methods* (state exam physics) were taken over by PD Dr. R. Valiullin and PD Dr. F. Stallmach, respectively. In September 2014 after six years of funding by DFG the successful cooperation within the the DFG Priority Research Program *Porous Metal-Organic Frameworks* (SPP 1362) came to an end. Our group continues to contribute to the DFG Priority Research Programs *Porous Media with Defined Pore Structures - Modeling, Application and Synthesis* (SPP 1570). In 2014, the collaborative research project *WasserMod* was started. This project, which is jointly financed by the Ministries of Research and Education of Germany (BMBF) and Greece (GRST) is coordinated by our group and opens us the opportunity to extend our research expertise into the vastly developing area of renewable energy process optimization.

After finishing their studies within the IRTG *Diffusion in Porous Materials*, Phillip Zeigerman, Christian Reichenbach, Alexander Shakhov and Anne-Kirstin Push obtained their PhD degrees in 2014. Christian, Phillip and Alexander left our group and continued their careers elsewhere.

PD Dr. F. Stallmach

4.2 High-Pressure Low-Field ^{1}H NMR Relaxometry in Nanoporous Materials

C. Horch, S. Schlayer F. Stallmach

We recently proposed to use low-field NMR relaxometry at elevated methane pressures to characterize the gas storage properties and pore structures of innovative nanoporous materials [1, 2]. For this purpose, an NMR sensor with NdFeB permanent magnets (B_0 = 118 mT) and a pressure cell made of PEEK (4 cm outer diameter) were designed (see Fig. 4.1). It is suitable for ^{1}H NMR studies of adsorbed molecules at pressures of up to 300 bar.

The system was used to investigate methane uptake of microporous metal-organic frameworks and nanoporous activated carbon [1, 2]. T_2 relaxation time distribution of pure methane and of methane under co-adsorption of carbon dioxide show that the host-guest interaction lead to a relaxation time contrasts, which may be used to distinguish between the gas phase and the different adsorbed phases of methane. Adsorption isotherms, exchange of methane between adsorbent particles and the surrounding gas phase, successive displacement of methane from adsorption sites by co-adsorption of carbon dioxide and CO_2/CH_4 adsorption separation factors were determined from the observed NMR relaxation time distributions. For more details we refer the reader to ref. [2].

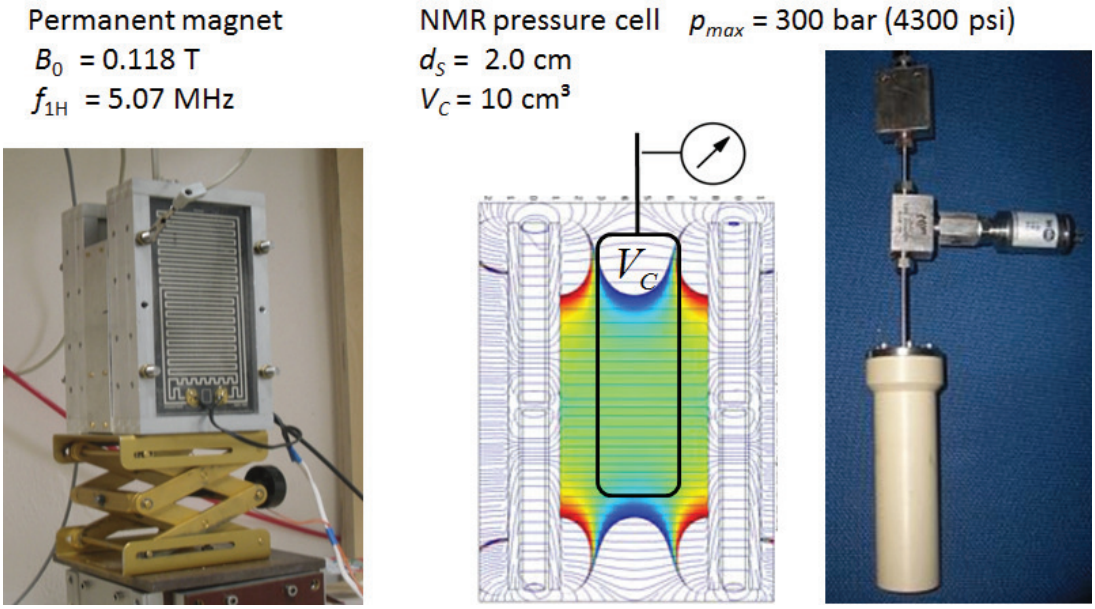

Figure 4.1: Low-field NMR sensor and pressure cell for ^{1}H relaxation time studies in nanoporous materials using hydrocarbons or water as pore fluids at static pressures of up to 300 bar. [2].

[1] L. Arnold et al., Chemie Ingenieur Technik **85**, 1726 (2013).
[2] C. Horch et al., J. Magn. Reson. **240**, 24 (2014).

4.3 Ferrocene in the metal-organic framework MOF-5 studied by homo- and heteronuclear correlation NMR and MD simulation

M. Wehring, F. Stallmach, P.C.M.M. Magusin*, S. Amirjalayer†, R. Schmid†

*Centre for Surface Chemistry and Catalysis, KU Leuven University, Belgium
†Organometallics and Materials Chemistry, Ruhr-Universität Bochum, Germany

Advanced solid-state 2D NMR spectroscopy and Molecular Dynamics computation are employed to investigate the interaction between adsorbed ferrocene molecules and the MOF-5 lattice. Relayed ^{13}C-^{1}H heteronuclear correlation (HETCOR) 2D NMR spectra clearly indicate short-distance contacts between the ferrocene guests and the benzene-1,4-dicarboxylic-acid linkers, mediated via intermolecular ^{1}H spin diffusion. By use of 2D ^{1}H-^{1}H correlation spectroscopy the distances between ^{1}H nuclei in the guests and the linkers are estimated to be shorter than 0.5 nm. MD computer simulations support the interpretation of the 2D solid state NMR studies. Moreover, they suggest a wide distribution of intermolecular distances in this host-guest system with the shortest intermolecular hydrogen-hydrogen distances of 0.15 nm. For more details we refer the reader to ref. [1]

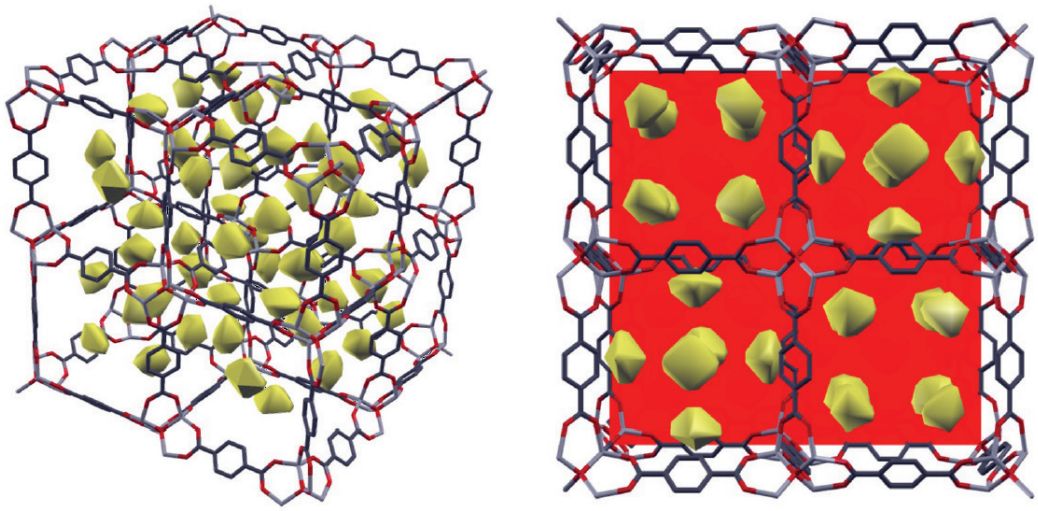

Figure 4.2: Centers of mass (corresponding to the positions of the iron atoms) of ferrocene molecules in the A and B cells of MOF-5 as obtained by analyzing trajectories of MD computer simulations. The experimental 2D NMR investigations confirm the location of the ferrocene molecules in the MOF-5 lattice.

[1] M. Wehring, P.C.M.M. Magusin, S. Amirjalayer, R. Schmid, F. Stallmach, Micropor. Mesopor. Mater. **186**, 130 (2014).

4.4 ^{13}C NMR study of diffusion anisotropy of carbon dioxide adsorbed in nanoporous DMOF-1

M. Peksa, F. Stallmach, J. Lang*,

*Department of Low Temperature Physics, Charles University in Prague, Czech Republic

DMOF-1 ($Zn_2(bdc)_2dabco$) is a metal-organic framework with tetragonal symmetry. It contains parallel one-dimensional channels with a diameter of about 0.75 nm interconnected by smaller windows. For carbon dioxide adsorbed in the nanochannels the chemical shift tensor and the diffusion tensor were investigated by ^{13}C NMR. The spectra acquired under static conditions reveal a powder pattern with a residual chemical shift anisotropy of $\langle \Delta\delta \rangle = -55$ ppm. The collinearity of the axisymmetrical residual chemical shift and the diffusion tensors was utilized to assess the diffusion anisotropy via the diffusion attenuation of the ^{13}C PFG NMR powder pattern. The results show that carbon dioxide is highly mobile in DMOF-1. The apparent diffusion coefficient (the trace of diffusion tensor) is $(6.2 \pm 1.0) \times 10^{-9}$ m^2 s^{-1} at 298 K and the corresponding anisotropy expressed as $D_\parallel/D_\perp$ is approximately equal to 3. For more details we refer the reader to ref. [1]

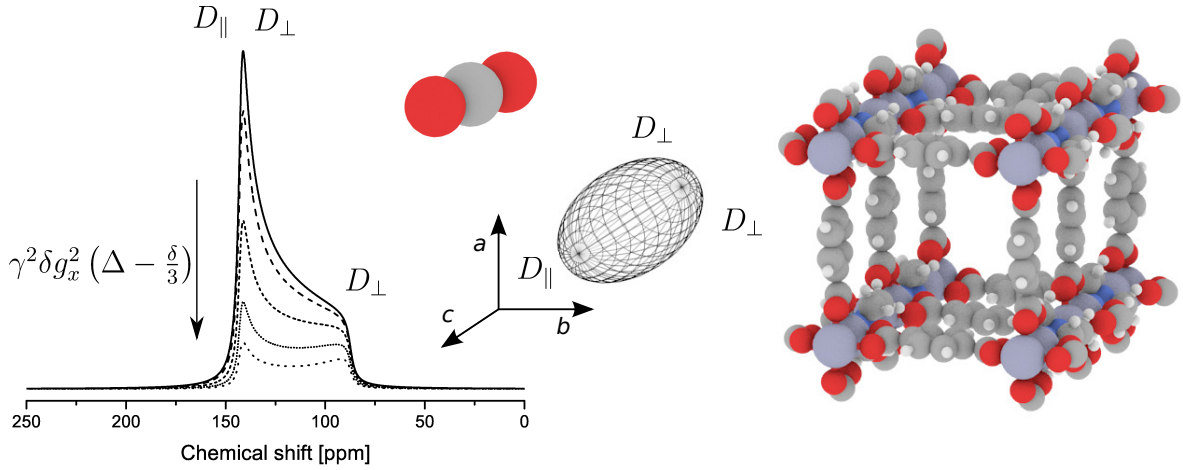

Figure 4.3: Diffusion attenuated ^{13}C PFG NMR spectra of carbon dioxide in DMOF-1. The diffusion weighting of the spectra by using pulsed field gradients allows us to determine the self-diffusion of CO_2 along ($D_\parallel$) and perpendicular ($D_\perp$) to the channel direction of the DMOF-1.

[1] M. Peksa, J. Lang, F. Stallmach, Micropor. Mesopor. Mater. **205**, 11 (2015).

4.5 Symmetry breaking in nanocapillary filling

Schneider D., Valiullin R.

Understanding fluid transport on nanoscale is a key factor in the development of modern technologies. Although different aspects of fluid phase equilibria under nanoscopic confinement have extensively been addressed by means of theory and experiment, exploration of dynamical properties has remained less covered. In our work we have studied the filling dynamics of model capillaries using dynamic mean field theory of lattice gas and Kawasaki dynamics simulations. We have found two different scenarios for filling of capped nanocapillaries from the the vapor phase. By means of dynamic mean field theory of confined lattice gas we have shown that capillary filling of capped nanochannels from vapor phase can occur via two different mechanisms, which are accompanied by totally different dynamics [1]. The first, well-known one refers to the filling by the meniscus detachment from the capped end and its progressive advancement towards the channel opening (see Figure 4.4. In striking contrast, for other sets of thermodynamic and structural parameters, the filling can instead be accompanied by the formation of a liquid bridge in the proximity of the open end, followed by capillary filling by via recession of the meniscus on the internal side of the liquid bridge towards the capped end. In this case the dynamics is found to slow down dramatically. Further on, we have applied dynamic mean field theory to study relaxation dynamics in linear pores with side streams and with ink bottle structures, mimicking real porous materials possessing intrinsic structural disorder [2]. Our results show several mechanisms for how the pore structure affecting the dynamics. An important conclusion of this work is that features like side-streams and ink bottle segments can substantially slow the equilibration of confined fluids, leading to the formation of transient metastable states.

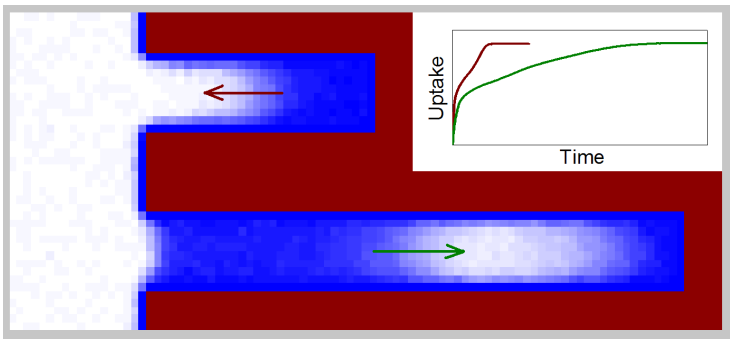

Figure 4.4: Two scenarios for the filling capped nanocapillaries accompanied by different dilling dynamics.

[1] D. Schneider, R. Valiullin, P. Monson, Langmuir **30**, 1290 (2014).
[2] D. Schneider, R. Valiullin, P. Monson, Langmuir **31**, 188 (2015).

4.6 Adsorption and diffusion in MOF Co_2(dhtp): The interplay of open metal sites, small paraffins and olefins

C. Chmelik*, J. Kärger*, P. D. C. Dietzel†, A. Mundstock‡, J. Caro‡

*University of Leipzig
†University of Bergen
‡University of Hannover

The metal organic framework (MOF) structure of the composition M_2(dhtp)$(H_2O)_2 \cdot 8H_2O$ ($dhtp^{4-}$ = dioxidoterephthalate derived from H_4dhtp as dihy-droxyterephthalic acid, M=Zn, Co, Ni, Mg, Mn, Fe, Cu; the compounds in the series are typically also labeled as M-MOF-74, CPO-27-M, or M_2(dobdc)) became one of the most studied MOFs for the storage and separation of gas molecules due to their high concentration of coordinatively unsaturated metal sites. The cobalt containing structure Co_2(dhtp) has been identified as a promising candidate for the adsorptive separation of ethylene/ethane and propylene/propane mixtures. The adsorption and diffusion patterns of the paraffins and olefins were found to be closely related to the availability of coordinatively unsaturated metal sites which act as preferential adsorption sites for the olefins (see fig. 4.5). Another objective of this study was to investigate the pronounced sensitivity of Co_2(dhtp) towards humid air [1].

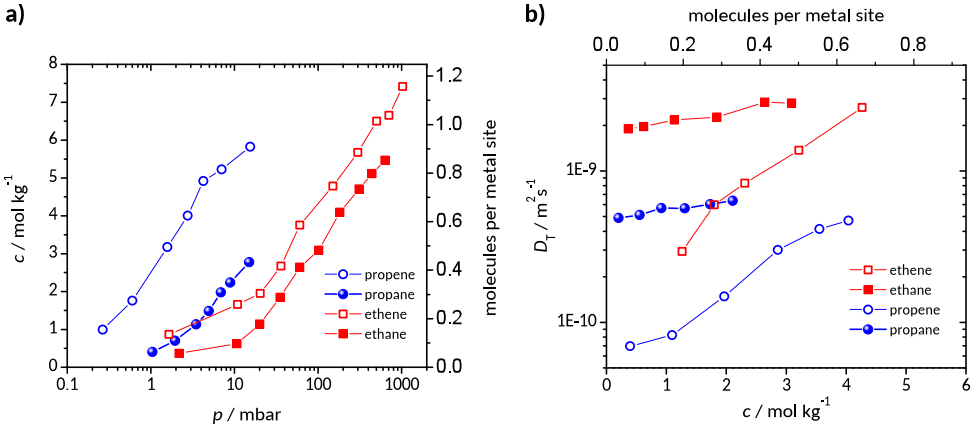

Figure 4.5: (a) Adsorption isotherms of the C2 and C3 paraffins and olefins in Co_2(dhtp) at 298 K. (b) The adsorption characteristics has direct implications for the loading dependence of the transport diffusivities.

[1] C. Chmelik et al., Micropor. Mesopor. Mater. **183**, 117 (2014) .

4.7 Microimaging of transient concentration profiles of reactant and product molecules during catalytic conversion in nanoporous materials

T. Titze*, C. Chmelik*, J. Kullmann*, L. Prager†, E. Miersemann*, R. Gläser*, D. Enke*, J. Weitkamp‡, J. Kärger*,

*University of Leipzig
†Leibniz Institute of Surface Modification
‡University of Stuttgart

Microimaging by IR microscopy is applied to the recording of the evolution of the concentration profiles of reactant and product molecules during catalytic reaction, notably during the hydrogenation of benzene to cyclohexane by nickel dispersed within a nanoporous glass (see fig. 4.6). Being defined as the ratio between the reaction rate in the presence of and without diffusion limitation, the effectiveness factors of catalytic reactions were previously determined by deliberately varying the extent of transport limitation by a changing suitably chosen system parameters, such as the particle size and by comparison of the respective reaction rates. With the novel options of microimaging, effectiveness factors become accessible in a single measurement by simply monitoring the distribution of the reactant molecules over the catalyst particles [1]. With the realistic option of attaining resolutions in the range of seconds and a few micrometers and reaction temperatures up to several hundred centigrade, microimaging offers promising prospects for application in both fundamental research and catalyst development.

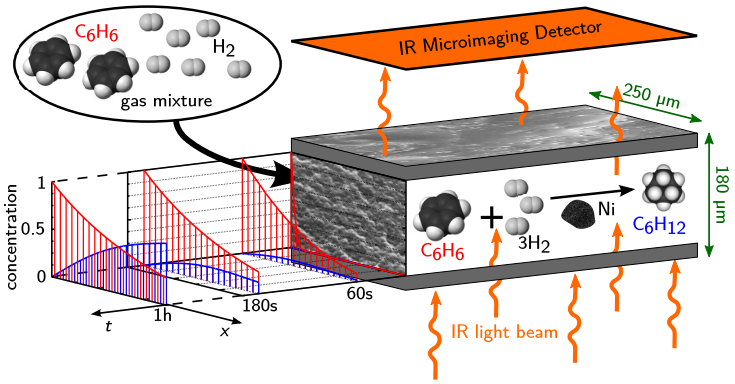

Figure 4.6: Monitoring reactant and product concentration profiles during the conversion of benzene (red) into cyclohexane (blue) in nanoporous materials by microimaging, with the arrows in green indicating the spatial extensions relevant for our experiments.

[1] T. Titze et al., Angew. Chem. Int. Ed. (2015) in press. (DOI: 10.1002/anie.201409482)

4.8 Funding

Water vapor sorbed in porous solids - Experimental study of its equilibrium and transport rate for adsorptive heat transformation, supported by computer modeling.
PD Dr. F. Stallmach (coordinator), Dr. Ch. Chmelik
BMBF FKZ: 03SF0469A

Fundamental Host-Guest Interactions in Porous Metal Organic Frameworks. A Combined Experimental and Theoretical Approach.
PD Dr. F. Stallmach
DFG STA 648/1-2, within SPP 1362 MOFs

Knowledge-based development of supported ZIF membranes for liquid mixture separation by pervaporation
Dr. Ch. Chmelik, Prof. Dr. J. Kärger,
DFG CH 778/1-2, within SPP 1362 MOFs

Separating mixutures of chiral anesthetic gases by modified porous glasses
Dr. Ch. Chmelik
DFG CH 778/2-1 and 778/2-2, within SPP 1570

Measuring Intracrystalline Profiles of Diffusion and Reactions in Zeolites by IR Microscopy
Prof. Dr. J. Kärger, Dr. Ch. Chmelik
DFG KA 953/20-2

NMR relaxation time studies on sediment samples at elevated methane gas pressures
PD Dr. F. Stallmach
Baker Hughes Inc., Houston, USA

NMR-Untersuchungen an verstrangten Katalysatoren
PD Dr. F. Stallmach
BASF SE Ludwigshafen

Driven diffusion in nanoscaled materials
Dr. R. Valiullin
DFG VA 463/5-2

Correlating diffusion processes in complementary pore spaces using NMR and theoretical modelling
Prof. Dr. J. Kärger, Prof. Dr. A. Bunde, Dr. R. Valiullin
DFG KA 953/30-1

4.9 Organizational Duties

Frank Stallmach

- deputy chair and member of the steering committee of the MRPM Division of the Groupement AMPERE; conference series "Magnetic Resonance in Porous Media" (MRPM)

- faculty board member, member of several commissions of the faculty board
- referee: Micropor. Mesopor. Mat., Angewandte Chemie, J. Magnetic Resonance, J. Phys. Chem., Chemical Engineering Technology, Surface Geophysics

Jörg Kärger
- Membership in the Programme Committee of the "FEZA conference" (Leipzig, 2014), in the Scientific Committee of the conference "Diffusion Fundamentals VI" (Dresden, 2015) and in the Structural Committee "Spreading in Nature, Techology and Society" of the Saxonian Academy of Sciences in Leipzig
- Editor: Diffusion Fundamentals; Membership in Editorial Boards: Adsorption, Micropor.Mesopor.Mat.
- Referee: Nature, Phys. Rev., Phys. Rev. Lett., Angew. Chem., Europhys. Lett., J. Chem. Phys., J. Phys. Chem., Langmuir, Micropor. Mesopor. Mat., Phys. Chem. Chem. Phys., J. Magn. Res.
- Project Reviewer: Deutsche Forschungsgemeinschaft

Rustem Valiullin
- Editorial Board Online Journal "Diffusion Fundamentals", Editorial Board "Dataset Papers in Physical Chemistry"
- Referee: J. Phys. Chem., J. Am. Chem. Soc., Adsorption, Micropor. Mesopor. Mat., Phys. Rev. B, Phys. Rev. E, Phys. Rev. Lett., Langmuir, Soft Matter, Chem. Soc. Rev.

Christian Chmelik
- Membership in the Scientific Committee of the conference "Diffusion Fundamentals VI" (Dresden, 2015) and in the Structural Committee "Spreading in Nature, Techology and Society" of the Saxonian Academy of Sciences in Leipzig
- Editorial Board Online Journal "Diffusion Fundamentals"
- Co-Guest-Editor of the Open-Access-Journal "Materials"
- Referee: J. Phys. Chem., Micropor. Mesopor. Mat., Ind. Eng. Chem. Res., J. Am. Chem. Soc.

4.10 External Cooperations

Academic

- Delft University, Inst.Chem. Tech., Delft, The Netherlands
  Prof. Kapteijn
- Institut de Recherches sur la Catalyse, CNRS, Villeurbanne, France
  Dr. Jobic
- Max Planck Institut für Kohlenforschung, Mülheim
  Dr. Schmidt, Prof. Schüth
- Ruhr-Universität Bochum, Lehrstuhl für Anorganische Chemie 2, Organometallics and Materials Chemistry
  PD Dr. Schmid
- Universität Hannover, Dept. Phys. Chem., Hannover
  Prof. Caro, Prof. Wiebcke

- Universität Leipzig, Institut für Technische Chemie, Leipzig
  Prof. Einicke, Prof. Gläser, Prof. Enke
- Universität Leipzig, Institut für Anorganische Chemie, Leipzig
  Prof. Krautscheid
- Universität Leipzig, Institut für Medizinische Physik und Biophysik, Leipzig
  Prof. Huster
- TU Dresden, Inst. Biophysik, Dresden
  Prof. Brunner
- Universität Stuttgart, Institut für Technische Chemie, Stuttgart
  Prof. Klemm, Prof. Hunger
- University Athens, Dept Chem. Engn., Athens, Greece
  Prof. Theodorou, Prof. Papadopoulos
- University of Amterdam, Faculty of Science, The Netherlands
  Prof. Krishna
- University of Maine, Dept. Chem. Eng., USA
  Prof. Ruthven
- Victoria University of Wellington, MacDiarmid Institute for Advanced Materials and Nanotechnology, School of Chemical and Physical Sciences, New Zealand
  Dr. Galvosas
- LMU München, Dept. Chemistry and Biochemistry
  Prof. Bräuchle, Dr. C. Jung
- University of Massachusetts, Dept. of Chemical Engineering, Amherst, USA
  Prof. P.A. Monson
- Northwestern University, Dept. of Chem. Eng., Evanston, USA
  Prof. Snurr
- University of Florida, Dept. of Chem. Eng., Gainesville (FL), USA
  Prof. Vasenkov
- University College London, UK
  Prof. Coppens
- Otto-von-Guericke-Universität Magdeburg, Institut für Verfahrenstechnik, Magdeburg
  Prof. Seidel-Morgenstern

Industry

- BASF SE, Ludwigshafen, Germany
  Dr. U. Müller, Dr. Andrei-Nicolae Parvulescu
- Baker Hughes INTEQ GmbH, Celle, Germany
  Dr. Th. Kruspe, Dr. H. Thern
- Baker Hughes Inc., Houston, USA
  Dr. A. G. Mezzatesta, Dr. B. Li

- Clariant, Berlin, Germany
  Dr. Tissler, Dr. Tufar, Dr. Lutz, Dr. Rakoczy
- Sortec AG, Halle, Germany
  Dr. R. Herrmann
- Fraunhofer Institut für solare Energiesysteme (ISE), Freiburg, Germany
  Dr. S. Henninger, G. Füldner
- SINTEF, Oslo, Norway
  Prof. Stöcker

4.11 Publications

Journals

A. Shakhov, J. Kärger, R. Valiullin: *Diffusion properties of liquid crystal-based microemulsions*, Colloid Polym Sci **292**, 1961-1969 (2014).

J. Kärger: *In-depth study of surface resistances in nanoporous materials by microscopic diffusion measurement*, Microporous Mesoporous Materials **189**, 126-135 (2014).

D. Schneider, R. Valiullin, P. A. Monson: *Filling Dynamics of Closed End Nanocapillaries*, Langmuir **30**, 1290-1294 (2014).

D. Mehlhorn, R. Valiullin, J. Kärger, K. Schumann, A. Brandt, B. Unger: *Transport enhancement in binderless zeolite X- and A-type molecular sieves revealed by PFG NMR diffusometry*, Microporous Mesoporous Materials, **188**, 126-132 (2014).

D. Mehlhorn, A. Inayat, W. Schwieger, R. Valiullin, J. Kärger: *Probing Mass Transfer in Mesoporous Faujasite-Type Zeolite Nanosheet Assemblies*, ChemPhysChem **15**, 1681-1686 (2014).

N. Fatkullin, R. Valiullin: *Short-time diffusion behavior of Brownian particles in porous solids*, Magnetic Resonance in Solids **16**, 14202 (2014).

M. R. Bonilla, R. Valiullin, J. Kärger, S. K. Bhatia: Understanding Adsorption and Transport of Light Gases in Hierarchical Materials Using Molecular Simulation and Effective Medium Theory, J Phys Chem C **118**, 14355-14370 (2014).

T. Chokbunpiam, R. Chanajaree, T. Remsungnen, O. Saengsawang, S. Fritzsche, C. Chmelik, J. Caro, W. Janke, S. Hannongbua: *N2 in ZIF-8: Sorbate induced structural changes and self-diffusion*, Microporous Mesoporous Materials **187**, 1-6 (2014).

J. Kärger, T. Binder, C. Chmelik, F. Hibbe, H. Krautscheid, R. Krishna, J. Weitkamp: *Microimaging of transient guest profiles to monitor Mass transfer in nanoporous materials*, Nat. Mater. **13**, 333-343 (2014).

S. Begum, Z. Wang, A. Donnadio, F. Costantino, M. Casciola, R. Valiullin, C. Chmelik, M. Bertmer, J. Kärger, J. Haase, H. Krautscheid: *Water-Mediated Proton Conduction in a Robust Triazolyl Phosphonate Metal-Organic Framework with Hydrophilic Nanochannels*, Chem. Eur. J. **20**, 8862-8866 (2014).

C. Horch, St. Schlayer, F. Stallmach: *High-Pressure Low-Field 1H NMR Relaxometry in Nanoporous Materials*, Journal of Magnetic Resonace **240** 24-33 (2014).

T. Titze, C. Chmelik, J. Kärger, J. M. van Baten, R. Krishna: *Uncommon Synergy between Adsorption and Diffusion of Hexane Isomer Mixtures in MFI Zeolite Induced by Configurational Entropy Effects*, J. Phys. Chem. C **118** 2660-266 (2014).

M. Wehring, P.C.M.M. Magusin, S. Amirjalayer, R. Schmid, F. Stallmach: *Ferrocene in the metal-organic framework MOF-5 studied by homo- and heteronuclear correlation NMR and MD simulation*, Microporous and Mesoporous Materials **186**, 130-136 (2014)

C. Chmelik, A. Mundstock, P.D.C. Dietzel, J. Caro: Idiosyncrasies of Co2(dhtp): *In situ-annealing by methanol*, Microporous and Mesoporous Materials **183**, 117-123 (2014).

Books

none

Talks

F. Stallmach: *Transport and storage of gases, liquids and electrolytes in porous media studied by NMR*, BASF SE, Ludwigshafen F. Stallmach, 07th January 2014.

F. Stallmach: *NMR responses from pore fluids in micro- and mesoporous materials*, NMR school of the 12th Conference on Magnetic Resonance in Porous Materials (MRPM12), Wellington, NZ, 9th - 13th February 2014.

F. Stallmach: *Access molecular mobility in high-tec nanoporous materials by NMR*, 12th Conference on Magnetic Resonance in Porous Materials (MRPM12), Wellington, NZ, 9th - 13th February 2014.

M. Peksa, F. Stallmach, J. Lang: *Investigation of molecular motion of CO_2 in MOF Zn2(bdc)2dabco by* $^{1}3C$ *NMR and MD*, 12th Conference on Magnetic Resonance in Porous Materials (MRPM12), Wellington, NZ, 9th - 13th February 2014.

C. Chmelik: *Adsorption kinetics*, MIC/ZAE Workshop "Charakterisierung nanoporöser Materialien", Würzburg, Germany, April 8 - 9, 2014

J. Kärger: *Ausbreitungsphänomene in Natur, Technik und Gesellschaft*, Plenarvortrag at *Sächsischen Akademie der Wissenschaften zu Leipzig*, June 13, 2014

J. Kärger: *Experimental Evidence of Single-File Constraintsin Nanoporous Host-Guest Systems:Mysteries of Guest Diffusionin the Channel Network of Zeolites*, Majorana Conference about Single-File Dynamics in Biophysics and Related Fields, Erice (Sicily), Italy, July 4 - 9, 2014

J. Kärger: *Guest Diffusion in Nanoporous Solids: Messages for Fundamental Research and Material Science*, Conference DIMAT 2014, Münster, Germany, August 17 - 22, 2014

R. Valiullin: *Diffusion measurements in pore hierarchies*, FEZA Pre-School, Lichtenfels, Germany, 5th-7th September, 2014

F. Stallmach: *Einsatz interaktiver Vorlesungsfragen in der Experimentalphysik*, LiT.Shortcut Aktivierung im Hörsaal, HDS, Universität Leipzig, 17th December, 2014.

Posters

C. Horch, F. Stallmach, J.-H. Chen, B. Li, B. Zhang, H. Thern: *Methane uptake of oil shale plugs at elevated pressures studied by NMR relaxometry*, 12th Conference on Magnetic Resonance in Porous Materials (MRPM12), Wellington, NZ, 9th - 13th February 2014.

T. Splith, F. Stallmach: *NMR study of self-diffusion of methane and carbon dioxide in ZSM-58*, 26. Deutsche Zeolith-Tagung, Paderborn, Germany, February 26 - 28, 2014

T. Munkelt, C. Hamel, C. Küster, C. Chmelik, D. Enke, A. Seidel-Morgenstern: *Modified porous glass beads as stationary phase of a preparative separation process for volatile anaesthetic gases*, 26. Deutsche Zeolith-Tagung, Paderborn, Germany, February 26 - 28, 2014

C. Chmelik, P.D.C. Dietzel, A. Mundstock, J. Caro: *Distinctive features in the adsorption and diffusion characteristics of small paraffins and olefins in MOF Co2(dhtp)*, 26. Deutsche Zeolith-Tagung, Paderborn, Germany, February 26 - 28, 2014

C. Chmelik, P.D.C. Dietzel, A. Mundstock, J. Caro: *Adsorption and diffusion in MOF Co2(dhtp): The interplay of open metal sites and small paraffins and olefins*, 6th FEZA Conference 2014, Leipzig, Germany, September 8 - 11, 2014

A. Mundstock, J. Caro, C. Chmelik, U. Böhme, M. Hartmann, P.D.C. Dietzel: *The idiosyncrasies of M2(dhtp)*, 6th FEZA Conference 2014, Leipzig, Germany, September 8 - 11, 2014

A. Lauerer, P. Zeigermann, J. Lenzner, C. Chmelik, R. Valiullin, J. Kärger: *IR microimaging of mesoporous silicon as a model system for the investigation of hysteresis phenomena*, 6th FEZA Conference 2014, Leipzig, Germany, September 8 - 11, 2014

M. Goepel, H. Kabir, C. Küster, P. Zeigermann, R. Valiullin, C. Chmelik, D. Enke, J. Kärger, R. Gläser: *Mass-transfer investigation on aromatics hydrogenation using platinum supported on controlled pore glass*, 6th FEZA Conference 2014, Leipzig, Germany, September 8 - 11, 2014

T. Titze, C. Chmelik, J. Kärger, J.M. van Baten, R. Krishna: *Desorption with increasing partial pressure: The remarkable uptake patterns of hexane isomer mixtures in zeolite MFI*, 6th FEZA Conference 2014, Leipzig, Germany, September 8 - 11, 2014

J. Cousin Saint Remi, J. Denayer, J. Kärger: *Diffusion of small guest molecules in SAPO-34 crystals: single and multiple crystals measurments*, 6th FEZA Conference 2014, Leipzig, Germany, September 8 - 11, 2014

C. Chmelik, P.D.C. Dietzel, A. Mundstock, J. Caro: *Adsorption and Diffusion of Small Paraffins and Olefins in MOF Co2(dhtp)*, Conference MOF2014, Kobe, Japan, September 28 - October 1, 2014

4.12 Graduations

Habilitation

- none

Doctorate

- Phillip Zeigerman
  Diffusion in Mesoporous Solids under Conditions of Inhomogeneous Fluid Distribution
  January 2014
- Christian Reichenbach
  Poröse Glaskugeln als Modellsysteme für die Gasadsorption: Herstellung, Untersuchung von Sorptionsmechanismen und vergleichende Charakterisierung
  Juni 2014
- Alexander Shakhov
  Structure-dynamics relationships in complex fluids and disordered porous solids assessed using NMR
  September 2014
- Anne-Kristin Pusch
  NMR-Untersuchungen zur Diffusion von Einzelstoffen und Gemischen in modernen porösen Materialien
  October 2014

Master

- Friederike Pielenz
  Isotrope Diffusionswichtung mittels q-MAS PFG NMR in porösen Systemen
  Dezember 2014

Bachelor

- S. Cerniauskas
  Untersuchung der Adsorptions- und Desorptionseigenschaften von Wasser im Zeolith SAPO-34 mittels IR-Mikroskopie
  October 2014

4.13 Guests

- Martin Gelenter
  University of Florida, Gainesville, USA
  May 28 - August 10, 2014
- Dr. J. Cousin
  Vrije Universiteit Brussel, Belgium
  May 01 - June 30, 2014

5

Soft Matter Physics

5.1 Introduction

The Division of Soft Matter Physics strives to perform ground breaking research at the interdisciplinary forefront of Nanosciences, Biophysics as well as Medicine. Our research is aimed to understand the role of cell and molecular biomechanics in tumor progression, which is an important part of the emerging Physics of Cancer. In view of the fact that the group's work aims at the unique combination of Soft Matter Physics, Biophotonics and Medical Physics, it has a redefining impact on medical diagnosis and therapy. This could bring new perspectives to cancer research and trigger efforts to begin to understand the potential physical underpinnings of cancer. In addition to the enormously complex molecular networks required for the functioning of normal cells, tumors have an inherently high molecular diversity due to the stochastic nature of the mutations that cause cancer. Moreover, all cells in a tissue can be motile and are viscous on long time scales, behaving very much like a liquid droplet. Consequentially, tissue boundaries are comparable to fluid boundaries and can be described as a new form of fluid matter, which is a significant topic in the novel research area of active soft matter physics.

Our work focuses on the study of mechanical properties and behavior of polymer networks as well as whole biological cells. It is our primary objective to investigate the underlying physical mechanisms responsible for the observed active and passive behavior of biological soft matter. Special attention is given to the exploration of cancer as well as neuronal growth. Several research projects within our group investigate the function of biological cells from nanometer to macroscopic length scales. The aim is to understand the underlying mechanisms and forces that are required for cell motion and function such as proliferation. Moreover, how and to what extent can cellular mechanisms change during malignant transformation and how these changes can be described from a physical perspective, is the most important research aim.

Josef A. Käs

5.2 Dynamic membrane structure induces temporal pattern formation

J. Lippoldt, C. Händel, U. Dietrich, J.A. Käs

The understanding of temporal pattern formation in biological systems is essential for insights into regulatory processes of cells. Concerning this problem, the present work introduces a model to explain the attachment/detachment cycle of MARCKS and PKC at the cell membrane, which is crucial for signal transduction processes. Our model is novel with regard to its driving mechanism: Structural changes within the membrane fuel an activator-inhibitor based global density oscillation of membrane related proteins. Based on simulated results of our model, phase diagrams were generated to illustrate the interplay of MARCKS and PKC. They predict the oscillatory behavior in the form of the number of peaks, the periodic time, and the damping constant depending on the amounts of MARCKS and PKC, respectively. The investigation of the phase space also revealed an unexpected intermediate state prior to the oscillations for high amounts of MARCKS in the system. The validation of the obtained results was carried out by stability analysis, which also accounts for further enhanced understanding of the studied system. It was shown, that the occurrence of the oscillating behavior is independent of the diffusion and the consumption of the reactants. The diffusion terms in the used reaction-diffusion equations only act as modulating terms and are not required for the oscillation. The hypothesis of our work suggests a new mechanism of temporal pattern formation in biological systems. This mechanism includes a classical activator-inhibitor system, but is based on the modifications of the membrane structure, rather than a reaction-diffusion system.

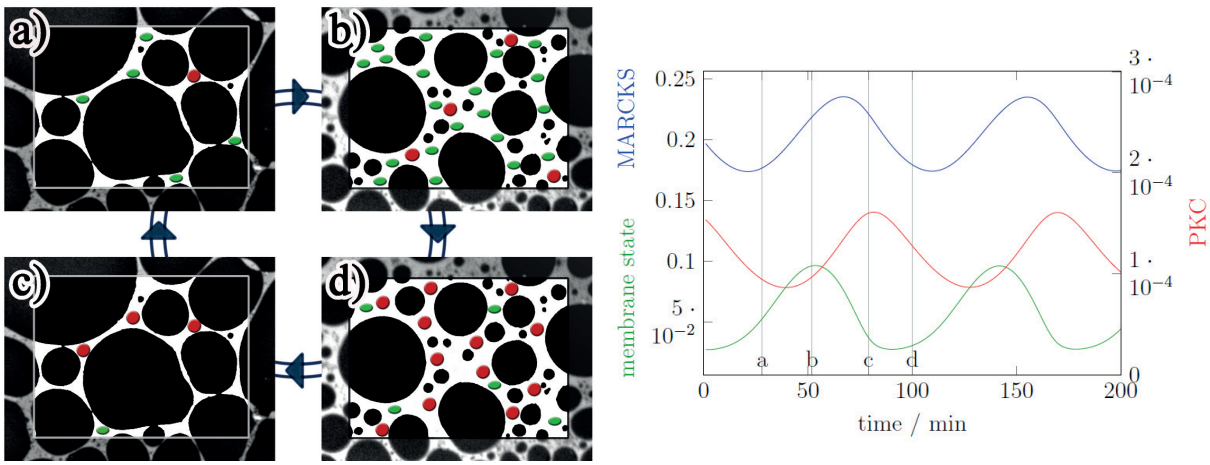

Figure 5.1: The left figure is a sketch, illustrating the membrane structure and protein attachment during different phases (a-d) of the oscillation. The bright parts of the background symbolise the disordered phase of the membrane and the dark parts the ordered phase. The green dots indicate MARCKS molecules while the red dots stand for PKC. The right figure shows the membrane associated variables 'amount of membrane bound MARCKS' in green, 'amount of membrane bound PKC' in red and the 'membrane state' in blue during a simulated oscillation within an open system. The time evolution of the observables is matching the left sketch.

5.3 Causes of Retrograde Flow in Fish Keratocytes

T. Fuhs, M. Gögler, C.A. Brunner, C.W. Wolgemuth, J.A. Käs

Confronting motile cells with obstacles doubling as force sensors we tested the limits of the driving actin-and-myosin-machinery. We could directly measure the force necessary to stop actin polymerization as well as the force present in the retrograde actin flow. Combined with detailed measurements of the retrograde flow velocity and specific manipulation of actin and myosin we found that actin polymerization and myosin contractility are not enough to explain the cells behavior. We show that ever-present depolymerization forces, a direct entropic consequence of actin filament recycling, are sufficient to fill this gap, even under heavy loads.

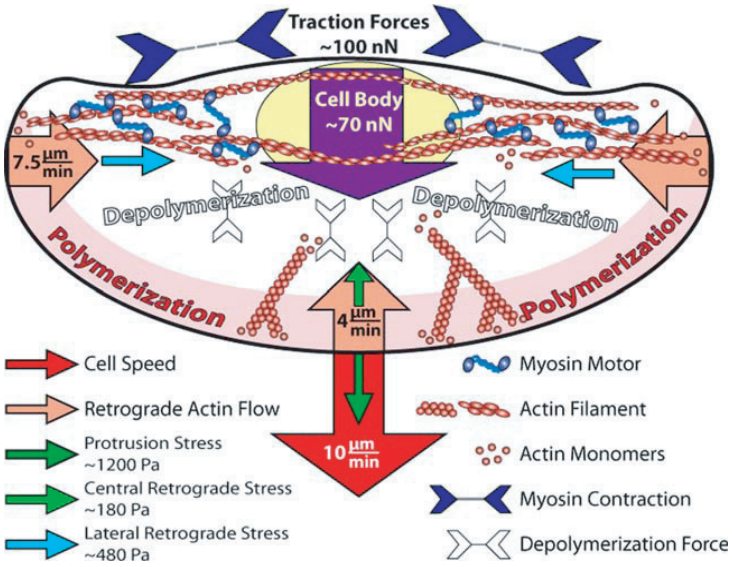

Figure 5.2: Illustration of the measured parameters for a migrating fish keratocyte. The force measurements and the characterization of the internal actin dynamics result in an almost complete physical picture for this cell type. Cell body force (violet), lamellipodium velocity and stall stress (red), retrograde actin flow, and stress in the central lamellum (light blue) and inward actin flow, and stress in the lateral lamellum (dark blue) are illustrated.

5.4 Thermal instability of cell nuclei

E. Warmt, T.R. Kießling, R. Stange, A.W. Fritsch, M. Zink, J.A. Käs

DNA is known to be a mechanically and thermally stable structure. In its double stranded form it is densely packed within the cell nucleus and is thermo-resistant up to 70 °C. In contrast, we found a sudden loss of cell nuclei integrity at relatively moderate temperatures ranging from 45 to 55 °C. In our study, suspended cells held in an optical double beam trap were heated under controlled conditions while monitoring the nuclear shape. At specific critical temperatures, an irreversible sudden shape transition of the nuclei was observed. These temperature induced transitions differ in abundance and intensity for various normal and cancerous epithelial breast cells, which clearly

characterizes different cell types. Our results show that temperatures slightly higher than physiological conditions are able to induce instabilities of nuclear structures, eventually leading to cell death. This is a surprising finding since recent thermorheological cell studies have shown that cells have a lower viscosity and are thus more deformable upon temperature increase. Since the nucleus is tightly coupled to the outer cell shape via the cytoskeleton, the force propagation of nuclear reshaping to the cell membrane was investigated in combination with the application of cytoskeletal drugs.

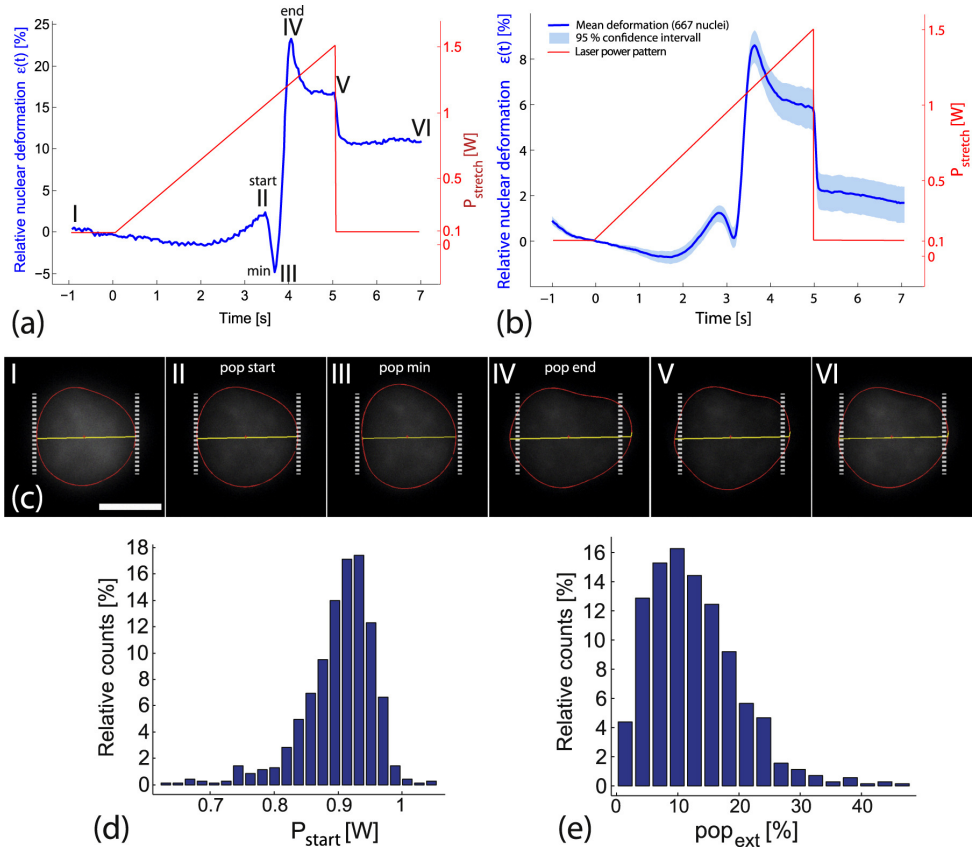

Figure 5.3: (a) Typical deformation curve of an individual MCF-7 cell nucleus (blue) in response to a linearly increasing stretch laser power (red). At low laser powers up to approximately t = 2 s (corresponding T_{eff} = 41 °C), the nuclear width slightly decreases despite increasing optical stress. Subsequently, the nucleus starts to extend, indicating initial nuclear reshaping. During further temperature increase, the nuclear elongation reaches a local maximal value (II), further denoted as the starting point of the nuclear pop event (T_{start} = 47 °C). Subsequently, the nucleus contracts to a minimal width (III) (T_{min} = 49 °C) followed by a drastic increase of nuclear elongation (≈ 30%) to a new local maximal value (IV) (corresponding to an effective temperature of T_{end} = 52 °C), where the nuclear pop ends. **(b)** Deformation data of 667 individual MCF-7 cell nuclei. The blue line shows the mean deformation and the surrounding patch indicates the 95% confidence interval. Note, this deformation curve is qualitatively similar to **(a)** while the extension of the mean elongation (from 'min' to 'end') is only about 9%. **(c)** Fluorescence images of the nucleus shown in **(a)** at characteristic points. The detected nuclear edge is shown in red, elongation in laser direction in yellow, and the initial diameter (t = 0) is indicated by dashed lines. The scale bar represents 10 μm. **(d)** Distribution of the pop start event (II) for 667 measured MCF-7 nuclei. **(e)** Shows the distribution for the pop extension (the nuclear elongation from minimal nuclear size (III) to maximal size (IV)).

5.5 Interfacing cells and iron-palladium - *Theory and experiments on various Coating Strategies*

U. Allenstein A. Weidt, A. Arabi-Hashemi*, F. Szillat*, M. Zink, S.G. Mayr*

*Leibniz-Institut für Oberflächenmodifizierung, Translationszentrum für Regenerative Medizin

Recent decades have seen a huge turn in implantology and biomaterial development towards regenerative medicine. The approach in orthopedic surgery is no longer to just replace damaged tissue by a passive implant that evokes the least possible interference with biological tissue, but rather to provide active stimulation and actuation. Fe-Pd ferromagnetic shape memory alloys are promising smart materials with a unique set of properties. They are superelastic and respond to external magnetic fields with deformations and strains up to 5%. Additionally, they are very ductile and, as we showed earlier, biocompatible [1]. Since interfacing living cells with a biomaterial is always paired with the usage of a suitable coating for enhanced initial adhesion, our further focus lay on investigating the interaction of Fe-Pd and typically used adhesive ligands. As reviewed in [2], we investigated the amino acid sequence RGD, which is a component of fibronectin and the selective binding motif to integrin receptors on the cell surface mediating cellular adhesion. In addition to cell tests, self-designed delamination tests, in which the interaction force of RGD ligands with Fe-Pd films was probed, showed a strong link between substrate and coating. Theoretical *ab initio* considerations supported these results. As counterpart to this specific binding motif, we developed an improvement of Poly-L-lysine as one of the most used non-specific binding agents in cell adhesion [3]. We found, that plasma treatment of the lysine monomer not only enhances cellular adhesion, but also improves robustness and ductility. *Ab initio* free energy calculations enabled us to explain the cleavage of L-lysine monomers inside the argon plasma, while also showing the preferred way to reassemble and crosslink on the surface. In vitro cell tests with NIH/3T3 murine fibroblasts showed an increased focal adhesion density in comparison to conventionally produced poly amino acid coatings. Additionally, we performed scratch tests on the plasma polymerized coating by penetrating the surface with a spherical nanoindenter up to a certain normal force and then pulling it horizontally through the film. This test revealed that a much higher resistivity against rupturing forces can be achieved with this highly cross-linked form of the polymer. These approaches prove that both the RGD and the plasma polymerized L-lysine coating bind strongly to FePd - an important prerequisite for applications in biomedical fields.

[1] U. Allenstein et al.: Acta Biomater. **2013** 9, 5845-53
[2] M. Zink et al.: Mater. Sci. Tech. **2014** 30, 1579-89
[3] U. Allenstein et al.: J. Mater. Chem. B **2014** 2, 7739-46

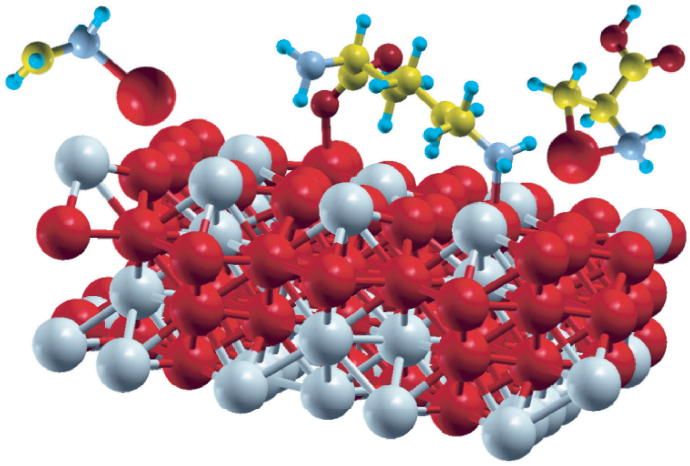

Figure 5.4: Poly-L-lysine molecule on the surface of Fe-Pd from *ab initio* calculations.

5.6 Tailoring the material properties of gelatin hydrogels by high energy electron irradiation

E.I. Wisotzki [*†] M. Hennes[†], C. Schuldt[*], F. Engert[†], W. Knolle[†], U. Decker[†], J.A. Käs[*], M. Zink[*], S.G. Mayr[*†‡]

[*]Universität Leipzig, Fak. f. Physik u. Geowiss., EXP I
[†]Leibniz-Institut für Oberflächenmodifizierung
[‡]Translationszentrum für Regenerative Medizin

Derived from the naturally prevalent protein collagen, gelatin is a highly interesting biomaterial for application in areas of regenerative medicine to bioengineering. Reagent-free treatment methods to tune the properties of hydrogels such as gelatin are highly desirable in order to preserve existing biocompatibility and biodegradability of the material, while tuning properties as required for specific applications. Electron irradiation can be used to crosslink gelatin without the addition of other potentially toxic reagents.

The group of Prof. Mayr, in collaboration with Dr. Zink and Prof Käs investigated the effect of electron irradiation on mechanical properties of gelatin. Gelatin hydrogels were synthesized and irradiated by a 10 MeV linear accelerator in order to induce chemical crosslinks. Electron irradiation was shown to control important material properties including the rheology, swelling and thermal stability.

Quantification of the degree of crosslinking was carried out by rheological measurements and swelling behaviour to observe hydrogel strengthening and elasticity. From this data, rubber elasticity theory and the Flory-Rehner equation for isotropically swollen elastomers were used to estimate the crosslinking densities and mesh size. Fourier transform infrared spectroscopy and scanning electron microscopy were used to analyze changes of the gelatin structure with respect to the irradiation dose. Gel fraction tests confirmed shifting of the sol-gel transition temperature from 37 °C dependent on the dose and concentration.

Overall, systematic approaches to precisely tune these material properties for de-

sired applications were demonstrated with respect to irradiation dose and gelatin concentration.

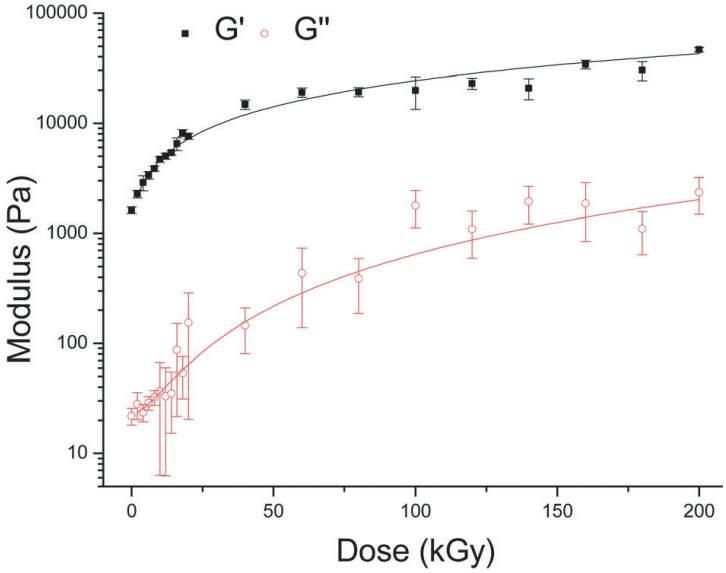

Figure 5.5: Effect of dose on storage (G) and loss moduli (G) of 4 wt% gelatin, with power law fits.

5.7 Cell membrane softening in human cancer cells

C. Händel, B.U.S. Schmidt, J. Schiller*, U. Dietrich, T.R. Kießling, L.-C. Horn†, M. Höckel‡, M. Zink, J.A. Käs

*Institut für Medizinische Physik und Biophysik
†Institut für Pathologie
‡Klinik und Poliklinik für Frauenheilkunde

Determining biomechanical properties of cellular membranes is a key step for understanding cellular functions like cell division or cell motility that are connected to cancer progression and other diseases, such as the Hermansky-Pudlak syndrome and the Niemann-Pick disease [1]. Mechanical properties of cytoskeleton have been intensively studied in cells and model systems. However, the role of membrane rigidity during cancer progression is not well understood and rigidity measurements exist only for vesicles composed of artificial lipids. In this project, we studied thermal shape fluctuations of giant plasma membrane vesicles (GPMVs) produced from primary tissue (figure 5.6, left) as well as cell lines by vesiculation or blebbing [2]. GPMVs contain a larger variety of membrane lipids and peptides than any artificial membrane and have to be regarded as more physiological model system. Based on a self-developed gradient-based edge detection algorithm, the bending rigidity was calculated by a Fourier analysis of thermal vesicle shape fluctuations [3]. The experimental results show that membranes

of malignant cells are significantly softer than those of their normal counterparts (figure 5.6, right). This cell membrane softening could be attributed to a decrease of fluid raft forming lipids in malignant cells. Moreover, this finding indicates that cancer may directly influence the membrane composition and its mechanical properties.

[1] A. Fritsch et al.: Nature Physics **2010** 6, 730-32
[2] A. Baumgart et al.: Proc. Natl. Acad. Sci. **2007** 104, 3165-70
[3] P. Duwe et al.: J. Phys. France **1990** 51, 945-62

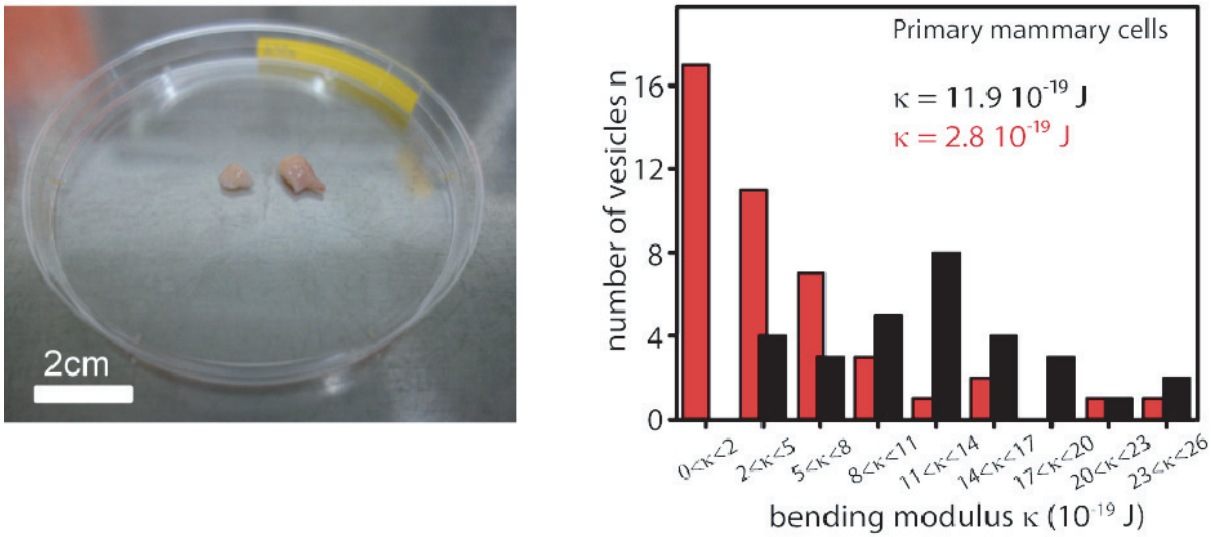

Figure 5.6: (left) Pieces of a human breast tumor obtained from Leipzig university hospital, **(right)** Biomechanical behavior of human carcinoma cell membranes (red) in contrast to membranes obtained from non-malignant cells (black). Distribution of bending elastic moduli κ of GPMVs obtained from primary breast epithelial cells.

5.8 Funding

Leipziger Schule der Naturwissenschaften - Bauen mit Molekülen und Nano-Objekten (BuildMoNa)
Prof. Dr. E. Hey-Hawkins, Prof. Dr. M. Grundmann und Prof. Dr. J. A. Käs
GSC 185/1

InterNeuro
Prof. Dr. J. A. Käs, Mitglied im DFG-Graduiertenkolleg "InterNeuro", Projekte 5 und 7
GRK 1097

Von lokalen Einschränkungen bis zum makroskopischen Transport - From local constraints to macroscopic transport
Prof. Dr. J. Käs, Dr. Stephan Diez et al.
DFG Forschergruppe FOR 877, Teilprojekt 6, KA 1116/ 7-1

Light propagation through the retina: Vertebrate retinal optics
Prof. Dr. J. A. Käs, Prof. Dr. A. Reichenbach et al.
DFG, RE 849/15-1

Untersuchung funktioneller Änderungen von Tumorzellen als Ursache unsymmetrischer Verteilungsfunktionen des Zelldeformationsverhaltens
Prof. Dr. J. A. Käs, Dr. M. Zink
DFG, KA 1116/9-1

Nanostrukturierte Substrate zur organotypischen Langzeitkultivierung adulter Gewebe: Neuartige Verfahren für in vitro Wirkstoffscreening am Beispiel von Augenerkrankungen
Dr. M. Zink, Prof. Dr. J. A. Käs, Prof. Dr. A. Robitzki (BBZ)
SAB,100121467

Invasion und initiale Schritte bei der Metastasierung solider Tumore (Karzinome)
Prof. Dr. J. A. Käs
ESF-Nachwuchsforschergruppe, SAB, 100147954

Werkzeuge und Technologien für die rationale Wirkstoffentwicklung
Prof. Dr. J. A. Käs
ESF-Nachwuchsforschergruppe, SAB, 100148830

Peptid-vermitteltes Tumortargeting: Diagnostik und Therapie
Prof. Dr. J. A. Käs, Prof. Dr. A. Beck-Sickinger, Prof. Dr. E. Hey-Hawkins, Prof. Dr. A. Robitzki
SMWK 70

Erforschung und Entwicklung eines Sortier-Chips zur Analyse seltener Zellen
Prof. Dr. J. A. Käs, Cellastix GmbH (S. Rönicke, R. Stange, B. Hofmann)
SMWK, 4-7531.60/32/2

Dynamisch-mechanische Manipulation and Charakterisierung von Zellen mit Hilfe magnetischer Dehnung
Dr. M. Zink
DFG, Zi-1330/2-1

5.9 Organizational Duties

Prof. J. A. Käs

- Senator der Universität Leipzig
- Direktor des Instituts für Experimentelle Physik I
- Member of the Organizing Committee: 5th Annual Symposium - Physics of Cancer, Leipzig, October 2014
  involved organizers: Prof. H. Herrmann, Prof. P Janmey, Jun.-Prof. Franziska Lautenschläger
- PWM Winterschool Spindlermühle CZ, March 2014
- Journal review: Nature, Science, Cell, Physical Review Letters, Biophysical Journal, Biophysica and Proceedings of the National Academy of Science, Langmuir, Angewandte Chemie, Nature Physics, Journal of Biophotonics, Cytoskeleton, Optics Express, New Journal of Physics

- Grant review: National Science Foundation, Div. of Materials Research; National Science Foundation, Div. of Cellular Organization; National Science Foundation, Div. of Computational Biology; National Science Foundation, Div. of Physics, Special Programs; Deutsche Forschungsgemeinschaft, Alexander von Humboldt Foundation, Deutsche Studienstiftung, Centre National de Recherche
- Fellow, American Physical Society
- Full Member, Saxonian Academy of Sciences

5.10 External Cooperations

Academic

- Syracuse University, USA
  Prof. M. E. Manning
- Syracuse University, USA
  Prof. M. C. Marchetti
- Princeton University, USA
  Prof. Dr. R. Austin
- Deutsche Gesellschaft für Zellbiologie (DGZ)
  Prof. Dr. H. Herrmann
- Max-Delbrück-Zentrum für molekulare Medizin
  Dr. M. Falcke
- Charité Berlin, MR Elastographie
  Prof. Dr. I. Sack
- Ludwig-Maximilians-Universität München, Fakultät für Chemie und Pharmazie
  Prof. Dr. A. Vollmar
- Technische Universität Braunschweig, Zoologisches Institut
  Prof. Dr. K. Rottner
- Universität Leipzig, Paul-Flechsig-Institut für Hirnforschung
  Prof. Dr. A. Reichenbach
- Universität Leipzig, Klinik u. Poliklinik für Frauenheilkunde
  Prof. Dr. M. Höckel
- Universität Leipzig, Institut für Pathologie
  Prof. Dr. L.-C. Horn
- Universität Leipzig, Institut für Anorganische Chemie
  Prof. Dr. E. Hey-Hawkins
- Universität Leipzig, Institut für Biochemie
  Prof. Dr. A. Beck-Sickinger
- Universität Leipzig, Klinik u. Poliklinik f. Mund-, Kiefer- u. Plast. Gesichtschirurgie
  Dr. T. Remmerbach
- Universität Leipzig, Klinik u. Poliklinik f. Dermatologie, Venerologie u. Allergologie
  Prof. Dr. J. Simon

- Universität Leipzig,Translationszentrum für Regenerative Medizin
  Prof. Dr. T. Magin
- Universität Leipzig, Klinik u. Poliklinik f. Dermatologie, Venerologie u. Allergologie
  Prof. Dr. M. Kunz
- Universität Leipzig, Abteilung für Neuroradiologie
  Prof. Dr. K.-T. Hoffmann
- Universität Leipzig, Institut für Biochemie
  Prof. Dr. T. Pompe
- Universität Leipzig, Institut für Experimentelle Physik I
  Prof. Dr. C. Mierke

Industry

- JPK Instruments, Berlin
  Dr. T. Müller
- RS Zelltechnik GmbH, Leipzig
  S. Rönicke
- Nanosurf AG, Liestal, Switzerland

5.11 Publications

Journals

M. Zink, S. G. Mayr: *Ferromagnetic shape memory alloys: synthesis, characterisation and biocompatibility of Fe-Pd for mechanical coupling to cells*, Materials Sciences and Technology **30**, Issue 13a, 1579-1589 (2014)

J. Lippoldt, C. Händel, U. Dietrich, J. A. Käs: *Dynamic membrane structure induces temporal pattern formation*, Biochim. Biophys. Acta (BBA) - Biomembranes, **1838**, Issue 10, 2380-2390 (2014)

E. Warmt, T. R. Kießling, R. Stange, A. W. Fritsch, M. Zink, J. A. Käs: *Thermal instability of cell nuclei*, New Journal of Physics **16**, Issue 7, 073009 (2014)

E. I. Wisotzki, M. Hennes, C. Schuldt, F. Engert, W. Knolle, U. Decker, J. A. Käs, M. Zink, S. G. Mayr: *Tailoring the material properties of gelatin hydrogels by high energy electron irradiation*, J. of Materials Chemistry B **2**, Issue 27, 4297-4309 (2014)

J. Runge, T. E. Reichert, A. Fritsch, J. A. Käs, J. Bertolini, T. W. Remmerbach: *Evaluation of single cell biomechanics as potential marker for oral squamous cell carcinomas: a pilot study*, Oral Diseases **20** Issue 3, e120-e127 (2014)

D. A. Minner, P. Rauch, J. A. Käs, C. A. Naumann: *Polymer-tethered lipid multi-bilayers: a biomembrane-mimicking cell substrate to probe cellular mechano-sensing*, Soft Matter **10**, Issue 8 (2014)

T. Fuhs, M. Gögler, C. A. Brunner, C. W. Wolgemuth, J. A. Käs: *Causes of retrograde flow in fish keratocytes*, Cytoskeleton **71**, Issue 1, 24-35 (2014)

M. Gyger, R. Stange, T. Kießling, A. Fritsch, K. B. Kostelnik, A. G. Beck-Sickinger, M. Zink, J. A. Käs: *Active contractions in single suspended epithelial cells*, European Biophysics Journal **43** Issue 1, 11-23 (2014)

Talks

A. Fritsch, J. A. Käs, K. Seltmann, T. Magin *The cytoskeleton significantly impacts invasive behavior of biological cells*, APS March Meeting, Denver, USA, 2014

T. Fuhs, M. Gögler, C. A: Brunner, C. W Wolgemuth, J. A. Käs *Causes of retrograde flow in fish keratocytes*, APS March Meeting, Denver, USA, 2014

J. A. Käs *Measurements of Active Cell Biomechanics*, 4th AFM EuroForum, Göttingen, March 2014 (invited talk)

T. Golde, C. Schuldt, J. Schnauß, D. Strehle, M. Glaser, J. A. Käs *Fluorescent beads disintegrate actin networks*, Annual conference BuildMona, Leipzig, March 2014

J. Schnauß, M. Glaser, C. Schuldt, T. Golde, J. A. Käs *Actin bundle contractility without molecular motors*, Annual conference BuildMona, Leipzig, March 2014

U. Allenstein, Y. Ma, A. Arabi-Hashemi, F. Szillat, M. Zink, S. G. Mayr *Biocompatibility of $Fe_{70}Pd_{30}$ ferromagnetic shape memory films for cell sensing*, DPG Spring Meeting, April 2014

T. Golde, C. Schuldt, J. Schnauß, D. Strehle, M. Glaser, J. A. Käs *Fluorescent beads disintegrate actin networks*, DPG Spring Meeting, Dresden, April 2014

U. Allenstein, Y. Ma, A. Arabi-Hashemi, F. Szillat, M. Zink, S. G. Mayr *Functionalization of FePd Ferromagnetic Shape Memory Alloys for Biomedical Applications - An Experimental and Theoretical Survey*, MRS Spring Meeting, San Francisco, April 2014

J. A. Käs *Physics of cancer*, SFB 937 - Seminarreihe "Collective behaviour in soft and biological matter", Göttingen, May 2014 (invited talk)

U. Allenstein *Why plasma treatment enhances functional groups for ultra durable biopolymer coatings*, Workshop Ionenstrahlen & Nanostrukturen, Paderborn University, July 2014

J. Schnauß, C. Schuldt, T. Golde, M. Glaser, S. Schmidt, D. Strehle, J. A. Käs *Contractile actin bundles without molecular motors*, Soft-FIRE conference, Cargese, France, August 2014

J. A. Käs *The cytoskeleton significantly impacts invasive behavior of biological cells*, Cell Physics 2014, Universität des Saarlandes, September 2014 (invited talk)

J. A. Käs *Prospective Outlook of mechanics in Oncology*, Strategies workshop "Mechanics in Oncology", Gaithersburg, USA, September 2014 (invited talk)

C. Schuldt, J. Lorenz, J. Schnauß, M. Glaser, J. A. Käs, D. M. Smith *Polymer Physics 2.0: Exploiting programmable nanomaterials to control material properties of soft matter*, DNA Nanotechnology Workshop Mitteldeutschland, Dresden, September 2014

J. A. Käs *Die Rolle der Zellmechanik im Voranschreiten von Krebs*, Physikalisches Kolloquium Bergische Universität Wuppertal, November 2014 (invited talk)

C. Schuldt, J. Lorenz, J. Schnauß, M. Glaser, J. A. Käs, D. M. Smith *Polymer Physics 1.1: Exploiting programmable nanomaterials to control material properties of soft matter*, DNA Nanotech Regional Workshop, Leipzig, December 2014

Posters

S. Pawlizak, A. Fritsch, T. Thalheim, D. Ahrens, J. A. Käs *Cellular adhesion - a key mechanism for compartmentalization and tumor spreading?* 58th Annual Meeting of Biophysical Society, San Francisco, February, 2014

A. Fritsch, K. Seltmann, T. Magin, J. A. Käs *Keratins significantly contribute to cell stiffness and impact invasive behavior*, 58th Annual Meeting of Biophysical Society, San Francisco, February, 2014

J. Lippoldt, M. Knorr, D. Strehle, J. A. Käs *Cell motility at the leading edge: Measuring membrane fluctuations with an optical tweezer setup*, Annual conference BuildMona, Leipzig, March 2014

J. Schnauß, M. Glaser, T. Golde, C. Schuldt, D. Strehle, J. A. Käs *Enthalpic contraction of actin bundles*, Annual conference BuildMona, Leipzig, March 2014

C. Schuldt , T. Golde, J. Schnauß, M. Glaser, J. A. Käs *Entropic Contraction of Actin Networks*, DPG Spring Meeting, Dresden, March/April 2014

J. Schnauß, C. Schuldt, T. Golde, M. Glaser, S. Schmidt, J. A. Käs *Contractile actin bundles without molecular motors*, Soft-FIRE conference, Cargese, France, August 2014

C. Schuldt, J. Lorenz, J. Schnauß, M. Glaser, J. A. Käs, D. M. Smith *Polymer Physics 2.0: Exploiting programmable nanomaterials to control material properties of soft matter*, 5th Annual Symposium - Physics of Cancer, Leipzig, October 2014

J. Schnauß, C. Schuldt, T. Golde, M. Glaser, S. Schmidt, J. A. Käs *Contractile actin bundles without molecular motors*, 5th Annual Symposium - Physics of Cancer, Leipzig, October 2014

B. U. S. Schmidt, S. Braig, K. Ferkaljuk, C. Händel, O. Werz, R. Müller, S. Zahler, A. Koeberle, J. A. Käs, A. M. Vollmar *Modulation of Membrane Rigidity Impacts Cell Migration and Invasion*, 5th Annual Symposium - Physics of Cancer, Leipzig, October 2014

C. Händel, B. U. S. Schmidt, J. Schiller, U. Dietrich, T. R. Kießling, S. Pawlizak, A. W. Fritsch, L.-C. Horn, S. Briest, M. Höckel, M. Zink, J. A. Käs *Plasma Membrane Softening in Human Breast and Cervical Cancer Cells*, 5th Annual Symposium - Physics of Cancer, Leipzig, October 2014

J. Lippoldt, M. Knorr, D. Strehle, J. A. Käs *Cell motility at the leading edge: Measuring membrane fluctuations*, 5th Annual Symposium - Physics of Cancer, Leipzig, October 2014

T. Golde, M. Glaser, C. Schuldt, J. Schnauß, H. Herrmann, J. A. Käs Composite networks of actin and intermediate filaments, BIOTEC Forum "Biomechaniscs across scales - molecules, cells, tissues", Dresden, December 2014

C. Händel, B. U. S. Schmidt, J. Schiller, U. Dietrich, T. R. Kießling, S. Pawlizak, A. W. Fritsch, L.-C. Horn, S. Briest, M. Höckel, M. Zink, J. A. Käs *Plasma Membrane Softening in Human Breast and Cervical Cancer Cells*, BIOTEC Forum "Biomechaniscs across scales - molecules, cells, tissues", Dresden, December 2014

B. U. S. Schmidt, S. Braig, K. Ferkaljuk, C. Händel, O. Werz, R. Müller, S. Zahler, A. Koeberle, J. A. Käs, A. M. Vollmar *Modulation of Membrane Rigidity Impacts Cell Migration and Invasion*, BIOTEC Forum "Biomechaniscs across scales - molecules, cells, tissues", Dresden, December 2014

C. Schuldt, J. Lorenz, J. Schnauß, T. Händler, M. Glaser, J. A. Käs, D. M. Smith *Scaling with persistence length: Expanding the accessible phase space of semi-flexible polymer networks via DNA tubes*, BIOTEC Forum "Biomechaniscs across scales - molecules, cells, tissues", Dresden, December 2014

J. Schnauß, T. Golde, C. Schuldt, S. Schmidt, M. Glaser, D. Strehle, J. A. Käs, C. Heussinger *Actin bundle contractions driven by depletion forces*, BIOTEC Forum "Biomechaniscs across scales - molecules, cells, tissues", Dresden, December 2014

5.12 Graduations

Doctorate

- Franziska Wetzel
  Biomechanical phenotyping of cells in tissue and determination of impact factors
  19.05.2014
- Dan Strehle
  Bundles of semi-flexible cytoskeletal filaments
  19.05.2014
- Melanie Knorr
  Stochastic fluctuations in cell motility - from leading edge to collective motion
  22.09.2014
- Tobias Kießling
  Thermorheology of living cells - the impact of temperature variations on cell mechanics
  22.09.2014
- Anatol Fritsch
  From individual cells to tumor aggregates - biomechanical and thermorheological studies
  20.10.2014

Master

- Lydia Reuter
  Time-dependent elasticity measurements on growth cones
  March 2014
- Iris Wenzel
  Cell deformability and its influence on cell dynamics in monolayers
  September 2014
- Tobias Eggebrecht
  Impact of small temperature variations on living cell migration
  December 2014
- Tobias Thalheim
  Role of keratin during cell-cell adhesion
  December 2014

Bachelor

- Florian Rämisch
  Metastable superparamagnetic bead chains of specific lengths
  June 2014

5.13 Guests

- Valentina Dallacasagrande M. Sc.
  EU-research assistant at the Paul-Flechsig-Institut for brain research and the Dept. Softmatter Physics, Universität Leipzig, March 2010 - 2014

6

Biological Physics

6.1 Introduction

Cellular Biophysics in the Field of Cancer Research Most cancer-related deaths during the malginant cancer progression are caused by the ability of cancer cells to metastasize. The process of metastasis follows a linear propagation of several steps. It starts with the spreading of cancer cells from the primary tumor, which then migrate into the local tumor microenvironment. The cancer cells can transmigrate into blood or lymph vessels (intravasation), get transported through the vessel flow, adhere to the endothelial cell lining, grow and form a secondary tumor directly inside the vessel or the cancer cells possibly transmigrate through the endothelial vessel lining (extravasation) into the extracellular matrix of connective tissue. After this step, the cancer cells migrate further into the targeted tissue (possibly another organ), grow and form a secondary tumor (i.e. the tumor metastasizes). Despite of all current findings based on biochemistry and even the novel approaches based on genomics and proteomics cancer research did not fundamentally change cancer death rates, but still improved clinical diagnosis substantially in the field of cancer research regarding the classification and detailed staging of tumors, numerous marker proteins and mapping of specific human cancer-types. Thus, a main criticism to these methods is that the expression levels of numerous genes and molecules, which are differently regulated during cancer progression, depend on the cancer disease stage. In particular, it is still not fully understood how they regulate cancer progression. A reason may be that these genomic and proteomic based methods do not account for the localization of the molecules in special compartments such as lipid rafts, their activation or assembly state, their life-time, turn-over-, modification- and recycling rate. Thus, we and others propose that the biomechanical properties are crucial for the efficiency and speed of cancer cell invasion and subsequently, for metastases formation. In more detail, classical physical approaches will be adopted to complex soft matter such as cancer cells and novel biophysical methods will be developed in order to adopt them to cancer research. These novel physical approaches have so far changed or will still alter the direction of recent cancer research. Moreover, even the role of the endothelium during the transmigration and invasion of cells is not clear, it has been seen as passive barrier, but this could not explain all novel findings as our finding that this endothelial layer of vessels can enhance the invasiveness of cancer cells. Thus, we will investigate how cancer cells alter the structural, biochemical and mechanical properties of the endothelium to regulate their own invasiveness through

extracellular matrices and hence, through the tissue microenvironment. Moreover, we will investigate how the mechanical properties of cancer cells regulate the functional properties such as cancer cell invasion and transendothelial migration. Finally, our research will shed light on the mechanical properties of cancer cells and the interacting endothelium and will point out the importance of the mechanical properties as a critical determinant for the efficiency of cancer cell invasion and the overall progression of cancer. In conclusion, we suggest that the regulation of the endothelial cells biomechanical properties by cancer cells and the mechanical properties of cancer cells are a critical determinants of cancer cell invasiveness and may affect the future development of new cancer treatments.

Claudia Mierke

6.2 The phenotype of cancer cell invasion controlled by fibril diameter and pore size of 3D collagen networks

J. Sapudom*, S. Rubner*, S. Martin*, T. Kurth, S. Riedel, C.T. Mierke, T. Pompe*

*Biophysical Chemistry Group, Institute of Biochemistry, Faculty of Biosciences, Pharmacy and Psychology

The behavior of cancer cells is strongly influenced by the properties of extracellular microenvironments, including topology, mechanics and composition. As topological and mechanical properties of the extracellular matrix are hard to access and control for in-depth studies of underlying mechanisms in vivo, defined biomimetic in vitro models are needed. Herein we show, how pore size and fibril diameter of collagen I networks distinctively regulate cancer cell morphology and invasion. Three-dimensional collagen I matrices with a tight control of pore size, fibril diameter and stiffness were reconstituted by adjustment of concentration and pH value during matrix reconstitution. At first, a detailed analysis of topology and mechanics of matrices using confocal laser scanning microscopy, image analysis tools and force spectroscopy indicate pore size and not fibril diameter as the major determinant of matrix elasticity. Secondly, by using two different breast cancer cell lines (MDA-MB-231 and MCF-7), we demonstrate collagen fibril diameter and not pore size to primarily regulate cell morphology, cluster formation and invasion. Invasiveness increased and clustering decreased with increasing fibril diameter for both, the highly invasive MDA-MB-231 cells with mesenchymal migratory phenotype and the MCF-7 cells with amoeboid migratory phenotype. As this behavior was independent of overall pore size, matrix elasticity is shown to be not the major determinant of the cell characteristics. Our work emphasizes the complex relationship between structural-mechanical properties of the extracellular matrix and invasive behavior of cancer cells. It suggests a correlation of migratory and invasive phenotype of cancer cells in dependence on topological and mechanical features of the length scale of single fibrils and not on coarse-grained network properties.

6.3 Physical View on the Interactions Between Cancer Cells and the Endothelial Cell Lining During Cancer Cell Transmigration and Invasion

C.T. Mierke

There exist many reviews on the biological and biochemical interactions of cancer cells and endothelial cells during the transmigration and tissue invasion of cancer cells. For the malignant progression of cancer, the ability to metastasize is a prerequisite. In particular, this means that certain cancer cells possess the property to migrate through the endothelial lining into blood or lymph vessels, and are possibly able to transmigrate through the endothelial lining into the connective tissue and follow up their invasion path in the targeted tissue. On the molecular and biochemical level the transmigration and invasion steps are well-defined, but these signal transduction pathways are not yet clear and less understood in regards to the biophysical aspects of these processes. To functionally characterize the malignant transformation of neoplasms and subsequently reveal the underlying pathway(s) and cellular properties, which help cancer cells to facilitate cancer progression, the biomechanical properties of cancer cells and their microenvironment come into focus in the physics-of-cancer driven view on the metastasis process of cancers. Hallmarks for cancer progression have been proposed, but they still lack the inclusion of specific biomechanical properties of cancer cells and interacting surrounding endothelial cells of blood or lymph vessels. As a cancer cell is embedded in a special environment, the mechanical properties of the extracellular matrix also cannot be neglected. Therefore, in this review it is proposed that a novel hallmark of cancer that is still elusive in classical tumor biological reviews should be included, dealing with the aspect of physics in cancer disease such as the natural selection of an aggressive (highly invasive) subtype of cancer cells displaying a certain adhesion or chemokine receptor on their cell surface. Today, the physical aspects can be analyzed by using state-of-the-art biophysical methods. Thus, this review will present current cancer research in a different light from a physical point of view with respect to cancer cell mechanics and the special and unique role of the endothelium on cancer cell invasion. The physical view on cancer disease may lead to novel insights into cancer disease and will help to overcome the classical views on cancer. In addition, in this review it will be discussed how physics of cancer can help to reveal and propose the functional mechanism which cancer cells use to invade connective tissue and transmigrate through the endothelium to finally metastasize. Finally, in this review it will be demonstrated how biophysical measurements can be combined with classical analysis approaches of tumor biology. The insights into physical interactions between cancer cells, the endothelium and the microenvironment may help to answer some old, but still important questions in cancer disease progression.

6.4 The fundamental role of mechanical properties in the progression of cancer disease and inflammation

C.T. Mierke

The role of mechanical properties in cancer disease and inflammation is still underinvestigated and even ignored in many oncological and immunological reviews. In particular, eight classical hallmarks of cancer have been proposed, but they still ignore the mechanics behind the processes that facilitate cancer progression. To define the malignant transformation of neoplasms and finally reveal the functional pathway that enables cancer cells to promote cancer progression, these classical hallmarks of cancer require the inclusion of specific mechanical properties of cancer cells and their microenvironment such as the extracellular matrix as well as embedded cells such as fibroblasts, macrophages or endothelial cells. Thus, this review will present current cancer research from a biophysical point of view and will therefore focus on novel physical aspects and biophysical methods to investigate the aggressiveness of cancer cells and the process of inflammation. As cancer or immune cells are embedded in a certain microenvironment such as the extracellular matrix, the mechanical properties of this microenvironment cannot be neglected, and alterations of the microenvironment may have an impact on the mechanical properties of the cancer or immune cells. Here, it is highlighted how biophysical approaches, both experimental and theoretical, have an impact on the classical hallmarks of cancer and inflammation. It is even pointed out how these biophysical approaches contribute to the understanding of the regulation of cancer disease and inflammatory responses after tissue injury through physical microenvironmental property sensing mechanisms. The recognized physical signals are transduced into biochemical signaling events that guide cellular responses, such as malignant tumor progression, after the transition of cancer cells from an epithelial to a mesenchymal phenotype or an inflammatory response due to tissue injury. Moreover, cell adaptation to mechanical alterations, in particular the understanding of mechano-coupling and mechano-regulating functions in cell invasion, appears as an important step in cancer progression and inflammatory response to injuries.

This may lead to novel insights into cancer disease and inflammatory diseases and will overcome classical views on cancer and inflammation. In addition, this review will discuss how the physics of cancer and inflammation can help to reveal whether cancer cells will invade connective tissue and metastasize or how leukocytes extravasate and migrate through the tissue.

In this review, the physical concepts of cancer progression, including the tissue basement membrane a cancer cell is crossing, its invasion and transendothelial migration as well as the basic physical concepts of inflammatory processes and the cellular responses to the mechanical stress of the microenvironment such as external forces and matrix stiffness, are presented and discussed. In conclusion, this review will finally show how physical measurements can improve classical approaches that investigate cancer and inflammatory diseases, and how these physical insights can be integrated into classical tumor biological approaches.

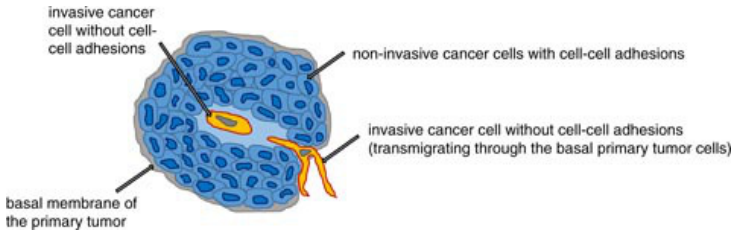

Figure 6.1: The initial step for the selection of an invasive cancer cell subtype. An invasive cancer cell loses its cell-cell adhesion and migrates through the primary tumor and the basement membrane into the connective tissue microenvironment

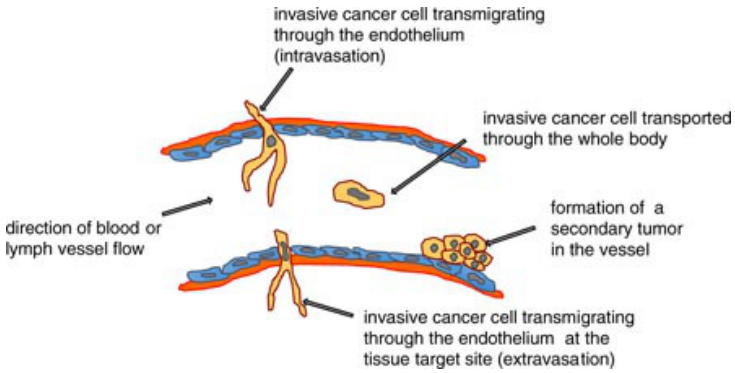

Figure 6.2: The transendothelial migration step of cancer cells during metastasis. The invasive and aggressive cancer cells transmigrate intercellularly through the basement membrane and the endothelial cell lining in blood or lymph vessels. The cancer cell is then transported by the vessel flow to targeted sites for secondary tumor formation. These sites can be the endothelial cell lining of blood or lymph vessels, or the invasive cancer cells can transmigrate through the endothelium and the basement membrane in order to invade the connective tissue

6.5 Funding

Functional Role of Endothelial Cells during transendothelial Migration and Invasion of Cancer Cells
Prof. C. T. Mierke
German Cancer Foundation (Deutsche Krebshilfe)

Invasion und initiale Schritte bei der Metastasierung solider Tumore (Karzinome) "Eine biochemische und biophysikalische Untersuchung der Tumorzellen bei dem epithelialen-mesenchymalen Übergangsprozess und der Tumor-Mikroumgebung zur Ermittlung neuer therapeutischer Ziele"
Prof. C. T. Mierke
ESF-SAB Research Group

6.6 Organizational Duties

C. T. Mierke

- Referee: Cancer Research, Journal of Cell Science, Advanced Biomaterials,Acta Biomaterials, British Journal of Cancer, Journal of Pharmacy and Pharmacology, Molecular Vision, International Journal of Nanomedicine, Plos One, Eur. J. Biophysics
- Special Issue Guest Editor for Physical Biology

6.7 External Cooperations

Academic

- Imperial College London, Department of Materials, London,UK
  Prof. Dr.-Ing. habil. Aldo R. Boccaccini
- Netherlands Cancer Institute Amsterdam, Netherlands
  Dr. Arnoud Sonnenberg
- University of Regensburg, Institute for Molecular and Cellular Anatomy, Regensburg, Germany
  Prof. Dr. Ralph Witzgall
- Philipps-University Marburg, Department of Neurosurgery, Germany
  Prof. Dr. J. W. Bartsch
- Department of Paediatric Kidney, Hannover medical School, Germany
  Prof. Dr. Hermann Haller , Dr. rer. nat. Wolfgang Ziegler
- University of Bonn, Institute of Genetics Actin Dynamics and Motility Unit, Germany
  Prof. Dr. Klemens Rottner
- University of Leipzig, Translational Center for Regenerative Medicine, Germany
  Prof. Dr. Thomas Magin
- University of Leipzig, Center for Biotechnology and Biomedicine (BBZ), Germany
  Prof. Dr. A. Robitzki

6.8 Publications

Journals

C. T. Mierke: *The fundamental role of mechanical properties in the progression of cancer disease and inflammation*, Reports on Progress in Physics **77**, 076602 (2014)

C. T. Mierke: *Physical View on the Interactions Between Cancer Cells and the Endothelial Cell Lining During Cancer Cell Transmigration and Invasion*, Biophysical Reviews and Letters DOI: 10.1142/S1793048015300017 (2014)

6.9 Graduations

Master

- Yadav Bashyal
  Effect of ADAM8 on the motility of cancer cells and other mechanical properties
  August 2014

Bachelor

- Alexander Hayn
  The role of $\alpha 2\beta 1$ integrins in cell motility and cell mechanics
  24. July 2014

II

Institute for Experimental Physics II

7

Magnetic Resonance of Complex Quantum Solids

7.1 Introduction

The electronic properties of quantum-solids in which the electrons exhibit strong correlations with each other or with the lattice are particularly rich and will be of special importance in future functional materials. In addition, such solids are challenging for experiment, aswell as theory, as the more than twenty five-year history of high-temperature superconductivity shows: we still do not understand the electronic structure of these systems. One particular aspect of strongly correlated electronic materials is their tendency towards nano-scale electronic phase separation. Even in perfect lattices, electronic nano-structures can form. The investigation of such materials requires the use of methods that can give detailed information. Here, magnetic resonance, on nuclei and electrons, is of particular interest as they not only have atomic scale resolution, but also yield bulk information in contrast to surface techniques. We explore the properties of these materials with tailored new techniques at the frontiers of magnetic resonance. For example, we are the leading laboratory when it comes to NMR at highest pressures and magnetic fields.

Jürgen Haase

7.2 High-Sensitivity Nuclear Magnetic Resonance at Giga-Pascal Pressures: A New Tool for Probing Electronic and Chemical Properties of Condensed Matter under Extreme Conditions

T. Meier, J. Haase

Nuclear Magnetic Resonance (NMR) is one of the most important techniques for the study of condensed matter systems, their chemical structure, and their electronic properties. The application of high pressure enables one to synthesize new materials, but the response of known materials to high pressure is a very useful tool for studying

their electronic structure and developing theories. For example, high-pressure synthesis might be at the origin of life; and understanding the behavior of small molecules under extreme pressure will tell us more about fundamental processes in our universe. It is no wonder that there has always been great interest in having NMR available at high pressures. Unfortunately, the desired pressures are often well into the Giga-Pascal (GPa) range and require special anvil cell devices where only very small, secluded volumes are available. This has restricted the use of NMR almost entirely in the past, and only recently, a new approach to high-sensitivity GPa NMR, which has a resonating micro-coil inside the sample chamber, was put forward. This approach enables us to achieve high sensitivity with experiments that bring the power of NMR to Giga-Pascal pressure condensed matter research. First applications, the detection of a topological electronic transition in ordinary aluminum metal and the closing of the pseudo-gap in high-temperature superconductivity, show the power of such an approach. Meanwhile, the range of achievable pressures was increased tremendously with a new generation of anvil cells (up to 10.1 GPa), that fit standard-bore NMR magnets. This approach might become a new, important tool for the investigation of many condensed matter systems, in chemistry, geochemistry, and in physics, since we can now watch structural changes with the eyes of a very versatile probe.

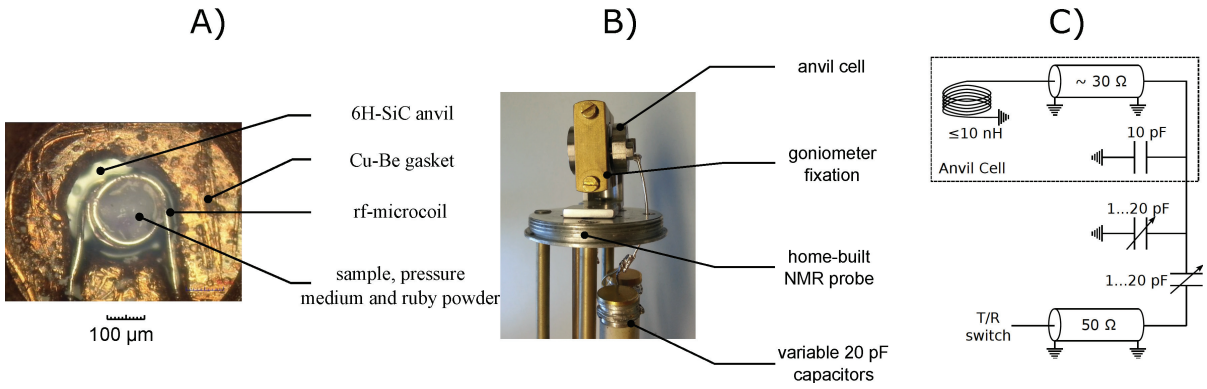

Figure 7.1: (A) Photograph of the high-pressure region with a 4-turn micro-coil filled with a liquid gallium sample, ruby powder and pressure transmitting medium. (B) Mounted LAC-TM1 on a home-built NMR probe. (C) Schematic wiring of the probe connecting the micro-coil in the high-pressure region, see also.

7.3 Moissanite anvil cell design for giga-pascal nuclear magnetic resonance

T. Meier, T. Herzig, J. Haase

A new design of a non-magnetic high-pressure anvil cell for nuclear magnetic resonance (NMR) experiments at Giga-Pascal pressures is presented, which uses a micro-coil inside the pressurized region for high-sensitivity NMR. The comparably small cell has a length of 22 mm and a diameter of 18 mm, so it can be used with most NMR magnets. The performance of the cell is demonstrated with external-force vs. internal-pressure experiments, and the cell is shown to perform well at pressures up to 23.5 GPa using

800 μm 6H-SiC large cone Boehler-type anvils. ^{1}H, ^{23}Na, ^{27}Al, ^{69}Ga, and ^{71}Ga NMR test measurements are presented, which show a resolution of better than 4.5 ppm, and an almost maximum possible signal-to-noise ratio.

7.4 Distribution of electrons and holes in cuprate superconductors as determined from ^{17}O and ^{63}Cu nuclear magnetic resonance

M. Jurkutat, D. Rybicki*, O.P. Sushkov†, G.V.M. Williams‡, A. Erb§, J. Haase

*AGH University of Science and Technology, Faculty of Physics and Applied Computer Science, Department of Solid State Physics, al. A. Mickiewicza 30, 30-059 Krakow, Poland
†School of Physics, University of New South Wales, Sydney, Australia
‡School of Chemical and Physical Sciences, Victoria University of Wellington, PO Box 600, Wellington 6140, New Zealand
§Walther Meissner Institute for Low Temperature Research, Walther-Meissner-Strasse 8, 85748 Garching, Germany

The local distribution of electrons and holes in the CuO_2 plane of the high-temperature superconducting cuprates is determined with nuclear magnetic resonance through the quadrupole splittings of ^{17}O and ^{63}Cu. Based on new data for single crystals of electron-doped $Pr_{2-x}Ce_xCuO_4$ (x=0, 0.05, 0.10, 0.15) as well as $Nd_{2-x}Ce_xCuO_4$ (x=0, 0.13) the changes in hole contents n_d of Cu $3d_{x2-y2}$ and n_p of O $2p_\sigma$ orbitals are determined and these account for the stoichiometrically doped charges, similar to hole-doped $La_{2-x}Sr_xCuO_4$. It emerges that while $n_d + 2n_p=1$ in all parent materials as expected, n_d and n_p vary substantially between different groups of materials. Doping holes increases predominantly n_p, but also n_d. To the contrary, doping electrons predominantly decreases n_d and only slightly n_p. However, n_p for the electron-doped systems is higher than that in hole-doped $La_{1.85}Sr_{0.15}CuO_4$. Cuprates with the highest maximum T_c's appear to have a comparatively low n_d and high n_p. The rather high oxygen hole content of the Pr_2CuO_4 and Nd_2CuO_4 with the low n_d seems to make them ideal candidates for hole doping to obtain a potentially high T_c.

7.5 Nuclear magnetic resonance at up to 10.1 GPa pressure detects an electronic topological transition in aluminum metal

T. Meissner, S.K. Goh*, J. Haase, M. Richter†, K. Koepernik‡, H. Eschrig‡§

*Cavendish Laboratory, University of Cambridge, JJ Thomson Avenue, Cambridge CB3 0HE, UK
†School of Chemical and Physical Sciences, Victoria University of Wellington, PO Box 600, Wellington 6140, New Zealand
‡IFW Dresden, PO Box 270116, D-01171 Dresden, Germany
§Deceased during writing of the paper.

High-sensitivity ^{27}Al nuclear magnetic resonance (NMR) measurements of aluminum metal under hydrostatic pressure of up to 10.1 GPa reveal an unexpected negative curvature in the pressure dependence of the electronic density of states measured through shift and relaxation, which violates free electron behavior. A careful analysis of the Fermiology of aluminum shows that pressure induces an electronic topological transition (Lifshitz transition) that is responsible for the measured change in the density of states. The experiments also reveal a sudden increase in the NMR linewidth above 4.2 GPa from quadrupole interaction, which is not in agreement with the metal's cubic symmetry.

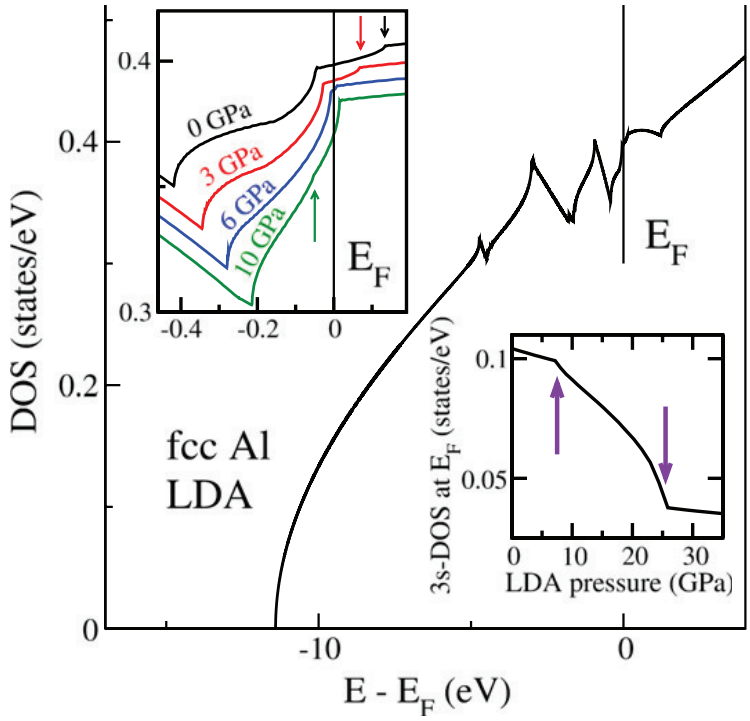

Figure 7.2: Electronic DOS of face centered cubic aluminum in LDA. (Main Panel) Zero-pressure DOS, the Fermi energy E_F is indicated by a vertical line. (Upper inset) Zoom near E_V for different pressures (see text). (Lower inset) Pressure dependence of N_{3s} (E_V), arrows indicate the positions of two ETT.

7.6 Local lattice distortions in oxygen deficient Mn-doped ZnO films, probed by electron paramagnetic resonance

M. Lorenz, R. Böttcher, S. Friedländer, A. Pöppl, D. Spemann, M. Grundmann

The structure and functional properties of metal oxide films for device applications are largely affected by oxygen vacancies. While the macroscopic relationship between functionality and oxygen supply during growth is easy to access, the local influence of changing oxygen content on the incorporated metal atoms has been rarely investigated.

As a model system, we use Mn as a local probe in hetero- and homoepitaxial ZnO thin films for electron paramagnetic resonance (EPR). Mn is expected to be incorporated as Mn^{2+} in the Zn-lattice site of ZnO films grown in a wide range of oxygen partial pressures. The zero field splitting (ZFS) parameter *D* depends on the crystallographic *c/a* ratio of ZnO : Mn lattice constants as it measures the trigonal distortion of oxygen tetrahedra at the Zn^{2+} site with respect to the Mn^{2+} site. The ZFS parameter *D* correlates linearly with displacement of Mn^{2+} ions along the *c*-axis in the MnO_4 tetrahedra and the corresponding bond lengths between the Mn^{2+} ions and the axial oxygen ion.

7.7 Ligand spheres in asymmetric hetero Diels-Alder reactions catalyzed by Cu(II) box complexes: experiment and modeling

V. Umamaheswari*, P. Cias*, A. Pöppl, M. Kaum†, G. Gescheidt*

*Institute of Physical and Theoretical Chemistry, Graz University of Technology, Stremayrgasse 9, 8010 Graz, Austria

†Technische Universität Berlin, Fakultät II, Institut für Chemie, Strasse des 17, Juni 135, 10623 Berlin, Germany

The stereoselective hetero Diels Alder reaction between ethyl glyoxylate and cyclohexadiene catalyzed by [Cu(II)t-Bu-(box)](OTf)$_2$ was investigated. The reaction was performed step-by-step and the geometry of the Cu(II) complexes formed in the course of the catalysis was analysed by EPR spectroscopy, advanced pulsed EPR methods (ENDOR, and HYSCORE) and DFT calculations. Our results show that one triflate counterion is directly coordinated to Cu(II) during the catalytic process (axial position). This leads to penta-coordinated Cu(II) complexes. Solvent molecules are able to alter the geometry of the Cu(II) complexes although their coordination is weak. These findings provide an explanation for the solvent and counterion effects observed in many catalytic reactions.

7.8 Tetrahalidocuprates(II) - structure and EPR spectroscopy. Part 2: tetrachloridocuprates(II)

A. Winter*, K. Thiel*, A. Zabel*, T. Klamroth*, A. Pöppl, A. Kelling*, U. Schilde*, A. Taubert*, P. Strauch*

*University of Potsdam, Institute of Chemistry, Karl-Liebknecht-Str 24-25, 14476 Potsdam, Germany

We present and discuss the results of crystallographic and electron paramagnetic resonance (EPR) spectroscopic analyses of five tetrachloridocuprate(II) complexes to supply a useful tool for the structural characterisation of the $[CuCl_4]^{2?}$ moiety in the liquid state, for example in ionic liquids, or in solution. Bis(benzyltriethylammonium)-,

bis(trimethylphenylammonium)-, bis(ethyltriphenylphosphonium)-, bis(benzyltriphenylphosphonium)-, and bis(tetraphenylarsonium)tetrachloridocuprate(II) were synthesised and characterised by elemental, IR, EPR and X-ray analyses. The results of the crystallographic analyses show distorted tetrahedral coordination geometry of all $[CuCl_4]^{2?}$ anions in the five complexes and prove that all investigated complexes are stabilised by hydrogen bonds of different intensities. Despite the use of sterically demanding ammonium, phosphonium and arsonium cations to obtain the separation of the paramagnetic Cu(II) centres for EPR spectroscopy no hyperfine structure was observed in the EPR spectra but the principal values of the electron Zeeman tensor, $g_{\|}$ and $g_{\perp}$, could be determined. With these EPR data and the crystallographic parameters we were able to carry out a correlation study to anticipate the structural situation of tetrachloridocuprates in different physical states. This correlation is in good agreement with DFT calculations.

7.9 A Continuous-Wave Electron Paramagnetic Resonance Study of Carbon Dioxide Adsorption on the Metal-Organic Frame-Work MIL-53

M. Mendt, B. Jee, D. Himsl*, L. Moschkowitz, T. Ahnfeldt†, N. Stock‡, M. Hartmann*, A. Pöppl

*Erlangen Catalysis Resource Centre, Friedrich Alexander University, Erlangen Nürnberg, Germany

†Faculty for Chemistry and Earth Sciences, University of Bayreuth, Bayreuth, Germany

‡Institute for Inorganic Chemistry, Christian Albrechts University Kiel, Kiel, Germany

Continuous-wave electron paramagnetic resonance spectroscopy is applied to explore the adsorption of carbon dioxide (CO_2) over the metal organic framework (MOF) MIL-53. Therefore, paramagnetic Cr^{3+} ions, which replace a small amount of the bulk Al^{3+} ions in MIL-53(Al/Cr), are used as magnetically active probes. CO_2 was adsorbed on samples of MIL-53(Al/Cr) at equilibrium pressures between 0 and 2.5 bar. The transformation from the large pore phase to the narrow pore phase of MIL-53 was observed by electron paramagnetic resonance spectroscopy at small CO_2 pressures between 0.2 and 0.4 bar, which is in accordance with adsorption results reported in literature. By analyzing the electron paramagnetic resonance signal intensities of the corresponding Cr^{3+} probes, the ratio between the amount of the narrow pore phase and the large pore phase before and after this phase transformation was quantified. A small fraction of the large pore phase remains even after this phase transition. CO_2 adsorption at 77 K indicates the occurrence of the transformation of this MOF from a narrow pore phase to a large pore phase triggered by the adsorbed CO_2. Similar observations were already made using powder X-ray diffraction or infrared spectroscopy. But in contrast to these methods electron paramagnetic resonance spectroscopy on Cr^{3+} seems to be very sensitive not only to large differences between crystallographic conformations like large pores and narrow pores but also to different amounts and configurations of CO_2 molecules trapped in the same structural phase of MIL-53, taking advantage of the high sensitivity of the fine structure interaction of Cr^{3+}.

7.10 ^{55}Mn pulsed ENDOR spectroscopy of Mn^{2+} ions in ZnO thin films and single crystal

R. Böttcher, A. Pöppl, M. Lorenz, S. Friedländer, D. Spemann, M. Grundmann

^{55}Mn pulsed electron nuclear double resonance (ENDOR) experiments were performed at X-band on high spin S = 5/2 Mn^{2+} ions incorporated at zinc lattice sites in heteroepitaxial ZnO thin films. The films have been prepared by pulsed laser deposition and the manganese ions were doped during the growth process. We examine how the c/a lattice axes ratio of the ZnO films influences the ^{55}Mn hyperfine (hf) and nuclear quadrupole (nq) coupling parameters of the Mn^{2+} probe ions. The results are compared with those obtained for Mn^{2+} ions present as impurities in ZnO single crystals and revealed that the ^{55}Mn nq coupling monitors sensitively the structural distortions in the bonding environment of the Mn^{2+} ions. The experiments provided the full axially symmetric ^{55}Mn hf and nq interaction tensors. The latter is found to be very sensitive to small axial distortions of the MnO_4 tetrahedrons. In particular, the ^{55}Mn pulsed ENDOR spectra of the ZnO:Mn thin films are strongly subjected to strain effects in the nq coupling parameter indicating a variation of the local structural parameters for the heteroepitaxial films. In the analysis of the ^{55}Mn pulsed ENDOR spectra the axial and cubic zero field splitting of the Mn^{2+} ions was taken into account and intensity effects in the ENDOR spectra due to the zero field splitting effects were discussed.

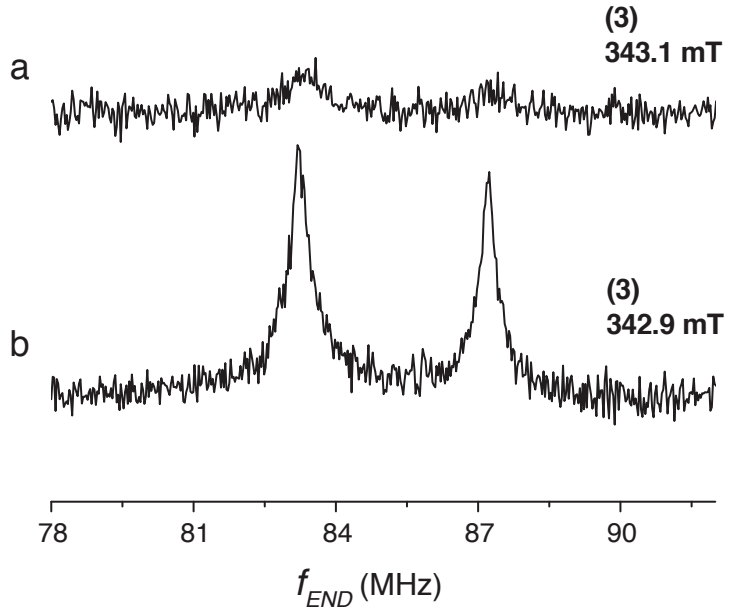

Figure 7.3: Experimental ^{55}Mn pulsed ENDOR spectra of the heteroepitaxial Zno:Mn film samples (a) G4005 and (b) G4008 recorded at the EPR observer transition (3) for $\vec{B} \parallel c$. Only ENDOR signals from the $m_s = -\frac{1}{2}$ manilfold are shown.

7.11 Study of charged defects for substitutionally doped chromium in hexagonal barium titanate from first-principles theory

S.K. Nayak[*], W.A. Adeagbo[*], H.T. Langhammer[†], W. Hergert[*], T. Müller[†], R. Böttcher

[*]Institute of Physics, Martin Luther University Halle-Wittenberg, Halle, Germany
[†]Institute of Chemistry, Martin Luther University Halle-Wittenberg, Halle, Germany

We have studied the defect properties of substitutionally doped chromium in hexagonal barium titanate using the density functional theory together with the generalized gradient approximation restricted to exclusively electronic compensation of the charged defect. The supercell used in our studies is large enough to mimic a chromium concentration of about 2 mol %, which corresponds to an amount typically applied in experiments. Chromium is found to prefer the Ti sites inside the face-sharing oxygen octahedra compared with the other non-equivalent Ti sites within the exclusively corner-sharing octahedra of the hexagonal host lattice. Analysis of formation energy, derived from the total energies of defective supercells in various charge states and systematic post-processing, shows that the charge state of -1 is stable for wide range of Fermi energy within the band gap. The charge state of 0 is only stable for a very low electron concentration, i.e. for highly oxidizing conditions.

7.12 Methane Activation on In-Modified ZSM-5 Zeolite. H/D Hydrogen Exchange of the Alkane with Bronsted Acid Sites

S.S. Arzumanov[*†], I.B. Moroz[†], D. Freude, J. Haase, A.G. Stepanov[*†]

[*]Boreskov Institute of Catalysis, Siberian Branch of the Russian Academy of Sciences, Novosibirsk, Russia
[†]Faculty of Natural Sciences, Department of Physical Chemistry, Novosibirsk State University, Novosibirsk, Russia

In relation to clarifying the pathway of methane activation on In-modified zeolites, a comparative analysis of kinetics of hydrogen (H/D) exchange between methane-d_4 and Brønsted acid sites (BAS) for both the pure acid form zeolite (H-ZSM-5) and In-modified zeolites (In^+/H-ZSM-5 and InO^+/H-ZSM-5) has been performed. Monitoring of the kinetics has been carried out with 1H magic-angle spinning NMR spectroscopy in situ within the temperature range of 453-568 K. While the rate of exchange on In^+/H-ZSM-5 is 1 order of magnitude larger than that on H-ZSM-5, the exchange occurs on InO^+/H-ZSM-5 by 2 orders of magnitude faster than that on H-ZSM-5. Significant increase of the rate and decrease of the activation energy (E_a = 74 ± 6 kJ mol^{-1}) and the temperature threshold (453 K) for the reaction of the exchange on InO^+/H-ZSM-5 compared to the rate, activation energy, and temperature threshold (543 K) for the

reaction on In^+/H-ZSM-5 (E_a = 127 ± 27 kJ mol^{-1}) and H-ZSM-5 (E_a = 118 ± 9 kJ mol^{-1}) have been rationalized in terms of involvement of both InO^+ and BAS in activation of methane molecules on the zeolite. Some transient intermediate complex of methane with the zeolite InO^+ species and BAS has been assumed to be formed within the zeolite pore. This complex is involved either in the reaction of H/D exchange with BAS of the zeolite or evolves further to offer indium methyl species.

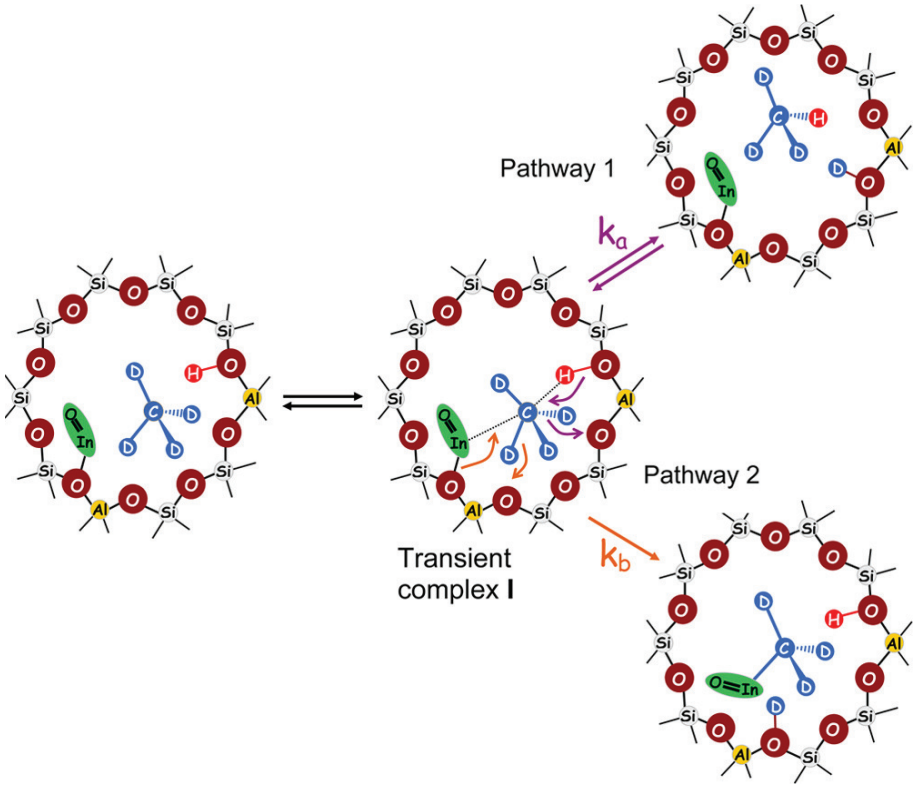

Figure 7.4: [a]H/D exchange of methane on InO^+/H-ZSM-5 zeolite is described bz the rate constant k_a, and concurrent methane conversion to CH_3-In=O species is described bz the rate constant k_b.

7.13 Rotational and Translational Motion of Benzene in ZIF-8 Studied by ^{2}H NMR: Estimation of Microscopic Self-Diffusivity and Its Comparison with Macroscopic Measurements

D.I. Kolokolov[*,†], L. Diestel[‡], J. Caro[‡], D. Freude, A.G. Stepanov[*,†]

[*]Boreskov Institute of Catalysis, Siberian Branch of the Russian Academy of Sciences, Novosibirsk, Russia
[†]Faculty of Natural Sciences, Department of Physical Chemistry, Novosibirsk State University, Novosibirsk, Russia
[‡]Institute of Physical Chemistry and Electrochemistry, Leibniz University Hannover, Hannover, Germany

In relation to unique properties of metal-organic framework (MOF) ZIF-8 to adsorb and separate hydrocarbons with kinetic diameters notably larger than the entrance windows of the porous system of this microporous material, the molecular dynamics of benzene adsorbed on ZIF-8 has been characterized and quantified with ^{2}H nuclear magnetic resonance. We have established that within the ZIF-8 cage the benzene molecule undergoes fast rotations, hovering in the symmetric potential of the spherical cage and relatively slow isotropic reorientations by collisions with the walls. Benzene performs also translational jump diffusion between neighboring cages characterized by an activation barrier $E_D = 38$ kJ mol^{-1} and a pre-exponential factor $\tau_{D0} = 4\times10^{-10}s$. This microscopic measurement of benzene mobility allows us to estimate the self-diffusion coefficient for benzene in ZIF-8 ($D^0_{self} \approx 4\times10^{-16}$ m^2 s^{-1} at $T = 323K$). Macroscopic measurements of diffusivities derived from membrane permeation studies ($3.5e-15ms^{-1}$ at $T = 298K$ for fractional occupancy $\ominus \approx 0.99$) and sorption uptake ($D_{i,MS} \approx 1e-20ms^{-1}$ at 323K) are several orders of magnitude larger or smaller than the microscopic self-diffusion coefficient D^0_{self}, which was derived from relaxation time analysis. This experimental finding is attributed to the limits of macroscopic measurements.

7.14 Funding

Aufklärung des Ladungstransports in funktionalisierten porösen Organsilikaten und Kompostmembranen mit MAS-NMR-Spektroskopie und Diffusometrie
Prof. Dr. Jürgen Haase, Prof. Dr. Michael Wark
DFG, HA 1893/9-1

Deuterium-Festkörper-NMR und 1H MAS PFG NMR-Untersuchungen der Beweglichkeit des Wirtsgerüsts und der Gastmoleküle in nanoporösen Materialien
Prof. Dr. Jürgen Haase
DFG, HA 1893/16-1

Micro-Imaging transienter Konzentrationsprofile von Gastgemischen in Zeolithkristallen
Prof. Dr. Jürgen Haase, Prof. Dr. Jörg Kärger
DFG, HA 1893/15-1

Metalle unter extremen Bedingungen
Prof. Dr. Jürgen Haase
DFG, HA 1893/12-1

Energy efficient MOF-based Mixed Matrix Membranes for CO_2 Capture
Prof. Dr. Jürgen Haase
EU, 608490

MOFs as carrier for nitric oxide delivery in biological systems - microscopic fundamentals of adsoprtion and controlled release studied by infrared and electron and nuclear spin resonance spectroscopy
PD Dr. Marko Bertmer, Prof. Dr. Andreas Pöppl, Prof. Dr. Martin Hartmann, Prof. Dr.

Michael Fröba
DFG, BE 2434/4-2, PO 426/8-2

Charakterisierung der [2+2]-Photodimerisierung von photoaktiven Substanzen auf der Basis von Zimtsäure eingebaut in Polymeren oder in supramolekularen Strukturen mit Festkörper-NMR-Spektroskopie
PD Dr. Marko Bertmer
DFG, BE 2434/2-3

Paramagnetic adsorption sites in microporous crystalline solids studied by electron paramagnetic resonance spectroscopy from single crystals to oriented thin films
Prof. Dr. Andreas Pöppl
DFG, PO 426/11-1

7.15 Organizational Duties

Professor Dr. Jürgen Haase
- Dean of the Faculty
- Vice Director of the Magnetic Resonance Center Leipzig
- Board Member of the Heisenberg Gesellschaft e. V.
- Full Member of the Saxonian Academy of Sciences in Leipzig
- Member of the German Physical Society
- Member of the American Physical Society
- Member of the "ICAM Board of Goveners" of the Institute for Complex Adaptive Matter
- Referee: Physical Review, Science, IOP, German-Israeli Foundation for Scientific Research and Developement

Prof. Dr. Andreas Pöppl
- Referee: Journal ofMagnetic Resonance, Journal ofAmericanChemical Society, Physical Chemistry Chemical Physics, Chemical Physics Letters
- Project Reviewer: German-Israeli Foundation for Scientific Research and Development

PD Dr. Marko Bertmer
- Referee: AngewandteChemie,Chemistry ofMaterials, Journal of PhysicalChemistry, Solid State Nuclear Magnetic Resonance

Prof. Dr. Dieter Michel
- Full Member of the Saxonian Academy of Sciences in Leipzig
- Member of the German Physical Society
- Member of the Society of German Chemists
- German Coordinator of the German-Russian Centre "Applied and Computational Physics (ACOPhys)" at the St. Petersburg State University
- Member at the International Advisory Committee of the International Meeting of Ferroelectricity
- Member at the International Advisory Committee of the European Meeting of Ferroelectricity

- Member at the International Advisory Committee of the Conference "NMR of Condensed Matter St. Petersburg"
- Member of the German-Israeli Foundation for Scientific Research and Developement
- Referee: Physical Review, Journal of Physics: Condensed Matter, Langmuir, Journal of Magnetic Resonance, Phys. Stat. Sol., Materials Chemistry and Physics, German-Israeli Foundation for Scientific Research and Developement

Prof. Dr. Rolf Böttcher

- Referee: Physical Review, Journal of Physics: Condensed Matter, Langmuir, Journal of Magnetic Resonance

7.16 External Cooperations

Academic

- Technical University Munich, Physics Department, Crystal Lab, Garching, Germany
  Prof. Dr. Andreas Erb
- Cavendish Laboratory, Cambridge, UK
  S. K. Goh, P. Alireza
- Washington University, St. Louis, MO, USA
  J. Schilling, M. Conradi
- Victoria University, Physics Department, Wellington, New Zealand
  Dr. Grant V. M. Williams
- Helmholtz-Zentrum Dresden-Rossendorf, Dresden, Germany
  Prof. Dr. J. Wosnitza
- University of Minnesota, School of Physics and Astronomy, USA
  Prof. Dr. M. Greven
- University of Illinois at Urbana-Champaign, Department of Physics, USA
  Prof. Dr. C. P. Slichter
- Laboratoire National des Champs Magnétiques Pulsès, Toulouse, France
  Prof. Dr. G. Rikken
- University of New South Wales, School of Physics, Sydney, Australia
  Prof. Dr. O. Sushkov
- Washington University, Department of Chemistry, St. Louis, MO, USA
  Sophia E. Hayes
- Universität Koblenz-Landau, Abteilung Chemie, Landau, Germany,
  Prof. Dr. Gabriele Schaumann
- Martin-Luther-Universität Halle-Wittenberg, Halle, Germany
  Dr. H. T. Langhammer
- Kazan State University, Tartastan, Russian Federation
  Prof. Dr. E. N. Kalabukhova

- Universität Erlangen-Nürnberg, Erlangen Catalysis Resource Center - ECRC, Erlangen, Germany
  Prof. Dr. Martin Hartmann
- Université du Maine, Laboratoire de Physique de l'Etat Condenseé, Le Mans, France
  Prof. Dr. A. Kassiba
- University of Vilnius, Faculty of Physics, Vilnius, Lithuania
  Prof. Dr. J. Banys
- Argonne National Laboratory, Illinois, USA
  Prof. Dr. P. Littlewood
- Georgetown University Department of Chemistry, Washington, DC, USA
  Prof. Dr. YuYe Tong
- Max Planck Institute of Solid State Research, Stuttgart, Germany
  Prof. Dr. B. Keimer
- University of Illinois at Chicago, USA
  Prof. Dr. D. K. Morr
- IFW-Dresden, Dresden, Germany
  M. Richter, H. Eschrig
- Ruhr-University Bochum, Bochum, Germany
  R. A. Fischer

Industry

- NMR-Service GmbH, Erfurt, Germany
  M. Braun
- Bruker BioSpin GmbH, Rheinstetten, Germany
  F. Engelke

7.17 Publications

Journals

T. Meier, J. Haase
High-Sensitivity Nuclear Magnetic Resonance at Giga-Pascal Pressures: A New Tool for Probing Electronic and Chemical Properties of Condensed Matter under Extreme Conditions
J. Vis. Exp. **92** (2014) e52243

T. Meissner, S.K. Goh, J. Haase, M. Richter, K. Koepernik, H. Eschrig
Nuclear magnetic resonance at up to 10.1 GPa pressure detects an electronic topological transition in aluminum metal
J. Phys.: Condens. Matter **26** (2014) 015501

T. Meier, T. Herzig, J. Haase
Moissanite anvil cell design for giga-pascal nuclear magnetic resonance
Rev. Sci. Instrum. **85** (2014) 043903

M. Jurkutat, D. Rybicki, O.P. Sushkov, G.V.M. Williams, A. Erb, J. Haase
Distribution of electrons and holes in cuprate superconductors as determined from 17O and 63Cu nuclear magnetic resonance
Phys. Rev. B **90** (2014) 140504

S.S. Arzumanov, I.B. Moroz, D. Freude, J. Haase, A.G. Stepanov
Methane Activation on In-Modified ZSM-5 Zeolite. H/D Hydrogen Exchange of the Alkane with Brønsted Acid Sites
J. Phys. Chem. C **118** (2014) 14427-14432

D.I. Kolokolov, L. Diestel, J. Caro, D. Freude, A.G. Stepanov
Rotational and Translational Motion of Benzene in ZIF-8 Studied by 2H NMR: Estimation of Microscopic Self-Diffusivity and Its Comparison with Macroscopic Measurements
J. Phys. Chem. C **118** (2014) 12873-12879

S. Begum, Z. Wang, A. Donnadio, F. Costantino, M. Casciola, R. Valiullin, C. Chmelik, M. Bertmer, J. Kärger, J. Haase, H. Krautscheid
Water-Mediated Proton Conduction in a Robust Triazolyl Phosphonate Metal?Organic Framework with Hydrophilic Nanochannels
Chem. Eur. J. **20** (2014) 8862-8866

M. Lorenz, R.Böttcher, S. Friedländer, A. Pöppl, D. Spemann, M. Grundmann
Local lattice distortions in oxygen deficient Mn-doped ZnO films, probed by electron paramagnetic resonance
J. Mater. Chem. C **2** (2014) 4947-4956

V. Umamaheswari, P. Cias, A. Pöppl, M. Kaupp, G. Gescheidt
Ligand spheres in asymmetric hetero Diels?Alder reactions catalyzed by Cu(II) box complexes: experiment and modeling
Dalton Trans. **43** (2014) 698-705

A. Winter, K. Thiel, A. Zabel, T. Klamroth, A. Pöppl, A. Kelling, U. Schilde, A. Taubert, P. Strauch
Tetrahalidocuprates(II) ? structure and EPR spectroscopy. Part 2: tetrachloridocuprates(II)
New J. Chem. **38** (2014) 1019-1030

M. Mendt, B. Jee, D. Himsl, L. Moschkowitz, T. Ahnfeldt, N. Stock, M. Hartmann, A. Pöppl
A Continuous-Wave Electron Paramagnetic Resonance Study of Carbon Dioxide Adsorption on the Metal-Organic Frame-Work MIL-53
Appl Magn Reson **45** (2014) 269-285

R. Böttcher, A. Pöppl, M. Lorenz, S. Friedländer, D. Spemann, M. Grundmann
55Mn pulsed ENDOR spectroscopy of Mn2+ ions in ZnO thin films and single crystal
J Magn Reson **245** (2014) 79-86

S.K. Nayak, W.A. Adeagbo, H.T. Langhammer, W. Hergert, T. Müller, R. Böttcher
Study of charged defects for substitutionally doped chromium in hexagonal barium titanate from first-principles theory
Phys. Status Solidi RRL (2014) 1-5

S.S. Naumov, W. Knolle, S.P. Naumov, A. Pöppl, I. Janovsky
The Dynamical Behavior of the s-Trioxane Radical Cation?A Low-Temperature EPR and Theoretical Study
Molecules **19** (2014) 17305-17313

V. Umamaheswari, P. Cias, A. Pöppl, G. Gescheidt
Catalytically Active Cu(II)-Pybox Complexes: Insights by EPR Spectroscopy and DFT Computations
Appl Magn Reson **45** (2014) 667-679

V.A. Ivanshin, T.O. Litvinova, N.A. Ivanshin, A. Pöppl, D.A. Sokolov, M.C. Aronson
Evolution of the 4f Electron Localization from YbRh2Si2 to YbRh2Pb Studied by Electron Spin Resonance
Journal of Experimental and Theoretical Physics **118** (2014) 760-764

B. Sarker, D.G. Papageorgiou, R. Silva, T. Zehnder, F. Gul-E-Noor, M. Bertmer, J. Kaschta, K. Chrissafis, R. Detsch, A.R. Boccaccini
Fabrication of alginate?gelatin crosslinked hydrogel microcapsules and evaluation of the microstructure and physico-chemical properties
J. Mater. Chem. B **2** (2014) 1470-1482

E. Halevas, A. Hatzidimitriou, M. Bertmer, A.A. Vangelis, A. Antzara, C. Mateescu, A. Salifoglou
Structure Lattice-Dimensionality and Spectroscopic Property Correlations in Novel Binary and Ternary Materials of Group 13 Elements with ?-Hydroxycarboxylic Benzilic Acid and Phenanthroline
Cryst. Growth Des. 14 (2014) 4041-4059

J. Kucerik, J. Schwarz, A. Jäger, M. Bertmer, G.E. Schaumann
Character of transitions causing the physicochemical aging of a sapric histosol
J Therm Anal Calorim **118** (2014) 1169-1182

F. Bauer, K. Ficht, M. Bertmer, W.-D. Einicke, T. Kuchling, R. Gläser
Hydroisomerization of long-chain paraffins over nano-sized bimetallic Pt?Pd/H-beta catalysts
Catal. Sci. Technol. **4** (2014) 4045-4054

D. Schneider, R. Valiullin, P. A. Monson
Filling Dynamics of Closed End Nanocapillaries
Langmuir **30** (2014) 1290-1294

Talks

J. Haase
The Cuprate Phase Diagram and NMR - Distribution of Electrons and Holes and the Uniform Spin Response
International Workshop on Correlated Oxides
Minneapolis, USA, 30.04. - 05.05.2014

J. Haase
Insight into Solids with Extreme NMR
GDCH Kolloquium
Aachen, Germany, 15.07.2014

A. Pöppl
CW AND PULSED EPR SPECTROSCOPY OF PARAMAGNETIC COMPLEXES IN METAL-ORGANIC FRAMEWOKS (MOF)
9th Meeting of the European Federation of EPR groups
Marseille, France, 07. - 11.09.2014

J. Haase
High-Pressure NMR and Correlated Electron Materials
International Workshop ?Pressure and Strain Effects in Correlated Electron Materials?
Dresden, Germany, 06. - 10.10.2014

A. Pöppl
CW EPR Spectroscopy with Dielectric Resonators - Small Single Crystals and Thin Films
DFG Priority Program SPP 1601 "New frontiers in sensitivity for EPR spectroscopy: from biological cells to nano materials" Annual Meeting
Schwerte, Germany, 07. - 10.10.2014

Posters

T. Meier, J. Haase
Electronic properties of metallic gallium up to 4 GPa - studied with new anvil-cell NMR
DPG-Führjahrstagung 2014
Dresden, Germany, 30.03. - 04.04.2014

D. Savchenko, E. Kalabukhova, A. Pöppl, E. Mokhov
ELECTRON SPIN RELAXATION TIMES OF NITROGEN DONORS IN SI-RICH 6H SIC
9th Meeting of the European Federation of EPR groups
Marseille, France, 07. - 11.09.2014

T. Meier, J. Haase
NMR at GPa pressures: A New Versatile Tool
Workshop "Pressure and Strain Effects in Correlated Electron Systems"

7.18 Graduations

Doctorate

- Anusree V. Kuttatheyil
  Mulinuclear Solid-state NMR Spectroscopy of Metal-Organic Frameworks
  May 2014

Master

- Mantas Simenas
  EPR spectroscopy of Cu(II) monomers and Cu(II) pairs in the $^{3}_{\infty}[Cu(I)_2Cu(II)_2\{H_2O_2\}\{(Metrz\text{-}mba)_2thio\}_2Cl_2]$ *metal-organic framework*
  October 2014

7.19 Guests

- Prof. Dr. Elena V. Charnaya
  St. Petersburg State University, Physics Faculty
  April 2014
- Denis Nefedov
  St. Petersburg State University, Physics Faculty
  March - April 2014, November 2014 - April 2015
- Andrey Uskov
  St. Petersburg State University, Physics Faculty
  March - April 2014
- Benno Meier
  University of Southampton, School of Chemistry
  May 2014
- Hiroshi Yasuoka
  Advanced Science Research Center, Japan Atomic Energy Agency
  November - December 2014

8

Nuclear Solid State Physics

8.1 Introduction

Quantum-sensor and quantum-information technology as well as superconducting systems require "placing" a well defined number of atoms at well defined positions in a crystal, with a tolerance of about one lattice constant. This is a challenging task but new developments in focusing technology allow today for the implantation of ions with low kinetic energies within nanometer resolution. A low kinetic energy is necessary to avoid ion beam straggling. Focusing is however only the first step; the second step is counting the ions to achieve deterministic single-ion implantation. The combination of focusing and counting is actually a real challenge. The goal is to produce a signal of a "flying by" ion without changing its direction and its kinetic energy. The measurement of the impact using secondary electrons is not possible for low-energy ions. Our first idea, based on a thin foil placed in the beam path as a "transparent detector", was to accelerate the ions in order to get a measurable secondary electron signal and then to slow down the ions selectively after the foil (kinetic energy correction). But calculations show that this would lead to a statistical increase of the divergence which would preclude any nanometer-size focusing. The new method that we are currently developing for counting single ions is based on space charge detection. The idea is to "pick up" the space charge produced by an ion while it is flying in close vicinity to a large number of metal structures, in order to detect the passage of the ion without changing its direction. Calculations show that the ions produce a very small high-frequency signal due to the influence of space charge, and new sophisticated electronics should be able to detect such a signal. During the literature research, we became aware that a quite similar method is already in use for mass detection. This also proves that the experimental realisation of our idea is feasible. A project within the Joint Lab with the IOM (in the order of 1.5 Mio Euro) is now starting to set up this already patented new device.

Beside the developments in single ion implantation, we could successfully set up a new optical system for optically-detected magnetic resonance (ODMR), set up a 100 kV accelerator (which allows us to implant all types of ions) and improve the nano-implanter with a new atomic force microscope (AFM). We also obtained promising results for the controlled switching of the charge state of single NV centers and, in cooperation with the ETH Zurich, we could produce single NV centres that are able to detect single proton spins placed at the surface of a diamond sample.

Jan Meijer

8.2 Passive charge state manipulation of NV centres

K. Groot-Berning*, N. Raatz, S. Pezzagna, J. Meijer

*Quantum, Institut für Physik, Universität Mainz

Due to various reasons such as charge transfer from other neighbouring defects, randomly terminated surface, or ionization during high-power laser irradiation, the charge state of NV defects becomes unstable and sporadically switches, e.g. between negative (NV^-) and neutral (NV^0) on small time scale. For this reason the development of the methods of stabilization of Fermi level in the vicinity of NV defects is one of the key areas of research. By now, the surface termination with O/H and the application of electric potential via electrolytic gate electrode have been shown as possible ways to resolve the issue with the instability of the charge state of the NV defects.

A high hole concentration is responsible for the switching of the charge state of shallow NV defects to the neutral NV^0 state. In contrast to H, O termination allows to find shallow NV centers in their negative charged state NV^-. This effect is shown in Fig. 8.1 for an ensemble of shallow NV defects created by low energy N ion implantation (5 keV, fluence between 1×10^{11} and 1×10^{14} cm^{-2}) in a high-purity CVD diamond. Fig. 8.1(d) shows that the NVs for an O-terminated surface at this implantation energy are mostly in the negative charge state NV^-, in contrast to the lower energies between $(0.5-1)$ keV. The fluorescence spectra for H- and O-terminated surface are compared. The surface of as-grown CVD diamond is H-terminated and retains this termination after annealing in vacuum at a temperature of 800 ℃. In order to obtain an O-terminated surface, the diamond is boiled in a $(1:1:1)$ mixture of sulfuric, perchloric and nitric acids for several hours. The fluorescence spectra taken from the area implanted with the least dose (1×10^{11} cm^{-2}) clearly show NV^0 center emission (*orange* curve in Fig. 8.1(b)) before the chemical treatment while it turns out to be clearly NV^- after the acid bath (*violet* curve in Fig. 8.1(b)). Although this switching effect is very pronounced at low implantation doses, it is not observed for high dose implantation (Fig. 8.1(c)). Areas implanted at high fluence were not sensitive to the surface termination and most of the created NV defects were found in the negative charge state irrespective of the surface treatment. This is probably due to the high concentration of the implanted N atoms, which act as donors and over-compensate the surface hole gas.

Note that the local N concentration surrounding each NV centre from the ensemble in the implanted area corresponds to 0.6 ppm (Fig. 8.1(b)) and to 170 ppm (Fig. 8.1(c)), to be compared with the intrinsic concentration of the sample below 5 ppb. Such an effect of the N concentration has also been experimentally shown and simulated in reference. In diamond, unlike in other semiconductors, point defects can be found in different charge states and the Fermi level should be defined locally, depending on the close environment of the defects. As a consequence, the implantation of dopants (like P, B or Li) in the vicinity of NV centres may be another way to passively control the charge of single defects [1]. First experiments on ensemble of NV centres are promising, showing that the co-implantation of P- or B-atoms are able to modify the charge state of NV centres towards NV^- or NV^0, respectively. Beside the charge state consideration,

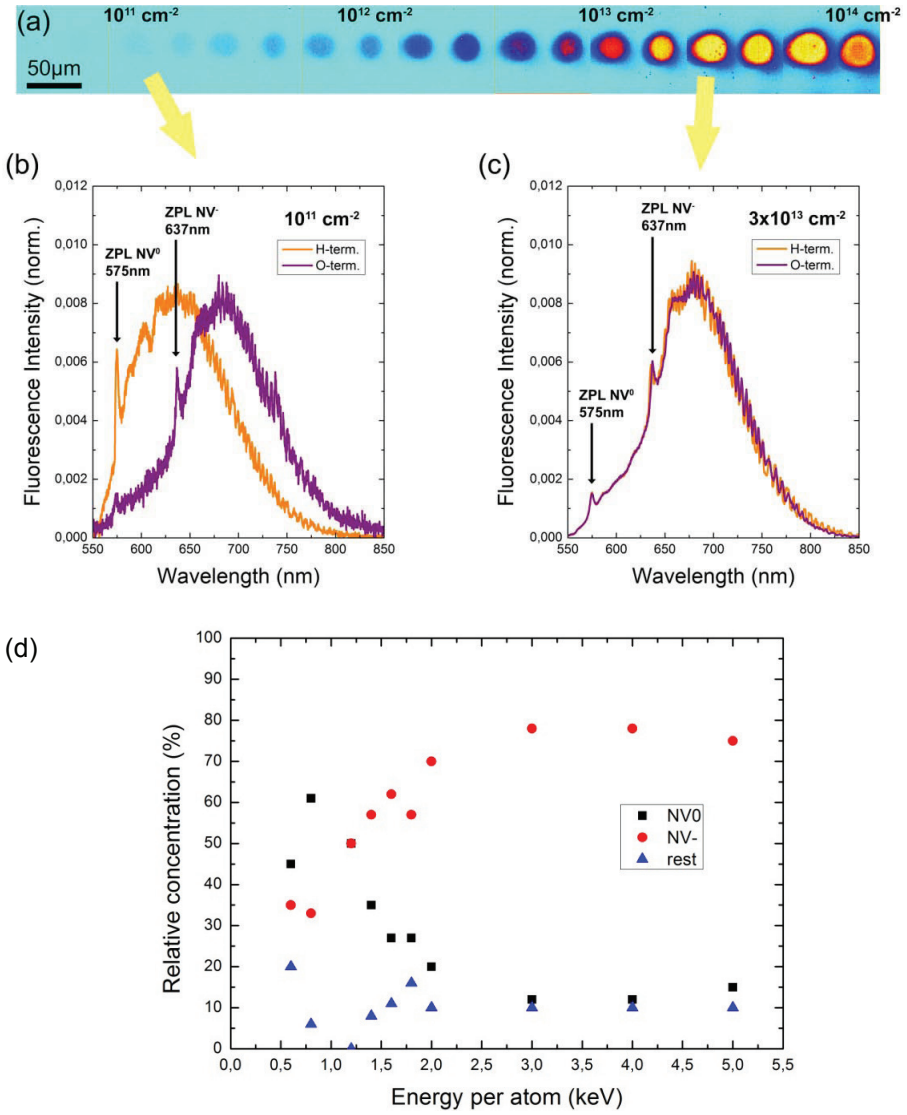

Figure 8.1: Surface-termination-induced charge state control of an ensemble of shallow implanted NV centres. **(a)** Fluorescence image of a diamond implanted with a 25 µm focused beam of 5 keV N^+ ions at different fluences from 6×10^{10} to 1×10^{14} cm^{-2}. **(b)** Fluorescence spectra taken from the region at 1×10^{11} cm^{-2} with either a H (*orange*) or O (*violet*) surface termination. The charge state is changed from NV^0 to NV^- when the surface termination is modified from H to O. **(c)** Fluorescence spectra taken from the region at 3×10^{13} cm^{-2} with either a H (*orange*) or O (*violet*) surface termination. At such a high fluence the surface termination does not influence the charge state anymore. **(d)** Average charge state of NV ensembles as a function of the implantation energy and for an O-terminated surface. Very shallow implanted NV can be found typically in NV^0 state [1].

the surrounding of the NV centres used as qubits or magnetic sensors has to be kept clean enough not to be detrimental to the fluorescence rate or to the coherence time. This has to be further investigated.

[1] K. Groot-Berning et al.: phys. stat. sol. a: Appl. Mater. Sci. **211**, 2268 (2014), doi:10.1002/pssa.201431308

8.3 Temperature treatment of NV centres

J. Rödiger*, N. Raatz, S. Pezzagna, A. Zaitsev†, J. Meijer

*RUBION, Ruhr-Universität Bochum

†College of Staten Island and the graduate college of CUNY, Staten Island, NY, USA

A drawback of ion implantation is the massive creation of point defects. The procedure to overcome this problem is a subsequent annealing step. Whereas for silicon the annealing leads to very good results, for diamond the procedure is much more subtle. The stable phase of diamond at room temperature is not the diamond sp^3 but graphite sp^2 bounds. The problem is to find the temperature and annealing time which are necessary to produce the optimal number of NV centers with large T_2 times.

To investigate the procedure, we implant CN^- molecules with fluences between 10^{12} and 10^{15} ions/cm^2 and a kinetic energy of 100 keV in an optical grade 3×3 mm^2 E6 diamond (Fig. 8.2). We use an optical grade diamond because of the high N content.

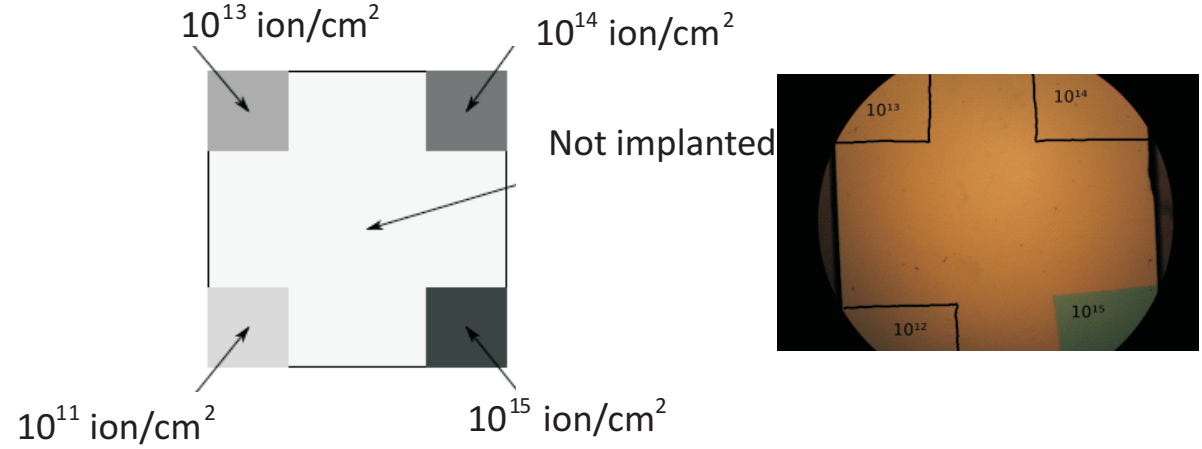

Figure 8.2: Scheme and picture of the implanted diamond sample with different N fluences [unpubl.].

Subsequently we anneal the diamond plate in a home build carbon vacuum furnace at different temperatures for 20 s for each step. The raise time to reach this temperature was 40 K/min. The furnace has a very small heat capacity, thus the cooling rate is very high and not taken into account. After the annealing, we measure the emission spectrum and repeat this procedure 13 times, in a temperature range from (800 – 1600) ℃.

Figure 8.3 shows the results of PL intensity of NV centers and other dominant defects in the area with the fluences of 10^{13} and of 10^{15} ion/cm^2 after the different annealing cycles. Please keep in mind that the PL intensities are not representing the absolute number of defects thus an absolute comparison of defects numbers is not permitted.

This method is able to investigate a general trend. Figure 8.3 shows an increase of NV centers until 1300 ℃ for low fluence implanted diamond. For heavily implanted diamond, we see an increase of NV^- until 1600 ℃, whereas the NV^0 shows a maximum at 1300 ℃. The 3H center representing a single point defect shows a sharp drop at a temperature of about 1000 ℃. Vacancies become mobile at 600 ℃ thus this behavior is not surprising. Additionally, the H3 center related to the N–N–V defect is formed at a temperature of 1300 ℃. These circumstance leads to the assumption that implanted N

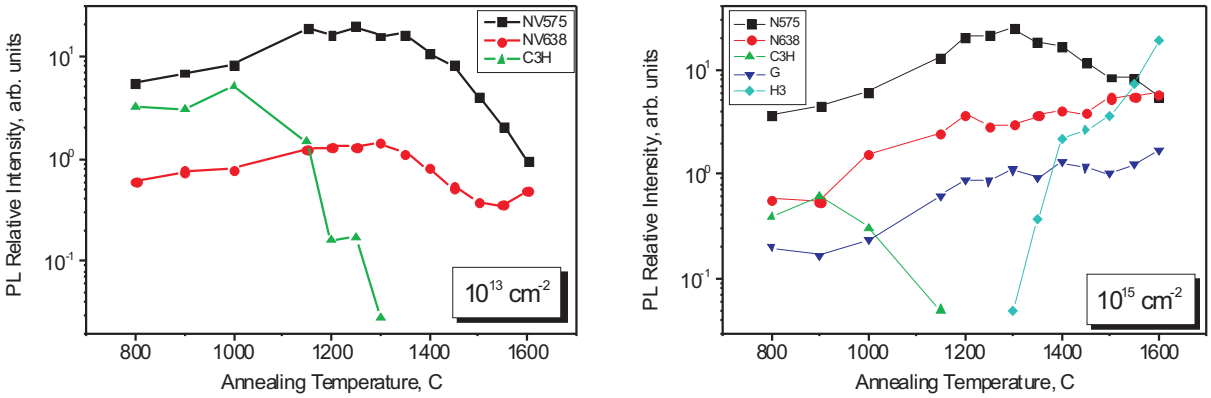

Figure 8.3: Photoluminescence of diamond implanted with 10^{13} and 10^{15} ion/cm^2 after different annealing steps. The zero phonon line structures (NV575 for NV^0 and NV638 for NV^-) as well as the defect band structures (3H, G, H3) are shown after background subtraction. Please pay attention that the intensity of the individual PL structures does not represent the absolute number of the individual defects [unpubl.].

atoms become mobile at these temperatures. We found H3 only for the highly doped area, which means that only implanted N becomes mobile. Several experiments lead to the assumption that dopants need vacancies for the diffusion. These experiments underline this assumption because the intrinsic N do not form any H3 center. Thus for area with low fluence, we do not see any H3 centers at all. The stability of the artificial NV center is found up to 1300 ℃. This is an important result. Experiments performed at very high annealing temperature mainly destroy the artificial NVs thus only the intrinsic NVs will remain.

The results lead to the assumption that the temperature window to produce artificial NVs is in the range between (800 – 1300) ℃. Below 800 ℃ the vacancies are immobile and above 1300 ℃ the N become mobile and form H3 (N–N) defects and destroy the NV centers.

In semiconductor industry, a fast annealing procedure (rapid thermal process (RTP)) is developed in order to avoid a diffusion of the implanted dopants. This could be also an option for diamond treatment. Further unknown is the time dependence of the annealing procedure. Because of the different activation energies of the defects this could be an additional parameter that has to be optimized in the future. Partially, this work is based on the master thesis of J. Rödiger, a publication is in preparation.

8.4 Overgrowth of NV centres

S. Pezzagna, M. Lesik*, N. Raatz, A. Tallaire†, J.-F. Roch*, J. Meijer

*Laboratoire Aimé Cotton, CNRS, Université Paris-Sud
and Ecole Normale Supérieure de Cachan, Orsay, France
†Laboratoire des Sciences des Procédés et des Matériaux, Université Paris 13,
Sorbonne Paris Cité, Villetaneuse, France

The overgrowth technique allows us to investigate the influence of the surface as well as to produce NV centers with high lateral resolution in the depth. The last point is not

as important for sensing but could be essential for quantum devices. The influence of the surface is shown in Fig. 8.4.

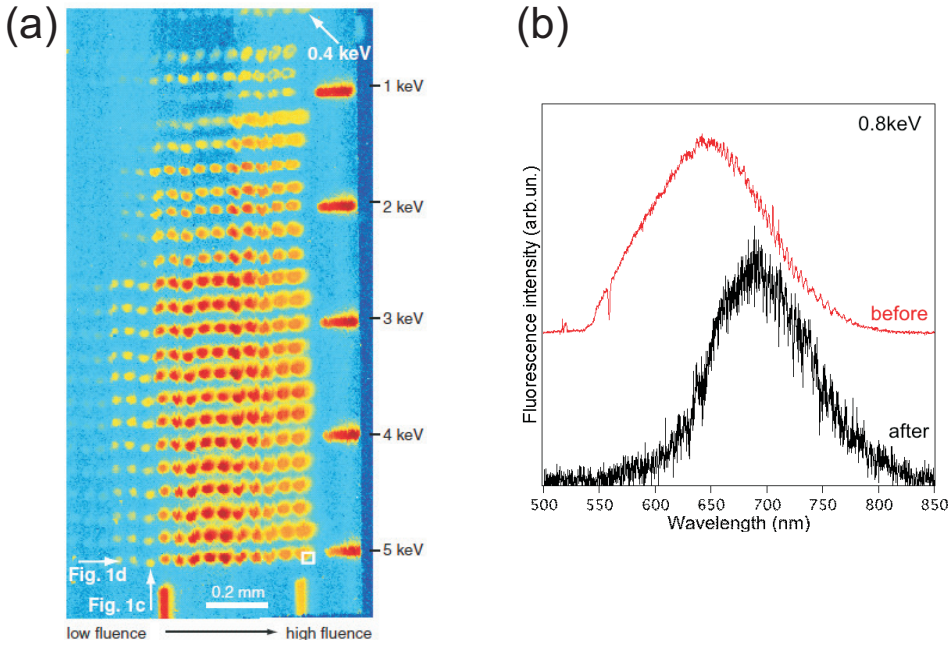

Figure 8.4: Implanted NV spots at different fluences and kinetic energies. **(a)** Evolution of spectral dependencies of typical NVs for different implantation energies. **(b)** NV spectra of the shallowest NVs (0.8 keV) before and after CVD overgrowth [1].

It is obvious that the creation yield decreases for shallow implanted NVs (Fig. 8.4(a)) and that the coupling of the surface phonons dominates more and more the spectra (Fig. 8.4(b)). Using CVD diamond overgrowth, the NV centers are buried in the depth and we expect a reduction of these influences. The effect is shown in Fig. 8.5. This experiment was performed using a polished diamond plate implanted with a nano-pattern as shown in Fig. 8.5. In order to investigate single NV we implanted a structure

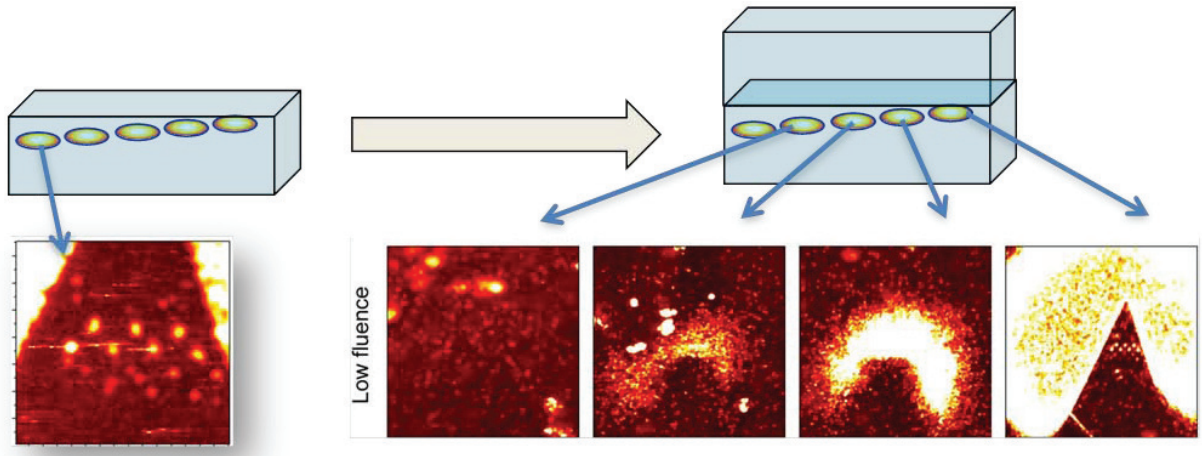

Figure 8.5: Overgrowth experiment: four implanted structures with energies between (1 – 5) keV were overgrown by using a CVD method at Villetaneuse. Surprisingly only the shallow implanted structure survived [unpubl.].

with "high" and "low" fluence. For the low fluence implanted structure we found one or two NV centers per spot. Subsequently the Villetaneuse group overgrew a 5 µm thick diamond layer using a modified CVD method. The main challenge was to start the CVD process without etching the implanted layer. After some trails the Villetaneuse group found suitable parameters. However the results are very surprising. As shown in Fig. 8.5 only the shallow implanted structure with energy of 1 keV (corresponding to 2 nm implantation depth) survived the overgrown process.

For the 1 keV implanted spot, the spectra before regrowth show no zero phonon line (ZPL). After regrowth, the NV^- ZPL appears on the spectra, similar to the case of deep implanted N (Fig. 8.4(b)). These results are complementary to the experiments performed at the Stuttgart group. For shallow implanted ions the main damaged layer is expected to be etched away at the regrowth start and thus there are less defects with spins (than for deeper NVs) to reduce the T2-time. This is also a possible explanation of the vanishing of the NVs in our experiments. The migration of N in diamond is assisted by defects. Deeper implanted NVs remain more defects and the chance that NVs survived is even higher. Additionally it has to be taken into account that the fluence of the 1 keV spot is by two orders of magnitude higher compared to the 5 keV due to the small conversion yield.

[1] M. Loretz et al.: Appl. Phys. Lett. **104**, 033102 (2014), doi:10.1063/1.4862749

8.5 Surface treatment of diamond

N. Raatz, S. Pezzagna, J. Meijer

The optimization of shallow implanted NVs requires a surface treatment before and after implantation. Unfortunately, a large number of properties have to be considered in order to optimize the NV centers. Therefore no ideal recipe with satisfactory results could be found up to now.

Commercially available diamond plates are polished by mechanical or/and chemical process steps. The companies keep details of this procedure secret and the parameters are mainly unknown. However, in all cases this process leads to a large number of defects, in some case we could find holes of several hundreds of nm in diameter.

There are two ways to overcome this problem, either using unpolished plates (labelled with "as grown") or removing the damaged layer. For a large number of application the last option is the only choice because as grown samples have a too high surface roughness. Possible treatments are Ar/Cl plasma or O etching at high temperature. The etching of a diamond surface in a smooth way is not yet solved. The main problem is to find a suitable method that allows describing the quality of the surface. But this is not only an open question for shallow NVs but is an important question to find optimal seeds to grow new diamond or to use a diamond as a detector.

During ion implantation, the charging up of the surface is a real issue and has to be taken into account especially for shallow implantation (with kinetic energies of a few keV only) at high fluence. Charge up voltages up to values of a few keV can be reached easily. It is possible to evaporate a thin conductive layer in order to prevent a charge up during the implantation. Additionally, the surface treatment changes the Fermi level

and could influence the creation of defects and the evolution of defects during the heat treatment. After implantation a heat treatment is performed to create the NV centers, which often leads to a contamination of the surface; thus a surface cleaning by O plasma is recommended (Fig. 8.6).

The heat treatment is described in Sect. 8.3. N starts to diffuse at a temperature of 1300 °C. Due to the proximity of the surface it is expected that N will disappear.

However after the heat treatment it is necessary to clean and terminate the surface. Up to now three different recipes are know: H, O and F. H termination can be induced by a plasma treatment. The "as grown" samples are typically found to be H terminated. O and F termination are achieved by plasma or acid treatment. O and F stabilize the NV in the NV-charge state. The T_2 time can be found between (3 – 70) µs depending on the depth for implanted N. For grown NVs the values are between (40 – 187) µs. The T_2 depends very strongly on the amount of ^{13}C. The isotopic concentration is crucial for deep as well as for shallow implanted NV centers.

An unsolved question is whether the termination could have an impact on the NV creation yield and other defect production mechanisms. This is for example the case in silicon and there are some ongoing investigations in this view.

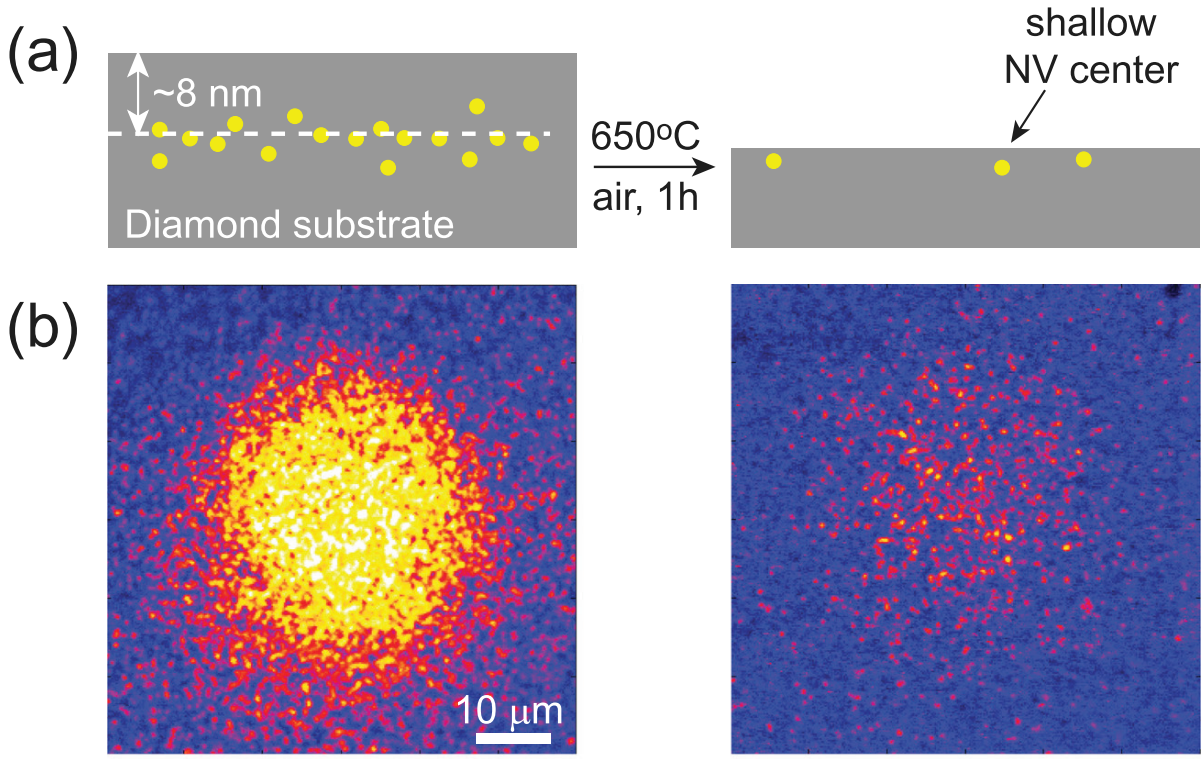

Figure 8.6: (a) NV centers before and after 650 °C O etching in dry air for 1 h. **(b)** shows a spot with 5 keV implanted NV before and after etching. The sample was before implantation treated with Ar/O plasma in order to remove the defect layer [1].

[1] M. Loretz et al.: Appl. Phys. Lett. **104**, 033102 (2014), doi:10.1063/1.4862749

8.6 Single ion implantation with high spatial resolution

N. Raatz, S. Pezzagna, Chr. Eames, J. Meijer

In the last years quantum information processing developed very fast and progressive. One way for the realization of a quantum computer is the doping of semiconductors with certain dopants. Despite the variety of doping possibilities the most prominent candidate for solid state quantum device is the Nitrogen Vacancy (NV) centre in diamond. One way to place single ions in solids is the method we use in the nanoimplanter.

The nanoimplanter is a combination of an atomic force microscope (AFM) with a pierced hollow tip and low energy source (keV range). The drilling of the AFM tip is made by a focussed ion beam. The collimation through this hole results in a very small ion beam about a few nanometers in diameter. An ion gun with a gas source provides a broad range of ion types and an integrated electron multiplier allows the detection of single ions.

This year we installed a new AFM system which works in contact and in non contact mode. Working in non contact mode increases the lifetime of each AFM tip a lot. In the first place it reduces the damage of the very sensitive tip and it allows us to make AFM scans before the implantation at a defined area (Fig. 8.7). In the case

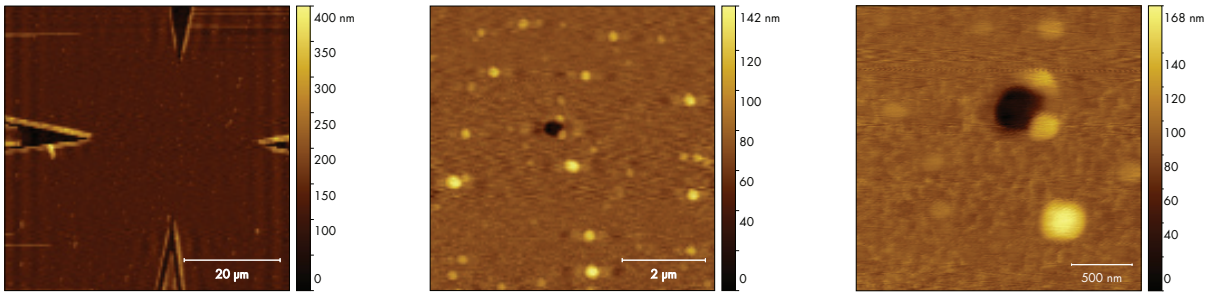

Figure 8.7: In this figure shows three AFM-scans of one structure in a ZnSe sample covered with a perforated metal mask. The four tips in the left scan are used as navigation markers to find the very small hole (about a few 100 nm) in the centre. Those three scans can be seen as a "zoom-in". In the first step we locate the implantation point (in this case the hole in the metal mask) and in the second step we move the tip over it and implant single ions through the pierced AFM tip.

of working in contact there is a change that the hole gets closed, because of dirt on the specimen surface. Furthermore we are able to implant single ions on high pillars without destroying the AFM tip. In the second place the new system allows us to implant ions through the hole in the tip on a PMMA surface (Fig. 8.8) to estimate the hole size directly in the chamber itself. We implanted a row of ions on PMMA and with non contact mode we are able to make an AFM scan of the very soft and sensitive PMMA surface (Fig. 8.8(b)). In the case of scanning in contact mode we would destroy the surface and, by association, the pattern. With the AFM scan in Fig. 8.8(c) one can then estimate the hole size of the pierced AFM tip. The implantation and the scanning on PMMA are also useful to measure the ion beam sculpting (Fig. 8.8(a)), which results in a reduced hole size.

In addition we made some tests to find the best settings for the best resolution of the topography of the test sample. The parameters depend not only on the cantilever itself

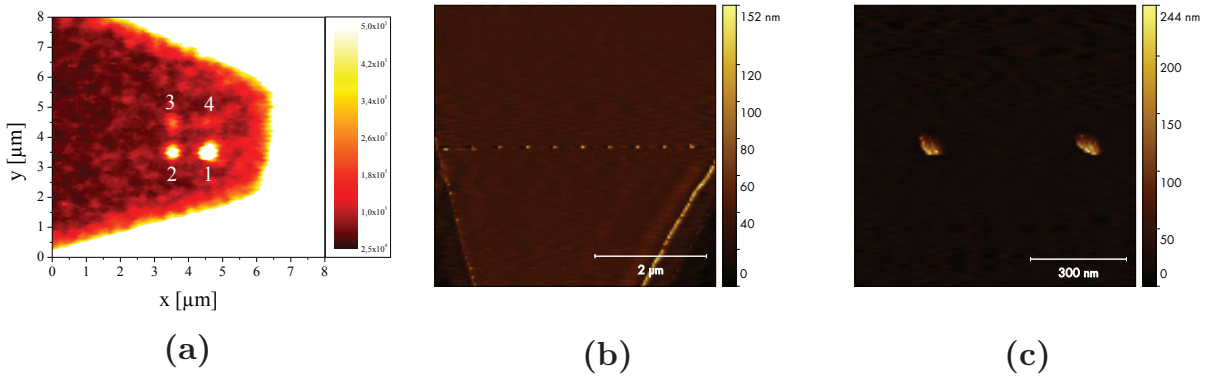

Figure 8.8: (a) Confocal scan of a pattern of NV centers in diamond to show the ion beam sculpting. The reduced brightness is a result of the reduced hole size. During the implantation of spot 4 the hole got closed. **(b)** Non contact AFM scan of an implanted row with 10 points on PMMA. **(c)** Non contact AFM scan of two spots of the pattern in (b). One can estimate the hole size directly in the nanobeam chamber.

but also on the material of the sample. One future point is to investigate the dependency of the parameters with respect to the materials.

8.7 3D engineering of conducting paths in diamond

J. Lehnert, M. Mensing, J. Zabaleta Llorens*, J. Meijer

*Max Planck Institute of Solid State Research, Stuttgart, Germany

While diamond becomes a more attractive host material for nuclear quantum computing and sensor applications, there sprouts a fundamental need for electrical access in the sub micrometer regime. This need can be extended to nuclear magnetic resonance (NMR) applications, where conducting paths in a diamond anvil cell can be used to determine its pressure. The graphitization of diamond by helium ion beam irradiation is a viable tool. To achieve this, the needed ion fluence had be determined. It is known that the defect (vacancy) concentration of 1×10^{22} cm^{-3} is necessary for a complete local graphitization [1]. To calculate the expected damage per ion, a monte-carlo simulation was carried out using `SRIM` [2]. For a range of fluences between $\left(1\times10^{18}-5\times10^{15}\right)$ cm^{-2} (area $1-6$, size 240×60 µm^2) the results are shown in Fig. 8.9(a). It can be observed that the depth and thickness of the conducting paths can be controlled via energy and the fluorescence, respectively. For the experiments used in this work, a ion energy of 1.6 MeV was used. The samples were annealed at 1200 ℃ for 3 h after the irradiation and cleaned by O plasma treatment for 30 min at 0.4 mbar before characterization. The I–V-curves illustrated in Fig. 8.9(b) where measured at a homebuilt point probe station. A significant increase of the conductivity was observed. For a fluence of 1×10^{18} cm^{-2} the resistance was 50 kΩ. Further, a narrow conduction path of length 100 µm was produced with a fluence of 1×10^{18} cm^{-2} (Fig. 8.9(c)). In order to contact it two pads were attached to it with the same fluence. The measured I–V-curve is shown in Fig. 8.9(d). The resistance was determined to be 7.1 kΩ.

[1] P. Olivero et al.: Adv. Mater. **17**, 2427 (2005), doi:10.1002/adma.200500752

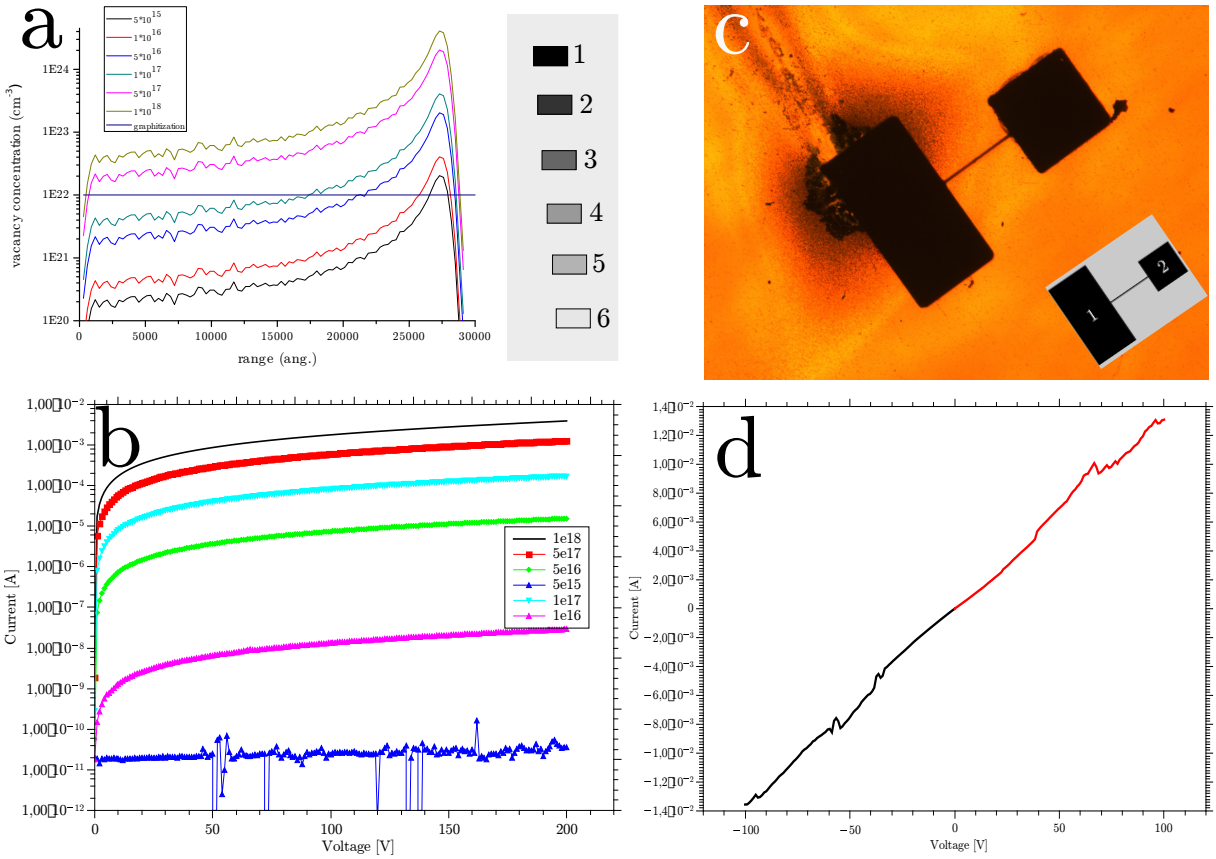

Figure 8.9: (a) Calculated vacancy concentration for different ion fluences as a function over the ion range and a scheme of the implanted pads (right). A darker shade indicates a higher fluence. **(b)** *I*–*V*-curves of the individual pads. **(c)** Transmission light microscopy image of an embedded conducting path and its contact pads in diamond. The pads are 240×60 µm^2 and 120×120 µm^2 big, respectively. **(d)** *I*–*V*-curve of the embedded conducting path from one contact to the other.

[2] J.F. Ziegler et al.: *SRIM – The Stopping and Range of Ions in Matter* (2008), http://www.srim.org

8.8 Coupling of color centers into macroscopic quantum systems with an atomic nano-assembler

J. Lehnert, R. John, S. Pezzagna, J. Meijer

The coupling of two NV centers can be achieved with very high quality [1]. However, to increase the number of NV centers in a scalable manner, the individual addressing and manipulation of the NV centers is necessary. One promising scheme is the use of the charge states of the NV centers [2]. Indeed, in its negative NV^- charge state, the associated electron spin can be manipulated and readout with optical and microwave fields. In its NV^+ state, the NV center is dark and not influenced by the electromagnetic fields. The idea is based on an individual and sequential switching of the charge state of the NV centers from NV^- to NV^+ after the spin state has been swap to the N nuclear

spin, where is can be much longer stored. The dark state (NV^+) has no paramagnetic moment, thus the state does not disturb the nuclear spin [3]. In order to switch the charge state of a NV center different methods are possible. One first method is based on the determined change of the Fermi-level position by applying an external gate voltage from 2.8 eV down to 0.6 eV (Fig. 8.10). This method has already been proved for very

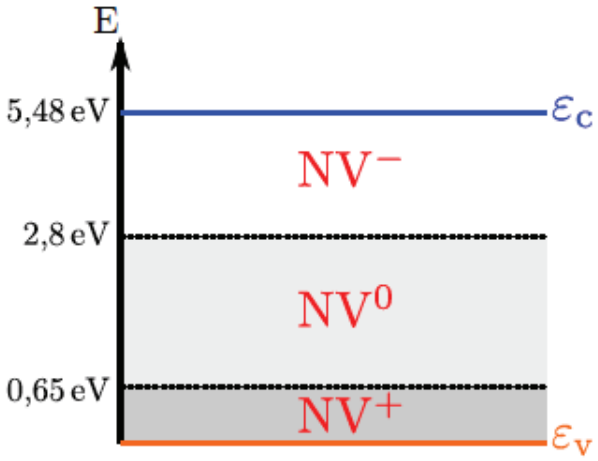

Figure 8.10: The Fermi-levels where different charge states are expected. However, due to the low charge carrier concentration and charged defects, the Fermi-level of NV centers in diamond is pinning. These restrain the switching of NV centers.

shallow NV centers using a H-terminated surface [2]. However, the coherence time (T_2) is very short, thus this method seems not to be appropriate. In order to passively control the Fermi level we investigate the influence of implantation of B and P [4]. The active switching of the charge state for deep NVs is studied using three different methods:

- The fabrication of an in-plane PIN junction and the implantation of NV centers into the intrinsic area.
- The use of metal contacts on the surface of the diamond and the use of shallow implanted NV centers.
- A local electron beam irradiation.

PIN junction An electronic grade diamond purchased from Element6 with a residual N concentration in the range of a few ppb was used as a substrate for the fabrication of p-i-n diode structures [5]. The structures were made by B- and P-ion implantation with a fluence of 2×10^{16} cm^{-2} and an energy of 70 keV for B and a fluence of 1×10^{16} cm^{-2} and an energy of 95 keV for P. After the implantation, the substrate was annealed in vacuum at a temperature of 1600 ℃. The resulting diode structure is shown in Fig. 8.11. The high-temperature annealing caused strong graphitization of the ion-damaged diamond layer. This layer covers the ion-doped non-graphitized areas, which are of p-type in case of B ions and n-type in case of P ions. Several diodes were subsequently implanted with CN^- with a fluence of 1×10^{12} cm^{-2} and an energy of 95 keV and then annealed at a temperature of 800 ℃ in order to create NV defects in their i-areas.

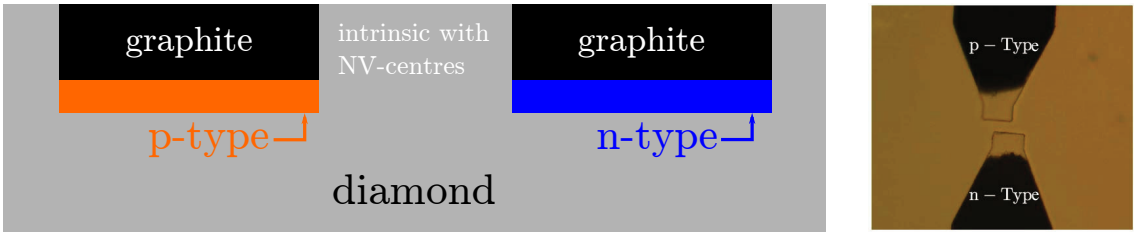

Figure 8.11: Scheme of the implanted B (p-type) and P (n-type) areas (*left*). The n- and p-type fingers with a gap distance of 10 µm (*right*).

The luminescence measurements have been performed at room temperature with a home-made confocal microscope working in the photon counting regime. The numerical aperture of the air objective is 0.95. The fabricated structures revealed typical behaviour of rectifying diodes. At forward bias, the diodes produced characteristic electroluminescence due to NV^0 centers imbedded into the i-area.

We studied the behaviour of the diode using the simulation `nextnano` software. In Fig. 8.12 the expected band bending in forward and backward direction is shown. Due to

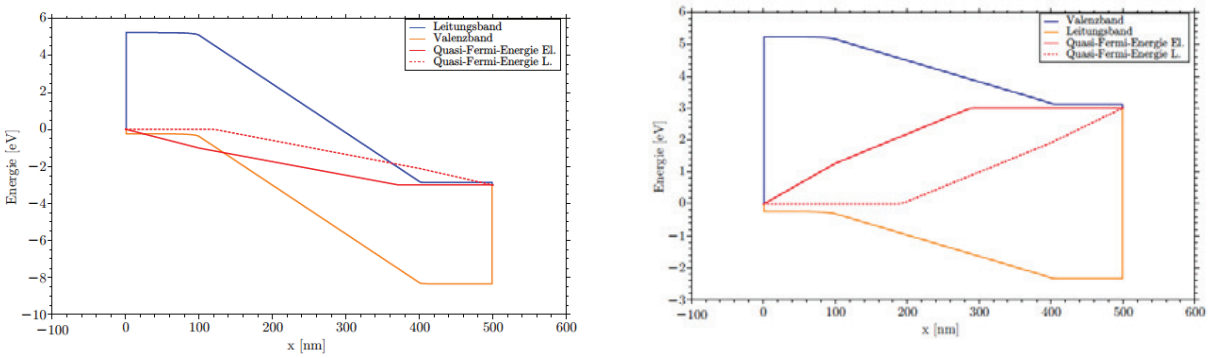

Figure 8.12: Simulated band bending and Fermi levels of the implanted pin diode to switch the NV centers.

the current flow, two quasi Fermi levels have to be considered. Although we expect from the simulation that the diode "opens" at 7 V, it was experimentally found that it opens at 20 V or even higher. This discrepancy can be explained by charge trapping. Additionally, further investigation is required whether a real n-type diamond is obtained. Whereas producing p-type diamond using B implantation is a well established method, n-type diamond using P implantation is still an open question. To prove this statement, we will perform Ion Beam Induced Charge (IBIC) measurements soon.

The luminescence of the i-area of one of the diodes was studied in regime of photoluminescence using excitation with 532 nm. It was found that the variation of applied bias from −30 V to +30 V considerably changed the intensity and the spectral content of the photoluminescence (Fig. 8.13).

Whereas the switching from NV^- to NV^0 forth and back is possible, we could not find any switching behaviour from NV^0 to NV^+. Actually we test NV centers in p-type diamonds and use additional laser pulses to switch the NV charge state. These experiments are looking very promising.

The work is based partly on the theses of J. Lehnert and of J. Vogel. Publications are in preparation.

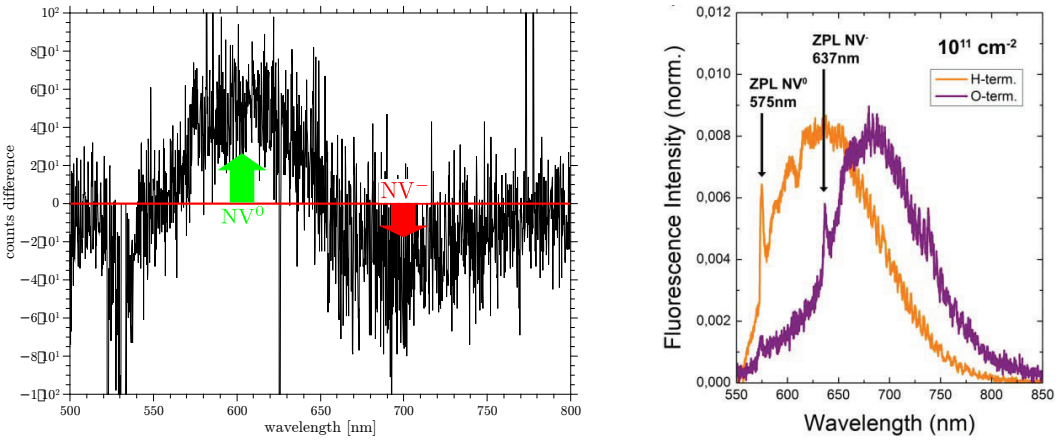

Figure 8.13: (a) Difference of NV center spectra inside the gap of the PIN diode. The spectra is taken for 30 V forward biased direction and −30 V in backward direction. It is clearly seen that the charge state of the NV center is changed. **(b)** NV fluorescence spectra for NV^- and NV^0. The NV^+ seems to be dark.

MOI contact Beside a PIN junction, it is possible to use a Shottky barrier to change the potential and the Fermi level of the NV center. In order to test this method, Au pads are evaporated on the diamond surface (Fig. 8.14(a)). Simulations show that the potential drop very fast inside the diamond thus very high potentials are necessary to switch the diamond (Fig. 8.14(b)). However we found a clear evidence that a switching is possible using this method (Fig. 8.14(c)). The work is partially based on the thesis of R. John.

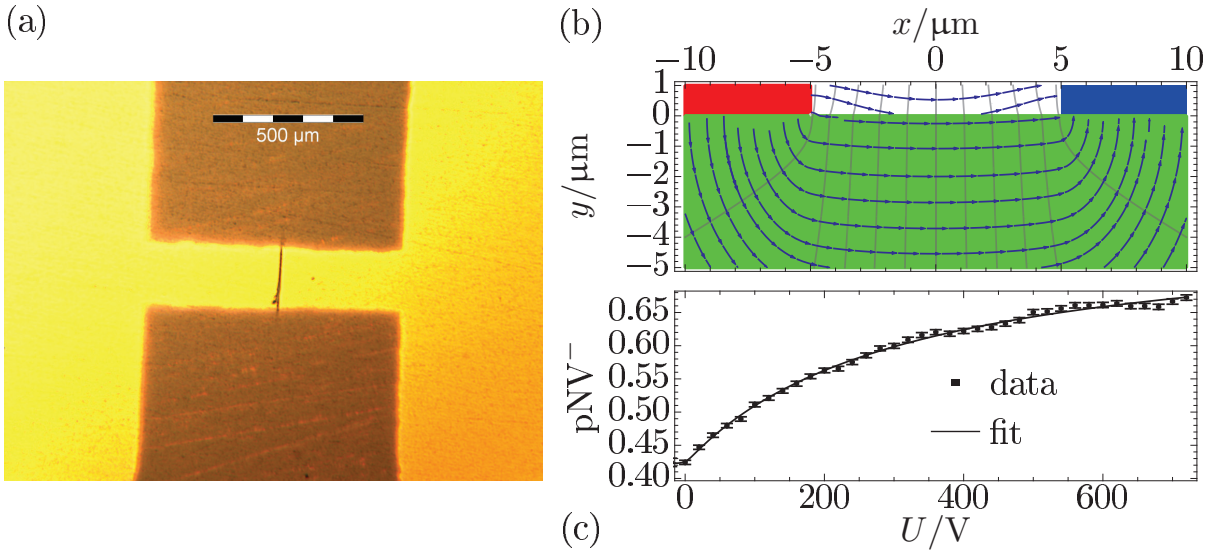

Figure 8.14: (a) Picture of two isolated Au contact areas with a gap size of 10 µm. **(b)** Calculated potential distribution. **(c)** NV^- percentage versus the applied voltage for an certain number of intrinsic NV centers found into the gap. The value is changed from 0.43 – 0.67 because at high voltage also deeper NV are switched to NV^-.

Switching NV by electron irradiation To manipulate the Fermi level we can also use an electron beam irradiation with an energy of 15 keV or less. This leads to a change of the charge state. However these results are very preliminary and have to be proved in detail.

Summary We show that P as well as B implantation influence the Fermi level and stabilize the charge state to NV^- or NV^+, respectively [4]. However the number of free carrier is found to be very low, so that the conductivity is almost zero. One possible explanation is that defects trap the charge carriers and lead to local inhomogeneous Fermi levels. These charged traps could also explain the failing gate structures and PIN junction, especially because a very deep Fermi level is necessary to achieve a NV^+ state. To overcome this problem, we will implant BN molecules at low kinetic energy. This will allow to place an acceptor very close to the NV center. Indeed, the first experiments show that the number of NV centers is very less and that only a few can be found in NV^0 state. The next step will be to implant these molecules into a gate and pin structure and apply a voltage, as well as irradiate these structures with electrons.

[1] F. Dolde et al.: Nat. Commun. **5**, 3371 (2014), doi:10.1038/ncomms4371
[2] M.V. Hauf et al.: Nano Lett. **14**, 2359 (2014), doi:10.1021/nl4047619
[3] B. Grotz et al.: Nat. Commun. **3**, 729 (2012), doi:10.1038/ncomms1729
[4] K. Groot-Berning et al.: phys. stat. sol. a: Appl. Mater. Sci. **211**, 2268 (2014), doi:10.1002/pssa.201431308
[5] A. Lohrmann et al.: Appl. Phys. Lett. **99**, 251106 (2011), doi:10.1063/1.3670332

8.9 Charge state switching of NV-centres with electrical fields

R. John, J. Meijer

Nitrogen–vacancy centres in diamond have proven beneficial for the future construction of quantum computers. These centers occur in the three different charge states NV^+, NV^0 and NV^- [1], where the latter possesses essential electronic properties for usage as a qubit in quantum computers [2]. It was shown using photoluminescence-spectroscopy that limited electrostatical manipulation of the charge state of the NV-centres is possible at or just below the surface of the host diamond as illustrated in Fig. 8.15. This effect could also be quantified using a simple ad-hoc band scheme where the low voltage sensitivity was attributed to the shielding effect of surface-near vacancies. Despite this low sensitivity which projects to about 1 MV/m of electric field needed for a mean change of the charge state, this effect may be usable with nano diamonds to detect local electric fields optically, for example at the surface of biological nerve cells while these perform neural activity.

[1] A. Lenef et al.: Phys. Rev. B **53**, 13441 (1996), doi:10.1103/PhysRevB.53.13441
[2] M.W. Doherty et al.: Phys. Rep. **528**, 1 (2013), doi:10.1016/j.physrep.2013.02.001

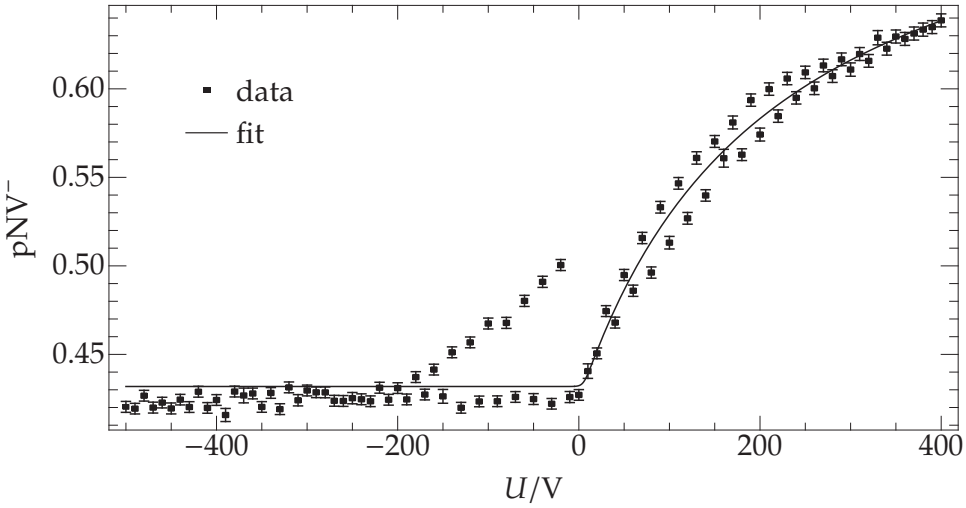

Figure 8.15: Dependence of the relative charge state of NV-centres (measured as relation of NV^-- to NV^0- and NV^--centres) at the surface of a 300 µm thick diamond to the voltage U which was applied to this and the opposing surface. The visible hysteresis is due to the electrical capacitance of the vacancies in combination with the electrical isolation of the diamond.

8.10 New setup for optically detected magnetic resonance (ODMR)

R. John, S. Pezzagna, J. Meijer

At the end of 2014 our department put another setup for confocal fluorescence microscopy into operation, which was additionally equipped for optically detected magnetic resonance (ODMR). For this purpose the sample is fixed on a printed circuit board containing grounded coplanar waveguides which are coupled to a thin (≈ 20 µm) Cu wire stretched over the sample. Using external connectors, continuous, pulsed or IQ-modulated microwave radiation with frequencies up to 6.4 GHz and powers up to ≈ 16 W PEP can thus be applied to the sample while it is illuminated by lasers with wavelengths of 532 nm and 594 nm which can be pulsed by acousto-optical modulators. Some of the impurities of certain hosts used as sample like the negatively charged nitrogen–vacancy centres in diamond show electron spin selective fluorescence which can be used to measure the spin state of these colour centres [1]. Using continuous ODMR spectroscopy the transition frequencies of these spin states are measurable, which enables the conduction of pulsed experiments like the application of microwave pulses of incrementally increasing lengths interleaved with laser pulses to measure Rabi-oscillations and thus the Rabi-frequency of the centre like in Fig. 8.16(*right*). With this further experiments like pulsed ODMR spectroscopy (see Fig. 8.16(*left*)) and spin echo are possible, which can resolve hyperfine structure, coupling to nearby spins like ^{13}C or spin-spin/spin-lattice relaxation. The setup also allows polarisation resolved measurement using two avalanche photodiodes (APD) as well as two-channel correlation to measure $g^{(2)}$-statistics, which allows the determination of single-photon-sources (SPS)[1]. The measurements are automatable for several days or weeks such that very

[1]Single fluorescent colour centres in this cases.

long or batch measurements are feasible. Magnetic manipulation is also possible.

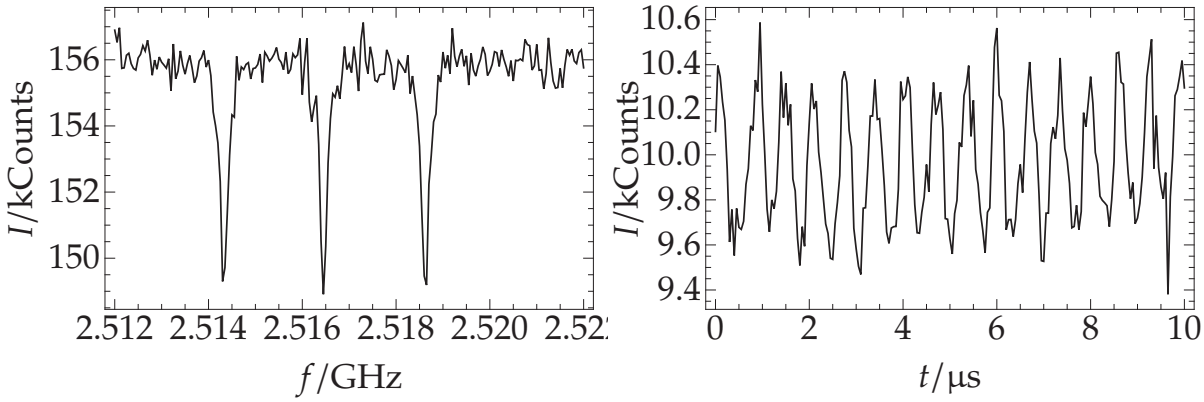

Figure 8.16: Pulsed ODMR-spectrum of an nitrogen–vacancy centre ^{14}N-core (*left*); application of microwave pulses of length t on this NV to measure its power-dependent Rabi-frequency (*right*).

[1] M.W. Doherty et al.: Phys. Rep. **528**, 1 (2013), doi:10.1016/j.physrep.2013.02.001

8.11 3D ion beam writing in diamond

R. Wunderlich, T. Lühmann, J.L. Barzola Quiquia*, J. Meijer

*Division of Superconductivity and Magnetism

Ion beam writing is a known technique for prototyping or sculpturing e.g. in PMMA. Here we use the high defect production cross section in the Bragg Peak of a focused 1.8 MeV He ion beam to induce a phase transition from the diamond lattice to a graphite-like structure. Due to the fact that the Bragg-Peak for this conditions is in a depth of about three micrometer we create buried graphite structures which are surrounded by diamond.

To generate structures in an arbitrary depth between the maximal penetration depth and the diamond surface we develop a novel mask method for an all-in-one process for the structure production. With the help of a mask revolver which holds a certain number of copper foils the Bragg-Peak can be shifted with respect to the copper foil thickness (Fig. 8.17). A Cu mesh with continuous ramps on each bar drags the graphitization peak to the diamond surface where a standard electric contact with e.g. Ag paste can be conducted (Fig. 8.18).

With this approach we create simple buried wires for electric characterization, where we can verify a variable range hopping mechanism (Fig. 8.19(*left*)) as well as more challenging structures like 3D stacks of graphitization loops with electric contacts, which can be used for the producing of a magnetic field in diamond.

For the investigation of the development of the irradiated diamonds with different fluences and subsequently different heating temperatures we apply confocal Raman spectroscopy and ellipsometry (Fig. 8.19(*right*)).

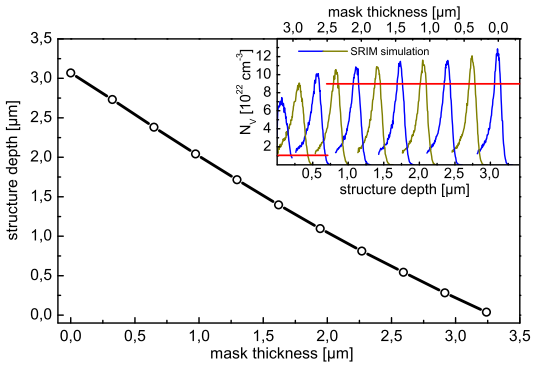

Figure 8.17: Dependence of the structure depth on the Cu mask thickness.

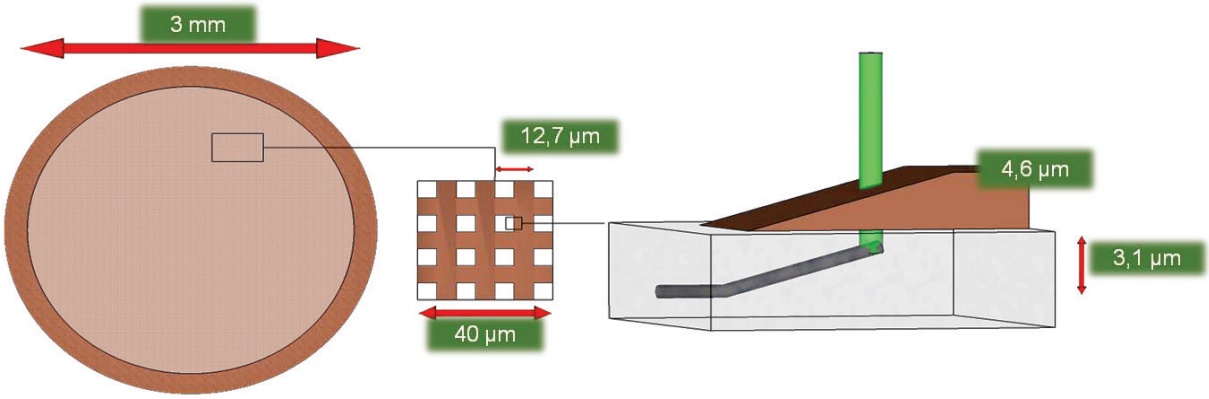

Figure 8.18: Cu mesh for the contacting of the buried structures with the surface.

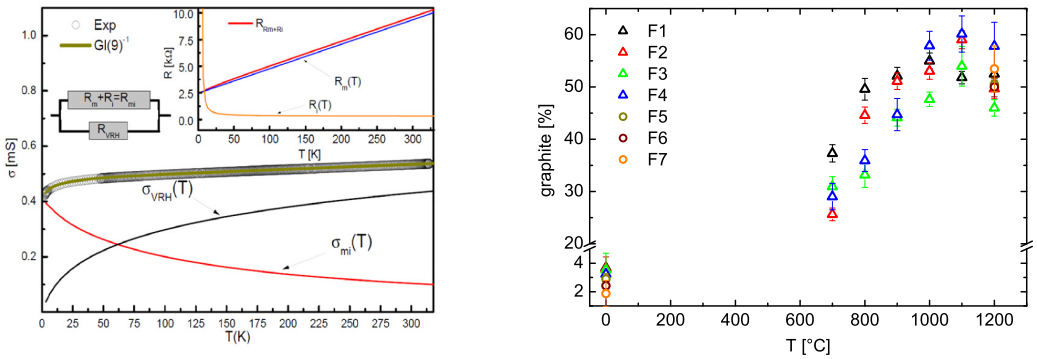

Figure 8.19: Conductance dependence of a buried graphite "wire" on the temperature (*left*). Graphite amount in buried graphite-like layers measured by ellipsometry, depending on annealing temperature (*right*).

8.12 Collimation of ion beams with help of muscovite foil

C. Scheuner, St. Jankuhn, J. Vogt, J. Meijer

For the creation of NV-centres in diamond and other important applications very tiny ion beams are needed. Thus, the collimation of ion beams with pores in muscovite

foil was studied. The foils were prepared at the GSI Darmstadt by irradiation with high energetic Sm-ions which penetrated the foil. This results in an amorphisation of the crystal structure of the muscovite along the tracks of the Sm-ions. After this the amorphous material got etched away with hydrofluoric acid and this created rhomb shaped pores with a side length of about 123 nm. One of them and the intact muscovite surface can be seen in Fig. 8.20. The foil had a thickness of 7 μm which would be enough

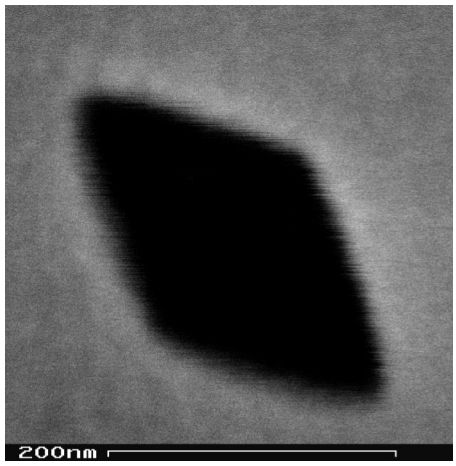

Figure 8.20: Scanning electron microscopy micrograph of a pore in the muscovite foil and the intact surface after the ion beam radiation.

to stop N-ions with energies up to 11 MeV.

Beams of N^+- and N^{++}-ions with 4 MeV, 2 MeV and 0.8 MeV were shot on the foil. The beams had a divergence that was as small as possible. The foil was mounted on a goniometer between ion beam and a particle detector in order to measure the number of transmitted ions with respect to the angle between ion beam and the pores. This angle distribution got treated in the same way as for ion channelling in a crystal lattice. A characteristic value of this process is the critical angle: the greatest angle where theoretically channelling can occur. The critical angles where determined out of the data from the experiment. Also theoretical predictions where done to predict the critical angles with respect to the ion energies. The theoretical values matched good to the experiment as can be seen in Fig. 8.21. Further the charge state of the N-ions seems to have no influence on the critical angle in the way the experiment was done.

In addition, the energy loss of the ions transmitted through the pores was measured and compared to values calculated out of the Rutherford-scattering theory. The data were also recorded with respect to the angle, and compared to the theory it could be seen that the behaviour of the energy loss and the value were about the same but the ions lost mostly less energy than predicted.

Also the change in the divergence of the ion beam was measured. Therefore the shape and size of the ion beam, that was transmitted through the pores, were measured in different distances to the foil with an alignment where the ion beam were as parallel to the pores as possible. The divergence recorded was much smaller than the critical angle.

In the end the foil was controlled to any damages caused by the ion beam but it seemed to have none.

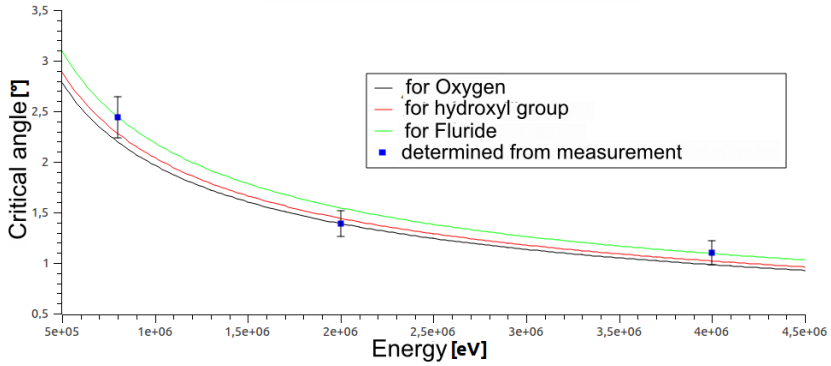

Figure 8.21: Energy-dependent plot of the critical angles determined out of the measurements are compared to the theoretical predictions for the three main scattering partners of the N-ion in the muscovite lattice.

8.13 Concept of single ion detector for deterministic ion implantation at the nanoscale

D. Spemann[*†], J.W. Gerlach[†‡], St. Rauschenbach[§], B. Rauschenbach[†‡¶], J. Meijer[*†]

[*]Division of Nuclear Solid State Physics
[†]Joint Single Ion Implantation Lab, Leipzig
[‡]Leibniz Institute of Surface Modification e.V., Leipzig
[§]Max Planck Institute for Solid State Research, Stuttgart
[¶]Institute for Experimental Physics II, Universität Leipzig

Nowadays, the ability to endow functionality to single atoms or molecules in materials becomes of increasing importance in nanotechnology. Atoms can be used as switches, single photon sources or quantum mechanical objects, e.g. for information processing and quantum computing. Deterministic ion implantation, i.e. the implantation of a counted number of ions, with a lateral accuracy of a few nanometers is one approach to achieve this goal. However, counting low-keV single ions with high detection efficiency is difficult – techniques used so far include secondary electron detection [1] or ion beam induced charge [2] caused by the ion impact. Ion traps have been used as single ion sources as well [3]. All these techniques have their individual limitations, e.g. the requirement for the implanted material to act as an efficient secondary electron emitter or particle detector or the restriction to specific atoms and substantial experimental effort in case of ion traps.

Our planned approach to deterministic ion implantation uses a commercial Focused Ion Beam (FIB) system equipped with a dedicated single ion source. The latter one comprises an ion source, an $\vec{E} \times \vec{B}$ filter and a single ion detector which allows to detect the ion prior to injection into the FIB system, making the ion detection independent from the properties of the implanted material. In order to be compatible with the very low acceptance of the FIB ion column a single ion detector based on image charge detection is envisaged to preserve the very low emittance of the ion source. The evaluation of an alternative detector concept using secondary electron emission from the ion passage through ultra-thin foils gave unacceptably large emittance values due to ion scattering.

[1] T. Matsukawa et al.: Appl. Surf. Sci. **117/118**, 677 (1997), doi:10.1016/S0169-4332(97)80163-8
[2] J.C. McCallum et al.: Adv. Mater. Sci. Eng. **2012**, 272694 (2012), doi:10.1155/2012/272694
[3] W. Schnitzler et al.: Phys. Rev. Lett. **102**, 070501 (2009), doi:10.1103/PhysRevLett.102.070501

8.14 PIXE-investigations of time-dependent intracellular disassembly of LbL biopolymer multilayers

M. Ritzschke, St. Jankuhn, J. Meijer, U. Reibetanz*

*Institute for Medical Physics and Biophysics

Due to an increasingly detailed understanding of molecular mechanism of diseases as well as the necessity of targeted transport of novel active agents, the development of specific and efficient drug delivery systems is highly relevant. In this context, modular biocompatible and biodegradable systems such as constructed of spherical biopolymer multilayer particles and capsules by Layer-by-Layer (LbL) technique are multifunctional and, therefore, particularly promising [1].

Beside construction, one important aspect of LbL-carriers is the controlled disassembly within targeted cell compartments with subsequent drug release, which can be achieved e.g. by the choice of biopolymers or their coupling mechanism.

Thus, particle-induced X-ray emission (PIXE) investigations of multilayer decomposition within cytoplasm of fibroblast-like Vero cells using nanoparticles (NPs) as multilayer constituents in different positions will help us to understand the time-dependent disassembly of the multilayer by detecting the NP re-distribution within the cell [2]. Using ion beam analysis for such investigations several parameters have to be considered, such as (i) ion beam diameter, (ii) carrier diameter and (iii) thickness of the multilayer (that is, number of polymer/NP layers). Time-dependent experimental studies of NP distribution have been compared to calculated model distribution to facilitate data interpretation. Taking those parameters into account, cross sections of detected elemental distributions have been studied. Fig. 8.22 exemplarily shows Ca and Fe cross sections of a $CaCO_3$ core (Ca) coated with 21 layers protamine sulfate and dextran sulfate with three integrated NP layers (Fe) after 48 h co-incubation with Vero cells. Compared to investigations after 72 h and 96 h co-incubation, the multilayer thickness decreases with increasing time illustrating the ongoing multilayer disassembly [3].

[1] U. Reibetanz et al.: Macromol. Biosci. **6**, 153 (2006), doi:10.1002/mabi.200500163
[2] U. Reibetanz et al.: Nucl. Instrum. Meth. Phys. Res. B **269**, 2281 (2011), doi:10.1016/j.nimb.2011.02.064
[3] M. Ritzschke: Bachelorarbeit, Universität Leipzig (2014)

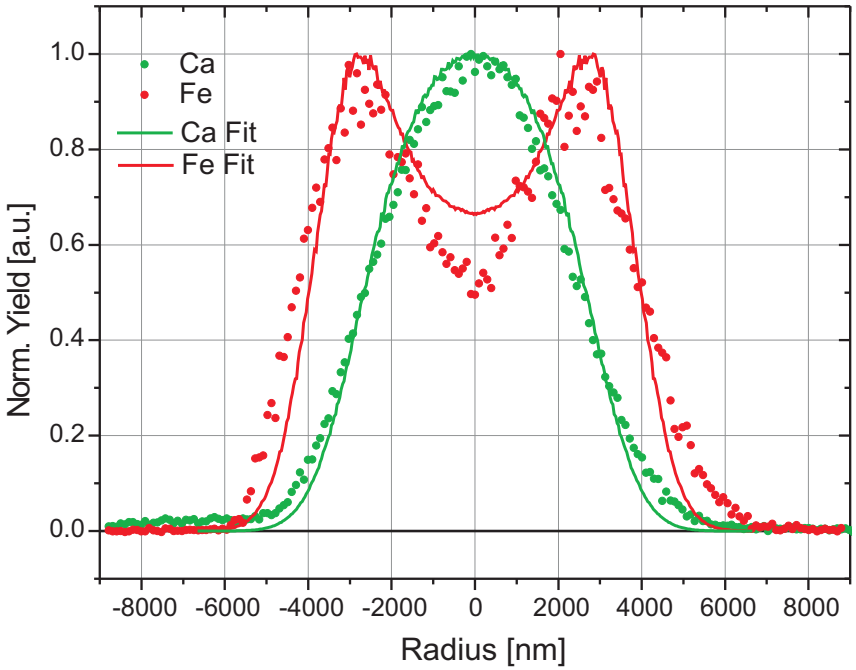

Figure 8.22: Ca and Fe cross sections of measured elemental distributions of a $CaCO_3$ core (Ca) coated with 21 layers protamine sulfate and dextran sulfate with three integrated NP layers (Fe) after 48 h co-incubation with Vero cells (*dotted lines*). The fits result in a Fe shell thickness of about 200 nm at the verified parameters ion beam diameter (3 µm) and carrier diameter (5 µm) (*solid lines*).

8.15 Funding

Integration of Molecular Components in Functional Macroscopic Systems: Coupling color centers into macroscopic quantum systems with an atomic nano-assembler
Prof. Dr. J. Meijer
VolkswagenStiftung

DIAmond Devices Enabled Metrology and Sensing (DIADEMS)
Prof. Dr. J. Meijer
EU FP7-ICT-2013.9.7 611143

Quantum Information with NV Centres (QINVC)
Prof. Dr. J. Meijer
CHIST-ERA VBP 01BQ1105

Diamond Materials for Quantum Application: Ultraprecise deterministic doping of diamond
Prof. Dr. J. Meijer
DFG FOR1493

Functionalized Nanodiamonds for Biomedical Research and Therapy
Prof. Dr. J. Meijer
VolkswagenStiftung

EXMAD – Extreme Sensitive Magnetometry using Nitrogen–Vacancy Centers in Diamond
Prof. Dr. U.L. Andersen/Prof. Dr. J. Meijer
The Danish Council for Strategic Research

Utilization of Ion Accelerators for Studying and Modelling of Radiation Induced Defects in Semiconductors and Insulators
Prof. Dr. J. Meijer
IAEA CRP F11016

Joint Lab "Einzelionenimplantation": "Sensorik mit einzelnen Atomen"
Prof. Dr. Dr. h.c. B. Rauschenbach/Prof. Dr. J. Meijer
Leibniz-Gemeinschaft/EU

8.16 Organizational Duties

J. Meijer
- User Selction Panel for the Ion Beam Center: Helmholtz-Zentrum Dresden–Rossendorf
- Advisory Board: ISTAC Croatian Nuclear Science
- Programme Committee: 14. International Conference on Nuclear Microprobe Technology and Applications, Padova, Italy, 07.–11.07.2014
- Referee: Several journals

J. Vogt
- Member of the Faculty Board

8.17 External Cooperations

Academic

- City University of New York, College of Staten Island, Department of Engineering Science and Physics, USA
  Assoc. Prof. Dr. A.M. Zaitsev
- Centre National de la Recherche Scientifique (CNRS), École normale supérieure (ENS), Laboratoire Aimé Cotton (LAC), Cachan, France
  Prof. Dr. J.-F. Roch
- Centre National de la Recherche Scientifique (CNRS), Laboratoire des Sciences des Procédés et des Matériaux (LSPM), Fabrication Processes of Advanced Materials (PEMA), Paris, France
  Prof. Dr. J. Achard
- Commissariat à l'énergie atomique et aux énergies alternatives (CEA), Institut Rayonnement Matière de Saclay (IRAMIS), Service de Physique de l'Etat Condensé (SPEC), Quantronique, Saclay, France
  Prof. Dr. D. Esteve

- ETH Zürich, Physikdepartement, Laboratorium für Festkörperphysik, Spin Physics and Imaging, Switzerland
  Prof. Dr. C. Degen
- Fraunhofer-Institut für Angewandte Festkörperphysik Freiburg, Mikro- und Nanosensoren
  Dr. C.E. Nebel
- Humboldt-Universität zu Berlin, Mathematisch-Naturwissenschaftliche Fakultät I, Institut für Physik, AG Nanooptik
  Prof. Dr. O. Benson
- Hungarian Academy of Sciences, Wigner Research Centre for Physics, Institute for Solid State Physics and Optics, Budapest, Hungaria
- Interuniversitair Micro-Electronica Centrum (imec) Leuven, Belgium
- Julius-Maximilians-Universität Würzburg, Fakultät für Chemie und Pharmazie, Institut für Organische Chemie
  Prof. Dr. A. Krüger
- Leibniz-Institut für Oberflächenmodifizierung e.V. Leipzig
  Prof. Dr. Dr. h.c. B. Rauschenbach, Prof. Dr. B. Abel
- Leibniz-Universität Hannover, Institut für Anorganische Chemie, AK Analytik
  Prof. Dr. C. Vogt
- Ludwig-Maximilians-Universität München, Fakultät für Physik, Experimentelle Quantenphysik
  Prof. Dr. H. Weinfurter
- Max-Planck-Institut für biophysikalische Chemie Göttingen, Karl-Friedrich-Bonhoeffer-Institut, Abt. NanoBiophotonik
  Prof. Dr. Dr. h.c. St.W. Hell
- Technische Universität München, Walter Schottky Institut, E25: Spins and Defects in Semiconductors
  Prof. Dr. M.S. Brandt
- Università di Torino, Dipartimento di Fisica Sperimentale, Gruppo di Fisica dello Stato Solido
  Prof. Dr. E. Vittone
- Universität Basel, Department of Physics, Quantum-Sensing Lab, Switzerland
  Prof. Dr. P. Maletinsky
- Universität Kassel
- Universität Konstanz, Mathematisch-Naturwissenschaftliche Sektion, Fachbereich Physik, Lehrstuhl für Ultrakurzzeitphysik und Photonik
  Prof. Dr. A. Leitenstorfer
- Universität Leipzig, Medizinische Fakultät, Institut für Medizinische Physik und Biophysik
  Prof. Dr. E. Donath, Dr. I. Estrela-Lopis, Dr. U. Reibetanz

- Universität Mainz, Fachbereich Physik, Mathematik und Informatik, Institut für Physik, Arbeitsgruppe Quanten-, Atom- & Neutronenphysik (QUANTUM)
  Prof. Dr. F. Schmidt-Kaler, Priv.-Doz. Dr. K. Singer
- Universität Stuttgart, Fakultät Mathematik und Physik, 3. Physikalisches Institut
  Prof. Dr. J. Wrachtrup
- Universität Ulm, Fakultät für Naturwissenschaften, Institut für Quantenoptik
  Prof. Dr. F. Jelezko
- Universität Ulm, Fakultät für Naturwissenschaften, Institut für Theoretische Physik, Controlled Quantum Dynamics Group
  Prof. Dr. M.B. Plenio
- University of Warwick, Department of Physics, Condensed Matter Physics, Magnetic Resonance Cluster, Coventry, UK
  Prof. Dr. M. Newton
- Universität Wien
- Westfälische Wilhelms-Universität Münster, Physikalisches Institut
  Prof. Dr. R. Bratschitsch

Industry

- ARTTIC Paris, France
- attocube systems AG München
- Element Six Ltd. Shannon, Co. Clare, Ireland
- THALES Research & Technology Palaiseau, France

8.18 Publications

Journals

D. Antonov, T. Häußermann, A. Aird, J. Roth, H.-R. Trebin, C. Müller, L. McGuinness, F. Jelezko, T. Yamamoto, J. Isoya, S. Pezzagna, J. Meijer, J. Wrachtrup: *Statistical investigations on nitrogen–vacancy center creation*, Appl. Phys. Lett. **104**, 012105 (2014), doi:10.1063/1.4860997

R. Böttcher, A. Pöppl, M. Lorenz, S. Friedländer, D. Spemann, M. Grundmann: ^{55}Mn *pulsed ENDOR spectroscopy of* Mn^{2+} *ions in* ZnO *thin films and single crystal*, J. Magn. Reson. **245**, 79 (2014), doi:10.1016/j.jmr.2014.05.012

S.K. Das, R. Guin, D. Banerjee, K. Johnston, P. Das, T. Butz, V.S. Amaral, J.G. Correia, M.B. Barbosa: *Perturbed Angular Correlation Study of the Static and Dynamic Aspects of Cadmium and Mercury Atoms Inside and Attached to a* C_{60} *Fullerene Cage*, Z. Naturforsch. **69a**, 611 (2014), doi:10.5560/ZNA.2014-0055

F. Dolde, V. Bergholm, Y. Wang, I. Jakobi, B. Naydenov, S. Pezzagna, J. Meijer, F. Jelezko, P. Neumann, T. Schulte-Herbrüggen, J. Biamonte, J. Wrachtrup: *High-fidelity spin entanglement using optimal control*, Nat. Commun. **5**, 3371 (2014), doi:10.1038/ncomms4371

F. Dolde, M.W. Doherty, J. Michl, I. Jakobi, B. Naydenov, S. Pezzagna, J. Meijer, P. Neumann, F. Jelezko, N.B. Manson, J. Wrachtrup: *Nanoscale detection of a single fundamental charge in ambient conditions using the NV^- center in diamond*, Phys. Rev. Lett. **112**, 097603 (2014), doi:10.1103/PhysRevLett.112.097603

M. Engler, F. Frost, S. Müller, S. Macko, M. Will, R. Feder, D. Spemann, R. Hübner, S. Facsko, T. Michely: *Silicide induced ion beam patterning of* Si*(001)*, Nanotechnol. **25**, 115303 (2014), doi:10.1088/0957-4484/25/11/115303

K. Groot-Berning, N. Raatz, I. Dobrinets, M. Lesik, P. Spinicelli, A. Tallaire, J. Achard, V. Jacques, J.-F. Roch, A.M. Zaitsev, J. Meijer, S. Pezzagna: *Passive charge state control of nitrogen-vacancy centres in diamond using phosphorous and boron doping*, phys. stat. sol. (a) **211**, 2268 (2014), doi:10.1002/pssa.201431308

M.V. Hauf, P. Simon, N. Aslam, M. Pfender, P. Neumann, S. Pezzagna, J. Meijer, J. Wrachtrup, M. Stutzmann, F. Reinhard, J.A. Garrido: *Addressing Single Nitrogen-Vacancy Centers in Diamond with Transparent in-Plane Gate Structures*, Nano Lett. **14**, 2359 (2014), doi:10.1021/nl4047619

C.C. Lo, S. Simmons, R. Lo Nardo, C.D. Weis, A.M. Tyryshkin, J. Meijer, D. Rogalla, S.A. Lyon, J. Bokor, T. Schenkel, J.J.L. Morton: *Stark shift and field ionization of arsenic donors in* ^{28}Si*-silicon-on-insulator structures*, Appl. Phys. Lett. **104**, 193502 (2014), doi:10.1063/1.4876175

M. Lorenz, R. Böttcher, S. Friedländer, A. Pöppl, D. Spemann, M. Grundmann: *Local lattice distortions in oxygen deficient* Mn*-doped* ZnO *thin films, probed by electron paramagnetic resonance*, J. Mater. Chem. C **2**, 4947 (2014), doi:10.1039/C4TC00407H

M. Loretz, S. Pezzagna, J. Meijer, C. L. Degen: *Nanoscale nuclear magnetic resonance with a* 1.9*-nm-deep nitrogen-vacancy sensor*, Appl. Phys. Lett. **104**, 033102 (2014), doi:10.1063/1.4862749

M. Loretz, T. Rosskopf, J.M. Boss, S. Pezzagna, J. Meijer, C. L. Degen: *Single-proton spin detection by diamond magnetometry*,
Science Express 16.10.2014, doi:10.1126/science.1259464

D. Spemann, P. Esquinazi, A. Setzer, W. Böhlmann: *Trace element content and magnetic properties of commercial HOPG samples studied by ion beam microscopy and SQUID magnetometry*, AIP Advances **4**, 107142 (2014), doi:10.1063/1.4900613

C. Stüber, M. Morawski, A. Schäfer, C. Labadie, M. Wähnert, C. Leuze, M. Streicher, N. Barapatre, K. Reimann, S. Geyer, D. Spemann, R. Turner: *Myelin and iron concentration in the human brain: A quantitative study of MRI contrast*, NeuroImage **93**, 95 (2014), doi:10.1016/j.neuroimage.2014.02.026

X. Zhou, M. Dorn, J. Vogt, D. Spemann, W. Yu, Z. Mao, I. Estrela-Lopis, E. Donath, C. Gao: *A quantitative study of the intracellular concentration of graphene/noble metal nanoparticle composites and their cytotoxicity*, Nanoscale **6**, 8535 (2014), doi:10.1039/c4nr01763c

Books

S. Pezzagna, J. Meijer: *Single-Ion Implantation in Diamond with a High Lateral Resolution: A Key Technology for the Fabrication of Quantum Devices*, In: V.K. Sarin (Ed.). Comprehensive Hard Materials, vol.3. Elsevier, Burlington, 321–336 (2014).
doi:10.1016/B978-0-08-096527-7.00050-7

Talks

M. Chipaux, A. Tallaire, S. Pezzagna, J. Meijer, J.-F. Roch, V. Jacques, T. Debuisschert
Magnetic imaging with an ensemble of NV centers in diamond
SBDD XIX: Hasselt Diamond Workshop, Hasselt, Belgium, 19.–21.02.2014

K. Groot-Berning, N. Raatz, I. Dobrinets, A. Tallaire, J. Achard, A.M. Zaitsev, J. Meijer, S. Pezzagna
Passive charge state control of nitrogen–vacancy centres in diamond using phosphorous and boron doping
SBDD XIX: Hasselt Diamond Workshop, Hasselt, Belgium, 19.–21.02.2014

D. Lehmann
Leipziger Uranmaschinen-Versuche
Weiterbildungsseminar, Bosch Sicherheitssysteme GmbH, Leipzig, 09.04.2014, invited

D. Lehmann
Start des Uranprojekts in Deutschland vor 75 Jahren
131. öffentliche Sonntagsvorlesung, Universität Leipzig, Leipzig, 26.10.2014, invited

J. Meijer
VolkswagenStiftung, Hannover, 13.01.2014

J. Meijer
Addressing individual NV centers for quantum computation
Physikalisches Kolloquium, Universität Paderborn, 23.01.2014, invited

J. Meijer
Addressing of single atoms using ion beams
Kolloquium, Göttingen, 27.01.2014

J. Meijer
Addressing of single atoms using ion beams
Physikalisches Kolloquium, TU Bergakademie Freiberg, 23.04.2014, invited

J. Meijer
Addressing of Single atoms
Chemie-Seminar, Universität Leipzig, 21.05.2014

J. Meijer
Functionalized single atoms addressed by ion beam implantation
Institutskolloquium, Leibniz-Institut für Oberflächenmodifizierung e.V., Leipzig, 05.06.2014

J. Meijer
Addressing of single ions using ion beam implantation
Joint Training Course on Ion Beam Microscopy, Legnaro, Italy, 03.–04.07.2014, invited

J. Meijer, S. Pezzagna
The functionalization of single atoms addressed by ion beam implantation
14. International Conference on Nuclear Microprobe Technology and Applications, Padova, Italy, 07.–11.07.2014, invited

J. Mejer
Radioaktivität
Lange Nacht der Wissenschaften, Leipzig, 27.06.2014

J. Meijer
Was ist ein Ionen-Mikroskop?
"Türen auf für die Maus", Universität Leipzig/WDR, Leipzig, 03.10.2014

J. Meijer
Quantencomputer und Quantensensoren
Physik am Samstag, Universität Leipzig, Leipzig, 08.11.2014, invited

J. Meijer
Defect Engineering and high power devices in diamond
IAEA CRP Meeting, Vienna, Austria, 11.11.2014, invited

M. Mensing, D. Spemann
Determination of the Point Spread Function of a Nuclear Microprobe
Physics Seminar, National University of Singapore, Singapore, 30.05.2014, invited

Chr. Müller, X. Kong, J. Cai, K. Melentijević, A. Stacey, M. Markham, D. Twitchen, J. Isoya, S. Pezzagna, J. Meijer, J. Du, M. Plenio, B. Naydenov, L. McGuinness, F. Jelezko
Few spin NMR of external spins using a strongly coupled sensor in diamond
DPG-Frühjahrstagung, Dresden, 30.03.–04.04.2014

Chr. Osterkamp, J. Scharpf, S. Pezzagna, J. Meijer, Th. Diemant, R.J. Behm, B. Naydenov, F. Jelezko
Increasing the creation yield of shallow nitrogen–vacancy centers by surface plasma termination
DPG-Frühjahrstagung, Dresden, 30.03.–04.04.2014

S. Pezzagna
Passive charge state control of nitrogen–vacancy centres in diamond using phosphorous and boron doping
SBDD XIX: Hasselt Diamond Workshop, Hasselt, Belgium, 19.–21.02.2014

S. Pezzagna
De la couleur du diamant à lÂ´optique quantique (From the colour of diamond to quantum optics)
Dolmetscher-Kolloquium, Universität Leipzig, Leipzig, 07/2014

S. Pezzagna
Creation and charge state control of optical centres in diamond
2nd Workshop "Diamond & New Technologies": Technological applications of artificial diamond, Torino, Italy, 16.09.2014

S. Pezzagna
Nanoscalability with NV centres in diamond
QINVC Final Meeting, CEA Saclay, France, 10/2014

S. Pezzagna
Entanglement-enhanced NV-array sensors for electric and magnetic fields
DFG FOR1493-2 Kick off Meeting, Berlin, 11/2014

T. Reinert, N. Barapatre, M. Jäger, M. Morawski
High Throughput PIXE for Large Area High Definition Elemental Imaging
23rd International Conference on the Application of Accelerators in Research and Industry, San Antonio, TX, USA, 25.–30.05.2014, invited

C. Schreyvogel, M. Wolfer, J. Meijer, C.E. Nebel
Tuned NV emission by in-plane Al-*Schottky junctions on hydrogen terminated diamond*
SBDD XIX: Hasselt Diamond Workshop, Hasselt, Belgium, 19.–21.02.2014

D. Spemann
Defect Induced Magnetism in Carbon
ECMP Seminar, The University of Melbourne, Melbourne, Australia, 03.07.2014, invited

R. Wunderlich, T. Lühmann, D. Diering, J. Barzola, J. Meijer
Ion beam writing on diamond in micrometer scale at the LIPSION nanoprobe
14. International Conference on Nuclear Microprobe Technology and Applications, Padova, Italy, 07.–11.07.2014

Posters

St. Jankuhn, O. Naumov, Ch. Lan, M. Ritzschke, J. Meijer, U. Reibetanz
Investigation of intracellular multilayer decomposition of Layer-by-Layer self-assembled particles by means of ion beam analysis
14. International Conference on Nuclear Microprobe Technology and Applications, Padova, Italy, 07.–11.07.2014

J. Lehnert, M. Mensing, R. Karsthof, C. Ronning, A. Lohrmann, M. Grundmann, S. Pezzagna, J. Meijer
Active charge state control of NV colour centres using planar pin-junctions in diamond
SBDD XIX: Hasselt Diamond Workshop, Hasselt, Belgium, 19.–21.02.2014

M. Mensing, J. Barzola, J. Meijer, D. Spemann
Improving the lateral resolution in ion beam analysis by deconvolution of the point spread function of a nuclear nanoprobe
14. International Conference on Nuclear Microprobe Technology and Applications, Padova, Italy, 07.–11.07.2014

N. Raatz, I.W. Rangelow, J.L. Barzola Quiquia, S. Pezzagna, J. Meijer
Writing and imaging nanostructures of single defects in diamond
14. International Conference on Nuclear Microprobe Technology and Applications, Padova, Italy, 07.–11.07.2014

R. Schirhagel, S. Gerstl, N. Raatz, J. Meijer, C.L. Degen
Determining implantation profiles in diamond by atom probe tomography
SBDD XIX: Hasselt Diamond Workshop, Hasselt, Belgium, 19.–21.02.2014

8.19 Graduations

Master

- J. Lehnert
  Untersuchung elektrischer Eigenschaften Diamant-basierter Bauelemente
  January 2014

Bachelor

- R. John
  Elektrostatische Beeinflussung des Ladungszustandes von NV-Zentren in Diamant
  July 2014
- M. Ritzschke
  Untersuchungen zur zeitabhängigen intrazellulären Auflösung einer Layer-by-Layer assemblierten Polyelektrolytmultischicht mittels Protonen-induzierter Röntgenemission
  October 2014
- L. Rogée
  Theoretical and Practical Ion Beam Focussing with Emphasis on Heavy Ions
  April 2014
- C. Scheuner
  Kollimation von Ionenstrahlen mittels Muskovitfolie
  October 2014

8.20 Guests

- Prof. Dr. F. Jelezko
  Universität Ulm, Fakultät für Naturwissenschaften, Institut für Quantenoptik
  28.01.2014
- Priv.-Doz. Dr. K. Singer
  Universität Mainz, Fachbereich Physik, Mathematik und Informatik, Institut für Physik, Arbeitsgruppe Quanten-, Atom- & Neutronenphysik (QUANTUM)
  04.02.2014

- Dipl.-Phys. E. Schmidt
  Friedrich-Schiller-Universität Jena, Institut für Festkörperphysik
  18./19.03.2014
- Prof. Dr. J.-F. Roch
  Centre National de la Recherche Scientifique (CNRS), École normale supérieure (ENS), Laboratoire Aimé Cotton (LAC), Cachan, France
  19./21.03.2014
- Assoc. Prof. Dr. J.C. McCallum
  University of Melbourne, School of Physics, Centre for Quantum Computation and Communication Technology, Australia
  06./07.06.2014
- Prof. Dr. A. Krüger
  Julius-Maximilians-Universität Würzburg, Fakultät für Chemie und Pharmazie, Institut für Organische Chemie
  25.06.2014
- Prof. Dr. M. Takeshi
  University of Osaka
  02./03.07.2014
- Prof. Dr. T. Reinert, J.K. Rami
  University of North Texas, Department of Physics, Denton, TX, USA
  16.–31.07.2014
- Prof. Dr. D.N. Jamieson
  University of Melbourne, School of Physics
  27.07.–08.08.2014
- Dr. T. Schenkel
  Lawrence Berkeley National Laboratory, Ion Beam Technology Group
  17./18.09.2014
- Dr. H.-W. Becker, Dr. C. Larue, Dr. D. Rogalla
  Ruhr-Universität Bochum, RUBION and Department of Plant Physiology
  24.–28.11.2014
- Dipl.-Phys. R. Feder
  Leibniz-Institut für Oberflächenmodifizierung e.V. Leipzig
  22.11.2014

9

Semiconductor Physics

9.1 Introduction

The TCO2014 conference brought together many national and international experts and students for exchanging and discussing the latest on oxide semiconductors and transparent conductive oxides (TCO). The meeting was held in honor of Karl Bädeker (1877-1914) who had discovered TCOs at Universität Leipzig in 1906.

In 2014 we have successfully extended our research on bipolar electronics; the type-II nature of n-ZnO/p-CuI and n-ZnO/p-NiO diodes was discovered and theoretically modeled. Bipolar diodes were also fabricated on n-In_2O_3 using p-type $ZnCo_2O_4$ (ZCO) which had already been previously used by us for highly rectifying diodes on n-ZnO. The ZnO/ZCO JFETs could be used to fabricate high gain inverters. The second type of oxide JFET was reported using ZnO/NiO gates. Finally, fully amorphous oxides pn-diodes were reported for zinc-tin-oxide, using a ZTO/ZCO structure, favorably with a thin i-ZTO layer at the interface.

The composition spread approach using pulsed laser depositionhas been used for $(In,Ga)_2O_3$ and $(Al,Ga)_2O_3$ for which structural (X-ray) and optical (ellipsometry, Raman spectroscopy) data were analyzed as a function of composition. Currently, diodes and photodetector properties are investigated.

Figure 9.1: Journal covers of 2014/15 publications of the semiconductor physics group

We like to point to the special volume of Semiconductor Science and Technology 2015 (Volume 30, Issue 2) on *Semiconductor Functional Oxides* edited by Saskia Fischer and Marius Grundmann. Discoveries and progress have been also made in various other systems including magnetic spinels, multiferroic heterostructures and oxide microcavities. Please find details in the following chapters.

We are largely indebted to our funding agencies in particular Deutsche Forschungsgemeinschaft (DFG) and European Social Fund (ESF). We are grateful for the continued funding of Sonderforschungsbereich SFB 762 "Functionality of Oxide Interfaces" (2012–2015) and our project on nanowire heterostructures in the Forschergruppe FOR 1616 "Nanowire Optoelectronics" which was extended for the second funding period (2015–2018). Also we thank Sächsische Aufbaubank to support our new work on Ga_2O_3 thin films and oxide solar cells. The generous support of Universität Leipzig allowed us to install in 2013 a new high resolution X-ray diffraction setup and a multi-target sputter chamber for oxides. In 2014 we could continue our work on ZCO and CuI bipolar electronics with two new DFG grants. A project on flexible oxide electronics was positively reviewed for inclusion in the new DFG SPP FFlexCom (SPP 1796). The work of our students and researchers together with our academic and industrial partners near and far was fruitful and enjoyable and thus it is with pleasure that the semiconductor physics group presents their progress report.

Marius Grundmann

9.2 Karl Bädeker (1877–1914) and the Discovery of TCO's

M. Grundmann

Karl Wilhelm Sali Bädeker was born 3.2.1877 in Leipzig as the second of five children to his father Friedrich Dietrich (Fritz) Bädeker (1844–1925), a publisher, and his mother Florentina Paulina Rosalia (Flöry) Baedeker, née Landfermann (1849–1916) from Koblenz. Karl's paternal grandfather was the rather famous publisher Karl Baedeker (1801–1859) who established the series of tour guides carrying his name, known for their precise information.

Karl Wilhelm grew up at the Bädeker residence in Leipzig at Plagwitzer Str. 30 (now Käthe-Kollwitz-Straße 64). After private schooling and elementary school he then went to the Thomasschule in Leipzig and received the high school exam (*Maturitätszeugnis*) Easter 1895. He pursued studies in Geneva, Heidelberg, Munich and Göttingen. Under Walther Nernst he earned a doctoral degree (Dr. phil.) with a thesis on the dielectric constant of gases and its temperature dependence. His oral exam on 2.8.1900 was conducted by professors Walther Nernst, Otto Wallach and Felix Klein.

After military training, Bädeker was inscribed 6.11.1901 at Universität Leipzig for attending Boltzmann's lecture 'Theorie der Elektrizität und des Magnetismus' and conducting laboratory work 'Selbständige physikalische Arbeiten für Fortgeschrittene' with Otto Wiener. Bädeker left Universität Leipzig 2.6.1902; upon recommendation of professor Theodor des Coudres, he worked June and July 1902 at Universität Würzburg with Wilhelm Wien and Des Coudres. On 1.10.1902 he started employment as II. Assistent at the Physikalische Institut of Universität Greifswald with Walter König. In front of the Royal Saxon Academy of Sciences he reported 8.6.1903 in Leipzig on the

absence of the influence of ultraviolet light on the conductivity of metals [1]. This work on metals, seemingly conducted 1902 in Leipzig, already contained major elements of his subsequent work on metal compounds, in particular the fabrication of metal thin films (platinum and antimony) on glass and the measurement of thin film conductivity with a Wheatstone bridge.

His position in Greifswald was extended for another two years, but starting 1.4.1905 Bädeker worked again in Leipzig, now at the Theoretisch-Physikalische Institut of Universität Leipzig. His research was supported by Theodor des Coudres from the Theoretisch-Physikalische Institut and by Otto Wiener with instruments from the *Sammlung* of the Physikalische Institut in Leipzig. Fig. 9.2 shows Bädeker with colleagues and Des Coudres. His habilitation thesis of 1906 [2] was refereed in Jena by professor Felix Auerbach. The *Probevorlesung* in Jena was held 2.2.1907 upon 'Die Elektronentheorie der Metalle'; subsequently Karl Bädeker became Privatdozent at the Physikalische Institut of Universität Jena.

Figure 9.2: Des Coudres (right at the table) with several coworkers including Karl Bädeker (4th from left) in the lecture hall of the Theoretisch-Physikalische Institut at Linnéstraße, presumably 1906. Adapted from [3].

In his 1907 paper [2], Bädeker reports on the fabrication of a number of simple metal compounds, namely CdO, CdS, CdSe, CuI, Cu_2O, CuO, CuS, Cu_2S, CuSe, Ag_2S, Ag_2Se, AgI, PbO, PbS and TlS. Nowadays, this reads like a nice list of semiconductors. The samples were made by fabricating *Metallspiegel durch kathodische Zerstäubung*, i.e. metal thin films by sputtering, on glass or mica. Oxidation was achieved in air (*an der Luft*

geröstet), iodization occured spontaneously and sulfur and selenization was performed at elevated temperature in the respective anion vapors. The thin film thickness was determined, using the known specific weight of the compound, by weighing of the thin film and substrate, removal of the thin film with suitable etching solution and (after drying) weighing of the substrate. The precision of the scale in the µg range allowed a precision of 2 nm for the thin film thickness. For CuI, the thickness was also estimated from the dielectric color (assuming an index of refraction of $n = 2$). The electrical conductivity was measured by pressing suitable contacts onto the film and using a Wheatstone bridge. In order to reduce contact phenomena, also a meandering current path was used.

CdO thin films were found transparent with orange-yellow hue and a specific resistivity of $1.20 \times 10^{-3}\ \Omega$ cm. The CuI films were transparent and clear. The resistivity of the best CuI film was found to be $4.56 \times 10^{-2}\ \Omega$ cm. Bädeker rightfully doubted that such small value can be due to electrolytic conduction. Nowadays it is clear that the conductivity of CuI is due to hole conduction. Both CdO, the mother of all TCO's, and CuI have recently found rising interest in the literature.

At Jena university, Karl Bädeker held various lectures about electricity. In 1910 he was appointed *außerordentlicher* professor at Universität Jena. His 1911 book on electrical properties of metallic conductors [4], treating electrons in a metal as a gas, became quite popular. Scientific work of Bädeker at Jena was related to thermionic emission of electrons from metals and thermopower in deformed steel rods. In 1912 he discussed doped semiconductors as artificial metals with variable electron concentration [5]. Bädeker gave his last lecture on 31.7.1914. The same day, Germany was declared into the state of war by the Kaiser.

Bädeker had to immediately leave his family and home at Jena, since he had received mobilization orders to report to Halberstadt. In the early morning hours of 6.8.1914, advancing on Belgian ground with troops towards Liége, he was killed together with general von Wussow between the villages of Retinne and Liéry. After three temporary burial sites, he found his final rest at the German war cemetery in Vladslo, Belgium.

Further details on Bädeker's life and work can be found in [6].

[1] K. Bädeker, *Über einen Versuch, eine Einwirkung ultravioletten Lichts auf den elektrischen Widerstand der Metalle zu finden*, Berichte über die Verhandlungen der Königlich sächsischen Gesellschaft der Wissenschaften zu Leipzig, Mathematisch-Physische Klasse **55**, 198–199 (1903), Sitzung vom 8.6.1903.

[2] K. Bädeker, *Über die elektrische Leitfähigkeit und die thermoelektrische Kraft einiger Schwermetallverbindungen*, Ann. Physik **327**, 749–766 (1907); or Vierte Folge Band 22.

[3] Private archive of Bädeker family, Corinna Schmidt-Thomé, Freiburg i. Br.

[4] K. Baedeker, *Die elektrischen Erscheinungen in metallischen Leitern (Leitung, Thermoelektrizität, galvanomagnetische Effekte, Optik)* (F. Vieweg & Sohn, Braunschweig, 1911).

[5] K. Baedeker, *Künstliche metallische Leiter*, Physikal. Zeitschrift **13**, 1080-1082 (1912). (Vortrag und Diskussion auf der 84. Versammlung deutscher Naturforscher und Ärzte in Münster i.W., 19.9.1912).

[6] M. Grundmann, *Karl Bädeker (1877-1914) and the Discovery of Transparent Conductive Materials*, phys. stat. sol. (a) **212**(7), 1409-1426 (2015).

9.3 International Conference: Transparent Conductive Oxides – Fundamentals and Applications (TCO 2014)

M. Grundmann, H. von Wenckstern

The international conference *Transparent Conductive Oxides – Fundamentals and Applications* was held in honor of the 100th anniversary of the death of Prof. Dr. Karl W. Bädeker from 29th September to 2nd October 2014 in Leipzig.

Nowadays transparent conductive oxides (TCO) are widely used as ohmic device within transparent contacts in displays and solar cells or electro-magnetic shielding. Research on TCOs is still very active for the fundamental understanding and optimization of known materials and the search for novel TCOs, including materials with higher mobility for more economic solutions, indium-free materials or p-type materials. Also semiconducting transparent oxides for diodes and transistors have gained tremendous interest over the last decade due to applications in transparent and flexible active electronics. In particular the high electron mobility of amorphous oxides provides a viable route to go beyond the limitations regarding cut-off frequencies and energy efficiency of amorphous silicon.

Figure 9.3: The conference was enjoyed and appreciated a lot by the participants not only due to the high ranking international speakers: Martin Allen, University of Canterbury, Christchurch; André Bikowski, Helmholtz-Zentrum Berlin; Keith Butler, University of Bath; Leonard J. Brillson, Ohio State University; Christian Elsässer, FhI Freiburg; Elvira Fortunato, Universidade Nova de Lisboa; Zbigniew Galazka, Leibniz-Institut für Kristallzüchtung, Berlin; Kee Hoon Kim, Seoul National University; Stephan Lany, NREL, Golden; David Look, Wright State University; Louis F. Piper, Binghamton University/SUNY; Bernd Szyszka, TU Berlin; John F. Wager, Oregon State University.

The TCO2014 conference focused on various aspects of current research on functional oxides, in particular the theory of oxide electronic materials, growth of bulk

semiconducting oxides, amorphous oxide thin films, metal-like n-type TCOs, p-type oxides, point defects in oxides, and oxide devices. The scientific program was anchored around invited talks from nine colleagues from abroad (US, Korea, New Zealand, UK, Portugal) and seven domestic speakers. Over a hundred participants followed the program of which major contributions are reported in the following papers. The presentations and the poster session provided a stimulating atmosphere for discussion and starting new collaborations. Also the guided tour through and on top of the Leipzig City Hall remains a memorable experience.

The announced Young Scientist Awards motivated students to present their best work (oral or poster). The first Young Scientist Award was bestowed on Kevin Stewart (Oregon State University) for his work on transparent, amorphous thin film transistors. The second prize went to Daniel Splith (Universität Leipzig) for his investigation of gallium oxide based rectifiers. The third prize was shared between Christian Lidig (Otto-von-Guericke-Universität Magdeburg) and Zhipeng Zhang (Universität Leipzig) for work on the anisotropic dielectric function of tin oxide and wavelength selective UV photodetectors with lateral composition gradient, respectively.

The organizers are grateful to the colleagues serving on the committees for the scientific program and the Young Scientist Awards and for financial support to Deutsche Forschungsgemeinschaft (Gr1011/29-1), Leipzig Graduate School of Natural Sciences BuildMoNa and the Research Profile Area "Complex Matter" of Universität Leipzig.

9.4 Bipolar wide band-gap heterodiodes with high rectification

H. von Wenckstern, F.-L. Schein, R. Karsthof, P. Schlupp, M. Grundmann

Transparent semiconducting oxides find application in transparent electrodes for touch screens, displays or thin film solar cells, as channel layer in transparent electronics or as detectors and sensors. These wide band-gap oxides are typically unipolar and *pn*-diodes can only be realized within heterojunctions. Here, we present several approaches towards wide band-gap heterodiodes involving *n*-type crystalline ZnO (c-ZnO), *n*-type amorphous zinc-tin oxide (a-ZTO), *p*-type crystalline CuI (c-CuI, the only "non-oxide" layer discussed) and *p*-type, amorphous $ZnCo_2O_4$ (a-ZCO) or NiO (a-NiO). The oxide layers were grown by pulsed laser deposition at 650 °C for the case of c-ZnO otherwise at room temperature. The c-CuI was grown by thermal evaporation of CuI-powder; the substrate was not heated. If c-ZnO was used as *n*-type material, we used ZnO:Al as transparent back contact (cf. fig. 9.4a), else a front-front contact configuration was used as illustrated in fig. 9.4b). The series resistance is for diodes with c-ZnO as *n*-type part below 1 kΩ due to the highly conducting ZnO:Al back-electrode (BE). For heterodiodes comprising a-ZTO the series resistance is because of the different diode layout with 76 kΩ considerably higher.

In principle, all heterojunctions investigated have low leakage currents, however, the comparatively high series resistance of the a-ZCO/a-ZTO heterodiodes limits their rectification to values of about 5 orders of magnitude (cf. table 9.1). For the heterodiodes with BE the rectification is more than seven orders of magnitude for c-CuI/c-ZnO and higher than ten orders of magnitude for a-NiO/c-ZnO and a-ZCO/c-ZnO. For each diode

Table 9.1: Rectification, ideality factor η and series resistance R_s, obtained from room-temperature *IV* - characteristics of bipolar heterojunction diodes.

Materials	Rectification	ideality factor	Series resistance (Ω)
c-CuI/c-ZnO	4×10^7	1.5	200
a-ZCO/c-ZnO	2×10^{10}	2	970
a-NiO/c-ZnO	1×10^{10}	1.6	500
a-ZCO/a-ZTO	1×10^5	2	76,000

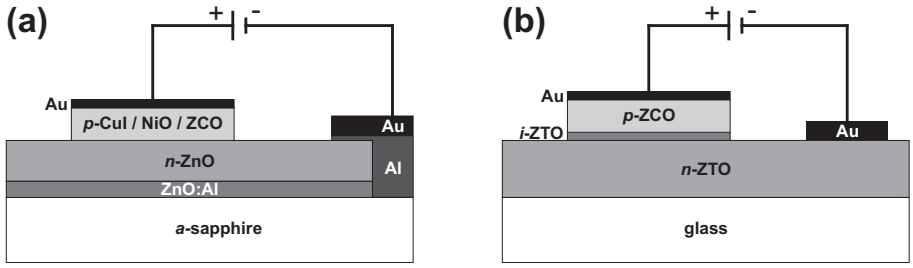

Figure 9.4: Schematic device layout for diodes comprising (a) c-ZnO and (b) a-ZTO.

type investigated, the rectification obtained defines the state of the art as illustrated in fig. 9.5 summarizing the literature on rectification of *pn*-diode for which at least one of the functional layers is an oxide. The diode with high rectification reported in 2007 was a p-NiO_x/n-TiO_y heterodiode with an ideality factor of 4.3 [2]. The ideality factor of our heterodiodes ranges from 1.5 to about 2 (cf. table 9.1).

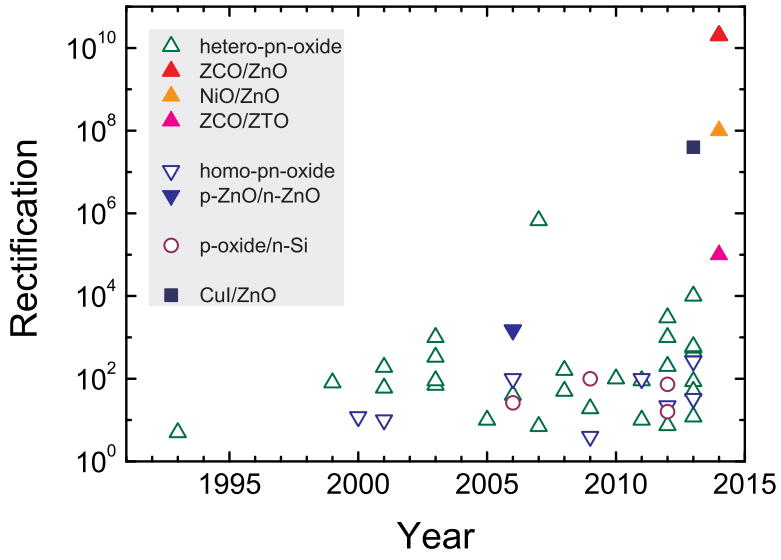

Figure 9.5: Historical development of the rectification of bipolar oxide diodes. Down triangles: homojunction diodes, up triangles: heterojunction diodes, circles: *p*-oxide/*n*-Si heterojunction diodes, full markers: results from Leipzig Semiconductor Physics Group. Data from ref. [1] and references therein.

So far, the a-ZCO/c-ZnO and a-NiO/c-ZnO diodes exhibit highest rectification; the

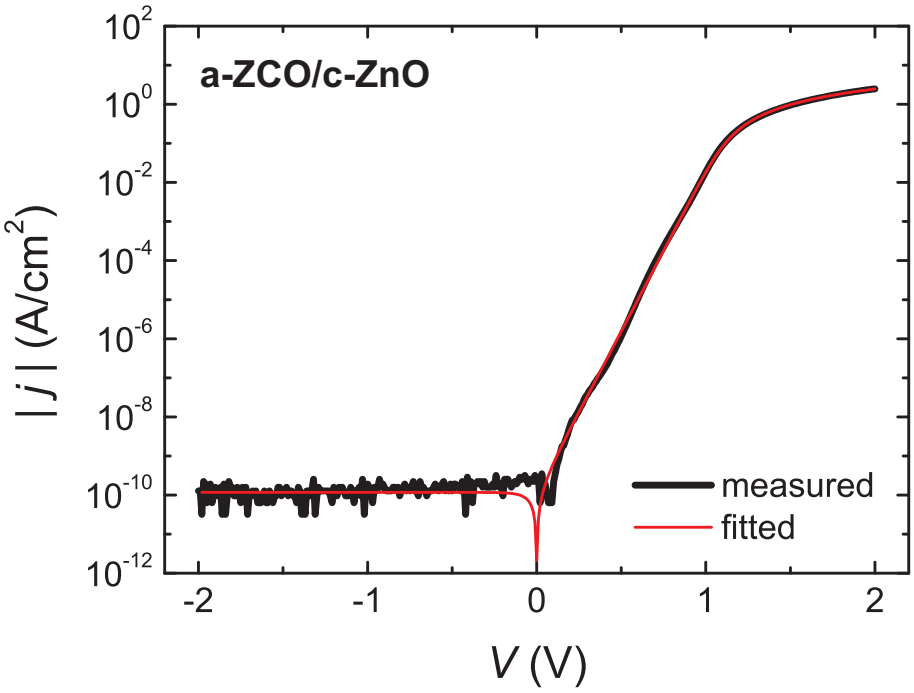

Figure 9.6: Experimental (black) and fitted (red) j - V characteristic of ZCO/ZnO diode with highest rectification.

room temperature current density-voltage characteristic of the best a-ZCO/c-ZnO diode is depicted in fig. 9.6. The reverse current density is with 10^{-10} A/cm^2 within the noise floor of measuring unit. The ideality factor of the diode is 2 as expected for type-II heterojunction diodes [3].

In summary we fabricated wide band-gap heterodiodes with very high rectification on crystalline and amorphous layers. The devices demonstrated define the state-of-the art for both heterodiodes with crystalline or amorphous *n*-type oxide layer.

[1] M. Grundmann, F.L. Schein, R. Karsthof, P. Schlupp, H. von Wenckstern, Adv. Sci. Technol. **93**, 252 (2014)
[2] M.-J. Lee, S. Seo, D.-C. Kim, S.-E. Ahn, D.-C. Seo, I.-K. Yoo, I.-G. Baek, D.-S. Kim, I.-S. Byun, S.-H. Kim, I.-R. Hwang, J.-S. Kim, S.-H. Jeon, B.-H. Park, Adv. Mater. **19**, 73 (2007)
[3] M. Grundmann, R. Karsthof, H. von Wenckstern, ACS Appl. Mat. & Interf. **6**, 14785 (2014)

9.5 Investigation of highly rectifying fully amorphous pn-heterojunction diodes.

P. Schlupp, F.-L. Schein, H. von Wenckstern, M. Grundmann

Room-temperature (RT) fabrication of semiconducting thin films is cost-efficient and allows the use of thermally unstable but flexible substrates. Due to their electronic

structure, oxide compounds of indium, gallium, zinc and tin show high electron mobility even in the amorphous state [1]. The most prominent candidate which is already exploited as channel layer material for transistors in pixel drivers of flat panel displays is gallium indium zinc oxide [2] However, indium and gallium are rare and have an unsure supply. Zinc tin oxide (ZTO) is a promising indium-free alternative [3, 4]. Beside *n*-type semiconducting films also *p*-type films are neccessary for active bipolar devices. Zinc cobalt oxide (ZCO) is one the few *p*-type oxides for which bipolar heterodiodes have already been demonstrated [5]. Here, we discuss electrical properties of all amorphous n-ZTO/p-ZCO heterojunction diodes fabricated entirely at RT.
The oxide thin films were grown by pulsed laser deposition at room-temperature and an 0.03 mbar oxygen atmosphere. To enhance the rectification of the diodes, an ultrathin semi-insulating ZTO layer was introduced at the heterointerface. Figure 9.7 depicts the temperature-dependent *jU*-characteristics of (a) a *pn*-diode and (b) a *pin*-diode from room temperature to 100°C. They were modeled using the Shockley equation.

$$j = \frac{I_0}{A}\left[\exp\left(e\frac{U - R_s I}{\eta k_B T}\right) - 1\right] + \frac{U - R_s I}{A R_p} + \frac{I_C}{A}. \tag{9.1}$$

A is the contact area, R_s is the series resistance, R_p is the parallel resistance, η is the ideality factor, k_B is the Boltzmann constant and T the absolute temperature. The current rectifications obtained at RT j(1.5V)/j(-1.5V) are about 5×10^4 for the *pn*-diodes and 1.1×10^6 for the *pin*-diodes, respectively. Since the leakage current of the *pn*-diodes

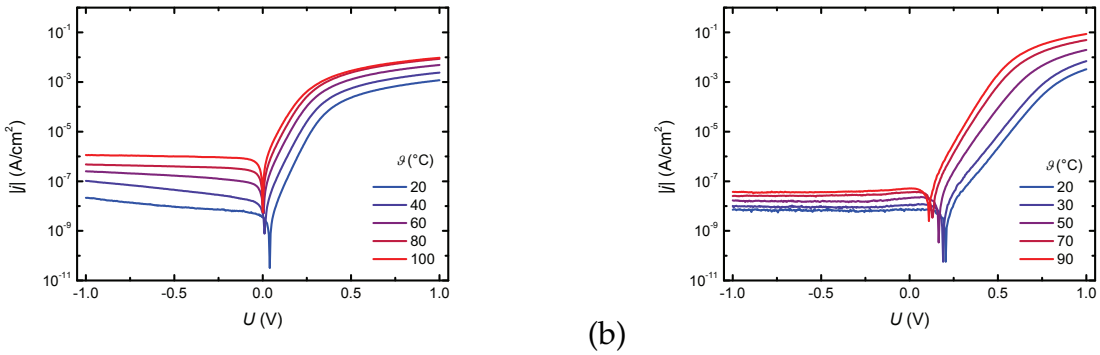

Figure 9.7: Temperature dependent *jU*-characteristics of a) a *pn*-diode and b) a *pin*-diode having an intrinsic insulating layer of about 5-10 nm at the heterointerface.

increases only slightly and less than the forward current with the temperature, the rectification is higher at elevated temperatures. The opposite holds true for the *pn*-diodes. The ideality factor of the *pn*-diode changes only slightly, from 1.27 to 1.17 with increasing temperature. In comparison to that it decreases from 2.0 to below 1.2 with increasing temperature for the *pin*-diodes. We assume that this higher ideality factor obtained at room temperature is due to more interface trap states caused by the intrinsic insulating ZTO layer and a broader distribution of the barrier which can be overcome by charge carriers more easily at higher temperatures [6].
The work was supported by the ESF(SAB 100124929) and Leipzig School of Natural Science (BuildMoNa).

[1] H. Hosono, N. Kikuchi, N. Ueda, H. Kawazoe: J. Non-Cryst. Solids. **198-200**, 165 (1996)
[2] J.-S. Park, H. Kim, I.-D. Kim: J. Electroceram. **32**, 117 (2014)
[3] M. K. Yajaraj, K. J. Saji, K. Nomura, T. Kamiya, H. Hosono: J. Vac. Sci. Technol. B **26**, 495 (2008)
[4] P. Schlupp, H. von Wenckstern, M. Grundmann: Mater. Res. Soc. Symp. Proc. **1633**, 101 (2014)
[5] F.-L. Schein, M. Winter, T. Böntgen, H. v. Wenckstern, M. Grundmann: Appl. Phys. Lett. **104**, 022104 (2014)
[6] P. Schlupp, F.-L. Schein,H. von Wenckstern,M. Grundmann: Adv. Electron. Mater. **1**, 1400023 (2015)

9.6 Current collection efficiency of semi-transparent ZnO/NiO UV solar cells

R. Karsthof, H. von Wenckstern, M. Grundmann

Transparent photovoltaic cells open new fields of application for solar energy conversion, e.g. as 'photovoltaic windows' transmitting the entire visible spectral range of the solar radiation and, at the same time, converting the energy of UV and IR photons into electrical energy as efficiently as possible. On the other hand, especially a UV-active device could also be employed to boost the efficiency of conventional solar cell technologies when applied as UV-enhancing partner in a tandem structure.

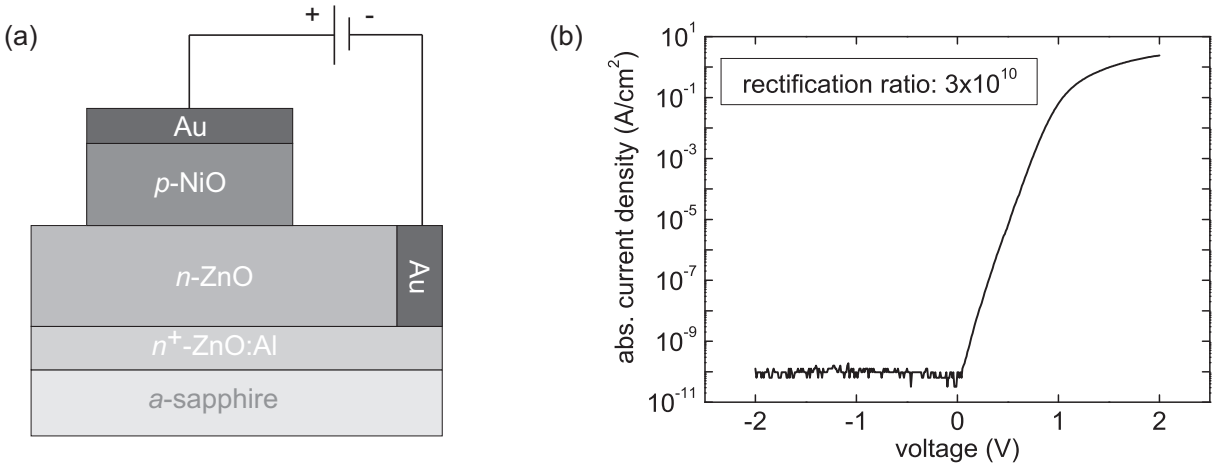

Figure 9.8: (a) schematic front view of sample structure, (b) jV characteristics of p-NiO/n-ZnO heterojunction diodes under dark conditions in log scale.

In this work we focused on the fabrication of UV-active solar cells based on p-NiO/n-ZnO heterojunctions. All oxide layers were grown by pulsed laser deposition (PLD). The nominally undoped ZnO absorber layer was grown on top of a-plane sapphire substrates with a highly Al-doped ZnO layer beneath which serves as transparent back contact. During this step the substrate temperature was kept at 670 ℃. Afterwards, we grew p-type NiO at room temperature (no intentional substrate heating) on top, and

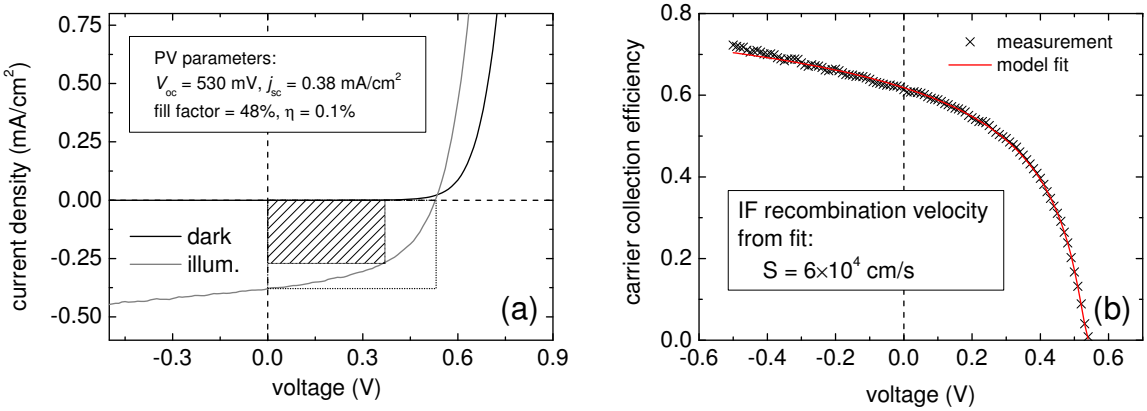

Figure 9.9: (a) comparison of jV characteristics in dark and under illumination and PV parameters, (b) charge carrier collection efficiency and respective fit

covered it with a 6 nm thin gold 'current-spreading layer' deposited by DC magnetron sputtering. Using standard UV photolithography, NiO/Au contacts with a circular shape were produced, enabling the characterization of individual sub-mm^2 cells. The average transmittance of the complete cell stack is around 50 % in the visible range (380 − 780 nm), dominated by absorption in the NiO layer. We have shown by X-ray diffraction measurements that the NiO films are X-ray amorphous, possibly causing strong band tails and thereby optical absorption in the visible spectral range.

Electrical characterization was carried out by means of current-voltage measurements under dark conditions and under illumination with a Xe lamp simulating solar radiation. In dark, the contacts show highly rectifying behavior with recification ratios of up to 10 orders of magnitude and above (see Fig. 9.8(b)). Upon illumination, open-circuit voltages of around 500 mV and short-circuit current densities of 0.4 mA/cm^2 have been measured. The fill factors of our devices were very low (only around 50 %), leading to conversion efficiencies of approximately 0.1 %. It is obvious that the absorption of light strongly deforms the current-voltage characteristics (Fig. 9.8(b)), leading to a strong voltage dependence of the current density in photovoltaic mode and thereby resulting in low fill factors.

To investigate the reasons for this behavior, we conducted an analysis of the collection efficiency of photo-generated charge carriers which can be responsible for a voltage dependence of the current under illumination. This was done by measuring jV characteristics at different levels of illumination; the details of the measurement principle can be read in the literature [1, 2]. We were able to fit our collection efficiency data with a model including recombination losses at the NiO/ZnO interface and within the depleted region of the junction (data and fit are shown in Fig. 9.9), and we conclude that the main reason for the observed deformation of the jV characteristics is fast recombination at the junction interface (recombination velocities of around $6x \times 10^4$ cm/s). To improve device performance, engineering of the interface properties is neccessary, e.g. by reduction of the interface defect density or by an optimization of the band alignment.

[1] K.W. Mitchell, A.L. Fahrenbruch, R.H. Bube, J. Appl. Phys. **48**, 4365 (1977)
[2] S. Hegedus, D. Desai, C. Thompson, Prog. Photovolt.: Res. Appl. **15**, 587 (2007)

9.7 Junction field-effect transistors based on NiO/ZnO heterojunctions

R. Karsthof, H. von Wenckstern, M. Grundmann

When compared to devices based on metal-insulator-semiconductor (MIS) or metal-semiconductor (MES) structures, junction field-effect transistors (JFETs) have advantages in certain fields of application. On one hand, in contrast to MISFETs, due to the absence of an insulating layer, high operating frequencies are possible. On the other hand, especially in the case of all-oxide devices, good performance also at elevated temperatures can be expected whereas ZnO-based MESFETs typically degrade when exposed to heat. Furthermore, the usage of large-band gap materials enables the fabrication of devices which are transparent for visible light. In our group, all-oxide JFETs based on *p*-$ZnCo_2O_4$(ZCO)/*n*-ZnO heterojunctions have already been demonstrated [1]. However, due to the band gap energy of ZCO being in the visible range, such devices are essentially opaque. For this reason we chose NiO as gate material. Due to its large band gap of around 3.7 eV, this material can in principle have high optical transmittance in the visible range.

All oxide layers of the device were grown by means of pulsed laser deposition. In all steps, UV photolithography was used to pattern the respective layers. First, a 20 nm thick ZnO layer was deposited on *a*-plane oriented sapphire substrate from which mesa structures were then produced by wet chemical etching in dilute phosphoric acid. These structures were used as channels. Next, source and drain contacts were grown from Ga-doped ZnO (4 at. % Ga) and the gate contact from NiO, in both cases at room temperature. Again, source, drain and gate contacts were finally covered with a 6 nm thick Au current-spreading layer (structure schematically shown in Fig. 9.10(a)).

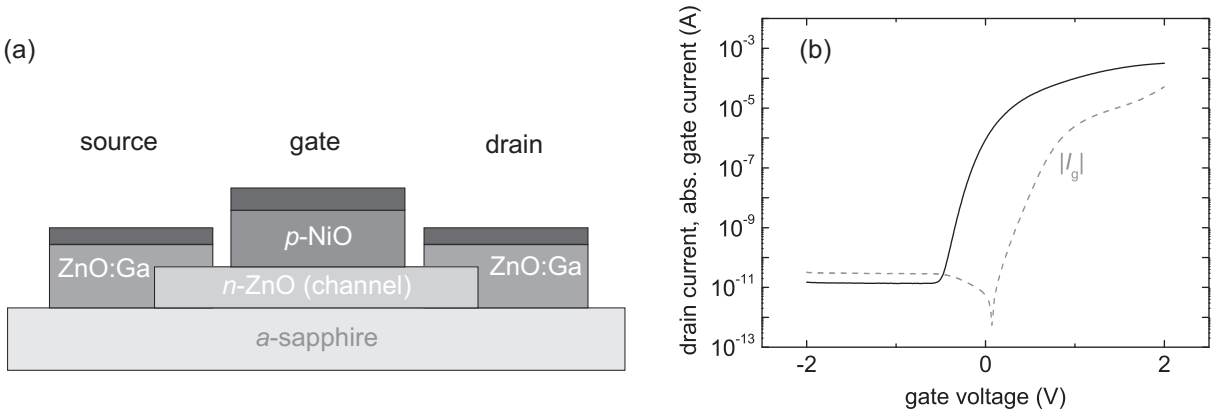

Figure 9.10: (a) schematic front view of transistor structure, (b) transfer characteristic and gate current of a selected device, measured at a drain voltage of 2 V

In Fig. 9.10(b) the transfer characteristic of the best device is shown. The typical current on/off-ratio was around 1×10^7 at ±2 V. Channel mobilities were approximately 4 cm^2/Vs and thus slightly lower than the values reported for our devices with ZCO gates. The best device showed a sub-threshold slope of 65 mV/dec which is only slightly above the theoretical minimum of 60 mV/dec. For the mentioned channel thickness of

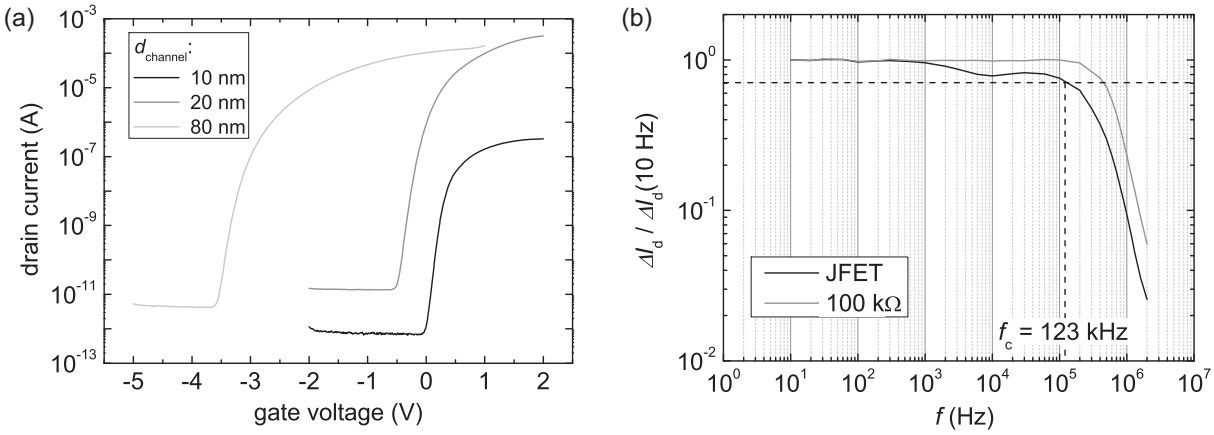

Figure 9.11: (a) transfer characteristics of devices with varying channel thickness, (b) drain current in dependence of gate operating frequency ('gate lag') and frequency response of a 100 kΩ resistor

20 nm, the on-voltage was around −0.5 V; by varying the thickness between 10 and 80 nm we could shift this value between approximately 0 V and −3.5 V (see Fig. 9.11(a)).

To check the high-frequency switching behavior of our transistors we investigated the so-called gate lag effect – i.e. the drain current was measured at a fixed drain voltage of 2 V while a sinusoidal signal of variable frequency was applied at the gate, quickly switching between the on- and off-state of the transistor. The frequency dependence of the drain current between 10 Hz and 20 MHz is shown in Fig. 9.11(b), together with the frequency response of the used amplifying circuit. A cutoff frequency of 123 kHz was determined for this device. We also investigated the temperature stability of the transistors in a range beween 10 °C and 100 °C, and we could show that the devices are thermally stable in this temperature regime with regard to their transfer characterstics: even though a slight increase of the off-current was observed, full operationality is conserved at elevated temperatures, and the occurring changes were shown to be almost completely reversible after room temperature was restored.

[1] F.-L. Schein, H. von Wenckstern, H. Frenzel, M. Grundmann, IEEE Electron. Device Letters **33**, 676 (2014)

9.8 Inverters based on ZnO JFETs with $ZnCo_2O_4$ gates

F.J. Klüpfel, A. Holtz, F.-L. Schein, H. von Wenckstern, M. Grundmann

Devices based on oxide semiconductors have received strong attention of the scientific community in recent years. Most reports on oxide based field-effect transistors (FETs) focus on metal-semiconductor-insulator FETs (MISFETs), which are the most common FET type in modern silicon technology. However, other FET types like metal-semiconductor FETs (MESFETs) and junction FETs (JFETs) have conceptual advantages concerning noise and switching speed. The fabrication of ZnO based MESFETs and JFETs has been presented by our group [1]. Also the realization of inverters using metal-semicondonductor FETs (MESFETs) has been reported [2].

Recently we demonstrated the fabrication of the first oxide based inverter using junction field-effect transistors (JFETs). We used *n*-type ZnO as channel material and *p*-type $ZnCo_2O_4$ (ZCO) as gate material. The devices were fabricated on *a*-plane sapphire, using pulsed laser deposition (PLD) at 650°C for the crystalline ZnO channels and PLD at room temperature for the amorphous ZCO layers.

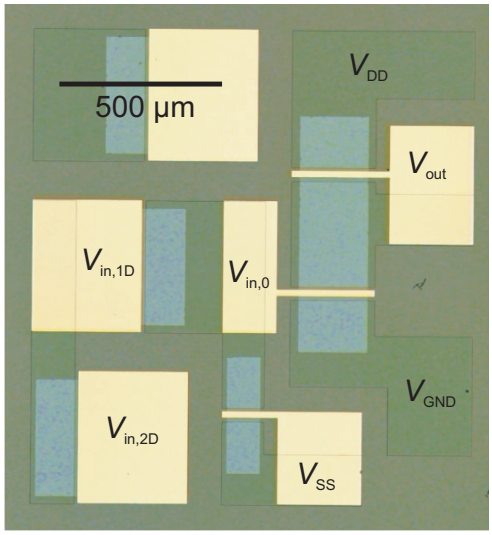

Figure 9.12: Microscope image of a full inverter. The blue areas are overlaps between ZnO channels and ohmic GaZnO contacts, the yellow areas consist of ZCO with Au capping.

Fig. 9.12 shows a microscope image of the inverter circuit. The operation voltage V_{DD} was between 1 V and 3 V and the pull-down voltage V_{SS} was fixed at -2 V. The input voltage can be applied at three different contacts, denoted $V_{in,0}$, $V_{in,1}$, and $V_{in,2}$ in Fig. 9.12. $V_{in,0}$ applies the input directly at the actual inverter circuit, while the voltage is shifted by 0.4 V and 0.9 V to more negative values for $V_{in,1}$ and $V_{in,2}$, respectively. The shift is realized by the voltage drop across one or two *p*-ZCO/*n*-ZnO heterodiodes.

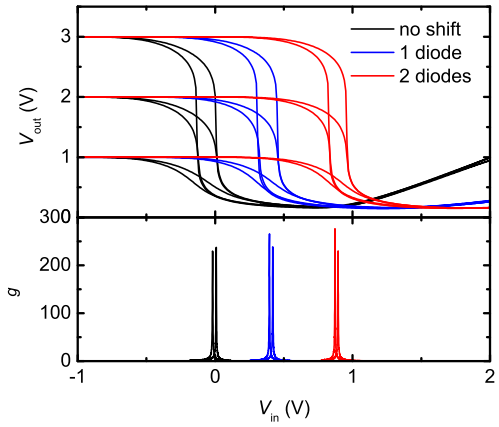

Figure 9.13: VTC of a full inverter based on ZnO channels with ZCO gates, shown for V_{DD} of 1 V, 2 V, and 3 V. Presented below is the gain of the device for V_{DD} = 3 V.

The resulting voltage transfer characteristics (VTC) are presented in Fig. 9.13. An important figure of merit is the gain of the inverters, which is calculated by

$g = -\partial V_{out}/\partial V_{in}$. For V_{DD} = 3 V the presented device has a gain of nearly 280, which is a record value for oxide semiconductor based inverters. It was shown theoretically, that the high gain is due to excellent current saturation of the JFETs for gate voltages around 0 V. To evaluate the usability of such inverters in logic circuits, the uncertainty range V_{uc} and the noise margins NM_H and NM_L were calculated. These quantities are derived from the points of the VTC, were the slope equals -1 (see e.g. [3]). A low uncertainty range indicates, that the two logic states of the inverter are well separated, and low voltages are sufficient to switch between these states. The noise margins are ideally equal to $V_{DD}/2$, and give a measure on how well the input voltage range matches the output voltage range. For the device presented in Fig. 9.13 we obtain V_{uc} = 0.35 V, NM_H = 1.85 V, and NM_L = 0.3 V at V_{DD} = 3 V. The uncertainty range is among the lowest values reported for oxide based devices. NM_H is close to the ideal value, while NM_L is comparably small. This reflects, that the input voltage shift with two diodes is not sufficient for V_{DD} = 3 V and should be increased. Nevertheless, the positive values demonstrate that the devices are suitable for logic circuits.

[1] Klüpfel *et al.*, IEEE Transactions on Electron Devices, **60**, 1828 (2013)
[2] Frenzel *et al.*, Applied Physics Letters, **96**, 113502 (2010)
[3] Heineck *et al.*, IEEE Electron Device Letters, **30**, 514 (2009)

9.9 Electrical and optical properties of long-throw magnetron sputtered zinc oxynitride thin films

A. Reinhardt, H. Frenzel, H. von Wenckstern, M. Grundmann

We have deposited zinc oxynitride (ZnON) thin films on glass substrates using a long-throw magnetron sputtering system. The large distance between target and substrate of about 25 cm assures droplet-free thin film growth resulting in smooth surfaces and thickness uniformity. The thin films were radio-frequency sputtered at room temperature from a metallic zinc target (purity: 99.99 %) in a reactive atmosphere consisting of Ar (gas flow: 10 sccm), N_2 (gas flow: 100 sccm) and O_2 (gas flow: 1 – 4 sccm). In order to obtain amorphous, semiconducting ZnON thin films the oxygen partial pressure was varied by adjusting the O_2:N_2 ratio as well as the total gas pressure in the range between 10^{-3} and 10^{-2} mbar.

Atomic force microscopy was used to investigate the surface morphology showing that all thin films have a very smooth surface with root-mean-square roughnesses ranging from 0.4 to 1.1 nm depending on deposition pressure. In order to determine the electrical properties of as-deposited films Hall effect measurements were performed at room temperature using the four-point probe van der Pauw technique. At a total gas pressure of 4×10^{-3} mbar in the sputtering chamber and a O_2:N_2 ratio of 1:100 we obtained n-type semiconducting thin films with carrier concentrations of about 10^{18} cm^{-3} and Hall mobilities up to 25 cm^2/Vs. At higher O_2:N_2 ratios the films become transparent and insulating with resistivities larger than 10^4 Ωcm. Therefore, at a constant O_2:N_2 ratio of 1:100 the deposition pressure was varied. With increasing pressure the resistivity increases as depicted in Fig. 9.14 (c). The structure of the thin films was determined

by means of X-ray diffraction that confirmed the formation of a ZnO phase at higher pressures as well as larger O_2:N_2 ratios leading to insulating films. However, the semiconducting thin films are X-ray amorphous as desired (see Fig. 9.14 (b)). Furthermore, Hall effect measurements revealed decreasing electron concentrations with increasing deposition pressure for the amorphous n-type semiconducting thin films with electron mobilities of $20-25\,cm^2/Vs$ (cf. Fig. 9.14 (d)). Fig. 9.14 (a) depicts the transmittance spectra of the films measured with a double-beam spectrometer. It turns out that the higher the deposition pressure the higher is the transparency of the films in accordance with the formation of ZnO. For the amorphous and semiconducting thin films an enhanced absorption of light in the entire visible spectral range is observed with an average transmittance around 50 %. The optical band gaps were estimated from the Tauc model. For the insulating thin films band gaps around 3.3 eV were determined which is comparable with the value for polycrystalline ZnO. The amorphous thin films revealed a strongly reduced band gap of 1.3 eV. This decrease in band gap value is properly due to the formation of Zn-N bonds which have smaller ionicity than Zn-O bonds.

In conclusion, by adjusting the O_2 flow rate and the deposition pressure we are able to deposit amorphous high-mobility ZnON thin films which are promising to realize high-performance thin-film transistors.

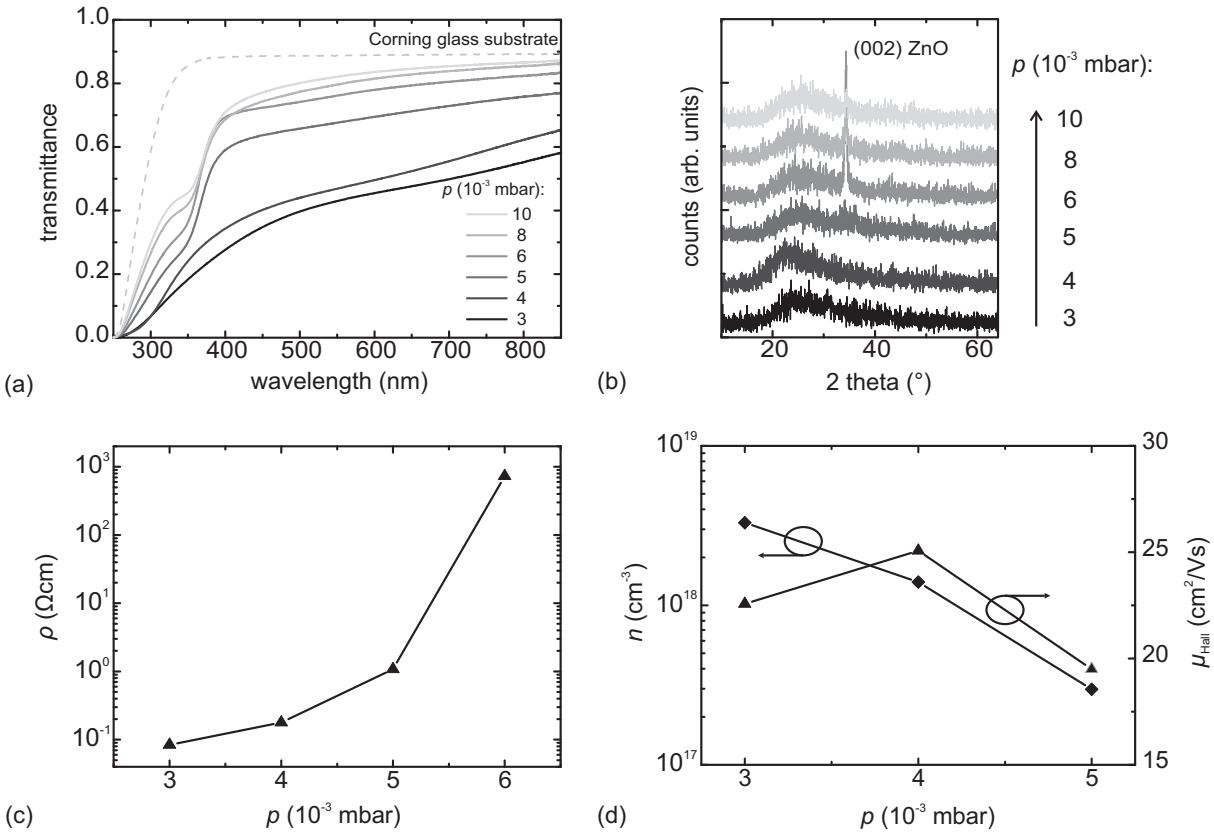

Figure 9.14: (a) Optical transmittance spectra, (b) X-ray diffraction pattern, (c) Resistivity and (d) Electron concentration and Hall mobility of ZnON thin films deposited at room temperature.

9.10 Long-throw magnetron sputtering of amorphous Zn-Sn-O-thin films at room temperature

H. Frenzel, T. Dörfler, P. Schlupp, H. von Wenckstern, M. Grundmann

We report on the fabrication of amorphous zinc tin oxide (ZTO) thin films by long-throw magnetron sputtering on glass substrate. In this growth technique, the distance between target and substrate is increased, such that only sputtered particles along the paraxial directions are deposited on the substrate. Droplets and other particles due to erosion of the target are naturally filtered by collisions with other particles during their movement to the substrate. With that, the thickness uniformity and surface roughness of thin films can be significantly improved however for the cost of a lower growth rate. In addition, energetic particles created in the discharge process can be completely thermalized by collisions and reach the substrate by diffusion. Film damages caused by bombardment of sputtered particles and negative ions as well as unintentional heating from the plasma can be reduced.

The ZTO thin films were deposited with a target-substrate distance of 25 cm. In the first approach, thin films were sputtered from a single ZTO-target (33 wt-% ZnO, 67 wt-% SnO_2) with a purity of 99.99 % and diameter 2 inch. Second, co-sputtering was performed from a SnO_2-target (99.9 % purity) and a ZnO-target (99.9 % purity). All films were fabricated using argon atmosphere only and at room temperature with no additional annealing.

In Fig. 9.15 a the resistivity of ZTO thin films is depicted, that were grown from a single target under different Ar working pressures. The resistivity revealed a narrow range for the total pressure between 0.2 and 0.3 Pa, where ZTO is n-type semiconducting with resistivity as low as 1.65×10^{-2} Ωm. In the semiconducting regime, Hall-effect measurements showed clearly a negative Hall coefficient. In this regime, the free charge carrier density was between 4×10^{17} and 1×10^{18} cm^{-3} and the mobility was between 2 and 6 cm^2/Vs. Outside of this range, the resistivity increases to values higher than 10^2 Ωm. There, the Hall coefficient showed alternating signs, i.e. the charge carrier density and mobility could not be analyzed. A similar pressure dependence has been previously observed for the growth of amorphous ZTO [1, 2]. However, the used method in these reports was pulsed-laser deposition and the conductivity window appeared at ten times higher pressures of oxygen. Furthermore, the lowest resistivities were in the range of 10^{-4} Ωm.

In order to further decrease the thin film's resistivity, a dc substrate voltage between −150 V and +600 V was applied at the Ar pressure of 0.22 Pa (Fig. 9.15 b). The resistivity is heavily dependent on the applied substrate voltage. It decreases for negative voltages by another order of magnitute to the lowest value of 2.4×10^{-3} Ωm, whereas for positive voltages the ZTO thin film is as resistive as for higher Ar pressures. This can be explained by the differently charged species in the plasma. For negative voltages, negatively charged O^{2-}-ions are repelled from the substrate and positively charged metal ions (Zn^{2+}, Sn^{4+}) are attracted to the substrate. The rate of incorporated differently charged zinc and tin ions should also be different. Thus, the ratio between oxygen and metal species and different metal species incorporated into the thin film is changed. Energy dispersive X-ray spectroscopy (EDX) revealed, that the amount of zinc and tin within the thin film is ideally stoichiometric for the sample with −150 V substrate voltage, i.e.

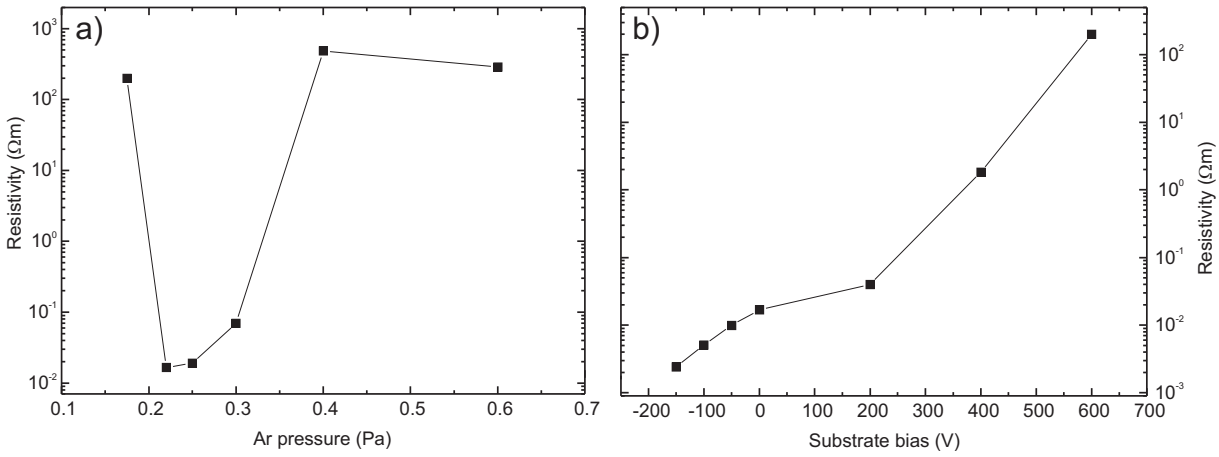

Figure 9.15: Resistivity of ZTO thin films grown from a single target in dependence of a) the working pressure and b) applied substrate bias at a working pressure of 0.22 Pa.

67 wt-% tin and 33 wt-% zinc.

The growth rate can be increased by co-sputtering from multiple targets. A power series has been performed with a constant power of 75 W for the ZnO-target and varying power for the SnO_2-target. The ZTO resistivity decreases with decreasing SnO_2 power, having a minimum at 35 W. From EDX measurements, the zinc amount of 32 wt-% and tin amount of 68 wt-% correspond well with the ideal values of 33 and 67 wt-%.

All ZTO films were found to be X-ray amorphous and showed atomically flat surfaces with rms roughnesses between 0.3 and 0.4 nm. The mean transmittance for a 30 nm thick film was 90 % in the VIS. These properties make the amorphous ZTO thin films suitable for low-cost, room-temperature fabrication of channel layers for transparent thin film transistors.

[1] P. Schlupp, H. von Wenckstern, and M. Grundmann, Proc. Mat. Res. Soc. **1633**, 101 (2014).
[2] M. K. Jayaraj, K. J. Saji, K. Nomura, T. Kamiya, and H. Hosono, Journal of Vacuum Science & Technology B **26**(2), 495 (2008).

9.11 Rectifying contacts on In_2O_3

D. Splith, H. von Wenckstern, F. Schmidt, M. Grundmann

Highly tin doped In_2O_3 is a material well know for its application as transparent conducting oxide used as an electrode in thin film solar cells, displays or as a contact layer in touch screens. However, the interest in the semiconducting properties of nominally undoped or only slightly doped crystalline In_2O_3 thin films or bulk crystals arose for fundamental reasons as well as for potential application in transparent electronic devices. For both of those, the fabrication of rectifying contacts which create a space charge region in the In_2O_3 is helpful or even necessary. With the use of a space charge region, defect spectroscopic measurements like capacitance voltage measurements, thermal admittance spectroscopy or deep level transient spectroscopy can be

applied to the material in order to characterize electronic defects in the material. On the other hand, contacts that create a space charge region are also needed in order to build active electronic devices like diodes or field-effect transistors. The realization of such contacts on In_2O_3 is non-trivial since for In_2O_3 the branch point energy lies within the conduction band and therefore, In_2O_3 tends to form a surface electron accumulation layer (SEAL) [1]. However, ZnO also tends to form a SEAL, but rectifying contacts can be fabricated by different methods. We employed the same methods known from ZnO in order to create rectifying contacts on In_2O_3.

9.11.1 Fabrication of Schottky contacts

D. Splith, H. von Wenckstern, F. Schmidt, M. Grundmann, O. Bierwagen[*†], J.S. Speck[†]

[*]Paul Drude Institut für Festkörperelektronik, Hausvogteiplatz 5-7, 10117 Berlin, Germany
[†]Materials Department, University of California, Santa Barbara, California 93106, USA

In order to fabricate Schottky contacts (SCs) on ZnO, a reactive sputtering process is needed [2], since the oxygen plasma is capable of removing the SEAL [3]. Bierwagen *et al.* showed that an oxygen plasma is also capable of removing the SEAL on In_2O_3 [4]. Therefore we used a reactive sputtering process in order to fabricate SCs on In_2O_3 [5].

The In_2O_3 thin films were grown by plasma-assisted molecular beam epitaxy on (001)-oriented yttria-stabilized zirconia (YSZ) substrates. Nominally undoped thin films have a free carrier concentration of $1.9 \times 10^{17}\,\mathrm{cm}^{-3}$. By doping with Sn, the free carrier concentration is increased to $8.5 \times 10^{17}\,\mathrm{cm}^{-3}$, while doping with Mg leads to a decreasing to $1.6 \times 10^{17}\,\mathrm{cm}^{-3}$. For the SCs Au, Pd and Pt were reactively sputtered in an half oxygen, half argon atmosphere on a nominally undoped, a Sn-doped and a Mg-doped In_2O_3 thin film.

In Fig. 9.16 (a) the *j*-*V*-characteristics of the different metals on the Mg-doped thin film are shown. A rectification of more than 3 orders of magnitude is observed for the Pt-SCs. The Au and the Pd-SCs also show a clear rectifying behaviour. By fitting with the model of thermionic emission the effective barrier heights and the ideality factors can be determined. Barrier heights range between 0.45 and 0.65 eV with the highest barrier heights and lowest ideality factors achieved for Pt contacts. However, in reverse direction, the measured characteristic deviates from the model, due to a leakage current. Temperature dependent measurements on a Pt-SC show linear dependence of the effective barrier height on T^{-1} in accordance to model of thermionic emission over a Gaussian broadened barrier [6] with a mean barrier height of 1.13 eV and a standard deviation of 0.17 eV. However, barrier height is decreased after temperature ramping up to 150 °C. Further, first thermal admittance spectroscopy (TAS) measurements show a defect with an activation energy of 290 meV and a apparent capture cross section of $6 \times 10^{-15}\,\mathrm{cm}^2$ as well as a shallow defect between 25 and 30 meV.

9.11.2 Fabrication of *pn*-heterojunction contacts

D. Splith, H. von Wenckstern, S. Lanzinger, F. Schmidt, S. Müller, P. Schlupp, R. Karsthof, M. Grundmann

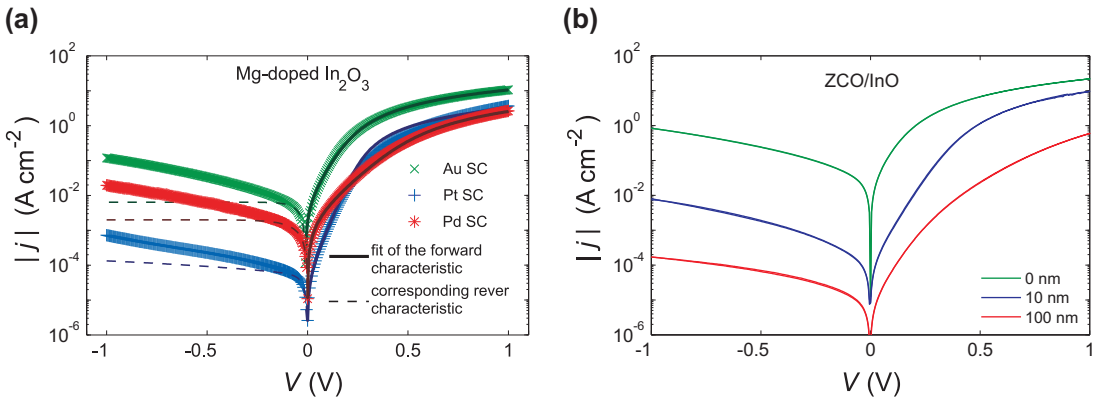

Figure 9.16: (a) *j-V* characteristics of reactively sputtered Au, Pt and Pd contacts on a Mg-doped In_2O_3 thin film. The *solid lines* shows the fit with the model of thermionic emission in forward direction, while the *dashed lines* show the corresponding reverse direction. (b) *j-V* characteristics of ZCO/In_2O_3 *pn*-heterojunctions for different thicknesses *d* of the Mg-doped In_2O_3 layer.

It was recently shown that *p*-type amorphous oxide semiconductors like $ZnCo_2O_4$ (ZCO) or NiO form rectifying *pn*-heterojunctions on ZnO [7]. We have shown that the same approach can be used in order to fabricate *pn*-heterojunctions on In_2O_3 [8].

The In_2O_3 thin films used in this study were grown by pulsed laser deposition (PLD) from a nominally undoped target on YSZ substrate. In order to reduce leakage currents, a Mg-doped thin film was grown on top of the undoped film. The thickness *d* of the Mg-doped layer was varied between 0, 10 and 100 nm. The contacts were fabricated by PLD of ZCO or NiO at room temperature. Here, only results for ZCO contacts will be discussed.

The *j-V* characteristics of ZCO contacts on the In_2O_3 thin film is shown in Fig. 9.16 (b) for different thicknesses *d* of the Mg-doped layer. Without the Mg-doped layer (d = 0 nm) the contacts show a rectification ratios between 10 and 50. By introducing the Mg-doped layer, the rectification of the heterojunctions can be increased to values larger than 3 orders of magnitude for both the 10 and the 100 nm thick Mg-doped layer. However, the series resistance of the contacts with the 100 nm thick Mg-doped layer is about an order of magnitude larger than for the other contacts, making this sample structure unsuited for further frequency dependent measurements due to the lower cut-off frequency. The ideality factors for d = 10 nm and d = 100 nm were determined using the Shockley equation and bunch around 2 as expected for a type-II heterojunction with interface recombination being dominant [9].

Capacitance-Voltage (CV) and TAS measurements were performed on a ZCO/In_2O_3 heterojunction with a 10 nm thick Mg-doped layer. The net doping profile calculated from the CV measurement shows a decrease of the net doping from 3×10^{18} cm^{-3} to 2×10^{18} cm^{-3} at a distance of about 10 nm due to the 10 nm thick Mg-doped layer. The TAS measurement revealed two defect levels at energies of 247 meV and 12 meV with apparent capture cross-sections of 2.2×10^{-14} cm^2 and 1.6×10^{-17} cm^2, respectively.

[1] P. King *et al.*, Phys. Rev. Lett. **101**, 116808 (2008)
[2] M. W. Allen *et al.*, Appl. Phys. Lett. **91**, 053512 (2007)
[3] B. J. Coppa *et al.*, J. Appl. Phys. **97**, 103517 (2005)
[4] O. Bierwagen *et al.* Appl. Phys. Lett. **98.17**, 172101 (2011)

[5] H. von Wenckstern *et al.* APL Mat. **2**, 046104 (2014)
[6] J. H. Werner and H. H. GÃ$\frac{1}{4}$ttler, J. Appl. Phys. **69**, 1522 (1991)
[7] M. Grundmann *et al.*, Adv. Sci. Technol. **93** (2014)
[8] H. von Wenckstern *et al.* Adv. Electron. Mater. (2015), DOI:10.1002/aelm.201400026
[9] M. Grundmann *et al.*, ACS Appl. Mater. Interfaces **6**, 14785 (2014)

9.12 Impact of strain on electronic defects in (Mg,Zn)O thin films

F. Schmidt, S. Müller, H. von Wenckstern, G. Benndorf, R. Pickenhain, M. Grundmann

Epitaxial strain strongly influences the material properties of thin film structures. In this study we report on a detailed investigation of the defect nature of (Mg,Zn)O thin films grown by by pulsed-laser deposition (PLD) on *a*-plane sapphire substrates [1]. The samples, having a thickness of approximately 1 μm, were grown using ceramic MgO/ZnO targets with admixtures of no, 0.10 wt.%, 0.25 wt.%, 1.00 wt.%, and 2.00 wt.% MgO. Prior to the ZnO layer, an about 200 nm thick aluminium doped (1 wt.%) ZnO (AZO) layer was deposited, which serves as ohmic back-contact and leads to low series resistance of the Schottky diode. The high Al-content within this functional layer leads to an increase of the *a*- and a decrease of the *c*-lattice constant compared to nominally undoped ZnO. The incorporation of Mg into the main layer leads to an increase of the fundamental bandgap and of the in-plane *a*-lattice. The Mg content in the thin films was estimated via low temperature photoluminescence (PL) by evaluating the bandgap shift determined from the energetic position of the I_6-line [3, 4]. Schottky contacts were realized by reactive dc-sputtering of PdO_y with a subsequent capping with metallic palladium [2].

In Fig. 9.17 we have compiled the PL data, please note the energy scale is shifted such that the I_6 transition lies at $E = 0$ eV for each Mg-content. This is done in order to allow direct comparison of PL features of the investigated samples. In this representation it is easily seen that the Y_0-line is present in all samples.

The structural defect-bound excitonic recombination Y_2 (Ref. [5]) is not present in samples with a Mg-content of $x \geq 0.8\%$. Brandt *et al.* showed that this line is connected to tensile strain in ZnO layers [6]. For the samples with a Mg-content of $x \leq 0.5\%$ and, of course, for binary ZnO the Y_2-line is clearly visible for the other samples with higher Mg-content it is not present. Relying on the fact that the appearance of the Y_2-line is connected to tensile strain in the layer and recalling that here the in-plane *a*-lattice constant increases in (Mg,Zn)O with increasing Mg-content we argue that the binary ZnO layer and the layers with a Mg-content up to 0.5% are under tensile strain. For Mg-contents of 0.8% and higher the in-plane *a*-lattice constant of the (Mg,Zn)O-layer is larger or equal to that of the ZnO:Al buffer layer [7].

The lattice constants were obtained by means of X-ray diffraction (XRD) using a PAN alytical X'Pert Pro diffractometer. The positions of the (00.2)- and (10.1)-reflexes were evaluated by fitting the data assuming Voigt profiles. The 2θ-ω scans are shown in Fig. 9.18, in which the fitted curves are shown as dashed solid lines, respectively.

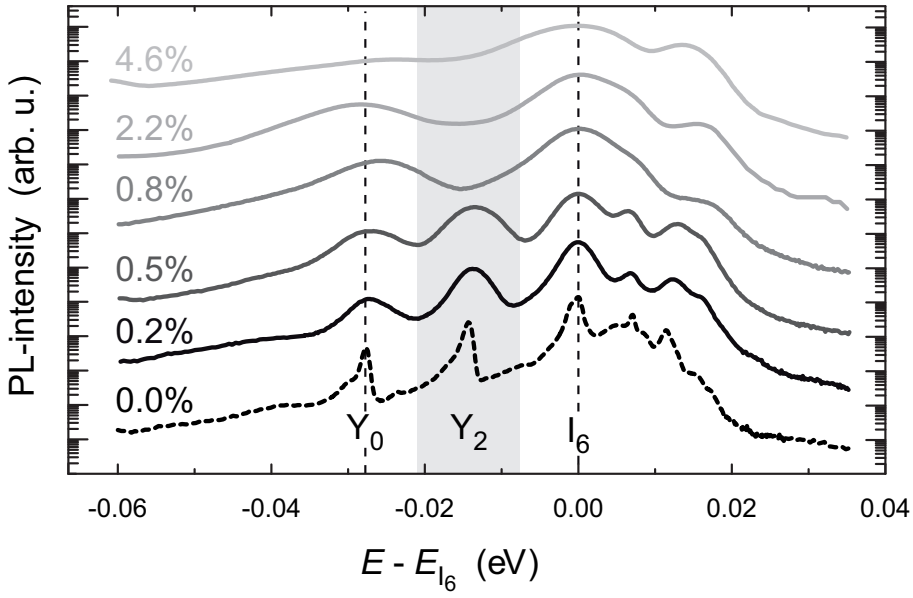

Figure 9.17: Low-temperature photoluminescence spectra (T = 2 K) of six (Mg,Zn)O alloys with $0 \leq x \leq 4.6\%$ as labeled grown on *a*-sapphire, respectively. The lines have been shifted for clarity in vertical and horizontal direction, as described in the text (adapted from Ref. [7]).

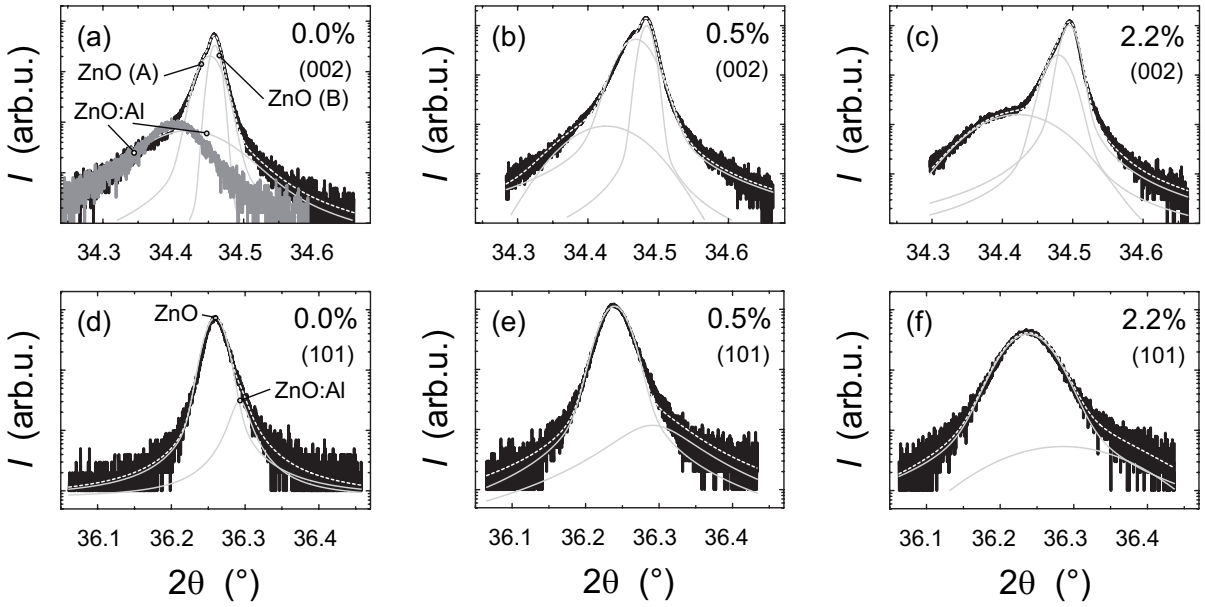

Figure 9.18: (a-c) scans of the (00.2)- and (d-f) (10.1)-reflex of three *c*-oriented (Mg,Zn)O alloys with x = 0, 0.5% and 2.2%. The dashed lines corresponds to fits of the data assuming Voigt-curves [7].

The (00.2)-peak of such a layer is shown for comparison in Fig. 9.18 (a) as a grey line and yields a *c*-axis lattice parameter of 5.2096 Å. The (10.1)-reflex is rather broad leading to a high inaccuracy in the *a*-lattice constant, which amounts to 3.2481 Å. The lineshape of the XRD peaks is asymmetric and reveals 3 contributions for the (00.2)-peaks and 2 underlying signals for the (10.1)-reflexes. The broad tail of the (00.2)-peak at lower angles is due to the AZO buffer layer, which is in accordance with the XRD

measurement of the 200 nm thick AZO reference sample (grey line in Fig. 9.18 (a)). This back-contact layer is also visible at higher 2θ-angles for the (10.1)-peaks, respectively. Furthermore, all (00.2)-peaks of the samples show a shoulder at lower angles.

The corresponding XRD-peak is labelled with "A", the main part of the signal with "B" in Fig. 9.18 (a). Since lower angles in the (00.2)-scan correspond to higher *c*-lattice constants, part A of the signal is related to a region A of the sample, which is more influenced by the underlying AZO buffer layer. Due to e.g. dislocations the strain is reduced in the (larger) region B, which is responsible for the lion's share of the XRD signal. This is the region probed by PL and by the space charge spectroscopic methods deep-level transient spectroscopy (DLTS), shown in the following section. The increase of the Mg-content in (Mg,Zn)O leads to an decrease of the *c*-lattice constant while the *a*-lattice constant increases.

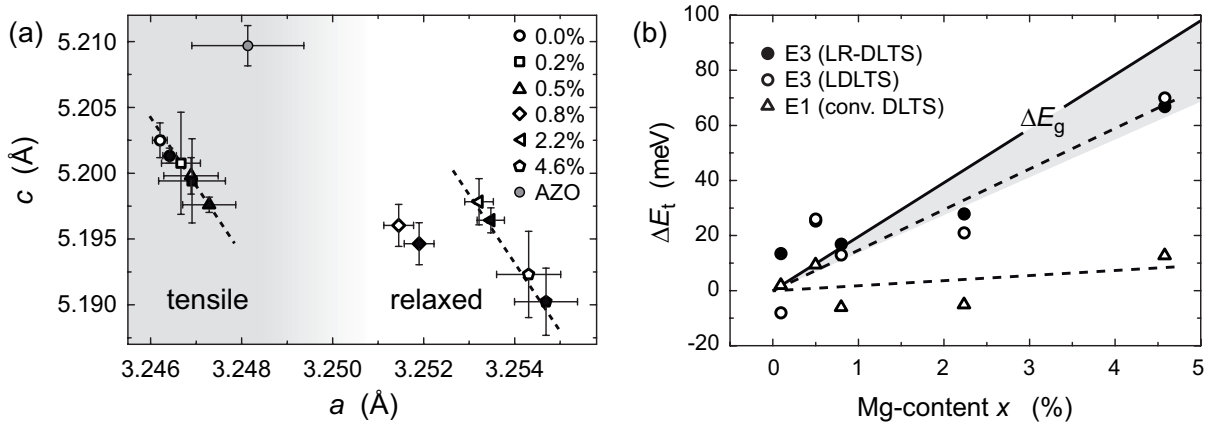

Figure 9.19: (a) *a*- and *c*-lattice constants of the *c*-(Mg,Zn)O thin films and an AZO buffer reference obtained from XRD scans as shown in Fig. 9.18. Open (solid) symbols represent the lattice constants steeming from region A (region B). (b) Change in thermal activation energy ΔE_t of the deep-levels E1 (triangles) and E3 (circles), respectively, over Mg content *x*. The data was obtained from LDLTS (open symbols) and LR-DLTS experiments (solid symbols). The shaded area represents the change of the conduction band-edge ΔE_c reported in the literature (adapted from Ref. [7]).

In Fig. 9.19 (a) the *a*- and *c*-lattice constants for all (Mg,Zn)O samples are compared. The open symbols represent lattice constants obtained from region A of the sample, while the solid markers show the corresponding constants obtained from region B. The *a*-lattice constant of the 200 nm thick AZO layer is higher compared to that of binary ZnO leading to tensile strain in those films. An increase of the Mg-content *x* reduces the tensile strain until the films grow unstrained on the AZO buffer, a further increase of *x* leads to relaxation of the thin films. From Fig. 9.19 (a) a change in the strain state can be expected between $0.5\% < x < 0.8\%$. Remarkably the samples with $0.0\% \leq x \leq 0.5\%$ and $x \geq 2.2\%$, i.e. before and after this transition, show the same slope in *a* over *c*, which is indicated by the dashed line in Fig. 9.19 (a). The observed values for the in- and out-of-plane lattice constants and the associated strain of the films are confirmed by the results obtained from the PL experiments, here the Y2-line is absent in samples which are not under tensile strain.

Electronic defects were studied by DLTS [9] in the temperature range from 10 K to 330 K using a helium flow cryostat. The DLTS scans are shown in Fig. 9.20 (a) with Mg-

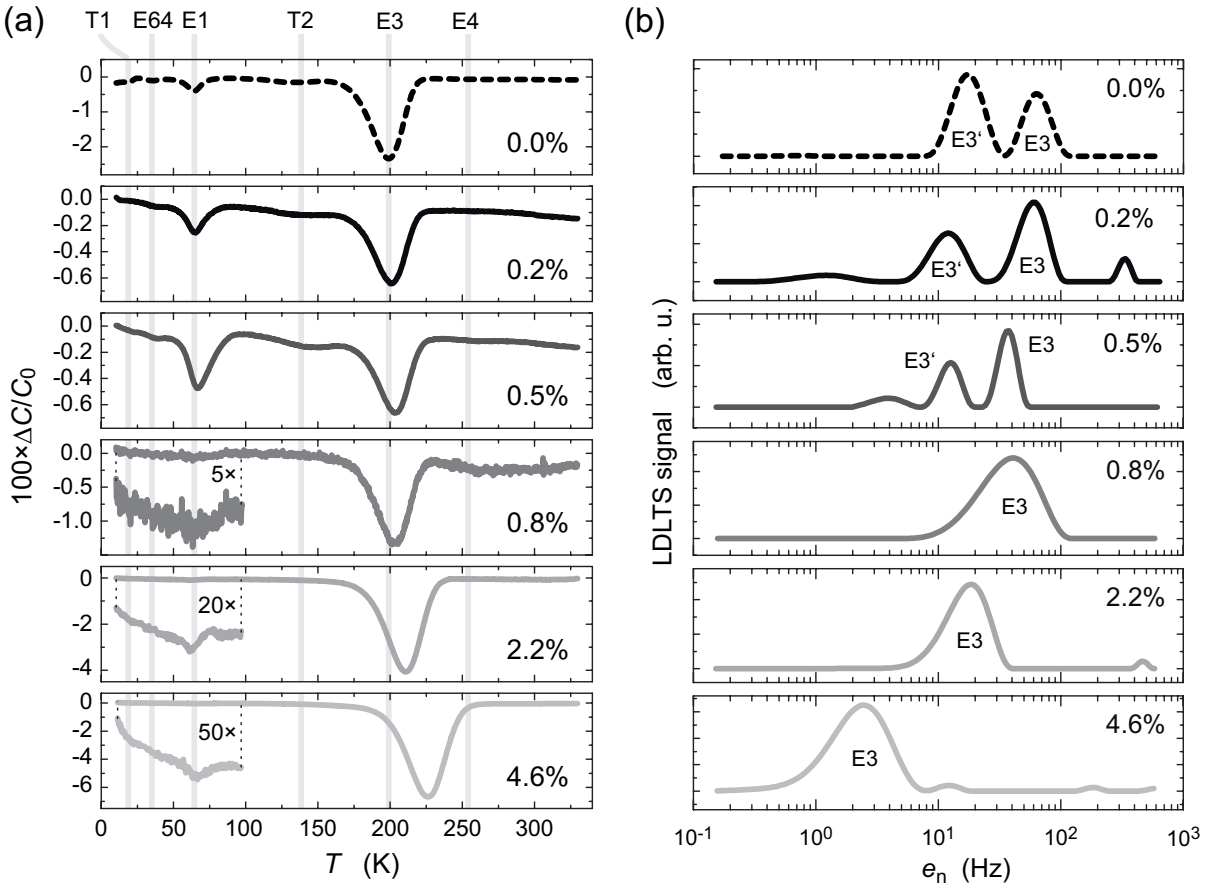

Figure 9.20: (a) DLTS scans of (Mg,Zn)O thin films with $0 \leq x \leq 4.6\%$ for a rate-window of 500 Hz. (b) LDLTS spectra of *c*-(Mg,Zn)O thin film samples, calculated from isothermal capacitance transients recorded at $T = 180$ K (adapted from Ref. [7]).

contents as labelled. For that a rate-window of 500Hz was applied. The measurements reveal peaks corresponding to deep levels commonly observed in PLD grown thin films, such as T1, E64, E1, T2, E3, E3' and E4. The defect E3 was detected in all samples and tends to increase with increasing Mg-content for samples with $x \geq 0.8\%$.

In as-grown ZnO thin films on AZO buffer a defect labeled E3' exists causing a DLTS signal in the vicinity of that of E3 [10, 11]. In order to investigate these defects unambiguously, a low-rate DLTS (LR-DLTS) setup was used in order to extend the applicable rate windows to the mHz regime [8]. Furthermore, high-resolution LDLTS was applied for all samples of this study. In Fig. 9.20 (b) LDLTS spectra calculated from isothermal capacitance transients recorded at $T = 180$ K are shown. It turns out that the signal of E3' is only detectable in samples with a Mg-content of $x \leq 0.5\%$, which are under tensile strain. It is absent in the relaxed (Mg,Zn)O samples with $x \geq 0.8\%$. The supposed idea of E3' beeing an extended defect goes along with the fact that it is only incorporated in tensile strained films grown on an AZO buffer layer, which in turn introduces structural defects like dislocations in the film.

Regarding the positions of E1 and E3 in Fig. 9.20 (a) in dependence of the Mg-content, the peak maximum of E1 occurs almost at the same temperature independent of x, while a shift to higher temperatures is visible for the peak position of E3 in the (Mg,Zn)O samples with increasing x. The reason for that is the increase of the fundamental

bandgap of (Mg,Zn)O with increasing x and the relative energetic difference between E1 and E3, respectively, with respect to E_c. Figure 9.19 (b) shows the change of the energetic position $\text{Œ}_t := E_{t,x} - E_{t,x=0}$ of the defects E1 and E3, respectively, versus x. The change of the bandgap energy is given by the slope of $E_{I_6}(x)$ and indicated in Fig. 9.19 (b) by the black solid line. The dashed lines represent the linear fits of $\text{Œ}_{t,E1}$ and $\text{Œ}_{t,E3}$ vs. x, respectively. While Œ_t increases with x for the defect E3, this value remains almost constant for E1. The increasing bandgap energy splits into a shift of the conduction band-edge Œ_c and valence band-edge Œ_v. The ratio of Œ_c to Œ_v amounts $\text{Œ}_c / \text{Œ}_v = 0.9/0.1$ to $0.6 = 0.4$ [13–16]. According to the literature, the corresponding range of Œ_c is shaded in Fig. 9.19 (b). Hence, the energetic position of E3 is fixed in the band and does not change with respect to the vacuum level, the change of Œ_c increases the thermal activation energy of the deep-level. E1, in contrast, shows only a minor change of its energetic position with respect to the conduction band-edge – the defect-level follows E_c. The electronic wavefunctions of E1 are with that predominantly derived from the conduction band which is not the case for the E3 defect.

[1] M. Lorenz, H. Hochmuth, C. Grüner, H. Hilmer, A. Lajn, D. Spemann, M. Brandt, J. Zippel, R. Schmidt-Grund, H. von Wenckstern, and M. Grundmann, Laser Chem., 140976 (2010).
[2] A. Lajn, H. von Wenckstern, Z. Zhang, C. Czekalla, G. Biehne, J. Lenzner, H. Hochmuth, M. Lorenz, M. Grundmann, S. Wickert, C. Vogt, and R. Denecke, J. Vac. Sci. Technol. B **27**, 1769 (2009).
[3] B. K. Meyer, H. Alves, D. M. Hofmann, W. Kriegseis, D. Forster, F. Bertram, J. Christen, A. Hoffmann, M. Straburg, M. Dworzak, U. Haboeck, and A. V. Rodina, phys. stat. sol. (b) **241**, 231 (2004).
[4] C. P. Dietrich, A. Müller, M. Stölzel, M. Lange, G. Benndorf, H. von Wenckstern, M. Grundmann, Mater. Res. Soc. Symp. Proc. 1201 (2010), 10.1557/PROC-1201-H03-08.
[5] M. R. Wagner, G. Callsen, J. S. Reparaz, J.-H. Schulze, R. Kirste, M. Cobet, I. A. Ostapenko, S. Rodt, C. Nenstiel, M. Kaiser, A. Hoffmann, A. V. Rodina, M. R. Phillips, S. Lautenschläger, S. Eisermann, and B. K. Meyer, Phys. Rev. B **84**, 035313 (2011).
[6] M. Brandt, H. von Wenckstern, G. Benndorf, M. Lange, C. P. Dietrich, C. Kranert, C. Sturm, R. Schmidt-Grund, H. Hochmuth, M. Lorenz, M. Grundmann, M. R. Wagner, M. Alic, C. Nenstiel, and A. Hoffmann, Phys. Rev. B **81**, 073306 (2010).
[7] F. Schmidt, S. Müller, H. von Wenckstern, G. Benndorf, R. Pickenhain, M. Grundmann, J. Appl. Phys. **116**, 103703 (2014).
[8] F. Schmidt, H. von Wenckstern, O. Breitenstein, R. Pickenhain, M. Grundmann, Solid-State Electron. **92**, 40 (2014).
[9] D. V. Lang, J. Appl. Phys. **45**, 3023 (1974).
[10] L. Dobaczewski, A. R. Peaker, K. B. Nielsen, J. Appl. Phys. **96**, 4689 (2004).
[11] F. D. Auret, W. Meyer, P. J. van Rensburg, M. Hayes, J. Nel, H. von Wenckstern, H. Schmidt, G. Biehne, H. Hochmuth, M. Lorenz, M. Grundmann, Physica B **401-402**, 378 (2007).
[12] M. Schmidt, H. von Wenckstern, R. Pickenhain, M. Grundmann, Solid-State Electron. **75**, 48 (2012).
[13] A. Ohtomo, M. Kawasaki, I. Ohkubo, H. Koinuma, T. Yasuda, and Y. Segawa, Appl. Phys. Lett. **75**, 980 (1999).

[14] G. Coli and K. K. Bajaj, Appl. Phys. Lett. **78**, 2861 (2001).
[15] F. Li, B. Yao, Y. M. Lu, B. H. Li, Y. Q. Gai, C. X. Cong, Z. Z. Zhang, D. X. Zhao, J. Y. Zhang, D. Z. Shen, and X. W. Fan, Appl. Phys. Lett. **92**, 192116 (2008).
[16] G. V. Rao, F. Säuberlich, and A. Klein, Appl. Phys. Lett. **87**, 032101 (2005).

9.13 Self-compensation in Al-doped (Mg,Zn)O thin films grown by pulsed laser deposition

A. Mavlonov, S. Richter, R. Schmidt-Grund, H. von Wenckstern, M. Grundmann

The ternary wide bandgap semiconducting oxide (Mg,Zn)O is a promising material for transparent electrode applications e.g. for thin film solar cells [1]. In order to achieve sufficient conductivity, doping by the group III element Al is commonly done but self-compensation (formation of acceptor-like intrinsic defects) has to be considered [2]. An experimental prove is involved because for such an investigation numerous samples with different doping levels would have to be grown under otherwise identical growth conditions. In this work, we report electrical properties of Al-doped $Mg_{0.05}Zn_{0.95}O$ thin films grown by PLD using a continuous composition spread (CCS) method [3]. The lateral variation of chemical composition was investigated by energy dispersive X-ray spectroscopy. To facilitate electrical characterization, $(5 \times 5)\,mm^2$ size pieces were cut from (Mg,Zn)O:Al films grown on 2-inch in diameter glass and/or sapphire substrates. All investigated films have a thickness ranging from 150 to 250 nm. The free charge carrier density n was obtained from Hall-effect measurement at room temperature (RT), which in degenerate materials immediately yields the following relationship: $n = [\mathrm{Al}] - zN_A$, where N_A is the density of compensating acceptors and z is their charge state. In highly doped (Mg,Zn)O the zinc vacancy (V_{Zn}), which is a doubly chargeable acceptor, is the dominant intrinsic defect [4]. We found that the films grown at lower growth temperatures (T_G = RT, 200°C and 300°C) have higher doping efficiency. The highest efficiency of 80.2 % is observed in the film grown at T_G = 200°C (cf. Fig. 9.21 a)). This is very interesting for TCO applications, however, from scientific point of view it is important to know the main limiting factors of doping efficiency at higher T_G. Therefore, all low temperature grown films were annealed at 400°C in vacuum (cf. Fig. 9.21 b)). As a general trend, the free charge carrier density of all films decreased with increasing annealing time. Interestingly, n saturated at $n \sim 2 \times 10^{20}\,cm^{-3}$ for the samples grown at T_G = 200, 300°C, the saturation carrier density is slightly lower for RT grown samples. As PLD is nonequilibrium growth method, unannealed films can be considered as metastable [5]. If we take into account that dopant concentration of $N_d = 1 \times 10^{21}\,cm^{-3}$ is constant for all films, in thermodynamic equilibrium conditions (after annealing) n is mainly changed due to an increase of N_A. Here, N_A is expected to be V_{Zn}, however, to proof this further optical and structural investigations are needed.

Funding: Islamic Development Bank (IDB), Merit Scholarship Programme for High Technology (A.M. Grant No. 91/UZB/P32).

[1] H. von Wenckstern *et al.*, The (Mg,Zn)O Alloy. Handbook of Zinc Oxide and Related Materials, Vol. 1 Materials. Taylor and Francis/CRC Press (2012).

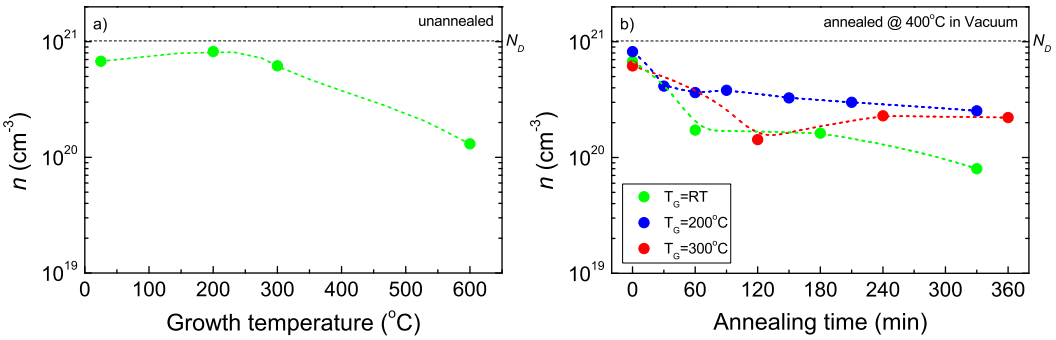

Figure 9.21: Free charge carrier density of Al-doped $Mg_{0.05}Zn_{0.95}O$ thin films as a function (a) growth temperature and (b) annealing time. N_D is the Al concentration in the films. Dashed lines are guides to the eye.

[2] D. C. Look *et al*. Phys. Rev. B **84**, (2011) 115202(6).
[3] H. von Wenckstern *et al*., CrystEngComm **15**, (2013) 10020-10027.
[4] F. Oba *et al*. Phys. Rev. B **77**, (2008) 245202(6).
[5] A. Ohtomo *et al*. Appl. Phys. Lett. **72**, (1998) 2466-2468.

9.14 Time-resolved luminescence of vapour deposited CuI thin films

M. Stölzel, K. Rudisch, G. Benndorf, M. Grundmann

Cuprous iodide (CuI) is a wide and direct band gap semiconductor that is a promising material for application in fully transparent electronics due to its intrinsic p-type conductivity [1]. We have studied the near band edge emission characteristics of a CuI thin film in the temperature range 2 – 295 K. The thin film was deposited on a rotated silica substrate by evaporation of CuI powder in a vacuum chamber with a base pressure of 5×10^{-5}mbar and has a thickness of about 300 nm.

Photoluminescence (PL) spectra at low temperatures show distinct excitonic features (Fig. 9.22 (a)). For $T = 2$ K the corresponding peak energies and binding energies E_B are listed in Fig. 9.22 (b). The temperature evolution of the spectra together with comparison to reflectance experiments on CuI single crystals [2] reveals the peaks **a** and **b** to result from the longitudinal and transverse free exciton (FX_L and FX_T). The sharp peaks **c** – **g** on the FXs' low energy side arise from bound excitons showing the expected decrease in intensity at higher temperatures. These excitons are bound to defects, such as the copper vacancy [3] or to deep centers.

Time-resolved PL measurements of these transitions at $T = 2$ K yielded mono- and bi-exponential decays for (**b** – **e**) and (**f**, **g**), respectively, as shown in Fig. 9.22 (c). The decay time of the free exciton **b** was determined to (20 ± 3) ps, being an upper bound as this time is close to our temporal resolution limit. A plot of the BXs' decay times vs. $E_B^{3/2}$ in Fig. 9.22 (d) shows linear behaviour as expected according to the theory developed by Rashba and Gurgenishvili [4]. Due to this good agreement we can conclude that

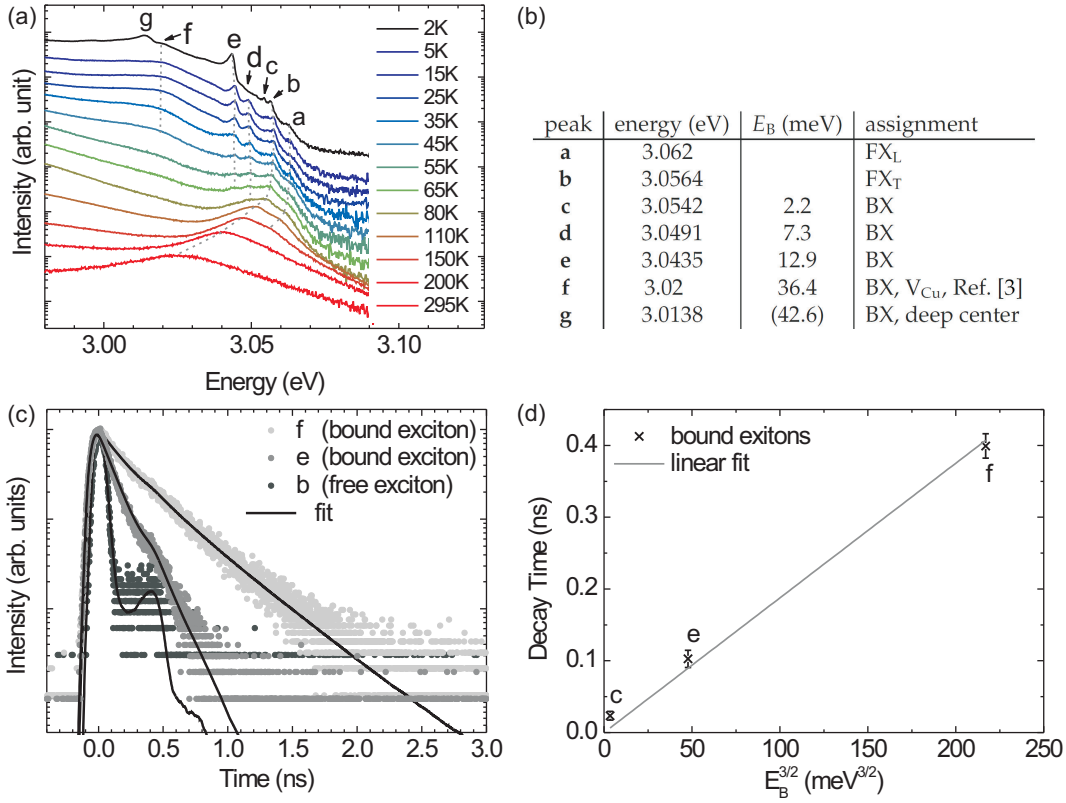

peak	energy (eV)	E_B (meV)	assignment
a	3.062		FX_L
b	3.0564		FX_T
c	3.0542	2.2	BX
d	3.0491	7.3	BX
e	3.0435	12.9	BX
f	3.02	36.4	BX, V_{Cu}, Ref. [3]
g	3.0138	(42.6)	BX, deep center

Figure 9.22: (a) Near band edge emission of a CuI thin film as a function of temperature. (b) Free (FX) and bound (BX) exciton transitions at $T = 2\,\mathrm{K}$. The energy of **b** serves as reference for the binding energies of the BX **c**–**g**. (c) Normalised transients of selected exciton transitions at $T = 2\,\mathrm{K}$ modeled by exponential and biexponential decay functions. (d) Determined decay times of the BX as a function of $E_B^{3/2}$ fitted linearly with a slope of $(1.8 \pm 0.2)\,\mathrm{ps/meV^{3/2}}$.

non-radiative decay channels are negligible and radiative decay dominates at low temperature.

This work has been supported by Deutsche Forschungsgemeinschaft (GR 1011/28-1).

[1] M. Grundmann et al., phys. stat. sol. (a) **210**, 1671 (2013), doi:10.1002/pssa.201370056
[2] M. Certier et al., Materials Science and Engineering: B **58**, 234 (1999), doi:10.1016/S0921-5107(98)00436-X
[3] T. Sauder and M. Certier, Physics Lett. A **101**, 55 (1984), doi:10.1016/0375-9601(84)90092-6
[4] E. Rashba and G. Gurgenishvili, Fiz. Tverd. Tela **4**, 1029 (1962)

9.15 Characterization and application of $(In,Ga)_2O_3$ and $(Al,Ga)_2O_3$

C. Kranert, H. von Wenckstern, R. Schmidt-Grund, D. Splith, M. Purfürst, Z. Zhang, H. Krauß, V. Zviagin, S. Müller, M. Jenderka, J. Lenzner, M. Lorenz, M. Grundmann

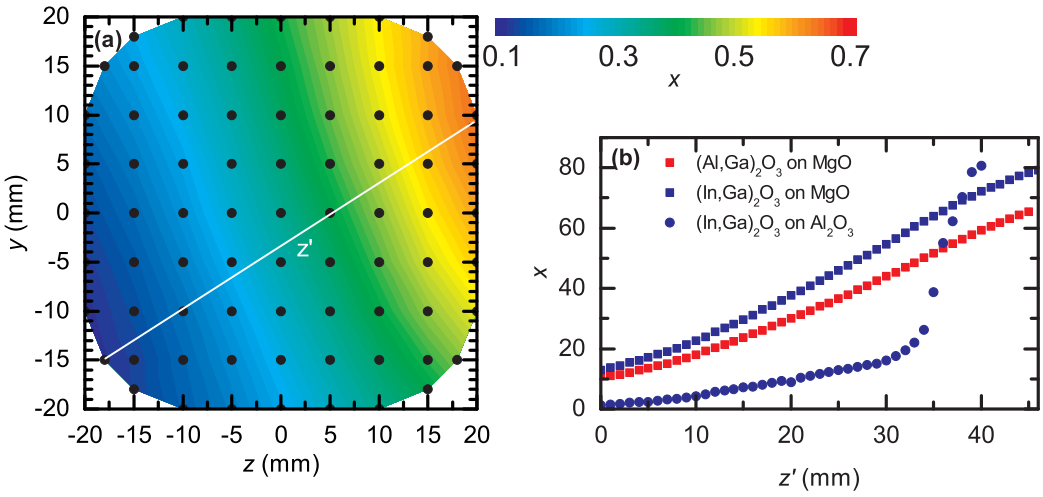

Figure 9.23: (a) Composition map of the $(Al_xGa_{1-x})_2O_3$ thin film determined by EDX. The *white line* indicates the position of the line scan measurements. **(b)** Al and In concentration x along the gradient of the $(Al_xGa_{1-x})_2O_3$ and $(In_xGa_{1-x})_2O_3$ thin films, respectively.

The bandgap energy of Ga_2O_3 can be decreased (increased) by substituting gallium ions by indium (aluminium). We investigated both alloys, $(In_xGa_{1-x})_2O_3$ and $(Al_xGa_{1-x})_2O_3$, covering a wide spectral range of the bandgap. We focused our research on the composition range for which the compound crystallizes in the monoclinic β-modification, which is the stable structure of Ga_2O_3.

For the fabrication of thin films, we made use of our continuous composition spread (CCS) approach for pulsed laser deposition (PLD) [1]. A target consisting of half-circular segments was used, one of which was made of binary Ga_2O_3 and the other either of binary In_2O_3 or Al_2O_3. The thin films were deposited on substrates with a diameter of 2 inch. For both compounds, MgO (100) substrates were used. Further, $(In, Ga)_2O_3$ was also deposited on α-Al_2O_3 (00.1). The composition of these thin films was determined by electron-dispersive X-ray spectroscopy (EDX) and covers the range of $0.1 < x < 0.7$ for $(Al_xGa_{1-x})_2O_3$ and an even wider range for $(In_xGa_{1-x})_2O_3$, as depicted in Fig. 9.23.

9.15.1 Structural properties

The structural properties of the compound materials were investigated by means of X-ray diffraction (XRD). For these experimental methods, ceramic samples with different aluminium and indium concentration, respectively, were prepared by sintering in order to obtain the reference data from bulk-like material. We acquired powder diffraction patterns of these samples and determined their lattice parameters by Rietveld refinement of the β-Ga_2O_3 unit cell. The obtained lattice parameters show a linear dependence on the alloy composition in agreement with Vegard's law. We found a stronger dependence of the parameters on the In concentration than on the Al concentration, which correlates with the smaller deviation between the ionic radii of Al and Ga than between In and Ga [2, 3].

XRD measurements of the thin films were carried out by means of a line scan along the composition gradient. We found single-phase material in the β-modification for an In concentration $x < 0.2$ for growth on Al_2O_3 and $x < 0.3$ for growth on MgO, and for

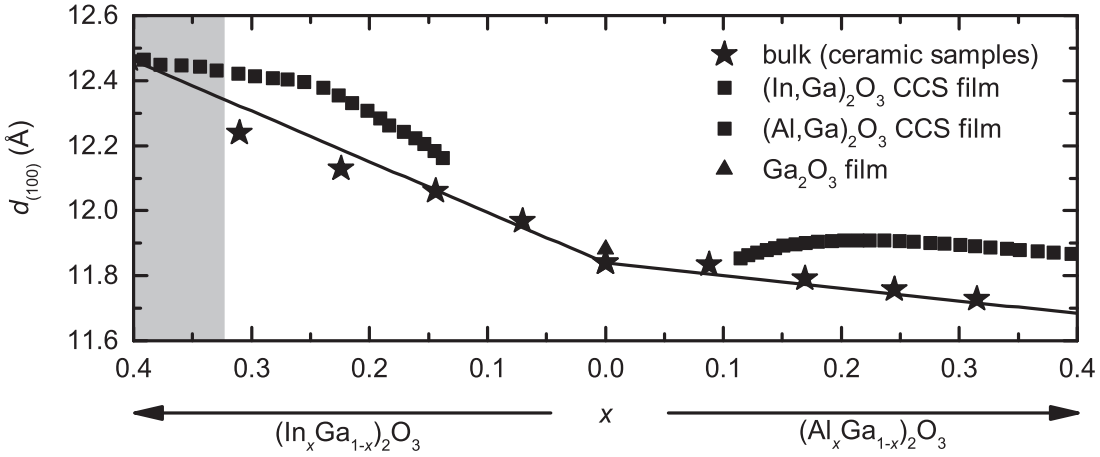

Figure 9.24: Spacing of the (100) planes of $(Al_xGa_{1-x})_2O_3$ and $(In_xGa_{1-x})_2O_3$. Data for thin film samples grown on MgO (*squares* and *circles*, respectively) are compared to the bulk values obtained from the ceramic samples (*stars*) and the corresponding linear approximation for the individual alloys (*solid lines*). Phase separation was observed for the thin films in the *grey-shaded area*.

an Al concentration $x < 0.5$ on MgO. For higher In concentrations, we observed the formation of the high-pressure phase $InGaO_3$ II and, for even larger x, that of bcc-In_2O_3. Higher Al concentrations led to the growth of γ-$(Al,Ga)_2O_3$. The lattice parameters of the thin films are increased relative to the bulk values as can be seen from Fig. 9.24. This expansion of the lattice increases with decreasing Ga concentration in the film for both alloys. Its origin is therefore assigned to defects and disorder due to the alloying.

9.15.2 Vibrational properties

Raman spectroscopy was applied to study the phonon energies in dependence on the composition. These values were again obtained for bulk material from the ceramic samples. The phonon energies shift mainly linear with the respective composition. The observed dependencies of the energies on x are similar for both compounds, opposite to the behaviour of the lattice parameters.

Analogously to XRD, the Raman scattering measurements of the thin films were carried out by means of a line scan along the composition gradient. In agreement to XRD, we observed exclusively Raman modes associated with the β-modification for sufficiently small x. For higher In concentration, additional modes occur which we assigned to the $InGaO_3$ II phase observed in EDX [2]. The Raman modes of γ-$(Al,Ga)_2O_3$ are too weak to be observed, thus the Raman spectrum vanishes for Al concentrations $x > 0.45$.

The phonon energies of the thin films are in good agreement to the bulk values despite the distinct deviation of the lattice spacings. This is shown exemplarily for two phonon modes in Fig. 9.25. Thus, a determination of the Al or In concentration by Raman spectroscopy appears feasible. However, some modes which appear to be more sensitive on the internal strain (e.g. the $A_g^{(3)}$ mode for $(In,Ga)_2O_3$ shown in Fig. 9.25(a) or the $A_g^{(10)}$ mode for $(Al,Ga)_2O_3$), exhibit a slight deviation from the expected linear dependence.

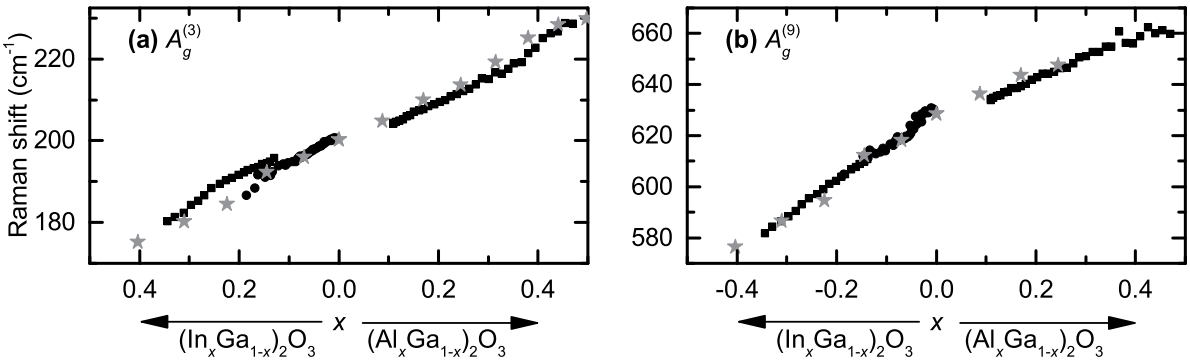

Figure 9.25: (a) and **(b)** Phonon energies for two Raman modes of β-$(In_xGa_{1-x})_2O_3$ and β-$(Al_xGa_{1-x})_2O_3$. Data for the CCS thin films on MgO (*black squares*) and on Al_2O_3 (*black circles*) are compared to bulk values obtained from ceramic samples (*grey stars*).

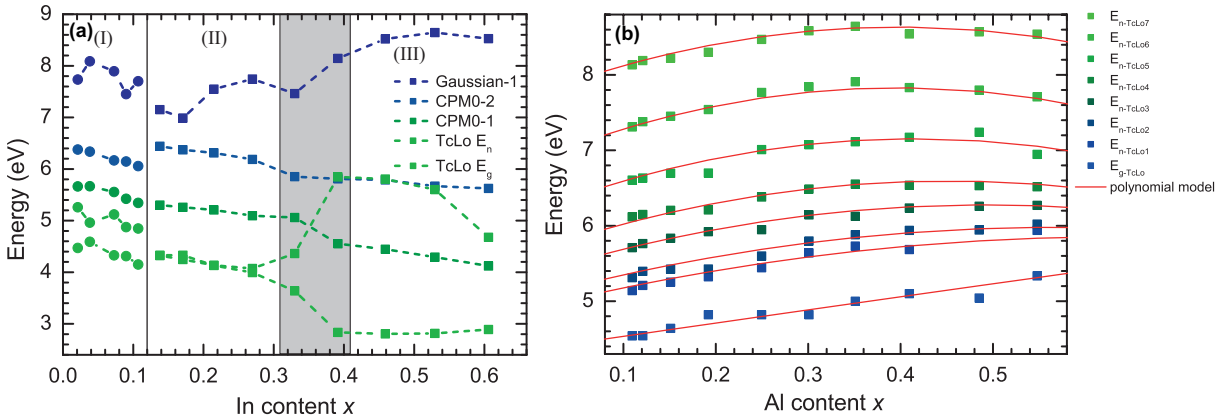

Figure 9.26: Energies of transitions used in the lineshape approximation of the dielectric function of **(a)** $(In_xGa_{1-x})_2O_3$ and **(b)** $(Al_xGa_{1-x})_2O_3$. The *roman numbers* in **(a)** refer to different regions on the samples (see text).

9.15.3 Optical properties

The optical properties of the thin films were investigated in the wide spectral range from 0.5 eV to 8.5 eV using spectroscopic ellipsometry [4, 5]. From a Kramers-Kronig-consistent numerical approximation to the experimental data, we calculated the complex dielectric function (DF) of the material in dependence on the composition. The refractive index of the material was found to increase slightly with incorporation of In and to decrease with increasing Al concentration. Thus, the thin films covered a range of the refractive index from 1.8 (Al, $x = 0.5$) to 1.92 (In, $x = 0.2$) for the β-phase.

The numerical DF was described by lineshape functions which correspond to electronic transitions. As expected, these transitions shift towards lower energies for the incorporation of In and towards higher energies for the incorporation of Al, which is accompanied by the respective shift of the absorption edge. The regions of different structural properties are also observed in the DFs, particularly for $(In_xGa_{1-x})_2O_3$. In Fig. 9.26(a), region (I) and (II) refer to a β-structure-like DF for the films grown on Al_2O_3 and MgO, respectively. The DF from region (III) is similar to that of bcc-In_2O_3[6], while no clear assignment is possible in the grey-shaded area, in which the phase separation of $InGaO_3$ II occurs.

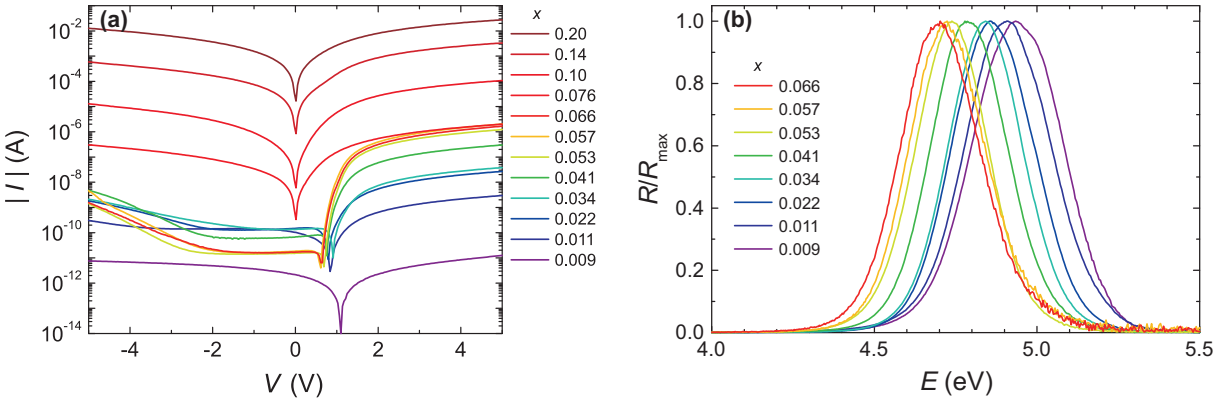

Figure 9.27: (a) *I-V*-characteristics of Schottky contacts on segments of the $(In, Ga)_2O_3$ thin film. **(b)** Normalized photoresponse of MSM photodetectors fabricated from the $(In, Ga)_2O_3$ thin film.

9.15.4 Photodetectors based on $(In,Ga)_2O_3$

The alloy $(In_xGa_{1-x})_2O_3$ is particularly interesting for the fabrication of solar-blind photodetectors. For these, the incorporation of In can be used to tune the lower cut-off energy of Ga_2O_3 towards the high-energy edge of the solar spectrum on earth. We prepared such devices based on segments cut from parts along the gradient of the $(In_xGa_{1-x})_2O_3$ thin film described above, which was deposited on Al_2O_3, using metal-semiconductor-metal (MSM) contacts [7].

Schottky contacts on the thin films were fabricated by reactive sputtering of Pt. Prior to that, additional ohmic contacts were realized by thermally evaporated Ti/Al, which were post-annealed at 500 ℃ in order to characterize the Schottky diodes. The *I-V*-characteristics obtained for these samples are shown in Fig. 9.27. Because the thin film is nominally undoped, almost no rectification is observed for the smallest In concentration due to the series resistance. The series resistance decreases with increasing In concentration, yielding a rectification ratio of over 10^4 in the range around $x \approx 0.05$. For higher In concentrations, the rectification ratio decreases again due to an decreasing parallel resistance.

The photodetectors were characterized by backside illumination through the Al_2O_3 substrate using monochromated light from a xenon lamp. As expected from the optical characterization, the cut-off energy systematically decreases with increasing In concentration. The responsivity maximum could be shifted from 4.95 eV for the lowest In concentration to 4.7 eV for $x = 0.066$.

CK was funded by the European Union and the Free State of Saxony. This work was supported within the framework of EFRE (SAB).

[1] H. von Wenckstern et al., CrystEngComm **15**, 10020 (2013), doi:10.1039/C3CE41327F
[2] C. Kranert et al., J. Appl. Phys. **116**, 013505 (2014), doi:10.1063/1.4886895
[3] C. Kranert et al., J. Appl. Phys. **117**, 125703 (2015), doi:10.1063/1.4915627
[4] R. Schmidt-Grund et al., J. Appl. Phys. **116**, 053510 (2014), doi:10.1063/1.4891521
[5] R. Schmidt-Grund et al., J. Appl. Phys. **117**, J. Appl. Phys. 117, 165307 (2015), doi:10.1063/1.4919088
[6] R. Schmidt-Grund et al., Appl. Phys. Lett. **105**, 111906 (2014), doi:10.1063/1.4896321

[7] H. von Wenckstern et al., Semicond. Sci. Technol. **30**, 024005 (2015), doi:10.1088/0268-1242/30/2/024005

9.16 Comparative Study of Optical and Magneto-Optical Properties of Normal, Disordered, and Inverse Spinel Type Oxide Thin Films

V. Zviagin, P. Richter *, T. Böntgen, M. Lorenz, M. Ziese, D.R.T. Zahn *, G. Salvan *, R. Schmidt-Grund, M. Grundmann.

*Technische Universität Chemnitz, Semiconductor Physics, Reichenheiner Str. 70, 09126 Chemnitz, Germany.

Spinel oxides consist of tetrahedrally and octahedrally coordinated cations within a cubic unit cell and crystalize in either normal structure, Co_3O_4 (CCO), $ZnCo_2O_4$ (ZCO), $ZnFe_2O_4$ (ZFO), inverse structure, $CoFe_2O_4$ (CFO), Fe_3O_4 (FFO), or a mixture of both, depending on the growth parameters such as temperature. This allows electronic and magnetic properties to be tuned, making them promising candidates for use in data storage, spintronic devices, biotechnology, and high-frequency applications such as telecommunications and radar systems [1, 2].

Optical and magneto-optical properties of the thin films were investigated by spectroscopic ellipsometry (SE), in the wide spectral range 0.5 – 8.5 eV, and magneto-optical Kerr effect (MOKE) spectroscopy, in the spectral range 1.5 – 5.5 eV with an applied magnetic field of 1.7 T, and in dependence on the deposition temperature. All samples were grown at high, ~ 600°C, (HT) and low, ~ 330°C, (LT) temperatures on MgO substrates, except for FFO which was grown only at ~ 550°C (HT) on a $MgAl_2O_4$ substrate, by pulsed laser deposition. Supported by structural characterization, properties of electronic transitions in the dielectric function spectra reflect the impact of disorder as well as symmetry distortion for films deposited at LT. For example, below ~ 1 eV, the crystal field (CF) transition within the tetrahedral Co^{2+} and an the inter-valence charge transfer (IVCT) transition between octahedral Fe^{3+} have higher oscillator strength for LT grown films compared to HT grown films. Based on the model dielectric function, deduced from SE, the measured MOKE response was used to obtain magnetically active off-diagonal elements of the complex dielectric tensor, ϵ_{xy}. The transitions visible in both optical and magneto-optical spectra are CF, IVCT, inter-sublattice charge transfer (ISCT) transitions, and transitions from O_{2p} bands to metal cation sites [3, 4]. However, it was found that not all transitions visible in the magneto-optical components ϵ_{xy} are as pronounced in the linear optical components ϵ_{xx} of the dielectric tensor and vice versa, (Fig. 9.28). Transitions showing the strongest magneto-optical response are IVCT and ISCT transitions involving Fe ions. Thus, since O_{2p} to Co or Zn cation transitions dominate the optical spectra for CCO and ZCO without magnetic field, no MOKE signal was recorded for those films. For spinels containing Fe ions, magneto-optical response is observed, which is highest for disordered normal and inverse structured spinels, in accordance with band structure calculations [5].

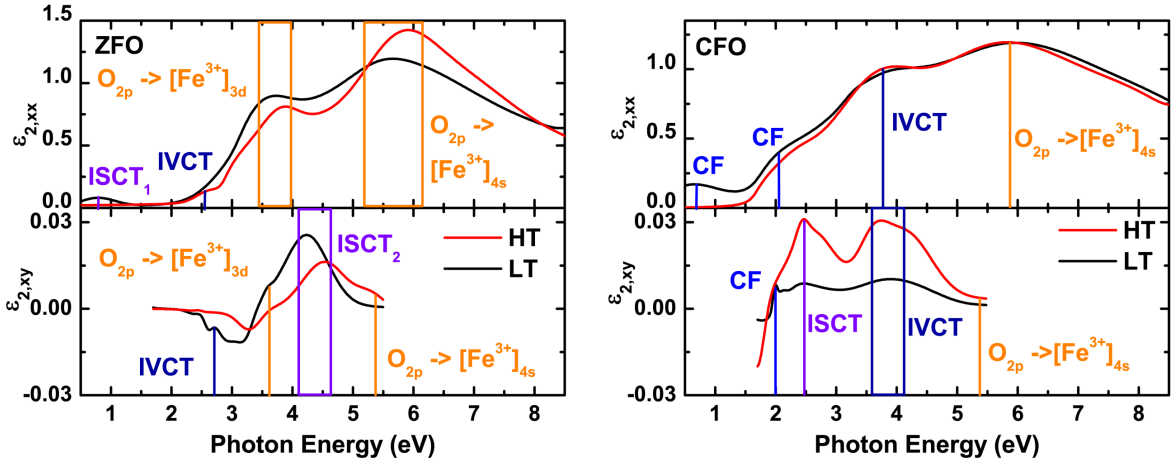

Figure 9.28: Imaginary part of diagonal, $\epsilon_{2,xx}$, and off-diagonal, $\epsilon_{2,xy}$, elements of the complex dielectric tensor for normal spinel ZFO (left) and inverse spinel CFO (right) with ISCT, IVCT, CF, and O_{2p} to Fe^{3+} cation transitions indicated by coloured vertical lines.

This work has been supported by Deutsche Forschungsgemeinschaft in the framework of SFB 762 "Functionality of Oxide Interfaces".

[1] M. Opel et al., Phys. Status Solidi (a) **208**, 232 (2011), doi:10.1002/pssa.201026403
[2] R. Valenzuela, Phys. Res. Int. (a) **2012**, 591839 (2011), doi:10.1155/2012/591839
[3] T. Böntgen et al., J. Appl. Phys. **113**, 073503 (2013), doi:10.1063/1.4790881
[4] K.J. Kim et al., J. Appl. Phys. **91**, 12 (2002), doi:10.1063/1.1480482
[5] S. Soliman et al., Phys. Rev. B **83**, 085205 (2011), doi:10.1103/PhysRevB.83.085205

9.17 Antiferromagnetic phase transition in the temperature-dependent dielectric function of hexagonal $YMnO_3$

S. Richter, S.G. Ebbinghaus*, C. Bundesmann†, M. Grundmann, R. Schmidt-Grund

*Martin-Luther-Universität Halle-Wittenberg, Institut für Chemie, Kurt-Mothes-Str. 2, 06120 Halle, Germany
†Leibniz-Institut für Oberflächenmodifizierung (IOM), Permoserstr. 15, 04318 Leipzig, Germany

Hexagonal $YMnO_3$ is well known for the co-occurrence of ferroelectricity and antiferromagnetism at low temperatures. However, the exact coupling mechanism leading to its multiferroicity is not completely understood yet. Especially the role of the Mn 3*d* orbitals affecting electronic and magnetic behavior perpendicular as well as along the crystallographic *c*-axis is not entirely clear. Based on the knowledge of the uniaxial dielectric function at room temperature [1] we used temperature-dependent spectroscopic ellipsometry at an *a*-plane oriented single crystal to show how the electronic transitions are affected by the antiferromagnetic phase transition at the Néel temperature around 80 K. Most interesting is the unusual temperature dependence of the

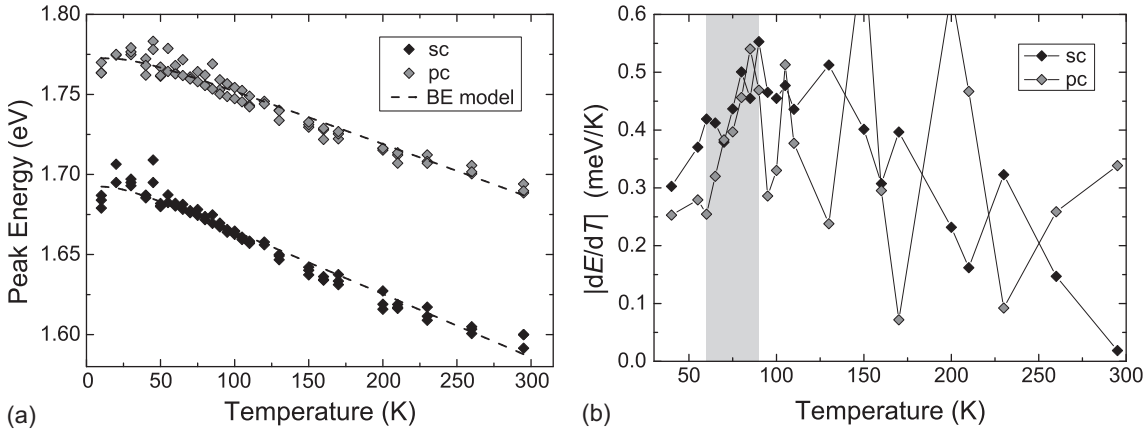

Figure 9.29: (a) Temperature dependence and Bose-Einstein model approximation of the deduced oscillator energies related to the interband charge transfer transitions. (b) Modulus of the derivative of these energies. The grayed area marks the range of literature values for the Néel temperature.

pronounced charge transfer transitions around (1.6 – 1.7) eV which are strongly connected to Mn 3*d* electrons [2]. If described with the semi-empiric Bose-Einstein model, the temperature dependency of their transition energies and broadenings is characterized by effective phonon energies not larger than 8 meV (Fig. 9.29 (a)). This is a hint for the occurrence of a soft phonon mode related to the antiferromagnetic phase transition and is observed in both tensor components of the dielectric function, parallel and perpendicular to the crystallographic *c*-axis. This strong connection can also be observed in the first derivative of the transition energies with respect to temperature which reveals a maximum around the Néel temperature that cannot be described by the Bose-Einstein model (Fig. 9.29 b)).

This work has been supported by Deutsche Forschungsgemeinschaft in the framework of SFB 762 "Functionality of Oxide Interfaces".

[1] R. Schmidt-Grund et al., RSC Adv. **4**, 33549 (2014), doi:10.1039/C4RA05036C
[2] S. Richter et al., arXiv:1503.04043 (2015)

9.18 Mueller matrix ellipsometry analysis of blazed gratings produced by reactive ion beam etching

L. Fricke, C. Bundesmann*, R. Fechner*, M. Burkhardt†, M. Helgert†, A. Gatto†, F. Frost*, M. Grundmann, R. Schmidt-Grund

*Leibniz-Institut für Oberflächenmodifizierung e.V. (IOM), Permoserstr. 15, D-04318 Leipzig, Germany.
†Carl Zeiss Jena GmbH, Jena, Germany.

We modelled the optical response of blazed gratings in fused silica using geometrical information of topography profiles obtained from atomic force microscopy (AFM) (Fig. 9.30 a)). The calculated spectra are in reasonable agreement with spectra measured

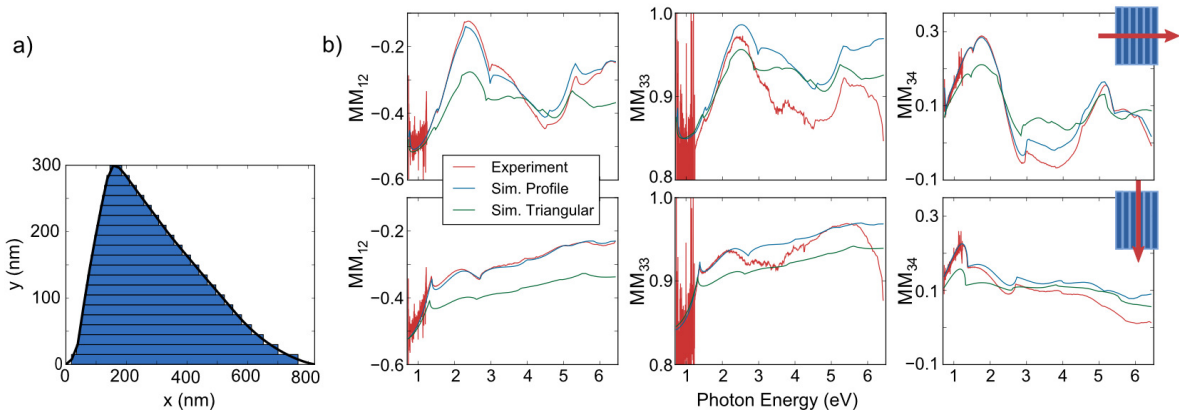

Figure 9.30: (a) Topography profile of the grating measured by means of AFM (solid line) and geometric slice model for the RCWA calculations (blue bars). (b) Experimental spectra (red lines) of selected Mueller matrix elements at an angle of oncidence of 75 ° along with the RCWA simulations using a triangular (green lines) and the exact (blue lines) profile for classical (top line) and diffraction geometry (bottom line). The light´s propagation direction with respect to the grating alignment is indicated in the sketches.

by Mueller matrix (MM) ellipsometry in the spectral range (0.7 − 6.5) eV at angles of incidence greater than 65° and different azimuthal orientations. The gratings were produced using interference lithography and reactive ion etching to transfer the pattern defined by lithography into the fused silica substrate [1]. The results show that MM ellipsometry is a useful tool to get information on the real geometrical shape of such structures, even for *in-situ* monitoring as fabrication process control.

For the simulation of the MM spectra we employed the rigorous coupled wave approach (RCWA). The dielectric function of fused silica was taken from a database, so that the whole modelling procedure is free of any adjustable parameter. A simple geometrical model approximation of the grating as triangular profile, already reproduces the correct spectral position of diffraction scattering anomalies (Fig. 9.30 b)). These can be recognized as cusps in the MM-spectra. But only the thorough representation of the real grating profile (Fig. 9.30 a)) results in simulations that reproduce the main features of the measured spectra correctly (Fig. 9.30 b)). The remaining differences between the magnitudes of the simulated and experimental Mueller-Matrix elements, we attribute to backside reflections from the double-side polished substrate. These backside reflections also lead to large depolarization of the incident light upon reflection at smaller incidence angles rendering the analysis with traditional RCWA impossible.

Experimental and simulated Mueller matrix spectra for a full in-plane rotation in steps of 18° are in excellent agreement with each other, respectively, and reveal the violation of the two-fold symmetry due to the grating asymmetry. Furthermore, the spectral positions of the diffraction anomalies shift in dependence on the rotation angle.

The authors acknowledge the support of the Sächsische Aufbaubank within the project "Precios" (Project-No. 100080120).

[1] F. Frost et al., Proceedings 3. Kolloquium "Dünne Schichten in der Optik", Leipzig (2012), pp. 345-349.

9.19 Twisted Nanowires

M. Grundmann

We have worked out the theory of the effect of torsion on [00.1]-oriented wurtzite and [111]-oriented zincblende nanowires with hexagonal cross-section [1]. The stresses (and strains) are determined via calculation of Prantl's stress function using a 2D solver and a boundary element method. The latter is computationally more economic and easily allowed us the extension to rounded corners and hollow shafts. In Fig. [**?**]a the (universal) shear stress distribution is depicted. The strain distribution in hexagonal nanowires with rounded corners depends on the curvature radius of the corners. For finite corner radius, the strain does no longer vanish at the corners.

The spatial variation of the valence band structure in the cross-section is evaluated in the framework of the 6×6 valence band Hamiltonian and deformation potential theory. We find that the shear strain induced potential leads to additional localization of holes in the center of the facets (Fig. [**?**]b).

In wurtzite wires, torsion does not evoke any piezoelectric charges or potentials (opposite to a statement in [2]) and thus does not impact the signal in piezotronic sensors. In zincblende wires, the second order piezoelectric effect causes piezoelectric charges with three-fold symmetry.

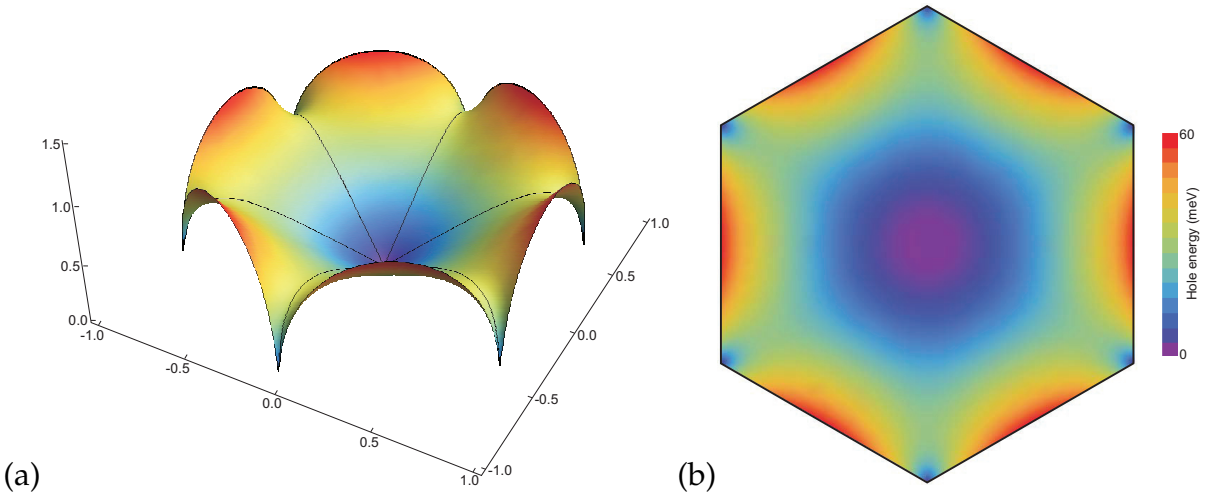

Figure 9.31: (a) 3D view of distribution of shear stress τ for hexagonal nanowire. (b) Energy shift of the top valence band (at Γ-point) in the cross-section of ZnO hexagonal nanowire for maximum shear strain of 2%.

[1] M. Grundmann, *Theory of Semiconductor Solid and Hollow Nano- and Microwires With Hexagonal Cross-Section Under Torsion*, phys. stat. sol. (b) **252**, 773-785 (2015), doi: 10.1002/pssb.201451431

[2] Z. Gao, J. Zhou, Y. Gu, P. Fei, Y. Hao, G. Bao, Z.L. Wang, J. Appl. Phys. **105**, 113707 (2009)

9.20 Non-linear deformation potential in uniaxially strained ZnO microwires

Sh. Khujanov, C. Sturm, J. Lenzner, M. Grundmann

The optical and piezoelectric properties of ZnO makes it interesting for devices such as strain generators [1]. Although the material properties of ZnO were intensively investigated in the last decades, there are only few reports about the determination of the deformation potentials and the strain induced change of the band gap energy. Especially the range, where the energy shift depends non-linear on the applied strain is limited to theoretical work [2]. Hexagonal ZnO microwires (MWs) were fabricated by the carbothermal vapor phase transport process (T = 1150 ℃) and selected single ZnO MWs with diameters ranging from 1.5 to 9 µm were transferred onto Si substrates. By bending the wires, we were able to induce strain up to ±3.5 %. The resulting shift of the near band-edge (NBE) emission was investigated by cathodoluminescence (CL) by making a line-scan from the compressive to the tensile part of the wire at a temperature T = 6 K (Fig. 9.32a). For strain values up to ±1.5 % we observe a linear dependence between strain and spectral shift of the NBE emission shift as reported by Dietrich *et al.* [3]. However, for larger strain values ($|\varepsilon| > 1.5\,\%$) the linear relation does not hold anymore. Furthermore, the induced spectral shift of the NBE depends on the sign of the strain, i.e. tensile or compressive strain (Fig. 9.32b): For tensile strain a maximum redshift of 78 meV, for compressive strain a maximum blueshift of 53 meV was observed. This difference can be attributed to the piezoelectric field induced by the bending of the wire [4]. The NBE emission energy as a function of the applied strain can be described by $E_{\mathrm{NBE}} = E_0 + D_1\epsilon + D_2\epsilon^2 + D_3\epsilon^3$ where E_0 is energy without an applied strain and the coefficients, D_1 and $D_{2,3}$ are the linear and nonlinear deformation potentials. By doing so, the averaged deformation potentials for the investigated MWs are $D_1 = (-2.65 \pm 0.22)$ eV, $D_2 = (-20.5 \pm 6.1)$ eV and $D_3 = (400 \pm 300)$ eV. Please note, the large uncertainty in D_3 is caused by the weak sensitivity due to the limited range of accessible strain.

SK acknowledges support from the Islamic Development Bank (IDB).

[1] Z.L. Wang et al., Adv. Funct. Mater. **14**, 10, (2004), doi:10.1002/adfm.200400180
[2] W. A. Adeagbo et al., Phys. Rev. B **89**, 195135 (2014), doi:10.1103/PhysRevB.89.195135
[3] C. P. Dietrich et al., Appl. Phys. Lett. **98**, 031105 (2011), doi:10.1063/1.3544939
[4] Sh. Xu et al., NanoLett. **12**, 5802-5807 (2012) , doi:doi.org/nl303132c

9.21 Low temperature PLD-growth of ZnO nanowires on $Zn_xAl_{1-x}O$

A. Shkurmanov, C. Sturm, H. Franke, H. Hochmuth, M. Grundmann

Self-organized grown ZnO micro- and nanostructures are promising for the implementation in devices with high spatial resolution, e.g. pressure sensors [1]. In order to

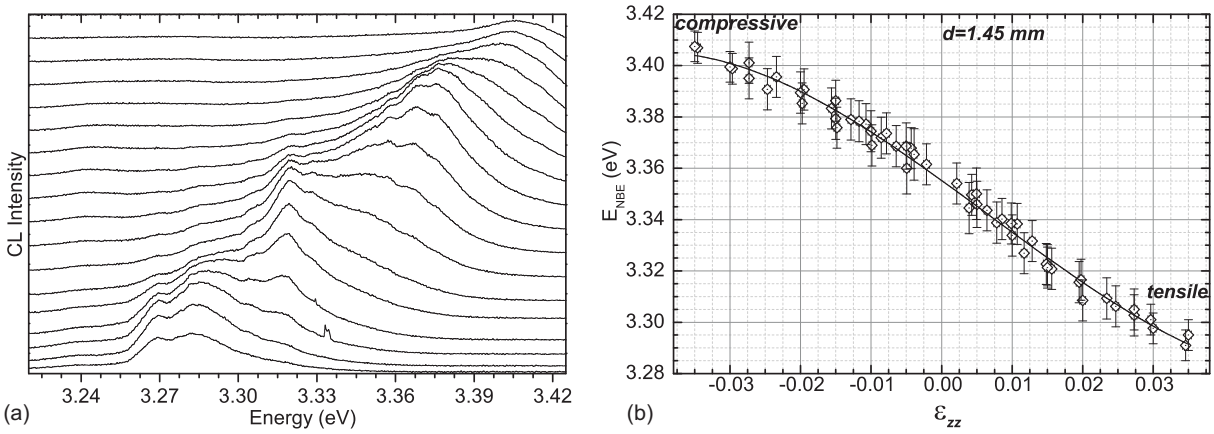

Figure 9.32: (a) The CL line scan spectra of a bent wire (d = 1.45µm) in the band gap energy region (the spectra were shifted along the vertical direction for better visibility). (b) The energy shift as a function of the induced strain. The solid line represents the polynomial fit used for the determination of the deformation potential.

integrate these nanostructures in CMOS technology, a growth temperature of less than 400 ℃ is required [2]. For nanowires (NWs) prepared by pulsed laser deposition (PLD) typically temperatures of about 900 ℃ are used [3] and a reduction of the temperature is quite challenging.

To read out an electronic signal from or charge the NWs, electrical contacts are needed. In the easiest way, this can be done by growing the NWs on a conductive layer, e.g. ZnO due to its intrinsic n-type behavior. Beside the usage as a contact, this layer has a strong influence on the growth of the NWs. For instance, a high density of NWs is observed on crystalline *a*-plane sapphire whereas on pure ZnO seed layer a low density growth of NWs is observable [3]. For the manipulation of the NWs growth we use $Al_xZn_{1-x}O$ films with an Al concentration varying from 0 at % to 7 at %.

At high growth temperatures ($T \approx 900$ ℃), a NWs growth was only observable for samples with a pure ZnO seed layer. For the films doped with Al a suppression of the NWs growth is obtained and the surface exhibits walls and honeycomb-like structures (Fig. 9.33a). An interesting effect arises by reducing the growth temperature down to 400 ℃. For samples with a seed layer consisting of 1 at % Al, an onset of a NWs growth at the edges of the walls and honeycombs is observed at intermediate temperatures ($T \approx 700$ ℃, Fig. 9.33b). A further reduction down to 400 ℃ leads to the growth of thin NWs with a diameter of about 5 nm and an aspect ratio of about 40 (Fig. 9.33c). Interestingly, at this low temperature a growth of NWs was neither observed for seed layers with larger nor lower Al concentration. This critical dependence of the NWs growth on the Al concentration and deposition temperature demonstrates the complex growth mechanism during the PLD process which is not fully understood until now.

[1] C. Pan, et al., Nature Phot. **7**, 752(2013), doi:10.1038/nphoton.2013.191
[2] S. Sedky et al., IEEE T Electron Dev. **48**, 377 (2001), doi:10.1109/16.902741
[3] C.P. Dietrich, M. Grundmann in Wide Band Gap Semiconductor Nanowires: Low-Dimensionality Effects and Growth, V. Consonni, G. Feuillet eds., p. 303-323 (Wiley-ISTE, Hoboken-London 2014), doi:10.1002/9781118984321.ch12

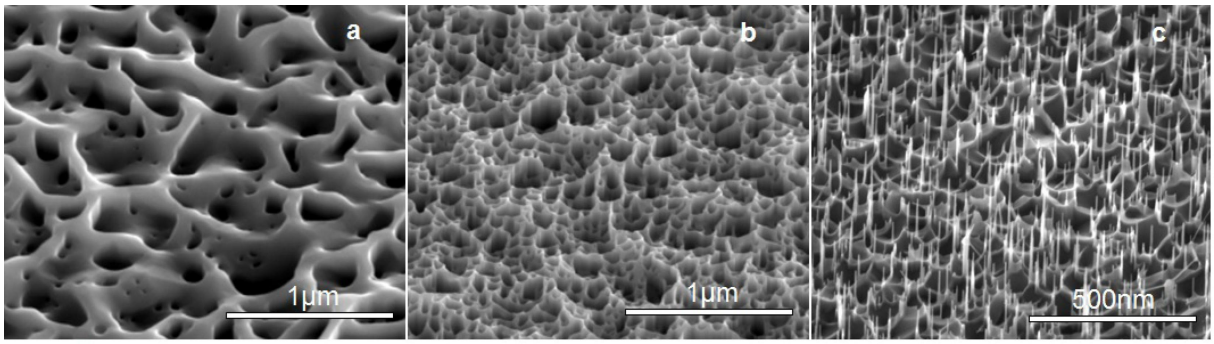

Figure 9.33: SEM images after the PLD NWs growth process for a seed layer with 1% of Al for (a) $T \approx 900\,°C$, (b) $T \approx 700\,°C$ and (c) $T \approx 400\,°C$.

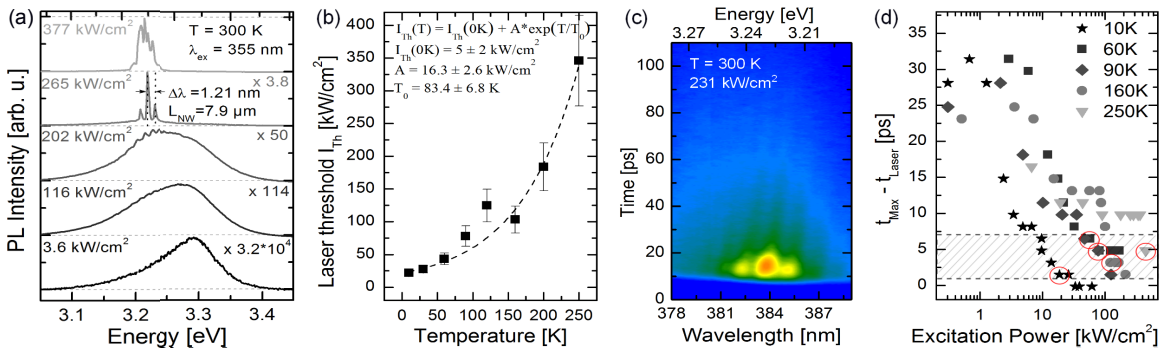

Figure 9.34: (a) Excitation power dependent PL spectra at 300 K. With increasing excitation power narrow laser modes appear around 3.21 eV. (b) The temperature dependence of the laser threshold power exhibits an exponential increase with increasing temperature. (c) Contour plot of PL decay at 300 K in a logarithmic color scale. (d) Excitation power dependent switch-on time. The switch-on time t_{on}^{laser} in the laser regime is marked by circles in the shaded region.

9.22 Lasing dynamics in ZnO nanowires

M. Wille, T. Michalsky, R. Schmidt-Grund, M. Grundmann

Zinc oxide nanowires (ZnO NWs) feature outstanding optical properties like waveguiding, light amplification and lasing under electrical and optical excitation. Indeed a ZnO NW provides all necessities for a laser system intrinsically: under high excitation the semiconductor material acts as active medium and the resonator geometry is provided by the end facets of the NW.

Figure 9.34(a) shows the photoluminescence (PL) emission out of a facet of a ZnO NW for several excitation powers at room temperature. The laser transition is characterized by the transition from broad spontaneous emission out of narrow resonator modes and a spectral red shift of the main emission intensity with increasing excitation power due to renormalization effects. Temperature dependent lasing experiments exhibit an exponential increase of the laser threshold power with increasing temperature (Fig. 9.34(b)). The dynamics of the laser process was investigated with time-resolved PL experiments using a streak camera with a temporal resolution of around 5 ps.

Figure 9.34(c) shows an example streak image at 300 K and at the laser threshold power. The drop of the PL intensity in time is described by a biexponential decay

model. The decay constants $\tau_1 < 5\,\text{ps}$ (decay out of an electron-hole plasma) and $\tau_2 = (50-200)\,\text{ps}$ (excitonic decay) do not change significantly in the investigated temperature range. Conspicuously the Fabry-Pérot modes exhibit a continuous spectral red shift in time, see Fig. 9.34(c). Indeed, the absolute value of this mode shift increases with increasing temperature ($(0.01-0.4)\,\text{meV/ps}$). This behavior can be qualitatively described by the temperature dependence and the temporal change of the refractive index dispersion after the optical excitation. Furthermore, we investigated the time between the impinging of the laser pulse and the built-up of maximal PL intensity. This time $t_{\text{max}} - t_{\text{laser}}$ is depicted in Fig. 9.34(d) in dependence on the excitation power and for different temperatures. It is observable that the switch-on time of the nano-emitter decreases with increasing excitation power. This is due to a faster scattering process with phonons and charge carriers at higher carrier densities. Because of the temporal resolution limit of our setup, the switch-on time of the nano-emitter in the laser regime (marked by the shaded region in Fig. 9.34(d)) can be assessed to be $t_{\text{on}}^{\text{laser}} < 5\,\text{ps}$.

This work was supported by the Deutsche Forschungsgemeinschaft within FOR1616 (SCHM2710/2-1).

9.23 Exciton-Polaritons in ZnO-based microcavities: temporal evolution, phase coherence and mode simulation

H. Franke, T. Michalsky, M. Thunert, S. Richter, O. Herrfurth, S. Lange, A. Holm, R. Buschlinger*, U. Peschel*, C. Sturm, M. Grundmann, R. Schmidt-Grund

*Friedrich-Schiller-Universität Jena, Institut für Festkörpertheorie und -optik,
Max-Wien-Platz 1,
07743 Jena

Polariton physics is still in the focus of current research, as it provides fascinating new effects but is also of considerable interest for applications in quantum information [1, 2]. The polaritons are quasi-particles arising from the strong coupling (SC) of light with matter, i.e. photons and excitons in the semiconductor, and are therefore easily manipulable.Their properties can be tuned by choosing the respective photonic or excitonic fraction or by interaction with their environment. As polaritons are bosons with a small effective mass, they can condense into a macroscopically occupied quantum state, analogous to an atomic Bose-Einstein condensate (BEC). In order to reach the SC regime and polariton condensation the active material, here ZnO, is sandwiched between two highly reflective Bragg reflectors (DBR) forming a so-called microcavity (MC) [6, 7, 13].

We have studied three different aspects in ZnO-based MC:

- For ZnO, it was found, that the relaxation of polaritons into the condensate is strongly enhanced by longitudinal optical (LO) phonons [3]. So, in the first part, Sec. 9.23.1, we have investigated the temporal decay of exciton-polaritons in a planar wedge-shaped MC and confirmed the strong influence of LO phonons on the scattering mechanism of polaritons.

- In the last decade, SC of polaritons and polariton BEC in MCs with strong disorder was realised, and therefore disorder effects have come into focus and are being explored on the quest for possible benefits [4]. In Sec. 9.23.2, we have carried out measurements with a Michelson interferometer on a planar MC and could prove, that condensed polaritons that are subject to significant disorder still preserve their phase coherence.

- Propagation of polariton condensates, i.e. superfluidity, at room temperature is an issue, which most promisingly can be reached by using one-dimensional ZnO nanostructures, as here weak disorder due to almost perfect crystallinity is present. So finally, in Sec. 9.23.3 we investigated ZnO-nanowire based MC with concentrical DBR shells. Here, we could prove the SC regime in coexistance with weakly coupled modes, which could be supported by finite difference time domain (FDTD) simulations.

9.23.1 Time-resolved polariton decay in a ZnO-based microcavity

The temporal decay of polaritons has been studied to some extent in GaAs-based microcavities (MC) [5]. It is expected that the polariton decay and relaxation processes in MC with a ZnO cavity differ qualitatively, because of the pronounced longitudinal optical (LO) phonon scattering. It has already been shown in the literature, that the lowest condensation threshold is reached, if the lower polariton branch (LPB) ground state is in energetic resonance with an LO phonon replica of an exciton [3].
The studied MC contains a wedge-shaped cavity layer, which allows to vary the energetical difference δE between the LPB ground state and the first LO phonon replica of the free A-exciton by probing on different positions on the sample (Fig. 9.35 (a)). It can be seen, that the LPB ground state shows maximal intensity when δE is small. Here, the LPB ground state is highly populated due to efficient LO phonon scattering of hot reservoir polaritons into the LPB ground state.

Time-resolved photoluminescence spectroscopy (PL) measurements were carried out at $T = 10\,\mathrm{K}$ and $130\,\mathrm{K}$. Thereby, a laser pulse creates off-resonantly a polariton ensemble in the MC decaying in (sub)pico-seconds. The luminescence resulting from their radiative recombination was measured energy and time resolved by k-space imaging using a streak camera. Transients were measured and modelled with a bi-exponential function to obtain characteristic decay times (Fig. 9.35 (b)). The transients revealed the slowest decay rate for $\delta E \approx 0$ at $T = 10\,\mathrm{K}$. This is related to efficient LO phonon scattering of reservoir polaritons into the ground state. As the reservoir states are fed continuously by slowly relaxing hot excitons, the LPB ground state is refilled continuously for a long time. This behaviour is not observed at $T = 130\,\mathrm{K}$. The reason for the difference might be inhomogeneities of the sample or a change of the scattering rate of polaritons with LO phonons.

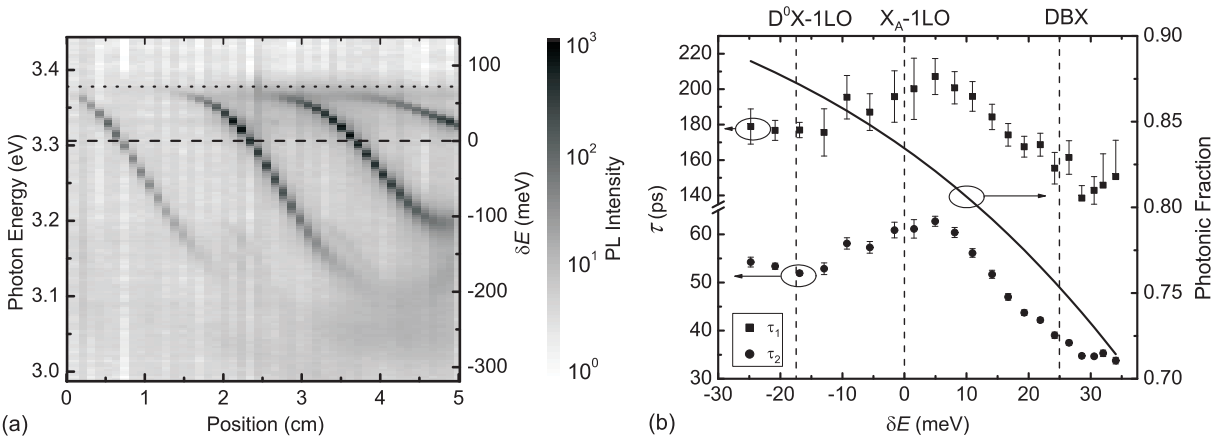

Figure 9.35: (a) PL linescan across the MC for zero in-plane wave vector at $T = 10\,\mathrm{K}$. (b) Decay times $\tau_{1,2}$ (*squares* respective *circles*) of the LPB ground state population at $T = 10\,\mathrm{K}$. The *solid* line shows the photonic fraction of the polaritons given by the corresponding Hopfield coefficient assuming a constant coupling strength of 40 meV, typical for ZnO MC [6]. The vertical *dashed* lines indicate the energies of excitonic transitions.

9.23.2 Coherence properties of disordered exciton-polariton Bose-Einstein condensates

In the last two years we reported on the influence of an effective disorder potential V_{dis} on the exciton-polariton BEC in a ZnO-based planar MC (see [7] for MC details). Experimentally, we observed pronounced intensity fluctuations within the far-field emission pattern even at high excitation powers. We found theoretically that this lack of BEC stabilization against increasing density or rather potential energy E_{pot} due to repulsive interaction relies on the driven dissipative nature of the condensate, leading to disorder-induced density-independent phase fluctuations [8, 9]. Thereby, the condensates phase fluctuation length is predominantly determined by the ratio $V_{\mathrm{dis}}/E_{\mathrm{pot}}$. If it exceeds a critical value, frequency detuning between different regions of the condensate sets in [10, 11], which may even result in spatial separation of uncorrelated BEC fragments [12].

To clarify, if the phase coherence of the disordered BEC in our MC is still preserved, we applied temporal coherence measurements of the BEC emission. For this purpose, we extended our μ-PL setup by a Michelson interferometer in plane mirror (PM) - retroreflector (RR) configuration. In doing so, we superimposed the far-field emission pattern $I(k_x, k_y)$ with its centrosymmetric counterpart. Thus, we superimpose beams with opposite emission angles θ, that originate from the decay of polaritons with opposite in-plane wave vector $k_{\|} \propto \sin\theta$. This allows us to determine the first-order correlation function $g^1(k, -k, \Delta t)$ with a temporal delay of Δt. The resulting interference pattern is determined by the geometry of the interferometer setup and the emission wavelength and can be adjusted by shifting the RR perpendicular to the optical axis.

The RR is mounted on a motorized linear stage with a maximum travel distance of 300 mm with sub-μm resolution. Thus, we are able to systematically vary the temporal delay between the emission from both interferometer arms up to $\Delta t_{\mathrm{max}} = 2 \times s_{\mathrm{max}}/c = 2\,\mathrm{ns}$ with sub-fs resolution. By analyzing the visibility $(I_1 - I_2)/(I_1 + I_2)$ of the interference patterns (Fig. 9.36 (a,b)) as a function of the temporal delay (path difference)

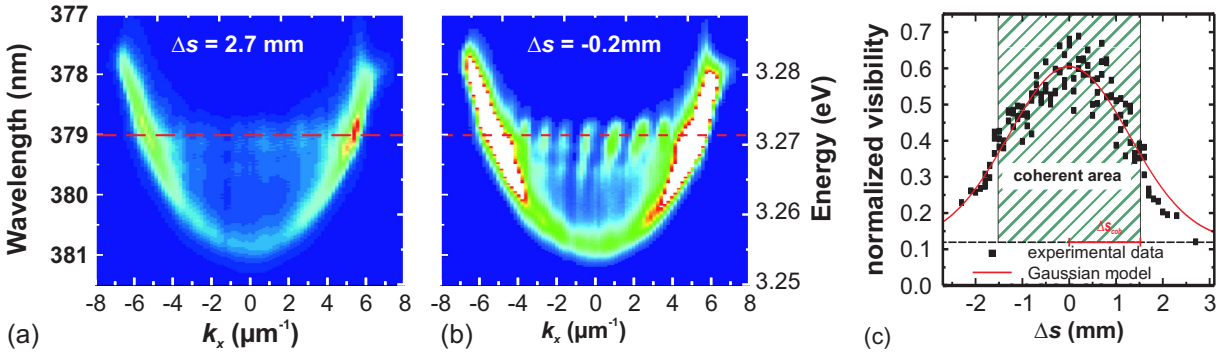

Figure 9.36: (a,b) *k*-space PL interference patterns: (a) large path difference Δs: uncorrelated far-field PL emission (basically the sum of the emission from the individual interferometer arms), (b) path differences close to zero: distinct interference fringes indicating mutual temporal coherence of the polariton emission. (c) Normalized visibility of the interference fringes as a function of the path difference for the condensate energy which is marked by the dashed red line in (a,b).

we deduced a coherence time of about $\tau_{\mathrm{coh}} = 5\,\mathrm{ps}$ for the polariton BEC emission (c.f. Fig. 9.36). This is more than 50 times larger than the lifetime of the uncondensed polaritons, which indicates coherence conservation during the multiple reabsorption and reemission processes of the investigated out-of equilibrium quantum system.

9.23.3 Light-matter interaction in a one-dimensional wire cavity

For the formation of polaritons being able to propagate only in one direction, we used high quality ZnO nanowires in combination with a radial symmetrical distributed Bragg reflector for a two dimensional lateral photonic confinement. The nanowire (NW) MC consists of a ZnO core wire grown by low vacuum pulsed laser deposition (PLD) surrounded concentrically by an all-oxide DBR shell. This shell consists of yttria stabilized zirconia (YSZ) and alumina layers and was made in a conventional PLD setup [13].

Photoluminescence (PL) measurements show that there is a rich diversity of photonic modes present in the NW MC structure as shown in Fig. 9.37: (a) A spatially resolved scan along the wire axis reveals the slight tapering of the NW diameter towards tip and foot and (b) depicts the dispersion of the resonator modes with angular resolution parallel to the wire axis. We generally can identify two types of modes. On the one hand we find weakly coupled photonic modes showing no strong interaction with the ZnO excitons. On the other hand there exist modes showing a clear anticrossing behaviour in their dispersion relations in the vicinity of the exciton resonances which proofs the achievement of the SC regime [1]. We also measured the temperature evolution of these modes from $10-300\,\mathrm{K}$. Modelling the polariton mode dispersion and its temperature evolution supposes that the SC regime is stable up to room temperature (Fig. 9.37 (c)).

Furthermore, excitation density dependent PL measurements show a nonlinear increase in intensity out of the weakly coupled modes (not shown here). Together with the underlying redshift of the gain profile and the relatively high threshold density of about $200\,\mathrm{kW/cm^2}$ even at $T = 10\,\mathrm{K}$, the gain mechanism for this lasing process is assumed to be an electron hole plasma.

To uncover the spatial mode distribution inside the NW MC we performed FDTD

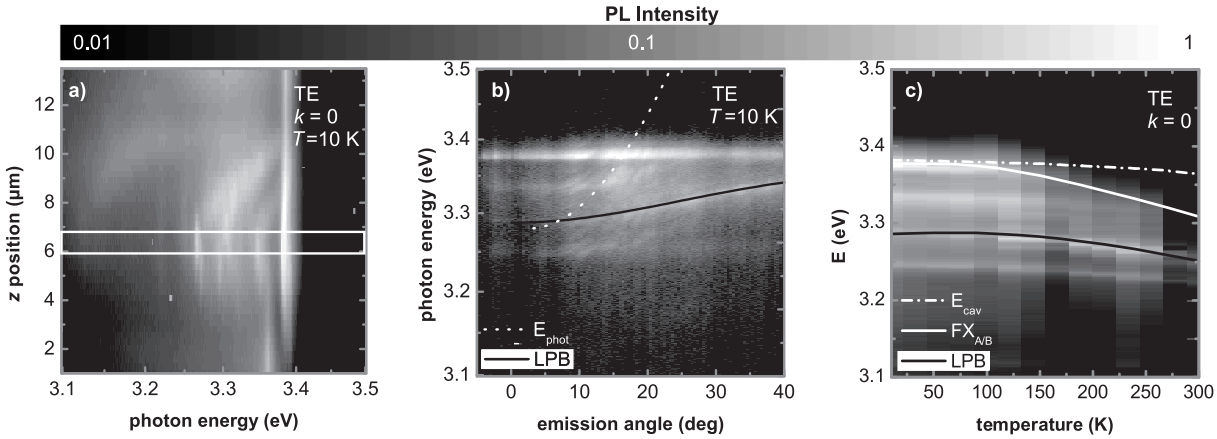

Figure 9.37: (a) Confocal PL linescan at $T = 10\,\mathrm{K}$ along the wire axis showing the locally varying cavity mode ground states. (b) Mode dispersion recorded from the spatial position highlighted by the white box in (a). The lines in (b) follow exemplarily one weakly (*white dotted*) and one strongly (*black*) coupled mode. (c) Temperature evolution of the resonator modes at $k = 0$ together with a polariton mode (*black*) which is modeled by coupling a bare cavity mode (*white solid*) with the ZnO A and B excitons (*white dotted*). (a) SEM images of the NW MC cross-sections, cut at different heights as indicated by the markings. Simulated cross-sectional field distributions in a circular (b) and hexagonal (c) geometry exemplarily for two mode energies.

simulations. Scanning electron microscopy (SEM) images of cross sections, cut perpendicular to the wire axis at various heights z, allowed to determine the geometry of the NW MC as shown in Fig. 9.38 (a). It turned out that the shape of the ZnO core wire changes from hexagonal over round back to hexagonal along the wire axis. Therefore FDTD simulations were performed for a circular (Fig. 9.38 (b)) and a hexagonal (Fig. 9.38 (c)) geometry. These simulations yield many resonant modes inside the resonator. It turnes out that here two relevant mode families are present. These are modes with and without overlap with the ZnO core wire, where the latter ones can be identified as the polariton modes. But a clear assignment between experiment and simulation remains unclear up to this point.

This work was supported by the Deutsche Forschungsgemeinschaft through project GR 1011/20-2 and within FOR1616 and by Deutscher Akademischer Austauschdienst within the project PPP Spain (ID 57050448). We acknowledge the cooperation regarding interferometry with María Dolores Martín and Luis Viña.

[1] D. Sanvitto and V. Timofeev, *Exciton-Polaritons in Microcavities*, Springer-Verlag 2012, doi:10.1007/978-3-642-24186-4
[2] T. Espinosa-Ortega and T.C.H. Liew, Phys. Rev. B **87**, 195305 (2013), doi:10.1103/PhysRevB.87.195305
[3] L. Orosz et al., Phys. Rev. B **85**, 121201 (2012), doi:10.1103/PhysRevB.85.121201
[4] M. Litinskaya, Phys. Lett. A **372**, 3898 (2008), doi:10.1016/j.physleta.2008.02.062
[5] B. Deveaud et al., Phys. Rev. Lett. **67**, 2355 (1991), doi:10.1103/PhysRevLett.67.2355
[6] H. Franke, PhD thesis, Universität Leipzig (2012), http://nbn-resolving.de/urn:nbn:de:bsz:15-qucosa-98174
[7] H. Franke et al., New. J. Phys. **14**, 013037 (2012), doi:10.1088/1367-2630/14/1/013037
[8] C. Sturm et al., in *The Physics Institutes of Universität Leipzig*, Report 2013, M. Grundmann (Ed.), pp. 222, Leipzig, 2014

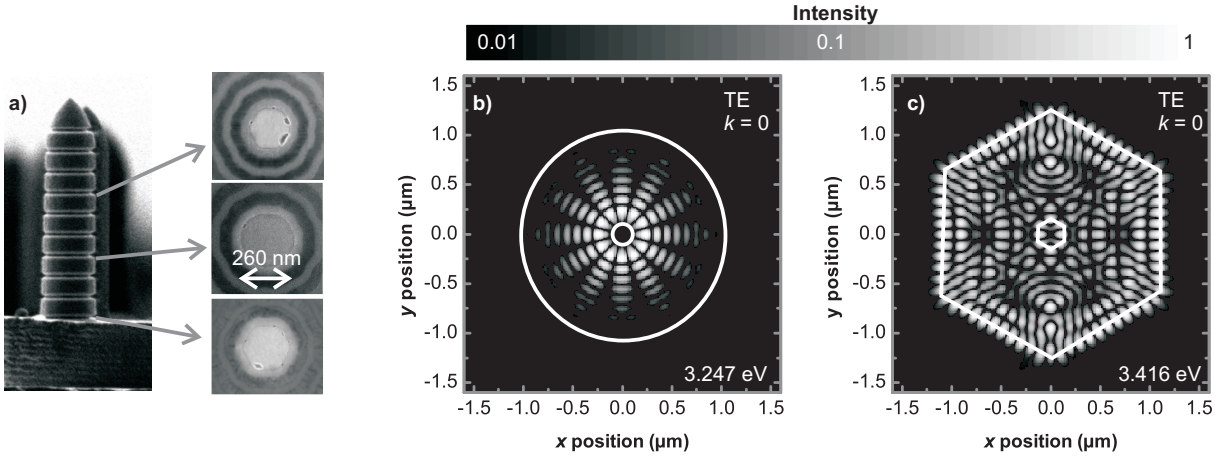

Figure 9.38: (a) SEM images of the NW MC cross-sections, cut at different heights as indicated by the markings. Simulated cross-sectional field distributions in a circular (b) and hexagonal (c) geometry exemplarily for two mode energies.

[9] M. Thunert, A. Janot et al., arxiv:1412.8667 (2014), submitted
[10] A. Baas et al., Phys. Rev. Lett. **100**, 170401 (2008), doi:10.1103/PhysRevLett.100.170401
[11] M. Wouters et al., Phys. Rev. B **77**, 121302 (2008), doi:10.1103/PhysRevB.77.121302
[12] D. Krizhanovskii et al., Phys. Rev. B **80**, 045317 (2009), doi:10.1103/PhysRevB.80.045317
[13] R. Schmidt-Grund et al., phys. stat. sol. B **247**, 1351 (2010), doi:10.1002/pssb.200945530

9.24 Modeling the conductivity around the dimensionality controlled metal-insulator transition in $LaNiO_3$ / $LaAlO_3$ (100) superlattices

H.M. Wei, M. Lorenz, M. Grundmann

$LaNiO_3$ (LNO) is an interesting material exhibiting Pauli paramagnetic metallic behavior in a wide temperature range. New properties can emerge in the LNO-based superlattices (SLs) by modifying the orbital, electronic, and magnetic structure of the bulk LNO [1]. Based on our form work on single LNO and LAO films, we fabricated (100)-oriented [LNO (d nm)/LAO (2 nm)]$_{10}$ SLs (therafter [d/2]$_{10}$).

The SL structure, thickness, and interfacial roughness was checked by various XRD methods. Fig. 9.39 (a) displays the XRD $2\theta-\omega$ scans of the [2/2]$_{10}$ SL on LSAT substrate. Satellite peaks up to third order are observed which indicate smooth interfaces between the LAO and the LNO layers. From the distance between adjacent satellite peaks, the thickness of one LNO/LAO double layer is estimated to be 4.00 ± 0.03 nm, which is fully consistent with our design of 2 nm LAO and 2 nm LNO. By fitting XRR curve as shown in the inset of Fig. 9.39 (a), the interfacial roughness is in between 0.37 and 0.54 nm. Fig. 9.39 (b) shows a typical RSM collected around the asymmetric (-103) LSAT

substrate peak. The RSM clearly reveals that the in-plane lattice parameter of the SL is identical to that of the substrate.

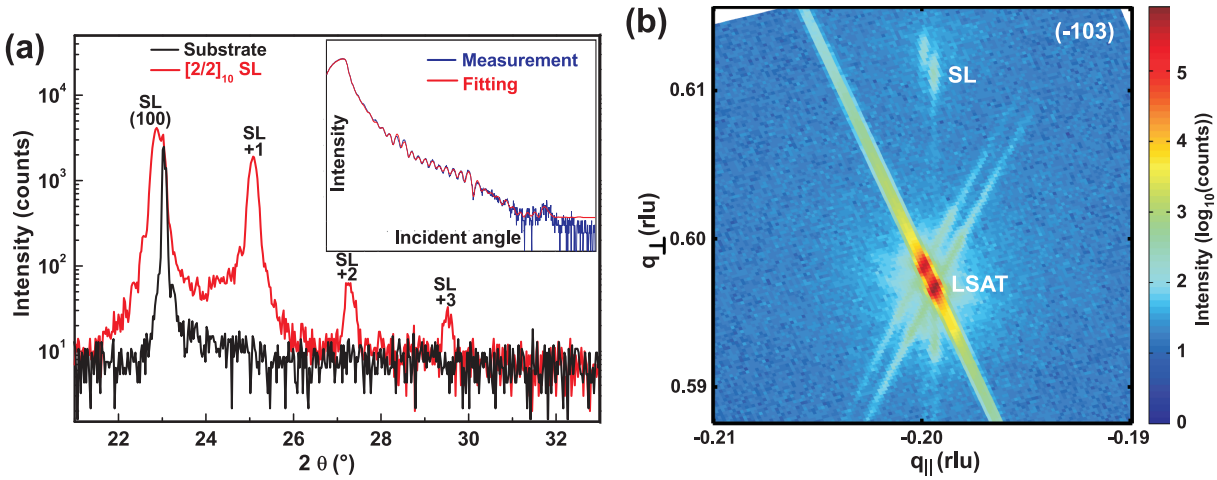

Figure 9.39: (a) XRD $2\theta - \omega$ scans of $[2/2]_{10}$ SL on LSAT (100) substrate. The inset show the corresponding X-ray reflectivity measurement and model fit. (b) RSM of $[2/2]_{10}$ SL around the asymmetric LSAT (-103) peak.

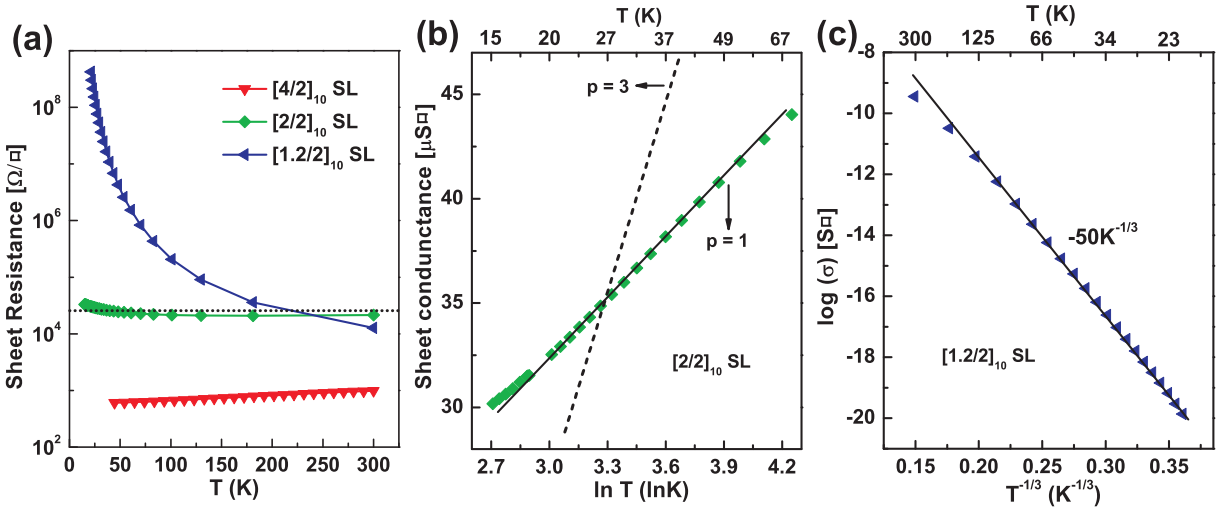

Figure 9.40: (a) Temperature-dependent resistivity of LNO/LAO SLs. (b) Sheet conductance versus the logarithm of temperature $\ln(T)$ for $[2/2]_{10}$ SL. (c) Logarithm of conductance $\log(\sigma)$ as a function of $1/T^{1/3}$ of $[1.2/2]_{10}$ SL.

The dependence of resistivity of the SLs with temperature is drastically changed as shown in Fig. 9.40 (a). The horizontal black dotted line in Fig. 9.40 (a) corresponds to 25.8 $k\Omega/\square$ which is the quantum of resistance in 2D state [2]. The sheet resistivity of $[4/2]_{10}$ SL is much lower than that value, and metallic behavior is found at all temperatures. When the sheet resistivity is close to 25.8 $k\Omega/\square$, the $[2/2]_{10}$ SL undergoes a transformation from metallic to insulating state. In contrast, the $[1.2/2]_{10}$ SL which is considered to be insulating shows a strong increase in resistance with decreasing temperature.

The temperature-dependent resistivity is fitted by appropriate models to clarify the intrinsic conductivity mechanism of the SLs for different LNO thickness. As shown in

Fig. 9.40 (b), the 2D zero-field conductivity shows a logarithmic increase as temperature increases: $\sigma = \sigma_0 + p\frac{e^2}{\pi h} ln(\frac{T}{T_0})$, where p is an index depending on scattering mechanism [3]. If the main inelastic relaxation mechanism is due to $el-el$ collisions, p=1, whereas $el-ph$ scattering gives p=3. The calculated p value of $[2/2]_{10}$ SL is close to 1 indicates the conductivity at low temperatures is dominated by $el-el$ collisions. In contrast, the temperature dependent resistivity of $[1.2/2]_{10}$ SL can be described using a 2D Mott variable range hopping model: $\sigma = \sigma_0 exp[-(T_0/T)^{1/3}]$ as shown in Fig. 9.40 (c) [4]. The relationship between hopping distance R and localization length a is given by: $R = \frac{1}{3}a(\frac{T_0}{T})^{1/3}$ [5]. The ratio of R/a is larger than 1 within the temperature range verifies the validity of the 2D VRH mechanism.

In summary, we have demonstrated epitaxial and lattice matched growth of LNO/LAO SLs. A clear quantum confinement effect on the electronic properties including a metal-insulator transition is demonstrated for decreasing LNO thickness. For more detailed information on the experiment and discussion of conduction mechanisms see Ref [6]. We thank the Deutsche Forschungsgemeinschaft (DFG) for financial support within the Collaborative Research Center SFB 762 "Functionality of Oxide Interfaces", and the project LO790/5-1 "Oxide topological insulator thin films".

[1] M. K. Stewart et al.: J. Appl. Phys. **110**, 033514 (2011), doi:10.1063/1.3614019
[2] R. Scherwitzl et al.: Phys. Rev. Lett. **106**, 246403 (2011), doi:10.1103/106.246403
[3] P. A. Lee et al: Rev. Mod. Phys. **57**, 287 (1985), doi:10.1103/RevModPhys.57.287
[4] W. Brenig et al: Philos. Mag. **27**, 1093 (1973), doi:10.1080/14786437308225819
[5] S. J. Lee et al.: Phys. Rev. B **46**, 12695 (1992), doi:10.1103/PhysRevB.46.12695
[6] H. M. Wei et al.: Appl. Phys. Lett. **106**, 042103 (2015), doi: 10.1063/1.4907011

9.25 Heteroepitaxial $YBiO_3$ thin films grown by pulsed laser depostion

M. Jenderka, M. Grundmann, M. Lorenz

The cubic perovskite $YBiO_3$ (YBO) was recently proposed to be a novel oxide topological insulator (TI) by first-principles calculations [1]. YBO has a high bulk resisitivity in the order of MΩm and a large band gap permitting room temperature operation. In contrast to earlier TIs, such as Bi_2Te_3 [2, 3], the insulating bulk promises the realization of truly surface-dominated transport and its direct measurement. TIs have the potential to realize structures with emergent exotic phenomena, such as Majorana Fermions, that are relevant for applications in spintronics, thermoelectricity and quantum computation [4, 5]. Originally, YBO was deposited on $LaAlO_3$ (LAO) as a buffer layer for the high-temperature superconductor $YBa_2Cu_3O_{7-\delta}$ [6] by aqueous chemical solution deposition. Here, we report on the heteroepitaxy of YBO thin films grown by pulsed laser deposition (PLD) on LAO(100) single crystalline substrates.

A polycrystalline YBO target was solid-state synthesized by sintering Y_2O_3 and Bi_2O_3 powders in a molar ratio of 1:1 in an oxygen atmosphere of 1 bar. X-ray diffraction (XRD) confirmed the presence of residual Y_2O_3 and Bi_2O_{3-x} in the light-orange target indicative of an incomplete reaction. Optimized PLD of single crystalline YBO

films on LAO(100) was performed at an oxygen partial pressure of 0.05 mbar, a growth temperature of 550°C and with 1875 laser pulses (thickness ~ 100 nm). The corresponding XRD 2Θ-ω pattern shown in Fig. 9.41(a) is indexed according to the fcc unit cell [7]. YBO grows on LAO(100) with (100) preferential orientation. The in-plane epitaxial relationship, investigated by ϕ-scans of the YBO(220) and LAO(111) reflections, is found to be YBO[110]||LAO[111], see inset in Fig. 9.41(a). The typical film surface has a root-mean-squared roughness of about 3.5 nm and shows droplets indicating a not optimally consolidated target.

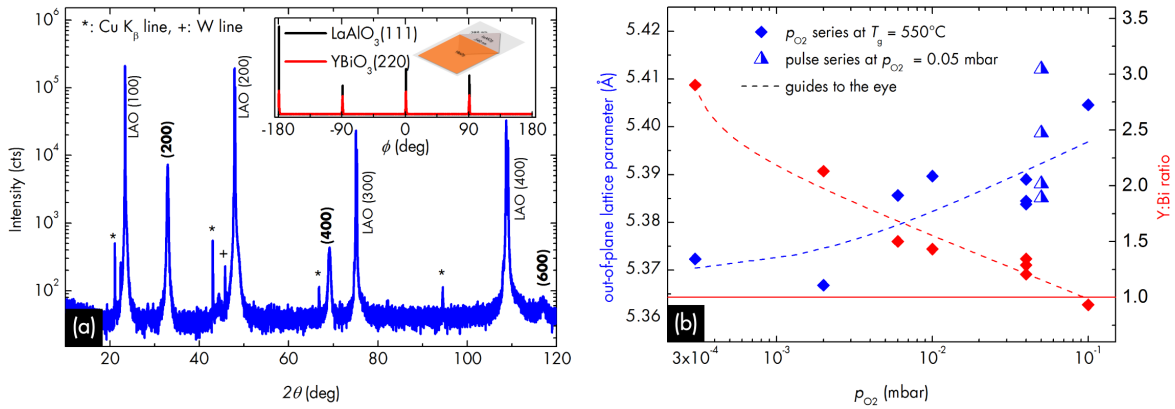

Figure 9.41: (a) XRD 2Θ-ω-scan confirms the (100) preferential orientation of YBO grown on LAO(100). Inset: The XRD ϕ-scan and the schematic illustrate the in-plane epitaxial relationship, i.e., YBO[110]||LAO[111]. (b) Dependence of out-of-plane lattice constant a_{out} and Y:Bi ratio on the oxygen partial pressure p_{O2} during PLD of YBO on LAO(100).

The structural properties of YBO films can be influenced by oxygen partial pressure (p_{O2}) and the number of laser pulses, i.e., film thickness. p_{O2} has impact on the out-of-plane lattice constant (a_{out}) and the Y:Bi ratio, see Fig 9.41(b). Low p_{O2} promotes O_2-vacancies and a sublimation of Bi and/or Bi_2O_3 thus effectively increasing the Y:Bi ratio in the film. The observed change of lattice dimensions can be understood by the different ionic radii of Bi and Y (1.03 and 0.90 Å) and the incorporation of said O_2-vacancies. XRD confirmed that thicker films have a reduced out-of-plane lattice constant and show an additional (111) preferential orientation.

[1] H. Jin et al.: Scientific Reports **3**, 1651 (2013), doi:10.1038/srep01651
[2] B. Skinner et al.: Phys. Rev. Lett. **109**, 176801 (2012), doi:10.1103/PhysRevLett.109.176801
[3] L. Barreto et al.: Nano Lett. **14**, 3755 (2014), doi:10.1021/nl501489m
[4] J.-H. Song et al.: Phys. Rev. Lett. **105**, 096493 (2010), doi:10.1103/PhysRevLett.105.096403
[5] C. Nayak et al.: Rev. Mod. Phys. **80**(3), 1083 (2008), doi:10.1103/RevModPhys.80.1083
[6] G. Li et al.: J. Mater. Res. **22**, 2398 (2007), doi:10.1557/jmr.2007.0320
[7] X.J. Zhang et al.: J. Supercond. Nov. Magn. **23**, 1011 (2010), doi:10.1007/s10948-009-0615-1

9.26 Strain influence on Magnetoresistivity in Sr_2FeMoO_6

P. Schwinkendorf, M. Lorenz, F. Bern, P. Esquinazi, M. Grundmann

Sr_2FeMoO_6 (SFMO) is a ferromagnetic double perovskite with Curie temperature (T_C) above 400 K. The cubic unit cell exhibits a lattice constant of 7.879 Å. The major reason for investigation on this material are its potentially 100 % spin polarized Fermi level electrons due to its half-metallic bandstructure [1] and the arising magnetoresistance (MR). Previous investigations point out intergrain tunneling as the main force behind this MR. Therefore, the grainsize is the most influencing parameter on its magnitude [2].
We investigated the possibile tunability of the MR by strain due to growth of thin SFMO films on different substrates. Our samples were fabricated by pulsed laser deposition (PLD) ablating a stochiometric polycrystalline target. SFMO then was deposited on either $LaAlO_3$ (LAO), MgO, $MgAl_2O_4$ or $SrTiO_3$ (STO) all of which were (00l) oriented. Growth parameters have been optimized in several attempts showing a strong influence of growth temperature and background pressure while laser energy and pulse frequency were not crucial.
X-ray diffraction of the films revealed a strong influence of the substrate on the out-of-plane lattice constant (fig. 9.42 (a)). The films appear to mainly consist of (00l) oriented SFMO. However, secondary phases such as Fe_3O_4 or $SrFeO_3$ can not always be excluded since the growth temperature window for single phase SFMO is as narrow as some 5 K around 1195 K. By SQUID-measurements the predicted ferromagnetism as well as the

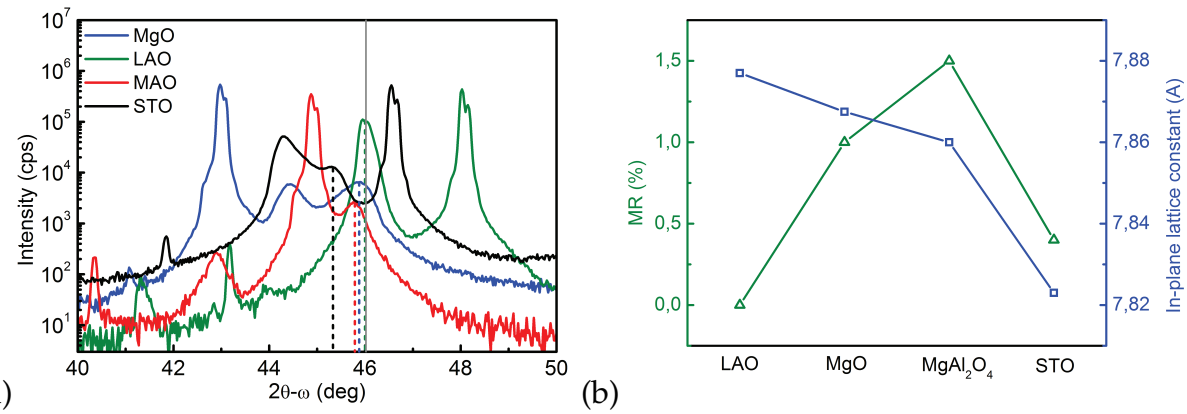

Figure 9.42: (a) XRD pattern of SFMO films on 4 different substrates (The grey line indicates the expected peak-position of relaxed SFMO.) (b) Relative MR of SFMO films measured at 0.75 T / 100 K and their in-plane lattice constants with respect to the corresponding substrate

$T_C > 400$ K could be confirmed.
Magnetoresistance differes largely between samples on different substrates but does not seem to correlate with the lattice constant of the SFMO. Figure 9.42 (b) shows in-plane film lattice constant as well as relative MR (100 K, 750 mT) for films on the indicated substrate. We therefore assume the substrate dependent grainsize of the SFMO to be responsible for this difference as this also matches the observations of AFM images. Figure 9.43 shows 5 μm × 5 μm AFM images of the sample surfaces. It reveals an epitaxial film with monolayer surface steps and without significant structural

defects in the case of LAO substrate (fig. 9.43 (b)). Considering the fully relaxed lattice constant (fig 9.42 (a)) this is reasonable and explains the lack of MR due to the lack of grain boundaries. The film on STO (fig. 9.43 (d)) shows a similar but not as perfect surface probably resulting in a higher grain boundary density and thus a higher MR. Nevertheless single grains seem still to be larger than 5 μm. This model applies for the samples grown on MgO (fig. 9.43 (a)) and $MgAl_2O_4$ (fig. 9.43 (c)) as here grains are in the range of 1 μm and MR is significantly increased. We thank N. Sobolev for preparation of the PLD target.

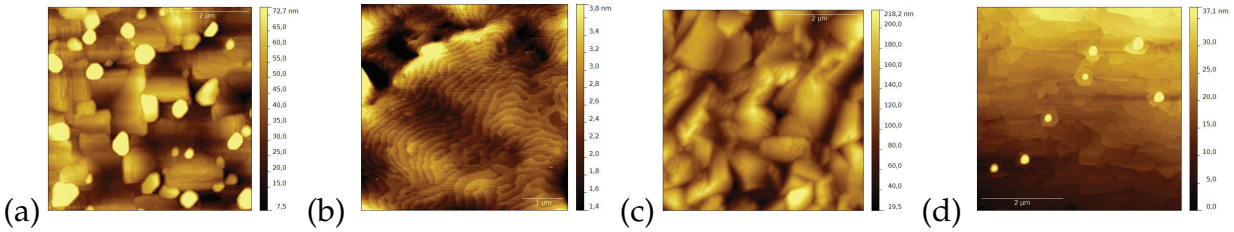

Figure 9.43: AFM images of SFMO films grown on (a) MgO (b) LAO (c) $MgAl_2O_4$ (d) STO

[1] K.-I. Kobayashi, T. Kimura, H. Sawada, K. Terakura, Y. Tokura; Nature **395**, p677 (1998)
[2] C. L. Yuan, S. G. Wang, W. H. Song, T. Yu, J. M. Dai, S. L. Ye, Y. P. Sun; Appl. Phys Lett. **75**, p3853 (1999)

9.27 PLD grown MgO-barriers for zinc ferrite based magnetic tunnel junctions

M. Bonholzer, M. Lorenz, M. Grundmann

Spinel oxides such as magnetite (Fe_3O_4) and zinc ferrite ($ZnFe_2O_4$) show promising properties for spintronic applications, i.e. semiconducting behavior and a high spin polarization [1–4]. We use zinc ferrite as ferrimagnetic electrode in order to realize room temperature operation of oxide based magnetic tunnel junctions (MTJs). The structure of our test-devices for characterization of the MgO-barriers is MgO(Substrate)/TiN/$ZnFe_2O_4$/MgO-barrier. This structure is grown epitaxially by pulsed laser deposition (PLD). On top we deposited Au-contacts by RF-sputtering. Also samples with a $ZnFe_2O_4$ top layer were grown for XRR-thickness analysis.
TiN is used as a highly conductive interlayer in order to reduce the series resistance of the device. The TiN [5] and $ZnFe_2O_4$ layers can be grown epitaxially with a high crystalline quality and atomically flat surfaces on in-situ annealed MgO-substrates.
On top of $ZnFe_2O_4$ we grow MgO with different thicknesses (variation of the number of PLD pulses). The appearance of RHEED intensity oscillations during deposition suggest two-dimensional growth of these layers (see Figure 9.44, a). Analysis of oscillation periods gives a growth rate of 0.95 nm per 100 pulses leading to the MgO thicknesses given in Table 9.2.

	XRR	RHEED	Brinkman-fit
TiN	19		
$ZnFe_2O_4$	27		
MgO 300 pulses	2.7	2.9	1.3
500 pulses	4.5	4.8	1.8
700 pulses	6.2	6.7	2.7
$ZnFe_2O_4$	14		

Table 9.2: Layer thicknesses (all values in nm) determined by X-ray reflectivity (XRR) performed on samples with a $ZnFe_2O_4$ top layer, by RHEED-intensity oscillation period during MgO deposition and by fitting the Brinkman model to the I-V curves of the tunnel junctions.

Table 9.2 also presents the results of X-ray reflectivity (XRR) measurements of layer stacks with a $ZnFe_2O_4$ top layer (see Figure 9.44, b). The values of MgO-thickness from XRR measurements are in a good agreement to the ones of the RHEED oscillation analysis.
We measured current-voltage characteristics of the tunnel junctions and determined the effective tunnel thickness by fitting the Brinkman model to the obtained data [6]. The mean values of the determined thicknesses for different pulse numbers are presented in the third row of Table 9.2. These values are smaller than the ones obtained by RHEED and XRR. This can be explained by small inhomogeneities in the thickness of the MgO layer. Tunneling resistance depends exponentially on the barrier thickness. Thinner areas therefore have a much smaller resistance and contribute more to the resulting current than thicker areas. The macroscopic measurement over the whole contact area gives an average value, resulting in smaller effective thicknesses.
The resistance area (RA) over effective thickness plot (Figure 9.44, c) gives a barrier height of $\phi \approx 0.4\,\mathrm{eV}$. This value is also reported in literature for MgO barriers achieving a TMR-value higher than 100% in metal based MTJs [7]. Therefore our barriers are suitable for use in oxide based MTJs.

[1] M. Opel *et al.*, Phys. Status Solidi A **208**, 232 (2011)
[2] C.E. Rodríguez Torres *et al.*, Phys. Rev. B **84**, 064404 (2011)
[3] K. Brachwitz *et al.*, Appl. Phys. Letters **102**, 172104 (2013)
[4] M. Lorenz *et al.*, Phys. Status Solidi RRL **5**, 438 (2011)
[5] M. Bonholzer *et al.*, Phys. Status Solidi A **211**, 2621 (2014)
[6] W. F. Brinkman *et al.*, J. Appl. Phys. **41**, 1915 (1970)
[7] F. Schleicher *et al.*, Nature Communications **5**, 4547 (2014)

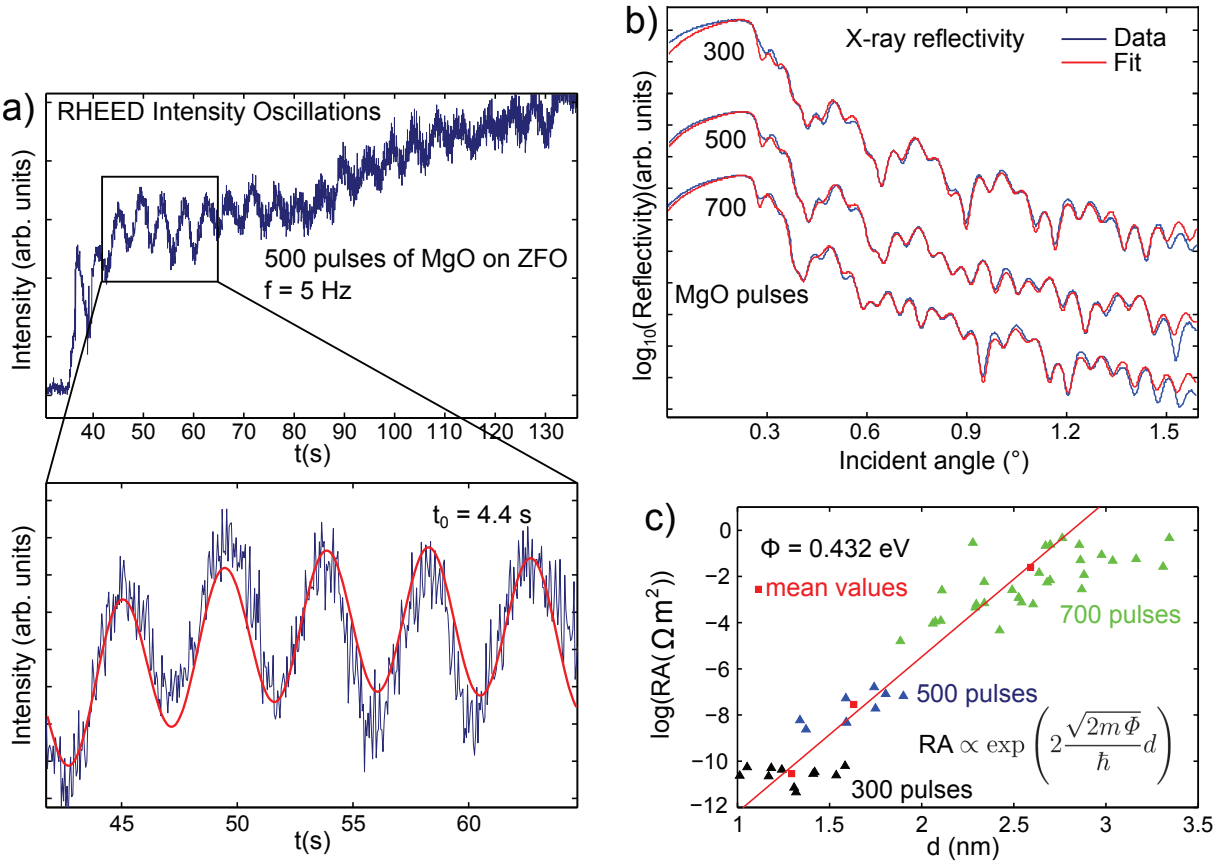

Figure 9.44: a) RHEED intensity over time during pulsed laser deposition (PLD) of MgO on top of $ZnFe_2O_4$. RHEED intensity oscillations are clearly visible indicating a two dimensional growth mode. The zoomed part shows the sine fit for determination of period time. This gives a growth rate of 0.95 nm per 100 pulses.
b) X-ray reflectivity measurements on samples with a $ZnFe_2O_4$ layer on top of the MgO barrier. Model fits are shown in red, obtained thickness values are presented in Table 9.2. Graphs are shifted for clarity.
c) Resistance area product over effective barrier thickness determined by fitting the Brinkman model to the I-V curves of several of our tunnel junctions. Colors indicate contacts on the same sample with specific numbers of PLD pulses (three samples). Linear fit was done on the corresponding mean values (red squares). Using the formula shown in the graph (R(V=0) from [6]) gives a barrier height of $\phi \approx 0.4$ eV.
The film thicknesses determined by all three methods are summarized in Table 9.2.

9.28 Funding

Leipzig School of Natural Sciences - Building with Molecules and Nano-objects (BuildMoNa)
Prof. Dr. M. Grundmann
DFG GS 185/2

Polarisationswechselwirkung in Laser-MBE Wurtzit-Perowskit-Heterostrukturen
Prof. Dr. M. Lorenz
SFB 762/2-2012, TP A2 within SFB 762 *Funktionalität Oxidischer Grenzflächen*

Optische Untersuchungen zu magneto-elektro-optischen Wechselwirkungen in ihrer Dynamik in oxidischen Heterostrukturen
Dr. Rüdiger Schmidt-Grund
SFB 762/2-2012, TP B03 within SFB 762 *Funktionalität Oxidischer Grenzflächen*

Lateraler Transport in oxidischen Feldeffekt-Strukturen
Dr. H. von Wenckstern, Prof. Dr. M. Grundmann
SFB 762/2-2012, TP B04 within SFB 762 *Funktionalität Oxidischer Grenzflächen*

Spinabhängiges Tunneln in oxidischen Heterostrukturen
Prof. Dr. M. Grundmann, Prof. Dr. I. Mertig (Martin-Luther-Universität Halle-Wittenberg)
SFB 762/2-2012, TP B06 within SFB 762 *Funktionalität Oxidischer Grenzflächen*

Bose-Einstein-Kondensation und Supraflüssigkeit von Exziton-Polaritonen bei Raumtemperatur
Prof. Dr. M. Grundmann, Dr. R. Schmidt-Grund
DFG GR 1011/20-2

Extrem verzerrte Nano- und Mikrodrähte
Prof. Dr. M. Grundmann
DFG GR 1011/23-1

Quantum Gases and Liquids in Semiconductor Rods conformally coated with Bragg Mirrors
Dr. R. Schmidt-Grund, Prof. Dr. M. Grundmann
DFG SCHM 2710/2-1, TP P1 within FOR 1616 *Dynamics and Interactions of Semiconductor Nanowires for Optoelectronics*

Oxidische topologische Isolator-Dünnfilme – Darstellung und elektronische Eigenschaften
Prof. Dr. M. Lorenz
DFG LO 790/5-1

Whispering Gallery Moden: Einfluss der Resonatorform auf Lasing-Eigenschaften
Prof. Dr. M. Grundmann
DFG GR 1011/26-1

Amorphe Spinelle als p-Typ Halbleiter
Prof. Dr. M. Grundmann
DFG GR 1011/27-1

Cupferiodid: Epitaxie, Dioden und Ferromagnetismus
Prof. Dr. M. Grundmann
DFG GR 1011/28-1

Ortsaufgelöste nanomechanische Eigenschaften funktionaler Oberflächen – Experiment und Simulation

Prof. Dr. M. Grundmann, Prof. Dr. Dr. B. Rauschenbach (Leibniz-Institut für Oberflächenmodifizierung e. V.), Prof. Dr. S. Mayr (Leibniz-Institut für Oberflächenmodifizierung)
SAW-2011-IOM-2

Graduiertenschule: Wolken, Aerosole und Strahlung am Beispiel des Mineralstaubes
Prof. Dr. M. Grundmann, Prof. Dr. A. Macke (Leibniz-Institut für Troposphärenforschung e. V.)
SAW-2012-IfT-4

3D in situ Ellipsometrie
Dr. R. Schmidt-Grund, Dr. C. Bundesmann (Leibniz-Institut für Oberflächenmodifizierung e. V.)
Forschungs- und Entwicklungsvertrag im Rahmen der Förderung aus dem Europäischen Sozialfonds

Transparente photovoltaische Zellen
Prof. Dr. M. Grundmann
Europäischer Fonds für regionale Entwicklung (EFRE) Energie und Klimaschutz – RL EuK 2007

Leistungselektronik auf Basis von Galliumoxid
Prof. Dr. M. Grundmann
Europäischer Fonds für regionale Entwicklung (EFRE) Energie und Klimaschutz – RL EuK 2007

Effiziente Energienutzung: Neue Konzepte und Materialien
Prof. Dr. M. Grundmann
ESF-Nachwuchsforschergruppe des Freistaates Sachsen im Rahmen des Europäischen Sozialfonds

Elektron-Phonon-Wechselwirkung in Mikro- und Nanonadeln
Dipl.-Phys. Christian Kranert
Landesinnovationspromotionsstipendium des Freistaates Sachsen im Rahmen des Europäischen Sozialfonds

Magnetotunnel-Widerstände mit oxidischen Kontakten
Michael Bonholzer, M.Sc.
Landesinnovationspromotionsstipendium des Freistaates Sachsen im Rahmen des Europäischen Sozialfonds

Transparente MESFET für digitale Anwendungen
Prof. Dr. M. Grundmann, Dr. H. Frenzel
BMBF 03V0509

High-resolution fingerprint sensing with piezoelectric nanowire matrices: PiezoMat
Prof. Dr. M. Grundmann
European Union, Seventh Framework Programme 611019

Postdoctoral scholarship: Investigation of vertically stacked functional oxides
Dr. O. Sviridova
European Union: Stipendienprogramm Erasmus Mundus WEBB

Working Interships in Science and Engineering (WISE)
Kaustav Dey and Dr. H. von Wenckstern
DAAD A1377677

PPP Spanien: Kohärenzeigenschaften kondensierter Exziton-Polaritonen
Dr. R. Schmidt-Grund
DAAD 57050448

9.29 Organizational Duties

M. Grundmann

- Prodekan Forschung der Fakultät für Physik und Geowissenschaften
- Direktor des Instituts für Experimentelle Physik II
- Stellvertretender Sprecher der Graduiertenschule "Leipzig School of Natural Sciences - Building with Molecules and Nano-objects" (BuildMoNa), http://www. buildmona.de
- Stellvertretender Sprecher des Sonderforschungsbereiches "Funktionalität Oxidischer Grenzflächen" (SFB762), http://www.physik.uni-halle.de/sfb762
- Sprecher der Fächerübergreifenden Arbeitsgemeinschaft Halbleiterforschung Leipzig (FAHL), http://www.uni-leipzig.de/~fahl
- Mitglied des wissenschaftlichen Beirats des Leibniz-Instituts für Oberflächenmodifizierung e. V., Leipzig (IOM)
- Organizer MRS Fall Meeting, Boston, Symposium "Oxide Semiconductors"
- Project Reviewer: Deutsche Forschungsgemeinschaft (DFG), Alexander von Humboldt-Stiftung (AvH), Schweizerischer Nationalfonds zur Förderung der wissenschaftlichen Forschung (FNSNF), Fonds zur Förderung der Wissenschaften (FWF), EU, Österreichische Forschungsförderungsgesellschaft mbH (FFG), Agence Nationale de la Recherche (ANR, France)
- Referee: Appl. Phys. Lett., Electr. Lett., J. Appl. Phys., Nature, Physica E, Phys. Rev. B., Phys. Rev. Lett., Phys. Stat. Sol., Adv. Materials, u.a.

M. Lorenz

- Editorial Board Member Journal of Physics D: Applied Physics (IOP, Bristol, U.K.)
- Project referee: Alexander von Humboldt-Stiftung
- Referee: Advanced Materials, Applied Physics Letters, Applied Physics A, Applied Surface Science, Chemical Communications, IEEE Photonics, Technology Letters, J. of Physics D: Applied Physics, J. Materials Chemistry C, J. Materials Science, J. Physical Chemistry, J. Applied Physics, Nanoscale (RSC), Phys. Chem. Chem. Phys. (RSC), Phys. Stat. Sol. Rapid Research Letters, Thin Solid Films

H. von Wenckstern

- Project Reviewer: U.S. Department of Energy – Office of Science, National Research Fondation RSA

- Referee: Appl. Phys. Lett., J. Appl. Phys., Thin Solid Films, Solid State Electron., Phys. Stat. Sol., Superlatt. Microstruct., J. Electron. Mater., Turk. J. Phys., J. Mater. Sci., Mater. Electron., J. Vac. Sci. Technol., Mater. Sci. Eng. B, J. Nanosci. Nanotechnol., Microelectron. Eng., J. Phys. D, J. Cryst. Growth, Surf. Sci.

R. Schmidt-Grund

- Vice Chair of the German Association on Ellipsometry (Arbeitskreis Ellipsometrie – Paul Drude e.V.)
- Project Reviewer: Deutsche Forschungsgemeinschaft (DFG), US Department of Energy – Office of Science
- Referee: Thin Solid Films, Current Applied Physics, Phys. Stat. Sol. C, Nature Communications, Appl. Phys. Lett., Optics Express, Journal of Electromagnetic Waves and Applications, Opt. Materials, ACS Applied Materials & Interfaces

H. Frenzel

- Referee: IEEE Electronic Device Letters, Thin Solid Films, Applied Physics Letters, ETRI Journal, Journal of Applied Physics, Japanese Journal of Applied Physics, Advanced Materials, physics status solidi (a)

9.30 External Cooperations

Academic

- Leibniz-Institut für Oberflächenmodifizierung e. V., Leipzig, Germany
  Prof. Dr. B. Rauschenbach, Prof. Dr. S. Mayr, Dr. J. Gerlach, Dr. C. Bundesmann, Dr. A. Lotnyk
- Universität Leipzig, Fakultät für Chemie und Mineralogie, Germany
  Prof. Dr. H. Krautscheid, Prof. Dr. R. Denecke
- Universität Halle-Wittenberg, Germany
  Prof. Dr. I. Mertig, Prof. Dr. W. Widdra, Prof. Dr. S.G. Ebbinghaus, Prof. Dr. W. Hergert
- Max-Planck-Institut für Mikrostrukturphysik, Halle/Saale, Germany
  Dr. O. Breitenstein, Dr. A. Ernst, Dr. P. Werner, Prof. Dr. D. Hesse
- Forschungszentrum Dresden-Rossendorf, Germany
  Prof. Dr. M. Helm, Dr. K. Potzger
- Technische Universität Berlin, Germany
  Prof. Dr. D. Bimberg, Prof. Dr. A. Hoffmann
- University of Aveiro, Portugal
  Prof. N. A. Sobolev
- Universität Magdeburg, Germany
  Dr. J. Bläsing, Prof. Dr. J. Christen
- Universität Jena, Germany
  Prof. Dr. C. Ronning
- University of Pretoria, South Africa
  Prof. F. D. Auret

- University of Canterbury, Christchurch, New Zealand
  Prof. Dr. M. Allen
- Centre de Recherche sur l' Hétéro-Epitaxie et ses Applications (CNRS-CRHEA), Valbonne, France
  Dr. J. Zúñiga-Pérez
- Western Michigan University, USA
  Prof. Dr. S. M. Durbin
- Katholieke Universiteit Leuven, Belgium
  Dr. V. Lazenka, Prof. Dr. K. Temst

Industry

- Solarion AG, Leipzig Germany
  Dr. A. Braun, Dr. A. Rahm
- Freiberger Compound Materials GmbH, Freiberg, Germany
  Dr. G. Leibiger

9.31 Publications

Journals

S. Acharya, S. Chouthe, H. Graener, T. Böntgen, C. Sturm, R. Schmidt-Grund, M. Grundmann, G. Seifert: *Ultrafast dynamics of the dielectric functions of ZnO and $BaTiO_3$ thin films after intense femtosecond laser excitation*, J. Appl. Phys. **115**, 053508 (9 pages) (2014)

M. Bonholzer, M. Lorenz, M. Grundmann: *Layer-by-layer growth of TiN by pulsed laser deposition on in-situ annealed (100) MgO substrates*, phys. stat. sol. (a) **211**(11), 2621-2624 (2014)

R. Böttcher, A. Pöppl, M. Lorenz, S. Friedländer, D. Spemann, M. Grundmann: *^{55}Mn Pulsed ENDOR Spectroscopy of Mn^{2+} Ions in ZnO Thin Films and Single Crystal*, J. Magn. Res. **245**, 79-86 (2014)

J.L. Cholula-Díaz, J. Barzola-Quiquia, H. Krautscheid, C. Kranert, T. Michalsky, P. Esquinazi, M. Grundmann: *Conducting behavior of chalcopyrite-type $CuGaS_2$ crystals under visible light*, Phys. Chem. Chem. Phys. **16**, 21860-21866 (2014)

C.P. Dietrich, M. Grundmann: *Pulsed-laser deposition growth of ZnO NWs*, Wide Band Gap Semiconductor Nanowires: Low-Dimensionality Effects and Growth, Vincent Consonni, Guy Feuillet eds., p. 303-323 (2014) (Wiley-ISTE, 2014), ISBN 978-1-84821-597-9

L. Fricke, T. Böntgen, J. Lorbeer, C. Bundesmann, R. Schmidt-Grund, M. Grundmann: *An extended Drude model for the in-situ spectroscopic ellipsometry analysis of ZnO thin layers and surface modifications*, Thin Solid Films **571**, 437-441 (2014)

M. Grundmann, R. Karsthof, H. von Wenckstern: *The recombination current in type-II heterostructure bipolar diodes*, ACS Appl. Mat. & Interf. **6**(17), 14785-14789 (2014)

M. Grundmann, F.-L. Schein, R. Karsthof, P. Schlupp, H. von Wenckstern: *Several Approaches to Bipolar Oxide Diodes With High Rectification*, Adv. Sci. Technol. **93**, 252-259 (2014)

M. Grundmann, M. Scheibe, M. Lorenz, J. Bläsing, A. Krost: *X-ray multiple diffraction of ZnO substrates and heteroepitaxial thin films*, phys. stat. sol. (b) **251**(4), 850-863 (2014)

T. Jakubczyk, H. Franke, T. Smolenski, M. Sciesiek, W. Pacuski, A. Golnik, R. Schmidt-Grund, M. Grundmann, C. Kruse, D. Hommel, P. Kossackiy: *Inhibition and Enhancement of the Spontaneous Emission of Quantum Dots in Micropillar Cavities with Radial Distributed Bragg Reflectors*, ACS Nano **8**(10), 9970-9978 (2014)

M. Kneiß, M. Jenderka, K. Brachwitz, M. Lorenz, M. Grundmann: *Modeling the electrical transport in epitaxial undoped and Ni-, Cr-, and W-doped TiO_2 anatase thin films*, Appl. Phys. Lett. **105**, 062103 (5 pages) (2014)

C. Kranert, R. Schmidt-Grund, M. Grundmann: *Raman active phonon modes of cubic In_2O_3*, phys. stat. sol. RRL **8**(6), 554-559 (2014)

C. Kranert, J. Lenzner, M. Jenderka, M. Lorenz, H. von Wenckstern, R. Schmidt-Grund, M. Grundmann: *Lattice parameters and Raman-active phonon modes of $(In_xGa_{1-x})_2O_3$ for $x < 0.4$*, J. Appl. Phys. **116**, 013505 (7 pages) (2014)

M. Lorenz, M. Lange, C. Kranert, C.P. Dietrich, M. Grundmann: *Optical properties of and optical devices from ZnO-based nanostructures*, Zinc Oxide Nanostructures: Advances and Applications, p. 43-99 (2014), M. Willander, ed. (Pan Stanford Publishing, Singapore, 2014), ISBN 9789814411332

M. Lorenz, R. Böttcher, S. Friedländer, A. Pöppl, D. Spemann, M. Grundmann: *Local lattice distortions in oxygen deficient Mn-doped ZnO thin films, probed by electron paramagnetic resonance*, J. Mat. Chem. C **2**, 4947-4956 (2014)

M. Lorenz, A. de Pablos-Martin, C. Patzig, M. Stölzel, K. Brachwitz, H. Hochmuth, M. Grundmann, T. Höche: *Highly textured fresnoite thin films synthesized by pulsed laser deposition with CO_2 laser direct heating*, J. Phys. D: Appl. Phys. **47**(3), 034013 (9 pages) (2014)

M. Lorenz, V. Lazenka, P. Schwinkendorf, F. Bern, M. Ziese, H. Modarresi, A. Volodin, M. van Bael, K. Temst, A. Vantomme, M. Grundmann: *Multiferroic $BaTiO_3$-$BiFeO_3$ composite thin films and multilayers: Strain engineering and magnetoelectric coupling*, J. Phys. D: Appl. Phys. **47**(13), 135303 (10 pages) (2014)

T. Michalsky, M. Wille, C.P. Dietrich, R. Röder, C. Ronning, R. Schmidt-Grund, M. Grundmann: *Phonon-assisted Lasing in ZnO Microwires at Room Temperature*, Appl. Phys. Lett. **105**, 211106 (4 pages) (2014)

S. Müller, H. von Wenckstern, D. Splith, F. Schmidt, M. Grundmann:

Control of the conductivity of Si-doped β-Ga_2O_3 thin films via growth temperature and pressure, phys. stat. sol. (a) **211**(1), 34-39 (2014)

S. Müller, H. von Wenckstern, F. Schmidt, D. Splith, R. Heinold, M. Allen, M. Grundmann: *Method of choice for fabrication of high-quality ZnO-based Schottky diodes*, J. Appl. Phys. **116**, 194506 (12 pages) (2014)

S. Puttnins, S. Jander, A. Wehrmann, G. Benndorf, M. Stölzel, A. Müller, H. von Wenckstern, F. Daume, A. Rahm, M. Grundmann: *Breakdown characteristics of flexible Cu(In,Ga)Se_2 solar cells*, Sol. Energy Mat. Sol. Cells **120**, 506-511 (2014)

F.-L. Schein, M. Winter, T. Böntgen, H. von Wenckstern, M. Grundmann: *Highly rectifying p-$ZnCo_2O_4$/n-ZnO heterojunction diodes*, Appl. Phys. Lett. **104**, 022104 (4 pages) (2014)

P. Schlupp, H. von Wenckstern, M. Grundmann: *Amorphous zinc-tin oxide thin films fabricated by pulsed laser deposition at room temperature*, Proc. Mat. Res. Soc. **1633**, 101-104 (2014)

F. Schmidt, H. von Wenckstern, O. Breitenstein, R. Pickenhain, M. Grundmann: *Low Rate Deep Level Transient Spectroscopy: A powerful tool for defect characterization in wide bandgap semiconductors*, Sol. St. Electr. **92**, 40-46 (2014)

F. Schmidt, S. Müller, R. Pickenhain, H. von Wenckstern, S. Geburt, C. Ronning, M. Grundmann: *Defect studies on Ar-implanted ZnO thin films*, phys. stat. sol. (b) **251**(5), 937-941 (2014)

F. Schmidt, P. Schlupp, S. Müller, C.P. Dietrich, H. von Wenckstern, M. Grundmann, R. Heinhold, H.-S. Kim, M.W. Allen: *A DLTS study of ZnO microwire, thin film and bulk material*, Proc. Mat. Res. Soc. **1633**, 51-54 (2014)

F. Schmidt, S. Müller, H. von Wenckstern, G. Benndorf, R. Pickenhain, M. Grundmann: *Impact of strain on defects in (Mg,Zn)O thin films*, J. Appl. Phys. **116**, 103703 (9 pages) (2014)

R. Schmdit-Grund, S. Richter, S.G. Ebbinghaus, M. Lorenz, C. Bundesmann, M. Grundmann: *Electronic transitions and dielectric function tensor of a $YMnO_3$ single crystal in the NIR-VUV spectral range*, RSC Adv. **4**(63), 33549-33554 (2014)

R. Schmidt-Grund, C. Kranert, T. Böntgen, H. von Wenckstern, H. Krauß, M. Grundmann: *Dielectric function in the NIR-VUV spectral range of $(In_xGa_{1-x})_2O_3$ thin films*, J. Appl. Phys. **116**, 053510 (7 pages) (2014)

R. Schmidt-Grund, H. Krauß, C. Kranert, M. Bonholzer, M. Grundmann: *Temperature dependence of the dielectric function in the spectral range (0.5-8.5) eV of an In_2O_3 thin film*, Appl. Phys. Lett. **105**, 111906 (4 pages) (2014)

P. Schwinkendorf, M. Lorenz, H. Hochmuth, Z. Zhang, M. Grundmann: *Interface charging effects in ferroelectric ZnO-$BaTiO_3$ field-effect transistor heterostructures*, phys. stat. sol. (a) **211**(1), 166-172 (2014)

D. Splith, S. Müller, F. Schmidt, H. von Wenckstern, J.J. van Rensburg, W.E. Meyer, M. Grundmann: *Determination of the mean and the homogeneous barrier height of Cu Schottky contacts on heteroepitaxial β-Ga_2O_3 thin films grown by pulsed laser deposition*, phys. stat. sol. (a) **211**(1), 40-47 (2014)

M. Stölzel, A. Müller, G. Benndorf, M. Lorenz, M. Grundmann, C. Patzig, T. Höche: *Determination of the spontaneous polarization of wurtzite (Mg,Zn)O*, Appl. Phys. Lett. **104**, 192102 (4 pages) (2014)

C. Tessarek, R. Röder, T. Michalsky, S. Geburt, H. Franke, R. Schmidt-Grund, M. Heilmann, B. Hoffmann, C. Ronning, M. Grundmann, S. Christiansen: Improving the optical properties of self-catalyzed GaN microrods towards whispering gallery mode lasing, ACS Photonics **1**(10), 990-997 (2014)

M. Thunert, A. Janot, H. Franke, C. Sturm, T. Michalsky, M.D. Martín, L. Viña, B. Rosenow, M. Grundmann, R. Schmidt-Grund: *Cavity Polariton Condensate in a Disordered Environment*, arXiv:1412.8667 (12 pages) (2014)

H. von Wenckstern, Z. Zhang, J. Lenzner, F. Schmidt, M. Grundmann: *A continuous composition spread approach towards monolithic, wavelength-selective multichannel UV-photodetector arrays*, Proc. Mat. Res. Soc. **1633**, 123-129 (2014)

H. von Wenckstern, D. Splith, F. Schmidt, M. Grundmann, O. Bierwagen, J.S. Speck: *Schottky contacts to In_2O_3*, APL Mat. **2**, 046104 (7 pages) (2014)

Z. Zhang, H. von Wenckstern, M. Grundmann: *Monolithic multichannel ultraviolet photodiodes based on (Mg,Zn)O thin films with continuous composition spreads*, IEEE J. Sel. Top. Quantum Electr. **20**(6), 3801606 (6 pages) (2014)

Talks

C.P. Dietrich, R. Johne, T. Michalsky, C. Sturm, P. Eastham, H. Franke, M. Grundmann, R. Schmidt-Grund: *Bose-Einstein condensation of whispering gallery mode exciton-polaritons in ZnO micro-wire resonators*, 32nd International Conference on the Physics of Semiconductors, Austin, Texas, USA, August 2014

H. Frenzel, M. Lorenz, F. L. Schein, A. Lajn, H. von Wenckstern, **M. Lorenz**, M. Grundmann: *Transparente Transistoren und ihre Anwendungen*, Seminar zur Lehrerfortbildung, Universität Leipzig, Fakultät für Physik und Geowissenschaften, Leipzig, Germany, January 2014

M. Grundmann: *Transparent Electronics: Physics, Materials and Devices*, Institut für Elektronik und Sensor Materialien, TUBA Freiberg, Germany, January 2014 (invited)

M. Grundmann: *Bipolar Oxide Electronics - Materials and Devices*, The 41st Int. Symp on Compound Semiconductor (ISCS 2014), Montpellier, France, May 2014 (invited)

M. Grundmann: *Semiconducting Oxides: Novel Materials and Applications*, Seminar des Fraunhofer Institut für Werkstoffmechanik (IWM), Halle/S, Germany, June 2014 (invited)

M. Grundmann: *Recent Developments in the Research and Application of Transparent Conducting and Semiconducting Oxides*, CIMTEC 2014, 6th Forum on New Materials, Symposium FH, Montecatini Terme, Italy, June 2014 (invited)

M. Grundmann: *Amorphous oxides and oxide heterostructures for electronic applications*, CECAM International Workshop "Nanostructured Zinc Oxide and related materials", Bremen, Germany, June 2014 (invited)

M. Grundmann: *Innovative Oxid-Materialien*, Netzwerk Energie & Umwelt e.V., HHL Leipzig, Germany, July 2014 (invited)

M. Grundmann: *Bipolar Oxide Electronics: Materials and Devices*, Wright State University/ Wright-Patterson Air Force Base, Dayton, OH, USA, July 2014 (invited)

M. Grundmann: *Bipolar Oxide Electronics: Materials and Devices*, Ohio State University, Columbus, OH, USA, July 2014 (invited)

M. Grundmann: *Transparent Electronics*, 13th European Vacuum Conference (EVC-13), Aveiro, Portugal, September 2014 (plenary talk, invited)

M. Grundmann: *Bipolar Oxide Electronics – Materials and Devices*, MRS Fall Meeting, Symp. O "Oxide Semicondcutors", Boston, USA, December 2014 (invited)

T. Jakubczyk, H. Franke, T. Smolenski, M. Sciesiek, W. Pacuski, A. Golnik, R. Schmidt-Grund, M. Grundmann, C. Kruse, D. Hommel, P. Kossacki: *Inhibition & Enhancement of the Spontaneous Emission of Quantum Dots in Micropillar Cavities with Radial Bragg Reflectors*, 32nd International Conference on the Physics of Semiconductors, Austin, Texas, USA, August 2014

R. Karsthof, P. Räcke, Z. Zhang, H. von Wenckstern, M. Grundmann: *Charge carrier collection in ZnO/NiO UV solar cells*, Spring Meeting of the German Physical Society 2014, Dresden, Germany, April 2014

R. Karsthof, P. Räcke, Z. Zhang, H. von Wenckstern, M. Grundmann: *Semi-transparent ZnO/NiO UV solar cells*, EMRS Spring Meeting, Lille, France, May 2014

R. Karsthof, H. von Wenckstern, M. Grundmann: *Cu-doped nickel oxide as p-type TCO*, Transparent Conductive Oxides Workshop, Leipzig, Germany, September/October 2014

C. Kranert, J. Lenzner, M. Jenderka, M. Lorenz, H. von Wenckstern, R. Schmidt-Grund, M. Grundmann: *Phonon Modes and Structural Properties of* $(In,Ga)_2O_3$ *Thin Films*, Transparent Conductive Oxides Workshop, Leipzig, Germany, September/October 2014

C. Kranert, R. Schmidt-Grund, M. Grundmann: *Probing Surface Charges in* ZnO *by Raman Spectroscopy*, 8th International Workshop on Zinc Oxide and Related Materials 2014, Niagara Falls, Ontario, Canada, September 2014

C. Kranert, R. Schmidt-Grund, M. Grundmann: *Resonant Raman scattering by LO phonons in wurtzite semiconductors – the role of the surface and point defects*, XXIV. International Conference on Raman Spectroscopy, Jena, Germany, August 2014

M. Lorenz: *PLD of functional oxides – magnetoelectric coupling and magnetoresistance in multiferroic composites*, KU Leuven, Department of Physics, IKS, Leuven, Belgium, March 2014 (invited)

M. Lorenz: *PLD of functional oxides: Recent activities on transparent semiconductors, highly correlated iridates and multiferroic composites*, Universität Leipzig, Faculty of Physics and Earth Science, MQF-Group Prof. J. Haase, Magnetic Resonance and Materials Science (MaReMaS) Seminar, Leipzig, Germany, June 2014 (invited)

M. Lorenz: *Pulsed laser deposition of functional oxides – towards a transparent electronics*, International Union of Crystallography IUCr2014 Materials or Minerals, Symposium MS-94 - Recent Development of Widegap Materials; Semiconductor and Oxides, Montreal, Canada, August 2014 (invited)

M. Lorenz, H. von Wenckstern, H. Frenzel, M. Grundmann: *Pulsed laser deposition of transparent conducting thin films for future oxide electronics*, Transparent Conductive Oxides Workshop, Leipzig, Germany, October 2014

M. Lorenz: *Novel functional semiconductor materials and devices grown by large-area pulsed laser deposition*, Taishan Academic Forum – Environment and Energy Materials, University of Jinan, Jinan, China, November 2014, appointed as Guest Professor of University of Jinan (invited)

A.A. Mavlonov, S. Richter, H. von Wenckstern, R. Schmidt-Grund, J. Lenzner, M. Grundmann: *Investigation of dopant limitations in (Mg,Zn)O:Al/Ga*, Transparent Conductive Oxides Workshop, Leipzig, Germany, October 2014

T. Michalsky, S. Lange, C.P. Dietrich, R. Röder, M. Wille, H. Franke, R. Schmidt-Grund, M. Grundmann: *Phonon-assisted lasing in ZnO microwires*, Spring Meeting of the German Physical Society 2014, Dresden, Germany, April 2014

S. Müller, H. von Wenckstern, D. Splith, F. Schmidt, M. Grundmann: *Structural and Electrical Properties of Si-doped β-Ga_2O_3 Thin Films*, 8th International Workshop on Zinc Oxide and related Materials, Niagara Falls, Canada, September 2014

K. Rudisch: *Investigation of electronic properties of CuI thin films*, Spring Meeting of the German Physical Society 2014, Dresden, Germany, April 2014

F.-L. Schein, F. Schmidt, T. Böntgen, J. Lenzner, M. Lorenz, H. von Wenckstern, M. Grundmann: *Transparent p-CuI/n-ZnO heterojunction diodes*, 8th International Workshop on Zinc Oxide and Related Materials, Ontario, Canada, September 2014

F.-L. Schein, D. Splith, M. Winter, T. Böntgen, H. von Wenckstern, M. Grundmann: *Highly rectifying p-$ZnCo_2O_4$/n-ZnO heterojunction diodes*, 8th International Workshop on Zinc Oxide and Related Materials, Ontario, Canada, September 2014

F.-L. Schein, P. Schlupp, M. Winter, T. Böntgen, H. von Wenckstern, M. Grundmann: *Highly rectifying p-$ZnCo_2O_4$/n-ZnO heterojunction diodes*, 56th Electronic Materials Conference, Santa Barbara (CA), USA, June 2014

F.-L. Schein, T. Böntgen, J. Lenzner, M. Lorenz, H. von Wenckstern, M. Grundmann: *Transparent p-CuI/n-ZnO heterojunction diodes*, Transparent Conductive Oxides Workshop, Leipzig, Germany, October 2014

P. Schlupp, F.-L. Schein, H. von Wenckstern, M. Grundmann: *Highly rectifying contacts on amorphous zinc-tin-oxide thin films consisting of metals and p-type zinc-cobalt-oxide*, Spring Meeting of the German Physical Society 2014, Dresden, Germany, April 2014

P. Schlupp, F.-L. Schein, H. von Wenckstern, M. Grundmann: *Unipolar and all amorphous bipolar diodes comprising n-type zinc-tin oxide*, 56th Electronic Materials Conference, Santa Barbara, USA, June 2014

P. Schlupp, F.-L. Schein, H. von Wenckstern, M. Grundmann: *All Amorphous Bipolar Heterodiodes Consisting of n-type Zinc-Tin Oxide and p-type Zinc-Cobalt Oxide*, 8th International Workshop on Zinc Oxide, Niagara Falls, USA, September 2014

P. Schlupp, F.-L. Schein, H. von Wenckstern, M. Grundmann: *All Amorphous Bipolar Heterodiodes Consisting of n-type Zinc-Tin Oxide and p-type Zinc-Cobalt Oxide*, Transparent Conductive Oxides Workshop, Leipzig, Germany, October 2014

P. Schlupp, S. Bitter, H. von Wenckstern, M. Grundmann: *Electrical and optical properties of PLD grown amorphous zinc-tin oxide thin films with different Sn/Zn ratios using a continuous composition spread approach*, MRS Fall Meeting, Boston, USA, December 2014

R. Schmidt-Grund, S. Richter, S.G. Ebbinghaus, M. Lorenz, C. Bundesmann, M. Grundmann: *Electronic transitions and dielectric function tensor in the NIR-VUV spectral range of a* $YMnO_3$ *single crystal*, 32nd International Conference on the Physics of Semiconductors, Austin, Texas, USA, August 2014

R. Schmidt-Grund, C. Kranert, H. Krauß, T. Böntgen, H. von Wenckstern, J. Lenzner, M. Grundmann: *NIR-VUV dielectric function of* $(In, Ga)_2O_3$ *thin films*, 32nd International Conference on the Physics of Semiconductors, Austin, Texas, USA, August 2014

D. Splith, S. Müller, H. von Wenckstern, O. Bierwagen, J.S. Speck, M. Grundmann: *Schottky contacts on* β*-*Ga_2O_3 *and* In_2O_3 *thin films*, Spring Meeting of the German Physical Society 2014, Dresden, Germany, April 2014

D. Splith, H. von Wenckstern, F. Schmidt, S. Müller, O. Bierwagen, J.S. Speck, M. Grundmann: *Schottky Contacts on* In_2O_3 *Thin Films grown by Molecular Beam Epitaxy*, 56th Electronic Materials Conference, Santa Barbara, USA, June 2014

D. Splith, S. Müller, H. von Wenckstern, M. Grundmann: *Schottky contacts on* β*-*Ga_2O_3 *thin films grown by pulsed laser deposition*, 8th International Workshop on Zinc Oxide, Niagara Falls, Canada, September 2014

D. Splith, S. Müller, H. von Wenckstern, M. Grundmann: *Schottky contacts on* β*-*Ga_2O_3 *thin films grown by pulsed laser deposition*, Transparent Conductive Oxides Workshop, Leipzig, Germany, October 2014

M. Thunert, A. Janot, C. Sturm, H. Franke, B. Rosenow, R. Schmidt-Grund, M. Grundmann: *Inuence of disorder on polariton BEC*, Spring Meeting of the German Physical Society 2014, Dresden, Germany, April 2014

V. Zviagin, P. Richter, T. Böntgen, M. Lorenz, D.R.T. Zahn, G. Salvan, R. Schmidt-Grund, M. Grundmann: *Ellipsometric study of* $ZnFe_2O_4$, $CoFe_2O_4$, *and* $ZnCo_2O_4$ *spinel oxides*, 8th Workshop Ellipsometry, Dresden, Germany, March 2014

Posters

M. Bonholzer, M. Lorenz, M. Grundmann: *Bottom electrode for zinc ferrite based magnetic tunnel junctions*, Annual Conference of the Graduate School BuildMoNa, Leipzig, Germany, March 2014

M. Bonholzer, M. Lorenz, M. Grundmann: *Bottom electrode for zinc ferrite based magnetic tunnel junctions*, International Workshop - Functionality of Oxide Interfaces, Monestary Irsee, Germany, March 2014

M. Bonholzer, M. Lorenz, M. Grundmann: *High quality TiN as bottom electrode for zinc ferrite based magnetic tunnel junctions grown by pulsed laser deposition*, Spring Meeting of the German Physical Society 2014, Dresden, Germany, April 2014

M. Bonholzer, M. Lorenz, M. Grundmann: *Bottom electrode for zinc ferrite based magnetic tunnel junctions*, Transparent Conductive Oxides Workshop, Leipzig, Germany, October 2014

C.P. Dietrich, R. Johne, T. Michalsky, H. Franke, C. Sturm, M. Lange, P. Eastham, M. Grundmann, R. Schmidt-Grund: *One-dimensional multimodal whispering-gallery exciton-polariton Bose Einstein condensation*, Conference on Physics of Light-Matter Coupling in Nanostructures, Montpellier, France, June, 2014

K. Dorywalski, D. J. Gawryluk, R. Schmidt-Grund, L. Fricke, M. Grundmann, M. Berkowski, M. Piasecki: *Optical features of* $FeTe_{1-x}Se_x$ *superconductors probed by spectroscopic ellipsometry*, 8th Workshop Ellipsometry, Dresden, Germany, March 2014

E.L. Fricke, C. Grüner, C. Bundesmann, R. Schmidt-Grund, M. Grundmann: *Rigorous simulations and analysis of the optical response of silica sculptured thin films*, Spring Meeting of the German Physical Society 2014, Dresden, Germany, April 2014

E.L. Fricke, C. Grüner, C. Bundesmann, R. Schmidt-Grund, M. Grundmann: *Rigorous simulations and analysis of the optical response of silica sculptured thin films*, 8th Workshop Ellipsometry, Dresden, Germany, March 2014

J. Hartmann, H. Franke, M.S. Mohajerani, J. Ledig, X. Wang, F. Steib, M. Straßburg, H.-H. Wehmann, R. Schmidt-Grund, M. Grundmann, A. Waag: *Towards vertically emitting InGaN/GaN 3D nano-LEDs*, E-MRS Spring Meeting 2014, Strasbourg, France, May 2014

M. Jenderka, R. Schmidt-Grund, M. Grundmann, M. Lorenz: *Heteroepitaxial* Li_2IrO_3 *Thin films – Electrical and Optical Properties*, Spring Meeting of the German Physical Society 2014, Dresden, Germany, April 2014

M. Jenderka, R. Schmidt-Grund, M. Grundmann, M. Lorenz: *Heteroepitaxial* Li_2IrO_3 *Thin films – Electrical and Optical Properties*, New Trends in Topological Insulators 2014, Berlin, Germany, July 2014

M. Jenderka, R. Schmidt-Grund, M. Grundmann, M. Lorenz: *Heteroepitaxial* Li_2IrO_3 *Thin films - Electrical and Optical Properties*, Helmholtz virtual institute new states of matter and their excitations 2014 (HVINSM14), Dresden, Germany, September 2014

R. Karsthof, P. Räcke, Z. Zhang, H. von Wenckstern, M. Grundmann: *Carrier collection in semi-transparent n-ZnO/p-NiO UV solar cells*, Annual Conference of the Graduate School BuildMoNa, Leipzig, Germany, March 2014

F.J. Klüpfel, H. von Wenckstern, M. Grundmann: *Low frequency noise in ZnO-based MESFETs*, Spring Meeting of the German Physical Society 2014, Dresden, Germany, April 2014

F.J. Klüpfel, H. von Wenckstern, M. Grundmann: *Low frequency noise in ZnO-based MESFETs*, Transparent Conductive Oxides Workshop, Leipzig, Germany, October 2014

C. Kranert, C. Dähne, J. Lenzner, H. von Wenckstern, R. Schmidt-Grund, and M. Grundmann: *Raman scattering in* $(In, Ga)_2O_3$ *thin films*, Annual Conference of the Graduate School BuildMoNa, Leipzig, Germany, March 2014

C. Kranert, C. Dähne, J. Lenzner, H. von Wenckstern, R. Schmidt-Grund, M. Grundmann: *Raman scattering in* $(In, Ga)_2O_3$ *thin films*, Spring Meeting of the German Physical Society 2014, Dresden, Germany, April 2014

C. Kranert, J. Lenzner, M. Jenderka, M. Lorenz, H. von Wenckstern, R. Schmidt-Grund, M. Grundmann: *Raman scattering in* $(Ga, In, Al)_2O_3$ *thin films*, Transparent Conductive Oxides Workshop, Leipzig, Germany, September/October 2014

C. Kranert, J. Lenzner, M. Jenderka, M. Lorenz, H. von Wenckstern, R. Schmidt-Grund, M. Grundmann: *Phonon Modes and Structural Properties of* $(In, Ga)_2O_3$ *Thin Films*, 8th International Workshop on Zinc Oxide and Related Materials 2014, Niagara Falls, Ontario, Canada, September 2014

C. Kranert, J. Lenzner, M. Jenderka, M. Lorenz, H. von Wenckstern, R. Schmidt-Grund, M. Grundmann: *Raman scattering in* $(Ga, In, Al)_2O_3$ *thin films*, XXIV. International Conference on Raman Spectroscopy, Jena, Germany, August 2014

C. Kranert, J. Lenzner, M. Jenderka, M. Lorenz, H. von Wenckstern, R. Schmidt-Grund, M. Grundmann: *Raman scattering in* $(Ga, In, Al)_2O_3$ *thin films*, 32nd International Conference on the Physics of Semiconductors, Austin, Texas, USA, August 2014

H. Krauß, T. Böntgen, H. von Wenckstern, J. Lenzner, R. Schmidt-Grund, M. Grundmann: *NIR-VUV dielectric function of* $(In, Ga)_2O_3$ *thin films with lateral composition spread*, Spring Meeting of the German Physical Society 2014, Dresden, Germany, April 2014

M. Lorenz, H. Frenzel, H. von Wenckstern, M. Grundmann: *Functional oxide heterostructures by large-area PLD*, Towards Oxide-Based Electronics TO-BE COST Action MP1308, 2014 Fall Meeting, Rome, Italy, September 2014

A.A. Mavlonov, S. Richter, H. von Wenckstern, R. Schmidt-Grund, M. Grundmann: *Electrical and optical properties of (Mg,Zn)O:Al thin films for solar cell application*, Spring Meeting of the German Physical Society 2014, Dresden, Germany, April 2014

A.A. Mavlonov, S. Richter, H. von Wenckstern, R. Schmidt-Grund, J. Lenzner, M. Grundmann: *Effective electron masses in (Mg,Zn)O:Al/Ga thin films derived from wafers with lateral composition spread*, 8th International Workshop on ZnO and Related Materials, Niagara Falls, Canada, September 2014

A.A. Mavlonov, S. Richter, H. von Wenckstern, R. Schmidt-Grund, J. Lenzner, M. Grundmann: *Revisiting dopant efficiency of Al and Ga in (Mg,Zn)O alloy by a continuous composition approach (CCS)*, Transparent Conductive Oxides Workshop, Leipzig, Germany, October 2014

A.A. Mavlonov, S. Richter, H. von Wenckstern, R. Schmidt-Grund, M. Grundmann: *Electrical, optical and structural properties of Al- and Ga-doped (Mg,Zn)O determined from thin films with lateral composition spreads*, 5th International Symposium on Transparent Conducting Materials, Crete, Greece, December 2014

T. Michalsky, H. Franke, R. Schmidt-Grund, T. Jakubczyk, T. Smoleński, W. Pacuski, P. Kossacki, C. Kruse, D. Hommel, M. Heilmann, C. Tessarek, S. Christiansen, M. Grundmann: *Lateral confinement of 1D and 0D cavities by conformal distributed Bragg reflector coating*, 32nd International Conference on the Physics of Semiconductors, Austin, Texas, USA, August 2014

S. Müller, H. von Wenckstern, F. Schmidt, R. Heinhold, M. Allen, M. Grundmann: *Method of choice for the fabrication of high-quality ZnO-based Schottky-diodes*, International Workshop Functionality of Oxide Interfaces, International Workshop – Functionality of Oxide Interfaces, Monestary Irsee, Germany, March 2014

S. Müller, H. von Wenckstern, F. Schmidt, R. Heinhold, M. Allen, M. Grundmann: *Method of choice for the fabrication of high-quality ZnO-based Schottky-diodes*, Spring Meeting of the German Physical Society 2014, Dresden, Germany, April 2014

S. Müller, H. von Wenckstern, F. Schmidt, D. Splith, R. Heinhold, M. Allen, M. Grundmann: *Method of choice for the fabrication of high-quality ZnO-based Schottky-diodes*, 8th International Workshop on Zinc Oxide and related Materials, Niagara Falls, Canada, September 2014

S. Müller, H. von Wenckstern, F. Schmidt, D. Splith, R. Heinhold, M. Allen, M. Grundmann: *Structural and Electrical Method of choice for the fabrication of high-quality ZnO-based Schottky-diodes*, Transparent Conductive Oxides Workshop, Leipzig, Germany, October 2014

A. Reinhardt, H. von Wenckstern, M. Grundmann: *Properties of MIS-diodes based on Si-doped β-Ga_2O_3*, International Workshop - Functionality of Oxide Interfaces, Monestary Irsee, Germany, March 2014

A. Reinhardt, H. von Wenckstern, M. Grundmann: *Properties of MIS-diodes based on Si-doped β-Ga_2O_3*, Spring Meeting of the German Physical Society 2014, Dresden, Germany, April 2014

S. Richter, C. Sturm, H. Franke, R. Schmidt-Grund, and M. Grundmann: *Polarization studies of exciton-polaritons in a planar microcavity*, Annual Conference of the Graduate School BuildMoNa, Leipzig, Germany, March 2014

S. Richter, C. Sturm, H. Franke, R. Schmidt-Grund, M. Grundmann: *Time-resolved photo-ellipsometry studies of exciton-polaritons in a planar ZnO-based microcavity*, Spring Meeting of the German Physical Society 2014, Dresden, Germany, April 2014

S. Richter, C. Sturm, H. Franke, R. Schmidt-Grund, M. Grundmann: *Time-resolved ellipsometry studies of exciton-polaritons in a ZnO-based planar microcavity under pulsed excitation*, 8th Workshop Ellipsometry, Dresden, Germany, March 2014

S. Richter, C. Sturm, H. Franke, R. Schmidt-Grund, M. Grundmann: *Tensorial g-Factor Model for Exciton-Polariton Pseudospin in Magnetic Fields*, International Conference on Problems of Strongly Correlated and Interacting Systems, Saint-Petersburg, Russia, May 2014

S. Richter, C. Sturm, H. Franke, R. Schmidt-Grund, M. Grundmann: *g-factor of exciton-polaritons*, European Conference on Physics Of Magnetism, Poznań, Poland, June 2014

K. Rudisch, F.-L. Schein, G. Benndorf, M. Lorenz, M. Grundmann: *Optical characterization of CuI films*, Spring Meeting of the German Physical Society 2014, Dresden, Germany, April 2014

F.-L. Schein, T. Böntgen, J. Lenzner, M. Lorenz, H. von Wenckstern, M. Grundmann: *Transparent p-CuI/n-ZnO heterojunction diodes*, Spring Meeting of the German Physical Society 2014, Dresden, Germany, April 2014

F.-L. Schein, M. Winter, T. Böntgen, H. von Wenckstern, M. Grundmann: *Highly rectifying p-$ZnCo_2O_4$/n-ZnO heterojunction diodes*, International Workshop - Functionality of Oxide Interfaces, Monestary Irsee, Germany, March 2014

F.-L. Schein, M. Winter, T. Böntgen, H. von Wenckstern, M. Grundmann: *Highly rectifying p-$ZnCo_2O_4$/n-ZnO heterojunction diodes*, Annual Conference of the Graduate School BuildMoNa, Leipzig, Germany, March 2014

R. Schmidt-Grund, C.P. Dietrich, T. Michalsky, R. Johne, P. Eastham, H. Franke, C. Sturm, M. Lange, M. Grundmann: *Parametric scattering in a multimode polariton system*, Spring Meeting of the German Physical Society 2014, Dresden, Germany, April 2014

P. Schlupp, F.-L. Schein, H. von Wenckstern, M. Grundmann: *A fully amorphous heterostructure pn-diode consisting of zinc-tin-oxide and zinc-cobalt-oxide fabricated at room-temperature*, Annual Conference of the Graduate School BuildMoNa, Leipzig, Germany, March 2014

D. Splith, S. Müller, H. von Wenckstern and M. Grundmann: *Schottky contacts on β-Ga_2O_3 thin films grown by pulsed laser deposition*, Annual Conference of the Graduate School BuildMoNa, Leipzig, Germany, March 2014

M. Thunert , A. Janot, T. Michalsky, C. Sturm, B. Rosenow, M.D. Martín, L. Viña, H. Franke, R. Schmidt-Grund, M. Grundmann: *Influence of disorder on polariton BEC*, Annual Conference of the Graduate School BuildMoNa, Leipzig, Germany, March 2014

M. Thunert , A. Janot, T. Michalsky, H. Franke, C. Sturm, B. Rosenow, M.D. Martín, L. Viña, R. Schmidt-Grund, M. Grundmann: *Influence of disorder on exciton-polariton Bose-Einstein-Condensates (BEC)*, International Conference on Problems of Strongly Correlated and Interacting Systems, Saint-Petersburg, Russia, May 2014

M. Wille, C. Czekalla, C.P. Dietrich, S. Geburt, C. Ronning, R. Schmidt-Grund, M. Grundmann: ZnO *Nano- and Microwires as Building Blocks for Optoelectronic Devices*, Annual Conference of the Graduate School BuildMoNa, Leipzig, Germany, March 2014

M. Wille, T. Michalsky, S. Geburt, C. Ronning, R. Schmidt-Grund, M. Grundmann: *Lasing in* ZnO *Nano- and Microwires*, Transparent Conductive Oxides Workshop, Leipzig, Germany, September/October 2014

M. Wille, T. Michalsky, H. Franke, R. Schmidt-Grund, C. Tessarek, M. Grundmann: *Hexagonal nano- and microwire resonators*, CECAM, Bremen, Germany, June 2014

V. Zviagin, P. Richter, T. Böntgen, M. Lorenz, D.R.T. Zahn, G. Salvan, R. Schmidt-Grund, M. Grundmann: *NIR-VUV Spectroscopic Study of* $ZnFe_2O_4$, $CoFe_2O_4$, *and* $ZnCo_2O_4$ *Thin Films*, Spring Meeting of the German Physical Society 2014, Dresden, Germany, April 2014

V. Zviagin, C. Kranert, P. Richter, T. Böntgen, M. Lorenz, D.R.T. Zahn, G. Salvan, R. Schmidt-Grund, M. Grundmann: *Optical and Magneto-Optical Properties of Charge-Transfer Transitions in Normal and Inverse Spinel Oxide Thin Films*, 32nd International Conference on the Physics of Semiconductors, Austin, Texas, USA, August 2014

9.32 Graduations

Doctorate

- Kerstin Brachwitz
  Defekt-induzierte Leitungsmechaismen und magnetische Eigenschaften spinellartiger Ferrite
  March 2014
- Christian Kranert
  Investigation of wide-bandgap semiconductors by UV Raman spectroscopy: resonance effects and material characterization
  December 2014
- Florian Schmidt
  Raumladungsspektroskopische Methoden zur Charakterisierung von weitbandlückigen Halbleitern
  December 2014
- Marko Stölzel
  Photolumineszenz von Exzitonen in polaren ZnO/MgZnO-Quantengrabenstrukturen
  May 2014

Master

- David Diering
  Electrical Properties of the wide-gab semiconductor β-Ga_2O_3 *and related transparent oxides*
  August 2014

- Tobias Dörfler
  Long-throw magnetron sputtering of amorphous transparent oxides
  December 2014
- Agnes Holtz
  ZnO basierte Inverter und Elektrolyt-Gate Transistoren als Biosensoren
  September 2014
- Hannes Krauß
  Dielektrische Funktion von Indiumoxid und Galliumoxid Dünnschichten im Temperaturbereicht 10K bis 300K
  November 2014
- Lisa Paller
  Drive-Level Capacitance Profiling on Cu(In,Ga)Se_2-based Thin Film Solar Cells
  September 2014
- Katharina Rudisch
  Characterization of electronic properties of CuI thin films
  December 2014
- Thorsten Schultz
  Untersuchung der Photolumineszenz von MgZnO/ZnO Quantengräben bei angelegem elektrischen Feld
  November 2014
- Vitali Zviagin
  Optical, Magneto-optical and structural properties of Spinel Oxide Thin Films in Dependece on Deposition Temperatures
  September 2014

Bachelor

- Rafael Deichsel
  Untersuchung von Fe^{3+}-Zentren in Zinkoxid mittels Photolumineszenz
  November 2014
- Oliver Herrfurth
  Exciton-Polaritons in ZnO-based Microresonators: Relaxation and Recombination Processes
  September 2014
- Alexander Holm
  Aufbau und Test eines Interferometermessplatzes zur Untersuchung von Exzitonen-Polaritonkondensaten
  November 2014
- Silvia Kunz
  Electrical and Optical Characterization of Aluminium-Doped Amorphous ZTO Thin Films
  May 2014

- Steffen Lanzinger
  pn-Heterodioden auf Indiumoxidbasis
  August 2014
- Paul Räcke
  Characterisation of Semi-Transparent p-NiO/n-ZnO Heterojunctions Working as UV-Solar Cells
  May 2014
- Anna Werner
  Strukturelle und elektrische Eigenschaften von Si-dotierten $(Ga,In)_2O_3$ Dünnfilmen
  August 2014

9.33 Guests

- Dr. Olga Sviridova
  Odessa National Polytechnic University, Ukraine
  September 2013 – July 2014
- Dr. Chandrahas Bharati
  CSIR-Central Glass and Ceramic Research Institute, India
  July 2014 – September 2014
- Kaustav Dey
  Indian Institute of Science Education and Research, India
  May 2014 – July 2014
- Dr. Lasse Vines
  University Oslo, Norway
  March 2014

10

Superconductivity and Magnetism

10.1 Introduction

The main interests of the group at the division are phenomena related to superconductivity and magnetism in solids. In the last few years the research activities in superconductivity have been mainly concentrated in searching for its existence in graphite, especially at graphite interfaces between Bernal-like crystalline regions. This research issue started in our division in Leipzig in the year 2000 and became supporting experimental evidence quite recently, indicating the existence of superconductivity at temperatures above 100 K. Future work will be concentrated in the localization of the superconducting phases and the increase of the superconducting yield.

Our division was the first to show that atomic lattice defects can produce magnetic order in graphite without the need of magnetic ions. This phenomenon is known nowadays as Defect-Induced Magnetism and it is found in a broad spectrum of different materials. We are involved in a collaborative research project with the aim of triggering this phenomenon in nominally non-magnetic oxides, via vacancies and/or hydrogen doping. Further research topic is the study of the electrical and magnetic properties of oxide multilayers of thickness starting from a few unit cells. Main research issues are related to the magnetic coupling at the interfaces of oxide layers, i.e. exchange bias phenomena, with different magnetic properties.

Pablo Esquinazi

10.2 Study of non-linear Hall effect in nitrogen grown ZnO microstructure and the effect of H^+-implantation

Y. Kumar, J. Barzola-Quiquia, I. Lorite, F. Bern, P. Esquinazi

We have studied the Hall effect measurements of the microstructured ZnO film grown by pulsed laser ablation, in N_2 atmosphere, on *a*-plane Al_2O_3 single crystal and also the effect of low energy H^+-implantation on these properties. It has been observed that Hall resistance, for the film before and after H^+-implantation, varies non-linearly with the applied magnetic field, whereas this non-linearity decreases with the rise in temperature Fig. 10.1. Two-band model relates this effect to the conduction of different

type of charge carriers through two parallel channels. Reduced non-linearity after H^+-implantation in the grown film is due to shallow-donor effect of the doped hydrogen giving rise to increment in the electron concentration. Parameters obtained from fitting of Hall resistance curves show an increase in relative concentration of electrons with the temperature, again reducing the effect of other channel and resulting in the reduction of non-linearity.

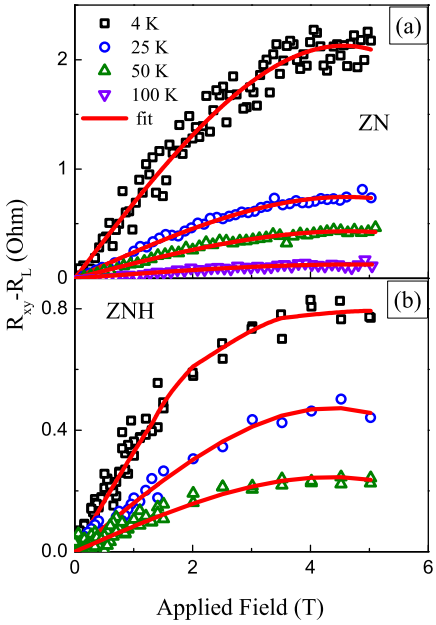

Figure 10.1: Magnetic field dependence of the Hall resistance after subtracting a linear slope ($R_{xy} - R_L$) at various temperatures for (a) as-grown ZnO film and (ZN) (b) after H^+-implantation (ZNH).

10.3 Umkehr effect observed in the magnetothermoelectric power of graphite

S. Muiños-Landín, I. Lorite, W. Böhlmann, P. Esquinazi

Recently many different studies have been done in highly oriented pyrolitic graphite (HOPG). Interesting properties such as defect induced magnetism, high magnetoresitance or different evidences of high temperature superconductivity where found in different experiments, and are directly related with the existence of the already known well defined metallic-like internal interfaces inside different graphite samples. In this work, taking into account several previous resistance and magnetoresistance measurements, we explore now a related property, the thermoelectric power (TEP), to improve the understanding of the mechanisms behind these internal interfaces. The thermoelectric power, also known as Seebeck effect, is the longitudinal voltage generated by an also longitudinal temperature gradient applied to any material. An interesting aspect of this measurement in our case is the response of the Seebeck coefficient to an applied

magnetic field. This point becomes particularly interesting if we take a look at the behavior of the thermolectric power in bismuth and bismuth/antimonium compounds when a magnetic field is present. There, it is possible to see a not yet well studied phenomenon which is called Umkehr effect. It consists in the asymmetry of the magnetothermoelectric power (MTEP) of a sample once the sign of the applied magnetic field is reversed. Given the relationship between the existence of the Umkehr effect with the internal structure of bismuth and the similarities between bismuth and graphite, a possible observation of the Umkehr effect seems to be interesting in a similar system like HOPG.

With this objective two different samples of HOPG where prepared and different electric, thermoelectric and thermomagnetic measurements were done in order to find any relationship between a possible anomalous response of the magnetothermoelectric power and the density of internal interfaces inside the HOPG samples. After a characterization of both samples, a difference in the density of internal interfaces was observed. A clear non-symmetric response, see Fig. 10.2, was obtained only for the sample which presents a high density of interfaces.

We propose as well a simple model which considers the contributions to the thermoelectric power that comes from the semiconducting regions and the one that comes from the metallic-like internal interfaces. Being possible this way to study their variation with temperature and the applied magnetic field.

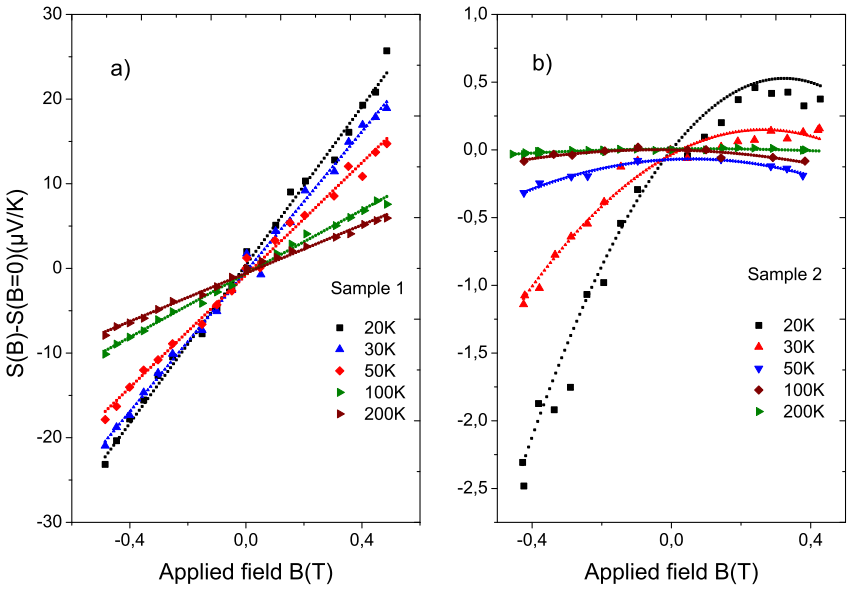

Figure 10.2: Magnetothermoelectric power of two different samples. a) Small density of interfaces b) High density of interfaces. A linear contribution from the Nernst effect is present in both samples, whereas only for the sample with a high density of interfaces there is an extra contribution.

10.4 Hydrogen influence on the electrical and optical properties of ZnO thin films grown under different atmospheres

I. Lorite, J. Wasik, T. Michalsky, R. Schmidt-Grund, P. Esquinazi,

In this work we studied the changes of the electrical and optical properties after hydrogen plasma treatment of polycrystalline ZnO thin films grown under different atmosphere conditions. The obtained results show that the gas used during the growth process plays an important role in the way hydrogen is incorporated in the films, see Fig. 10.3. The hydrogen doping can produce radiative and non-radiative defects that reduce the UV emission in ZnO films grown in oxygen atmosphere but it passivates defects created when the films are grown in nitrogen atmosphere. Impedance spectroscopy measurements show that these effects are related to regions where hydrogen is mostly located, either at the grain cores or boundaries. We discuss how hydrogen strongly influences the initial semiconducting behavior of the ZnO thin films.

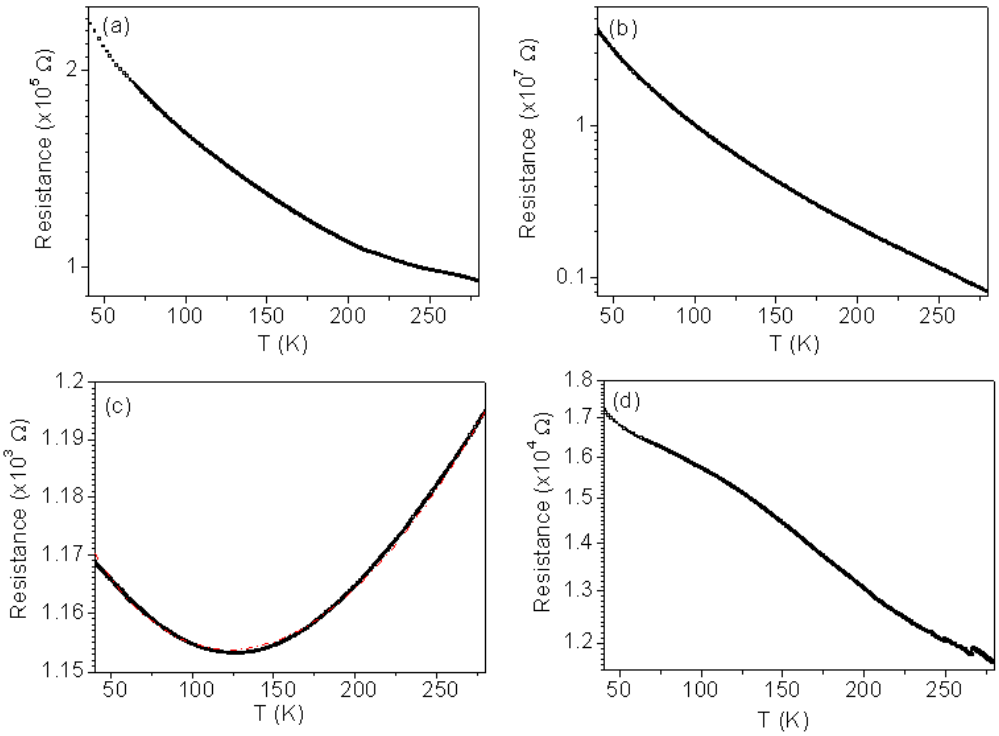

Figure 10.3: Temperature dependence of the resistance of ZnO grown in: a) Nitrogen, b) Oxygen, c) ZnO grown in nitrogen and H^+ treated and d) ZnO grown in oxygen and H^+ treated.

10.5 Transport properties of hydrogenated ZnO microwires

I. Lorite, P. Esquinazi, C. Zapata, S.P. Heluani,

We have studied the magnetoresistance (MR) of hydrogen plasma-treated pure ZnO wires of tens of micrometer diameter at different temperatures, see Fig. 10.4. A negative MR of 1% at 8 T applied field is measured for all wires at 4 K, independent of the temperature (300 K . . . 773 K) used during the hydrogen treatment. However, a positive MR develops, the higher the treatment temperature. The MR can be explained with a semi-empirical model taking into account local magnetic moments and the $s - d$ exchange interaction. These results together with field anisotropy in the MR indicate the appearance of magnetic order due to the hydrogen treatment in agreement with recently published reports on the influence of hydrogen in bulk ZnO single crystals. Hydrogen doping may provide a way to trigger defect-induced magnetism in small oxide structures.

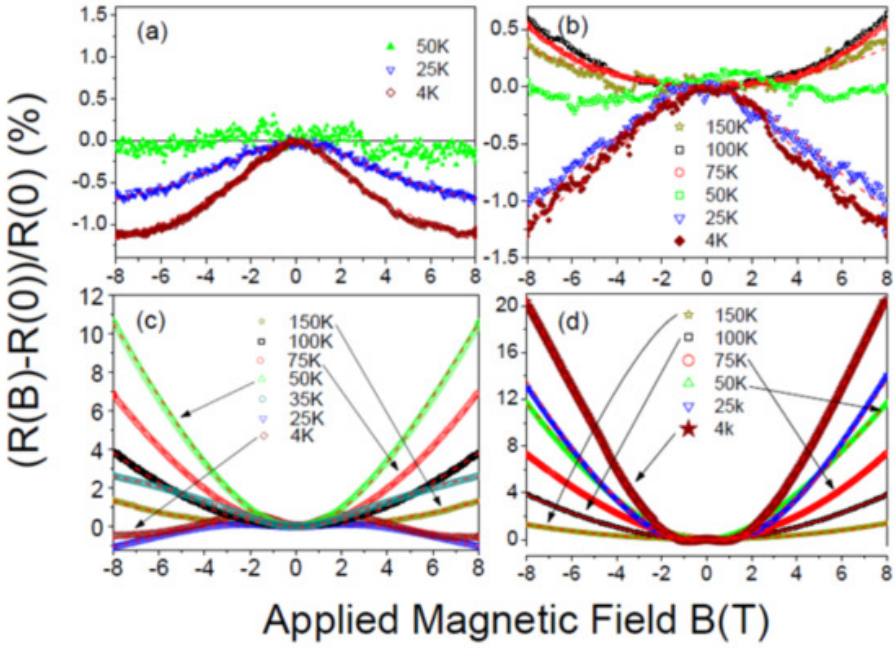

Figure 10.4: Comparison of the MR (in percentage) in perpendicular (black squares) and nearly parallel (blue squares) direction of the applied magnetic field of ZnO wires treated at: (a) RT (ZRT), (b) 100°C (ZF1), (c) 300°C (ZF3), and (d) 500°C (ZF5) for 1 h in H-plasma. All the measurements were done at 4 K.

10.6 Funding

Defect-induced Magnetism in Oxides
Prof. Dr. Pablo Esquinazi
DFG SFB 762/2, B1

Magnetic and electric properties of oxide superlattices with ultrathin single layers
Prof. Dr. Pablo Esquinazi and Prof. Dr. Michael Ziese
DFG SFB 762/2, B5

Development of nanostructured ZnO Biosensors for the detection of very low concentration of analytes in Biomedical Applications

Prof. Dr. Pablo Esquinazi
BMBF-NANOTEC (ARG 11/033

Superconducting Properties of Graphite Interfaces
Prof. Dr. Pablo Esquinazi
DAAD-PROBRAL

Effiziente Energienutzung: Neue Konzepte und Materialien
Prof. Dr. Pablo Esquinazi, M. Sc. Santiago Muiños Landín
ESF-NFG

10.7 Organizational Duties

P. Esquinazi

- Project Reviewer: Deutsche Forschungsgemeinschaft (DFG), National Science Foundation (USA), German-Israeli Foundation (GIF), Israel Science Foundation, Department of Energy (Washington), DAAD
- Referee: Phys. Rev. Lett, Phys. Rev. B., Appl. Phys. Lett., Chem. Phys. Lett., Nature Physics, Nature Materials, Physica C, Phys. Lett. A, phys. stat. sol., J. Low Temp. Phys., Carbon, J. Chem. Phys., Eur. J. Phys. B, J. Magn. Magn. Mater.

M. Ziese

- Head of the Undergraduate Physics Laboratory
- Dean of Studies
- Referee: Phys. Rev. Lett., Phys. Rev. B., Adv. Mater., Appl. Phys. A, Current Nanoscience, Eur. Phys. J. B, IEEE Trans. Magn., J. Phys.: Condens. Matter, J. Phys. D: Appl. Phys., J. Alloys Comp., J. Appl. Phys., J. Am. Ceram. Soc., J. Magn. Magn. Mater., J. Mater. Research, J. Mater. Science, Materials Science and Engineering B, Nanotechnology, phys. stat. sol., Thin Solid Films

W. Böhlmann

- Referee: J. Physical Chemistry, J. of American Chemical Society, Microporous and Mesoporous Materials

10.8 External Cooperations

Academic

- State University of Campinas, Campinas, Brazil
  Prof. Dr. Yakov Kopelevich
- Max-Planck Institute for Solid State Research, Stuttgart, Germany
  Dr. Ionela Vrejoiu
- Max-Planck Institute of Microstructure Physics, Halle, Germany
  Prof. Dietrich Hesse
- Max-Planck Institute of Microstructure Physics, Halle, Germany
  Dr. Marin Alexe

- Max-Planck Institute of Microstructure Physics, Halle, Germany
  Dr. Arthur Ernst
- Martin-Luther Universität Halle-Wittenberg, Halle, Germany
  Prof. Ingrid Mertig
- Martin-Luther Universität Halle-Wittenberg, Halle, Germany
  Prof. Wolfram Hergert
- Martin-Luther Universität Halle-Wittenberg, Halle, Germany
  Dr. Angelika Chassé
- Martin-Luther Universität Halle-Wittenberg, Halle, Germany
  Dr. Manfred Dubiel
- Stanford Synchrotron Radiation Laboratory, USA
  Dr. Hendrik Ohldag
- Max-Planck-Institut für Metallforschung, Stuttgart, Germany
  Dr. Eberhard Goering
- Laboratorio de Física de Sistemas Pequeños y Nanotecnologíia, Consejo Superior de Investigaciones Científicas, Madrid, Spain
  Prof. N. García (Madrid)
- Forschungszentrum Dresden-Rossendorf e.V., Institut für Ionenstrahlphysik und Materialforschung, Germany
  Dr. W. Anwand
- Forschungszentrum Dresden-Rossendorf e.V., Institut für Ionenstrahlphysik und Materialforschung, Germany
  Dr. G. Brauer
- Tucuman University, Argentina
  Prof. S. P. de Heluani
- University of La Plata, Argentina
  Dr. C. E. Rodriguez Torres
- Universidad Autónoma de Madrid, Spain
  Prof. Dr. Miguel Angel Ramos
- University of Ioannina, Greece, Ioannina, Greece
  Prof. I. Panagiotopoulos
- Bar Ilan University, Israel
  Dr. G. D. Nessim

10.9 Publications

Journals

I. Lorite, J. Wasik, T. Michalsky, R. Schmidt-Grund, and P. Esquinazi:
Hydrogen influence on the electrical an optical properties of ZnO thin film grown under different atmospheres
Thin Solid Films **556**, 18 (2014)

A. Ballestar, P. Esquinazi, J. Barzola-Quiquia, S. Dusari, F. Bern, R.R. da Silva, and Y. Kopelevich:
Possible superconductivity in multi-layer-graphene by application of a gate voltage
CARBON **72**, 312 (2014) 312

M. Lorenz, V. Lazenka, P. Schwinkendorf, F. Bern, M. Ziese, H. Modarresi, A. Volodin, M. J. Van Bael, K. Temst, A. Vantomme, and M. Grundmann:
Multiferroic $BaTiO_3$-$BiFeO_3$ composite thin films and multilayers: strain engineering and magnetoelectric coupling
J. Phys. D: Appl. Phys. **47**, 135303 (2014)

C. E. Rodríguez Torres, G. A. Pasquevich, P. Mendoza Zélis, F. Golmar, S. P. Heluani, Sanjeev K. Nayak, Waheed A. Adeagbo, Wolfram Hergert, Martin Hoffmann, Arthur Ernst, P. Esquinazi, and S. J. Stewart:
Oxygen-vacancy-induced local ferromagnetism as a driving mechanism in enhancing the magnetic response of ferrites
Phys. Rev. B **89**, 104411 (2014)

G. Grinblat, F. Bern, J. Barzola-Quiquia, M. Tirado, David Comedi, and Pablo Esquinazi:
Luminescence and electrical properties of single ZnO/MgO core/shell nanowires
Appl. Phys. Lett. **104**, 103113 (2014)

M. Villafuerte, J. M. Ferreyra, C. Zapata, J. Barzola-Quiquia, F. Iikawa, P. Esquinazi, S. P. Heluani, M. M. de Lima, Jr., and A. Cantarero:
Defect spectroscopy of single ZnO microwires
J. Appl. Phys. **115**, 133101 (2014)

A. Paul, C. Reitinger, C. Autieri, B. Sanyal, W. Kreuzpaintner, J. Jutimoosik, R. Yimnirun, F. Bern, P. Esquinazi, P. Korelis, and P. Böni:
Exotic exchange bias at epitaxial ferroelectric-ferromagnetic interfaces
Appl. Phys. Lett. **105**, 022409 (2014)

M. Ojeda, A. M. Balu, A. A. Romero, P. Esquinazi, J. Ruokolainen, H. Sixta, and R. Luque:
MAGBONS: Novel Magnetically Separable Carbonaceous Nanohybrids from Porous Polysaccharides
ChemCatChem, **6**, 2847 (2014)

J. L. Cholula-Díaz, J. Barzola-Quiquia, C. Kranert, T. Michalsky, P. Esquinazi, M. Grundmann, and H. Krautscheid:
Conducting behavior of chalcopyrite-type $CuGaS_2$ crystals under visible light
Phys. Chem. Chem. Phys. **16**, 21860 (2014)

A. Ballestar, T. T Heikkilä, and P. Esquinazi:
Size dependence of the Josephson critical behavior in pyrolytic graphite TEM lamellae
Supercond. Sci. Technol. **27**, 115014 (2014)

D. Spemann, P. Esquinazi, A. Setzer, and W. Böhlmann:
Trace element content and magnetic properties of commercial HOPG samples studied by ion beam microscopy and SQUID magnetometry
AIP Advances **4**, 107142 (2014)

P. Esquinazi, J. Krüger, J. Barzola-Quiquia, R. Schönemann, T. Herrmannsdörfer, and N. García:
On the low-field Hall coefficient of graphite
AIP ADVANCES **4**, 117121 (2014)

P. Esquinazi, T. T. Heikkili, Y. V. Lysogorskiy, D. A. Tayurskii, and G. E. Volovik:
On the Superconductivity of Graphite Interfaces
JETP Lett. **100**, 336 (2014)

D. Preziosi, I. Fina, E. Pippel, D. Hesse, X. Marti, F. Bern, M. Ziese, and M. Alexe:
Tailoring the interfacial magnetic anisotropy in multiferroic field-effect devices
Phys. Rev. B **90**, 125155 (2014)

Talks

Superconductivity in graphite
P. Esquinazi
Weizmann Institute of Science Israel

Defect-induced magnetism in solids
P. Esquinazi
Tel Aviv University / Israel

Search for superconductivity in differently treated graphite powders
P. Esquinazi, DPG Conference 2014 Dresden

Unusual Hysteresis Observed in the Magnetoresistance of Multiwall Carbon Nanotubes Bundles
J. Barzola-Quiquia
DPG Conference 2014 in Dresden

Magnetic order triggered by hydrogenation of Li-doped ZnO microwires
I. Lorite
DPG Conference 2014 Dresden

Superconductivity and interfaces in graphite
P. Esquinazi
ICSM 2014 Ankara, Turkey

Size-dependences of the Josephson-behavior of interfaces
P. Esquinazi
DIAM 2014 Madrid, Spain

Superconductivity in graphite
P. Esquinazi
Universidade de São Paulo, Brasil

Posters

Raman Spectroscopy of Few-Layer Graphene after Oxygen Plasma Etching
M. Zoraghi, J. Barzola-Quiquia, and P. Esquinazi
DPG Conference 2014 Dresden

Effect of external magnetic field on the photoresistance of ZnO based wires
I. Lorite, C. I. Zandalazini, S. Perez, and P. Esquinazi
DPG Conference 2014 Dresden

Magnetic properties in hydrogenated Li doped ZnO microwires
I. Lorite, C. I. Zandalazini, S. Perez, and P. Esquinazi
DPG Conference 2014 Dresden

Transport Properties of Single TiO_2 Nanotubes
M. Stiller, J. Barzola-Quiquia, I. Lorite, P. Esquinazi, R. Kirchgeorg, S. P. Albu, and P. Schmuki
DPG Conference 2014 Dresden

Sample size dependence of the Josephson behavior of the interfaces in pyrolytic graphite
A. Ballestar and P. Esquinazi
DPG Conference 2014 Dresden

Room temperature ferromagnetism after low energy H^+ implantation in Li-doped ZnO microwires
I. Lorite
IBMM 2014 in Leuven, Belgium

10.10 Graduations

Doctorate

- M. Sc. Ana Isabel Ballestar Balbas
  Superconductivity at Graphite interfaces
  26.03.2014

10.11 Guests

- Prof. Dr. Claudia Rodriguez Torres
  Universidad Nacional de La Plata, Argentina
  14. - 22.03.2014
- Prof. Dr. Nicolás García García
  Lab. de Física de Sistemas Pequenos, CSIC, Madrid, Spain
  04. - 31.05.2014
- Prof. Dr. Ana Melva Champi Farfán
  Universidade Federal do ABC, Santo André, Brasil
  26.05. - 26.06.2014

- Prof. Dr. Yakov Kopelevich
  Universidade Estadual de Campinas-UNICAMP, Bairro Barão Geraldo, Brasil
  02.07.2014 - 17.02.2015
- Dr. Bruno Camargo
  Universidade Estadual de Campinas-UNICAMP, Bairro Barão Geraldo, Brasil
  10.08.2014 - 31.07.2015
- PhD Ramita Wisutmitnakorn
  Mahidol University Bangkok, Thailand
  14.07. - 13.10.2014

III

Institute for Theoretical Physics

11

Computational Quantum Field Theory

11.1 Introduction

The Computational Physics Group performs basic research into classical and quantum statistical physics with special emphasis on phase transitions and critical phenomena. In the centre of interest are the physics of spin glasses, diluted magnets and other materials with quenched, random disorder, soft condensed matter physics with focus on fluctuating paths and interfaces, biologically motivated problems such as protein folding, aggregation and adsorption as well as related properties of homopolymers, and the intriguing physics of low-dimensional quantum spin systems.

The methodology is a combination of analytical and numerical techniques. The numerical tools are currently Monte Carlo and Molecular Dynamics computer simulations as well as exact enumeration techniques. The computational approach to theoretical physics is expected to gain more and more importance with the future advances of computer technology, and is likely to become the third cornerstone of physics besides experiment and analytical theory as sketched in Fig. 11.1. Already now it often helps to bridge the gap between experiments and the often necessarily approximate calculations in analytic approaches. To achieve the desired high efficiency of the numerical studies we develop new algorithms and, to guarantee the flexibility required by basic research, all computer codes are implemented by ourselves. The technical tools are Fortran, C, C++, and Python programs running under Unix or Linux operating systems and computer algebra using Maple or Mathematica. The software is developed and tested at the Institute on a cluster of PCs and workstations, where also most of the numerical analyses are performed. Currently we are also exploring the possibilities of the rapidly developing graphics card computing, that is computer simulations on graphics processing units (GPUs) with many cores. Large-scale simulations requiring vast amounts of computer time are carried out at the Institute on quite powerful compute servers, at the parallel computers of the Saxon computing centre in Dresden, and, upon successful grant application at the national supercomputing centres in Jülich, Stuttgart and München on parallel supercomputers. This hierarchy of various platforms gives good training opportunities for the students and offers promising job perspectives in many different fields for their future career.

Our research activities are closely integrated into the Graduate School “Build-

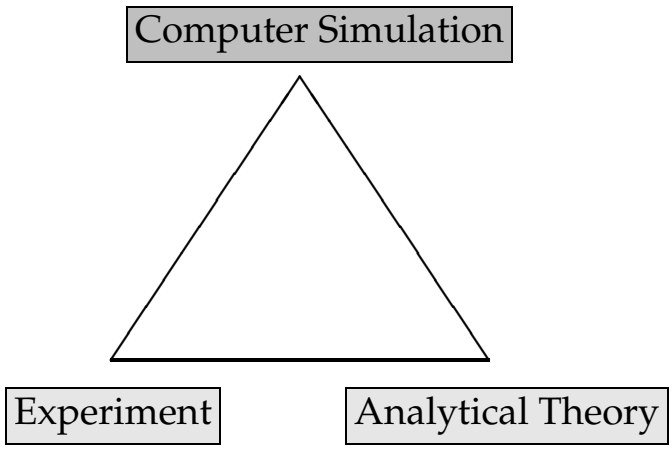

Figure 11.1: Sketch of the "triangular" relationship between experiment, analytical theory and computer simulation.

MoNa": Leipzig School of Natural Sciences – *Building with Molecules and Nano-objects*, two ESF Junior Research Groups, the International Max Planck Research School (IMPRS) *Mathematics in the Sciences*, and the International Graduate School *Statistical Physics of Complex Systems* with Université de Lorraine in Nancy, France, supported by the Deutsch-Französische Hochschule (DFH-UFA). In the second funding period 2011–2013, Coventry University in England has been integrated as an associated partner, and in the current third funding period 2014–2016, also the National Academy of Sciences of Ukraine in Lviv has joined as another associated partner institution, offering our PhD students now several interesting options for secondments. For instance, in 2014, one PhD student started a "co-tutelle de thèse" jointly supervised with a colleague from Coventry University. The three Graduate Schools are all "Classes" of the Research Academy Leipzig (RALeipzig), providing the organizational frame for hosting visiting students and senior scientists, offering language courses, organizing childcare and for many other practical matters.

At a more post-graduate level our research projects are embedded into the "Sächsische DFG-Forschergruppe" FOR877 *From Local Constraints to Macroscopic Transport* jointly with the universities in Chemnitz and Dresden, and the Sonderforschungsbereich/Transregio SFB/TRR 102 *Polymers under Multiple Constraints: Restricted and Controlled Molecular Order and Mobility* together with Halle University. Our group also actively contributes to two of the top level research areas ("Profillinien") and the Centre for Theoretical Sciences (NTZ) of the University. Beside "BuildMoNa" the latter structures are particularly instrumental for our cooperations with research groups in experimental physics and biochemistry on the one hand and with mathematics and computer science on the other.

On an international scale, our research projects are carried out in a wide net of collaborations which are currently mainly funded by the Alexander von Humboldt Foundation through an Institute Partnership with the National Academy of Sciences in Lviv, Ukraine, on *Polymers in Porous Environments and on Disordered Substrates* and the EU IRSES Network DIONICOS: *Dynamics of and in Complex Systems*, a consortium of 6 European and 12 non-European partners, including sites in England, France

and Germany as well as in Russia, Ukraine, India, the United States and Venezuela, which commenced work in 2014. Further close contacts and collaborations are established with research groups in Armenia, Austria, China, France, Great Britain, India, Israel, Italy, Japan, Poland, Russia, Spain, Sweden, Taiwan, Turkey, Ukraine, and the United States. These contacts are refreshed and furthered through topical Workshops, Advanced Training Modules and Tutorials, and our International Workshop series *CompPhys: New Developments in Computational Physics*, taking annually place at the end of November just before the first advent weekend.

Wolfhard Janke

11.2 Effects of bending stiffness on a coarse-grained polymer model

M. Marenz, W. Janke

To investigate the generic behavior of polymers and proteins with computer simulations, it is common to use generic models. On the one hand, these models neglect chemical details, which means that one cannot observe any specific behavior. Instead the general behavior for the type of polymer is exposed. However, using these coarse-grained models is the only possibility to investigate the physical system on a large time scale, length scale or parameter range. One of the most common coarse-grained models is the so called bead-stick polymer. The Hamiltonian is given by

$$H = 4 \sum_{i=1}^{N-2} \sum_{j=i+2}^{N} \left(\frac{1}{r_{ij}^{12}} - \frac{1}{r_{ij}^{6}} \right) + \kappa \sum_{\theta_i} (1 - \cos \theta_i) \ , \tag{11.1}$$

where r_{ij} is the distance between non-adjacent monomers, and θ_i is the angle of two adjacent bonds. The Hamiltonian allows us to modify the bending stiffness by varying κ, so that the simulated polymer can be anything between flexible, semi-flexible or stiff.

To simulate the system in the complete (T, κ)-plane we used two advanced Monte Carlo algorithms. A two-dimensional replica-exchange method, which simulates the system in parallel in the T and κ direction, is able to generate well equilibrated canonical mean values. These simulations are supported by the parallel multicanonical algorithm [1] combined with a one-dimensional replica exchange in the κ direction. Employing both algorithms, we calculated surface plots of various observables (energy, end-to-end distance, radius of gyration, eigenvalues of gyration tensor) to construct the full pseudo-phase diagram for several polymer lengths ($N = 14, 28, 42$).

Despite the simplicity of the model, the phase diagram is remarkably rich, see Fig. 11.2. Many of theses phases are comparable to conformations which have been observed for real polymers and proteins. Compared to former work simulating similar coarse-grained models, we observed a novel type of pseudo-phases which are best described by thermodynamically stable knots (noted by KC_n in Fig. 11.2) [2]. The transitions into these knot phases exhibit some surprising characteristics. Although we observed a clear phase coexistence between the knotted and unknotted phases, the transitions show no latent heat. Instead the two sub-energies, the Lennard-Jones energy and the bending energy, are transformed into each other as the knots form.

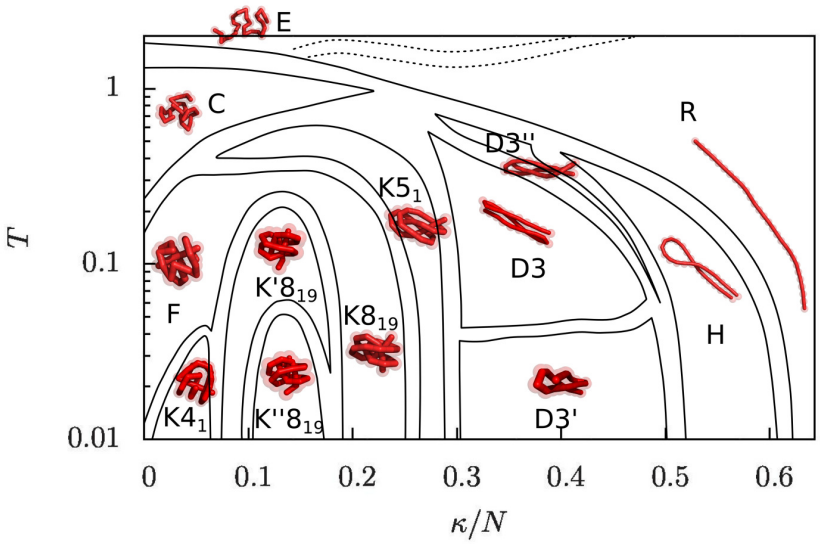

Figure 11.2: The pseudo-phase diagram for the bead-stick model with 28 monomers. The different pseudo phases are labeled as follows: E - elongated, R - rod-like, C - collapsed, F - frozen, KC$_n$ - knotted phase with the corresponding knot type, DN - $(N-1)$ times bent polymers, H - hairpin.

[1] J. Zierenberg et al.: Comput. Phys. Comm. **184**, 1155 (2013)
[2] M. Marenz, W. Janke: *Knots as topological order parameter for semi-flexible polymers*, Leipzig preprint (May 2015), submitted

11.3 The role of stiffness on structural phases in polymer aggregation

J. Zierenberg, W. Janke

We have investigated the role of stiffness in polymer aggregation leading from amorphous aggregates for rather flexible polymers to polymer bundles for stiffer polymers [1]. Employing parallel multicanonical simulations [2], we were able to map out generic T-κ structural phase diagrams describing an entire class of coarse-grained semiflexible polymers. Figure 11.3 (a) shows such a diagram for 8 polymers of length $N = 13$, exhibiting both amorphous aggregates and polymer bundles well-described by an end-to-end correlation parameter $C_R \approx 1/3$ and $C_R \approx 1$, respectively. A microcanonical analysis supports the first-order like transition characteristics of polymer aggregation, the transition line at higher temperatures.

A first-order (like) transition is usually accompanied by a free-energy barrier. We compared the microcanonical free energy for the available stiffness range, guided by a recent claim that the free energy of amorphous aggregation is lower than the formation of ordered structures such as fibrils [3]. Indeed Fig. 11.3 (b) shows that the free-energy barrier (local maximum) increases with increasing stiffness already for a finite system of 8 semiflexible polymers, supporting the previous claim.

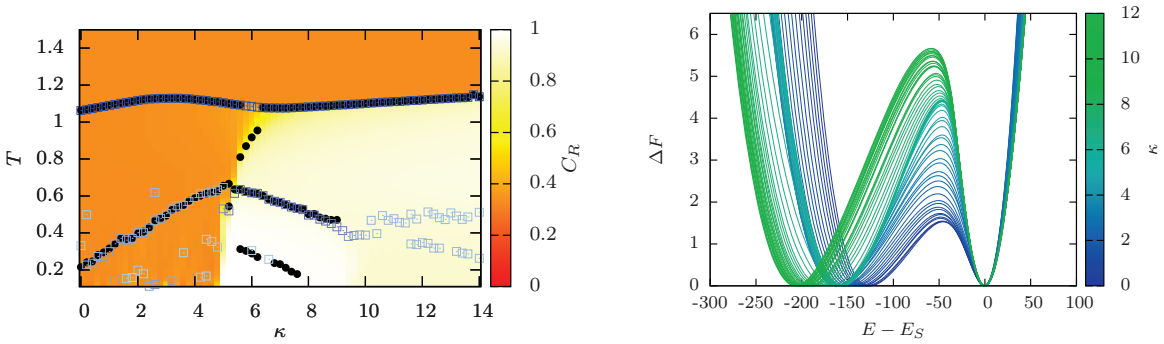

(a) (b)

Figure 11.3: (a) Full temperature-stiffness structural phase diagram of 8 polymers with 13 monomers each, combining the surface plot of a correlation parameter (1 = correlated; 1/3 = uncorrelated) with the peak locations of the heat capacity (black) and the thermal derivative of the phase separation parameter (blue). (b) Free-energy barrier of the same system at equal height temperature for several bending-stiffness parameters $\kappa \in [0, 12]$ encoded in the line color. Figures adapted from Ref. [1].

The numerical data was generated on the supercomputer JUROPA at Jülich Supercomputing Centre (JSC) under Grant No. HLZ21.

[1] J. Zierenberg, W. Janke: Europhys. Lett. **109**, 28002 (2015)
[2] J. Zierenberg et al.: Comput. Phys. Comm. **184**, 1155 (2013)
[3] Y. Yoshimura et al.: Proc. Natl. Acad. Sci. U. S. A. **109**, 14446 (2012)

11.4 Aggregation of θ-polymers in spherical confinement

J. Zierenberg, M. Mueller, P. Schierz, M. Marenz, W. Janke

This project aims for a better understanding of the influence of external confinement onto the physical properties of a small number of polymers [1]. We therefore investigated the change of the aggregation temperature for few polymers enclosed in a sphere, see the left of Fig. 11.4. This enables a systematic variation of the available space by only one parameter, the radius of the sphere. The enclosing sphere is steric, leading at most to an effective repulsion, without introducing technical difficulties with self-interactions imposed by periodic boundaries.

With this setup, we are thus able to explore the influence of the density onto the aggregation transition temperature. We simulated this system of θ-polymers (which means they are parametrized by a model that allows a single polymer to undergo a collapse transition) in the multicanonical ensemble. This allows us to reweight our data to a whole range of different temperatures of the surrounding heat bath, hence the notion of *multi*-canonical simulations. We conducted such simulations in a highly parallelized way [2, 3] for several different radii of the sphere and with that we vary the

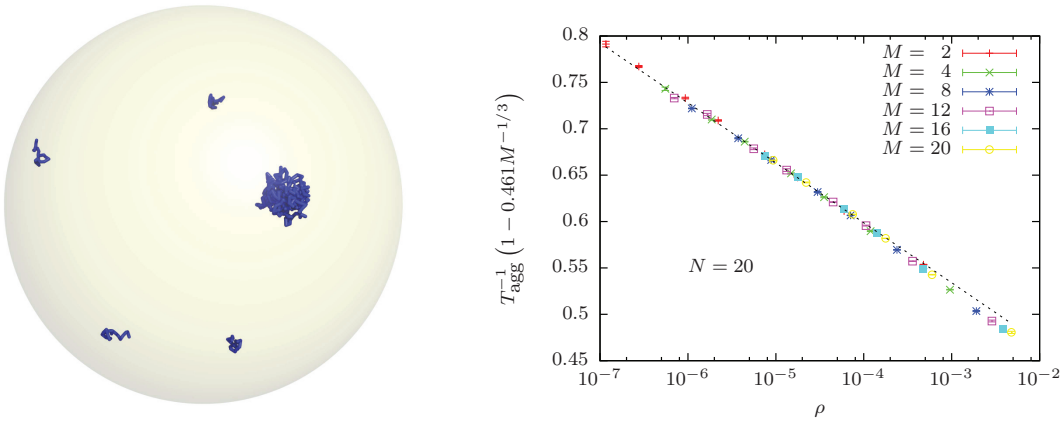

(a) (b)

Figure 11.4: (a) We enclose a small number M of polymers in a sphere and vary its radius, watching closely the aggregation transition temperature. (b) Combining entropic and energetic arguments, and respecting the typical length scale of the aggregate, we find an empirical data collapse of the inverse transitions temperatures over a broad range of densities.

volume accessible to the system. In the canonical picture we find that the aggregation temperature shifts in dependence of the radii.

To gain a quantitative understanding of this shift, we note that the spatial entropy available to the *aggregate* is in a first approximation independent from the radius of the surrounding sphere. In the separated regime the polymers can be treated similar to an ideal gas. Here, we can thus relate the entropy to the volume of the system, and with that to the radius of the sphere and the system's density. With the Gibbs construction we then relate the entropy difference of the two regimes to the microcanonical temperature T_{agg}, allowing the derivation of an explicit relation of the inverse transition temperature to the logarithm of the density,

$$1/T_{\mathrm{agg}}(\rho) = \frac{S(E_{\mathrm{sep}},\rho) - S(E_{\mathrm{agg}},\rho)}{\Delta E} \sim \frac{S(E_{\mathrm{sep}},\rho)}{\Delta E} =\sim -\ln\rho + \mathrm{const}\,, \tag{11.2}$$

under the assumption that, for fixed M and N, the latent heat $\Delta E = E_{\mathrm{sep}} - E_{\mathrm{agg}} = M\Delta e$ is almost constant.

For *flexible* polymers, the aggregate of M polymers with N monomers can be approximated by a single polymer with length $M \times N$, and this defines a "typical" length scale $R \sim (NM)^{-1/3}$ of the polymer aggregate, which may be exploited to derive an empirical scaling law for the inverse temperature in Eq. (11.2) in dependence of the *number of polymers*. With this we gain some insight into the nature of the finite-size effects in such a system enabling the empirical data collapse for a broad range of densities for different numbers of polymers in the right plot of Fig. 11.4.

For *stiffer* polymers this typical length scale is not as easy to determine. Here, we found interesting structural properties that are already visible in a very intuitive order-parameter [4], the so-called phase-separation parameter. This is essentially the average center-of-mass distance of the different polymers, and in the aggregate, it becomes smaller for stiffer polymers. This is at first sight counter-intuitive, but can be traced back to the formation of polymer bundles [5] which allow the polymers' center-of-masses to get closer as the polymers align.

[1] J. Zierenberg et al.: J. Chem. Phys. **141**, 114908 (2014)
[2] J. Zierenberg et al.: Comput. Phys. Comm. **184**, 1155 (2013)
[3] J. Zierenberg et al.: in *Computer Simulation Studies in Condensed-Matter Physics XXVI*, eds. D.P. Landau, H.-B. Schüttler, S. Lewis, M. Bachmann, Physics Procedia **53**, 55 (2014)
[4] M. Mueller et al.: *Probing the effect of density on the aggregation temperature of semi-flexible polymers in spherical confinement*, Leipzig preprint (March 2015), to appear in Physics Procedia (2015), in print
[5] J. Zierenberg, W. Janke: Europhys. Lett. **109**, 28002 (2015)

11.5 Polymer adsorption onto a stripe-patterned substrate

M. Möddel*, M. Bachmann†, W. Janke

*Present address: Blue Yonder GmbH, Karlsruher Str. 88, 76139 Karlsruhe, Germany
†Center for Simulational Physics, The University of Georgia, Athens, Georgia 30602, USA

Most naturally occuring substrates contain heterogeneities not just on the macroscopic scale but also on the micro- or nanoscopic level. Consequently, after we developed an in-depth understanding of the statistical equilibrium behaviour of a generic self-attracting polymer model close to an attractive homogeneous substrate in recent years [1–5], the question arose how this behaviour gets modified if hetereogeneities are introduced on the substrate.

The goal was to see the influence on the level of the whole pseudo-phase diagram, where "pseudo" refers to the finiteness of the simulated chain length. Since already the phase diagram of the polymer near the homogeneous substrate is very rich in transitions (cf. Fig. 11.5(a)), to extract any meaningful results the chosen surface heterogeneity needs to be easily controllable and preferably simple.

Our choice was to add to the previously investigated [1–5] bulk energy term and 9-3 Lennard-Jones (LJ) attraction between each monomer and the substrate an attractive cosine-square potential of distance $D = 5$ such that the energy of the system in total is

$$E_{\text{bulk}} = 4 \sum_{i=1}^{N-2} \sum_{j=i+2}^{N} \left(r_{ij}^{-12} - r_{ij}^{-6} \right) + \frac{1}{4} \sum_{i=1}^{N-2} (1 - \cos \vartheta_i) \ , \tag{11.3}$$

that is strongly dominated by a 12-6 Lennard-Jones (LJ) attraction between non-neighboring monomers, and

$$E_{\text{sur, stripe}}(x,z) = \begin{cases} \left(\frac{2}{15} z^{-9} - z^{-3}\right) \left[\epsilon_s + \epsilon_{\text{stripe}} \cos^2 \left(\pi \left(\text{mod} \left(x + \frac{D}{2}, D \right) - \frac{D}{2} \right) \right) \right], & \text{if } \left| \text{mod} \left(x + \frac{D}{2}, D \right) - \frac{D}{2} \right| \leq \frac{1}{2} \\ \left(\frac{2}{15} z^{-9} - z^{-3}\right) \epsilon_s \, , & \text{else} \, . \end{cases} \tag{11.4}$$

The impact of those stripes was described in detail with an emphasis on the onset of the "recognition" transition below which the polymer perfectly adapts the shape of the stripe. Figure 11.5(b) shows that despite some striking differences, many conclusions drawn for the adsorption of a single polymer on a homogeneous substrate remain valid in the more general heterogeneous case [6].

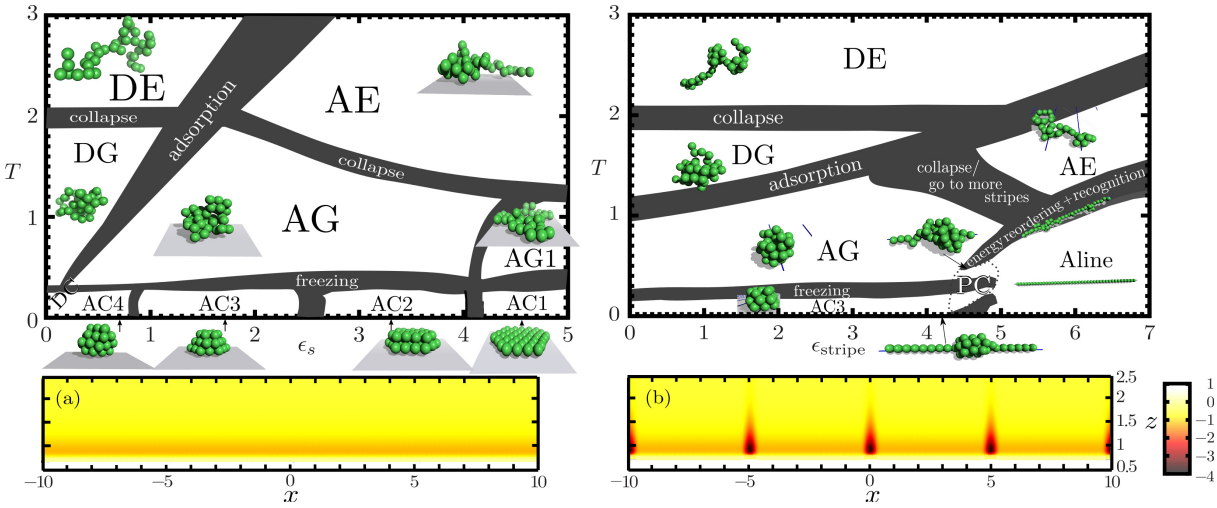

Figure 11.5: (a) Pseudo-phase diagram for polymer adsorption to a homogeneous substrate ($\epsilon_{\text{stripe}} = 0$) in the temperature ($T$) – surface attraction ($\epsilon_s$) plane and a "heat map" of the substrate potential for $\epsilon_s = 1$. (b) Analogous pseudo-phase diagram for the stripe patterned case in the T–ϵ_{stripe} plane for $\epsilon_s = 1$. Phases with "A/D" are adsorbed/desorbed, while "E", "G", and "C" denote phases with increasing order: expanded, globular, and compact. "PC" stands short for a region with phase coexistence.

[1] M. Möddel et al.: J. Phys. Chem. B **113**, 3314 (2009)
[2] M. Möddel et al.: Phys. Chem. Chem. Phys. **12**, 11548 (2010)
[3] M. Möddel et al.: Macromolecules **44**, 9013 (2011)
[4] M. Möddel et al.: Comput. Phys. Comm. **182**, 1961 (2011)
[5] M. Möddel et al.: in Proceedings of the *NIC Symposium 2012*, eds. K. Binder, G. Münster, M. Kremer, John von Neumann Institute for Computing, Jülich, NIC Series, Vol. **45**, p. 277 (2012)
[6] M. Möddel et al.: Phys. Rev. Lett. **112**, 148303 (2014)

11.6 Poly(3-hexylthiophene) (P3HT) adsorption on reconstructed Au(001)

M. Ivanov, J. Gross, W. Janke

Regioregular Poly(3-hexylthiophene) (P3HT) is a very well studied conjugated polymer due to its interesting electronic and optical properties [1]. Recently P3HT has attracted attention for the use in donor/acceptor blends for photovoltaic applications [2–4]. Studies of P3HT on the microscopic level are of great importance for a fundamental understanding of the tuneability of electronic properties and their dependence on external constraints, e.g., the adsorption on electrode surfaces. Hence a number of experimental studies addressed for example the influence of structure formation by polymer self-assembly on ideal surfaces on the electronic properties of oligo- and polythiophenes [5, 6]. Due to the complexity of these macromolecules the experimental findings have not been supported with simulations so far, which in contrast is well-established for studies of small organic molecules. This study reported on an

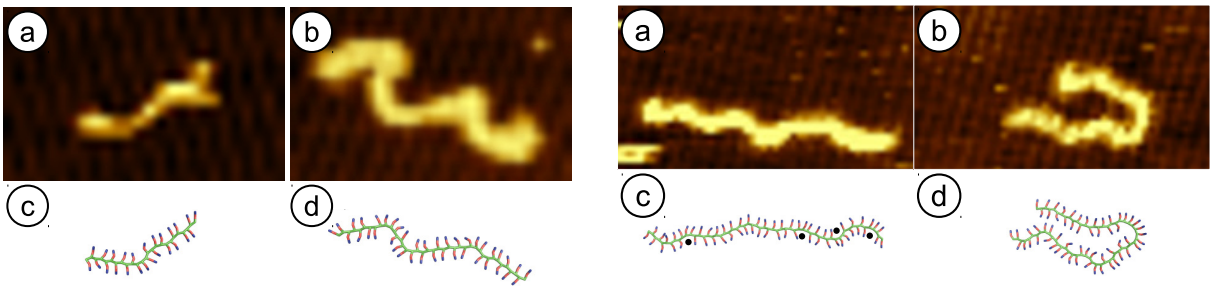

Figure 11.6: Left: Typical conformation of P3HT chains with (a, c) 25 and (b, d) 40 monomers observed in experiment (upper row) and simulation (lower row). Right: Similar comparison for (a, c) elongated coil and (b, d) collapsed hairpin conformations of a 60 monomer chain. Flipped side chains are marked with black dots in (c).

collaborative effort within the DFG SFB/TRR 102 project to combine the experimental observation of polymer chain conformations adsorbed on a metal surface with Monte Carlo simulations of the coarse-grained P3HT model developed by Huang *et al.* [8].

In a previous experimental study it has been shown that two different adsorption behaviours can be observed for in-situ deposited P3HT molecules on an Au(001) surface [7]. The polymer molecules adsorb either as weakly bonded random chains or as stronger interacting entities which locally lift the Au(001) reconstruction. The former random chain conformation is metastable at room temperature. It allows a molecular diffusion on the surface and was in the focus of the present work.

P3HT chains with a maximum length of 60 monomers were simulated in contact with an Au(001) surface. Their shapes were found in qualitative agreement with experimentally obtained chain conformations of in-situ deposited P3HT molecules on Au(001) as observed with scanning tunneling microscopy (STM), cf. Fig. 11.6. For a quantitative comparison the end-to-end distance as well as the radius of gyration of the molecules were determined. The results are published in Ref. [9].

[1] X. Bai, S. Holdcroft: Macromolecules **26**, 4457 (1993); Z. Bao et al.: Appl. Phys. Lett. **69**, 4108 (1996); M.R. Andersson et al.: J. Mater. Chem. **9**, 1933 (1999); B.W. Boudouris et al.: Macromolecules **44**, 6653 (2011)
[2] J.M. Frost et al.: Nano Letters **6**, 1674 (2006)
[3] M. Campoy-Quiles et al.: Nat. Mater. **7**, 158 (2008)
[4] A.M. Ballantyne et al.: Adv. Funct. Mater. **18**, 2373 (2008)
[5] Z.-Y. Yang et al.: ACS Nano **2**, 743 (2008)
[6] Y.-F. Liu et al.: Nanoscale **5**, 7936 (2013)
[7] S. Förster, W. Widdra: J. Chem. Phys. **141**, 054713 (2014)
[8] D.M. Huang et al.: J. Chem. Theory Comput. **6**, 526 (2010)
[9] S. Förster et al.: J. Chem. Phys. **141**, 164701 (2014)

11.7 Cluster growth during a polymer collapse

S. Majumder, W. Janke

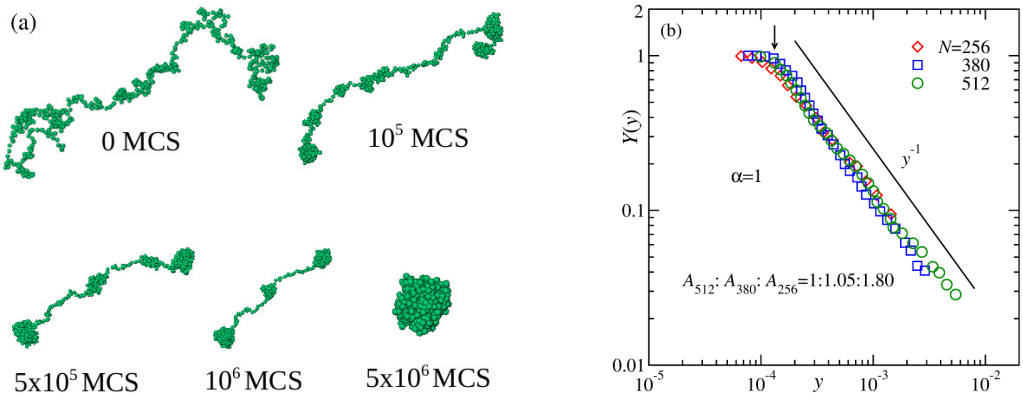

Figure 11.7: (a) Snapshots of a flexible polymer at different times showing the sequence of events occurring during the collapse, after being quenched from a high temperature expanded state to temperature below the theta transition [1]. (b) Finite-size scaling plots showing the collapse of data for different chain lengths confirming the linear growth of the average cluster size [1].

A polymer undergoes a collapse transition when it is quenched from a high-temperature expanded coil state (or in good solvent) to a low-temperature compact globule (in poor solvent)[1]. Understanding the kinetics of the collapse of a polymer is an important physical problem considering its potential connections to many biological phenomena such as protein folding. A polymer collapses via the formation, growth and subsequent coarsening or coalescence of clusters of monomers to form a single compact globule [2] as shown in Fig. 11.7(a). During this coarsening the average cluster-size (average number of monomers within a cluster), $C_s(t)$, is expected to follow a power law. In spite of the fact that the relaxation dynamics during the collapse have been studied in previous works [2], there exist no simulation studies which quantify the growth exponent unambiguously.

In this work we have addressed this issue from state of the art Monte Carlo simulations of a model polymer with the primary goal of quantifying the growth exponent for the cluster coarsening stage of the collapse. In the light of other coarsening systems we analyze our results via the application of finite-size scaling techniques in the nonequilibrium context [3]. Figure 11.7(b) shows such a scaling plot where the decay of the master curve suggests a linear growth of the average cluster size, confirming the universal Lifshitz-Slyozov mechanism of cluster growth, in contradiction to the previous theoretical and simulation results of Ref. [4].

[1] S. Majumder, W. Janke: *Cluster coarsening during polymer collapse: Finite-size scaling analysis*, Leipzig preprint (February 2015), to appear in Europhys. Lett., in print
[2] A. Halperin, P. Goldbart: Phys. Rev. E **61**, 565 (2000)
[3] S. Majumder, S.K. Das: Phys. Rev. E **81**, 050102(R) (2010); Phys. Rev. E **84**, 021110 (2011)
[4] Yu.A. Kuznetsov et al.: J. Chem. Phys. **103**, 4807 (1995); J. Chem. Phys. **104**, 3338 (1996)

11.8 Hysteresis and scaling of periodic driven DNA

S. Kumar*, R. Kumar, W. Janke

*Department of Physics, Banaras Hindu University, Varanasi 221 005, India

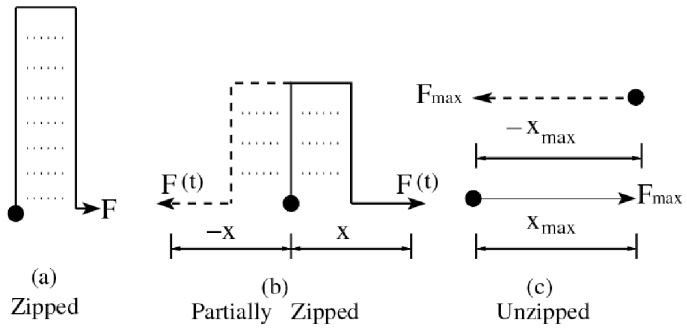

Figure 11.8: Schematic representations of DNA: (a) zipped, (b) partially zipped, (c) unzipped state. One end is kept fixed (indicated by the solid circle), while the other end may move.

Much attention has been paid in recent years to the understanding of biological processes, e.g., transcription and replication of nucleic acids, packing of DNA in a capsid, synthesis and degradation of proteins etc., which are driven by different types of molecular motors *in vivo* [1]. Experiments on biomolecules using single molecule force spectroscopy (SMFS) techniques have enhanced our understanding about these processes [2]. Unlike *in vivo*, where these motors are driven by oscillatory forces resulting from the periodic consumption of ATP to ADP [1], a constant force or loading rate as used in SMFS experiments provides a limited picture of these processes *in vitro*. This has been highlighted in recent studies, where it was suggested that by varying the amplitude and frequency of the applied force, new aspects of a force-driven transition can be introduced [3–5], which otherwise would not be possible in the case of a steady force.

In this project, we have shown within a simplified model the existence of a dynamical transition in a system of driven DNA under the influence of an oscillatory force of amplitude F and frequency ω [6], for a sketch see Fig. 11.8. A detailed comparison of the full Langevin equation with the Langevin equation in the over-damped limit has been performed. This shows that the scaling does not change by applying this approximation. For a chain of finite length, we observe that the area of hysteresis loops shown in Fig. 11.9 scales with the same exponents as proposed in the recent study of a semi-microscopic model [3]. However, in the true thermodynamic limit, we find that the high-frequency scaling regime extends to lower frequencies for larger chain length L, and the system has only one scaling regime where the area of the hysteresis loop scales with $\omega^{-1}F^2$. This indicates that a true dynamical transition may not exist in the thermodynamic limit. The scaling properties appear to be independent of temperature. Hence, the model proposed by us is accurate enough to study scaling properties, and at the same time it provides a possibility of analytic studies within certain limits.

[1] B. Alberts et al.: *Molecular Biology of the Cell* (Garland Publishing, New York, 1994)

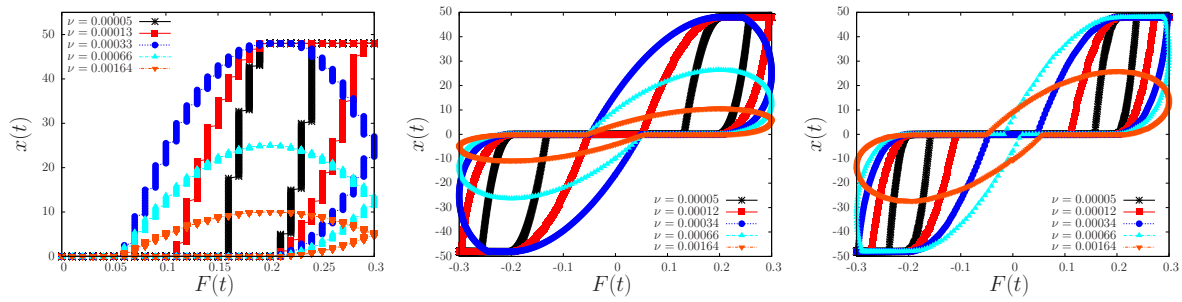

(a) (b) (c)

Figure 11.9: Hysteresis loop for the model with parameters $L = 24$ and $F = 0.3$ for (a) a staircase-like and (b, c) a sinusoidal periodic force. (c) shows the effect of the over-damped limit.

[2] S. Kumar, M.S. Li: Phys. Rep. **486**, 1 (2010)
[3] S. Kumar, G. Mishra: Phys. Rev. Lett. **110**, 258102 (2013)
[4] G. Mishra et al.: Phys. Rev. E **87**, 022718 (2013)
[5] R.K. Mishra et al.: J. Chem. Phys. **138**, 244905 (2013)
[6] S. Kumar et al.: *Driven DNA: Does a dynamical transition exist in the thermodynamic limit?*, Varanasi/Leipzig preprint (May 2015), to be published

11.9 Self-avoiding walks on critical percolation clusters

N. Fricke, W. Janke

We investigate self-avoiding walks (SAWs) in the fractal disorder landscape of a diluted lattice at the percolation threshold. This well-established model for flexible polymers in disordered environments [1] poses a formidable challenge that has long eluded efficient numerical treatment.

Recently, we developed an exact enumeration algorithm which makes use of the self-similar, finitely-ramified structure of the system [2]. Through a properly targeted decomposition of the critical clusters, we are able to overcome the exponential complexity that is usually inherent to exact enumeration methods, enabling us to handle SAWs of several thousand steps on critical clusters of arbitrary dimensionality [3].

Enumerating walks of $N = 25$ to $N = 12800$ steps on over 5×10^4 clusters for each individual length we could precisely determine the exponent ν describing the asymptotic scaling behaviour of the quenched average of the mean squared end-to-end distance via

$$\left[\left\langle R_{\mathrm{ee}}^2 \right\rangle\right] \sim N^{2\nu}. \tag{11.5}$$

This was done for the full incipient percolation clusters and the so-called cluster backbones, substructures without singly-connected dangling ends. As can be seen in Fig. 11.10 for the three-dimensional system, the asymptotic behaviour is identical in both cases but only truly reveals itself after about $N = 800$ steps. Previous numerical studies [4, 5] had therefore yielded significantly larger results than our own [6]. Another surprising finding of our investigation concerns the average number of conformations,

which turned out to follow a scaling law of the form $[Z] \sim \mu^{N+bN^{\xi}}$ instead of the widely assumed $[Z] \sim \mu^N N^{\gamma-1}$. This unusual behavior is related to the fact that the entropy on each cluster is typically dominated by only one or two small regions, towards which the vast majority of SAWs of a fixed length gravitate via designated flow channels; see Fig. 11.11.

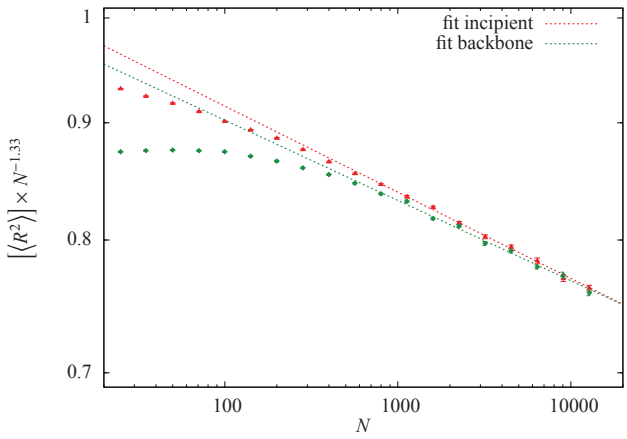

Figure 11.10: Mean squared end-to-end distance vs number of steps for SAWs on incipient critical clusters (red) and backbones (green) on a log-log scale. The lines show the results from least-squares fits of Eq. (11.5) over the ranges N = 800–12800 (incipient) and N = 1131–12800 (backbone). The factor $N^{-1.33}$ ($\approx N^{-2\nu}$) serves to magnify the differences.

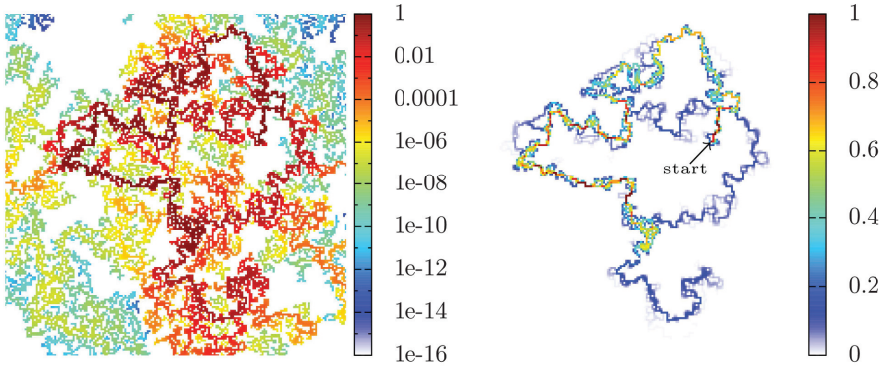

Figure 11.11: Fraction of SAW conformations passing through each site of a critical percolation cluster plotted on logarithmic (left) and linear color scale (right). Here the walks originate from the appendage in the upper right region and have a total length of N = 800 steps. Most conformations end in the dark red / yellowish region below the center.

[1] B. Barat, B.K. Chakrabarti: Phys. Rep. **258**, 377 (1995)
[2] N. Fricke, W. Janke: Europhys. Lett. **99**, 56005 (2012)
[3] N. Fricke, W. Janke: Phys. Rev. Lett. **113**, 255701 (2014)
[4] A. Ordemann et al.: Phys. Rev. E **61**, 6858 (2000)

[5] V. Blavatska, W. Janke: Europhys. Lett. **82**, 66006 (2008)
[6] V. Blavatska et al.: Condens. Matter Phys. **17**, 33604 (2014)

11.10 Semiflexible polymers in a hard-disk fluid: Persistence-length renormalization

S. Schöbl*, S. Sturm†, W. Janke, K. Kroy†

*Present address: d-fine GmbH, An der Hauptwache 7, 60313 Frankfurt, Germany
†Research Unit "Theory of Condensed Matter (TKM)"

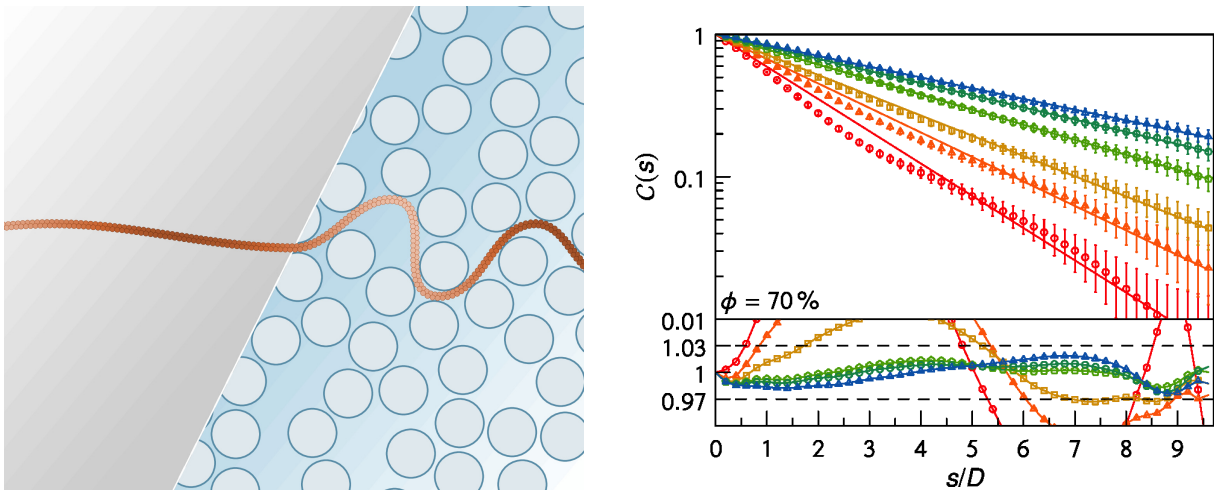

(a) (b)

Figure 11.12: (a) Sketch of semiflexible polymers exposed to the quenched environment of a hard-disk fluid. Due to the randomly distributed obstacles the polymers bend more strongly (right) than their unconstrained counterparts in free space (left). (b) The numerically determined tangent-tangent correlations decay exponentially in the limit $\ell_p/D \to \infty$ (here shown for $\ell_p/D = 2, 3, 4, 6, 8, 10$ and a background filling fraction of 70%), and decay more quickly for higher disorder filling fractions ϕ. The relative deviations of our exponential fits to the data shown in the lower panel nowhere exceed $\approx 3\%$ above $\ell_p = 6D$. Reproduced from Ref. [5].

Single-molecule experiments have established the wormlike chain (WLC) as a standard model for semiflexible polymers [1]. Exploiting the analogy of the WLC with a one-dimensional Heisenberg ferromagnet, it can be shown that the equilibrium tangent-tangent correlation function decays exponentially. The decay rate defines the *thermal* persistence length ℓ_p.

When the same polymer is embedded in a quenched, disordered environment, this property may change quantitatively or even qualitatively. We addressed this problem by performing extensive numerical simulations of semiflexible polymers in a quenched equilibrium hard-disk fluid which represents the (correlated) disordered environment. Only the space between the hard disks is accessible to the polymer. The extreme strength and density of the environmental constraints are a great challenge

to conventional Monte Carlo simulation schemes, which we found hard to overcome even with a sophisticated multicanonical histogram reweighting procedure [2]. We have therefore adopted a breadth-first chain-growth algorithm [3] that resolves this difficulty by *circumventing* energy barriers instead of trying to cross them [2, 4].

As a main result we find that the wormlike chain statistics apparently still applies to the quenched, disordered environment, albeit with a renormalized persistence length ℓ_p^* [5]. For an illustration see Fig. 11.12. We identify a universal form of this disorder renormalization by showing that the observed ℓ_p^* fall onto a single master curve l_p^D defined through

$$\frac{1}{\ell_p^*} = \frac{1}{\ell_p} + \frac{1}{\ell_p^D}, \tag{11.6}$$

where the "disorder persistence length" ℓ_p^D depends only on the disorder filling fraction. We argue that this novel effect may provide a useful quantitative measure of molecular crowding.

[1] O. Otto et al.: Nature Comm. **4**, 1780 (2013)
[2] S. Schöbl et al.: Phys. Rev. E **84**, 051805 (2011)
[3] T. Garel, H. Orland: J. Phys. A: Math. Gen. **23**, L621 (1999)
[4] S. Schöbl et al.: J. Phys. A: Math. Theor. **45**, 475002 (2012)
[5] S. Schöbl et al.: Phys. Rev. Lett. **113**, 238302 (2014)

11.11 Random heteropolymer models

V. Blavatska*, W. Janke

*Institute for Condensed Matter Physics, National Academy of Sciences of Ukraine, Lviv, Ukraine

The conformational properties of long heteropolymer chains are a subject of great interest in both chemical and biological physics. Typical examples are proteins, consisting of sequences of amino acid residues connected by peptide bonds. The conformations of individual macromolecules are controlled by the type of monomer-monomer interactions. In general, the constituents (monomers) of macromolecules in an aqueous environment can be characterized as hydrophilic or hydrophobic, depending on their chemical structure. Hydrophilic residues tend to form hydrogen bonds with surrounding water molecules, whereas the hydrophobic monomers effectively attract each other and tend to form a dense hydrophobic core.

We studied the conformational transitions of quenched, random heteropolymers within a lattice model containing N_A monomers of type A and $N_B = N - N_A$ monomers of type B. Such a model can describe in particular the sequences of hydrophobic and hydrophilic residues in proteins [1] and polyampholytes with oppositely charged groups [2]. Restricting ourselves only to short-range interactions between any pair of monomers residing on neighboring lattice sites that are not connected by a covalent bond, we considered 5 different parametrizations of this model. In particular, model 1 ($\varepsilon_{AA} = \varepsilon_{BB} = 1, \varepsilon_{AB} = -1$) where like monomers repel and opposite ones attract each

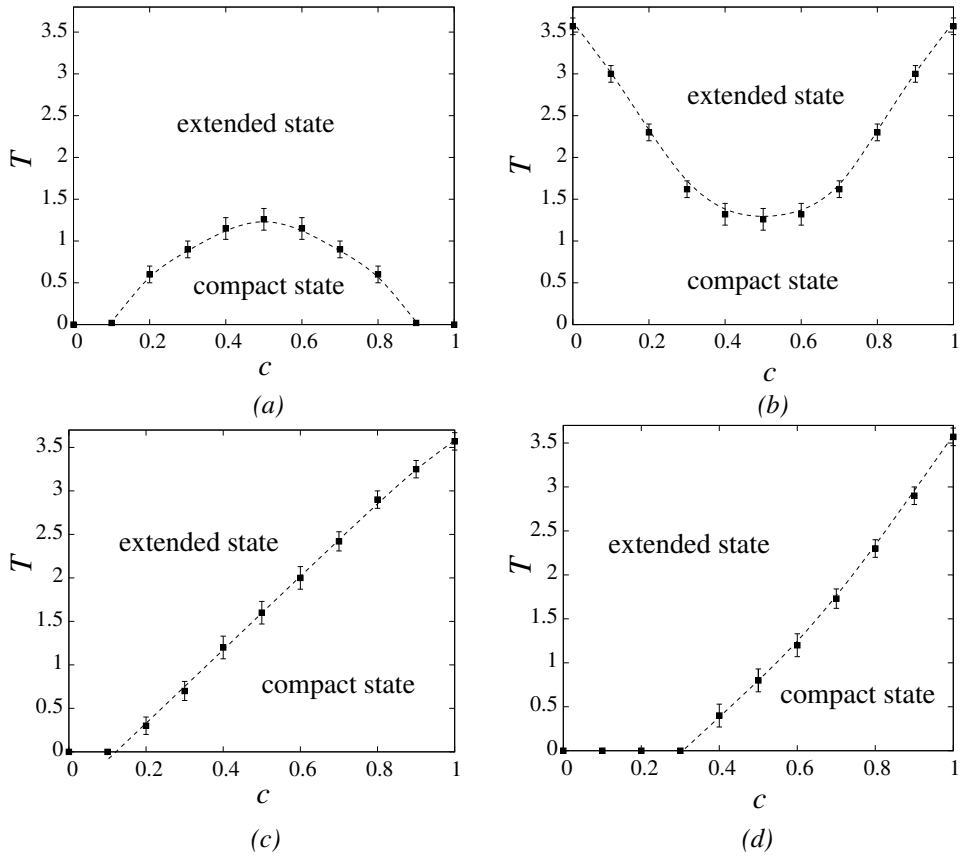

Figure 11.13: Phase diagrams of quenched, random heterogeneous polymer chains in T-c space. (a) model 1, (b) model 2, (c) model 4, (d) model 5.

other, refers to strongly screened Coulomb interactions [2]. The model 3 ($\varepsilon_{AA} = 1, \varepsilon_{BB} = \varepsilon_{AB} = 0$) is a particular case of model 1 and corresponds to a polymer chain containing charged (A) and neutral (B) monomers. Model 4 ($\varepsilon_{AA} = -1, \varepsilon_{BB} = \varepsilon_{AB} = 0$) refers to the (minimal) HP model [1] with hydrophobic (A) and hydrophilic (B) monomers. Models 2 ($\varepsilon_{AA} = \varepsilon_{BB} = -1, \varepsilon_{AB} = 1$) and 5 ($\varepsilon_{AA} = -1, \varepsilon_{BB} = 1, \varepsilon_{AB} = 0$) can be considered as generalizations of the two above mentioned cases.

Applying the pruned-enriched Rosenbluth chain-growth algorithm (PERM) [3] we analyzed numerically the transitions from an extended into a compact state as function of the inhomogeneity ratio $c = N_A/N$ for all five heteropolymer chain models [4]. In model 3, unlike the other models, the polymer chain expands its size with lowering the temperature due to the repulsion between monomers, and the polymer chain remains in an extended state at any temperature. Figure 11.13 shows that in model 2, the θ-transition is always present at any value of inhomogeneity ratio c, whereas models 1, 4 and 5 remain in an extended state when the concentration of attracting monomers is too small to cause a transition into the compact state. Note also that at small concentration of attractive monomers, the chains can attain the compact state only when they are long enough and have enough attractive nearest-neighbour contacts to overcome the conformational entropy. Models 2, 4 and 5 describe homogeneous polymer chains with nearest-neighbour attractions in the limiting case $c = 1$ (for model 2 also $c = 0$) with known value of the transition temperature $T_\theta = 3.717(3)$ [3].

[1] K.A. Dill: Biochemistry **24**, 1501 (1985); K.F. Lau, K.A. Dill: Macromolecules **22**, 3986 (1989)
[2] Y. Kantor, M. Kardar: Europhys. Lett. **28**, 169 (1994)
[3] P. Grassberger: Phys. Rev. E **56**, 3682 (1997)
[4] V. Blavatska, W. Janke: J. Chem. Phys. **140**, 034904 (2014)

11.12 Morphing the energy landscape of spin glasses

S. Schnabel, W. Janke

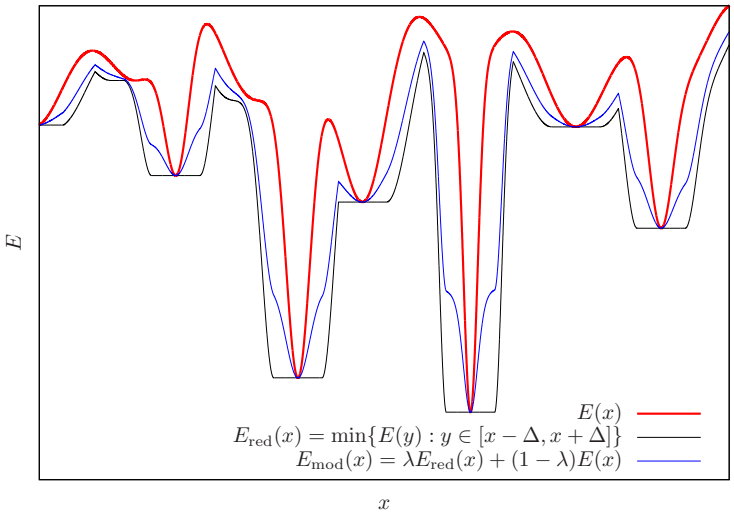

Figure 11.14: This sketch shows how a new variable (blue) with favorable characteristics can be composed from the energy (red) and a minimized energy (black).

Among the numerous systems that became accessible for investigation with the introduction of Monte Carlo simulations, spin glasses have proven to be among the most challenging. This becomes apparent when the Edwards-Anderson model [1] is studied. While being closely related to the very thoroughly examined and well-understood Ising model the introduction of disorder,

$$\mathcal{H} = \sum_{\langle ij \rangle} J_{ij} S_i S_j \,, \tag{11.7}$$

in the form of random couplings J_{ij} leads to an energy landscape that is characterized by an excessive number of local minima separated by energy barriers. This severely hampers Monte Carlo simulations since a random walker has to change frequently between high and low energies in order to sample a representative part of the state space. In consequence both the search for the ground state and the investigation of thermodynamic properties can only be performed for relatively modest system sizes. While for the former new methods keep being introduced, at least in the last two decades progress in the latter has exclusively been achieved due to an increase of computational resources.

We propose a novel technique related to the basin hopping algorithm [2]. In addition to the energy of a given configuration we evaluate the energy of the system after a short energy minimization and attribute this energy to the original configuration as well. Combining these two values, it is possible to obtain a variable that retains the minima of the Hamiltonian but alters the shape of the surrounding valleys (see Fig. 11.14), thus facilitating the simulation and reducing autocorrelation time. We obtain ground-state energies that correspond well with data from the literature. Furthermore, we are able to reach lower energies in balanced simulations than possible before.

[1] S.F. Edwards, P.W. Anderson: J. Phys. F **5**, 965 (1975)
[2] D.J. Wales: J. Phys. Chem. A **101**, 5111 (1997)

11.13 Finite-size scaling of three-dimensional lattice gas

J. Zierenberg, M. Wiedenmann, W. Janke

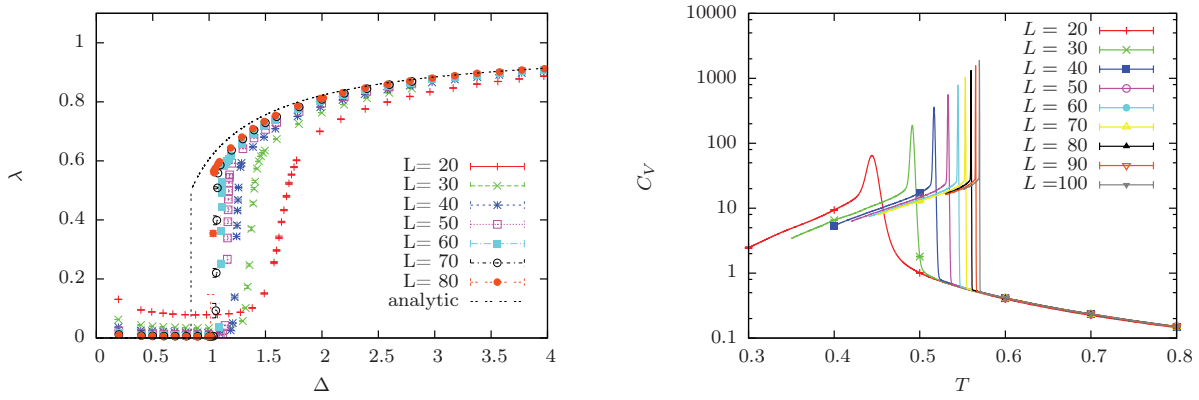

(a) (b)

Figure 11.15: (a) Fraction λ of excess particles in the largest cluster versus "dimensionless" density Δ at fixed temperature $T = 0.5$. (b) Canonical specific-heat curves at fixed density $\rho = 0.01$.

We studied the condensation/evaporation transition of the three-dimensional (3D) lattice gas on a cubic lattice [1, 2]. The lattice gas models particles as occupied sites on the lattice and is equivalent to the Ising model at fixed magnetization. The condensation/evaporation transition is usually discussed and described at fixed temperature, where analytic predictions exist, including rigorous results for the two-dimensional Ising lattice gas [3]. Figure 11.15(a) shows results for the 3D lattice gas varying a rescaled density compared to analytic predictions. This rescaling already includes the leading-order finite-size corrections and it may be anticipated that in the limit of large system sizes the analytic curve will describe the condensation/evaporation behaviour.

An alternative approach is to consider a fixed density and to identify the condensation transition temperature as the peak of the specific heat in Fig. 11.15(b). This may be considered as an orthogonal direction, where the finite-size scaling corrections have

the same size-dependence but may vary in amplitude [2]. We employed parallel multicanonical simulations [4], which allowed to obtain precise transition point estimates for relatively large system sizes including up to 10 000 particles. For the 3D lattice gas it seems that higher-order finite-size corrections are less pronounced in this approach, such that the largest system sizes were well described by the leading-order scaling predictions [2].

[1] J. Zierenberg et al.: J. Phys: Conf. Ser. **510**, 012017 (2014)
[2] J. Zierenberg, W. Janke: *Exploring different regimes in finite-size scaling of the droplet condensation/evaporation transition*, Leipzig preprint (April 2015), submitted to Phys. Rev. E
[3] M. Biskup et al.: Europhys. Lett. **60**, 21 (2002); Commun. Math. Phys. **242**, 137 (2003)
[4] J. Zierenberg et al.: Comput. Phys. Comm. **184**, 1155 (2013)

11.14 Nonstandard finite-size scaling at first-order phase transitions

M. Mueller, W. Janke, D.A. Johnston*

*Department of Mathematics and the Maxwell Institute for Mathematical Sciences, Heriot-Watt University, Edinburgh, UK

Albeit first-order phase transitions being omnipresent in nature their generic features in numerical studies are rarely discussed compared to the universal aspects of second-order phase transitions. Numerical investigations rely in principle on observations of finite systems due to the finiteness of the memory of computers. Of physical interest, however, are the properties of macroscopic systems. In the limit of infinite system size, first-order phase transitions are characterized by jumps in the order parameter and δ-function like divergences in response functions such as the specific heat or susceptibilities. In finite systems these singularities in observables are rounded and shifted much alike the effects in critical phenomena. These effects are systematic and thus a finite-size scaling theory was developed in the 1980's, which describes how the thermodynamic (many-particle or infinite-size) limit is approached. A rigorous solution for a class of models, including the Potts model under periodic boundary conditions has been found [1].

It is well established that the finite-size corrections at a first-order phase transition under periodic boundary conditions scale with the inverse system *volume*, that is $1/L^3$ for an $L \times L \times L$ lattice in three dimensions. The amplitudes of the correction terms are proportional to the logarithm $\ln q$ of the degeneracy q of the low-temperature phase, which is not particularly important in many standard models, such as the q-state Potts model, where that degeneracy is just a constant. However, if the degeneracy q of the low-temperature phase depends on the system size, oblique effects may disturb the traditional scaling ansatz with the inverse volume, leading to potentially wrong transition temperatures, latent heat and other observables.

In an extreme case with a macroscopic degeneracy $q \propto e^L$, the standard $1/L^3$ correction becomes $1/L^2$ [2]. One model with such a feature is the $3d$ plaquette-only gonihedric

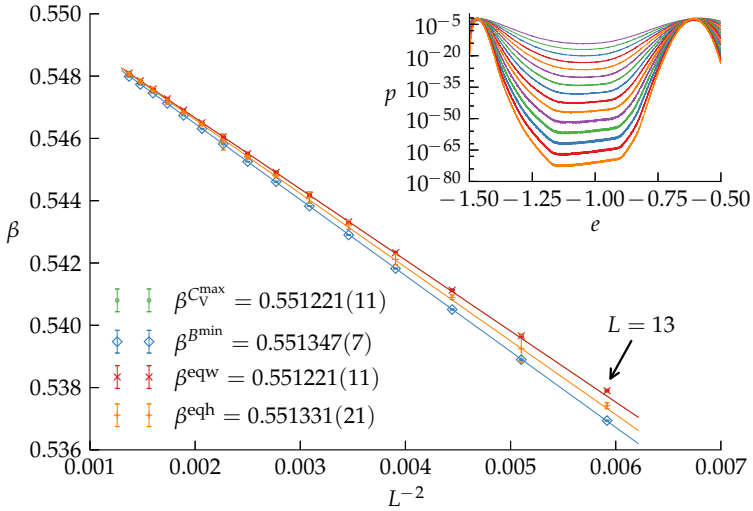

Figure 11.16: Fits that show clearly the leading $1/L^2$ scaling behaviour for the transition temperature obtained by different observables for the gonihedric Ising model. The inset shows the typical double-peaked energy probability density near the first-order phase transition temperature for different lattice sizes.

Ising model [3]. This is a member of a family of Hamiltonians that were originally formulated as a lattice discretization of string-theory actions in high-energy physics, which solely depend on the extrinsic curvature of the worldsheet [4].

We used multicanonical simulations of this model to generate high-precision data which indeed provides strong confirmation of the nonstandard finite-size scaling law [2], see Fig. 11.16. We checked for consistency in the amplitudes of higher-order corrections [5] and peak values of the specific heat or Binder's energy minimum [6]. The dual to the gonihedric model, which is an anisotropically coupled Ashkin-Teller model [7], has a similar degeneracy and also displays the nonstandard scaling law.

Our observation for the gonihedric model and its dual applies generically to any models which have a low-temperature phase degeneracy that depends exponentially on the system size. Potential examples range from ANNNI models to topological "orbital" models in the context of quantum computing. Numerous other systems, such as the Ising antiferromagnet on a $3d$ FCC lattice, have an exponentially degenerate number of ground states but a small number of true low-temperature phases. Nonetheless, they do possess an exponentially degenerate number of low-energy excitations so, depending on the nature of the growth of energy barriers with system size, an *effective* modified scaling could still be still be seen at a first-order transition for the lattice sizes accessible in typical simulations.

[1] C. Borgs et al.: J. Stat. Phys. **62**, 529 (1991)
[2] M. Mueller et al.: Phys. Rev. Lett. **112**, 200601 (2014)
[3] R. Pietig, F. Wegner: Nucl. Phys. B **466**, 513 (1996); *ibid.* **525**, 549 (1998)
[4] R.V. Ambartzumian et al.: Phys. Lett. B **275**, 99 (1992); G.K. Savvidy, K.G. Savvidy: Int. J. Mod. Phys. A **8**, 3393 (1993); Mod. Phys. Lett. A **8**, 2963 (1993)
[5] M. Mueller et al.: Nucl. Phys. B **888**, 214 (2014)
[6] M. Mueller et al.: in *Computer Simulation Studies in Condensed-Matter Physics*

XXVII, eds. H.-B. Schüttler, S. Lewis, M. Bachmann, D.P. Landau, Physics Procedia **57**, 68 (2014)
[7] D.A. Johnston, R.P.K.C Malmini: J. Phys. A: Math. Theor. **44**, 295004 (2011)

11.15 Equilibrium properties of the gonihedric plaquette model

M. Mueller, W. Janke, D.A. Johnston*

*Department of Mathematics and the Maxwell Institute for Mathematical Sciences, Heriot-Watt University, Edinburgh, UK

The plaquette model is a special case of a family of Hamiltonians called gonihedric Ising model, that originates from high-energy physics as a possible discretization of the area swept out by a string worldsheet moving through spacetime. The name comprises the greek words gonia (angle) and hedra (face) as a reminder of the origin, see [1] for a review.

The Hamiltonian of the plaquette-only gonihedric Ising model looks unobtrusive,

$$H = \sum_{[i,j,k,l]} \sigma_i \sigma_j \sigma_k \sigma_l \ , \tag{11.8}$$

but features very interesting properties. The first-order phase transition apparent in the system [2] is a very strong one and thus canonical simulations get easily trapped in one of the phases, potentially spoiling estimators for the transition temperature and latent heat. In addition, only very recently we found that the finite-size scaling behaviour for this model is changed due to the exponential degeneracy in the low-temperature phase [3].

Applying the nonstandard finite-size scaling ansatz we found an overall consistent inverse transition temperature of the infinite system $\beta = 0.551\,334(8)$ that incorporates estimators from both periodic and fixed boundary simulations as well as an estimator coming from a dual representation of the model. Furthermore, our high-precision multicanonical simulations allowed the estimation of the interface tension $\sigma = 0.12037(18)$ of the model, along with great consistency in the amplitudes of higher-order corrections [4, 5]. The puzzling effect of obtaining different latent heats for different boundary conditions could be traced back to extraordinary huge boundary effects [6], see Fig. 11.17.

To gain a deeper understanding of the properties of the transition, we investigated a recent suggestion in [7, 8] for a candidate order parameter coming from an anisotropic limit of the model. Indeed, we found that this planar order parameter is well suited to distinguish between the different phases [9]. Also, this parameter is subject to the nonstandard finite-size effects, as depicted in the right plot of Fig. 11.17.

With our multicanonical simulations in collaboration with the nonstandard finite-size scaling, the equilibrium properties of both energetic and magnetic quantities of the $3d$ plaquette gonihedric Ising model are now under good numerical control and the order parameter has been clearly identified. The *non*-equilibrium properties, in

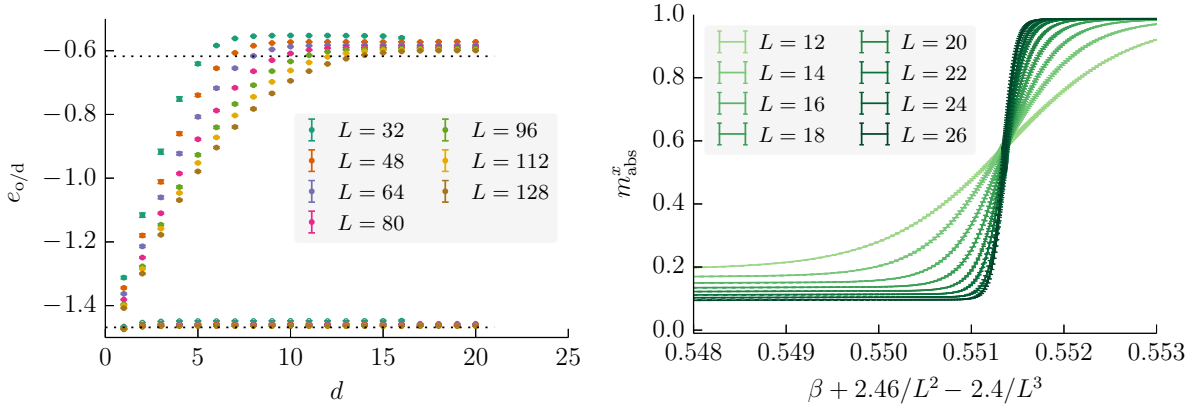

(a) (b)

Figure 11.17: (a) The disordered (upper) energies in layers at a distance d to the boundary are severely influenced when applying fixed boundaries, leading to biased latent heats for smaller lattices. This long-range order is also reflected in the definition of the planar order parameter of the model. (b) One of the planar order parameters as a function of inverse temperature, showing a sharp jump at the phase-transition point.

particular earlier suggestions that the model might serve as a generic example of glassy behaviour, even in the absence of quenched disorder, still pose open questions.

[1] D.A. Johnston et al.: in *Rugged Free Energy Landscapes: Common Computational Approaches to Spin Glasses, Structural Glasses and Biological Macromolecules*, ed. W. Janke, Lecture Notes in Physics **736** (Springer, Berlin, 2008), p. 173
[2] D. Espriu et al.: J. Phys. A: Math. Gen. **30**, 405 (1997)
[3] M. Mueller et al.: Phys. Rev. Lett. **112**, 200601 (2014)
[4] M. Mueller et al.: Nucl. Phys. B **888**, 214 (2014)
[5] M. Mueller et al.: in *Computer Simulation Studies in Condensed-Matter Physics XXVII*, eds. H.-B. Schüttler, S. Lewis, M. Bachmann, D.P. Landau, Physics Procedia **57**, 68 (2014)
[6] W. Janke et al.: *Finite-size scaling and latent heat at the gonihedric first-order phase transition*, Leipzig/Edinburgh preprint (Dezember 2014), to appear in J. Phys. Conf. Ser., in print
[7] D.A. Johnston: J. Phys. A: Math. Theor. **45**, 405001 (2012)
[8] Y. Hashizume, M. Suzuki: Int. J. Mod. Phys. B **25**, 73 (2011); *ibid.* **25**, 3529 (2011)
[9] M. Mueller et al.: Nucl. Phys. B **894**, 1 (2015); D.A. Johnston et al.: *Macroscopic degeneracy and order in the 3d plaquette Ising model*, Edinburgh/Leipzig preprint (December 2014), to appear in Mod. Phys. Lett. B, in print

11.16 First-order directional ordering transition in the three-dimensional compass model

M.H. Gerlach*, W. Janke

*Institut für Theoretische Physik, Universität zu Köln, Germany

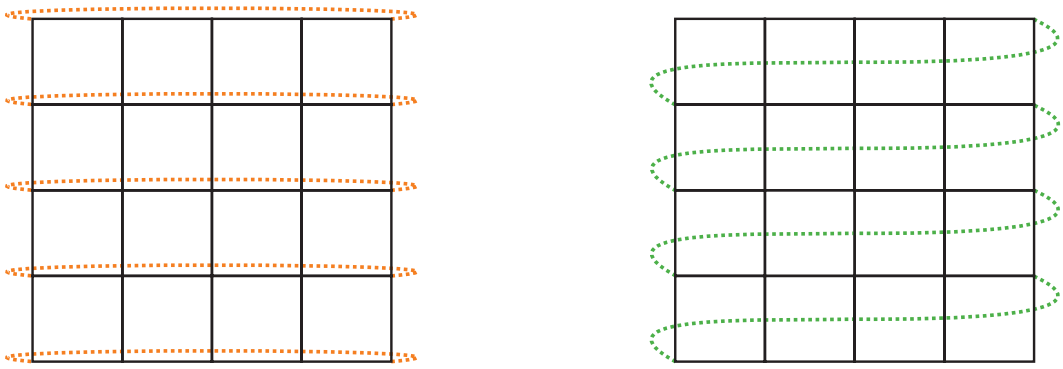

(a) PBC (b) SBC

Figure 11.18: Sketch of (a) periodic (PBC) and (b) screw-periodic boundary conditions (SBC) along the x-axis of a two-dimensional lattice. In the SBC picture the link between the lower right and the upper left corner is not shown. Equivalent boundary conditions are applied to the y-direction. Here a screw parameter of $S = 1$ is used.

Both the classical and the quantum version of the compass model have recently attracted much interest in the literature. The resaon is its connection to interesting quantum phenomena ranging from orbital order in transition metal compounds to topologically protected qbits [1–3]. In three dimensions the classical model is defined by the Hamiltonian

$$\mathcal{H} = J \sum_{i=1}^{N} \left(\sigma_i^x \sigma_{i+e_x}^x + \sigma_i^y \sigma_{i+e_y}^y + \sigma_i^z \sigma_{i+e_z}^z \right), \tag{11.9}$$

where $\sigma = (\sigma^x, \sigma^y, \sigma^z)$ are three-dimensional unit spin vectors, e_x, e_y, and e_z are unit vectors in x, y, and z direction, and J is a coupling constant. Although simple looking at first sight, surprisingly little is known about this model in three dimensions. Most studies so far focused on the two-dimensional analogue which still turned out to be rather hard to study numerically. It was shown to possess rich physics ranging from highly degenerate ground states to quantum phase transitions to an exciting thermal phase transition [4, 5].

In recent analyses of high-temperature series expansions of the three-dimensional quantum model (where the classical spins are replaced by Pauli matrices) it was claimed that this model does not exhibit a phase transition at any finite temperature [6]. This motivated us to consider first the three-dimensional classical model and to investigate whether this model exhibits a phase transition [7]. To this end we employed state-of-the-art Monte Carlo computer simulations using Metropolis, cluster, and parallel tempering (PT) techniques. From our previous studies in two dimensions [5] we knew that employing so-called screw-periodic boundary conditions [8] sketched in Fig. 11.18 considerably improves the finite-size scaling behaviour of this model. As a result we obtained convincing numerical evidence for a phase transition of first-order at the temperature $T_0 = 0.098328 \pm 0.000003$. This value is in good agreement with a brief

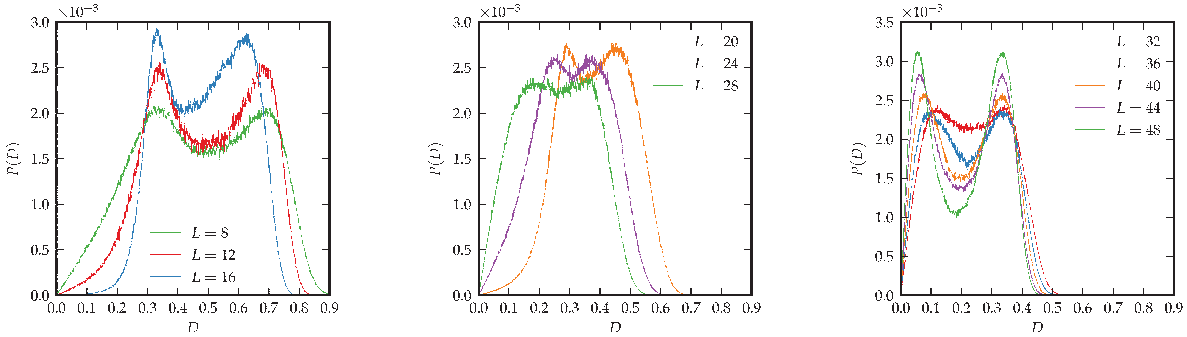

Figure 11.19: Histograms of the directional order parameter D in the three-dimensional compass model with screw-periodic boundary conditions for various lattice sizes L.

remark in Ref. [9]. The nature of the phase transition can be read off from the histograms of the directional order parameter D of the model in Fig. 11.19 which exhibit for large lattice sizes L a characteristic double-peak structure. Note the nonmonotonic behaviour as function of lattice size: Initially, the double peak becomes *less* pronounced until $L \approx 28-32$, and only from then on it becomes more pronounced with further increasing L. By analyzing the ratio of peak maximum to peak minimum, we arrive at a definitely nonzero, albeit small value for associated interface tension, $\sigma_{\mathrm{od}} \approx 3 \times 10^{-4}$.

[1] K.I. Kugel, D.I. Khomskii: Sov. Phys. Usp. **25**, 231 (1982)
[2] B. Douçot et al.: Phys. Rev. B **71**, 024505 (2005)
[3] A. Kitaev: Ann. Phys. **321**, 2 (2006)
[4] S. Wenzel, W. Janke: Phys. Rev. B **78**, 064402 (2008); see also "Publisher's Note" in Phys. Rev. B **78**, 099902(E) (2008) [Fig. 1 selected for Phys. Rev. B "Kaleidoscope" August 2008]
[5] S. Wenzel et al.: Phys. Rev. E **81**, 066702 (2010)
[6] J. Oitmaa, C.J. Hamer: Phys. Rev. B **83**, 094437 (2011)
[7] M.H. Gerlach, W. Janke: Phys. Rev. B **91**, 045119 (2015)
[8] E. Bittner et al.: Nucl. Phys. B **820**, 694 (2009)
[9] S. Wenzel, A.M. Läuchli: Phys. Rev. Lett. **106**, 197201 (2011)

11.17 Parallel multicanonical study of the three-dimensional Blume-Capel model

J. Zierenberg, N.G. Fytas*, W. Janke

*Applied Mathematics Research Centre, Coventry University, UK

We studied the three-dimensional (3D) Blume-Capel model [1, 2] on a cubic lattice, a spin-one Ising model in a crystal field described by the Hamiltonian

$$\mathcal{H} = -J \sum_{\langle ij \rangle} \sigma_i \sigma_j + \Delta \sum_i \sigma_i^2 = E_J + \Delta E_\Delta \,. \tag{11.10}$$

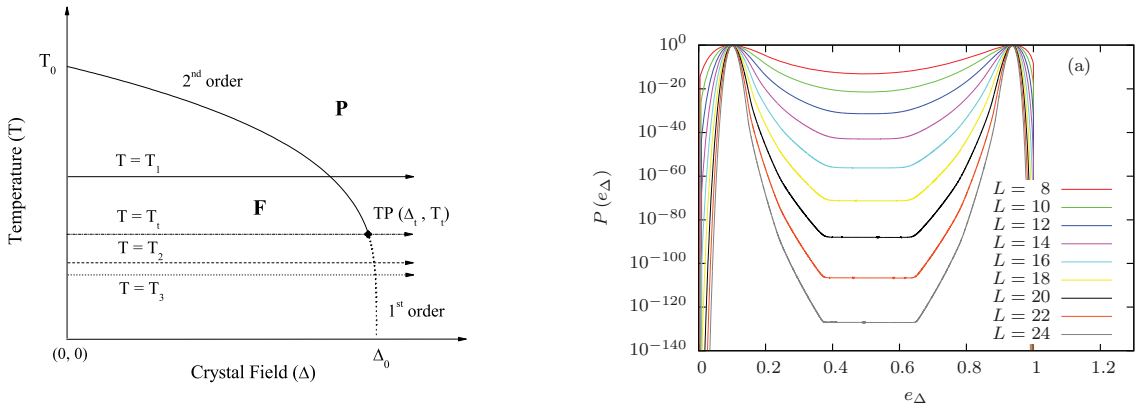

Figure 11.20: (a) Sketch of the 3D Blume-Capel phase diagram in the temperature – crystal field plane showing both a second-order (solid) and first-order (dashed) phase transition between the ferromagnetic (**F**) and paramagnetic (**P**) phase. (b) Fixed-temperature ($T_3 = 0.9$) probability distributions at the transition field Δ_{eqh} with respect to $e_\Delta = E_\Delta/V$.

Using a multicanonical based approach, we study the first- and second-order phase transition at fixed temperature along the crystal field axis [3], see Fig. 11.20(a). This exploits the numerical advantage of integer "magnetization" and the systematic advantage of a broad first-order regime over a wide range of temperatures, compared to a fixed-Δ approach.

Looking at a specific-heat like field-derivative of the spin-spin interaction term, $C(\Delta) = -\beta\Big[\langle E_J E_\Delta\rangle - \langle E_J\rangle\langle E_\Delta\rangle\Big]$, we performed finite-size scaling analyses in both the second-order ($T_1 = 2$) and first-order ($T_2 = 1$, $T_3 = 0.9$) regime as well as in the vicinity of a tricritical point estimate $T_t = 1.4182$ [4]. We verified the expected $\sim L^d$ scaling behavior in the first-order regime and the expected Ising universality class in the second-order regime with this orthogonal approach. A feature of this approach is the efficient study of the first-order regime, a tricky numerical task. Using a generalized-ensemble method, where also otherwise suppressed regions are sampled, see Fig. 11.20(b), allowed to even estimate accompanied free-energy like barriers. These may be related to spin-0 droplets/strips and vanish as one approaches the tricritical point. Our results at the tricritical estimate indicated its accuracy and yielded the expected Ising tricritical exponents from extrapolations of effective exponents.

[1] M. Blume: Phys. Rev. **141**, 517 (1966)
[2] H.W. Capel: Physica (Utr.) **32**, 966 (1966)
[3] J. Zierenberg et al.: Phys. Rev. E **91**, 032126 (2015)
[4] M. Deserno: Phys. Rev. E **56**, 5204 (1997)

11.18 Tunable condensate shapes in a stochastic transport model

H. Nagel, E. Ehrenpreis, W. Janke

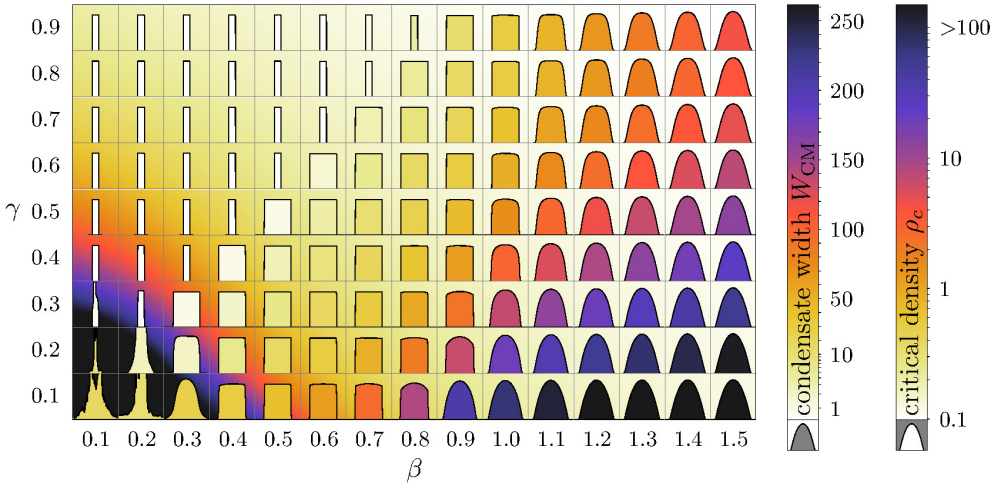

Figure 11.21: Numerically determined characteristic condensate shapes for systems of various β and γ at a condensate volume of about 10^5 particles. The shapes are formed by rescaling the width and height of all measured condensate sample shapes and only then averaging them. The fill colour inside the condensate shapes encodes the average width while the background colour around the shapes gives the critical density of the condensation. The shapes in the single-site regime are plotted narrowed to give a better distinction to the extended condensate shapes.

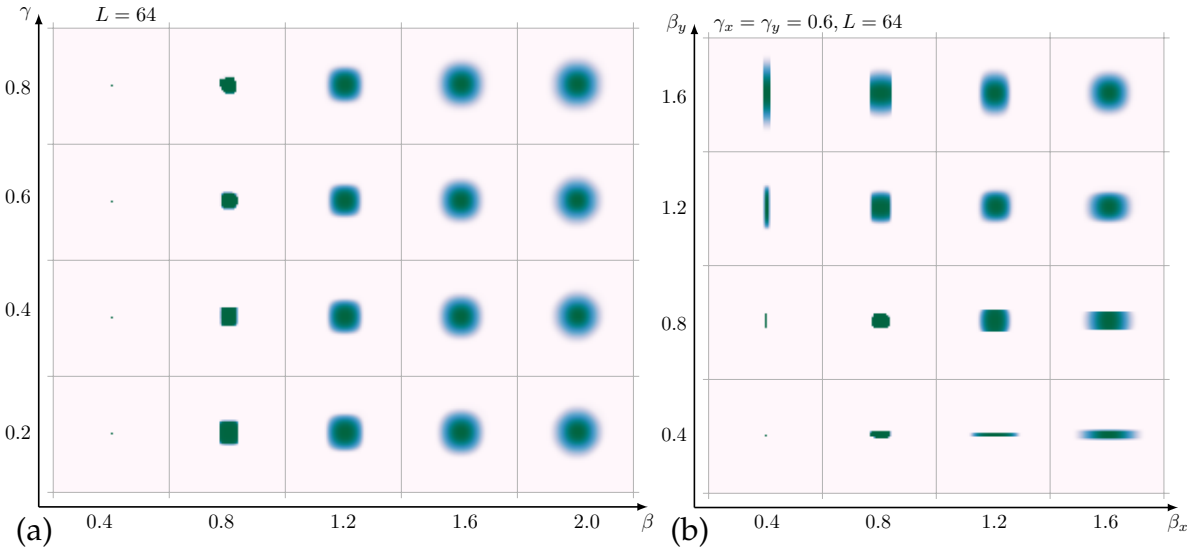

Figure 11.22: Mean condensate shapes for various values of the coupling constants β and γ of the considered condensation model in two dimensions for (a) isotropic and (b) anisotropic couplings (with $\gamma = 0.6$).

Condensation phenomena are observed in a broad range of physical processes on every length scale. While they are originally associated with the transition of matter from gas to some liquid or solid state, they are more generically realizations of nucleation and coarsening phenomena. A versatile approach to study such generic condensation mechanisms is the framework of stochastic transport processes with specific models such as the (asymmetric) simple exclusion process (ASEP), the zero-range process (ZRP) or the pair-factorized steady states (PFSS) transport model as a generalization of the ZRP with short-range interactions [1]. In this work, we consider a generic stochastic transport process with tunable nearest-neighbour interactions

$$g(m,n) = \exp[-|m-n|^{\beta} - 1/2(|m|^{\gamma} + |n|^{\gamma})]\,, \tag{11.11}$$

with the coupling constants β and γ for short-range and zero-range interactions, respectively. As predicted in previous analytical work [2, 3], these interactions lead to a steady state that features the formation of spatially extended particle condensates of various shapes and sizes for strengths of the zero-range coupling in the range $0 < \gamma < 1$. Single-site condensates with properties similar to those of the ZRP are observed for weak nearest-neighbour couplings $\beta < \gamma$. Extended condensates are observed with rectangular shape for $\gamma < \beta < 1$ and with smooth parabolic shape for $\beta > 1$. Using Monte Carlo simulations we validated the predictions concerning characteristic shapes (see Fig. 11.21) and scaling laws of the condensate size of the emerging condensates in most parts of the β-γ plane with very good agreement to the predicted scaling exponent α [4]. To simulate the technically challenging regime of rectangular condensates we proposed and successfully used a collective update method to overcome large barriers in the state space in between. Finally we extended the model to a two-dimensional system to systematically check how the mean condensate shape and the scaling of the its size is affected under change of the the coupling constants β and γ, see Fig. 11.22.

[1] M. Evans et al.: Phys. Rev. Lett. **97**, 010602 (2006)
[2] B. Wacław et al.: Phys. Rev. Lett. **103**, 080602 (2009)
[3] B. Wacław et al.: J. Stat. Mech. **2009**, P10021 (2009)
[4] E. Ehrenpreis et al.: J. Phys. A: Math. Theor. **47**, 125001 (2014)

11.19 Boundary drive induced phase transitions in stochastic transport condensation models

H. Nagel, H. Christiansen, W. Janke

Stochastic mass transport processes such as the asymmetric simple exclusion process (ASEP) or the zero-range process (ZRP) are simple transport models for particle hopping aiming to improve the understanding of basic phenomena in the dynamics of particles in driven diffusive systems. An important class of such phenomena that can be studied and understood on an abstract level is the emergence of generic condensates. In this project we systematically studied the phase diagram of such a transport process under driven particle exchange through open boundaries. While boundary drive

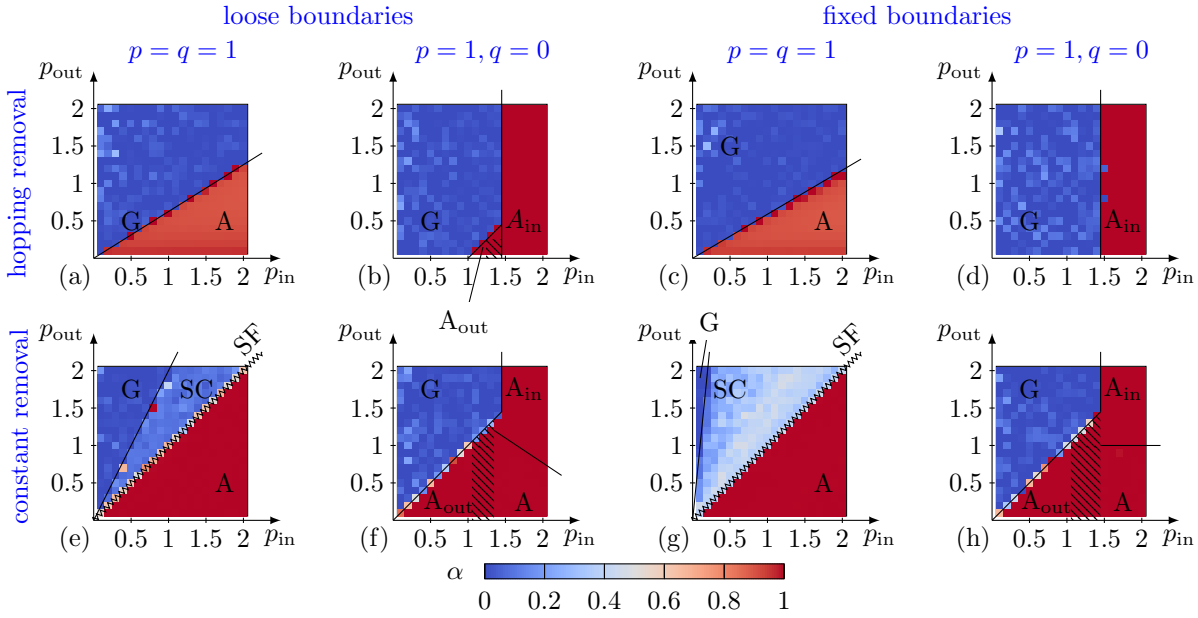

Figure 11.23: Phases induced by driven particle exchange through open boundary conditions of the system. With respect to the specific implementation of the interaction at the boundary, different phase diagrams are observed.

induced phase transitions are long known for the ASEP, the research for the ZRP with condensation dynamics is more recent [1].

We considered a transport process with tunable weights [2] as well as various types of interactions at the boundaries to study these effects on a much broader scale. The tunable model allowed us to effectively interpolate between ZRP-type as well as strong short-range interactions. At the boundaries we considered the existence of fixed versus loose couplings as well as different approaches to particle injection and removal rates. For the generated cases we produced the phase diagrams under differing strengths of the driven particle exchange at the boundaries for symmetric and totally asymmetric dynamics [3]. The main phases, as shown in Fig. 11.23, are: a thin particle gas (G), formation of aggregate condensates (A) and the spanning bulk condensate (SC). While the phase diagrams with vanishing as well as stronger short-range interactions are very similar except for the SC phase, we observed a qualitatively different mechanism for aggregate condensate formation with short-range interactions.

[1] E. Levine et al.: J. Stat. Phys. **120**, 759 (2005)
[2] B. Wacław et al.: Phys. Rev. Lett. **103**, 080602 (2009)
[3] H. Nagel et al.: Physics Procedia **57**, 77 (2014)

11.20 A simple non-equilibrium model for Stranski-Krastanov growth

J.K. Ochab*, H. Nagel, W. Janke, B. Wacław†

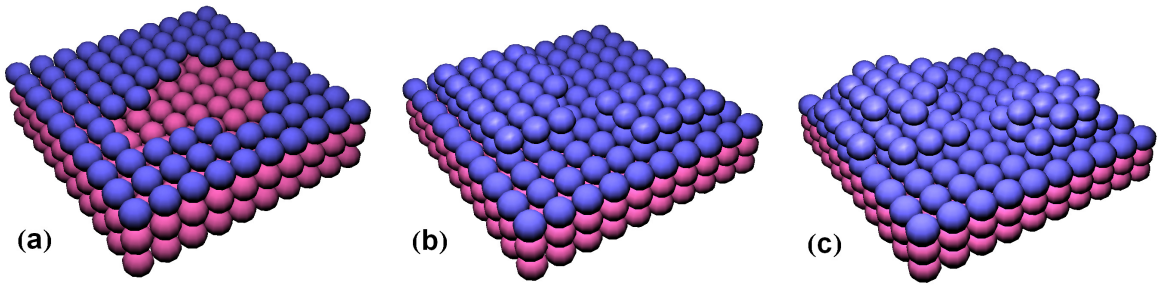

Figure 11.24: Schematic stages of Stranski-Krastanov growth. (a) The substrate (purple spheres) is covered with an increasing number of adatoms (blue spheres), starting from an incomplete monolayer. (b) As the density of adatoms increases, the adatoms form a complete monolayer and a partially filled second layer. (c) Upon further density increase, islands of variable height begin to form on the monolayer. Here the critical density of adatoms above which islands occur equals one adatom per one substrate site.

*Marian Smoluchowski Institute of Physics and Mark Kac Complex Systems Research Center, Kraków, Poland
†School of Physics and Astronomy, University of Edinburgh, Scotland, UK

We consider a simple non-equilibrium model of mass condensation with Lennard-Jones interactions between particles and a substrate. This model is an extension of the zero-range process to nearest-neighbour interactions, similar to that of Refs. [1–3], where particles interact when they are at the same site or at neighbouring sites. Although the model can be driven far from equilibrium, it is closely related to the equilibrium solid-on-solid (SOS) model [4]. A remarkable feature of this stochastic process is that the steady state factorises over pairs of neighbouring sites, also in dimensions higher than one, and thus it is called the pair-factorised steady state (PFSS) process. This property facilitates analytical calculations in the one-dimensional version of the model and, in certain cases, also in more than one dimension [5].

We show that when some number of particles is deposited onto the surface and the system is left to equilibrate, particles condense into an island if the density of particles becomes higher than some critical density [6]. We illustrate this with numerically obtained phase diagrams for (2+1)-dimensional systems. We also solve a (1+1)-dimensional counterpart of this model analytically and show that not only the phase diagram but also the shape of the cross-sections of (2+1)-dimensional condensates qualitatively matches the (1+1)-dimensional predictions [2, 3, 7]. Furthermore, when particles are being deposited with a constant rate, we demonstrate that the system has two phases: a single condensate for low deposition rates, and multiple condensates for fast deposition [6]. The behaviour of our model is thus similar to that of thin film growth processes, and in particular to Stranski-Krastanov growth.

[1] M. Evans et al.: Phys. Rev. Lett. **97**, 010602 (2006)
[2] B. Wacław et al.: Phys. Rev. Lett. **103**, 080602 (2009)
[3] B. Wacław et al.: J. Stat. Mech. **2009**, P10021 (2009)
[4] S.T. Chui, J.D. Weeks: Phys. Rev. B **23**, 2438 (1981)
[5] B. Wacław et al.: J. Phys. A: Math. Theor. **42**, 315003 (2009)

[6] J.K. Ochab et al.: *A simple non-equilibrium, statistical physics toy model of thin-film growth*, Kraków/Leipzig/Edinburgh preprint (March 2015), to be published
[7] E. Ehrenpreis et al.: J. Phys. A: Math. Theor. **47**, 125001 (2014)

11.21 NVE-WHAM and the bridge between molecular dynamics and Monte Carlo simulations for liquid-gas like phase transitions

P. Schierz, J. Zierenberg, W. Janke

Molecular dynamics (MD) and Monte Carlo (MC) simulations are starting from two distinct physical points of view. While MD numerically integrates Newton's equations of motion, MC samples according to known ensemble probabilities from statistical physics. The foundation of statistical physics states that both approaches should give the same results in equilibrium.

MD simulations are normally considered to sample the NVE ensemble which is not entirely correct. Here N stands for the particle number, V denotes the volume, and $E = E_{\text{kin}} + E_{\text{pot}}$ is the total energy of the system. Since MD simulations without a thermostat encounter total linear and total angular momentum conservation, the available phase space for an MD simulation is restricted in comparison to the microcanonical ensemble. This results in a deviating behaviour of MD simulation data in comparison to NVE MC [1, 2] simulations for a small number of degrees of freedom. The simulation of a liquid-gas like phase transition becomes especially complicated with an MD simulation with periodic boundary conditions (PBC). For the gas phase the PBC will lead to a nonconserved angular momentum where the ensemble is described by: particle number, volume, total energy and total linear momentum P (NVEP ensemble [3]). For the liquid phase the PBC will not change the total angular momentum J which results in an ensemble where the angular momentum is additionally conserved (NVEPJ ensemble [4]).

Nonetheless it was possible to develop a method which allows to estimate the density of states of the simulated systems for the relevant potential energies of the liquid-gas like transitions [5]. For an illustration, see Fig. 11.25. This method was adapted from the known "Weighted Histogram Analysis Method" (WHAM) for the canonical ensemble [6]. The canonical weight in the WHAM method is replaced by the appropriate ensemble weights of the NVEP and NVEPJ ensemble. Therefore it is possible to estimate the density of states.

The density of states can be used to calculate the behaviour in the NVT ensemble and therefore to investigate phase transitions with varying temperature. Since the NVE ensemble shows very good sampling in the potential energy range of canonical first-order phase transitions it seems possible to estimate the NVT phase-transition behaviour by performing many NVE simulations at various total energies. In this way it is possible to distribute the computational effort to many computer cores. Since this method estimates the density of states, it is also a promising approach for the estimation of free-energy barriers for first-order phase transitions with MD.

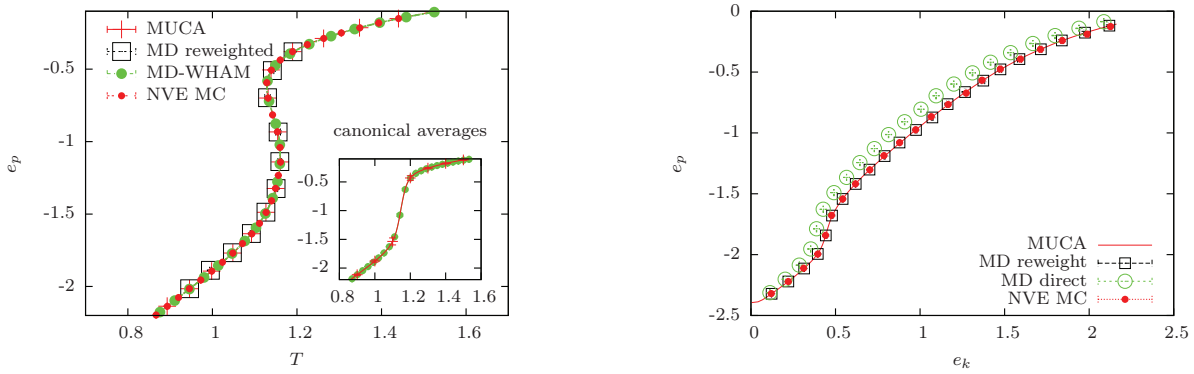

(a) (b)

Figure 11.25: (a) The potential energy vs. temperature for 8 polymers with 13 monomers each, simulated with two Monte Carlo techniques and MD. (b) The potential energy vs kinetic energy for a single polymer with 13 monomers. The MD data is once evaluated directly (NVEPJ ensemble) and once reweighted to the NVE ensemble.

[1] J.R. Ray: Phys. Rev. A **44**, 4061 (1991)
[2] R. Lustig: J. Chem. Phys. **109**, 8816 (1998)
[3] R. Lustig: J. Chem. Phys. **100**, 3048 (1994)
[4] F. Calvo et al.: J. Chem. Phys. **112**, 10350 (2000)
[5] P. Schierz et al.: *Molecular Dynamics and Monte Carlo simulations in the microcanonical ensemble: Quantitative comparison and reweighting techniques*, Leipzig preprint (May 2015), to be published
[6] A.M. Ferrenberg, R.H. Swendsen: Phys. Rev. Lett. **63**, 1195 (1989)

11.22 Application of the parallel multicanonical method to a broad range of problems

J. Zierenberg, M. Wiedemann, M. Marenz, W. Janke

We applied our recently refined parallel multicanonical method [1] to a broad range of problems and investigated the scaling properties including the Ising spin model, the q-state Potts model and bead-spring polymers [2], as well as the lattice gas model [3]. In all cases, we find a close to linear scaling with slope one for up to 128 cores used. This means that doubling the number of involved processors would reduce the wall-clock time necessary by a factor of two. Moreover, it is a straightforward and simple implementation especially if wrapped around an existing multicanonical simulation.

A detailed analysis of optimized parameters per degree of parallelization for the q-state Potts model in the range $q = \{2, 8\}$ suggests that there exists a limit depending on emerging barriers and associated increasing integrated autocorrelation times [1, 2].

For any real-life application, we continue to consider a fixed number of sweeps per multicanonical iteration that is distributed onto the number of cores. This is the only possibility to assess larger or more complicated systems and shows the expected scaling also for first-order transitions like gas condensation in two and three dimensions, see

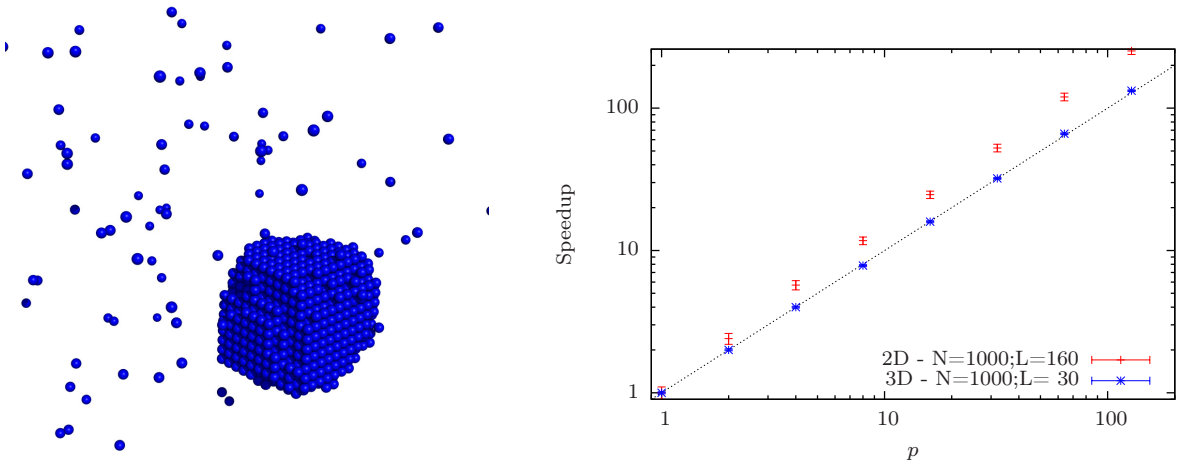

Figure 11.26: (a) Lattice gas in the droplet phase as an example for (b) the speedup in a day-to-day application.

Fig. 11.26 [3]. With this method, we were able to show that in three dimensions lattice gas condensation shows an unexpected deviation from the analytic predictions which may be explained by finite-size effects but needs additional investigations.

Altogether, this demonstrates the broad range of application of this parallel version of multicanonical simulations to problems in hard and soft condensed matter in any parameter that occurs linear in the Hamiltonian (temperature, field, etc.).

[1] J. Zierenberg et al.: Comput. Phys. Comm. **184**, 1155 (2013)
[2] J. Zierenberg et al.: Physics Procedia **53**, 55 (2014)
[3] J. Zierenberg et al.: J. Phys.: Conf. Ser. **510**, 012017 (2014)

11.23 Status of our framework for programming Monte Carlo simulation (βMC).

M. Marenz, J. Zierenberg, W. Janke

Monte Carlo (MC) computer simulations are a very powerful tool for investigating and understanding the thermodynamic behaviour of a wide variety of physical systems. These systems range from such simple ones like the Ising spin model to complex ones like the adsorption properties of proteins on surfaces [1]. In contrast to Molecular Dynamics (MD) simulations, the other important class of algorithm to simulate microscopic systems, MC simulations are not suitable to investigate dynamical properties. On the other hand, the ability of modern MC methods to explore effectively the phase space of physical systems, especially those with a phase transition, makes them a very powerful and indispensable tool.

Another difference to MD simulations is the lack of a widely used program package for generic MC simulations. One reason for this lack is the versatility of modern MC

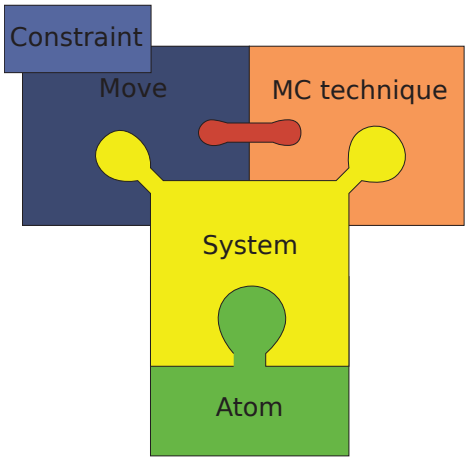

Figure 11.27: The 5 basic building blocks.

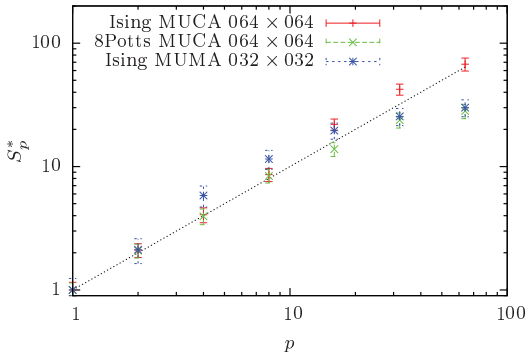

Figure 11.28: Scaling properties of the parallel multicanonical algorithm as a function of the number of processors p.

algorithms – there are various different algorithm and many different possibilities to adjust a MC simulation to a specific problem. This was the starting point for the development of our framework for advanced MC algorithms. The aim of the framework is to enable the programmer to implement specific simulations in an easy and efficient way, without the need to implement all the tricky details for every new problem. The framework is implemented in the C++ programming language and is designed such that it separates basics parts of a MC algorithm in separate building blocks. These building blocks can be used by the programmer to implement a specific simulation.

There are 5 basic building blocks as illustrated in Fig. 11.27: The first one is the "system", which defines the Hamiltonian and the structure of the physical system. This means that the "system" building block encapsulates the energy calculation and the structure of the considered physical problem. For off-lattice system this block contains a smaller subpart, the "atom" block, which encodes the geometry of the system (e.g., boundary conditions). As systems we have implemented so far different kinds of coarse-grained homopolymers, the Lennard-Jones gas, the TIP4P water model, lattice polymers and the Potts model in different dimensions. On top of the "system" are the last two other building blocks, the "move" and the "MC technique". A "move" defines a single update proposal, propagating the system from the current state to the next one. Additionally a "constraint" can be added to every "move" in order to simulate efficiently systems with geometrical confinements. The "MC technique" implements the Monte Carlo algorithm itself. At the moment we have implemented various algorithms such as Metropolis MC, parallel tempering, multicanonical MC, multimagnetic MC and the Wang-Landau MC algorithm. One of the most advanced MC algorithms we have implemented is a parallel version of the multicanonical algorithm [2], see Fig. 11.28.

The boundaries between these blocks are well defined, so that one can easily exchange one of them. For example one can use two different algorithm to simulate a specific system without implementing a completely new program. The framework is already in practical use for different studies, for example the investigation of the influence of bending stiffness on a coarse-grained homopolymer, the influence of a spherical confinement to pseudo-phase transitions of homopolymers, and the study of polymer aggregation of several polymers for a large set of parameters (temperature, bending

stiffness). Thus, the framework is very useful and has let already to the publication of several papers [2–6].

[1] M. Bachmann et al.: Angew. Chem. Int. Ed. **49**, 9530 (2010) [Angew. Chem. **122**, 9721 (2010), in German]
[2] J. Zierenberg et al.: Comput. Phys. Comm. **184**, 1155 (2013)
[3] M. Marenz et al.: Condens. Matter Phys. **15**, 43008 (2012)
[4] J. Zierenberg et al.: J. Phys.: Conf. Ser. **510**, 012017 (2014)
[5] J. Zierenberg et al.: J. Chem. Phys. **141**, 114908 (2014)
[6] J. Zierenberg, W. Janke: Europhys. Lett. **109**, 28002 (2015)

11.24 Funding

Graduate School *"BuildMoNa": Leipzig School of Natural Sciences – Building with Molecules and Nano-objects*
W. Janke (Principal Investigator)
Deutsche Forschungsgemeinschaft (DFG), Excellence Initiative Grant GSC185

Graduate School *Statistical Physics of Complex Systems*
W. Janke (with B. Berche, Nancy)
Deutsch-Französisches Doktorandenkollegium (DFDK) with "Co-tutelle de Thèse", jointly with Université de Lorraine, Nancy, France, and Coventry University, UK, and National Academy of Sciences of Ukraine, Lviv, Ukraine, as associated partner
Deutsch-Französische Hochschule (DFH-UFA), Grant No. CDFA-02-07

International Max Planck Research School (IMPRS) *Mathematics in the Sciences*
W. Janke (Scientific Member)
Max Planck Society and Klaus Tschira Foundation

Forschergruppe 877 *From Local Constraints to Macroscopic Transport*
W. Janke (Principal Investigator, project P9 in collaboration with K. Kroy, Research Unit "Theory of Condensed Matter (TKM)")
Deutsche Forschungsgemeinschaft (DFG), Grant No. JA 483/29-1

Sonderforschungsbereich/Transregio SFB/TRR 102 *Polymers under Multiple Constraints: Restricted and Controlled Molecular Order and Mobility*
W. Janke (Principal Investigator, project B04)
Deutsche Forschungsgemeinschaft (DFG)

Junior Research Group ("Nachwuchsforschergruppe") *Werkzeuge und Technologien für die rationale Wirkstoffentwicklung*
J. Bock, W. Janke
Europäischer Sozialfond (ESF)

Junior Research Group ("Nachwuchsforschergruppe") *Funktion durch Selbstorganisation: Emergente Eigenschaften von Atom- und Molekülaggregaten*
P. Schierz, W. Janke
Europäischer Sozialfond (ESF)

Molecular Conformation Mechanics of Proteins and Polymers
W. Janke
Deutsche Forschungsgemeinschaft (DFG), Grant No. JA 483/24-3

Mass Transport Models on Networks
W. Janke (twin project with H. Meyer-Ortmanns, Jacobs University Bremen)
Deutsche Forschungsgemeinschaft (DFG), Grant No. JA 483/27-1

Institute Partnership with the Institute for Condensed Matter Physics of the National Academy of Sciences of Ukraine, Lviv, Ukraine, *Polymers in Porous Environments and on Disordered Substrates*
W. Janke (with V. Blavatska, Lviv)
Alexander von Humboldt Foundation (AvH)

Marie Curie IRSES Network *DIONICOS: Dynamics of and in Complex Systems*
W. Janke (Principal Investigator, head of Leipzig node)
European Union (EU)

Aggregation and Collapse of Polymers in Confinement
W. Janke, M. Marenz, J. Zierenberg
NIC Jülich (computer time grant for "JUROPA"), Grant No. HLZ21

11.25 Organizational Duties

Wolfhard Janke

- Director, Institute for Theoretical Physics (ITP), Universität Leipzig
- Director, Naturwissenschaftlich-Theoretisches Zentrum (NTZ), Universität Leipzig
- Member of Department Council ("Fakultätsrat"), Faculty for Physics and Earth Sciences, Universität Leipzig
- Member of the Steering Committee ("Direktorium") of the Graduate Centre *Mathematics/Computer Science and Natural Sciences*, Research Academy Leipzig
- Principal Investigator of the Graduate School "BuildMoNa"
- Scientific Member of the International Max Planck Research School (IMPRS) *Mathematics in the Sciences*
- Principal Investigator of the DFG Sonderforschungsbereich/Transregio SFB/TRR 102 *Polymers under Multiple Constraints: Restricted and Controlled Molecular Order and Mobility*
- Principal Investigator of the DFG Forschergruppe FOR877 *From Local Constraints to Macroscopic Transport*
- Principal Investigator of "Profillinie" *Complex Matter*, Universität Leipzig
- Principal Investigator of "Profillinie" *Mathematical and Computational Sciences*, Universität Leipzig
- Spokesperson of the German-French Graduate College *Statistical Physics of Complex Systems* with Nancy (France), and associated partners in Coventry (England, UK) and Lviv (Ukraine), of the Deutsch-Französische Hochschule (DFH-UFA)
- Spokesperson of the German-Ukrainian Institute Partnership Leipzig-Lviv of the Alexander von Humboldt Foundation (AvH)

- External Member of the Jagiellonian University Graduate School *International Ph.D. Studies in Physics of Complex Systems*, Krakow, Poland
- *International Visiting Professor* of Coventry University, England, UK
- Permanent Member of the International Advisory Board for the Annual *Conference of the Middle European Cooperation in Statistical Physics (MECO)*
- Co-organizer of the "BuildMoNa" Modul 2014-B3 *Basic Concepts in Physics* (with F. Cichos and P. Esquinazi), Universität Leipzig, 7./14./15. May 2014
- Member of the International Scientific Committee for the *Humboldt Kolleg: German-Turkish Cooperation in Physics: New Challenges in Science*, Ankara University, Ankara, Turkey, 11.–13. June 2014
- Chair of Program Committee *Classical Statistical Mechanics and Complex Systems* of the XXVI IUPAP *Conference on Computational Physics* CCP2014, Boston, Massachusetts, USA, 11.–14. August 2014
- Organizer of the Workshop *CompPhys14* – 15th International NTZ Workshop on *New Developments in Computational Physics*, ITP, Universität Leipzig, 27.–29. November 2014
- Organizer of the Workshop *CompPhys15* – 16th International NTZ Workshop on *New Developments in Computational Physics*, ITP, Universität Leipzig, 26.–28. November 2015
- Guest Editor (with Y. Holovatch (Lviv, Ukraine) and S. Turner (Vienna, Austria)) for the Special Issue of Condens. Matter Phys.: *Self-Organization and Collective Behaviour in Complex Systems*
- Editor "Computational Physics", Central European Journal of Physics, Krakow, Poland
- Member of Editorial Board, Condens. Matter Phys., Lviv, Ukraine
- External Reviewer for Deutsche Forschungsgemeinschaft (DFG), Humboldt-Stiftung (AvH), Studienstiftung des deutschen Volkes, Fond zur Förderung der wissenschaftlichen Forschung (FWF), Österreich, The Royal Society, UK, The Engineering and Physical Sciences Research Council (EPSRC), UK, Israel Science Foundation, Israel, National Science Foundation (NSF), USA, Natural Sciences and Engineering Research Council of Canada (NSERC), Canada, The Jeffress Memorial Trust, Bank of America, Virginia, USA, Universität Mainz, Germany, The University of Warwick, England, UK, Coventry University, England, UK, CECAM, Lyon, France
- Referee for Physical Review Letters, Physical Review B, Physical Review E, Journal of Chemical Physics, Europhysics Letters, Physics Letters A, Physics Letters B, The European Physical Journal B, Physica A, Proceedings of the Royal Physical Society, Journal of Physics A, Computer Physics Communications, JSTAT, Condens. Matter Phys., PLOS ONE, New Journal of Physics, International Journal of Modern Physics C

11.26 External Cooperations

Academic

- Institute of Physics, Jagiellonian University, Kraków, Poland
  Prof. Dr. Piotr Białas, Dr. Leszek Bogacz, Prof. Dr. Zdzisław Burda

- CEA/Saclay, Service de Physique Théorique, France
  Dr. Alain Billoire
- Institut für Physik, Universität Mainz, Germany
  Prof. Dr. Kurt Binder, Andreas Nußbaumer, Prof. Dr. Friderike Schmid
- Max Planck Institute for Polymer Research, Mainz, Germany
  Dr. Hsiao-Ping Hsu, Prof. Dr. Kurt Kremer
- Institut für Theoretische Physik, Universität Heidelberg, Germany
  Dr. Elmar Bittner
- Laboratoire de Physique des Matériaux (UMR CNRS No 7556), Université de Lorraine, Nancy, France
  Prof. Dr. Bertrand Berche, Dr. Christophe Chatelain, Dr. Olivier Collet, Prof. Dr. Malte Henkel, Prof. Dr. Dragi Karevski
- Groupe de Physique des Matériaux (UMR CNRS No 6634), Université de Rouen, France
  Dr. Pierre-Emmanuel Berche
- SUPA, School of Physics and Astronomy, University of Edinburgh, Scotland, UK
  Dr. Richard A. Blythe, Prof. Dr. Martin R. Evans, Dr. Bartłomiej Wacław
- Istituto Nazionale di Fisica Nucleare, Sezione di Milano-Bicocca, Milano, Italy
  Prof. Dr. Pablo Butera
- Jülich Supercomputing Centre (JSC), Forschungszentrum Jülich, Germany
  Prof. Dr. Peter Grassberger, PD Dr. Thomas Neuhaus
- IAC-1, Universität Stuttgart, Germany
  Prof. Dr. Rudolf Hilfer, Prof. Dr. Christian Holm
- Complex Systems Division, Department of Theoretical Physics, Lunds Universitet, Lund, Sweden
  Prof. Dr. Anders Irbäck, Simon Mitternacht
- Department of Mathematics and the Maxwell Institute for Mathematical Sciences, Heriot-Watt University, Edinburgh, Scotland, UK
  Prof. Dr. Desmond A. Johnston
- Applied Mathematics Research Centre, Coventry University, England, UK
  PD Dr. Christian von Ferber, Dr. Nikolaos G. Fytas, Prof. Dr. Ralph Kenna, Dr. Thierry Platini, Dr. Martin Weigel
- Inst. für Theoretische Physik, FU Berlin, Germany
  Prof. Dr. Hagen Kleinert
- Atominstitut, TU Wien, Austria
  Prof. Dr. Harald Markum
- Jacobs Universität Bremen, Germany
  Prof. Dr. Hildegard Meyer-Ortmanns, Darka Labavić
- Applied Mathematics, Universitat Pompeu Fabra, Barcelona, Spain
  Dr. Ramon Villanova
- CERN (PH-SFT), Geneva, Switzerland
  Dr. Sandro Wenzel

- Department of Engineering of Physics, Ankara University, Turkey
  Prof. Dr. Handan Arkın (Olgar), Mustafa Bilsel, Buket Taşdizen
- Dept. of Physics, Hacettepe University, Ankara, Turkey
  Prof. Dr. Tarik Çelik, Gökhan Gökoğlu
- Institute for Condensed Matter Physics, National Academy of Sciences, Lviv, Ukraine
  Dr. Viktoria Blavatska, Prof. Dr. Yurij Holovatch
- Yerevan Physics Institute, Yerevan, Armenia
  Prof. Dr. David B. Saakian
- Landau Institute for Theoretical Physics, Chernogolovka, Russia
  Dr. Lev Barash, Prof. Dr. Lev N. Shchur
- Center for Simulational Physics, The University of Georgia, Athens, USA
  Prof. Dr. Michael Bachmann, Prof. Dr. David P. Landau
- Dept. of Physics, Florida State University, Tallahassee, USA
  Prof. Dr. Bernd A. Berg
- Dept. of Chemistry and Biochemistry, University of Oklahoma, Norman, USA
  Prof. Dr. Ulrich H.E. Hansmann
- Los Alamos National Laboratory, Los Alamos, USA
  Dr. Christoph Junghans, Dr. Thomas Vogel
- Dept. of Physics and Astronomy, Texas A&M, College Station, USA
  Prof. Dr. Helmut G. Katzgraber
- Dept. of Physics, Virginia Tech, Blacksburg, USA
  Prof. Dr. Michel Pleimling, Prof. Dr. Royce K.P. Zia
- Physics Department, Carnegie Mellon University, Pittsburgh, USA
  Prof. Dr. Robert H. Swendsen
- Jawaharlal Nehru Centre for Advanced Scientific Research (JNCASR), Jakkur, India
  Prof. Dr. Subir K. Das
- Computational Chemistry Unit Cell (CCUC), Department of Chemistry, Chulalongkorn University, Bangkok, Thailand
  Prof. Dr. Supot Hannongbua, Dr. Oraphan Saengsawang
- Laboratory of Statistical and Computational Physics, Institute of Physics, Academia Sinica, Nankang, Taipei, Taiwan
  Prof. Dr. Chin-Kun Hu
- The University of Tokyo, Japan
  Prof. Dr. Nobuyasu Ito
- Banaras Hindu University, Varanasi, India
  Prof. Dr. Sanjay Kumar
- Nagoya University, Japan
  Dr. Tetsuro Nagai, Prof. Dr. Yuko Okamoto
- Zhejiang Institute of Modern Physics, Zhejiang University, Hangzhou, P.R. China
  Prof. Dr. He-Ping Ying, Prof. Dr. Bo Zheng

11.27 Publications

Journals

V. Blavatska, N. Fricke, W. Janke: *Polymers in Disordered Environments*, Condens. Matter Phys. **17**, 33604-1–11 (2014)

V. Blavatska, W. Janke: *Conformational Transitions in Random Heteropolymer Models*, J. Chem. Phys. **140**, 034904-1–7 (2014)

T. Chokbunpiam, R. Chanajaree, T. Remsungnen, O. Saengsawang, S. Fritzsche, C. Chmelik, J. Caro, W. Janke, S. Hannongbua: *N_2 in ZIF-8: Sorbate Induced Structural Changes and Self-Diffusion*, Microporous Mesoporous Mater. **187**, 1–6 (2014)

E. Ehrenpreis, H. Nagel, W. Janke: *Numerical Survey of the Tunable Condensate Shape and Scaling Laws in Pair-Factorized Steady States*, J. Phys. A: Math. Theor. **47**, 125001-1–16 (2014)

S. Förster, E. Kohl, M. Ivanov, J. Gross, W. Widdra, W. Janke: *Polymer Adsorption on Reconstructed Au(001): A Statistical Description of P3HT by Scanning Tunneling Microscopy and Coarse-Grained Monte Carlo Simulations*, J. Chem. Phys. **141**, 164701-1–8 (2014)

N. Fricke, W. Janke: *Asymptotic Scaling Behavior of Self-Avoiding Walks on Critical Percolation Clusters*, Phys. Rev. Lett. **113**, 255701-1–5 (2014)

J. Gross, T. Neuhaus, T. Vogel, M. Bachmann: *Statistical Analysis of the Influence of Interaction Ranges on Structural Phases of Flexible Polymers*, in: *Computer Simulation Studies in Condensed-Matter Physics XXVI*, eds. D.P. Landau, M. Bachmann, S.P. Lewis, H.-B. Schüttler, Physics Procedia **53**, 50–54 (2014)

M. Marenz, W. Janke: *Effect of Bending Stiffness on a Homopolymer Inside a Spherical Cage*, in: *Computer Simulation Studies in Condensed-Matter Physics XXVII*, eds. H.-B. Schüttler, S. Lewis, M. Bachmann, D.P. Landau, Physics Procedia **57**, 53–57 (2014)

M. Möddel, W. Janke, M. Bachmann: *Adsorption and Pattern Recognition of Polymers at Complex Surfaces with Attractive Stripe-like Motifs*, Phys. Rev. Lett. **112**, 148303-1–5 (2014)

M. Mueller, W. Janke, D.A. Johnston: *Nonstandard Finite-Size Scaling at First-Order Phase Transitions*, Phys. Rev. Lett. **112**, 200601-1–5 (2014)

M. Mueller, W. Janke, D.A. Johnston: *Transmuted Finite-Size Scaling at First-Order Phase Transitions*, in: *Computer Simulation Studies in Condensed-Matter Physics XXVII*, eds. H.-B. Schüttler, S. Lewis, M. Bachmann, D.P. Landau, Physics Procedia **57**, 68–72 (2014)

M. Mueller, D.A. Johnston, W. Janke: *Multicanonical Analysis of the Plaquette-Only Gonihedric Ising Model and its Dual*, Nucl. Phys. B **888**, 214–235 (2014)

H. Nagel, D. Labavić, H. Meyer-Ortmanns, W. Janke: *Open Boundary Conditions in Stochastic Transport Processes with Pair-Factorized Steady States*, in: *Computer Simulation Studies in Condensed-Matter Physics XXVII*, eds. H.-B. Schüttler, S. Lewis, M. Bachmann, D.P. Landau, Physics Procedia **57**, 77–81 (2014)

J.C.S. Rocha, S. Schnabel, D.P. Landau, M. Bachmann: *Identifying Transitions in Finite Systems by Means of Partition Function Zeros and Microcanonical Inflection-Point Analysis: A Comparison for Elastic Flexible Polymers*, Phys. Rev. E **90**, 022601-1–10 (2014)

J.C.S. Rocha, S. Schnabel, D.P. Landau, M. Bachmann: *Leading Fisher Partition Function Zeros as Indicators of Structural Transitions in Macromolecules*, in: *Computer Simulation Studies in Condensed-Matter Physics XXVII*, eds. H.-B. Schüttler, S. Lewis, M. Bachmann, D.P. Landau, Physics Procedia **57**, 94–98 (2014)

S. Schöbl, S. Sturm, W. Janke, K. Kroy: *Persistence-Length Renormalization of Polymers in a Crowded Environment of Hard Disks*, Phys. Rev. Lett. **113**, 238302-1–5 (2014)

J. Zierenberg, M. Marenz, W. Janke: *Scaling Properties of Parallelized Multicanonical Simulations*, in: *Computer Simulation Studies in Condensed-Matter Physics XXVI*, eds. D.P. Landau, M. Bachmann, S.P. Lewis, H.-B. Schüttler, Physics Procedia **53**, 55–59 (2014)

J. Zierenberg, M. Mueller, P. Schierz, M. Marenz, W. Janke: *Aggregation of Theta-Polymers in Spherical Confinement*, J. Chem. Phys. **141**, 114908-1–9 (2014)

J. Zierenberg, M. Wiedenmann, W. Janke: *Application of the Parallel Multicanonical Method to Lattice Gas Condensation*, J. Phys.: Conf. Ser. **510**, 012017-1–8 (2014)

Books

Y. Holovatch, W. Janke, S. Thurner (Editors): *Self-Organization and Collective Behaviour in Complex Systems*, Special issue in memory of Professor Alexandr Olemskoi, Condens. Matter Phys., Vol. **17**, No. 3, 2014

in press

M.H. Gerlach, W. Janke: *First-Order Directional Ordering Transition in the Three-Dimensional Compass Model*, Phys. Rev. B **91**, 045119-1–8 (2015)

M. Mueller, W. Janke, D.A. Johnston: *Planar Ordering in the Plaquette-Only Gonihedric Ising Model*, Nucl. Phys. B **894**, 1–14 (2015)

P. Schierz, S. Fritzsche, W. Janke, S. Hannongbua, O. Saengsawang, C. Chmelik, J. Kärger: *MD Simulations of Hydrogen Diffusion in ZIF-11 with a Force Field Fitted to Experimental Adsorption Data*, Microporous Mesoporous Mater. **203**, 132–138 (2015)

T. Vogel, J. Gross, M. Bachmann: *Thermodynamics of the Adsorption of Flexible Polymers on Nanowires*, J. Chem. Phys. **142**, 104901-1–8 (2015)

J. Zierenberg, W. Janke: *From Amorphous Aggregates to Polymer Bundles: The Role of Stiffness on Structural Phases in Polymer Aggregation*, Europhys. Lett. **109**, 28002-1–6 (2015)

J. Zierenberg, N.G. Fytas, W. Janke: *Parallel Multicanonical Study of the Three-Dimensional Blume-Capel Model*, Phys. Rev. E **91**, 032126-1–8 (2015)

N. Fricke, S. Sturm, M. Lämmel, S. Schöbl, K. Kroy, W. Janke: *Polymers in Disordered Environments*, to appear in Diff. Fundam. (2015), in print

W. Janke: *Computer Simulation Studies of Polymer Adsorption and Aggregation – From Flexible to Stiff*, to appear in: *Computer Simulation Studies in Condensed-Matter Physics XXVIII*, eds. H.-B. Schüttler, S.P. Lewis, M. Bachmann, D.P. Landau, to appear in Physics Procedia (2015), in print

W. Janke, M. Mueller, D.A. Johnston: *Finite-Size Scaling and Latent Heat at the Gonihedric First-Order Phase Transition*, to appear in J. Phys.: Conf. Ser. (2015), in print

D.A. Johnston, M. Mueller, W. Janke: *Macroscopic Degeneracy and Order in the* $3d$ *Plaquette Ising Model*, to appear in Mod. Phys. Lett. B (2015), in print

S. Majumder, W. Janke: *Cluster Coarsening During Polymer Collapse: Finite-Size Scaling Analysis*, to appear in Europhys. Lett. (2015), in print

M. Mueller, J. Zierenberg, M. Marenz, P. Schierz, W. Janke: *Probing the Effect of Density on the Aggregation Temperature of Semi-Flexible Polymers in Spherical Confinement*, to appear in: *Computer Simulation Studies in Condensed-Matter Physics XXVIII*, eds. H.-B. Schüttler, S.P. Lewis, M. Bachmann, D.P. Landau, to appear in Physics Procedia (2015), in print

Talks

N. Fricke, W. Janke: *Self-Avoiding Walks and Θ-Polymers on Critical Percolation Clusters*, DPG Frühjahrstagung, Dresden, Germany, 31. March – 04. April 2014

N. Fricke, W. Janke: *True Asymptotics of Self-Avoiding Walks on 3D Percolation Clusters*, 15th International NTZ-Workshop on *New Developments in Computational Physics – CompPhys14*, Leipzig, Germany, 27.–29. November 2014

J. Gross, M. Bachmann: *Monte Carlo Study of Polymer Adsorption on Nanocylinders*, DPG Frühjahrstagung, Dresden, Germany, 31. March – 04. April 2014

J. Gross, M. Ivanov, W. Janke: *Poly(3-hexylthiophene) Adsorption on Au(001)*, 15th International NTZ-Workshop on *New Developments in Computational Physics – Comp Phys14*, Leipzig, Germany, 27.–29. November 2014

W. Janke: *Monte Carlo Simulations of Polymer Adsorption and Aggregation in Generalized Ensembles*, invited talk, VI International Conference BIFI2014 *Exploring the Role of Computation in Science: From Biology to Physics*, Zaragoza, Spain, 22.–24. January 2014

W. Janke: *Transmuted Finite-Size Scaling at First-Order Phase Transitions with Extensive Low-T Degeneracies*, 27th CSP Workshop on *Recent Developments in Computer Simulation Studies in Condensed Matter Physics*, The University of Georgia, Athens, Georgia, USA, 24.–28. February 2014

W. Janke: *Simulated Tempering and Magnetizing Monte Carlo Study of Crossover Scaling in the 2d 3-State Potts Model*, DPG Frühjahrstagung, TU Dresden, Germany, 30. March – 04. April 2014

W. Janke: *Scaling Properties of a Parallel Implementation of the Multicanonical Algorithm*, Physics Seminar, TU Chemnitz, Germany, 23. April 2014

W. Janke: *Introduction to Basic Concepts of Statistical Physics, Thermodynamics, and Computer Simulations*, BuildMoNa Scientific Module 2014-B3 *Basic Concepts in Physics*, Universität Leipzig, Germany, 07. May 2014

W. Janke: *Non-Standard Finite-Size Scaling at First-Order Phase Transitions*, Workshop *Statistical Physics and Low Dimensional Systems – SPLDS*, Pont-à-Mousson, France, 21.–23. May 2014

W. Janke: *Computer Simulation Studies of Polymers – Adsorption and Aggregation from Flexible to Stiff*, invited talk, Humboldt Kolleg 2014 *German-Turkish Cooperation in Physics: New Challenges in Science*, Ankara University, Turkey, 11.–13. June 2014

W. Janke: *Non-Standard Finite-Size Scaling at a First-Order Phase Transition*, XXVI IUPAP *Conference on Computational Physics CCP2014*, Boston University, Massachusetts, USA, 10.–14. August 2014

R. Kumar, S. Kumar, W. Janke: *Dynamical Transition in Driven DNA Under Oscillatory Force: Hysteresis and Scaling*, Seminar of the cdfa-dfdk, Coventry University, England, UK, 15. October 2014

M. Marenz, W. Janke: *Effect of Bending Stiffness on a Homopolymer Inside a Spherical Cage*, 27th CSP Workshop on *Recent Developments in Computer Simulation Studies in Condensed Matter Physics*, The University of Georgia, Athens, Georgia, USA, 25. February 2014

M. Mueller: *Pedantic Fitting and Why it Matters*, Seminar of the cdfa-dfdk, Leipzig, Germany, 23. January 2014

M. Mueller, D.A. Johnston, W. Janke: *Macroscopic Degeneracy Influences the Finite-Size Scaling at First-Order Phase Transitions*, 15th International NTZ-Workshop on *New Developments in Computational Physics – CompPhys14*, Leipzig, Germany, 27.–29. November 2014

H. Nagel, D. Labavic, H. Meyer-Ortmanns, W. Janke: *Open Boundary Conditions in Stochastic Transport Processes with Pair-Factorized Steady States*, 27th Annual Workshop of the Center for Simulational Physics, Athens, Georgia, USA, 25. February 2014

P. Schierz, J. Zierenberg, W. Janke: *Comparison of Microcanonical MD and MC Simulations for Liquid-Gas Like Phase Transitions*, 15th International NTZ-Workshop on *New Developments in Computational Physics – CompPhys14*, Leipzig, Germany, 27.–29. November 2014

S. Schnabel, W. Janke: *Trying to Flip the Right Spins in the Edwards-Anderson Model*, Seminar talk at Texas A&M, College Station, Texas, USA, 09. September 2014

J. Zierenberg, W. Janke: *Exploring Different Regimes in Finite-Size Scaling of the Droplet Condensation/Evaporation Transition*, Seminar of the cdfa-dfdk, Coventry University, England, UK, 15. October 2014

J. Zierenberg, M. Mueller, P. Schierz, M. Marenz, W. Janke: *Aggregation of Semiflexible Polymers Under Constraints*, 15th International NTZ-Workshop on *New Developments in Computational Physics – CompPhys14*, Leipzig, Germany, 27.–29. November 2014

Posters

E. Bittner, W. Janke: *MuCa vs WL: A Tight Race*, Conference MECO 39, Coventry University, England, UK, 08.–10. April 2014

J. Bock, N. Fricke, W. Janke: *Kinetic Growth Random Walks*, DPG Frühjahrstagung, Dresden, Germany, 31. March – 04. April 2014

J. Bock, W. Janke: *Computer Simulations of Semiflexible Polymers in Disordered Media*, XXVI IUPAP *Conference on Computational Physics CCP2014*, Boston University, Massachusetts, USA, 11.–14. August 2014

J. Bock, W. Janke: *Computer Simulations of Semiflexible Polymers in Disordered Media*, 15th International NTZ-Workshop on *New Developments in Computational Physics – CompPhys14*, Leipzig, Germany, 27.–29. November 2014

M. Ivanov, J. Gross, M. Mueller, W. Janke: *Polymers Interacting with Substrates*, SFB/TRR 102, 3rd Retreat, Wittenberg, Germany, 17. March 2014

M. Ivanov, J. Gross, W. Janke: *P3HT Molecules Interacting with Au(001) Substrates*, SFB/TRR 102, Satellite Meeting Makro 2014, Jena, Germany, 16. September 2014

M. Ivanov, J. Gross, W. Janke: *P3HT Molecules Interacting with Au(001) Substrates*, 15th International NTZ-Workshop on *New Developments in Computational Physics – CompPhys14*, Leipzig, Germany, 27.–29. November 2014

M. Ivanov, M. Möddel, W. Janke: *Polymer Adsorption onto a Stripe-Patterned Surface*, DPG Frühjahrstagung, Dresden, Germany, 31. March – 04. April 2014

W. Janke, J. Zierenberg: *From Amorphous Aggregates to Polymer Bundles: The Role of Stiffness on Structural Phases in Polymer Aggregation*, Conference MECO 39, Coventry University, England, UK, 08.–10. April 2014

M. Marenz, J. Zierenberg, W. Janke: *Semiflexible Polymer in a Spherical Cage*, NIC Symposium, Forschungszentrum Jülich, Germany, 12.–13. February 2014

M. Marenz, N. Fricke, J. Zierenberg, W. Janke: *Revisiting Percolation on Power-Law Correlated Disorder*, 15th International NTZ-Workshop on *New Developments in Computational Physics – CompPhys14*, Leipzig, Germany, 27.–29. November 2014

M. Mueller, W. Janke, D.A. Johnston: *Transmuted Finite-Size Scaling at First-Order Phase Transitions with Exponential Degeneracy of Ordered States*, DPG Frühjahrstagung, Dresden, Germany, 31. March – 04. April 2014

H. Nagel, D. Labavic, H. Meyer-Ortmanns, W. Janke: *Open Boundary Conditions in Stochastic Transport Processes with Tunable Short-Range Interaction*, 15th International NTZ-Workshop on *New Developments in Computational Physics – CompPhys14*, Leipzig, Germany, 27.–29. November 2014

P. Schierz, J. Zierenberg, W. Janke: *A Comparison of Molecular Dynamics and Multicanonical Simulations in the NVE Ensemble*, 7th Annual BuildMoNa Conference, Leipzig, Germany, 03.–04. March 2014

P. Schierz, W. Janke: *3D-Visualisierung von Polymeren - oder wie verkleben Spaghetti*, Lange Nacht der Wissenschaften, Leipzig, Germany, 27. June 2014

S. Schnabel, W. Janke: *Sampling Low-Energy States of the Edwards-Anderson Model*, Conference MECO 39, Coventry University, England, UK, 08.–10. April 2014

J. Zierenberg, M. Mueller, P. Schierz, M. Marenz, W. Janke: *Aggregation of Theta-Polymers in Spherical Confinement*, Biannual Meeting of the GDCh-Division of Macromolecular Chemistry *Polymers and Energy – Synthesis, Engineering, Characterisation and Applications*, Jena, Germany, 14.–16. September 2014

J. Zierenberg, M. Mueller, P. Schierz, M. Marenz, W. Janke: *Aggregation of Theta-Polymers in Spherical Confinement*, Satellite Meeting of the SFB Transregio 102 "Polymers under multiple constraints" *Self-Assembly in Synthetic and Biological Polymers: Similarities and Differences*, Jena, Germany, 15.–16. September 2014

11.28 Graduations

Bachelor

- Dorian Nothaaß
  Algorithmen für Spindynamik Simulationen
  28. July 2014
- Henrik Christiansen
  Stochastic Transport Processes with Open Boundaries
  11. August 2014
- Karl Horn
  Exact Enumeration of Lattice Polymers in Geometric Confinement
  22. September 2014

- David Oberthür
  Metropolis-Simulationen von Gitterheteropolymeren mit korrelierter Struktur, die einem langreichweitigen Potenzgesetz folgt
  22. September 2014
- Franz Paul Spitzner
  Generating Long-range Power-law Correlated Disorder
  07. October 2014

11.29 Guests

- Prof. Dr. Subir K. Das
  Jawaharlal Nehru Centre for Advanced Scientific Research, India
  NTZ/DFH-UFA Colloquium (05. May 2014)
  Kinetics of Phase Separation in Fluids
  04.-06. May 2014
- Dr. Viktoria Blavatska
  Institute for Condensed Matter Physics, Lviv, Ukraine
  Alexander von Humboldt Foundation Institute Partnership Programme
  NTZ/DFH-UFA Colloquium (30. October 2014)
  Conformational Properties of Complex Polymers: Rosette vs. Star-Like Structures
  October – November 2014
- Prof. Dr. A. Peter Young
  University of California, Santa Cruz, USA
  Physics Colloquium (04. November 2014)
  Numerical Studies of the Quantum Adiabatic Algorithm
  04. November 2014
- Prof. Dr. Anastasios Malakis
  University of Athens, Greece
  Anistropic Spin-Glass Models
  25. November – 01. December 2014
- Dr. Francesco Parisen Toldin
  Universität Würzburg, Germany
  Fermionic Quantum Criticality in Honeycomb and π-Flux Hubbard Lattice Models
  26.–28. November 2014
- Dr. Andreas Tröster
  TU Wien, Austria
  Fourier Monte Carlo Renormalization Group Approach to Crystalline Membranes
  26.–28. November 2014
- Prof. Dr. Michael Bachmann
  Center for Simulational Physics, The University of Georgia, Athens, USA
  Physics Colloquium (27. November 2014)
  A 20th Century Physics No-No Problem: The Reasons of us Being
  26.–29. November 2014

- Prof. Dr. Bertrand Berche
  Université de Lorraine, Nancy, France
  Subtleties of Gauge Theory in Aharonov-Bohm Rings
  26.–29. November 2014
- Dr. Hsiao-Ping Hsu
  MPI für Polymerforschung, Mainz, Germany
  Lattice Monte Carlo Simulations of Polymer Melts
  26.–29. November 2014
- M.Sc. Tomas Koci
  Center for Simulational Physics, The University of Georgia, Athens, USA
  Effects of the Bond Elasticity on the Structural Transitions of a Flexible Polymer
  26.–29. November 2014
- M.Sc. Marjana Krasnytska
  National Academy of Sciences of Ukraine, Lviv, Ukraine
  Lee-Yang-Fisher Zeros for the Ising Model on Complex Network
  26.–29. November 2014
- M.Sc. Matthew Williams
  Center for Simulational Physics, The University of Georgia, Athens, USA
  Structural Transitions in Helical Polymers
  26.–29. November 2014
- Dr. Nikolaos Fytas
  Coventry University, England, UK
  Universality in the Three-Dimensional Random-Field Ising Model
  26.–30. November 2014
- Prof. Dr. Malte Henkel
  Université de Lorraine, Nancy, France
  Spherical Models of Interface Growth
  26.–30. November 2014
- Prof. Dr. Ferenc Iglói
  Institute of Theoretical Physics, Research Institute for Solid State Physics and Optics, Budapest, Hungary
  Random Transverse-Field Ising Chain with Long-Range Interactions
  26.–30. November 2014
- Dr. Nikolay Izmailyan
  Yerevan Physics Institute, Yerevan, Armenia
  Corner Contribution to Free Energy for 2D Dimer Model
  26.–30. November 2014
- Prof. Dr. Desmond A. Johnston
  Heriot-Watt University, Edinburgh, Scotland, UK
  (Z2) Lattice Gerbe Theory
  26.–30. November 2014
- Dr. Martin Weigel
  Coventry University, England, UK

Fragmentation of Fractal Random Structures
26.–30. November 2014

- Prof. Dr. Lev Shchur
  Landau Institute, Chernogolovka, Moscow Region, Russia
  On the Accuracy of the Wang-Landau Algorithm
  26. November – 03. December 2014
- PD Dr. Thomas Neuhaus
  Jülich Supercomputing Centre, Forschungszentrum Jülich, Germany
  27.–29. November 2014
- Dr. Elmar Bittner
  Universität Heidelberg, Germany
  27.–29. November 2014

12

Quantum Field Theory and Gravity

12.1 Vacuum interaction between topological objects

M. Bordag

Boundary conditions play an important role in quantum field theory. On the one hand side they are generalizations of interactions which are concentrated on a region of higher co-dimensions. On the other hand, boundary conditions appear naturally when considering topological objects, for example boundary conditions can be found in some treatments of quantum field in black hole backgrounds, in the quantum Hall effect, in the physics of graphene etc. An interesting question appears about the vacuum quantum interaction of topological objects. As a first example in a larger project on this topic the vacuum interaction energy of two kinks was calculated. The results were extended to the vacuum interaction of two cosmic strings. Here the problem appears, that the background changes the topology of the space-time, thus providing a long range interaction. As a consequence it is not clear a'priori whether the subtraction of the empty space contribution will be sufficient to remove the ultraviolet divergences. This question was investigated in detail by two methods, the heat kernel expansion and a mode sum calculation. Both confirm, after nontrivial compensation, the validity of the subtraction procedure.

12.2 Casimir repulsion in sphere-plate geometry

M. Bordag

The electromagnetic vacuum energy is considered in the presence of a perfectly conducting plane and a ball with dielectric permittivity ε and magnetic permeability μ, $\mu \neq 1$. The attention is focused on the Casimir repulsion in this system caused by the magnetic permeability of the sphere. In the case of a perfectly permeable sphere, $\mu = \infty$, the vacuum energy is estimated numerically. The short- and long-distance asymptotes corresponding to the repulsive force and respective low-temperature corrections and high-temperature limits are found for a wide range of μ. The constraints on the Casimir repulsion in this system are discussed. This work was supported by the Heisenberg-Landau program. Within this project one publication resulted.

I.G. Pirozhenko, M. Bordag. Casimir repulsion in sphere-plate geometry. *Phys. Rev. D*, 87:085031, 2013.

12.3 Deformations of quantum field theories, mathematical structure of low-dimensional quantum field theories, integrable models, QFT on noncommutative spaces

G. Lechner, J. Schlemmer, Y. Tanimoto, S. Waldmann, R. Longo, H. Grosse, R. Verch, T. Ludwig, S. Alazzawi, A. Andersson, C. Schützenhofer, A. Huber

In the project "deformations of quantum field theories" we pursue the question how to obtain models of interacting quantum fields by deformation procedures, sidestepping the problems of quantization and renormalization. In collaboration with J. Schlemmer (Vienna) and Y. Tanimoto (Göttingen), we investigated the equivalence of certain deformation procedures arising in the context of chiral field theories and massless integrable models, respectively. These results provide further evidence to the effect that the symmetric inner functions appearing in the context of Longo-Witten endomorphisms are closely connected to elastic two-particle S-matrices.

Another aspect of this circle of ideas is being developed in collaboration with R. Longo (Rome). Here we start from a field theory and investigate the structure of its half-localized endomorphism subnets arising from subnets of modular localized real subspaces. As in the context of existence proofs for local observables by modular nuclearity, the crucial question is here under which conditions on the underlying inner function compactly localized subspaces are still cyclic.

An extension of the algebraic construction of integrable models on two-dimensional Minkowski space to the case of a general particle spectrum transforming under some global gauge group was given in collaboration with C. Schützenhofer (Vienna). My PhD student S. Alazzawi (Vienna) analyzes the inverse scattering problem in this context, i.e. which two-particle S-matrices arise from local relativistic quantum field theories.

Regarding quantum field theory on noncommutative space(-times), I pursued two different research projects. Together with R. Verch, T. Ludwig, and H. Grosse (Vienna) we established an operator-algebraic version of the Wick rotation for quantum fields on Moyal space(-time) with commuting time. Together with S. Waldmann (Erlangen), there is ongoing research on the formulation of quantum field theories on spacetime manifolds which behave noncommutative only locally. Also the PhD student A. Andersson will be involved in this project.

There is also a project on the structure of thermal equilibrium states of certain deformed quantum field theories. Diploma student A. Huber (Vienna) contributed to this in his thesis, and could show that such models possess a wealth of KMS-functionals. However, the positivity aspects of these functionals, as required for a probability interpretation of the theory, are not settled yet, and are still analyzed in collaboration with J. Schlemmer (Vienna).

12.4 Structure of the gauge orbit space and study of gauge theoretical models

G. Rudolph, Sz. Charzynski[*], E. Fuchs, H. Grundling[†], J. Huebschmann[‡], P. Jarvis[§], J. Kijowski[*], M. Schmidt

[*]U Warsaw
[†]U Sydney
[‡]U Lille
[§]U Hobart

The investigation of gauge theories in the Hamiltonian approach on finite lattices with emphasis on the role of nongeneric strata was continued.

As a further step towards a generalization of the results of [1] on stratified Kähler quantization to larger lattices, the defining relations for lattice gauge models with gauge group SU(2) have been derived [2]. E. Fuchs worked on the formulation of stratified Kähler quantization in terms of coherent states.

Based on [3] and [4], in collaboration with H. Grundling, the investigation of the structure of the algebra of observables and its representations for specific models of quantum lattice gauge theory in terms of gauge invariant quantities was continued.

[1] J. Huebschmann, G. Rudolph, M. Schmidt, Commun. Math. Phys. **286**, Nr. 2 (2009) 459–494
[2] F. Fürstenberg, G. Rudolph, M. Schmidt: Defining relations for the orbit type strata of SU(2)-lattice gauge models (submitted to J. Geom. Phys.).
[3] J. Kijowski, G. Rudolph, J. Math. Phys. **43** (2002) 1796–1808;
J. Kijowski, G. Rudolph, J. Math. Phys. **46** (2005) 032303; Rep. Math. Phys. **55** (2005) 199
P. Jarvis, J. Kijowski, G. Rudolph, J. Phys. A **38** (2005) 5359
[4] Commun. Math. Phys. 318 (2013) 717-766

12.5 Quantum field theory on non-commutative geometries, quantum field theory and cosmology, thermal states in quantum field theory

R. Verch, G. Lechner, D. Buchholz, C.J. Fewster, M. Gransee, M. Hänsel

In non-commutative quantum field theory, wave-equations on non-commutative spacetimes have been studied through scattering with non-local (in space and time) external potential terms. A complete solution theory has been developed for such a scenario in collaboration with G. Lechner. The relationship of the resulting non-commutative spacetime relations for quantum field operators to the popular approaches of quantum field deformormations is being investigated in a project with D. Bahns (Universität Göttingen).

Fundamental aspects of stability in cosmology (pertaining to solutions to the semiclassical Friedmann equations) are under investigation together with M. Hänsel.
A new description of local thermal equilibrium is being investigated together with M. Gransee and N. Pinamonti (University of Genova). Fundamental aspects of the Unruh effect are studied together with D. Buchholz (Universität Göttingen).
Together with C.J. Fewster (University of York), a chapter for a book project on quantum field theory on manifolds has been written.

12.6 Funding

Vacuum interaction between topological objects
Priv.-Doz. Dr. M. Bordag
DFG-Einzelprojekt BO1112/18-1

Spectral Zeta Functions and Heat Kernel Technique in Quantum Field Theory with Nonstandard Boundary Condition
M. Bordag
Heisenberg-Landau programme

New Trends and Applications of the Casimir Effect (CASIMIR)
Research Networking Program der ESF (European Research Foundation)
M. Bordag, member of the Steering Committee

Yang-Mills moduli spaces over a surface via Fréchet reduction
T. Diez
Auslandsstipendium der Studienstiftung des deutschen Volkes (Université des Sciences et Technologies de Lille)

Quantum Theory of Lattice Gauge models
E. Fuchs
IMPRS fellowship

Local thermal equilibrium in quantum field theory
M. Gransee
IMPRS fellowship, MPI-MIS

Stability in cosmology M. Hänsel
Uni Leipzig

Deformations of quantum field theories
G. Lechner, external collaborators at Vienna University
FWF project P22929-N16

12.7 Organizational Duties

Priv.-Doz. Dr. Michael Bordag

- Referee: J. Phys. A, Phys. Rev. D, J. Math. Phys.

- Member of the Steering Committee of the ESF Research Networking Program *New Trends and Applications of the Casimir Effect (CASIMIR)*

Dr. Gandalf Lechner
- Referee for Annales Henri Poincaré, Foundations of Physics, Communications in Mathematical Physics, Journal of Mathematical Physics, Journal of Noncommutative Geometry, Physical Review D, Journal of Modern Physics, Letters in Mathematical Physics, Reviews in Mathematical Physics, Forum of Mathematics, the Templeton Foundation, and mathscinet

Prof. Dr. G. Rudolph
- Referee: Class. Quant. Grav., J. Math. Phys., J. Geom. Phys., J. Phys. A, Rep. Math. Phys., Commun. Math. Phys.
- Referee for the German Research Council (DFG) and the Alexander von Humboldt Foundation

Dr. Matthias Schmidt
- Referee: J. Phys. A, Int. J. Mod. Phys. A, Class. Quant. Grav.

Prof. Dr. Rainer Verch
- Ansprechpartner, Forschungsprofilbereich "Mathematical and Computational Sciences", Universität Leipzig
- Berufungsbeauftragter des Rektorats
- Book Series Editor, Fundamental Theories of Physics (Springer)
- IMPRS Board Member
- Referee for DFG and for AvH Stiftung
- Referee: Ann. H. Poincaré, Commun. Math. Phys., Found. Phys., Class. Quantum Grav., Gen. Rel. Grav.

12.8 External Cooperations

Academic

- II. Inst. f. Theoretische Physik, Universität Hamburg
  Prof. Dr. K. Fredenhagen
- Universität Göttingen
  Prof. Dr. D. Bahns, Prof. Dr. D. Buchholz, Dr. Y. Tanimoto
- Universität München
  Dr. S. Alazzawi,
- Mathematisches Institut, Universität Münster
  Prof. Dr. R. Wulkenhaar
- Institut für Mathematik, Universität Paderborn
  Dr. Ch. Fleischhack
- Universität Würzburg
  Prof. Dr. S. Waldmann

- Universität Wien
  Prof. Dr. Harald Grosse, Dr. J. Schlemmer
- Department of Mathematics, University of York, England
  Dr. C.J. Fewster
- Universitá di Roma "Tor Vergata"
  Prof. Dr. R. Longo
- Dipartimento di Matematica, Universitá di Genova, Italy
  Prof. Dr. N. Pinamonti
- Université des Sciences et Technologies de Lille
  Prof. Dr. J. Huebschmann
- Polish Academy of Sciences, Center for Theoretical Physics, Warsaw
  Prof. Dr. J. Kijowski
  Dr. Sz. Charzynski
- National University, Dnepropetrovsk
  Prof. V. Skalozub
- VIK Dubna
  Dr. V. Nesterenko, Dr. I. Pirozhenko
- University of Tokyo
  Dr. Yoh Tanimoto
- University of New South Wales, Sydney
  Prof. H. Grundling
- Dep. of Mathematics, University of Wollongong, Australien
  Prof. Dr. A. Rennie
- University of Tasmania, Hobart
  Prof. Dr. P. Jarvis

12.9 Publications

Journals

G. Lechner, R. Longo: *Localization in Nets of Standard Spaces*, Preprint:1403.1226, Comm. Math. Phys. 336 (1), 27-61 (2015)

G. Lechner, C. Schützenhofer: *Towards an operator-algebraic construction of integrable global gauge theories*, Annales Henri Poincaré 15, 648-678 (2014)

In press

G. Lechner, R. Verch: *Linear hyperbolic PDEs with non-commutative time*, arXiv: 1307.1780, in press with J. Noncommutative Geom.

Talks

G. Lechner: *Construction of quantum field theories by deformation techniques*, DPG Spring conference, main talk QFT session, Berlin, Germany, March 2014

G. Lechner: *Operator algebras and the construction of models in quantum field theory*, Conference FJIM 2014, Bilbao, Spain, July 2014

G. Lechner: *Hyperbolic PDEs with non-commutative time*, Conference Frontiers in Fundamental Physics, Marseille, France, July 2014

G. Lechner: *The structure of the field algebra in non-commutative QFT and uniqueness of its KMS states*, Conference Quantum Mathematical Physics, Regensburg, Germany, September 2014

G. Lechner: *Reflection Positivity and Operator Algebras in Quantum Field Theory*, MFO Workshop: Reflection Positivity in Representation Theory, Stochastics, and Physics, Oberwolfach, Germany, December 2014

G. Rudolph: *Singular reduction and quantum gauge models*, Two invited talks at the University of Tasmania at Hobart, Australia, April 2014

G. Rudolph: *Symplectic reduction and quantum gauge theory*, Invited talk at the Center of Advanced Studies at the Warsaw University of Technology, Polska, September 2014

R. Verch: *Black holes, horizons, quantum fields*, Invited Main Talk, DPG-Frühjahrstagung, Fachsitzung MP, Berlin, Germany, March 2014

R. Verch: *PDEs with non-commutative space and time*, Conference "Operator and Geometric Analyis in Quantum Theory", Levico, Italy, September 2014 (invited)

R. Verch: *Wave equations with non-commutative space and time*, Conference and Workshop "Noncommutative Geometry in Mathematics and Physics", Hausdorff Center of Mathematics, Bonn, Germany, September 2014 (invited)

R. Verch: *Wave equations with non-commutative space and time*, Conference "Quantum Mathematical Physics", Universität Regensburg, Germany, Oktober 2014, (invited)

R. Verch: *Seminar Talk, Fachbereich Mathematik*, Universität Potsdam, Germany, November 2014, (invited)

12.10 Graduations

Doctorate

- Sabina Alazzawi
  Deformations of Quantum Field Theories and the Construction of Interacting Models
  Universität Wien, November 26, 2014

Master

- Tobias Diez
  Slice theorem for Fréchet group actions and covariant symplectic field theory
  January 2014

Bachelor

- Stanislaw Kazmin
  Kohärente Zustände
  Oktober 2014
- Richard Neidhardt
  Quantenobservablen für die Gittereichtheorie
  September 2014

13

Statistical Physics

The focus of research in the SPT group is on low-dimensional and mesoscopic interacting systems. These systems are fascinating because on the one hand they allow to study fundamental questions of quantum statistical mechanics, and on the other hand they have a great potential for technological applications. The interplay of a reduced dimensionality with enhanced interaction effects, non-equilibrium physics, and possibly disorder allows the observation of many interesting phenomena, which pose a stimulating challenge for theoretical analysis. The mathematical language used for the description of these systems is quantum field theory, including techniques like functional integrals, renormalization group, instanton calculus, the Keldysh technique for non-equilibrium situations, and the replica method for disordered systems. These analytical tools are supplemented by the use of computer algebra (Mathematica) and numerical calculations (Matlab, Perl, C++). We try to combine the analysis of theoretically interesting problems with relevance to experiments on nanostructures.

Fractional quantum Hall (QH) systems display perhaps the richest and most beautiful physics of all condensed matter systems. They are a prime example for the idea that the whole is more than the sum of its parts, as low lying excitations of a fractional QH fluid carry only a fraction of the electron charge and are thus qualitatively different from the system constituents. Recently, interest in fractional QH physics has been reinvigorated by the prospect that quasiparticles (QPs) of the fractional QH state at filling fraction 5/2 may be non-abelian anyons, i.e. their braiding may not only give rise to a multiplication of the wave function with a complex phase, but in addition corresponds to a unitary transformation of the highly degenerate ground state. Due to the topological nature of braiding, these unitary transformations are robust against local perturbations and guarantee a high degree of stability of the quantum weave of braids, lending it to the construction of topological quantum bits. Future research in this field will concentrate on both the analysis of qualitative properties of topologically ordered systems and the description of experimentally relevant consequences in nanostructured systems.

Similarly to the edge states of QH systems, in single channel nanowires interactions strongly modify the dynamics of electrons. In the presence of strong spin-orbit coupling and in proximity to a superconductor, nanowires can support a topologically ordered state suitable for the formation of topological quantum bits. In multimode nanowires, a quantum phase transition between superconductor and diffusive metal can occur, which is tuned by an external magnetic field and is experimentally realized in niobium

and molybdenum-germanium systems. Comparatively small changes in the external magnetic field can give rise to a large change in conductivity. Quantum mechanical fluctuations of the superconducting phase can restore part of the density of states, which is reduced due to scattering of electrons off the superconducting order parameter.

B. Rosenow

13.1 Topological Polaritons in a Quantum Spin Hall Cavity

A. Janot, B. Rosenow, G. Refael*

*Institute of Quantum Information and Matter, Department of Physics, California Institute of Technology, Pasadena, CA 91125, USA

We focus on the topological properties possible in a solid-state system due to the interaction of light and matter and consider topological polartions in a hybrid system of a 2-dimensional quantum spin Hall insulator [1] embedded in an optical cavity. In particular, we try to identify the topological index that protects topological polartions. As opposed to Fermionic topological phenomena, where time reversal is the natural symmetry that protects edge states [2], in bosonic systems time reversal cannot serve this role. Our work [3] characterizes the emergent spinfull polaritons in the quantum spin Hall cavity, clarifies their relation to the electronic edge states present in the wells, and explains how to explore them experimentally. Most importantly, we identify the topological invariant which guarantees the existence of the topological polaritons. We

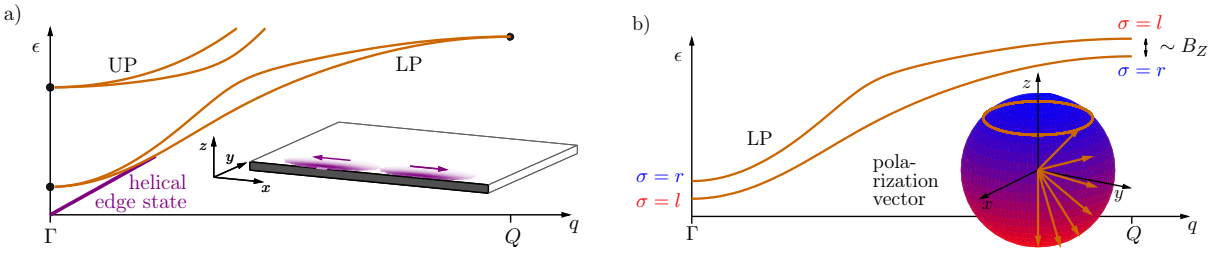

Figure 13.1: Defining properties of a topologically nontrivial polariton: a) the lower polariton (LP) and upper polariton (UP) branches (orange lines) are split by spin-orbit coupling, except at the time reversal invariant momenta (Γ, Q) (thick black dots). For a topological polariton we predict helical edge states (thick purple line) with helical excitons and p-polarized photons. b) with a time reversal breaking Zeeman field $B_Z \neq 0$, the polarization vector $\vec{n}$ of each LP-dispersion branch can be tracked over the whole Brillouin zone. The polariton is topologically nontrivial if $\vec{n}$ covers the entire Bloch sphere (inset). Here, the north (south) pole (blue (red) color) stands for right (left) circular polarization, while the x-y plane represents linearly polarized light.

have identified two criteria for topological polaritons in a quantum spin Hall cavity. First, we predict helical polaritonic edge-states with energies below the lower polariton branch, see left panel of Fig. 13.1. These edge states are topologically protected by non-vanishing Chern numbers [4] of the lower polariton branch (for details see Ref. [3]).

Second, we have shown that the number of wrappings of the Bloch sphere by the polarization vector of the bulk polaritons is equivalent to these Chern numbers.

Applying an external Zeeman field allows an experimental extraction of this topological invariant although time reversal symmetry is broken, see right panel of Fig. 13.1. Thus, we have demonstrated that a topologically nontrivial quantum spin Hall insulator coupled to cavity photons is a candidate for topological polaritons.

[1] B. A. Bernevig, T. L. Hughes, and S.-C. Zhang, Science **314**, 1757 (2006).
[2] C. Kane, and E. Mele, Phys. Rev. Lett. **95**, 146802 (2005).
[3] A. Janot, B. Rosenow, and G. Refael, preprint arXiv:1501.04092 (2015).
[4] D. J. Thouless, M. Kohmoto, M. P. Nightingale, and M. den Nijs, Phys. Rev. Lett. **49**, 405 (1982).

13.2 Topological superconductivity in Quantum Hall–superconductor hybrid systems

B. Zocher, B. Rosenow

In Ref. [1], we develop a scenario to engineer a topological superconductor (SC) whose zero-energy quasiparticles are Majorana fermions (MFs). In contrast to previous proposals [2–4], we consider the strong magnetic field limit where a $\nu = 1$ integer quantum Hall (QH) system is proximity coupled to an s-wave SC via a spin sensitive barrier. Due to the spin sensitivity of the barrier, an effective p-wave pairing potential is induced in the spin-polarized lowest Landau level (LLL). In the presence of an external magnetic field necessary to reach the QH regime, the superconducting pairing potential has a triangular Abrikosov vortex lattice imprinted, with a flux of $h/2e$ per vortex. In the LLL, there is one electronic state per flux quantum h/e threading the system, such that there are two superconducting vortices per electronic state. This lattice system can be described by a pair of commuting generalized translation operators $\mathcal{T}_x$ and $\mathcal{T}_y$ which define a Bloch problem with generalized momenta $\mathbf{k}$, despite the absence of translational invariance of the Hamiltonian for electrons in a magnetic field.

The superconducting pairing couples momenta $\mathbf{k}$ and $-\mathbf{k}$ with an amplitude $\Delta_{\mathbf{k}}$, similar to the situation without magnetic field. Interestingly, there are ten unpaired momenta in the Brillouin zone, since $\Delta_{\mathbf{k}}$ is represented as $\Delta_{\mathbf{k}} \sim \partial_x \Delta(\mathbf{r} = l_B^2 \mathbf{k} \times \hat{z})$, with $\Delta(\mathbf{r})$ denoting an s-wave superconducting pair potential with an imprinted Abrikosov vortex lattice. The unpaired momenta arise due to the four maxima and six saddle points of $|\Delta(\mathbf{r})|$. The zeroes of $\Delta(\mathbf{r})$ all have a finite slope since superconducting vortices correspond to simple zeroes, and hence do not give rise to unpaired momenta. The first Brillouin zone can be decomposed into two hexagons, each associated with one vortex of the unit cell. Drawing an analogy between one such hexagon and the Brillouin zone of the honeycomb lattice in graphene, the three unpaired momenta originating from the saddle points correspond to the M points, and the remaining two correspond to the K and K' points. Due to the degeneracy of symmetry related unpaired momenta, the hybrid system has an even particle number parity, and hence is topologically trivial (see Fig. 13.2(a)). However, it can be driven into a topologically nontrivial phase by changing the parity of the ground state, i.e. by moving an odd number of unpaired momenta through the Fermi level. We show that this can be realized by appropriately coupling

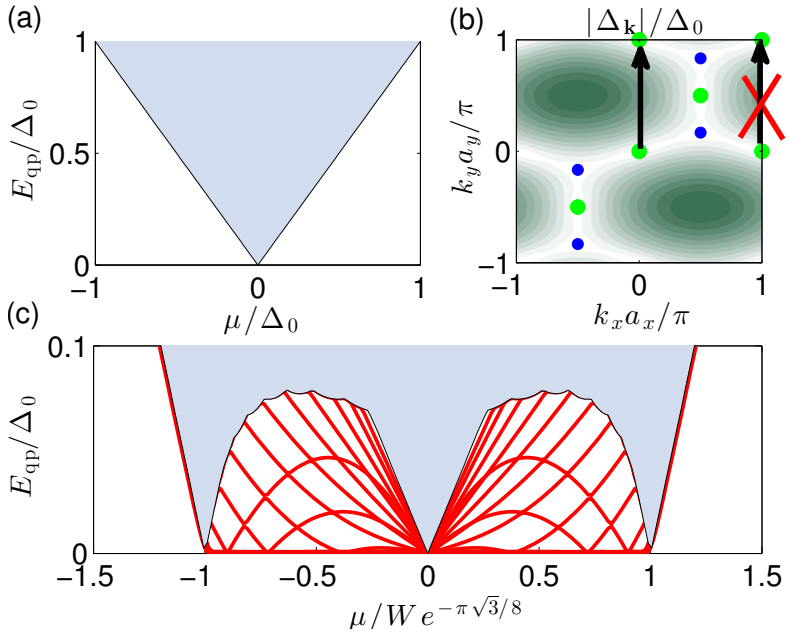

Figure 13.2: (a) Excitation spectrum $E_{\mathbf{k}} = |\Delta_{\mathbf{k}}|$. All unpaired momenta have zero energy. (b) Coupling of unpaired momenta $(0,0)$ and $(0,\pi)$ by the external potential $V(\mathbf{r}) = W\cos(yQ_y/2)$ lifts their degeneracy, and (c) excitation spectrum as function of chemical potential for $W = \Delta_0/2$. Shaded: Bulk spectrum for periodic boundary condition in x direction. Lines: Majorana edge mode for open boundary condition in x direction.

either one or three pairs of unpaired momenta $\mathbf{k}_1$ and $\mathbf{k}_2$, thus lifting the degeneracy between them (see Fig. 13.2(b),(c)). Experimentally, this can be achieved by engineering a periodic potential $V(\mathbf{r})$ with Fourier components for momenta $\mathbf{q}$ connecting $\mathbf{k}_1$ and $\mathbf{k}_2$. Consequently, breaking the symmetry of the vortex lattice is a necessary criterion for driving the system into a topologically nontrivial superconducting phase. Since it turns out that the momenta corresponding to the K and K' points cannot be split pairwise, the external potential needs to couple one or three pairs of M points.

[1] B. Zocher, B. Rosenow, arXiv: 1408.6148.
[2] J. D. Sau, R. M. Lutchyn, S. Tewari, and S. Das Sarma, Phys. Rev. Lett. **104**, 040502 (2010).
[3] R. M. Lutchyn, J. D. Sau, and S. Das Sarma, Phys. Rev. Lett. **105**, 077001 (2010).
[4] Y. Oreg, G. Refael, and F. von Oppen, Phys. Rev. Lett. **105**, 177002 (2010).

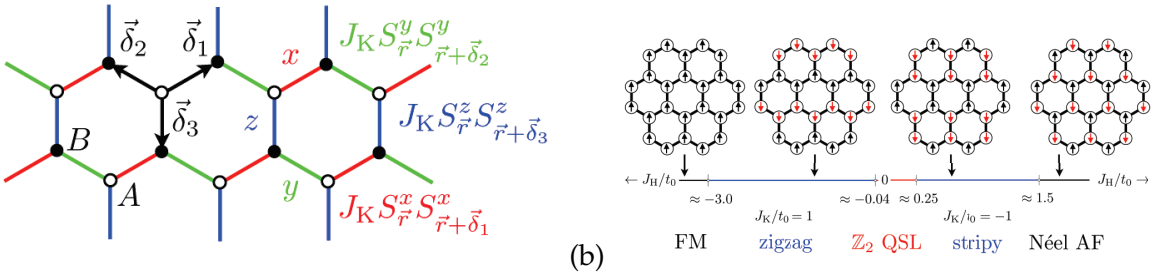

Figure 13.3: (a) the Kitaev exchange interaction on the honeycomb lattice: the different colors of the various bonds linking neighboring sites encode the bond-specific nearest-neighbor interaction of the frustrated, Ising-like Kitaev exchange. Along an x bond (in red), only the x components of neighboring spin-1/2 operators are coupled. The conventions for y and$z$ bonds are analogous. (b) Phase diagram [2] of the Kitaev-Heisenberg Hamiltonian for Kitaev exchange $J_K = \pm t_0$ and $J_H > 0$ and $J_H < 0$, respectively. The $\mathbb{Z}_2$ quantum spin liquid (QSL) ist destabilized by sufficiently strong Heisenberg interaction strength.

13.3 Unconventional pairing and electronic dimerization instabilities in the doped Kitaev-Heisenberg model

D. D. Scherer, M. M. Scherer*, G. Khaliullin†, C. Honerkamp‡, B. Rosenow

*Institut für Theoretische Physik, Universität Heidelberg, D-69120 Heidelberg, Germany
†Max-Planck-Institut für Festkörperforschung, D-70569 Stuttgart, Germany
‡Institute for Theoretical Solid State Physics, RWTH Aachen University, D-52056 Aachen, Germany and JARA - FIT Fundamentals of Future Information Technology, Germany

A paradigmatic example for the intricate interplay of spin-orbit coupling and correlations in electronic systems is provided by the honeycomb iridate compound Na_2IrO_3. This material might provide a promising route to study interaction induced topological insulators and superconductors together with their topologically protected boundary or surface modes. Experimentally, it was shown to order magnetically below 15 K in a so-called zigzag pattern [1]. A low-energy theory that captures the magnetic properties in Na_2IrO_3 and that can be obtained from a strong-coupling expansion features so-called Kitaev and Heisenberg exchange terms [2]. The Kitaev exchange Hamiltonian (see Fig. 13.3 (a)) on a honeycomb lattice is known to host a quantum spin liquid ground-state with Majorana fermions as quasiparticle excitations. The Heisenberg exchange, however, destabilizes the quantum spin liquid, as can be seen in the phase diagram displayed in Fig. 13.3 (b). As several state-of-the-art experimental techniques to dope this and related spin-orbit coupled materials are coming to the fore [3, 4], we analyzed the phase diagram of a hole-doped Kitaev- Heisenberg model on the honeycomb lattice. By computing the one-particle irreducible part of the effective interaction with the functional renormalization group [5], we unveiled the competition between several particle-hole and particle-particle instabilities beyond mean-field theory. Our results [6] on the leading instabilities inferred from renormalization group flows to strong coupling are collected in Fig. 13.4.

Most notably, we find extended regions of p-wave triplet instabilities. For sufficient hole doping, a superconducting p-wave condensate indeed provides for another route

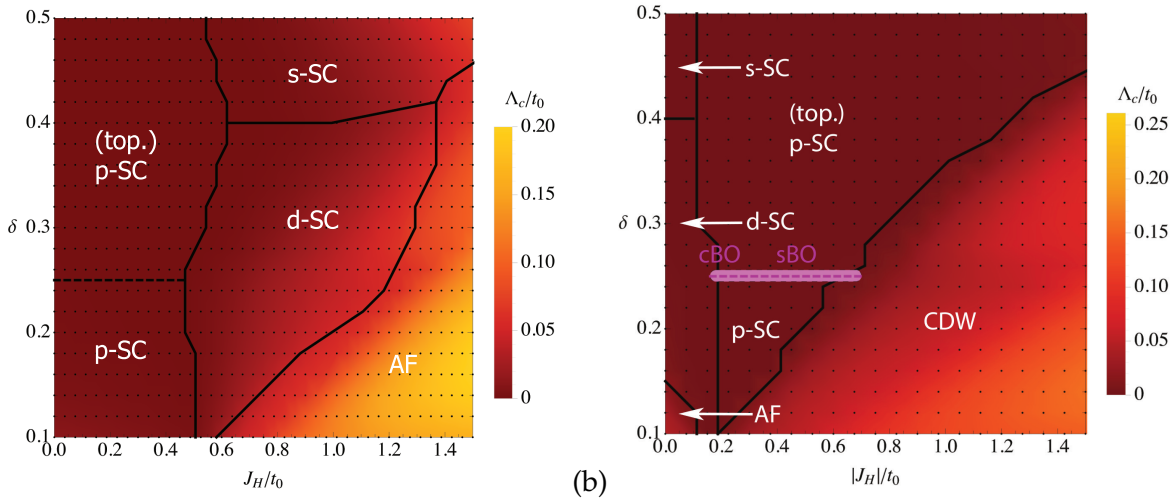

Figure 13.4: Tentative phase diagram of the doped Kitaev-Heisenberg model with simple nearest-neighbor hopping in the parameter space spanned by Heisenberg interaction strength $|J_H|$ in units of the bare hopping amplitude t_0 and hole-doping level δ: (a) with $J_K = -t_0$ (b) and $J_K = +t_0$. The charge (cBO) and spin bond-order (sBO) instabilities appear only for ferromagnetic Heisenberg and antiferromagnetic Kitaev exchange and the doping level tuned to van Hove-filling $\delta = 1/4$. The dashed line marks the gap-closing transition from the trivial to the topologically non-trivial p-wave superconductor (p-SC). Other instabilities are antiferromagnetic spin-density wave (AF), charge-density wave (CDW) as well as superconducting s-wave (s-SC) and d-wave (d-SC) instabilites in the singlet channel. The critical scale Λ_c, where we observe renormalization group flow to string coupling, serves as an estimate for critical temperatures.

to exotic Majorana quasiparticles. Through a gap-closing transition at a critical hole doping, the p-wave superconductor turns into a topologically nontrivial superconductor with Majorana edge states at the boundary by a change in a $\mathbb{Z}_2$ topological invariant, the so-called Kramers' parity. Our results suggest, that the doped Kitaev-Heisenberg model indeed allows for topological superconducting phases beyond simple mean-field arguments. We further uncovered a previously overlooked electronic dimerization instability driven by Fermi surface nesting and an enhancement of the single-particle density of states due to van Hove singularities in the doped Kitaev-Heisenberg model [6].

In an extension of this work, we recently incorporated a density functional theory derived band structure [7] for Na_2IrO_3 into the low-energy model describing the doped system. Interestingly, we find that for the realistic band structure, the Kramers' parity enabling topological superconductivity occurs in the low doping regime, as opposed to the regime of large doping for the simplified band structure alluded to above. An instability analysis will thus shed further light on the question of whether topological superconductivity could be realized in doped Na_2IrO_3 thin films.

[1] X. Liu *et al.*, Phys. Rev. B **83**, 220403(R) (2011)
[2] J. Chaloupka, G. Jackeli, and G. Khaliullin, Phys. Rev. Lett. **110**, 097204 (2013)
[3] R. Comin *et al.*, Phys.Rev.Lett. **109**, 266406 (2012)
[4] Y. K. Kim *et al.*, Science **345**, 187 (2014)
[5] W. Metzner *et al.*, Rev. Mod. Phys. **84**, 299 (2012)
[6] D. D. Scherer *et al.*, Phys. Rev. B *90*, 045135 (2014)
[7] K. Foyevtsova *et al.*, Phys. Rev. B **88**, 035107 (2013)

13.4 Transmission phase lapses through a quantum dot in a strong magnetic field

Y. Dinaii*, Y. Gefen*, B. Rosenow

*Department of Condensed Matter Physics, The Weizmann Institute of Science, Rehovot 76100, Israel

The phase of the transmission amplitude through a mesoscopic system contains information about the system's quantum mechanical state and excitations thereof. In the absence of an external magnetic field, abrupt phase lapses occur between transmission resonances of quantum dots and can be related to the signs of tunneling matrix elements. They are smeared at finite temperatures. By contrast, we show here that in the presence of a strong magnetic field, phase lapses represent a genuine interaction effect and may occur also on resonance. We identify a relevant physical regime where these phase lapses are robust against finite temperature broadening [1].

Probability amplitudes, which are the building blocks of quantum mechanics, are complex entities. This simple fact can be regarded as responsible for much of the quantum phenomena in Nature. The need to measure such complex entities is thus of substantial importance. Such measurements, performed on the transmission amplitude of electrons passing through a quantum dot (QD), revealed an intriguing phenomenon: the associated phase jumped abruptly between transmission peaks. The origin of these so-called *phase lapses* has been heatedly debated. The explanation relies on the presence of intra-dot interactions, which lead to *population switching*: an abrupt "swap" of two level occupations as the gate voltage is varied. In addition, quantum chaos correlations in the QD may be invoked.

Here we find that (i) phase lapses may occur also in this regime of a strong magnetic field, but that the underlying physics is utterly different from the zero field case. Importantly, these phase lapses represent a genuine many-body effect, resulting from the interaction between the inner and outer edge channels (the inner edge channel may also be represented by an orbital level or a compressible puddle). (ii) In the standard case, zero transmission and phase lapses are due to the coherent addition of two or more transmission amplitudes through the quantum dot. In contradistinction, in the strong magnetic field case phase lapses are due to true dephasing as an internal degree of freedom fluctuates inside the quantum dot. (iii) For zero magnetic field phase lapses acquire a width $\sim T^2$ at a finite temperature T [2]. By contrast we find that for a realistic, experimentally relevant physical regime, strong magnetic field phase lapses are robust against broadening at finite temperatures.

[1] Y. Dinaii, Y. Gefen, and B. Rosenow, Phys. Rev. Lett. **112**, 246801 (2014).
[2] A. Silva, Y. Oreg, and Y. Gefen, Phys. Rev. B **66**, 195316 (2002).

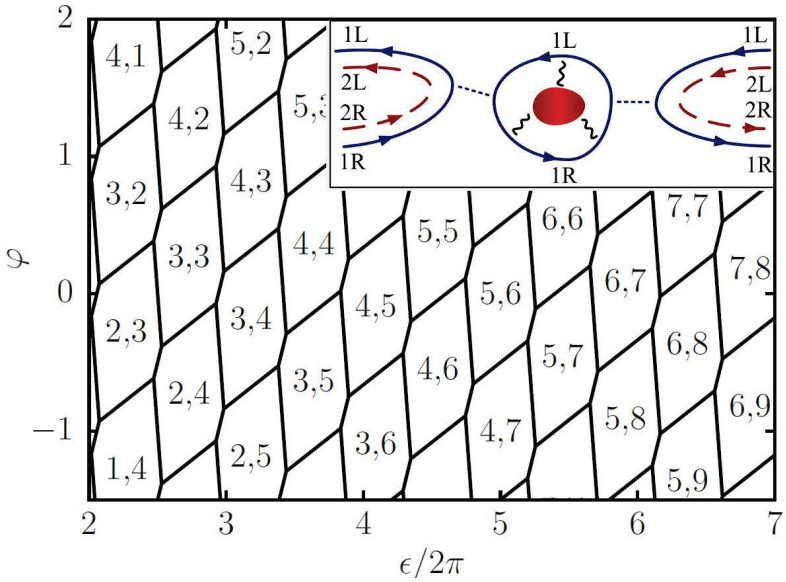

Figure 13.5: Example of a stability diagram describing the charge distribution in the quantum dot (QD) in the strong coupling regime. The pairs of numbers denote the charge in the outer and inner parts. Inset: A gate-defined QD operating in the quantum Hall regime (filling factor $\nu = 2$). The transmission amplitude of electrons traveling along channel 1R towards the dot is measured by embedding it in one arm of a Mach-Zehnder interferometer (not shown).

13.5 Dephasing suppression and phase lapses in the fractional quantum Hall regime

Y. Dinaii*, Y. Gefen*, B. Rosenow

*Department of Condensed Matter Physics, The Weizmann Institute of Science, Rehovot 76100, Israel

A charge fluctuator which is electrostatically coupled to a conducting channel may fully dephase quantum transport through the latter. Here, we address the case where a quantum dot (QD), playing the role of a charge fluctuator, is tunnel-coupled to an additional channel. In the case where the latter may support fractional charge, distinct differences from the integer case arise : Abrupt phase lapses of the transmission through the conducting channel occur (which may or may not be equal to π). This is accompanied by a cusp-like suppression of the interferometer's visibility, yet no full dephasing. We interpret our findings in terms of the entanglement between the fluctuator and the conducting channel [1].

Interference between possible paths is a fundamental quantum mechanical phenomenon. Its realization via an electronic Mach-Zehnder interferometer (MZI) and an electronic Fabry-Pérot interferometer plays an important role in investigating basic physics phenomena such as the Aharonov-Bohm effect, action-free measurement, correlations among particles, and fractional statistics of Abelian and non-Abelian anyons. Understanding the degradation of quantum interference (dephasing) is crucial for nanoelectronic technologies, and is of profound importance for clarifying the elusive transition from a quantum behavior to a classical one. Dephasing of interferometry signal due to the interaction with a detector is intimately related to the entanglement

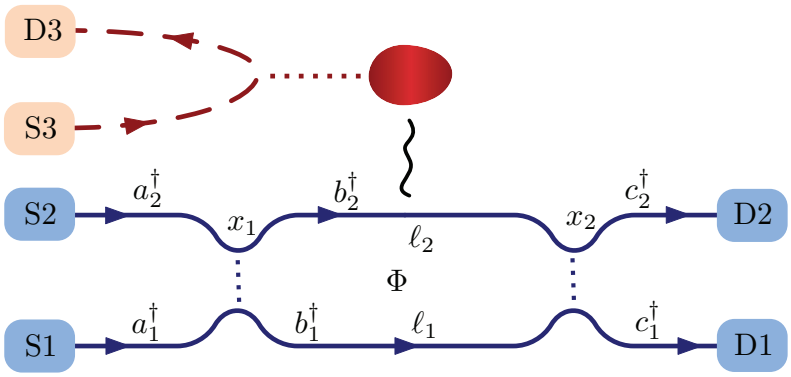

Figure 13.6: Schematics of the setup. A quantum dot (red solid puddle) is capacitively coupled (black wiggly line) to an arm of a Mach-Zehnder interferometer (MZI) (blue solid lines). The QD is tunnel-coupled (red dots) to a chiral Luttinger liquid lead (red dashed line). Tunneling between the two MZI arms is denoted by blue dotted lines. Magnetic flux Φ is enclosed by the "lower" and "upper" MZI arms whose lengths are ℓ_1 and ℓ_2, respectively. The arrows denote the direction of the chiral motion from the sources ("S") towards the drains ("D"). Creation operators associated with the various regions of each channel are designated in the figure.

between them. It is often associated with acquiring information about which path the interfering particle has taken.

Here we study a paradigmatic controlled-dephasing setup of a MZI interacting with a fluctuator, but with a twist: the fluctuator operates in the fractional quantum Hall regime. The fluctuator is realized by a quantum dot (QD) (cf. Fig. 13.6), which is electrostatically coupled to the upper arm of the MZI. Since the QD has two charging states ("empty" and "occupied"), the fluctuation pattern of the charge on it defines quantum telegraph noise. Consequently, the phase accumulated along the upper arm of the MZI fluctuates between two values (θ and $\theta+\delta$). The QD is weakly tunnel-coupled to a channel that supports fractional charge. This is to be contrasted with previous studies, which examined a QD that was tunnel-coupled to regular electron reservoirs. We find that: (i) When the gate voltage applied on the QD is varied smoothly, a sharp jump in the phase of the transmission amplitude through the upper arm of the MZI occurs. (ii) For a symmetric arrangement of the QD ($\delta = \pi$, see below), the abrupt phase lapse is π. (iii) Unlike the integer case, even for $\delta \neq \pi$ (asymmetric arrangement), a *sharp* phase lapse will appear, which differs from π. (iv) The visibility of the MZI is minimal at the point where a phase lapse occurs, but generically it cannot be fully suppressed. (v) The visibility is a monotonically decreasing function of the entanglement between the MZI and the QD. The protection against full dephasing is a consequence of the inability of the MZI and the QD to fully entangle.

[1] Y. Dinaii, Y. Gefen, and B. Rosenow, Phys. Rev. Lett. **112**, 246801 (2014).

13.6 Funding

Phasenrelaxation und Gegenstsrom-Dissipation in Quanten-Hall Doppellagen
B. Rosenow
DFG-Projekt RO 2247/7-1

Engineering the coherency of fractional and non-abelian electronic interferometers
B. Rosenow
DFG-Projekt RO 2247/8-1

Robustheit geschützter Randzustände in topologischen Isolatoren
B. Rosenow (Teilprojektleiter)
ESF-Projekt 100124929

13.7 Organizational Duties

B. Rosenow

- Member of the Qualitätssicherungskommission of the Faculty of Physics and Earth Sciences
- Referee for Science, Phys. Rev. Lett., Phys. Rev. B, Europhys. Lett. Adv. Con. Matter, JSTAT, Physica A, NSF, Studienstiftung des Deutschen Volkes

B. Zocher

- Referee for Phys. Rev. X, Phys. Rev. B, Journal of Physics: Condensed Matter, Studienstiftung des deutschen Vokes

13.8 External Cooperations

Academic

- University of Vermont, USA
  A. Del Maestro
- Universität Heidelberg, Germany
  Dr. Michael M. Scherer
- Max-Planck-Institut für Festkörperforschung, Stuttgart, Germany
  G. Khaliullin
- RWTH Aachen, Germany
  Prof. Dr. Carsten Honerkamp
- Universiteit Leiden, Netherlands
  Dr. Timo Hyart
- School of Physics and CRANN, Trinity College, Ireland
  Prof. Paul Eastham
- Weizmann Institute for Science, Israel
  Prof. Yuval Gefen, Prof. Ady Stern
- Harvard University, USA
  Prof. Bert Halperin

13.9 Publications

Journals

T. Hyart, A. R. Wright, and B. Rosenow, *Zeeman-field-induced topological phase transitions in triplet superconductors*, Phys. Rev. B **90**, 064507 (2014)

D. D. Scherer, M. M. Scherer, G. Khaliullin, C. Honerkamp, B. Rosenow, *Unconventional pairing and electronic dimerization instabilities in the doped Kitaev-Heisenberg model*, Phys. Rev. B **90**, 045135 (2014)

Y. Dinaii, Y. Gefen, and B. Rosenow, *Transmission Phase Lapses through a Quantum Dot in a Strong Magnetic Field*, Phys. Rev. Lett. **112**, 246801 (2014)

Y. Dinaii, Y. Gefen, and B. Rosenow, *Suppression of dephasing and phase lapses in the fractional quantum Hall regime*, Phys. Rev. B **89**, 241402(R) (2014)

in press

C.W. von Keyserlingk, S.H. Simon, B. Rosenow, *Enhanced bulk-edge Coulomb coupling in Fractional Fabry-Perot interferometers*

M. Thunert, A. Janot, H. Franke, C. Sturm, T, Michalsky, M. D. Martin, L. Vina, B. Rosenow, M. Grundmann, R. Schmidt-Grund, *Cavity Polariton Condensate in a Disordered Environment*

P-F Duc, M. Savard, M. Petrescu, B. Rosenow, A. Del Maestro, G. Gervais,*Critical Flow and Dissipation in a Quasi-One-Dimensional Superfluid*

L. Kimme, T. Hyart, B. Rosenow, *Symmetry-protected topological invariant and Majorana impurity states in time-reversal invariant superconductors*

B. Zocher, B. Rosenow, *Topological superconductivity in Quantum Hall-superconductor hybrid systems*

Talks

D. D. Scherer, *Unconventional pairing and electronic dimerization instabilities in the doped Kitaev-Heisenberg model*, ERG 2014 - 7th International Conference on the Exact Renormalization Group, Lefkada, September 2014

A. Janot, *Superfluid Stiffness of a Driven Dissipative Condensate with Disorder*, Workshop on coherent phenomena in disordered optical systems, ICTP Trieste, May 2014

L. Kimme, *Symmetry-protected topological invariant and Majorana impurity states in time-reversal invariant superconductors*, DPG Frühjahrstagung, Dresden, April 2014

B. Zocher, *Crossed Andreev reflection and noise through Majorana bound states*, Weizmann Institute, February 2014.

B.Rosenow, *Workshop Topological Phenomena in Low-Dimensional Quantum Systems*, University of Oslo, December 2014.

B. Rosenow, *Workshop Topology and Entanglement in Correlated Quantum Systems*, Max- Planck Institute for Complex Systems Dresden, July 2014.

B. Rosenow, *Conference Emergent Phenomena in Quantum Hall Systems 5*, Weizmann Institute of Science, July 2014.

B. Rosenow, *Workshop Topological matter, Superconductivity and Majorana*, Institute for Advanced Study, Hong Kong university, January 2014.

Posters

L. Kimme, *Effects of non-magnetic impurities in time-reversal invariant superconductors*, Boulder Summer School for Condensed Matter and Materials Physics, Boulder, Colorado, July 2014

M. Treffkorn, *Theoretical description of scanning gate microscopy on quantum Hall point contacts*, DPG Frühjahrstagung, Dresden, April 2014

A. Janot, *Polaritons in a Quantum Spin Hall Insulator*, DPG Frühjahrstagung, Dresden, April 2014

A. Janot, *Polaritons in a Quantum Spin Hall Insulator*, Annual Conference BuildMoNa, Leipzig, March 2014

D. D. Scherer, *Unconventional pairing and bond-order states in the doped Kitaev-Heisenberg model*, MPIPKS Focus Workshop Topological Matter out of Equilibrium, Dresden, March 2014

13.10 Guests

- Prof. Joachim Krug
  Universität Köln
  December 16
- Prof. Yuval Gefen
  Weizmann Institute for Science, Israel
  October 6 - 7
- Prof. Alessandro Romito
  Freie Universität Berlin, Germany
  October 6 - 7

14

Theory of Condensed Matter

14.1 Introduction

Major research topics of our groups include nonequilibrium phenomena and pattern formation in systems of various nature, e.g. in soft condensed matter and in biological systems. Modern analytic methods of statistical physics and computer simulations complement and stimulate each other. Cooperations with mathematicians, theoretical and experimental physicists, biologists and medical researchers in Germany, Europe and around the world are well established. Our emeritus Dieter Ihle is still very active and was, together with five local colleagues, in 2014 awarded with the first prize of the Joint Institute of Nuclear Research Dubna for their work on "Theory of Spin Fluctuations and High-Temperature Superconductivity in Cuprates".
More specifically, we are interested in the following problems.

Stochastics and pattern formation (Behn). Noise induced phenomena like non-equilibrium phase transitions are studied with analytical and cumputational methods in stochastically driven nonlinear systems with many degrees of freedom. Methods of nonlinear dynamics and statistical physics are used to formulate and investigate mathematical models of the adaptive immune system. We describe the randomly driven evolution of idiotypic networks of the B-lymphocyte subsystem and investigate its role in the control of autoreactive clones.

Non-equilibrium dynamics in soft-condensed-matter systems (Kroy). Much of what we do can be summarized as Soft Mesoscopics, the study of of emerging properties in soft and biological matter. Studied phenomena range from desert dunes and ripples spontaneously developing as a generic consequence of aeolian sand transport, through non-equilibrium dynamics of hot nanoparticles, proteins and polymers, the viscoelastic and inelastic mechanics of the cytoskeleton, to the tension propagation in single DNA molecules under strong external fields. (Related experimental work is currently in progress at EXP1: MON, MOP, PWM.) A common theme is the presence of strong fluctuations and stochastic dynamics on the microscale. The emergence of the mesoscopic structure and transport is to be understood. The applied methods comprise a broad statistical mechanics toolbox including stochastic (integro-)differential equations, liquid-state theories, effective hydrodynamic equations, various systematic coarse-graining techniques, and massively parallel numerical simulations on GPUs.

Ulrich Behn, Klaus Kroy

14.2 Stochastic Phenomena in Systems with Many Degrees of Freedom

U. Behn, R. Kürsten

Arrays of coupled nonlinear dynamical systems driven by multiplicative or additive noise show close analogies to phase transitions in equilibrium, cf. e.g. [1].

For an infinite array of globally coupled overdamped anharmonic oscillators subject to additive Gaussian white noise a mean-field like description is exact. We have proved the existence of a well-behaved critical manifold in the parameter space which separates a symmetric phase from a symmetry broken phase and calculated exact, optimal bounds of the critical value of the control parameter [2]. The method can be extended to models with higher order saturation showing a continuous phase transition and to models with competing interactions to characterize a tricritical point [3].

We further developed a numerical method which allows, by a suitable decomposition of the state space, an efficient computer simulation of nonlinear stochastic differential equations to sample probability densities also in sparsely visited regions of the support, see for example Fig. 14.1. The scheme exploits exact properties of so-called truncated Markov chains with detailed balance and can be extended to systems without detailed balance [4].

Rüdiger Kürsten also investigated Bernoulli bond percolation on random recursive trees, for a few related results see [5]. Random recursive trees are obtained from a root node by repeatedly attaching nodes randomly to one of the existing nodes. A stochastic coupling is exploited to obtain exact results for Bernoulli bond percolation on random recursive trees of fixed size. For example, the expectation values of the root cluster size, of the number of nodes in the n-th gerneration clusters, and of the number of clusters of size one can be obtained. Some combined limits of system size and percolation probability are considered and compared to previous results.

[1] F. Sagués, J. García-Ojalvo, J.M. Sancho: Rev. Mod. Phys. **79**, 829 (2007)
[2] R. Kürsten, S. Gütter, U. Behn: Phys. Rev. E **88**, 022114 (2013)
[3] R. Kürsten, U. Behn: *Critical Manifold and Tricritical Point of Nonlinear Globally Coupled Systems with Additive Noise*, in preparation.
[4] R. Kürsten, U. Behn: *Sampling Stochastic Differential Equations Using a Decomposition of the State Space*, in preparation.
[5] R. Kürsten: *Comment on 'Anomalous diffusion induced by enhancement of memory'*, arXiv:1503.03302

14.3 Randomly Driven Evolution of Idiotypic Networks

U. Behn, N. Preuß, H. Schmidtchen, R. Schulz, B. Werner*

*Max Planck Institute for Evolutionary Biology, Plön

The paradigm of idiotypic networks conceptualized a few decades ago by Niels Jerne [1] finds today a renewed interest mainly from the side of systems biology and from clinical research, cf. e.g. the recent reviews [2, 3].

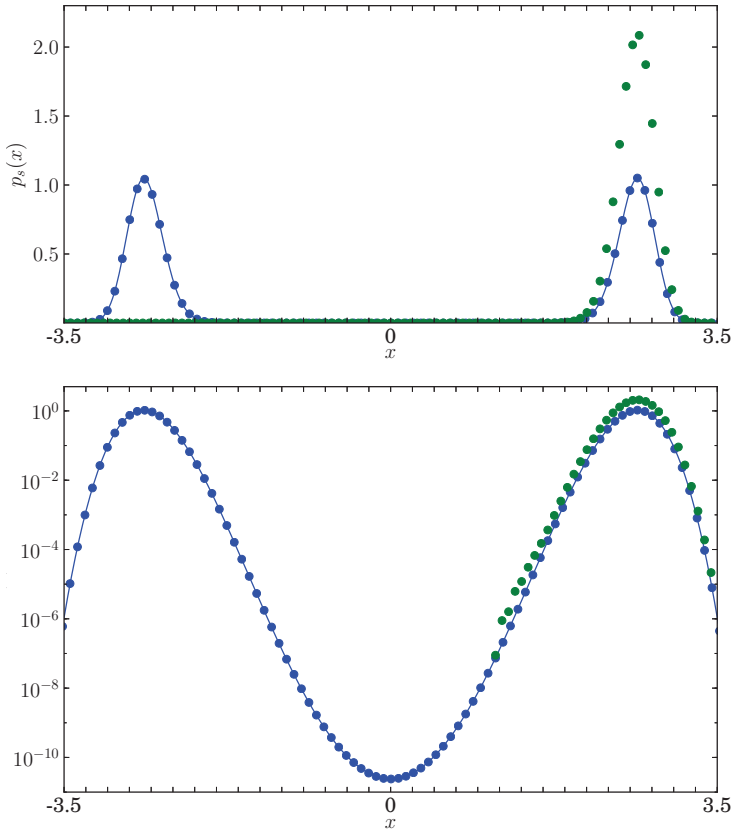

Figure 14.1: Stationary probability density of the process generated by the stochastic differential equation $\dot{x} = ax - x^3 + \xi(t)$ where $\xi(t)$ is a Gaussian white noise of strength σ ($a = 5$, $\sigma = 1$). The plot compares the analytical solution (blue line) with histograms obtained by simulations of comparable length utilizing a Euler-Maruyama scheme. The conventional simulation (green dots) starts at $x = 1$ and after a thermalization period 3×10^9 time steps are recorded. Our decomposition of the state space (blue dots) uses 32 intervals and for each interval 10^8 time steps. Note that in the conventional simulation the left peak is completely missed. The bottom figure is a logarithmic plot of the same data and demonstrates the perfect agreement of our data with the analytical result over 10 orders of magnitude.

In our group we have developed a minimalistic model of the idiotypic network [4–6]. In this model a node represents a clone of B lymphocytes with certain idiotype. The model network evolves, driven by the random influx of new idiotypes from the bone marrow, towards a highly organized modular architecture where groups of nodes which share statistical characteristics can be identified. The most interesting architecture, found in a certain regime of parameters, consists of a connected part (densely linked core groups and a hereto linked periphery), a hereof disconnected part (singletons), and groups of suppressed clones (stable holes), see Fig. 14.2.

We have considered the problem of self tolerance in the frame of our model [9]. The role of self is played by permanently occupied nodes. We found in simulations that in the presence of self the architecture evolves such that the neighbors of self are only weakly occupied, i.e. self is tolerated. The simulation results are corroborated by an analytical modular mean field theory which includes correlations [7].

Our results support the view that autoreactive clones which naturally occur also in

healthy organisms are controlled by anti-idiotypic interactions, and could be helpful to understand network aspects of autoimmune disorders, cf. the comment of immunologist Véronique Thomas-Vaslin [10] to our paper [9].

We further considered model experiments to understand minimal requirements which should be met in order to infer statistical characteristics such as the size of idiotype repertoire and the degree distribution of the idiotypic network from samples, taken at a certain time and covering only a part of the network, cf. part III of [8].

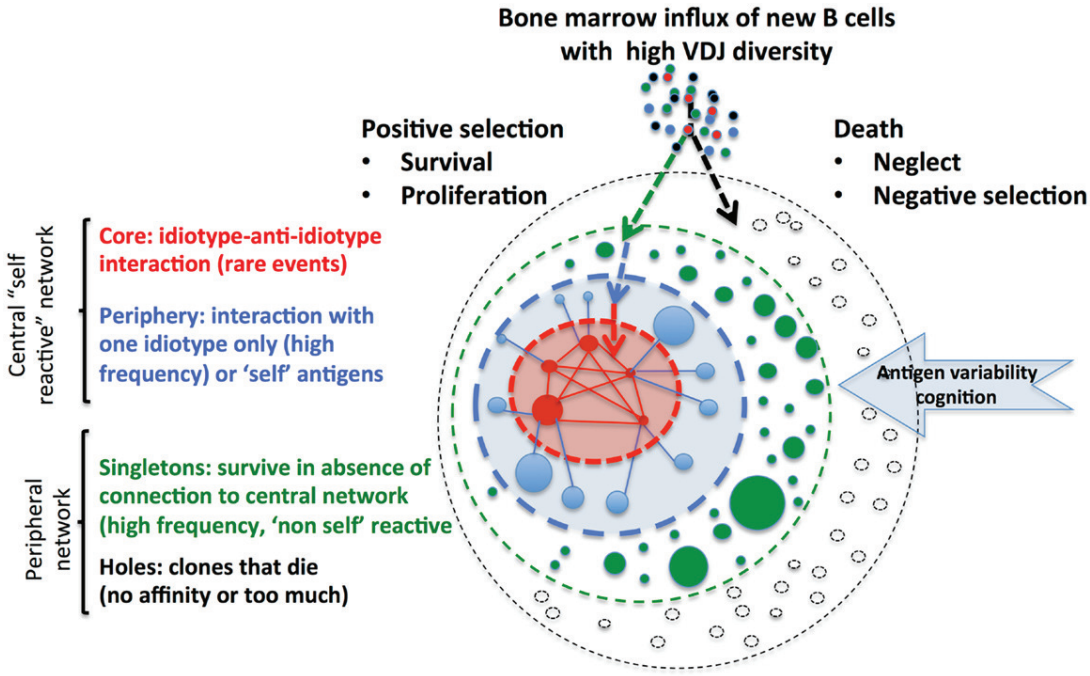

Figure 14.2: Metadynamics and lymphocyte integration within the central idiotypic and peripheral network in our model as seen by V. Thomas-Vaslin [10]. Figure from [10] under Creative Commons license.

[1] N.K. Jerne: Ann. Inst. Pasteur Immunol. **125C**, 373 (1974)
[2] U. Behn: Immunol. Rev. **216** 142 (2007)
[3] U. Behn: *Idiotype Network*, in: Encyclopedia of Life Sciences, John Wiley & Sons, Ltd, Chichester, doi:10.1002/9780470015902.a0000954.pub2 (2011)
[4] M. Brede, U. Behn: Phys. Rev. E **67**, 031920 (2003)
[5] H. Schmidtchen, M. Thüne, U. Behn: Phys. Rev. E **86**, 011930 (2012)
[6] H. Schmidtchen, U. Behn: Phys. Rev. E **86**, 011931 (2012)
[7] N. Preuß, Master Thesis, Universität Leipzig, 2014
[8] H. Schmidtchen, Dissertation, Universität Leipzig, 2015.
[9] R. Schulz, B. Werner, U. Behn: Frontiers in Immunology **5**, 00086 (2014), doi: 10.3389/fimmu.2014.00086
[10] V. Thomas-Vaslin, Frontiers in Immunology **5**, 00369 (2014), doi:10.3389/fimmu.2014.00369

14.4 Inelastic Mechanics of Biopolymer Gels, Cells and Cell Aggregates

A. Kramer, M. Gralka*, K. Kroy

*Department of Physics, University of California, Berkeley, USA

Whereas classical viscoelastic models can often be applied to describe the mechanical response of biomaterials to small deformations, they cannot adequately be used to model the response to large deformations. Here, the transient breaking of bonds, e.g. crosslinks in biopolymer networks or cell-cell adhesions in cell aggregates, leads to a new class of response reminiscent of plastic phenomenology.

We developed a schematic modeling framework for the construction of inelastic models for biological materials by extracting a simplified version of the inelastic Glassy Wormlike Chain (iGWLC) [1]. Our model consists of a combination of an inelastic model for the bonds and a viscoelastic model, the choice of which depends on the experimental set-up and protocol. The total strain is decomposed into a visoelastic and a slip part, where the latter is associated with the transient breaking of bonds, which is described by a first-order rate equation with force-dependent rates. Therewith we were able to provide a qualitative explanation of the nonlinear response measured for fibrin and collagen gels, cells and cell aggregates [2, 3] on a unified theoretical basis.

[1] L. Wolff *et al.*: New J. Phys. **12**, 053024 (2010), doi:10.1088/1367-2630/12/5/053024
[2] S. Münster *et al.*: PNAS **110**, 12197 (2013), doi:10.1073/pnas.1222787110
[3] T.V. Stirbat *et al.*: Eur. Phys. J. E **36**, 84 (2013), doi:10.1140/epje/i2013-13084-1

14.5 Rapid force spectroscopy

K. Kroy, J.T. Bullerjahn, S. Sturm

Dynamic force spectroscopy is a well-established technique that allows the experimentalist to determine the free energy landscape of single molecules by probing their rupture behavior under external force. Conventional theories of dynamic force spectroscopy [1] rely on a quasistatic model of bond breaking that is well justified for current experimental setups, but fails to cover the high loading rates amenable to full-scale molecular dynamics simulations and, possibly, future high-speed force spectroscopy assays [2]. We extended these theories to rapid force spectroscopy protocols by explicitly resolving the non-equilibrium internal bond dynamics. Our analytical predictions are exact for fast loading protocols and reduce to established quasistatic results in the limit of slow external loading. Our results are directly applicable to experimental or numerical data and have been published in "Nature Communications" [3]. A separate in-depth account of the underlying theory has moreover been published in a special issue of the "European Physical Journal" [4].

[1] O. K. Dudko *et al.*: Phys. Rev. Lett. **96**, 108101 (2006), doi:10.1103/PhysRevLett.96.108101

[2] M. Rief, H. Grubmüller: ChemPhysChem **3**, 255–261 (2002), doi:10.1002/1439-7641(20020315)3
[3] J. T. Bullerjahn, S. Sturm, K. Kroy: Nature Communications **5**, 4463 (2014), doi:10.1038/ncomms5463
[4] S. Sturm, J. T. Bullerjahn, K. Kroy: EPJ ST, **223**.14, 3129-3144 (2014), doi:10.1140/epjst/e2014-02323-7

14.6 Renormalized persistence length of semiflexible polymers in disorder

K. Kroy, W. Janke, S. Schöbl, S. Sturm

The most conspicuous property of a semiflexible polymer is its persistence length, defined as the decay length of tangent correlations along its contour. Using an efficient stochastic growth algorithm to sample polymers embedded in a quenched two-dimensional hard-disk fluid, we find that the disorder-averaged polymer conformations again exhibit Wormlike Chain statistics, albeit with a renormalized persistence length. For stiff polymers, this renormalized persistence length defines a "disorder persistence length" that depends only properties of the background disorder and provides us with a novel, quantitative measure of molecular crowding. Our results have been published in "Physical Review Letters" [1].

[1] S. Schöbl, S. Sturm, W. Janke, K. Kroy: Phys. Rev. Lett. **113**, 238302 (2014), doi:10.1103/PhysRevLett.113.238302

14.7 Inelastic mechanics of the cytoskeleton and cell morphology

M. Kettner, G. Zecua, K. Kroy

Cell shape relies on a structure that supports pressure and tension differences between the cell and its environment, the cytoskeleton. Its dominant substructure, the actin-cortex, is responsible for an effective surface tension. In the long time limit it behaves as a viscous fluid. This motivates a description of cell shape in analogy to a liquid drop with a given surface tension. The governing equation is the Young-Laplace equation which relates the local mean curvature to the pressure difference through the surface. In equilibrium, the cell should accordingly take the shape of a minimal surface, i.e., a surface with vanishing mean curvature.

Based on experimental observations [1] with cells attached to discrete points on stiff flat substrates, we develop a three dimensional theorie for the cell shape projected onto the substrate that accounts for the experimental results.

The liquid drop analogy can be extended to tissues. We propose a perturbation theory around the equilibrium minimal surface as a model for tissue growth, which

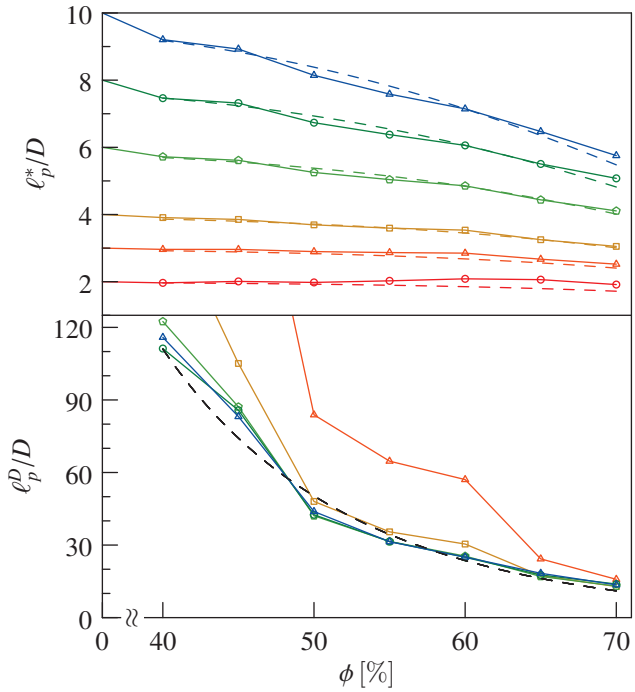

Figure 14.3: Exposure to a quenched hard-disk fluid of increasing background filling fraction ϕ successively decreases the renormalized persistence length ℓ_p^* (as determined from the exponentially decaying tangent-tangent correlation function) below its intrinsic value ℓ_p, here ranging from 2 to 10 disk diameters D. The *disorder persistence length* ℓ_p^D, defined via $1/\ell_p^D = 1/\ell_p^* - 1/\ell_p$, collapses onto a single master curve for large ℓ_p.

corresponds to the mathematical model of mean curvature flow, considering the coupling of the curvature with the underlying stresses of the polymer network, as has been done recently for the actin-cortex in the elastic limit [2].

[1] I.B. Bischofs, *et al.*: Phys. Rev. Lett., **103**, 048101 (2009)
[2] H. Berthoumieux, *et al.*: New J. Phys. **16**, 065005 (2014), doi:10.1088/1367-2630/16/6/065005

14.8 Self-propelled swimmers

G. Zecua, G. Falasco, M. Guthardt, A. Würger*, K. Kroy

*Laboratoire Ondes et Matiere d'Aquitaine, Université de Bordeaux, France

Previous work has been related to the propulsion velocities of spherical particles driven by self-thermophoresis. Using the Lorentz reciprocal theorem, we extend the approach to compute the translational and angular velocity for particles of any shape and assemblages in the form of a balance of energy dissipation. Our result can be applied also for many particle systems, including coupling between translational and rotational motions.

We find out that hydrodynamic interactions split into two parts. One part is related to the change of the thermophoretic slip layer around the particle, while the second

part is related to the mobility matrix for Stokesian drag in a many-particle system. We can also apply the theory to computations of the drift velocity for tandems of active swimmers and inert particles. This has been tested for the case of an assemblage consisting of an active Janus particle and an inert cargo. Then, it is possible to write down a Smoluchowsky equation for the probability density with respect to the position and orientation of an ensemble of Janus particles [1]. The thermal field of each particle induces a correction to the translational and angular of it neighbors, which can lead to self-polarization. This model is being currently tested in collaboration with the experimental group MON.

[1] T. Bickel, *et al.*: Phys.Rev. E **89**, 050303(R) (2014)

14.9 Packing structure of biopolymer solutions

M. Lämmel, K. Kroy, E. Jaschinski*, R. Merkel*

*Forschungszentrum Jülich (ICS-7: Biomechanics), Jülich, Germany

Stiff and semiflexible polymers are fundamental structural and functional building blocks of biological matter. They provide the constituents for nature to construct bioscaffolds, like the cytoskeleton or fibrous tissue. Our work focuses on solutions of stiff polymers in the semi-dilute regime, where the physics of the network is dominated by its *tight entanglements* [1] that constrain the thermal motion of each constituent filament to a tube-like cage formed by surrounding filaments. On the mean-field level, the tube is represented by a harmonic potential that confines the transverse fluctuations of a test polymer. The tube size, corresponding to the strength of the harmonic potential, is obtained from a self-consistently solved binary collision approximation proposed by Morse [2]. A local version [3] of this theory that predicts spatial tube radius fluctuations fared very well in comparison with extensive experiments on F-actin solutions [4].

Presently, we investigate the effect of shearing on the networks' packing structure, especially on the tube size. We extend our theoretical description to account for both shear-induced nematic ordering and tube bending and compare its predictions to extensive hybrid Monte Carlo/Brownian dynamics (MC/BD) simulations and new experiments with F-actin performed by our collaborators from the group of R. Merkel (Forschungszentrum Jülich).

Besides the influence of nematic order on the mean tube size, we also investigate how the experimental preparation process can change the statistics of the tube size. The binary collision approach predicts the relative variations of the tube size to be unchanged by imposed nematic order, which is indeed in agreement with the experimental data. Upon larger straining deformations, however, (non-local) tube bending might affect the shape of the tube size distribution. Following Fernández *et al.* [5], we estimate the shear induced tube deformation by minimizing the free energy of a test tube clamped between two neighbor tubes that change their positions according to the applied strain. Equipartition of the bending and the confinement contribution to the test polymer's free energy leads to shear-induced tube-widening. Moreover, starting from an equilibrium distribution of tube conformations that represent the unstrained

solution, we obtain that the tube size distribution becomes narrower as the strain increases.

[1] D.C. Morse: Macromolecules **31**, 7030 (1998), doi:10.1021/ma9803032
[2] D.C. Morse: Phys. Rev. E **63**, 031502 (2001), doi:10.1103/PhysRevE.63.031502
[3] J. Glaser and K. Kroy: Phys. Rev. E **84**, 051801 (2011), doi:10.1103/PhysRevE.84.051801
[4] J. Glaser *et al.*: Phys. Rev. Lett. **105**, 037801 (2010), doi:10.1103/PhysRevLett.105.037801
[5] P. Fernandez *et al.*: Soft Matter **5**, 2047 (2009), doi:10.1039/B816510F

14.10 Aeolian sand sorting and ripple formation

M. Lämmel, A. Meiwald, K. Kroy

Sand is driven along riverbeds or blown across beaches and deserts by turbulent flows. This seemingly chaotic process creates a whole hierarchy of structures ranging from ripple patterns over dunes to vast wavy sand seas. Moreover, by the very same process, the sand is constantly being sorted, because smaller grains advance faster while their heavier companions trail behind. Starting from the grain-scale physics, we model the sorting dynamics at the surface of the sand bed by grain-size- and wind-dependent erosion and illustrate how it creates the characteristic bimodal grain size distributions that are a prerequisite for the formation of so-called megaripples [1].

The separation into small and big grains has remarkable consequences for the transport physics of the wind-blown sand and gives rise to a very rich phenomenology. For such a bidisperse mixture, we derive different transport regimes as a function of wind strength and grain size ratio. Most importantly, we obtain a parameter range where only the small grains perform large hops whereas the big ones, driven by both the wind and the bombardment of fine grains, are set into a creep-like motion. The presence of the two transport modes provides the essential condition to create ripple patterns and suggests that these structures have a lot in common with their bigger relatives, aeolian sand dunes, whose physics is much better understood. This enables us to adapt a well established dune model [1] to predict formation, morphology, and dynamics of the sand ripples. Preliminary tests against field data strongly support our approach, which, moreover, provides a roadmap for future systematic field and laboratory measurements.

[1] G. Qian *et al.*: Sedimentology 59, 1888 (2012), doi:10.1111/j.1365-3091.2012.01330.x
[2] K. Kroy *et al.*: Phys. Rev. Lett. 88, 054301 (2002), doi:10.1103/PhysRevLett.88.054301

14.11 Stability of Dune Fields

S. Auschra, M. Lämmel, M. Will, K. Kroy

Arid regions on Earth and Mars are often covered with vast assemblies of crescent-shaped sand dunes, so-called barchans. The observation that single barchans either shrink or grow indefinitely if fed by a constant homogeneous influx of sand [2], makes the existence and stability of barchan fields a conundrum [3]. Several interaction mechanisms between adjacent barchans have been studied in the past in order to explain the observed well-selected dune sizes and distances within a field [3, 4]. As there is still no uncontroversial final answer to the miracle of stable barchan fields, we decided to have closer look at the interdune sand exchange.

We investigate the steady-state configuration of consecutive barchan dunes interacting by wind-driven sand transport. Based on well-established equations for isolated dunes [1, 2] we derive a coarse-grained description of the dominant pair interactions within a dune field. Sand supplied from the horns of a windward dune to its downwind neighbors initiates a complex response in their shape and mass. On the basis of a dimensionally reduced description which is justified by a close-by shape attractor, a fixed point equation for the mass balance of a fed dune was derived and analysed in view of stable solutions. We provide evidence that this process is a good candidate for explaining the stabilization of barchan dunes in the field.

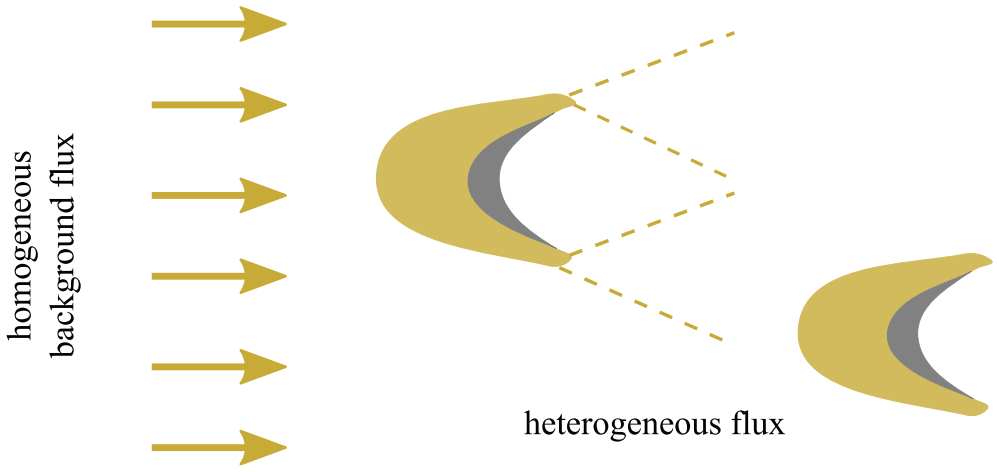

Figure 14.4: Inter-dune sand exchange. The downwind dune is fed by the homogeneous background flux plus a laterally spreading heterogeneous flux that escapes from the horns of the upwind dune.

[1] K. Kroy *et al.*: Phys. Rev. Lett. 88, 054301 (2002), doi:10.1103/PhysRevLett.88.054301
[2] S. Fischer, M. E. Cates, K. Kroy: Phys. Rev. E **77**, 031302, (2008), doi:10.1103/PhysRevE.77.031302
[3] H. Elbelrhiti, B. Andreotti, P. Claudin.: J. Geophys. Res. **113**, F02S15, 2008, doi:10.1029/2007JF000767
[4] M. Génois *et al.*: Eur. Phys. J. B **86**, 447, 2013, doi:10.1140/epjb/e2013-40710-2

14.12 Aeolian Sand Transport – Mesoscale Modelling and Pattern Formation

K. Kroy, M. Lämmel, A. Meiwald

When driven by wind, sand in the desert or at the beach generates an impressive zoo of structures ranging from delicate ripples to wavy sand seas spanning orders of magnitude in their size. To understand how these structures emerge, it is essential to thoroughly describe the underlying, seemingly chaotic, hopping motion of the sand grains. A mean-field approach that represents the distribution of grain trajectories by a single effective path was successfully used in the past to explain the formation and dynamics of sand dunes [1]. Sand ripples, however, whose typical wavelengths coincide with the characteristic hop lengths of the wind-blown grains, require information about mesoscale transport properties that are not accessible within this substantially reduced approach. We therefore extended it into develop a two-species framework that maps the ensemble of grain paths onto two populations representing fast saltating grains and slow reptating grains [3]. This provides a conceptionally transparent and computation-

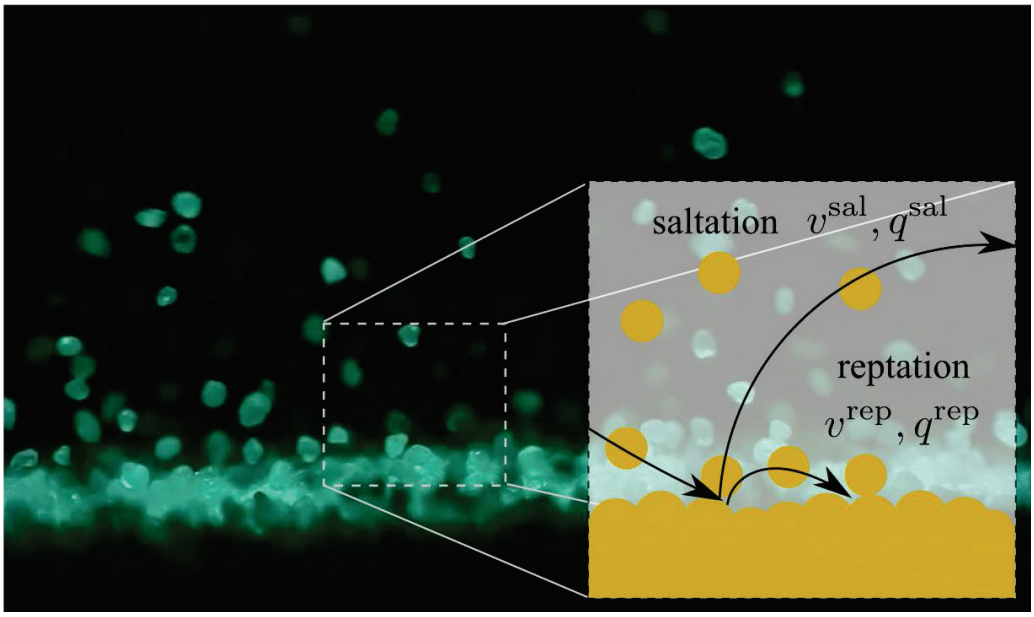

Figure 14.5: The two-species picture of aeolian sand transport maps the ensemble of mobile grains onto two representative species: high-energetic saltating grains and low-energetic reptating grains which in contrast to the saltating grains do not cause a splash of particles when impacting the sand bed. (Background picture by A. Valance, Universite de Rennes, France.)

ally efficient formulation and, most importantly, gives access to the wanted mesoscale structure of aeolian sand transport. We obtain model predictions of mesoscopic observables, e.g., the mean particle velocity at the ground, the mean particle hop length and the mean transport layer height, that are in remarkable agreement with various experimental data.

On this basis, we can also resolve a long-standing debate about the synthetic characteristic length scale that emerges in this processes. This so-called saturation length controls the size of sand dunes [1]. With the two-species prediction of the saturation

length the deduced minimal dune size is found to be in exceptional agreement with experimental field measurements.

[1] K. Kroy *et al.*: Phys. Rev. Lett. 88, 054301 (2002), doi:10.1103/PhysRevLett.88.054301
[2] B. Andreotti: J. Fluid Mech. **510**, 47-70 (2004), doi:10.1017/S0022112004009073
[3] M. Lämmel *et al.*: New J. Phys. **14**, 093037 (2012), doi:10.1088/1367-2630/14/9/093037

14.13 Non-isothermal Brownian motion

G. Falasco, M.V. Gnann*, K. Kroy

*International Max Planck Research School Mathematics in the Sciences, Leipzig, Germany

We extend the theory of hot Brownian motion to colloidal particles placed in externally imposed temperature gradients. We derive the fluctuating hydrodynamic equations suitable to describe sub-micron particles in nonisothermal Newtonian solvents under typical experimental conditions [3]. Upon elimination of the hydrodynamic fields we arrive at generalized Langevin equations for the translation and rotation of the particle [4]. The strength of thermal fluctuations turns out to be given by a tensorial frequency-dependent noise temperature, resulting from the dynamical coupling between the temperature gradient in the fluid and the hydrodynamic modes exited by the particle itself. Moreover, we study the particle linear response and derive non-isothermal fluctuation-dissipation formulas. Exploiting these relations, we show that a particle held in a harmonic trap can be turned into a genuine thermospectrometer, i.e. the energy modes of the thermal spectrum can be measured, by varying the trap stiffness, as the ratio of correlation and response.

[1] K. Kroy *et al.*: Phys. Rev. Lett. 88, 054301 (2002), doi:10.1103/PhysRevLett.88.054301
[2] G. Falasco, *et al.* Phys. Rev. E 90, 032131 (2014) doi:10.1103/PhysRevE.90.032131
[3] G. Falasco, K. Kroy, Preprint, arxiv.org/abs/1503.04025
[4] G. Falasco, M. V. Gnann, K. Kroy: Preprint, arxiv.org/abs/1406.2116

14.14 Funding

German-Israeli Foundation for Scientific Research and Development
A. Meiwald
Grant No. 4411-1.02/8.44

Sächsische DFG-Forschergruppe 877, "From local constraints to macroscopic transport"
M. Lämmel, S. Sturm, G. Falasco

Leipzig Graduate School "Building with Molecules and Nano-objects"
G. Falasco

Europäischen Sozialfonds (ESF), Nachwuchsforschergruppe "Lösungen und Netzwerke steifer Polymere"
M. Lämmel

Europäischen Sozialfonds (ESF), Nachwuchsforschergruppe "Funktion durch Selbstorganisation: Emergente Eigenschaften von Atom- und Molekülaggregaten"
G. Falasco

Europäischen Sozialfonds (ESF), Nachwuchsforschergruppe "Werkzeuge und Technologien für die rationale Wirkstoffentwicklung"
G. Zecua

Leipzig Graduate School "Building with Molecules and Nano-objects"
G. Falasco

Nonlinear Stochastically Driven Systems with Many Degrees of Freedom
R. Kürsten, M.Sc.
IMPRS Fellowship

14.15 Organizational Duties

Ulrich Behn
- Speaker of the Condensed Matter Theory Group
- Vertrauensdozent für die Nobelpreisträgertagungen in Lindau
- Bibliotheksbeauftragter of the Faculty
- Member of the Library Commission of the university
- Member of Research Profile Area "Mathematical and Computational Sciences"
- Scientific Member of the International Max Planck Research School "Mathematics in the Sciences"
- Referee: Europhysics Letters
- Reviewer: CEA Saclay

Klaus Kroy
- Member of the graduate grants committee of the university
- Study counselor for physics
- Member of the research associations "Complex Matter", "Mathematical and Computational Sciences", "Molekulare und zelluläre Kommunikation in Therapie und Diagnostik"
- PI in DFG FOR 877 and Leipzig School of Natural Sciences Building with Molecules and Nano-objects (BuildMoNa)
- Scientific Member of the International Max Planck Research School Mathematics in the Sciences
- Referee for Nature Physics, Nature Nanotechnology, Nature Communications, Science, PNAS, PRL, PRE, JCP, Soft Matter, Physica A, EPJE, Aeolian Research, Journal Physics of Fluids, Aeolia, Geomorphology, and various funding organizations (DFG, Academy of Finland)

Andrea Kramer
- Scientific Coordinator DFG Research Unit 877 *From Local Constraints to Macroscopic Transport*

- Scientific Manager Graduate School BuildMoNa

14.16 External Cooperations

Academic

- University of California, Berkeley, USA
  M.Sc. M. Gralka
- Forschungszentrum Jülich GmbH, Germany
  Prof. Dr. R. Merkel, Dipl. E. Jaschinski
- University of Minnesota, USA
  Prof. Dr. David C. Morse
- Ben-Gurion University of the Negev, Israel
  H. Yizhaq, I. Katra and H. Tsoar
- Université de Rennes, France
  A. Valance
- Aarhus University, Denmark
  K.R. Rasmussen
- Université de Bordeaux, France
  Prof. Dr. A. Würger
- Institut für Klinische Immunologie
  Prof. Dr. G. Metzner
- Max Planck Institute for Evolutionary Biology, Plön
  Dr. B. Werner
- Joint Institute for Nuclear Research, Dubna, Russia
  Prof. Dr. N.M. Plakida

14.17 Publications

Journals

J. T. Bullerjahn, S. Sturm, K. Kroy: *Theory of rapid force spectroscopy*, Nature Communications **5**, 4463 (2014), doi:10.1038/ncomms5463

S. Sturm, J. T. Bullerjahn, K. Kroy: *Intramolecular relaxation in dynamic force spectroscopy*, EPJ ST **223**, 3129-3144 (2014), doi:10.1140/epjst/e2014-02323-7

S. Schöbl, S. Sturm, W. Janke, K. Kroy: *Persistence-Length Renormalization of Polymers in a Crowded Environment of Hard Disks*, Phys. Rev. Lett. **113**, 238302 (2014), doi:10.1103/PhysRevLett.113.238302

E.J.R. Parteli, K. Kroy, H. Tsoar, J.S. Andrade Jr., T. Pöschel: *Morphodynamic modeling of aeolian dunes: Review and future plans*, EPJ ST **223**, 2269–2283 (2014), doi:10.1140/epjst/e2014-02263-2

G. Falasco, M.V. Gnann, D. Rings, K. Kroy: *Effective temperatures of hot Brownian motion*, Phys. Rev. E 90 *3*, 032131 (2014), doi:10.1103/PhysRevE.90.032131

K. Kroy: *Levitating nanoparticles: Non-equilibrium nano-thermometry*, Nature Nanotechnology **9** (6), 415–417 (2014), doi:10.1038/nnano.2014.109

T. Bickel, G. Zecua, A. Würger: *Polarization of active Janus particles*, Phys.Rev. E **89**, 050303(R) (2014), doi:10.1103/PhysRevE.89.050303

R. Schulz, B. Werner, U. Behn: *Self tolerance in a minimal model of the idiotypic network*, Frontiers in Immunology **5**, 00086 (2014), 12 pp., doi:10.3389/fimmu.2014.00086

A.A. Vladimirov, D. Ihle, N.M. Plakida: *Magnetic susceptibility and short-range order in iron pnictides: Anisotropic J_1 - J_2 Heisenberg model*, Eur. Phys. J. B **87**, 112 (2014), 5pp., doi:10.1140/epjb/e2014-50152-y

A.A. Vladimirov, D. Ihle, N.M. Plakida: *Magnetic order and spin excitations in layered Heisenberg antiferromagnets with compass-model anisotropies*, Pis'ma Zh. Eksp. Teor. Fiz. **100**, 885–890 (2014), doi:10.7868/S0370274X14240059

Preprints

M. Lämmel, A. Meiwald, K.Kroy: *Analytical mesoscale modeling of aeolian sand transport*, arXiv:1405.0624v1

G. Falasco, K. Kroy: *Non-isothermal fluctuating hydrodynamics and Brownian motion*, arXiv:1503.04025

G. Falasco, M. V. Gnann, K. Kroy: *Non-Isothermal Fluctuation-Dissipation Relations and Brownian Thermometry*, arXiv:1406.2116

R. Kürsten: *Comment on 'Anomalous diffusion induced by enhancement of memory'*, arXiv:1503.03302

Posters

J. T. Bullerjahn, S. Sturm, K. Kroy: *Rapid force spectroscopy*, Annual BuildMoNa Conference, Leipzig, Germany, March 3–4, 2014

A. Meiwald, M. Lämmel, K. Kroy: *Mesoscale Modelling of Aeolian Sand Transport*, DPG-Frühjahrstagung, Dresden, Germany, March 30–April 5, 2014

S. Auschra, M. Lämmel, K. Kroy: *Stability of Barchan Dune Fields*, DPG-Frühjahrstagung, Dresden, Germany, March 30–April 5, 2014

G. Falasco, M. V. Gnann, K. Kroy: *Non-isothermal Brownian motion*, Seminar "Nonlinear Response in Complex Systems and Nonequilibrium Liquids", Cologne, Germany, September 1–5, 2014

G. Falasco, M. V. Gnann, K. Kroy: *Non-isothermal Brownian motion*, Conference "Venice meeting on fluctuations in small complex systems II ", Venice, Italy, September 9–13, 2014

G. Falasco, M. V. Gnann, K. Kroy: *Non-isothermal Brownian motion*, Workshop "Advances in Nonequilibrium Statistical Mechanics", Florence, Italy, May 26–June 13, 2014

R. Kürsten, U. Behn: *Optimal bounds on critical or tricritical points of nonlinear globally coupled systems with additive noise*, Sigma Phi 2014, International Conference on Statistical Physics, Rhodos, July 7–11, 2014

R. Kürsten, U. Behn: *Optimal bounds on critical or tricritical points of nonlinear globally coupled systems with additive noise*, IV Summerschool on Small and Complex Systems, IFISC, Palma de Mallorca, September 8–19, 2014

Talks

A. Kramer: *Melting of pectin gels*, Annual BuildMoNa Conference, Leipzig, Germany, March 3–4, 2014

S. Sturm: *Caged and released semiflexible polymers*, SFG Meeting, Dresden, Germany, March 24th 2014

J. T. Bullerjahn, S. Sturm, K. Kroy: *(Theory of) rapid force spectroscopy*, DPG-Frühjahrstagung, Dresden, Germany, March 30–April 5, 2014

M. Lämmel: *Nematic microstructure in biopolymer solutions*, DPG-Frühjahrstagung, Dresden, Germany, March 30–April 5, 2014

K. Kroy: *There is Music in the Noise. Structure from Stochastic Dynamics*, Workshop "Dynamic Systems: From Statistical Mechanics to Engineering Applications", Zürich, Switzerland, January 9–10, 2014

K. Kroy: *Hot Brownian Motion*, Ben Gurion University, Beer Sheva, Israel, March 11th, 2014

K. Kroy: *How to break a bond – theory of rapid force spectroscopy*, Workshop "Brownian Motion in Confined Geometries", Dresden, Germany, March 17–21, 2014

K. Kroy: *Mesoscale Modeling of Aeolian Sand Transport*, University of Erlangen, May 2nd, 2014

K. Kroy: *Inelastic Mechanics of Polymer Networks and Cells*, World Congress of Biomechanics, Boston, USA, June 6–11, 2014

K. Kroy: *Non-isothermal Brownian motion*, Wigner Kolloquium, TU-Berlin, June 5th, 2014

K. Kroy: Heraeus Workshop Nonlinear Response in Complex Systems and Nonequilibrium Liquids, DLR, Cologne, Germany, September 1–5, 2014

K. Kroy: *Non-isothermal Brownian Motion*, "Venice Meeting on Fluctuations in Small Complex Systems", Venice, Italy, October 9–13, 2014

K. Kroy: *Hot Brownian Motion*, "Advances in Live Cell Thermal Imaging and Manipulation", Okinawa, Japan, November 10–12, 2014

K. Kroy: *Non-isothermal Brownian Motion*, Kolloquium, University of Bayreuth, Germany, December 2nd, 2014

R. Kürsten, U. Behn: *Critical manifold and tricritical point of nonlinear globally coupled systems with additive noise*, DPG-Frühjahrstagung, Dresden, Germany, March 30 – April 5, 2014

R. Kürsten, U. Behn: *Critical manifold and tricritical point of nonlinear globally coupled systems with additive noise*, Workshop of the International Max Planck Reseach School Mathematics in the Sciences, Leipzig, July 16–17, 2014

14.18 Graduations

Master

- Sven Auschra
  Gegenseitige Stabilisierung von Sicheldünen
  December 2014
- Nicolas Preuß
  Self Tolerance and Correlations in Idiotypic Networks
  December 4, 2014

Bachelor

- Maik Weßling
  A geometrical description of the impact process of particles onto 2D granular packings
  March 2014
- Andreas Hübner
  Bestimmung der Dauer von S-Phasen und Zellzyklen mit Thymidinanaloga: Simulation und mathematisches Modell
  March 4, 2014
- Meike Will
  Computersimulation zur Dynamik von Dünenfeldern
  December 2014

14.19 Guests

- Prof. Dr. Michael Wilkinson
  The Open University
  February 12, 2014
- Dr. Marco Baiesi
  University of Padua
  May 8, 2014

- Prof. Dr. Michael Cates
  University of Edinburgh
  May 19, 2014
- Dipl. Phys. Evelin Jaschinski
  Forschungszentrum Jülich
  May 27, 2014
- Dr. Nikolaj Georgi
  Max Planck Institute for Mathematics in the Sciences, Leipzig
  June 10, 2014
- Prof. Dr. Leo van Hemmen
  TU München
  July 14–16, 2014
- Dr. Ithzak Katra, Hezi Yizhaq, B.Sc. Erez Schmerker
  Ben-Gurion University of the Negev, Israel
  September 9–11, 2014
- Dr. Stefan Münster
  Center for Systems Biology, Dresden
  October 1, 2014
- Dr. Claus Heussinger
  University of Göttingen
  November 4, 2014
- Prof. Dr. Max von Renesse
  University of Leipzig
  December 4, 2014

15

Theory of Elementary Particles

15.1 Introduction

Group Leader: Prof. S. Hollands

Our group is interested in the properties of matter at very high energies (small scales) or under other extreme conditions, covering a broad variety of research topics ranging from the study of elementary particles and their properties to the study of quantized matter fields in the presence of strong gravitational fields. The underlying theme of our research and teaching activity is the theory of such quantized fields in its various manifestations, and applications, including:

1. Quantum fields on discrete spacetimes (lattices) and their numerical and theoretical study
2. Quantum fields on curved spacetimes
3. Applications of ideas from integrable systems to the study of quantum gauge theories
4. Dualities and relation with classical General Relativity

Quantum field theories on lattices are natural discretized counterparts of continuum models that describe elementary particles in quantum field theoretic models such as the standard model of particle physics. They were introduced in order to investigate certain non-perturbative features of these models in a controlled approximation that are inaccessible by other means, such as perturbation theory. A substantial fraction of the current work being done in this area are numerical simulations and the development of new theoretical methods leading to improved numerical schemes. Quantum gauge theories such as the standard model can also be treated as continuum field theories, and can thereby be studied using perturbative methods. The task of finding improved ways of handling perturbative calculations is an important aspect of quantum field theory and is actively pursued in our group.

Quantum field theory in curved spacetime (QFTCS) is the theory of quantum fields propagating in a background, classical, curved spacetime. On account of its classical treatment of the metric, QFTCS cannot be a fundamental theory of nature. However,

QFTCS is expected to provide an accurate description of quantum phenomena in a regime where the effects of curved spacetime may be significant, but effects of quantum gravity itself may be neglected. In particular, it is expected that QFTCS should be applicable to the description of quantum phenomena occurring in the early universe and near (and inside of) black holes, provided that one does not attempt to describe phenomena occurring so near to singularities that curvatures reach Planckian scales and the quantum nature of the spacetime metric would have to be taken into account. Quantum field theory in curved spacetimes has provided important physical insights into the quantum nature of black holes, indicating that they should, if left alone, gradually evaporate due to the emission of quanta whose energies are distributed thermally at the famous Hawking temperature.

In parallel to direct approaches to quantum field theory via perturbative, or numerical, techniques, there are now also more indirect approaches via so-called "holographic dualities". Such dualities typically establish a connection with a quantum field theory living on some sort of boundary of a space and a classical, gravitational, theory living in the higher dimensional space itself. This type of duality is believed to probe rather different regimes of quantum field theory (strong coupling, "large N"), and is hence complementary to other methods. At the technical level, it motivates studies into higher dimensional gravity theories, which turn out to have a rather rich mathematical structure. The study of such structures is another research topic in our group.

More information may be found on the group's webpages, www.uni-leipzig.de/~tet

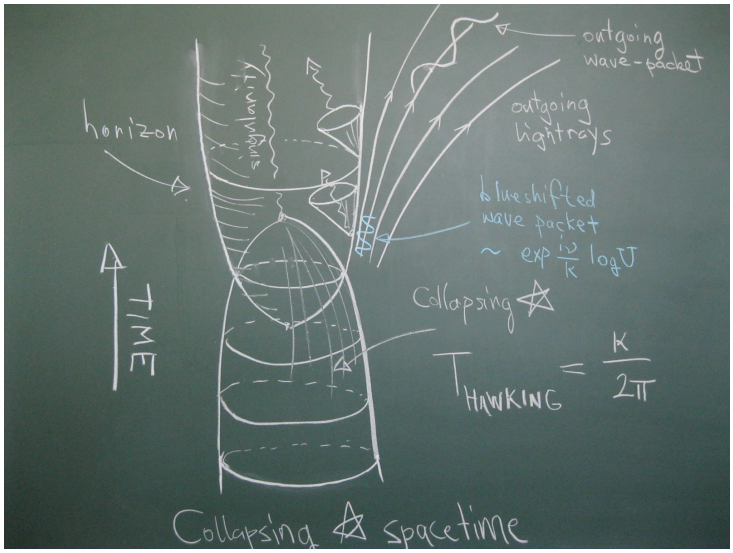

Figure 15.1: The Hawking Effect

15.2 Stability of higher dimensional black holes

S. Hollands

Holographic descriptions of quantum field theories require a good understanding of the corresponding solutions of the dual bulk gravity theories. Among these, black hole solutions enjoy a privileged status in the holographic duality. By now, many such

solutions have been constructed in various kinds of gravity and supergravity theories. It is of major interest to (a) get a mathematical classification and (b) a good understanding of the stability properties of the black holes in higher dimensions. For both problems, sophisticated methods are required. One strategy which can give a better conceptual understanding of instabilities of black holes is the "canonical energy method" [1]. This method is of an essentially variational nature, and relates "dynamical" stability properties of black holes very nicely to their "thermodynamical" stability, in the sense of the laws of black hole mechanics. When combined with other sophisticated techniques such as algebraically special properties of many known background solutions, and methods from geometric analysis, definite criteria for (in)stability of certain types of black holes could be established, for example (near) extremal ones [2].

[1] S. Hollands and R. M. Wald, "Stability of Black Holes and Black Branes," Commun. Math. Phys. **321** (2013) 629 [arXiv:1201.0463 [gr-qc]].
[2] "Instabilities of extremal rotating black holes in higher dimensions," arxiv:1408.0801, accepted for publication in Commun. Math. Phys.
[3] S. Hollands and A. Thorne, "Bondi mass cannot become negative in higher dimensions," Commun. Math. Phys. **333**, no. 2, 1037 (2015) [arXiv:1307.1603 [gr-qc]].

15.3 Operator product expansions in quantum field theory

S. Hollands, J.W. Holland, M.B. Fröb

All quantum field theories with well-behaved ultra violet behavior are believed to have an operator product expansion (OPE) [1]. This means that the product of any two local fields located at nearby points x and y in spacetime can be expanded in the form

$$O_A(x)O_B(y) \sim \sum_C C_{AB}^C(x-y)\, O_C(y), \tag{15.1}$$

where A, B, C are labels for the various local fields in the given theory (incorporating also their tensor character/spin), and where C_{AB}^C are certain numerical coefficient functions—or rather distributions—that depend on the theory under consideration, the coupling constants, etc. The sign "$\sim$" indicates that this can be understood as an asymptotic expansion: If the sum on the right side is carried out to a sufficiently large but finite order, then the remainder goes to zero fast as $x \to y$ in the sense of operator insertions into a quantum state, or into a correlation function. The operator product expansion is an important tool for calculations in asymptotically free quantum field theories (such as Quantum Chromo Dynamics, QCD). At a conceptual level, the OPE may be viewed as a kind of "skeleton" of quantum field theory, and its understanding may shed some light on fundamental open questions in this theory. Our work has been directed in the following directions:

1. We would like to understand the sense in which the coefficients in the OPE can be viewed as analogs of the structure constants in an algebra. As such, they

would have to satisfy powerful constraints corresponding to a kind of "Jacobi identity" (associativity law). We have understood in what sense such consistency conditions indeed hold.

2. One would like to understand whether there are ways to compute the OPE coefficients recursively order-by-order in a small coupling expansion around those for a conformal fixed point (e.g. free field theory). We have made great progress in finding such recursive formulas, which are intimately tied to the property of associativity. We are investigating whether, and how, such identities can establish the existence of quantum field theories at the non-perturbative level, in theories which are "asymptotically Gaussian" at short distances [Work in progress by SH and JWH].

3. We are trying to understand whether perturbations of the "OPE algebra" fit into the frameworks established for deformations of other kinds of algebraic structures in mathematics, in terms of notions such as "Hochschild cohomology".

4. We have generalized our analysis concerning the convergence properties of the OPE to theories with zero mass. Such theories are particularly interesting physically, but also particularly challenging due to their complicated behavior at large distances ("infra-red"). These difficulties have, consequently, forced us to invent a very significant extension of previous techniques. One of the main reasons for our interest in this direction lies in the fact that non-abelian gauge theories such as QCD must be treated by such methods. However, in such theories one faces also additional difficulties due to the local gauge symmetry characteristic for these models. We are currently trying to incorporate this kind of structure into our analysis of the OPE in order to obtain results of comparable power. [Work in progress by SH and MBF.]

This is a longer term research project. The following papers report on progress concerning some of these questions:

[1] K. G. Wilson and W. Zimmermann, "Operator product expansions and composite field operators in the general framework of quantum field theory," Commun. Math. Phys. **24**, 87 (1972).
[2] S. Hollands and R. M. Wald, "Quantum fields in curved spacetime," Phys. Rept. **574** (2015) 1 [arXiv:1401.2026 [gr-qc]].
[3] S. Hollands and C. Kopper, "The operator product expansion converges in massless φ^4_4 theory," Commun. Math. Phys. **313** (2012) 257 [arXiv:1411.1785 [hep-th]].
[4] J. Holland and S. Hollands, "Recursive construction of operator product expansion coefficients," arXiv:1401.3144 [math-ph].
[5] J. Holland and S. Hollands, "A small cosmological constant due to non-perturbative quantum effects," Class. Quant. Grav. **31** (2014) 125006 [arXiv:1305.5191 [gr-qc]].

15.4 Yangian Symmetry and scattering in gauge field theories

R. Kirschner, D. Chicherin, S. Derkachov

Integrable quantum systems are applied successfully to the study of the high-energy asymptotics and of the renormalization of composite operators in gauge theories.

These applications stimulated the development of the methods of integrable quantum systems. In the calculation of scattering amplitudes in maximally extended supersymmetric Yang Mills theory two superconformal symmetries have been discovered [1] which fit into the framework of Yangian symmetry [2].

In 2013 we have proposed a convenient formulatation of this symmetry relying on the Quantum Inverse Scattering Method and have developed efficient methods for solving of the symmetry condition [3, 4].

In continuation of this work we have obtained an extension in spectral parameters of a generic Yangain symmetric correlator by acting with Yang-Baxter operators on a trivial basic correlator. We have investigated the action of Yang-Baxter operators on such generic correlators and also the symmetric convolution of symmetric correlators. The relation of the latter to the on-shell intermediate particle or unitarity cut contribution to loop correction to amplitudes has been discussed [5].

[1] J. M. Drummond, J. Henn, G. P. Korchemsky and E. Sokatchev,
Dual superconformal symmetry of scattering amplitudes in N=4 super-Yang-Mills theory,
Nucl. Phys. B **828** (2010) 317, [arXiv:0807.1095 [hep-th]].
[2] J. M. Drummond, J. M. Henn and J. Plefka,
Yangian symmetry of scattering amplitudes in N=4 super Yang-Mills theory,
JHEP **0905** (2009) 046, [arXiv:0902.2987 [hep-th]].
[3] D. Chicherin and R. Kirschner, *Yangian symmetric correlators*,
Nucl. Phys. B **877** (2013) 484 [arXiv:1306.0711 [math-ph]].
[4] D. Chicherin, S. Derkachov and R. Kirschner,
Yang-Baxter operators and scattering amplitudes in N=4 super-Yang-Mills theory,
Nucl. Phys. B **881** (2014) 467, [arXiv:1309.5748 [hep-th]].
[5] R. Kirschner, "Yangian symmetric correlators, R operators and amplitudes," J. Phys. Conf. Ser. **563** (2014) 1, 012015.

15.5 Entanglement entropy of quantum fields

K. Sanders, S. Hollands

A typical state of a quantum field theory (QFT) may exhibit a lot of entanglement between spacelike separated regions. In Minkowski space this is due to the Reeh-Schlieder theorem, which has partial extensions to curved spacetimes [2]. In order to quantify the amount of entanglement of a state between two given regions, one may adopt the notion of entanglement entropy as used in quantum mechanics (QM). Computing entanglement entropies is difficult, even for free fields [3], but the results show some interesting features. E.g., when space is divided into two regions by a boundary surface S, the entanglement entropy of the vacuum is divergent and the coefficient of the leading divergent order is proportional to the area of S ("area law").

Unfortunately, the existing computations have a number of drawbacks: they often only work for ground states (using path integrals), and they introduce regulators and subtle computational tricks whose physical meaning is unclear (e.g. the replica

method). In this project we endeavour to provide an alternative approach to entanglement entropy, with a better physical motivation, and compare with the existing results. We focus on the following questions:

- The definition of entanglement entropy in terms of density matrices, familiar from QM, requires modification, due to the existence of inequivalent Hilbert space representations in QFT. For this reason we resort to the relative entropy of Araki [1], leading to a well-defined entanglement entropy in a very general setting, taking values in $[0, \infty]$.
- For two quasi-free states in QM, we obtained an explicit formula for their relative entropy, relying heavily on literature from quantum information theory [4]. This general result allows us to find upper and lower bounds for entanglement entropies.
- For quasi-free states of a free scalar QFT, we expect to find their relative entropy as a generalisation of the formula from QM, and the upper and lower bounds should generalise as well.
- In simple explicit cases, such as the Minkowski vacuum and spacelike separated regions with sufficiently simple geometry, it may be possible to evaluate or approximate the bounds on the entanglement entropy. This allows for a comparison of computational methods and results with the existing literature (e.g. the area law).

[1] H. Araki, Publ. Res. Inst. Math. Sci. **11** (1975/76), 809–833
[2] K. Sanders, Commun. Math. Phys. **288** (2009), no.1, 271–285
[3] S.N. Solodukhin, Living Rev. Relativity **14** (2011), no.8
[4] C. Weedbrook, S. Pirandola, R. García-Patrón, N.J. Cerf, T.C. Ralph, J.H. Shapiro and S. Lloyd, Rev. Mod. Phys. **84** (2012), no.2, 621–669

15.6 Modular nuclearity of scalar fields in curved spacetimes

K. Sanders, G. Lechner

Nuclearity conditions were introduced in quantum field theory by [1], and modular nuclearity, which makes use of Tomita-Takesaki theory, has recently played an important role in certain integrable interacting algebraic QFTs in two dimensional Minkowski space [2]. Although conditions of this sort are physically desirable, mathematically useful, and expected to hold quite generally, they have only been verified in very few cases, even for free fields.

The general formulation of a nuclearity condition requires a reference Hilbert space (obtained from a reference state), a (bounded) region of spacetime, and an operator representing the energy. For free scalar fields, the condition has been verified e.g.

- For the Hamilton operator in the ground state on an ultrastatic spacetime, using localisation in arbitrary bounded regions [3].

- For the modular operator of a wedge region in the Minkowski vacuum, using localisation in any smaller wedge region [2].

In this project we aim to expand our knowledge on nuclearity conditions in the following ways:

- In ultrastatic spacetimes we consider the relation between modular nuclearity and Hamiltonian nuclearity for ground states. Such a relation is known for the Minkowski vacuum, but its proof uses results by Bisognano and Wichmann that do not easily generalise to general ultrastatic spacetimes.

- In arbitrary globally hyperbolic spacetimes we will verify modular nuclearity for general quasi-free Hadamard states. We may define a modular operator associated to bounded open regions and verify the condition for any bounded sub-regions.

For both problems we have already achieved good results at the one-particle level, relying in part on the local quasi-equivalence of quasi-free Hadamard states [4].

[1] D. Buchholz and E. Wichmann, Commun. Math. Phys. **106** (1986), no.2, 321–344
[2] D. Buchholz and G. Lechner, Ann. Henri Poincaré **5** (2004), no.6, 1065–1080
[3] R. Verch, Lett. Math. Phys. **29** (1993), no.4, 297–310
[4] R. Verch, Commun. Math. Phys. **160** (1994), no.3, 507–536

15.7 Applications of numerical stochastic perturbation theory to lattice QCD

H. Perlt, A. Schiller

In collaboration with authors from different locations we have continued our research program using numerical stochastic perturbation theory (NSPT).

It is well known that lattice perturbation theory (LPT) is much more involved compared to its continuum QCD counterpart. The complexity of diagrammatic approaches increases rapidly beyond the one-loop approximation. By now only a limited number of results up to two-loop accuracy have been obtained.

Applying the standard Langevin dynamics [1, 2] to the problem of weak coupling expansions for lattice QCD, a powerful numerical approach for higher loop calculations – called numerical stochastic perturbation theory (NSPT) – has been proposed in [3].

With colleagues from the QCDSF collaboration we have calculated Wilson loops of various sizes up to 20 loops in SU(3) pure lattice gauge theory at different lattice sizes for Wilson gauge action using the technique of numerical stochastic perturbation theory [4]. This allowed us to investigate the perturbative series for various Wilson loops at high loop orders. In we have calculated [5] the SU(3) beta function from Wilson loops to 20th order numerical stochastic perturbation theory. An attempt has been made to include massless fermions, whose contribution is known analytically to 4th order. The question whether the theory admits an infrared stable fixed point is addressed.

The subtraction of hypercubic lattice corrections, calculated at one-loop order in lattice perturbation theory, is common practice, e.g., for determinations of renormalization constants in lattice hadron physics (see the next project). One may overcome the limitation to one-loop and calculate hypercubic corrections for any operator and action beyond the one-loop order using Numerical Stochastic Perturbation Theory (NSPT). Together with colleagues from Regensburg and Dubna we started [6] a first check whether NSPT can by used to subtract hypercubic lattice corrections and provide (in a parametrization valid for arbitrary lattice couplings) the lattice corrections up to three-loop order for the SU(3) gluon and ghost propagators in Landau gauge. In [7] we explored the practicability of such an approach to operators including fermions and considered, as a first test, the case of Wilson fermion bilinear operators in a quenched theory. Our results allow us to compare boosted and unboosted perturbative corrections up to three-loop order.

[1] G. Parisi and Y. s. Wu, Sci. Sin. **24** (1981) 483.
[2] G. G. Batrouni, G. R. Katz, A. S. Kronfeld, G. P. Lepage, B. Svetitsky and K. G. Wilson, Phys. Rev. D **32** (1985) 2736.
[3] F. Di Renzo, E. Onofri, G. Marchesini and P. Marenzoni, Nucl. Phys. B **426** (1994) 675 [arXiv:hep-lat/9405019].
[4] R. Horsley, G. Hotzel, E.-M. Ilgenfritz, R. Millo, Y. Nakamura, H. Perlt, P. E. L. Rakow, G. Schierholz and A. Schiller, Phys. Rev. D **86** (2012) 054502 [arXiv:1205.1659 [hep-lat]].
[5] R. Horsley, H. Perlt, P. E. L. Rakow, G. Schierholz and A. Schiller, Phys. Lett. B **728** (2014) 1 [arXiv:1309.4311 [hep-lat]].
[6] J. Simeth, A. Sternbeck, E. -M. Ilgenfritz, H. Perlt and A. Schiller, PoS LATTICE **2013** (2014) 459 [arXiv:1311.1934 [hep-lat]].
[7] J. Simeth, A. Sternbeck, M. Göckeler, H. Perlt and A. Schiller, arXiv:1501.06322 [hep-lat].

15.8 Aspects in the determination of renormalization constants on the lattice

H. Perlt, A. Schiller

Renormalization factors in lattice Quantum Chromodynamics (QCD) relate observables computed on finite lattices to their continuum counterparts in specific renormalization schemes. Therefore, their determination should be as precise as possible in order to allow for a reliable comparison with experimental results. One approach is based on lattice perturbation theory [1]. However, it suffers from its intrinsic complexity, slow convergence and the impossibility to handle mixing with lower-dimensional operators. Therefore, nonperturbative methods have been developed and applied. Among them the so-called regularization-invariant momentum (RI-MOM) scheme [2] is widely used because of its simple implementation.

Like (almost) all quantities evaluated in lattice QCD also renormalization factors suffer from discretization effects. One can attempt to cope with these lattice artifacts by

extrapolating the nonperturbative scale dependence to the continuum (see Ref. [3]) or one can try to suppress them by a subtraction procedure based on perturbation theory. Here we were dealing with the latter approach.

In a recent paper of the QCDSF/UKQCD collaboration [4] a comprehensive discussion and comparison of perturbative and nonperturbative renormalization have been given. Particular emphasis was placed on the perturbative subtraction of the unavoidable lattice artifacts. For the simplest operators and lattice actions this can be done with reasonable effort in one-loop order completely by computing the corresponding diagrams for finite lattice spacing numerically. An alternative approach can be based on the subtraction of one-loop terms of order a^2 with a being the lattice spacing. The computation of those terms has been developed by the Cyprus group [6] and applied to various operators for different actions.

In collaboration with colleagues from QCDSF and Cyprus university we have used in works [7] and [8] some of those results for the analysis of lattice Monte Carlo data of the QCDSF collaboration to determine as precisely as possible the renormalization constants in the so-called renormalization group invariant (RGI) scheme Z^{RGI}.

A novel method for nonperturbative renormalization of lattice nonsinglet as well as singlet operators has been introduced by our lattice collaboration [9], which is based on the Feynman-Hellmann relation (for more details see [10]). The Feynman-Hellmann technique offers a promising alternative for calculations of quark line disconnected contributions to hadronic matrix elements. The method involves computing two-point correlators in the presence of generalized background fields arising from introducing additional operators into the action. As a first application, and test of the method, we computed the renormalization factors of the axial vector current and the scalar densityfor both nonsinglet and singlet operators for three quark flavors of SLiNC fermions. For nonsinglet operators, where a meaningful comparison is possible, perfect agreement with recent calculations using standard three-point function techniques has been found.

[1] S. Capitani, Phys. Rept. **382** (2003) 113 [arXiv:hep-lat/0211036]
[2] G. Martinelli, C. Pittori, C. T. Sachrajda, M. Testa and A. Vladikas, Nucl. Phys. B **445** (1995) 81 [arXiv:hep-lat/9411010]
[3] R. Arthur and P. A. Boyle (RBC and UKQCD Collaborations), Phys. Rev. D **83** (2011) 114511 [arXiv:1006.0422 [hep-lat]].
[4] M. Göckeler, R. Horsley, Y. Nakamura, H. Perlt, D. Pleiter, P. E. L. Rakow, A. Schäfer, G. Schierholz, A. Schiller, H. Stüben and J. M. Zanotti, (QCDSF/UKQCD Collaboration) Phys. Rev. D **82** (2010) 114511 [Erratum-ibid. D **86** (2012) 099903] [arXiv:1003.5756 [hep-lat]].
[5] M. Göckeler, R. Horsley, E.-M. Ilgenfritz, H. Perlt, P. E. L. Rakow, G. Schierholz and A. Schiller, Phys. Rev. D **54** (1996) 5705 [arXiv:hep-lat/9602029].
[6] M. Constantinou, V. Lubicz, H. Panagopoulos and F. Stylianou, JHEP **0910** (2009) 064 [arXiv:0907.0381 [hep-lat]].
[7] M. Constantinou, M. Costa, M. Göckeler, R. Horsley, H. Panagopoulos, H. Perlt, P. E. L. Rakow, G. Schierholz and A. Schiller, Phys. Rev. D **87** (2013) 9, 096019 [arXiv:1303.6776 [hep-lat]].
[8] M. Constantinou, R. Horsley, H. Panagopoulos, H. Perlt, P. E. L. Rakow, G. Schier-

holz, A. Schiller and J. M. Zanotti, Phys. Rev. D **91** (2015) 1, 014502 [arXiv:1408.6047 [hep-lat]].
[9] A. J. Chambers *et al.* [QCDSF Collaboration], Phys. Lett. B **740** (2015) 30 [arXiv:1410.3078 [hep-lat]].
[10] A. J. Chambers *et al.* [CSSM and QCDSF/UKQCD Collaborations], Phys. Rev. D **90** (2014) 1, 014510 [arXiv:1405.3019 [hep-lat]].

15.9 Fuzzy extra dimensions in $\mathcal{N} = 4$ super Yang-Mills theory and matrix models

H. Steinacker*, J. Zahn

*Faculty of Physics, University of Vienna, Austria

The maximally supersymmetric $\mathcal{N} = 4$ $SU(N)$ super-Yang-Mills theory takes a special role among all 4-dimensional quantum field theories. It is arguably the most symmetric 4-dimensional gauge theory, it is perturbatively finite, and much research effort has been devoted in recent years to study various aspects of this model. Its 6 scalar fields are $N \times N$ matrix valued, and non-trivial configurations of these can be interpreted as fuzzy geometries embedded in $\mathbb{R}^6$ (with the eigenvalues of the matrices indicating the embedding coordinates). Such non-trivial vacua can be obtained by adding soft supersymmetry breaking terms to the potential. In particular, it is well-known that fuzzy spheres S^2_N [1] can arise in this way. These can be understood as quantized coadjoint orbits of $SU(2)$, i.e., quantized spheres S^2.

In our project [2], we found a new type of solutions, which can geometrically be understood as projections of quantized coadjoint orbits of $SU(3)$. These coadjoint orbits would naturally be embedded in $\mathbb{R}^8$, but the projection to $\mathbb{R}^6$ leads to singularities and self-intersections. This is illustrated in Figure 15.2 for one such coadjoint orbit, the projective space $\mathbb{C}P^2$.

We confirmed that our new solutions are stable in the sense that the spectrum of perturbations does not contain imaginary frequency modes. On the other hand, there are fermionic zero modes which link sheets with opposite orientation and carry a definite chirality. This may pave the way to constructing more realistic (chiral) models out of the highly symmetric $\mathcal{N} = 4$ super-Yang-Mills theory. Also the fact that the fermionic zero modes naturally organize in a $\mathbb{Z}_3$ family structure is reminiscent of the standard model.

[1] J. Madore, "The Fuzzy sphere," Class. Quant. Grav. **9**, 69 (1992).
[2] H. C. Steinacker and J. Zahn, "Self-intersecting fuzzy extra dimensions from squashed coadjoint orbits in $\mathcal{N} = 4$ SYM and matrix models," JHEP **1502**, 027 (2015) [arXiv:1409.1440 [hep-th]].

15.10 Quantum electrodynamics in external potentials

J. Zahn

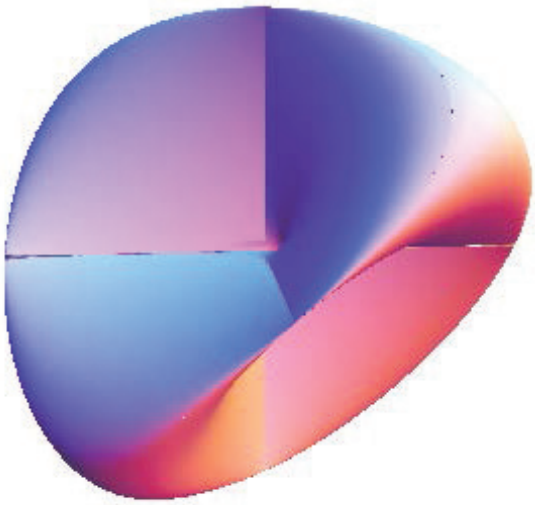

Figure 15.2: Three-dimensional section through the projected $\mathbb{C}P^2$.

Quantum electrodynamics in external potentials (QEDext) has received increasing interest in recent years, triggered in particular by the envisioned high intensity laser sources, c.f. [1] for a review. These may allow to experimentally study the creation of electron-positron pairs in strong external fields, the so-called Schwinger effect. As this is a non-perturbative effect, this opens the exciting possibility to experimentally probe quantum field theory in such a regime. On the other hand, the effect depends highly non-linearly on the external potential, so for interpretations of the experiments it is important to have reliable theoretical and computational tools at disposal.

The theory of quantum fields on curved spacetimes (QFTCS) has much in common with QEDext: For generic external potentials, tools such as Wick rotation or Fourier transformation, which are heavily exploited in quantum field theory on Minkowski space, are not available. QFTCS has witnessed tremendous progress during the last two decades, c.f. the review [2], so it is natural to revisit QEDext from this point of view. This already led to a new formula for the non-perturbative evaluation of vacuum polarization in static potentials [3] and of the vacuum current in time-dependent homogenous electric fields [4].

We plan to continue this line of research by further developing a method, already sketched in [4], to compute particle creation, i.e., the Schwinger effect, in time-dependent external potentials. In contrast to other schemes, it is in principle applicable to generic external potentials. Due to a different treatment of the inherent renormalization ambiguities, the method also circumvents some difficulties that are present in other schemes.

[1] G.V. Dunne, *New Strong-Field QED Effects at ELI: Nonperturbative Vacuum Pair Production*, Eur. Phys. J. D55 (2009) 327, [arXiv:0812.3163].

[2] S. Hollands and R.M. Wald, *Quantum fields in curved spacetime*, Phys. Rept. 574 (2015) 1, [arXiv:1401.2026].

[3] J. Schlemmer and J. Zahn, *The current density in quantum electrodynamics in external potentials*, accepted for publication in Ann. Phys., arXiv:1501.05912 [hep-th].

[4] J. Zahn, *The current density in quantum electrodynamics in time-dependent external potentials and the Schwinger effect*, arXiv:1501.06527 [hep-th].

15.11 Funding

ERC Starting Grant
Prof. S. Hollands
QC & C 259562

DFG Grant
Dr. A Schiller
SCHI 422/9-1

15.12 Organizational Duties

Prof. S. Hollands

- Group leader
- Group speaker
- Erasmus coordinator
- Kolloquium organizer
- Associate editor: General Relativity and Gravitation

Dr. A. Schiller

- Referee Phys. Rev. D
- Referee Europhysics Journal C

15.13 External Cooperations

Academic

- DESY Hamburg
  Prof. G. Schierholz (QCDSF collaboration)
- Edinburgh U., UK
  Dr. R. Horsley (QCDSF collaboration)
- Liverpool U., UK
  Dr. P.E.L. Rakow (QCDSF collaboration)
- Adelaide U., Australia
  Dr. J. Zanotti (QCDSF collaboration)
- Cyprus U. Nikosia
  Prof. H. Panagopoulos and collaborators
- Jena U.
  Dr. A. Sternbeck

- Dubna, Russia
  Dr. E.-M. Ilgenfritz
- U. Chicago, USA
  Prof. R. M. Wald
- Kinki U., Japan
  Prof. A. Ishibashi
- Perimeter Institute, Canada
  Dr. S. Greene
- Grenoble U., France
  Dr. M. Wrochna
- Vienna U., Austria
  Dr. H. Steinacker
- Dubna, Russia
  Prof. A. Isaev (Heisenberg-Landau grant)
- St. Petersburg, Steklov Inst., Russia
  Dr. S.E Derkachov
- Yerevan Phys. Inst., Armenia
  Dr. D. Karakhanyan

15.14 Publications

Journals

J. Holland and S. Hollands, "Recursive construction of operator product expansion coefficients," Commun. Math. Phys. **336** (2015) 3, 1555

S. Hollands and R. M. Wald, "Quantum fields in curved spacetime," Phys. Rept. **574** (2015) 1

S. Hollands and A. Thorne, "Bondi mass cannot become negative in higher dimensions," Commun. Math. Phys. **333**, no. 2, 1037 (2015)

J. Holland and S. Hollands, "A small cosmological constant due to non-perturbative quantum effects," Class. Quant. Grav. **31**, 125006 (2014)

K. Sanders, C. Dappiaggi and T. P. Hack, "Electromagnetism, Local Covariance, the Aharonov-Bohm Effect and Gauss' Law," Commun. Math. Phys. **328**, 625 (2014)

K. Sanders, "On the construction of Hartle-Hawking-Israel states across a static bifurcate Killing horizon," Lett. Math. Phys. **105**, no. 4, 575 (2015)

R. Horsley, H. Perlt, P. E. L. Rakow, G. Schierholz and A. Schiller, "The SU(3) Beta Function from Numerical Stochastic Perturbation Theory," Phys. Lett. B **728** (2014) 1

M. Constantinou, M. Costa, M. Göckeler, R. Horsley, H. Panagopoulos, H. Perlt, P. E. L. Rakow, G. Schierholz and A. Schiller, "Perturbatively improving renormalization constants," PoS LATTICE **2013** (2014) 310

J. Simeth, A. Sternbeck, E.-M. Ilgenfritz, H. Perlt and A. Schiller, "Discretization Errors for the Gluon and Ghost Propagators in Landau Gauge using NSPT," PoS LATTICE **2013** (2014) 459

A. J. Chambers, R. Horsley, Y. Nakamura, H. Perlt, D. Pleiter, P. E. L. Rakow, G. Schierholz, A. Schiller H. Stüben, R. D. Young and J. M. Zanotti, "A Feynman-Hellmann approach to the spin structure of hadrons," Phys. Rev. D **90** (2014) 014510

R. Horsley, J. Najjar, Y. Nakamura, H. Perlt, D. Pleiter, P. E. L. Rakow, G. Schierholz, A. Schiller, H. Stüben and J. M. Zanotti, [QCDSF-UKQCD Collaboration], "Determining Sigma - Lambda mixing," PoS LATTICE **2014** (2014) 110

A. J. Chambers, R. Horsley, Y. Nakamura, H. Perlt, P. E. L. Rakow, G. Schierholz, A. Schiller and J. M. Zanotti, "A novel approach to nonperturbative renormalization of singlet and nonsinglet lattice operators," Phys. Lett. B **740** (2015) 30

R. Horsley, J. Najjar, Y. Nakamura, H. Perlt, D. Pleiter, P. E. L. Rakow, G. Schierholz and A. Schiller *et al.*, "Lattice determination of Sigma-Lambda mixing," Phys. Rev. D **91** (2015) 7, 074512

D. Chicherin, S. Derkachov and R. Kirschner, "Yang-Baxter operators and scattering amplitudes in N=4 super-Yang-Mills theory," Nucl. Phys. B **881** (2014) 467

D. Bahns, K. Rejzner and J. Zahn, "The effective theory of strings," Commun. Math. Phys. **327**, 779 (2014)

J. Zahn, "The renormalized locally covariant Dirac field," Rev. Math. Phys. **26**, no. 1, 1330012 (2014)

H. C. Steinacker and J. Zahn, "An extended standard model and its Higgs geometry from the matrix model," PTEP **2014**, no. 8, 083B03 (2014)

J. Zahn, "Locally covariant chiral fermions and anomalies," Nucl. Phys. B **890**, 1 (2014)

H. C. Steinacker and J. Zahn, "Self-intersecting fuzzy extra dimensions from squashed coadjoint orbits in $\mathcal{N} = 4$ SYM and matrix models," JHEP **1502**, 027 (2015)

in press

J. Holland, S. Hollands and C. Kopper, "The operator product expansion converges in massless φ^4_4-theory," arXiv:1411.1785 [hep-th]. submitted to Commun. Math. Phys.

S. Hollands and A. Ishibashi, "Instabilities of extremal rotating black holes in higher dimensions," arXiv:1408.0801 [hep-th], accepted for publication in Commun. Math. Phys.

J. Schlemmer and J. Zahn, "The current density in quantum electrodynamics in external potentials," arXiv:1501.05912 [hep-th], accepted for publication in Ann. Phys.

Talks

For some talks of Prof. S. Hollands, see the TET group page
http://www.uni-leipzig.de/~tet/?page_id=551

R. Kirschner, "Yangian symmetric correlators, R operators and amplitudes," J. Phys. Conf. Ser. **563** (2014) 1, 012015. QSIS 21, Prag, June 2014.

15.15 Graduations

Master

- Ravinder Kumar
  Numerical Stochastic Perturbation Theory for SU(3) Gauge Theory on Asymmetric and Anisotropic Lattices
  February 19, 2014

15.16 Guests

- Prof. K.-H. Rehren
  U Göttingen
  January 28
- Prof. J. Yngvason
  U Vienna
  April 8
- Dr. M. Dütsch
  U Göttingen
  April 8
- Prof. B. Garbrecht
  TU München
  April 15-16
- Prof. P. Chrusciel
  U Vienna
  May 5-7
- Prof. J. Kunz
  U Oldenburg
  May 13
- Prof. M. Keyl
  TU München
  May 26-28
- Prof. H. Sahlmann
  U Erlangen
  June 3

- Dr. P. Figueras
  Cambridge
  June 9-12
- Dr. Y. Tanimoto
  U Göttingen / U Tokyo
  June 16-21
- Prof. M. Gaberdiel
  ETH Zürich
  July 8-9
- Dr. T. Igata
  Osaka City University
  August 18-31
- Prof. R.M. Wald
  U Chicago
  September 6-12
- Dr. R. Suzuki
  Kyoto U
  September 14-20
- Dr. J. Fuksa
  CTU Prague
  September 22 - October 4
- Prof. D Karakhanyan
  Yerevan State University
  September 29 - November 28
- Prof. K. Fredenhagen
  U Hamburg
  November 11
- Dr. K. Rejzner
  U York
  November 18-19
- Prof. S. Waldmann
  U Würzburg
  November 24-25
- Dr. W. Dybalski
  TU München
  December 2-3

Author Index

F

G

H

I

J

K

L

M

N

T

U

V

W

Z

ISSN 0370-1972
Phys. Status Solidi B
252 · No. 4 April
645–844 (2015)

physica status solidi b

www.pss-b.com

basic solid state physics

4
2015

Theory of semiconductor solid and hollow nano- and microwires with hexagonal cross-section under torsion

Marius Grundmann

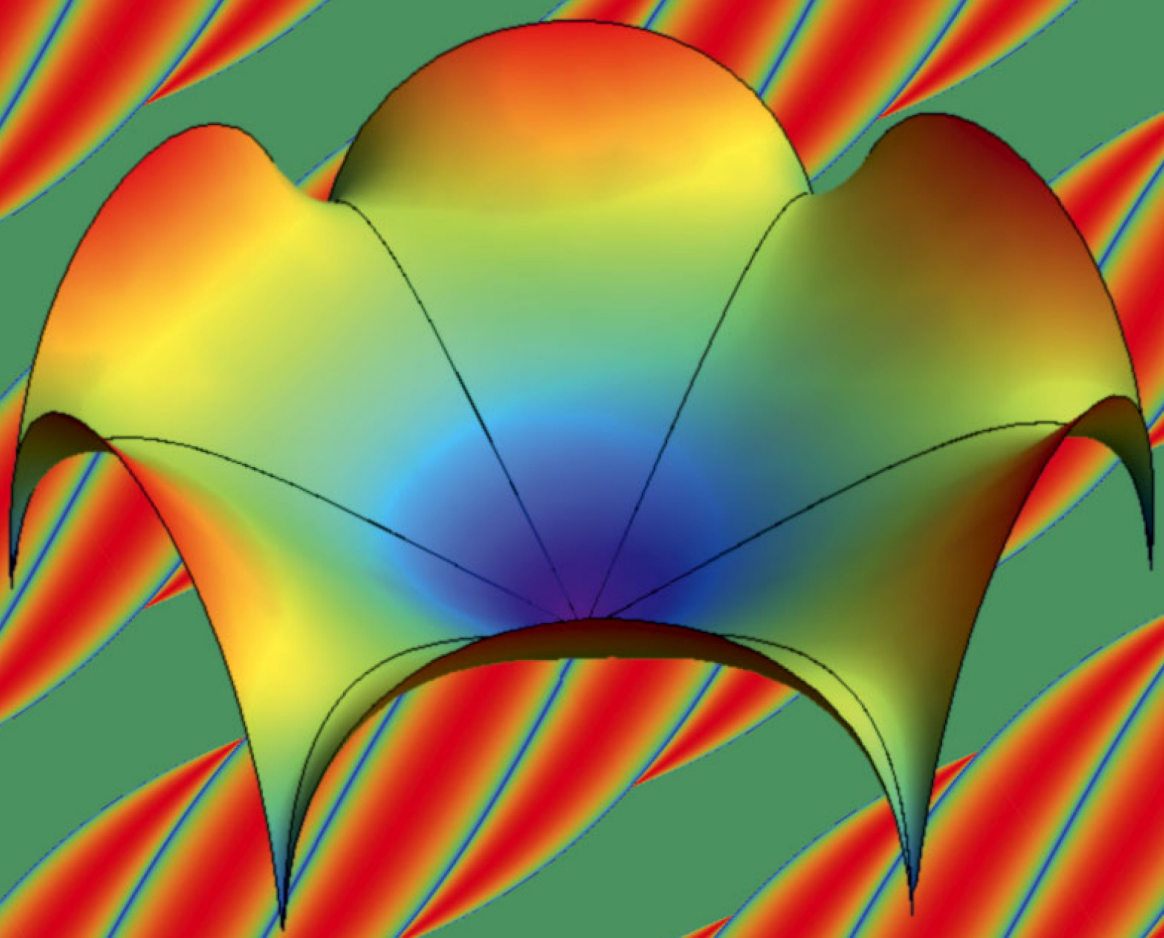

WILEY-VCH

6th Annual Symposium
Physics of Cancer
Leipzig, Germany
September 7 – 9, 2015

PoC

Organizing Committee:
Darius Köster (India)
Franziska Lautenschläger (Germany)
Harald Herrmann (Germany)
Josef A. Käs (Germany)
Joachim Spatz (Germany)

Invited Speakers include:
Eberhard Bodenschatz (Germany)
Aránzazu del Campo (Germany)
Kevin Chalut (UK)
Elisabeth Chen (USA)
Christian Dahmann (Germany)
Mourmita Das (India)
Tamal Das (Germany)
Magalie Faivre (France)
Jeffrey Fredberg (USA)
Jochen Guck (Germany)
Colin Jamora (India)
Laurent Kreplak (Canada)
Karsten Kruse (Germany)
Lisa Manning (USA)
Larry Nagahara (USA)
Maithreyi Narasimha (India)
Pierre Nassoy (France)
Ewa Paluch (UK)
Srikala Raghavan (India)
Heiko Rieger (Germany)
Monika Ritsch-Marte (Austria)
Amy Rowat (USA)
Ingolf Sack (Germany)
Kristine Schauer (France)
Christine Selhuber-Unkel (Germany)
Ralph Sinkus (UK)

Welcome!

This exciting conference assembles the scientific community seeking to understand how physical interactions change during cancer development, how these cause dramatic effects, and what we may be able to do about them. We look forward to meeting you in September 2015!

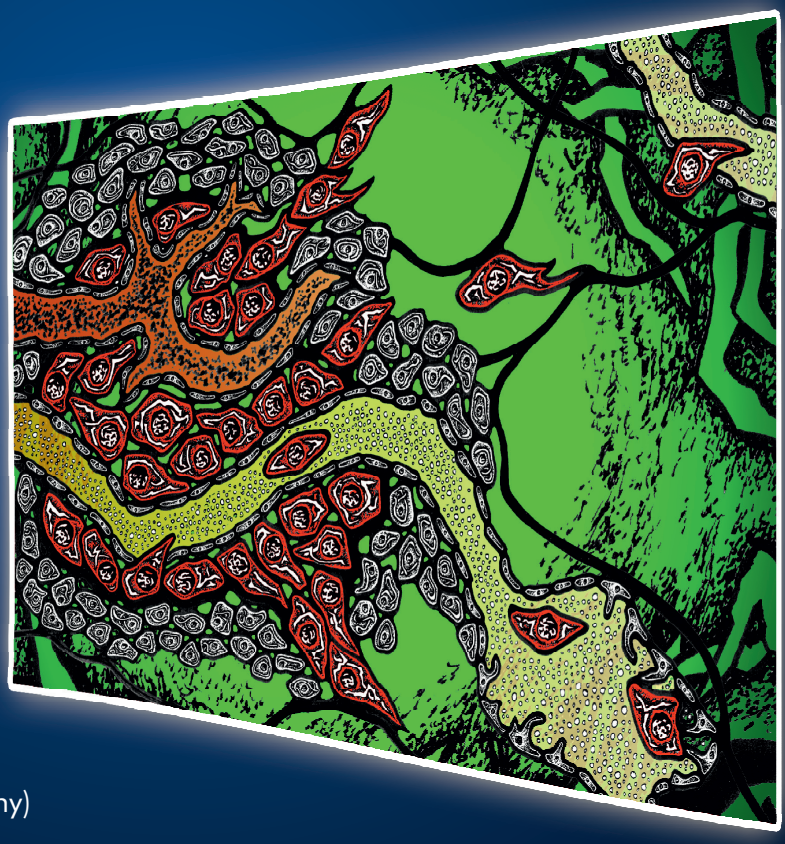

For more information and registration, visit the conference website:

conference.uni-leipzig.de/poc

UNIVERSITÄT LEIPZIG DFG dkfz. DGZ BuildMoNa